OEA

PCBs in the Upper Hudson River

Volume 2
A Model of PCB
Fate, Transport, and Bioaccumulation

Prepared for:

General Electric
Albany, New York

Job Number:
GENhud:131

May 1999

TABLE OF CONTENTS

TABLE OF CONTENTS (Cont.)

TABLE OF CONTENTS (Cont.)

TABLES

TABLES (Cont.)

FIGURES

FIGURES (Cont.)

FIGURES (Cont.)

FIGURES (Cont.)

FIGURES (Cont.)

FIGURES (Cont.)

FIGURES (Cont.)

FIGURES (Cont.)

FIGURES (Cont.)

FIGURES (Cont.)

FIGURES (Cont.)

PLATES

Plate 4-1. Cohesive sediment zones as defined by side scan sonar (reaches 6-8) and the sediment transport bed mapping (Reaches 1-5).

Introduction

Quantitative Environmental Analysis, LLC.

SECTION 1
INTRODUCTION

1.1 BACKGROUND

In 1990, the Region II office of the United State Environmental Protection Agency (USEPA Region II) began a reassessment of the 1984 "No-Action" decision for the sediments of the Upper Hudson River. Recognizing the complexity and dynamic nature of the links between the sediment polychlorinated biphenyl (PCB) levels and PCB levels in the water column and biota, the General Electric Company (GE) has undertaken the development of a mass balance model. The purpose of the model is to provide scientifically reliable estimates of future PCB levels by integrating available site data and the scientific knowledge of the physical, chemical and biological processes that govern PCB fate within the river. Properly constructed, the model can be used to assess, with greater confidence than any other method currently available, the potential impacts of various remedial scenarios on downstream PCB transport and PCB levels in fish. Without such a tool, the interpretation of data and the evaluation of remedial scenarios are subjective and open to considerable uncertainty.

The overall goal of the modeling efforts is to provide quantitative answers to the following questions:

- When will PCB levels in Upper Hudson River fish populations recover to levels meeting human health and ecological risk criteria under continued No Action?

- Can remedies other than No Action significantly shorten the time required to achieve acceptable risk levels?

- Are there sediments now buried and effectively sequestered from the food chain which are likely to become "reactivated" following a major flood, resulting in an increase in contamination of the fish population?

GE has completed a comprehensive model capable of addressing these questions. This report summarizes the development, calibration/validation and application of the model. There are four sub-models that describe:

1) hydrodynamics
2) sediment transport
3) PCB fate and
4) PCB bioaccumulation within the Upper Hudson River.

The four sub-models have each been calibrated/validated for the period from 1977 to 1998 using environmental monitoring data collected on the Hudson River.

1.2 MODELING APPROACH

PCB sources associated with the Hudson Falls plant site area (Figure 1-1) and historically contaminated sediments account for the water column loadings and fish PCB body burdens observed in the Upper Hudson River. However, most of the historically deposited sediment PCBs are now sequestered below the sediment surface, a consequence of the continual deposition of watershed derived particulate matter. The change in surface sediment PCB concentrations has been preserved in the vertical profile of PCB concentrations in areas of the river subject to continual accretion. Sediment cores collected from these locations and dated using radioactive tracers (USEPA 1997) generally show PCB maxima in the late 1960s and early 1970s, a rapid decline between the 1970s and mid 1980s, and a slower decline thereafter (Figure 1-2). The temporal changes preserved within the sediment record reflect the net result of a variety of dynamic processes governing the transport, transfer, and transformation of PCBs within the river (Figure 1-3):

- transport of PCBs to the river from external sources,
- influx of uncontaminated water and particulate matter from the surrounding watershed,
- deposition and erosion of particulate matter at the sediment surface,
- diffusion of PCBs within the sediment and between the sediment and overlying water column, and

- loss of PCBs through volatilization and biologically mediated reactions.

These processes represent the basic elements of a mass balance and are the framework of a conceptual model of PCB fate within the Upper Hudson River. The mass balance stems from the scientific principle of mass conservation and is the basis for the quantitative analysis of PCBs in the Hudson River.

The mass balance principle is applied to a given stretch of river by adding mass inflows from the upstream boundary, tributary inflows and the mass transferred from the bed and subtracting the sum of the mass outflow at the downstream boundary, the mass transfer by volatilization and burial, and the mass loss by microbial degradation.

The quantitative form of the mass balance concept contains the processes, expressed as mass transfer rates, defined as products of a transfer coefficient and either the concentration (advection process) or the concentration gradient (diffusive process). The transfer coefficients are functions of the fundamental properties of the interactive system: the river flow (velocity, depth and shear), the suspended and bed solids (size, density and composition) and the PCBs (molecular weight and structure, volatility and diffusivity). The functions are based on theoretical reasoning confirmed by laboratory experiments. Their extrapolation to the natural environment introduces a degree of uncertainty, thus, a degree of freedom, in assigning a numerical value, specific to a water body. Transfer coefficients are accepted or rejected by comparing the concentrations calculated with those observed.

To construct a mass balance for the water column, river bed, and food chain, the equations include local concentrations and concentrations in the contiguous regime. This is complicated by the fact that the process is dynamic. The settling flux, expressed in terms of water concentrations, is a source for the bed and, the scour of the bed is a source for the water column. It follows that the water and bed equation must be solved simultaneously. Furthermore, the time scale of interest is the long-term projection (years – decades) of PCB concentration in three regimes (water, bed, and biota). To assess annual variation it is necessary to examine seasonal changes in PCB concentration during periods influenced by high flow and low flow.

The high flow periods, typically in the spring, are the result of sporadic floods from snow melt or high rainfall, that occurs over intervals of hours to days. Low flow typically occurs in summer and early fall when the watershed has high evapotranspiration rates and less water enters the tributaries and the river. The late fall-winter periods may be characterized by either a high or low flow, depending on regional meteorological conditions. Thus, the numerical computation covers a spectrum of time scales from hours to decades.

1.3 OVERVIEW OF THE MODELS

The models described here are applied to a 40-mile section of the Upper Hudson River extending from Fort Edward at mile point (MP) 194 to Troy Dam (MP 154) (Figure 1-4). Mile points start with MP 0 at the southern tip of Manhattan at the Battery. This section of the river has eight dams that separate the river into eight reaches. These reaches are numbered from the Troy Dam (reach 1) in the upstream direction to the Thompson Island Pool (TIP) (Reach 8). The mile points at the boundaries of each reach and at other selected locations within the study area are shown in Table 1-1. The GE capacitor manufacturing plants and the Allen Mill are located just upstream of Reach 8 in the vicinity of Bakers Falls (approximately MP 197).

Table 1-1. Mile Points of Reach Boundaries and Other Selected Locations

Reach/Location	Mile Point*	Description
Reach 8	188.4-193.7	Fort Edward Dam to Thompson Island Dam
Reach 7	186.0-188.4	Thompson Island Dam to Fort Miller Dam
Reach 6	183.2-186.0	Fort Miller Dam to Northumberland Dam
Reach 5	168.0-183.2	Northumberland Dam to Stillwater Dam
Reach 4	165.8-168.0	Stillwater Dam to Mechanicville Dam
Reach 3	163.4-165.8	Mechanicville Dam to Lock 2
Reach 2	159.5-163.4	Lock 2 to Waterford Dam
Reach 1	153.9-159.5	Waterford Dam to Troy Dam
Fort Edward	194.6	Water Quality Sampling Station
Thompson Island Dam	188.5	Water Quality Sampling Station
Schuylerville	181.4	Water Quality Sampling Station
Stillwater	168.3	Water Quality Sampling Station
Waterford	156.5	Water Quality Sampling Station

*Mile point is measured in miles northward along the river channel beginning at the Battery on the southern tip of Manhattan.

The model has four sub-models that are discussed below.

- hydrodynamics
- sediment transport
- PCB fate and
- PCB bioaccumulation

1.3.1 Hydrodynamic Model

Hydrodynamics refers to the movement of water through the river and the friction or shear stress that this movement causes at the interface between the water and the sediment bed. A hydrodynamic model computes the velocity and water surface elevation, as well as the shear stress at the sediment-water interface, in response to upstream flows and to flows entering the river from tributaries. The conditions predicted by the hydrodynamic model are used in the sediment transport model to evaluate sediment scour, resuspension, and downstream transport. Additionally, the PCB fate model uses the hydrodynamic model output to compute overall downstream transport of PCBs.

Two hydrodynamic models were developed, calibrated, and validated in order to provide the necessary hydrodynamic input for the sediment transport and PCB fate models. A two-dimensional, vertically-integrated hydrodynamic model defines the distribution of shear stresses at the sediment-water interface that controls sediment transport. The one-dimensional hydrodynamic model was developed to define the average transport of PCBs within the water column.

1.3.2 Sediment Transport Model

Sediment transport includes the movement of suspended solids within the river and the deposition and resuspension that occurs at the sediment-water interface. The sediment transport model uses the output of the two-dimensional hydrodynamic model and the results of laboratory

and field studies to describe the resuspension and deposition processes of cohesive and non-cohesive sediments within the Upper Hudson River. The model takes into account solids loading from upstream of the study area, tributary loading, scour of cohesive and non-cohesive sediment, deposition of tributary and resuspended solids, and downstream transport. Results of the sediment transport model (in the form of a spatial and temporal matrix of total suspended solids (TSS) and as resuspension and deposition fluxes) are used directly by the PCB fate model.

1.3.3 PCB Fate Model

PCB fate includes the transport of PCBs dissolved in the water or sorbed to solids, transfer between the dissolved and sorbed phases, transfer between the water and atmosphere, and degradation that occurs biochemically. The PCB fate model includes mechanistic descriptions of these transport, transfer and reaction processes (Figure 1-3). PCBs are assumed to partition between dissolved and particulate phases, with partitioning assumed to be rapid, such that equilibrium conditions are generally well approximated. The dissolved phase is composed of freely dissolved PCBs and PCBs sorbed to dissolved and colloidal organic matter. Freely dissolved PCBs are transferred from the water column to the atmosphere by volatilization across the air-water interface. Particulate-phase PCBs settle from the water column to the sediment bed, and are resuspended from the sediment bed into the water column. Dissolved PCBs are exchanged between the water column and sediment bed and within the sediment in accordance with the laws of diffusion, that is, from a region of higher concentration to one of lower concentration, with the rate of transfer controlled by a mass transfer coefficient.

The output from the hydrodynamic and sediment transport models provide much of the information necessary to predict long-term PCB fate and transport trends in the Upper Hudson River. This information is supplemented by laboratory and field data to refine the relevant processes.

1.3.4 PCB Bioaccumulation Model

PCB bioaccumulation involves the uptake of water- and sediment-borne PCBs by invertebrates and the sequential transfer of those PCBs through the food web *via* predation. The bioaccumulation model consists of a simplified food web representative of the Upper Hudson River, empirically defined trophic transfer factors for calculating PCB levels in invertebrates, and a mechanistic, dynamic simulation framework for computing PCB levels in fish.

The model food web structure and the diet of each of the model species were developed based on site-specific information. The model food web contains four trophic levels: particulate matter (trophic level 1, or TL1), invertebrates (TL2), forage fish (TL3) and predators (TL4). TL1 includes water column and surface sediment particulate matter. TL2 is represented by two functional groups, benthic macroinvertebrates associated with the sediment bed (BMI) and phytophilous macroinvertebrates associated with particulate matter and periphyton in contact with the water column (PMI). TL3 is presented by two species, pumpkinseed and brown bullhead. TL4 is represented by largemouth bass.

The dynamic PCB bioaccumulation model is based on the principals of conservation of mass and energy and mechanistically describes the uptake and loss of PCBs by forage and predatory fish. PCBs are taken up during respiration and ingestion and are lost by diffusion across the respiratory surfaces. Rates of PCB uptake and loss are calculated from computed rates of feeding and respiration and empirically defined transfer efficiencies of PCBs. Finally, the dissolved and particulate PCB concentrations computed by the fate model provide the PCB exposure for the food web.

1.3.5 Calibration and Validation

The equations that comprise each of the models are general and can be applied to any river system. Application of these equations to the Upper Hudson River involved the determination of appropriate values for each of the parameters in the equations. Site-specific data were the basis for assigning values, either directly or by the process of model calibration. Each of the models was calibrated and validated using a data record that extends from 1977 to

the present. As described above, the models are interrelated with information generated by one model providing input for the next model in the sequence. A schematic of the interrelationships is presented on Figure 1-5.

1.3.6 PCB Constituents Modeled

PCBs are a mixture of 209 possible congeners that vary in the number and position of chlorine atoms bound to the biphenyl rings. PCBs containing the same number of chlorine atoms are chemical homologs (e.g. monochlorinated biphenyls are the group of PCB congeners containing one chlorine regardless of position). The number and position of the chlorine atoms affect the physical, chemical, and biological properties of the individual PCB congeners (e.g. Henry's Law Constant, octonal-water partition coefficient, and susceptibility to dechlorination) and consequently their environmental fate. Therefore, the environmental fate of PCBs in the Hudson River is dependant on the mix of PCB congeners present in the system.

PCB were not consistently quantified and reported within the historical PCB database. The historical Hudson River sediment, water column, and biota PCB databases were developed using packed column-based gas chromatographic (GC) techniques. These methods quantified PCBs within environmental samples based on subjective pattern matching between the chromatographs of commercial Aroclor mixtures and those of the samples. As a result, PCB identification varied among laboratories and over time within individual laboratories. Moreover, the methods employed were incapable of differentiating individual congeners and, due to co-elution of the sample and carrier solvent, did not quantify a significant fraction of the sample's mono- and dichlorinated PCBs. In contrast, capillary column-based GC analytical techniques, such as those employed by GE and the USEPA in recent years, resolve PCBs in Hudson River media at the individual congener level. This lack of consistency in quantifying PCBs between the different data sets necessitated the development of procedures to transform the data into a common measurement against which to compare model calculations.

GE and the USEPA determined that the fraction of PCBs containing three or more chlorines (heretofore represented as PCB_{3+}) represents the most common PCB equivalents within

the historical database. This selection was based upon rigorous evaluation of PCB analytical techniques employed by the different laboratories responsible for generating the historical PCB data. This work is documented in numerous technical memorandum written by Dr. John Butcher of Tetra-Tech, Inc. (Butcher 1996a, Butcher 1996b, Butcher 1997a, Butcher 1997b, Butcher 1998a, Butcher 1998b), on behalf of the USEPA and modified and substantiated by additional analyses and analytical measurements conducted by GE (HydroQual 1998, QEA 1999, GE 1997, GE 1998). The specifics of the transformations required to convert the data into PCB_{3+} equivalents are described in these documents.

The decision to model PCB_{3+} precludes evaluation of mono- and dichlorinated PCB fate and transport. Mono- and dichlorinated PCBs make up a significant proportion of total PCBs within Hudson River sediments, originating in large part from biologically-mediated reductive dechlorination. Moreover, due to their lower partition coefficients, mono- and dichlorinated PCBs account for a significant portion of pore water total PCB concentrations and consequently account for a significant portion of sediment/water column PCB exchange. However, mono- and dichlorinated PCBs do not significantly bioaccumulate in fish, typically constituting less than 5% of total PCBs in fish from the UHR. Therefore, the choice to model PCB_{3+} (as dictated by the historical data) does not significantly influence the predictive power of the models since the principal goal of the modeling effort is the future projections of PCBs in fish under different remedial action scenarios.

1.4 MODEL SENSITIVITY AND UNCERTAINTY

A model is an abstraction of reality and its predictions are estimations of future conditions. The inaccuracy in model prediction results from multiple sources:

1) the equations describing the relevant processes
2) the values assigned to the parameters of the equations
3) the assumptions regarding future conditions (e.g., river flows, soil erosion, PCB discharges to the river)

The equations are imperfect because they describe the relevant physical, chemical and biological processes using simplifications demanded by incomplete knowledge and computational constraints. The parameter values are imperfect because the data available are subject to error and generally do not characterize the full range of conditions at the site being modeled. Model calibration is the process by which parameter values are chosen to maximize the ability of the model to describe historical conditions for which data are available. In the absence of data limitations, the optimum model calibration defines the best estimates of the parameters (i.e., the parameter values that reduce uncertainty to that inherent in the equations). The extent to which calibration determines the "correct" value for each parameter depends on the robustness of the calibration data set and the sensitivity of the model to changes in the parameter. If the model is sensitive to a parameter then its uncertainty is small. Conversely, if the model is insensitive to a parameter then its uncertainty is high.

Equation and parameter inaccuracy can be estimated from the difference between the model and calibration data. Such an assessment is done routinely in regression analyses where parameter inaccuracy is specified by the uncertainty of the slope estimate and equation inaccuracy is specified by the component of data variance not accounted for by the model. Such uncertainty assessments yield upper bound estimates of inaccuracy because they assign all error to the model. In fact, a portion of the error is due to data error. Data error exists because data are a limited sampling of continuous processes and are subject to sampling and analysis inaccuracies.

A regression-like approach is not practical for the complex mechanistic models used to describe PCBs in the Hudson River. Approaches do exist for estimating the parameter uncertainty of water quality models. The most common approach is based on Bayes Theorem. Here, the distribution of possible parameter values is estimated by using the concordance between parameter values and the ability of the model to reproduce the calibration data to update an initial distribution developed from data or experience. In other words, the final distribution of parameter values includes only those that yield a model result statistically consistent with the data (e.g., the root mean square difference between model and data is within some defined limit).

Such an approach has been used with other water quality models, including a relatively simple model of PCB fate in the Upper Hudson River (Steinberg *et al.* 1996).

A formal Bayesian analysis to define the parameter uncertainty in the Hudson River models is difficult, if not impossible, because of the complexity of the equations and computational constraints. As a practical alternative we used the knowledge gained through development and calibration of the models to choose a subset of processes for investigation. The criteria for the inclusion in the subset was that the process is important to model prediction, but the parameter values used in the process description are not accurately known from measurement and were established by professional judgement or calibration.

Uncertainty of the selected parameters was estimated by a sensitivity analysis designed to determine the range over which the parameters can be varied without causing an increase in calibration error. The results of this analysis are presented as part of the discussions of model development in the sections that follow.

The sensitivity analysis was used to establish a bounding prediction. The purpose was to establish a lower bound estimate of natural recovery for comparison to the best estimate based on the base calibration. This bounding prediction is less likely because the parameters are shifted from their expected values.

Prediction error resulting from the inaccuracy of assumptions regarding future conditions was addressed by making several predictions that use differing assumptions regarding upstream PCB sources and river flow.

1.5 SCOPE OF MODELING EFFORT

The model developed for the Upper Hudson River addressed the questions posed in Section 1.1 by simulating the major processes that control PCB concentrations in water and sediment and the major processes that control the transfer of PCBs through the food web to top

predatory fish. It does this for the stretch of river between Rogers Island in Fort Edward and the Troy Dam.

There remains a suite of relevant questions whose answers are beyond the scope of the model. Although the model computes the PCB load delivered over the Troy Dam to the Lower Hudson River, it does not predict the contribution of Upper Hudson River PCBs to PCB levels observed in Lower Hudson River fish, sediment and water. Because the model represents PCBs as a single aggregate of all PCBs with three or more chlorine atoms, it does not predict changes in PCB toxicity that result from environmental transformations. Aggregation also precluded accurate assessment of PCB dechlorination mechanisms and rates. The bioaccumulation model simulates the average individual in a population and cannot address questions about the distribution of PCB levels within the population, the relationships between fish population dynamics and fish PCB levels, or the impacts of toxic stress on population growth or sustainability. Finally, the observed entry of PCB oil as a Dense Non-Aqueous Phase Liquid (DNAPL) into the river at Hudson Falls indicates that PCB fate and transport may be affected by the dissolution and transport characteristics of DNAPL. The model does not simulate DNAPL and cannot address questions related to these phenomena.

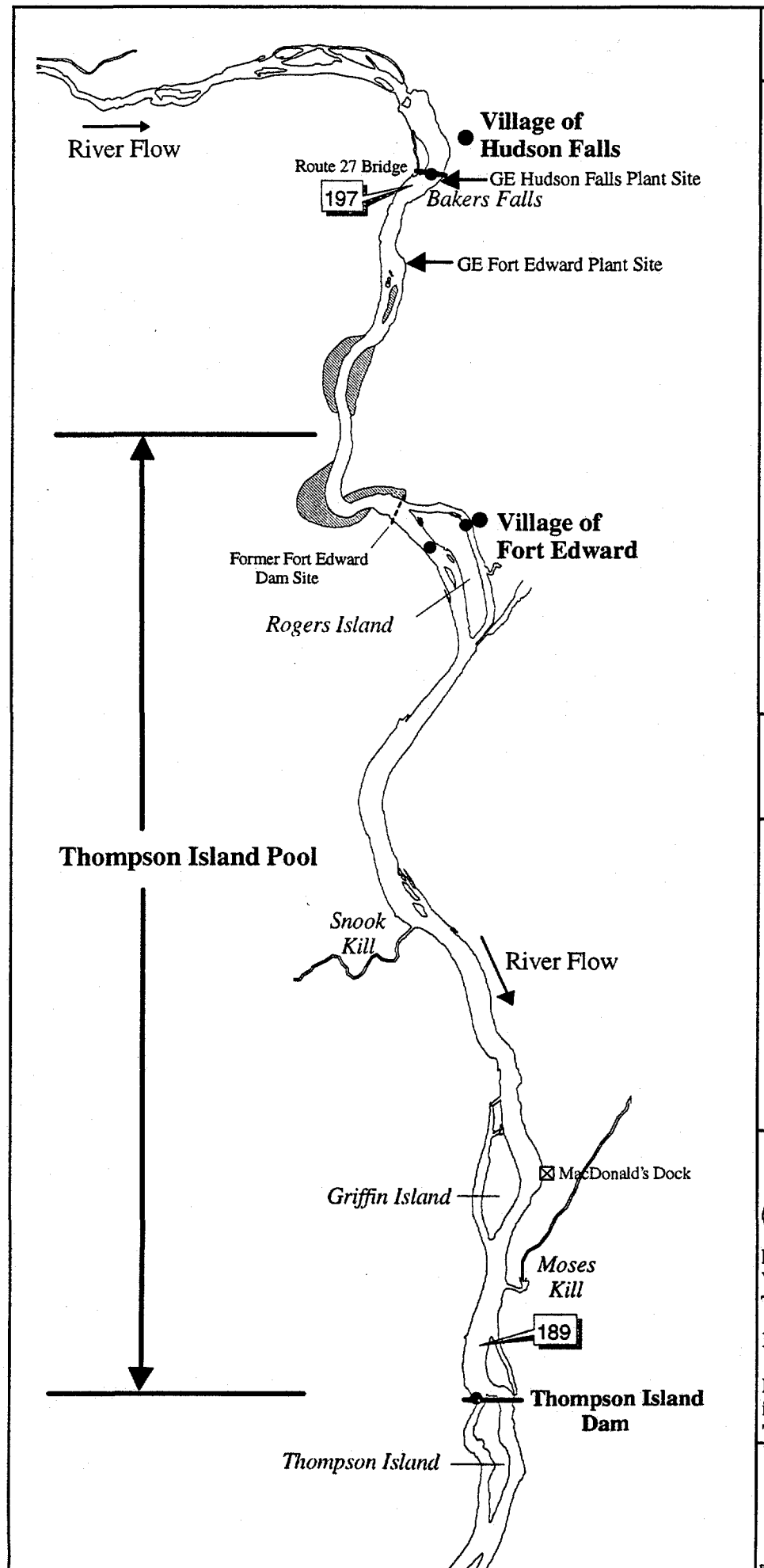

LOCATION MAP OF THE HUDSON RIVER

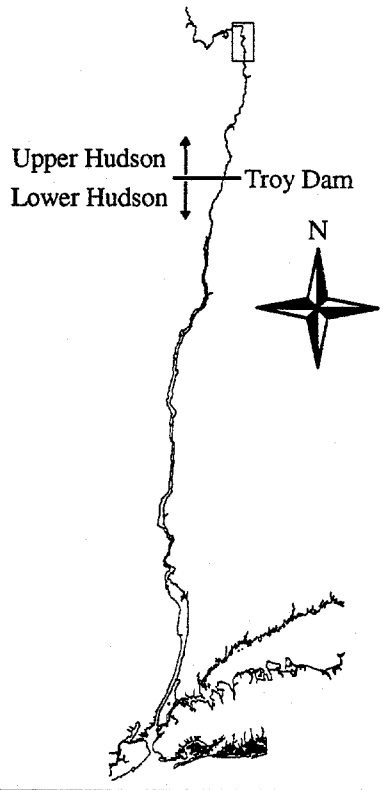

GRAPHIC SCALE

0.5 0 0.5 1 Miles

LEGEND

- GE Plant Sites
- Approximate Location of Remnant Deposits
- Approximate Mile Point from Battery in NYC
- Routine Water Column Monitoring Locations

GENERAL ELECTRIC COMPANY
Hudson River Project

PCBs in the Upper Hudson River
Volume 2. A Model of PCB Fate, Transport, and Bioaccumulation

Figure 1-1.

Portion of the Upper Hudson River including GE plant sites and Thompson Island Pool (Reach 8).

QEA
Quantitative Environmental Analysis, LLC

Project: GENhud 131 May 1999

\\Poseidon\d-drive\Genhud\Documents\Final_report\Vol_2\Section_1\UHR_TIP_Fig1_1

313650

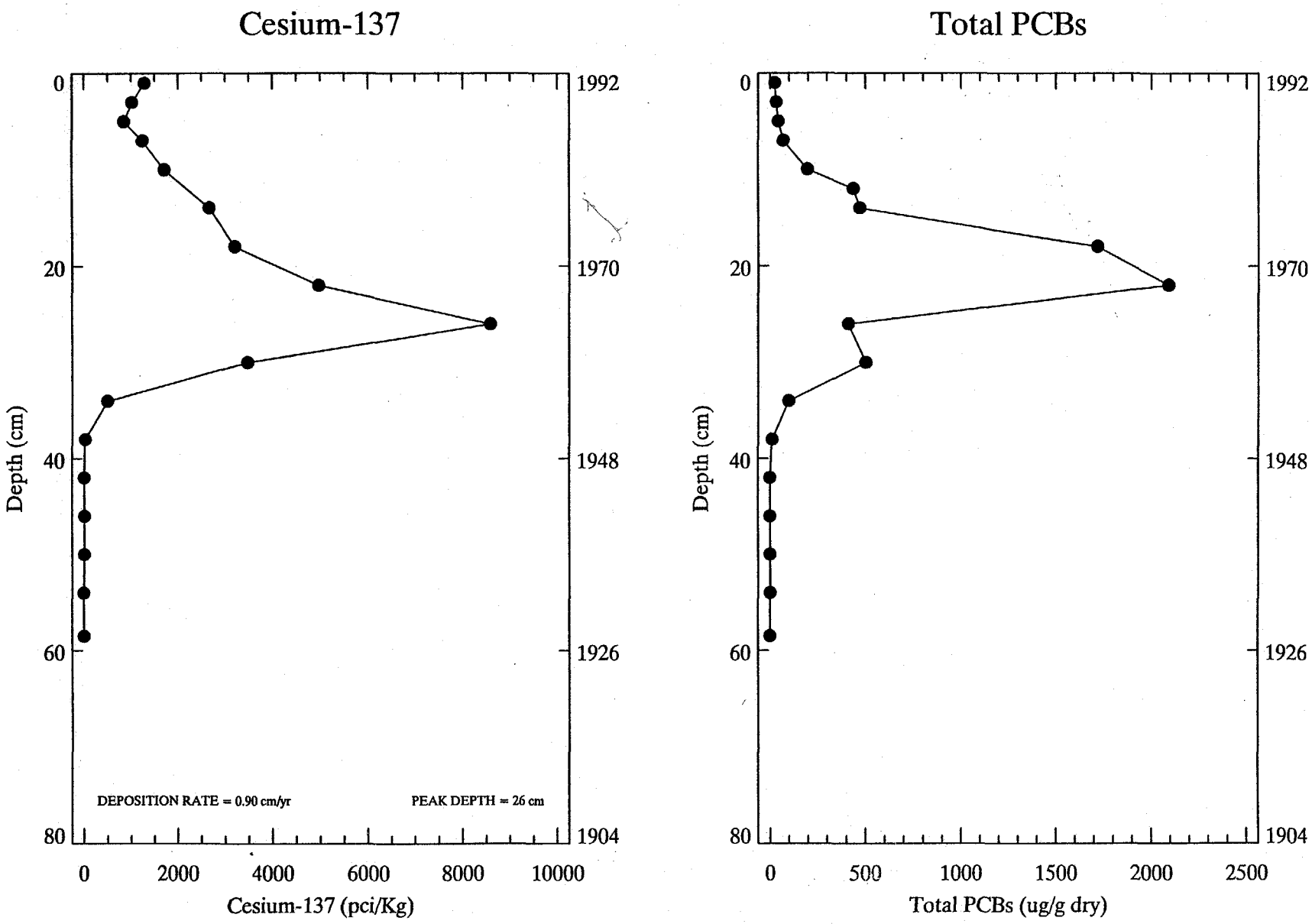

Note: Core shown is USEPA High Resolution Core HR-019 collected in Thompson Island Pool at RM 188.5.

Figure 1-2. PCB sediment time history as evidenced by a sediment core dated using ^{137}Cs.

MJW - D:\GENhud\analysis\Sediment\98HR_LR\cesium\csprof.pro
Thu Apr 15 02:24:24 1999

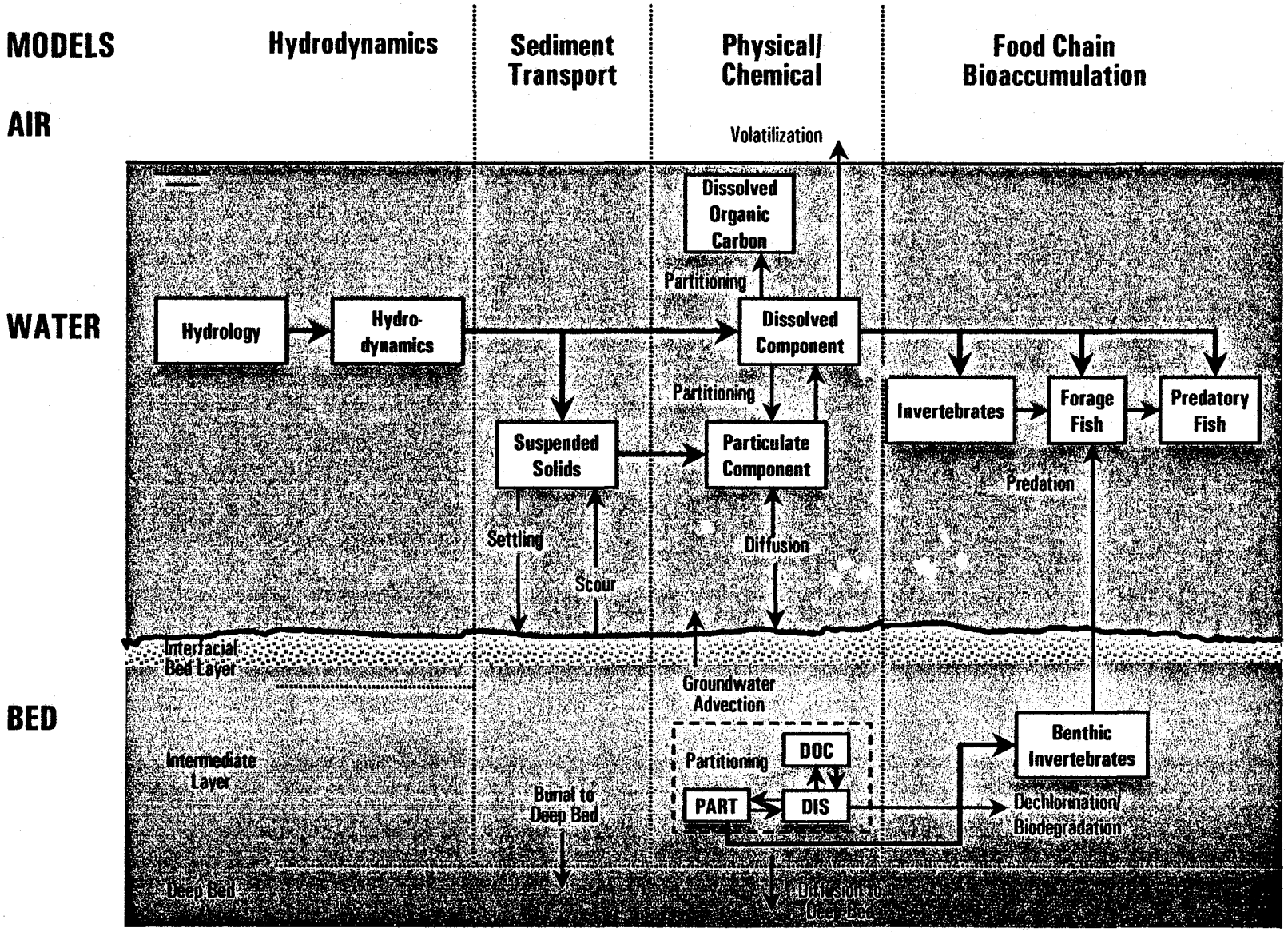

Figure 1-3. Dynamic processes governing fate, transport, and transformation of PCBs in the environment.

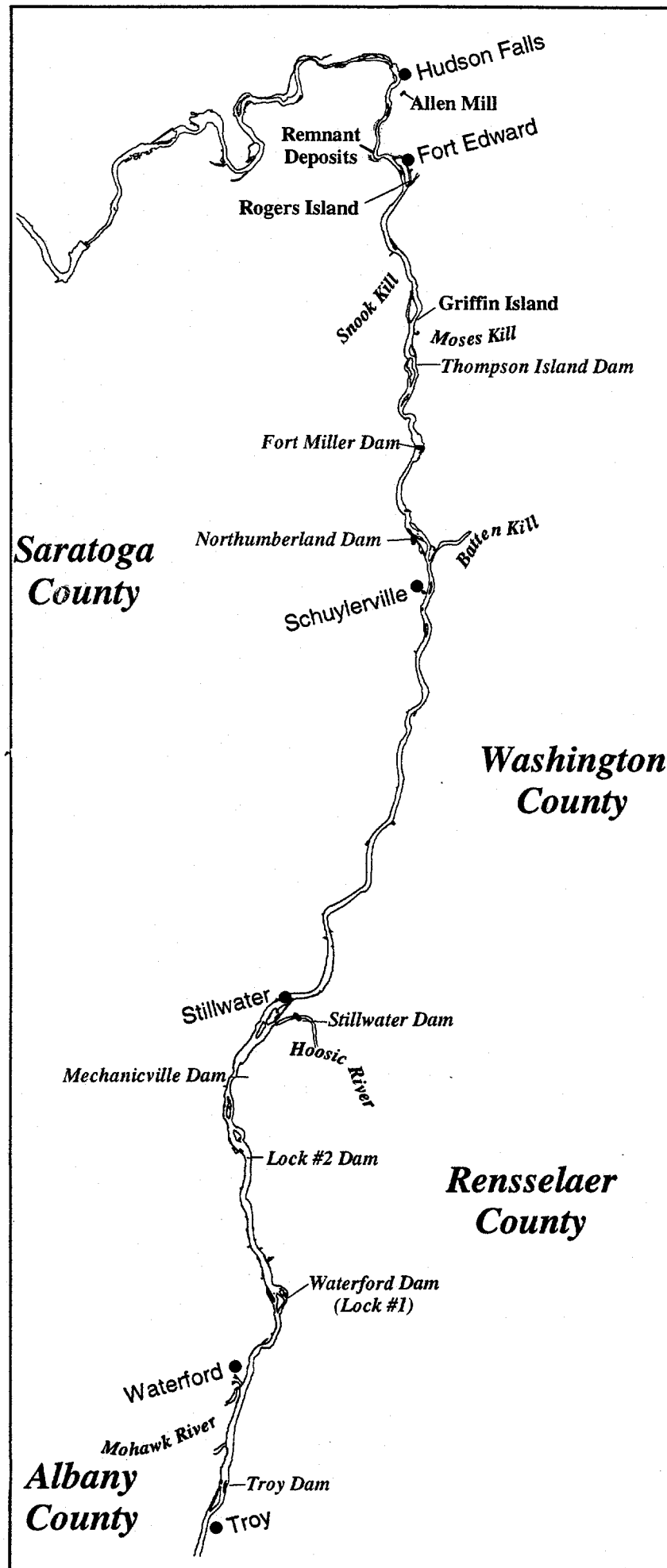

LOCATION MAP OF THE UPPER HUDSON RIVER

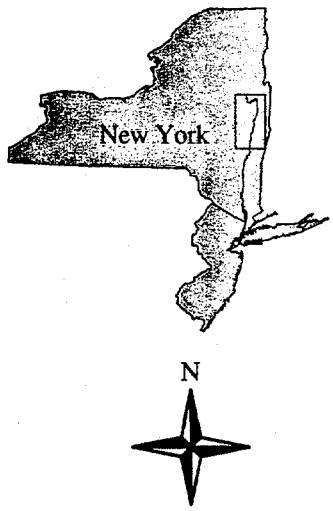

GRAPHIC SCALE

2 0 2 4 Miles

NOTES/DATA SOURCES

The USGS gauging stations of Fort Edward, Schuylerville, Stillwater, and Waterford can be approximated by the location of each respective city (green dots).

GENERAL ELECTRIC COMPANY
Hudson River Project

PCBs in the Upper Hudson River Volume 2. A Model of PCB Fate, Transport, and Bioaccumulation

Figure 1-4.

Upper Hudson River.

QEA
Quantitative Environmental Analysis, LLC

Project: GENhud 131 May 1999

313653

\\Poseidon\D_drive\Genhud\Documents\Final_Report\Vol_2\UHR_Fig1_4.apr

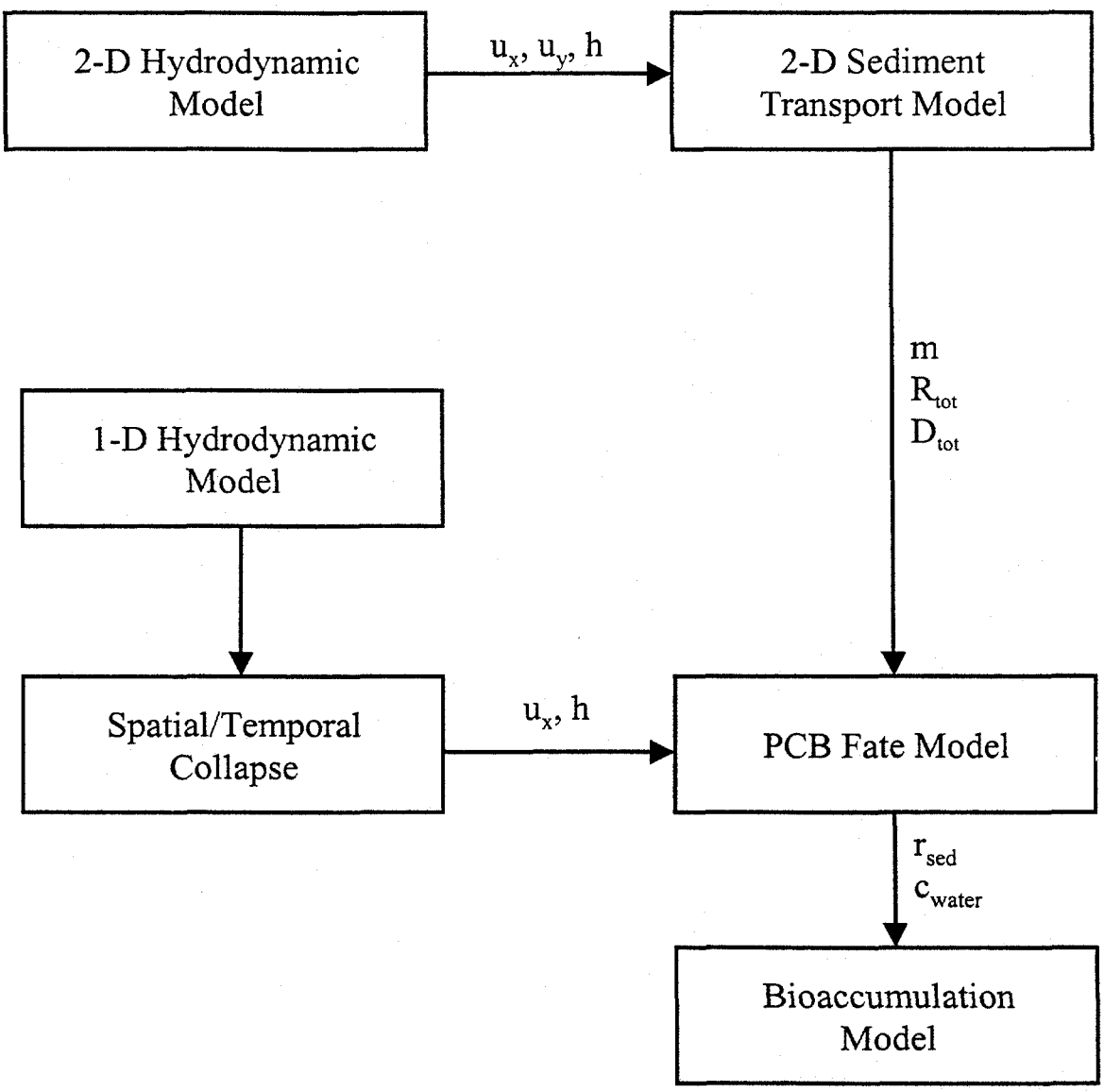

Figure 1-5. Model interrelationships.

\\Poseidon\D_drive\Genhud\Documents\Final_reportVol_2\Section_1\Fig1_5_model_inter.ppt

Hydrodynamic Models

Quantitative Environmental Analysis, LLC.

SECTION 2
HYDRODYNAMIC MODELS

2.1 MODEL STRUCTURE AND EQUATIONS

Hydrodynamic processes affect PCB transport in the Upper Hudson River on different spatial and temporal scales. For example, a relatively coarse numerical grid is sufficient to simulate accurately water column PCB transport along the main stem of the river. Accurate prediction of solids fluxes at the sediment-water interface requires a finer grid to resolve spatial variations in bathymetry, bottom shear stress and sediment bed properties. These variations in spatial and temporal scales necessitated development of two hydrodynamic models of the Upper Hudson River. A one-dimensional model was developed to provide transport information for the PCB fate model. A two-dimensional, vertically-averaged model was developed and coupled to the sediment transport model.

Other researchers have developed hydrodynamic models of the Upper Hudson River using one-dimensional models developed by the U.S. Army Corps of Engineers, i.e., HEC-2 or HEC-6. Previous modeling studies include, but are not limited to, the following: Zimmie's (1985) application of HEC-6 to the TIP and FEMA Flood Insurance Studies (e.g., FEMA 1995), which used HEC-2. While these two models can provide adequate simulations of water surface elevation gradients and cross-sectionally averaged velocities in the Upper Hudson River, both models cannot be used to calculate time-variable discharge as needed to meet the goals of this study.

2.1.1 One-Dimensional Model

Time-variable flow in the Upper Hudson River was described using a one-dimensional hydrodynamic model, i.e., laterally- and vertically-averaged. For a non-prismatic channel, as exists in this river, the one-dimensional conservation of mass and momentum equations are:

$$\frac{\partial A}{\partial t} + \frac{\partial (u_x A)}{\partial x} = 0 \qquad (2\text{-}1)$$

$$\frac{\partial u_x}{\partial t} + \frac{1}{2}\frac{\partial u_x^2}{\partial x} = -g\frac{\partial \eta}{\partial x} - g\frac{n^2}{R^{4/3}}u_x|u_x| \qquad (2\text{-}2)$$

where:

A	=	cross-sectional area (L^2)
u_x	=	cross-sectional average velocity (L/T)
η	=	water surface displacement from the reference depth (L)
n	=	Manning's coefficient ($T/L^{1/3}$)
R	=	hydraulic radius (L)
g	=	acceleration due to gravity (L/T^2)

These equations were solved numerically.

The Manning's n coefficient used in Equation (2-2) was assumed to be temporally and spatially constant in a particular reach. However, Manning's n did vary between reaches, with reach-specific values being determined during model calibration.

Solution of Equations (2-1) and (2-2) required development of functional relationships between the cross-sectional area and η and R for each numerical grid element. These functional relationships were determined from Upper Hudson River bathymetry and geometry data.

2.1.2 Two-Dimensional Model

The Upper Hudson River is relatively shallow and the flow is unstratified. These conditions make it reasonable to assume that the water column is vertically well-mixed. Thus, the two-dimensional, vertically-averaged equations are an accurate approximation to the general three-dimensional equations of motion for an incompressible fluid. The hydrodynamic equations

(conservation of mass and momentum) applied to the Upper Hudson River are (Ziegler and Nisbet 1994):

$$\frac{\partial \eta}{\partial t} + \frac{\partial (u_x h)}{\partial x} + \frac{\partial (u_y h)}{\partial y} = 0 \qquad (2\text{-}3)$$

$$\frac{\partial (u_x h)}{\partial t} + \frac{\partial (u_x^2 h)}{\partial x} + \frac{\partial (u_x u_y h)}{\partial y} = -gh\frac{\partial \eta}{\partial x} - C_f q u_x + \frac{\partial}{\partial x}\left(hB_H \frac{\partial u_x}{\partial x}\right) + \frac{\partial}{\partial y}\left(hB_H \frac{\partial u_x}{\partial y}\right) \qquad (2\text{-}4)$$

$$\frac{\partial (u_y h)}{\partial t} + \frac{\partial (u_x u_y h)}{\partial x} + \frac{\partial (u_y^2 h)}{\partial y} = -gh\frac{\partial \eta}{\partial y} - C_f q u_y + \frac{\partial}{\partial x}\left(hB_H \frac{\partial u_y}{\partial x}\right) + \frac{\partial}{\partial y}\left(hB_H \frac{\partial u_y}{\partial y}\right) \qquad (2\text{-}5)$$

where:

h	=	total water depth ($h_o + \eta$) (L)
h_o	=	reference water depth (L)
u_x, u_y	=	velocities along the x- and y-axes (L/T), respectively
q	=	$(u_x^2 + u_y^2)^{1/2}$ (L/T)
C_f	=	spatially variable bottom friction factor (non-dimensional)
B_H	=	horizontal eddy viscosity (L^2/T)

Note that the x-axis is oriented in the longitudinal (along-channel) direction and the y-axis is oriented in the lateral (cross-channel) direction. Equations (2-3) to (2-5) were transformed from Cartesian coordinates to orthogonal, curvilinear coordinates in order to resolve more accurately the complex geometry and bathymetry of the Upper Hudson River. The resulting equations were solved numerically.

Bed elevation changes due to sediment deposition and erosion cause changes in the reference water depth (h_o). Generally, sediment bed elevation changes are a small fraction of h_o for the time periods considered in this study and do not significantly affect hydrodynamics in the Upper Hudson River. However, small areas of high deposition, over decadal time scales, could cause enough change in h_o to affect flow patterns in localized areas of the river. Therefore,

changes in bed elevation predicted by the sediment transport model were used to adjust h_o during all simulations.

The bottom friction factor in Equations (2-4) and (2-5) is dependent on the local water depth and effective bottom roughness (Blumberg and Mellor 1983):

$$C_f = MAX\left[\frac{k^2}{\left(\ln\frac{h}{2z_o}\right)^2} \;,\; C_{f,\min}\right] \qquad (2\text{-}6)$$

where:

k	=	von Karman's constant (0.4)
$C_{f,min}$	=	minimum bottom friction factor
z_o	=	effective bottom roughness (L)

The bottom friction factor (C_f) thus varies both spatially and temporally due to changes in total water depth (h) and bottom roughness (z_o). As total water depth increases, due to changes in bathymetry (spatial variation in h_o) or water surface elevation (temporal variation in η), C_f decreases. Spatially variations in bottom roughness are also included by using different z_o values for cohesive and non-cohesive sediment bed types. It was assumed that bottom roughness in non-cohesive and hard bottom areas (which used the same z_o value) is greater than z_o in cohesive bed areas, which is consistent with the physical characteristics of those two bed types.

2.2 APPLICATION TO THE UPPER HUDSON RIVER

The Upper Hudson River is a run-of-the-river reservoir system comprised of a series of eight dams and associated backwaters, that extends from Fort Edward to Troy. Pool elevation varies from about 120 ft above MSL in the TIP (Reach 8) to about 16 ft above MSL in Reach 1 (Figure 2-1). Dam heights range from about 4 ft in the TIP to about 20 ft in Reach 4 (Mechanicville Dam). Mean flow rate in the Upper Hudson River increases by almost 60%

between Fort Edward (5,200 cfs) and Waterford (8,100 cfs). Mean velocities and water depths, based on model results for a 22-year simulation (1977 to 1998), for the eight reaches are shown in Figure 2-2. Additional discussion of Upper Hudson River hydrologic and hydraulic characteristics is presented in Volume 1, Section 1.

The hydrodynamic models of the Upper Hudson River extend from the Route 197 bridge at Rogers Island (Fort Edward) to the Federal Dam at Troy (Figure 1-4). Due to the discontinuity caused by the eight dams located along the river, each of the eight reaches was modeled separately. Thus, eight hydrodynamic models were developed to simulate flow in the Upper Hudson River. The upstream inflow used for a particular reach (downstream of TIP) was the predicted flow over the dam that defined the upstream boundary of that reach. This situation makes it necessary to run the models sequentially, from upstream to downstream.

Man-made flow structures and hydroelectric generating plants at some of the dams can cause localized circulation effects in various reaches of the Upper Hudson River (see Volume 1, Section 1 for more discussion). The spatial scale of these localized effects was assumed to be relatively small in this study. Thus, the hydrodynamic models neglected the effects of structures, i.e., bridges, and flow diversions due to hydroelectric generating plants. Seasonal changes in pool level, e.g., lower pool level in Reach 2 during the winter, were not included in the model simulations.

2.2.1 Representation of the River: One-Dimensional Model

The numerical grid for the one-dimensional model used a grid spacing (Δx) of 2,500 ft (762 m), with ½ cells (Δx = 1,250 ft) being used at the upstream and downstream boundaries of each reach. This grid spacing produced a total number of cells in a particular reach that ranged from 6 cells in Reaches 4 and 7 to 35 cells in Reach 5.

Cross-sectional geometry data were collected along 165 transects between Fort Edward and Troy by GE in 1991 (O'Brien & Gere 1993b). These transects were located along transects surveyed by Normandeau Associates in 1977. Bathymetry and geometry, i.e., A, $\eta = f_1(A)$ and

$R = f_2(A)$, were determined for each hydrodynamic grid cell using the transect data. If more than one transect was located in a grid cell, transect data in that cell were averaged. For cells containing no transect data, cell geometry was estimated using linear interpolation between the nearest upstream and downstream cells that contained transect data.

The datum used to determine reference water depths, i.e., $\eta = 0$, from transect data in a particular reach was the elevation of the dam crest. A similar procedure was used in developing bathymetry information for the two-dimensional hydrodynamic model.

2.2.2 Representation of the River: Two-Dimensional Model

The two-dimensional model in the TIP (Reach 8) extends from the Route 197 bridge at Rogers Island (MP 194.4) to TID (MP 188.5). This six-mile reach was discretized using 68 longitudinal and 10 lateral cells (Figure 2-3). Average longitudinal cell size was 140 m and typical lateral cell size was about 20-30 m. The hydrodynamic effects of the jetty at the entrance to the Champlain Canal near MP 189 were included in the model.

The two-dimensional numerical cells used in Reaches 1 to 7 are presented in Figures 2-4 to 2-10. In Reach 7, 10 lateral cells were used, while 5 lateral cells were employed in Reaches 1 to 6. A summary of grid cells for all reaches is presented in Table 2-1.

Table 2-1. Number of Longitudinal Cells in One- and Two-Dimensional Hydrodynamic Models

Reach	1-D Model	2-D Model
1	18	24
2	5	18
3	7	12
4	34	9
5	5	66
6	6	13
7	10	26
8	13	68

Bathymetric data collected in the TIP by GE in 1991 were used to specify values of h_o for model input (O'Brien & Gere 1993b). The 1991 bathymetric survey collected depth soundings at about 107,000 points throughout the TIP at river flows that ranged from about 1,700 to 2,700 cfs. The reference water depth (h_o) in a particular grid cell was calculated by averaging the 1991 sounding data located within that grid cell. The resulting bathymetric distribution used for TIP model input is presented in Figure 2-11. Bathymetric input for the two-dimensional models of Reaches 1 to 7 was developed from transect data collected during the same 1991 survey.

2.2.3 Boundary Conditions

The hydrodynamic models required specification of two types of time-variable boundary conditions: (1) inflows from upstream and tributary sources and (2) stage height at each dam. Flow rates measured by the U.S. Geological Survey (USGS) at the Fort Edward gauging station were used as input at the upstream boundary of the TIP model. The mean flow rate at this location is approximately 5,200 cfs and the 100-year flood has been estimated to be 47,330 cfs (daily average) (USEPA 1996). Daily average flow rates at Fort Edward between 1977 and 1998 are shown in Figures 2-12a and b. The mean flow rates at Stillwater and Waterford, locations of two other USGS gauging stations on the river, are approximately 6,600 and 8,100 cfs, respectively.

The Upper Hudson River between Fort Edward and Waterford receives tributary discharge contributions at an average runoff rate of 1.6 cfs/mi^2, from a 1,793 mi^2 drainage basin (Figure 2-13). A summary of the tributaries and associated drainage areas is presented in Table 2-2. Discharge is measured for less than 33% of the drainage area between Fort Edward and Waterford, making it necessary to estimate tributary flows for a large portion of this drainage basin.

Table 2-2. Estimated Tributary and Direct Drainage Discharge to the Upper Hudson River					
Tributary	Reach	I	Drainage Area (mi^2)	β_i	Mean Flow Rate (cfs)
Snook Kill	8	1	75	0.83	105
Moses Kill	8	2	55	0.61	77
Direct Drainage, R8	8	3	31	0.34	43
Direct Drainage, R7	7	4	15	0.17	21
Direct Drainage, R6	6	5	16	0.18	23
Batten Kill	5	6	431	4.8	601
Fish Creek	5	7	245	2.7	342
Flately Brook	5	8	8	0.016	14
Direct Drainage, R5	5	9	79	0.16	136
Hoosic River	4	10	720	1.4	1,353
Direct Drainage, R4	4	11	13	0.025	20
Anthony Kill	3	12	63	0.12	96
Direct Drainage, R3	3	13	13	0.025	20
Deep Kill	2	14	16	0.031	25
Direct Drainage, R2	2	15	13	0.025	20

Flow rate data collected at the USGS gauging stations at Fort Edward, Stillwater and Waterford were used to construct monthly-average flow balances for the Upper Hudson River. Tributary flows were assumed to be proportional to flows measured at USGS gauging stations located on either Kayaderosseras Creek or the Hoosic River (see Figure 2-13). Kayaderosseras Creek gauge data were used for tributaries entering between MP 180 and MP 194. Hoosic River gauge data were used for tributaries entering between MP 159 and MP 180. Direct drainage runoff was estimated by treating the total direct drainage in a particular reach as an additional tributary. The modified drainage area proration method, using the appropriate gauging station, i.e., Kayaderosseras Creek or Hoosic River, was applied to the direct drainage area for each reach to estimate direct runoff.

For month k, the flow balance between Fort Edward and Stillwater was calculated as:

$$ {}^{k}\overline{Q}_{ST} - {}^{k}\overline{Q}_{FE} = {}^{k}\alpha_{FS}\left(\sum_{i=1}^{7}\beta_i\,{}^{k}\overline{Q}_{KC} + \sum_{i=8}^{9}\beta_i\,{}^{k}\overline{Q}_{HR}\right) \qquad (2\text{-}7) $$

and between Stillwater and Waterford:

$$ {}^{k}\overline{Q}_{WA} - {}^{k}\overline{Q}_{ST} = {}^{k}\alpha_{SW} \sum_{i=10}^{15} \beta_i \, {}^{k}\overline{Q}_{HR} \qquad (2\text{-}8) $$

where:

${}^{k}\overline{Q}_{FE}$	=	mean flow rate at Fort Edward for month k
${}^{k}\overline{Q}_{ST}$	=	mean flow rate at Stillwater for month k
${}^{k}\overline{Q}_{WA}$	=	mean flow rate at Waterford for month k
${}^{k}\overline{Q}_{KC}$	=	mean flow rate at Kayaderosseras Creek gauge for month k
${}^{k}\overline{Q}_{HR}$	=	mean flow rate at Hoosic River gauge for month k
${}^{k}\alpha_{FS}$	=	drainage area proration adjustment factor for Fort Edward to Stillwater drainage basin for month k
${}^{k}\alpha_{SW}$	=	drainage area proration adjustment factor for Stillwater to Waterford drainage basin for month k
β_i	=	drainage area proration factor for tributary i between Fort Edward and Waterford

The drainage area proration factor is given by (Table 2-2):

$$ \beta_i = \begin{cases} \dfrac{DA_i}{DA_{KC}} & , \quad i < 8 \\ \dfrac{DA_i}{DA_{HR}} & , \quad i \geq 8 \end{cases} \qquad (2\text{-}9) $$

where:

DA_{KC}	=	drainage area at Kayaderosseras Creek gauge (90 mi^2)
DA_{HR}	=	drainage area at Hoosic River gauge (510 mi^2)
DA_i	=	drainage area for tributary i between Fort Edward and Waterford

Equations (2-7) and (2-8) were solved for ${}^k\alpha_{FS}$ and ${}^k\alpha_{SW}$ for each month (Table 2-3).

Table 2-3. Monthly Drainage Area Proration Adjustment Factors for Upper Hudson River Tributaries

Month	α_{FS}	α_{SW}
January	0.87	0.95
February	0.82	1.11
March	0.85	1.02
April	0.81	0.83
May	0.82	0.81
June	0.88	0.40
July	0.76	0.00
August	0.88	0.00
September	0.84	0.00
October	0.95	0.58
November	1.01	0.78
December	0.99	1.01

Tributaries flow rates, during month k, were estimated using:

$$Q_i = \begin{cases} {}^k\alpha_{FS}\beta_i Q_{KC} & , \quad i \le 7 \\ {}^k\alpha_{FS}\beta_i Q_{HR} & , \quad i = 8,9 \\ {}^k\alpha_{SW}\beta_i Q_{HR} & , \quad i > 9 \end{cases} \qquad (2\text{-}10)$$

where:

Q_i = estimated flow rate in tributary i between Fort Edward and Waterford

Q_{KC} = measured flow rate at Kayaderosseras Creek gauge

Q_{HR} = measured flow rate at Hoosic River gauge

Monitoring at the Kayaderosseras Creek gauge was discontinued in 1995. Discharge data collected at the USGS gauging station on Glowegee Creek (DA_{GC} = 26 mi^2, Figure 2-13) were used after this date:

$$Q_i = {}^k\alpha_{FS}\beta_i\left(\frac{90}{26}\right)Q_{GC} \quad , \quad i \le 7 \qquad (2\text{-}11)$$

where:

Q_{GC} = measured flow rate at Glowegee Creek gauge

A flow balance for the Upper Hudson River, including mean tributary flow rates, is presented in Figure 2-14. Mean discharge in the river increases by 56% between Fort Edward and Waterford. Increases in Upper Hudson River flow rate between Fort Edward and Waterford due to tributary discharge are shown in Figure 2-15, where the large impacts of Batten Kill (MP 182) and Hoosic River (MP 167), which together comprise 67% of the total tributary flow, are evident.

Stage heights measured by Champlain Canal personnel at the locks in each reach (T. Rathwell, New York State Thruway Authority, *personal communication* 1996) were used to develop a relationship between flow rate and water surface elevation at each dam (Figure 2-16). The dam rating curves developed from these data have the form:

$$\eta_{DAM} = DQ_{DAM}^{b} \qquad (2\text{-}12)$$

where:

η_{DAM} = water surface elevation above dam crest (m)

Q_{DAM} = flow rate at dam (cfs)

b = reach-dependent exponent

D = reach-dependent constant

Table 2-4. Stage Height Rating Curve Coefficients for Dams in Reaches 1 to 8

Reach	D	b
1	0.84	0.96
2	1.0	0.51
3	1.1	0.66
4	2.0	0.12
5	1.2	0.90
6	1.6	0.36
7	0.71	0.67
8	0.40	0.44

The stage height data, and associated rating curve, for Reach 4 (Figure 2-16) are considerably different from data collected in the other reaches. The hydroelectric plant at the Mechanicville Dam, which is the highest dam on the Upper Hudson River, primarily controls stage height in this reach. Operating procedures at the hydroelectric plant tend to keep the pool behind the dam at a relatively constant level over a wide range of flow rates.

No stage height data are available for Reach 7 as the Champlain Canal bypasses this section of the river. A simple weir equation was used to estimate water surface elevation variations at the Reach 7 dam. These dam rating curves were used to specify time-variable water surface elevation at the downstream boundary of the hydrodynamic models.

2.2.4 Coupling One-Dimensional Hydrodynamic Model to PCB Fate Model

The PCB fate model (see Section 4) required time-varying flow rates, volumes and depths calculated by the one-dimensional hydrodynamic model to solve the one-dimensional transport equation. The one-dimensional model thus provided hydrodynamic information for the PCB fate model that was used to simulate the water-column transport of PCBs in the Upper Hudson River. One-dimensional hydrodynamic model information was not used for sediment transport modeling purposes.

Coupling the one-dimensional hydrodynamic model to the PCB fate model required manipulation of the hydrodynamic model output such that it was consistent with the structure of the PCB fate model. Manipulation of the hydrodynamic output was done in four steps: (1) coupling hydrodynamic output from all eight reaches; (2) spatially collapsing the hydrodynamic model grid to the PCB fate model grid; (3) temporally averaging the hydrodynamic output; and (4) flow balancing.

The PCB fate model of the Upper Hudson River has a continuous grid that extends from Fort Edward to the Federal Dam at Troy. The first step of the model coupling involved taking the hydrodynamic output from the eight separate reaches and linking that information to produce

a continuous grid of hydrodynamic information for the river. The result of this coupling was a hydrodynamic grid containing 80 cells. The PCB fate model consists of 28 cells, each of which contain between one and seven hydrodynamic grid cells. Hence, the second step in the coupling process was to spatially collapse the one-dimensional hydrodynamic output to the PCB fate model grid. Information from the one-dimensional hydrodynamic model was output as daily average values for use in the PCB fate model. Finally, the coupling output was flow balanced to ensure mass conservation. This last step was necessary because coupling of the eight reaches caused small errors in mass conservation due to flux discontinuities between the coupled elements, i.e., elements immediately upstream and downstream of a dam.

2.2.5 Coupling Two-Dimensional Hydrodynamic Model to Sediment Transport Model

Information from the two-dimensional hydrodynamic model, i.e., current velocity, water depth and bottom friction coefficient, was transferred to the sediment transport model for use in simulating water column transport of suspended sediment and to calculate bottom shear stress. The two models performed simulations on the same numerical grid in a particular reach, so spatial collapsing of hydrodynamic model output was not necessary. Temporally, the two models used the same time step and no temporal averaging of hydrodynamic model output was done.

2.2.6 Summary

Development of model inputs for geometry (bathymetry and numerical grids) and boundary conditions used a large amount of Upper Hudson River data. Grid resolution for the one-dimensional model was adequate for simulating water column transport of PCBs. The two-dimensional model provides sufficient resolution, particularly in the TIP, to accurately represent lateral and longitudinal variations in bathymetry and bottom roughness (sediment bed type). Neglect of hydrodynamic effects due to dam operations and structures introduces some uncertainty into model results, but this approximation should only affect relatively small, localized areas in the Upper Hudson River.

Specification of tributary flow rates was done using an estimation procedure that employed discharge data from the available USGS gauging stations in the Upper Hudson River drainage basin. This method used a mass balance approach to ensure that the models would accurately represent long-term mean flow rates. However, the estimation method produces some uncertainty in tributary flow rate magnitude and timing on short time scales, e.g., daily variations. Time-variable stage heights at the downstream boundary of each reach were specified using data-based rating curves, except in Reach 7, where data were unavailable. Variability in rating curve data (Figure 2-16) introduces some uncertainty in the specified stage height at each dam for a particular flow.

2.3 HYDRODYNAMIC MODEL CALIBRATION

2.3.1 Calibration Strategy

Both hydrodynamic models were calibrated by adjusting friction coefficients in the models such that the best agreement between predicted and observed water surface elevation was achieved. The Manning's coefficient, n in Equation (2-2), and effective bottom roughness, z_o in Equation (2-6), were adjusted for the one- and two-dimensional models, respectively, to achieve best agreement with water surface elevation data collected at upstream locations in all reaches, expect Reach 7. Because calibration of the Reach 7 models was not possible due to a lack of data, the decision was made that friction coefficients determined for the TIP would be used in Reach 7.

Champlain Canal stage height data collected at Gauge 119, located near the lock entrance at Fort Edward, were used to develop a rating curve at this location, similar to the stage height rating curves generated at the dams. Calibration of the models in the TIP was accomplished by comparing predicted water surface elevations near Fort Edward to stage heights estimated from the Gauge 119 rating curve. A range of flows, from 2,500 to 35,000 cfs, was used to predict water surface elevations at the Gauge 119 location. The bottom friction coefficients were adjusted until the average error over the flow range was minimized.

Stage height data collected in Reaches 1 to 6 during high flow events in 1993 and 1994 were used to calibrate both models in those reaches. Similar to the TIP, calibration was achieved in these six reaches by adjusting the friction coefficients in the models so that the best agreement between observed and predicted stage heights at the upstream extent of a specific reach was achieved. Champlain Canal stage data collected at the downstream side of each lock were used for calibration purposes, e.g., Gauge 113 is located below Lock 5C, which is located at the upstream extent of Reach 5. Note that uncertainty exists in the accuracy of these data because stage heights were measured by visual observation and, generally, only one observation was made per day.

2.3.2 One-Dimensional Model Results

A Manning's n value of 0.019 was determined for the TIP based upon the best agreement between predicted and estimated stage heights at Gauge 119. The mean and median values of the relative error for the flow rate range of 2,500 to 35,000 cfs were 55 and 22%, respectively. The mean absolute error for this range of flows was 12 cm (0.39 ft), with minimum and maximum errors of –0.6 and 25 cm (-0.02 and 0.82 ft). Note that the stage height range at Gauge 119 was about 250 cm (~8 ft) for the flow range considered. The largest errors occurred for flow rates less than 15,000 cfs, with the mean relative and absolute errors being 93% and 14 cm, respectively, in that flow range. Gauge 119 stage heights ranged over about 80 cm (~2.7 ft) for flows less than 15,000 cfs. Uncertainty in specified stage height at the downstream (dam) boundary of the TIP during low flow rates may contribute to uncertainty, and corresponding error, in predicted stage height in the vicinity of Gauge 119. The model performed considerably better for high flow rates (> 15,000 cfs), with errors ranging from 0.5 to 39% (-0.6 to 20 cm) and a mean error of 16% (10 cm). For flow rates over 15,000 cfs, stage heights had a range of about 170 cm (~5.4 ft).

Calibration results for Reaches 1-4 and 6 during the 1993 spring flood are depicted in Figure 2-17. Reach 5 calibration results during the 1994 spring flood are given in Figure 2-18. Generally, predicted stage heights agree well with observed stage heights during both floods in

all six reaches. Manning's n coefficients in these six reaches were higher than the TIP Manning's n, with calibration values of 0.023 in Reach 5 and 0.025 in Reaches 1-4 and 6.

2.3.3 Two-Dimensional Model Results

The hydrodynamic model contains two adjustable parameters: horizontal eddy viscosity (B_H) and effective bottom roughness (z_o). The two-dimensional hydrodynamic model was run with the minimum value of B_H needed to ensure numerical stability, which was 0.5 m^2/s for the TIP and 1 m^2/s for the other seven reaches of the Upper Hudson River. No adjustment of B_H was made during model calibration or validation.

Spatially variable z_o and $C_{f,min}$ values depended on local bed type, i.e., cohesive, non-cohesive or hard bottom (rocky). The distribution of cohesive, non-cohesive and hard bottom bed areas in the Upper Hudson River is discussed in Section 3. The assumption was made that cohesive bed areas have lower bottom friction coefficients, corresponding to a smoother surface due to smaller median sediment particle size, than non-cohesive or hard bottom (rocky) bed areas. For all cohesive areas in the Upper Hudson River, z_o and $C_{f,min}$ were set at 75 μm and 0.0020, respectively, and were not adjusted during calibration.

For the TIP, the best calibration results were achieved with z_o = 1,500 μm and $C_{f,min}$ = 0.0035 in the non-cohesive/hard bottom areas. An average error of 4% resulted for these parameter values over the flow range of 2,500 to 35,000 cfs. These results are significantly better than those obtained during the one-dimensional model calibration. The primary reasons that the two-dimensional model performed better than the one-dimensional model were: (1) higher resolution numerical grid and (2) more accurate representation of reach geometry.

Model calibration indicated that using the TIP non-cohesive friction factors (z_o = 1,500 μm and $C_{f,min}$ = 0.0035) in Reaches 1 to 6 produced good results. Model-data comparisons for Reaches 1-4 and 6 during the 1993 spring flood are presented in Figure 2-19. The model generally predicted stage height accurately in all five reaches throughout the flood. Peak stage heights in Reaches 4 and 6 were under-predicted a few times but this disagreement may be due

to uncertainty in the downstream boundary condition, which was specified using a rating curve instead of data. Reach 5 calibration results (Figure 2-20) were very good for the entire 1994 spring flood simulation.

2.3.4 Summary

The one-dimensional model results for the seven calibrated reaches were acceptable for the purposes of this model, i.e., providing transport information for the PCB fate model. Model accuracy might be improved with increased grid resolution (smaller Δx) but such a modification would probably have a small effect on PCB fate model simulations. The Manning's n values determined for the TIP and Reaches 1-6 (ranging from 0.019 to 0.025) are consistent with Manning's coefficients determined during FEMA Flood Insurance Studies of the Upper Hudson River (FEMA 1995), which ranged from 0.015 to 0.030.

Very good results for the two-dimensional model calibration give confidence in the ability of the model to accurately simulate stage height over a wide range of flow rates. These results indicate that the geometry and bathymetry of the system are well represented by the model inputs. Consistency of bottom friction coefficient values throughout the seven reaches suggests that the model may be somewhat insensitive to this parameter, a topic that has been investigated and is discussed further in Section 2.5.

2.4 HYDRODYNAMIC MODEL VALIDATION

The hydrodynamic models and the tributary flow estimation procedure were validated using water surface elevation data obtained during the 1983 spring flood in the TIP. Further validation of the two-dimensional model was accomplished using current velocity data collected during August 1997 in the TIP. Bottom friction coefficients, i.e., n and z_o, were not adjusted during model validation, only model boundary conditions were changed, i.e., upstream and tributary flow rates and stage height at TID. Additional validation of the models was done through comparison of measured and predicted flow rates at Stillwater and Waterford between 1977 and 1992.

Stage height data collected during the 1983 spring flood at Gauge 119 were used to validate the hydrodynamic models in the TIP. This flood had a maximum flow rate at Fort Edward of 34,100 cfs, which represents a return period of approximately 10 years. The 1983 flood had the highest daily average flow rate measured at the Fort Edward gauge since the gauge became operational in 1977.

2.4.1 One-Dimensional Model Results

Results of the validation simulation are presented in Figure 2-21a. Predicted stage heights at Gauge 119 are in good agreement with observed stage heights during the 1983 spring flood (April 24 to May 16). However, the model under-predicted stage height during the peak of flood by about 15 cm (~0.5 ft), which should be compared to the stage height range of approximately 200 cm (~7 ft) during this flood. These results suggest that the Manning's coefficient for the TIP may depend upon discharge to some extent, with Manning's n being greater than 0.019 (the calibration value) for flow rates greater than about 30,000 cfs.

The one-dimensional model was run from March 1, 1977 to March 1, 1998 for use in the PCB fate model. Daily average flow rate data at Stillwater and Waterford are available from March 10, 1977 to June 30, 1992. Comparisons between predicted and observed daily average flow rates during this 5,592-day period were made at both locations, see Figures 2-22 and 2-23. Generally, the model accurately predicted discharge at both locations, with predicted values being within 30% of the measured values approximately 97 and 93% of the time at Stillwater and Waterford, respectively.

Another measure of the ability of the model to predict flow rates at Stillwater and Waterford, and also of the accuracy of the tributary flow estimation method, is through comparisons of predicted and observed monthly average flow rates. Improved model accuracy would be expected for monthly average discharge because difficulties with tributary flow estimation on a daily basis should have a small effect on mean values over the longer time scale. Model results indicate that this was the case, as is shown in Figure 2-24 and 2-25. Monthly

average flow rates were predicted quite accurately at both gauging stations. The predicted long-term average flow rate was within 1% of the measured mean value at both Stillwater and Waterford.

2.4.2 Two-Dimensional Model Results

The two-dimensional model validation results are shown in Figure 2-21b. Agreement between predicted and measured stage heights during this flood was excellent. The model slightly under-predicted stage height at Gauge 119 at the flood peak and slightly over-predicted stage height during a portion of the falling limb of the hydrograph (May 10 to 15). Successful calibration and validation of the model demonstrated that: (1) model geometry and bathymetry are accurately represented and (2) bottom friction factors used in the model are realistic.

Predicted and observed daily average flow rates at Stillwater and Waterford are compared in Figures 2-26 and 2-27, respectively. Predicted daily average flow rates were within 30% of measured values about 95 and 94% of the time at Stillwater and Waterford, respectively. The cause of the slightly degraded performance of the two-dimensional model, when compared to the one-dimensional model results, for predicting daily average flow rates at Stillwater and Waterford is uncertain. Monthly average flow rate comparisons are given in Figures 2-28 and 2-29. Similar to the one-dimensional results, the two-dimensional model predicted monthly average discharge more accurately than daily average discharge. The predicted long-term average flow rate is within 2% of the measured mean value at each location. These results, when combined with the one-dimensional model results, indicate that the tributary flow estimation method is credible and reasonably accurate.

GE collected velocity data in the TIP during August 1997 (O'Brien & Gere 1998). Current velocities were measured along five transects in the vicinity of Snook Kill (Figure 2-30). Velocities were measured at approximately 25 and 75% of the water depth at each sampling point along a transect. Data were collected on August 27 and 28, during which the instantaneous flow rate at Fort Edward varied from about 3,500 to 4,700 cfs. Flow rates in tributaries upstream

of the transect locations were not measured. Measured flow rates at the transects ranged from 3,550 to 5,040 cfs.

Steady-state circulation in the TIP was simulated with the two-dimensional model for each of the flow rates measured at the five transects. Comparisons of predicted and observed velocity distributions along each transect are presented on Figure 2-31. Velocity data on that figure are the mean values of measurements made at 25 and 75% of the water depth. A hand-held velocity meter was used to collect these data and, hence, uncertainty in measured velocities exists, e.g., due to current meter accuracy, operator error and orientation of the meter to the river current. Accuracy of the velocity meter is approximately ±3 cm/s and that uncertainty is depicted as error bars on the data in Figure 2-31. Additional uncertainty in the data cannot be quantified, but would probably be larger than the displayed error bars due to meter accuracy. Generally, fair agreement was achieved between predicted and observed velocity distributions. The model tended to over-predict velocities along the western shore and under-predict mid-channel velocities, which is probably due to poor grid resolution in the nearshore areas in this portion of the TIP.

Sensitivity of the velocity distributions to bathymetry and friction parameters was investigated to determine if the model predictions could be significantly improved. Bathymetry data collected along the August 1997 transects were used to modify model inputs in this portion of the TIP. Generally, the original model bathymetry agreed well with the transect data, except along the west shore, which the data indicated was shallower in the near shore region. Simulations using the modified bathymetry, however, did not produce velocity distributions significantly different from those predicted using the original bathymetry. The impact of model parameters, i.e., B_H and z_o, on the predicted velocity distributions was investigated by varying those parameters over large ranges. Similar to the bathymetry modification, parameter variation had a minimal effect on the velocity distributions. These results indicate that the probable cause of the disagreement between predicted and observed velocity distributions is poor resolution of the islands along the eastern shore. The islands across from Snook Kill complicate circulation patterns in this region of the TIP. Resolution of the islands, and the channels between them, is probably inadequate for accurately simulating flow patterns in this region. Increased grid

resolution, by at least a factor of two, would be needed to improve model performance in this region.

2.4.3 Summary

Both hydrodynamic models were able to predict stage height variations in the TIP during a large flood accurately. The one-dimensional model tended to under-predict stage height at Gauge 119 during the highest discharge, suggesting that the effective Manning's n for the TIP may increase for flow rates greater than about 30,000 cfs. Daily and monthly average flow rates at Stillwater and Waterford were predicted with adequate accuracy, with monthly average discharge being predicted more accurately than daily average flow. Velocity distributions in the vicinity of the TIP islands were not predicted with high accuracy. However, inability to adequately resolve the island geometry with the present two-dimensional numerical grid was probably the cause of discrepancies between observed and predicted velocity distributions in that region.

2.5 MODEL SENSITIVITY AND UNCERTAINTY

Sensitivity of the hydrodynamic models to bottom friction parameter values was evaluated using the 1983 spring flood simulation in the TIP. For the one-dimensional model, Manning's coefficient values of 0.015 and 0.023 were used in the sensitivity runs, which represented a range of $\pm$ 0.004 about the calibration value of 0.019. The effective bottom roughness, z_o, in the non-cohesive bed area was increased and decreased by a factor of two, i.e., 750 and 3,000 μm, for the two-dimensional model sensitivity analysis.

One-dimensional model sensitivity results are illustrated in Figure 2-32. The model is slightly more sensitive to decreasing Manning's n than to an equal increase in that parameter. The mean differences between predicted stage heights at Gauge 119, with respect to the original validation run, were 25 and –27% for high and low Manning's n values, respectively. These results show that the one-dimensional model is relatively sensitive to variations in Manning's n.

Thus, the Manning's n value of 0.019 determined during model calibration has a low degree of uncertainty associated with it.

The two-dimensional model was relatively insensitive to the factor of two changes in z_o investigated (Figure 2-33). Similar to the one-dimensional model, the model was more sensitive to increasing than decreasing z_o. Mean differences in predicted stage height were 1.3 and < -0.1% for the high and low bottom roughness values, respectively. Insensitivity of the two-dimensional model to variations in z_o indicates that TIP geometry inputs, i.e., bathymetry and shoreline, are the primary factors controlling water surface elevations calculated by the model. This result demonstrated that TIP geometry was accurately represented in the model. Note that careful examination of Figures 2-21b and 2-33a reveals that varying bottom roughness from 1,500 to 750 μm caused negligible changes in predicted stage height at Gauge 119. This result was due to the use of $C_{f,min}$ in Equation (2-6), and it indicated that $C_{f,min}$ was specified at many non-cohesive grid elements for bottom roughnesses of 750 and 1,500 μm.

These results, coupled with the two-dimensional model calibration results in Reaches 1 to 6, show that the value of the non-cohesive bottom roughness is relatively uncertain. This finding may have important implications for the sediment transport model because the bottom roughness coefficient affects bottom shear stress, which is a primary variable that controls resuspension and deposition. The effect of varying z_o on sediment transport simulations in the TIP was investigated, see Sections 3.4 and 3.5.

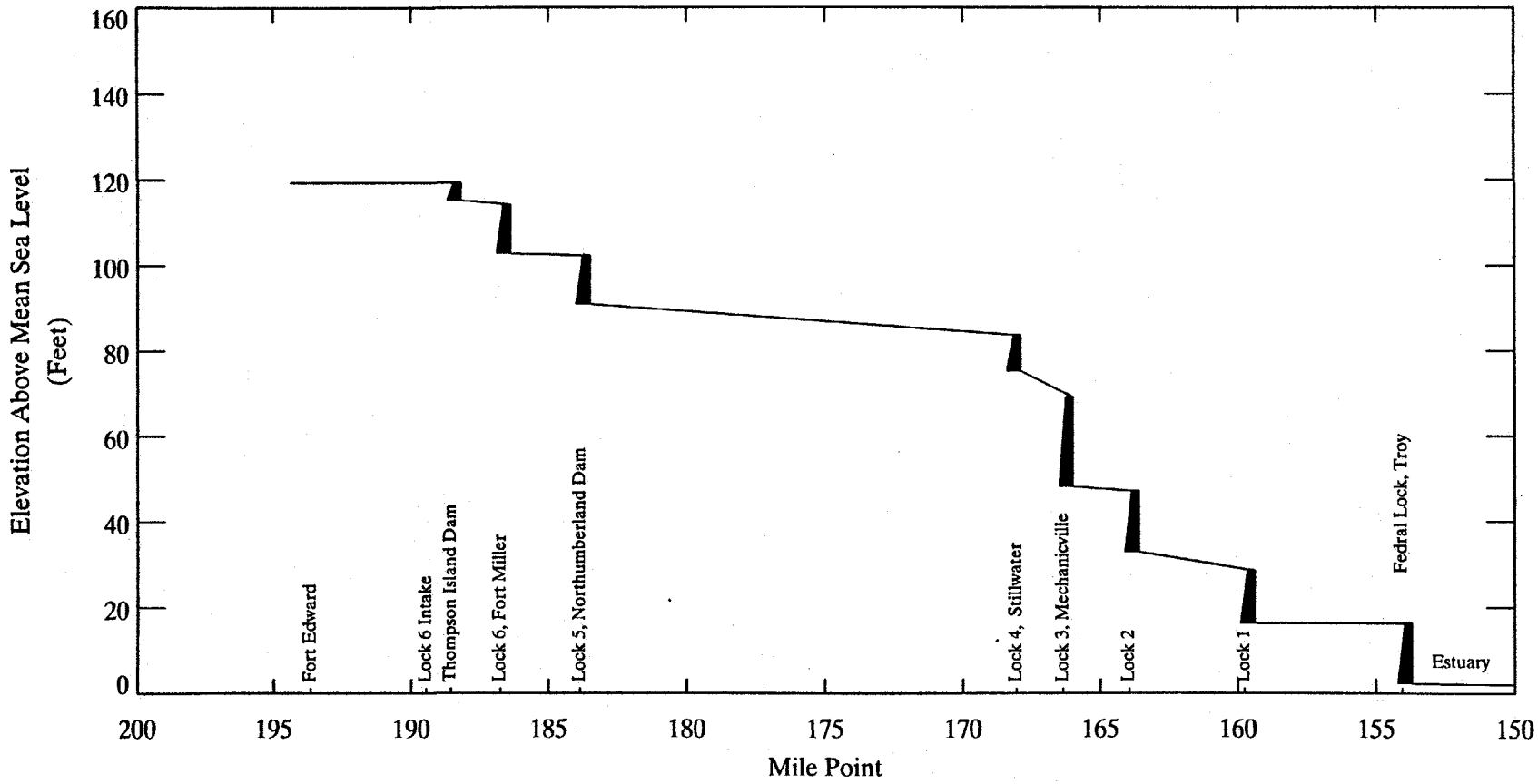

Figure 2-1. Approximate hydraulic gradient for the Upper Hudson River. Dam heights are approximate.

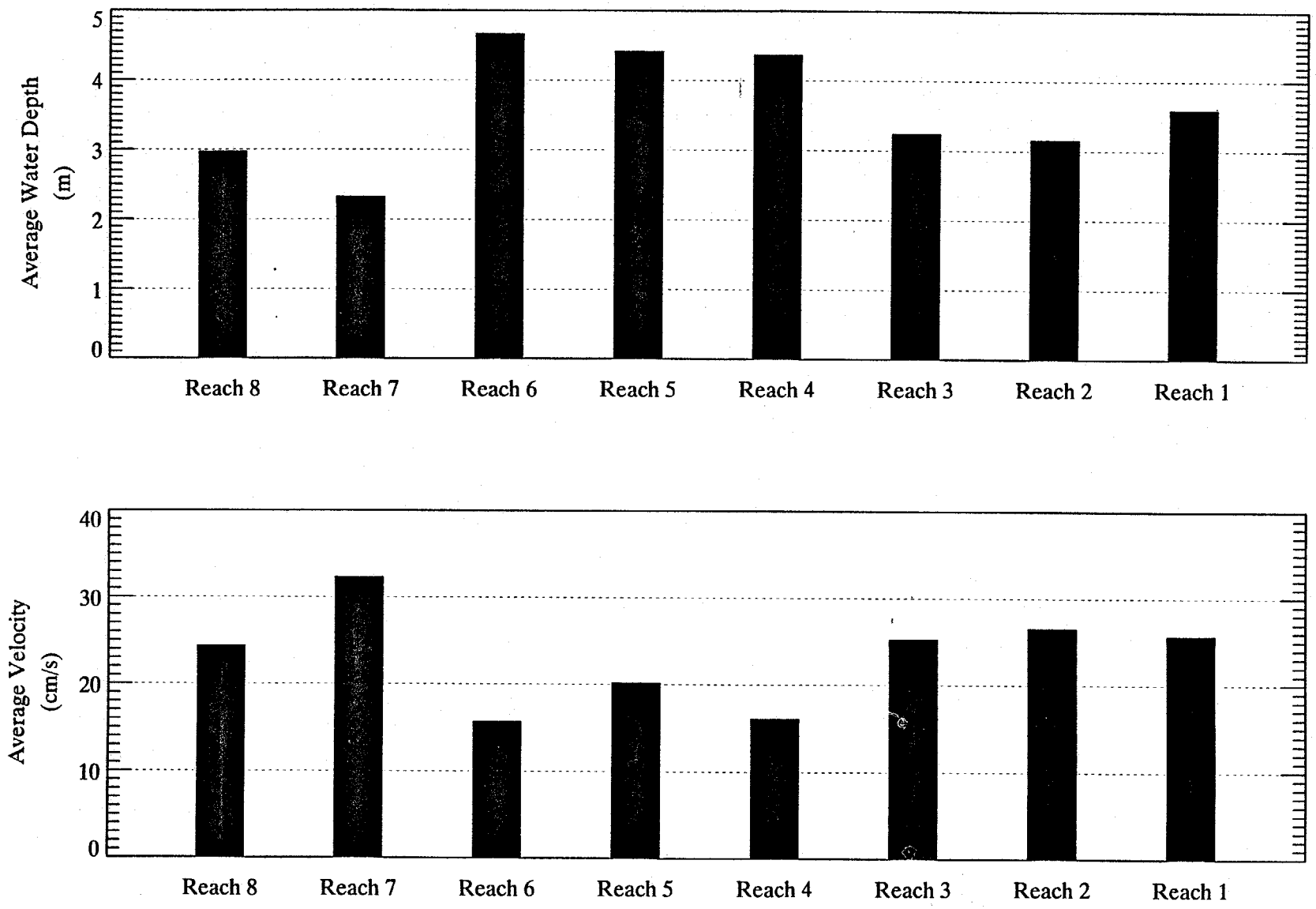

Figure 2-2. Average current velocity and water depth in Reaches 1 to 8.
Values were determined from model results averaged over 22-year simulation (1977-1998)

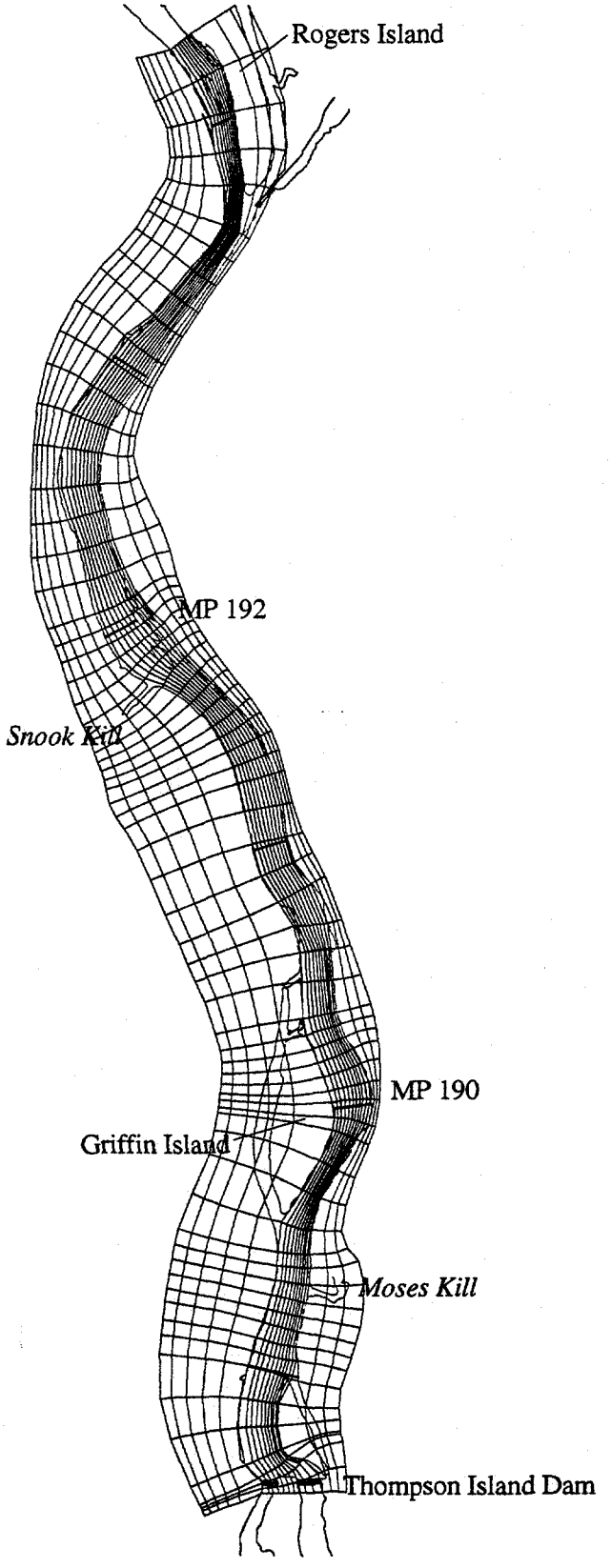

LOCATION MAP OF THE HUDSON RIVER

GRAPHIC SCALE

0.3 0 0.3 0.6 Miles

LEGEND

- Shoreline
- Mile Points
- Dams and Locks
- Reach 8 Grid
- Flood Plain Grid

GENERAL ELECTRIC COMPANY
Hudson River Project

PCBs in the Upper Hudson River
Volume 2. A Model of PCB Fate, Transport and Bioaccumulation

Figure 2-3.

Two-dimensional numerical grid for Reach 8 (Thompson Island Pool).

QEA
Quantitative Environmental Analysis, LLC

Project: Genhud 131 April 1999

313681

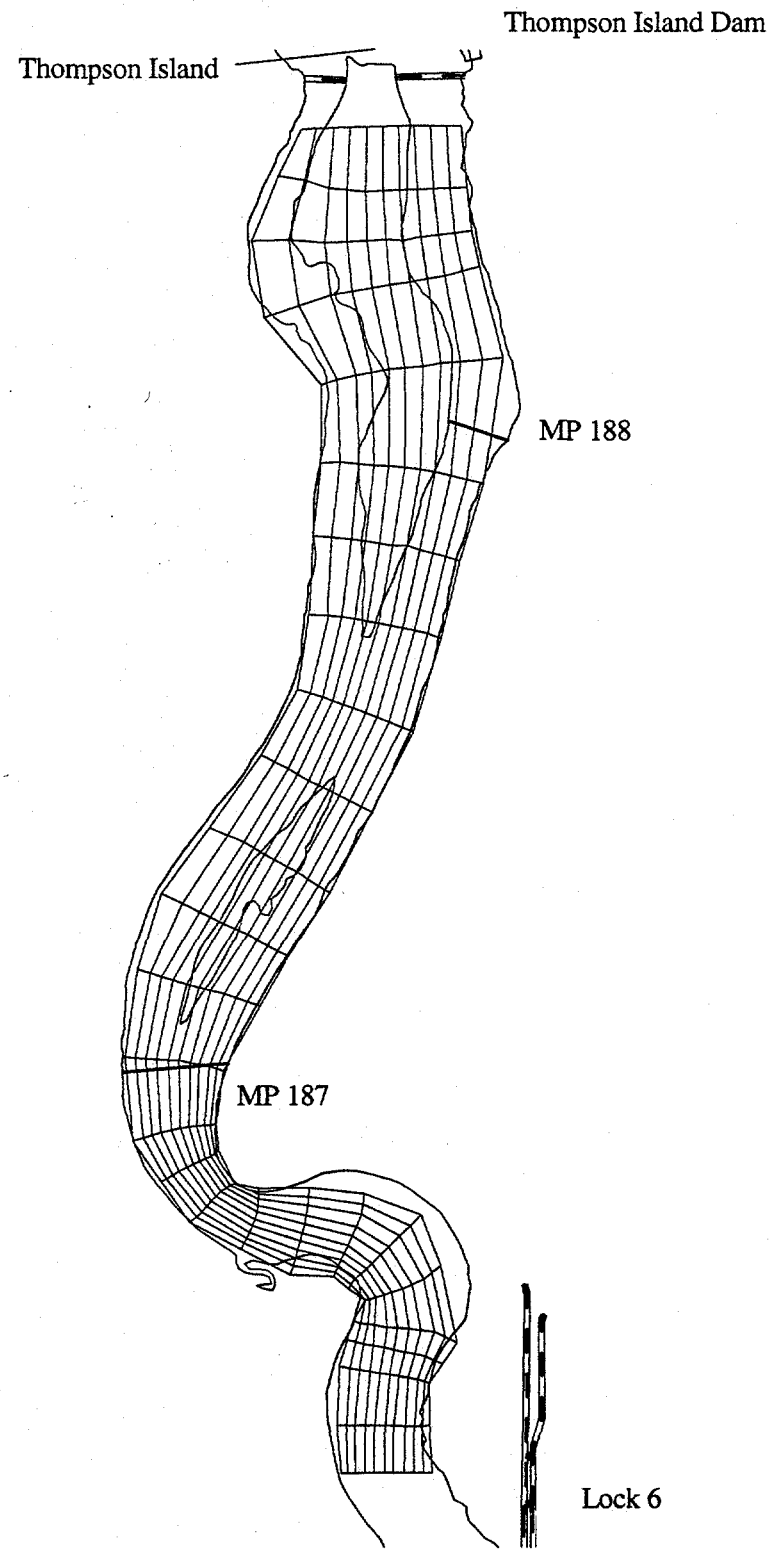

LOCATION MAP OF THE HUDSON RIVER

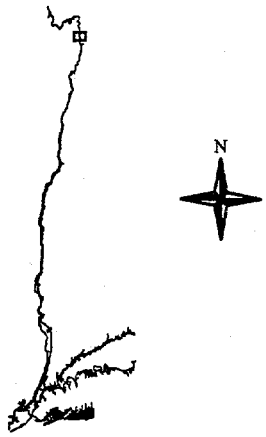

GRAPHIC SCALE

0.1 0 0.1 0.2 Miles

LEGEND

- Shoreline
- Mile Points
- Dams and Locks
- Reach 7 grid

GENERAL ELECTRIC COMPANY
Hudson River Project

PCBs in the Upper Hudson River
Volume 2. A Model of PCB Fate, Transport and Bioaccumulation

Figure 2-4.

Two-dimensional numerical grid for Reach 7.

QEA
Quantitative Environmental Analysis, LLC

Project: Genhud 131 April 1999

\\Poseidon\D_drive\GENhud\Documents\Final_Report\Vol_2\Section_2\Fig_3_to_10.apr

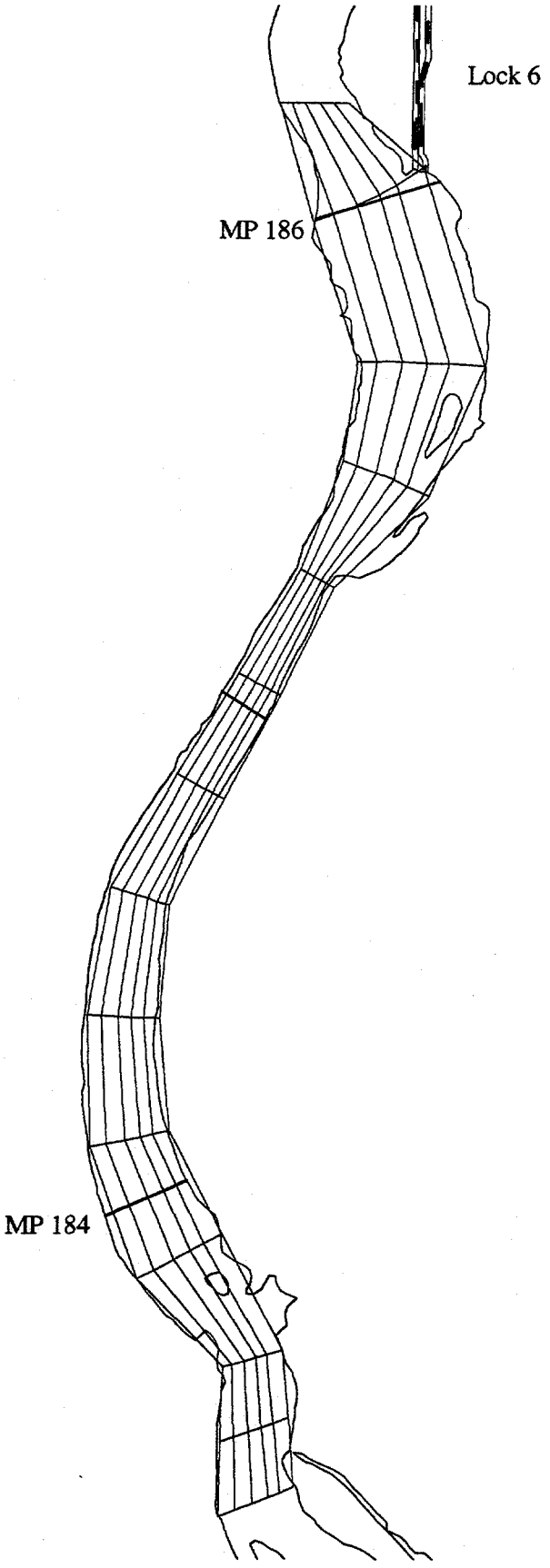

LOCATION MAP OF THE HUDSON RIVER

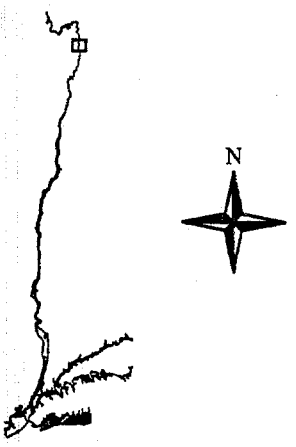

GRAPHIC SCALE

0.2 0 0.2 0.4 Miles

LEGEND

- Shoreline
- Mile Points
- Dams and Locks
- Reach 6 Grid

GENERAL ELECTRIC COMPANY
Hudson River Project

PCBs in the Upper Hudson River
Volume 2. A Model of PCB Fate, Transport and Bioaccumulation

Figure 2-5.

Two-dimensional numerical grid for Reach 6.

QEA
Quantitative Environmental Analysis, LLC

Project: Genhu April 1999

\\Poseidon\D_drive\GENhud\Documents\Final _report\Vol_2\Section_2\Fig_3_to_10

313683

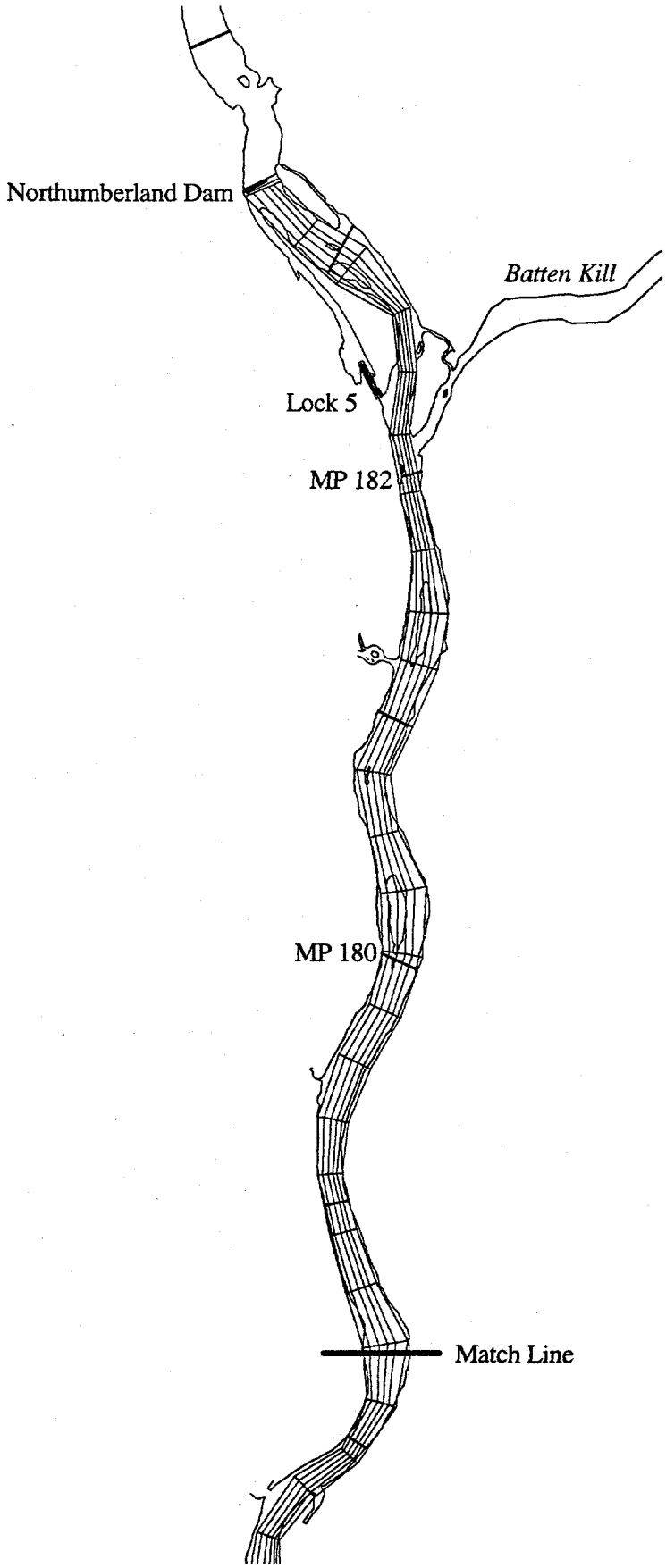

LOCATION MAP OF THE HUDSON RIVER

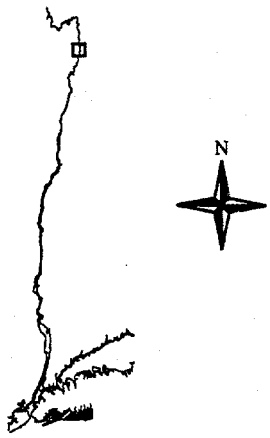

GRAPHIC SCALE

0.4 0 0.4 0.8 Miles

LEGEND

- Shoreline
- Mile Points
- Dams and Locks
- Reach 5 Grid

GENERAL ELECTRIC COMPANY
Hudson River Project

PCBs in the Upper Hudson River
Volume 2. A Model of PCB Fate, Transport and Bioaccumulation

Figure 2-6a.

Two-dimensional numerical model for Reach 5.

QEA
Quantitative Environmental Analysis, LLC

Project: Genhud 131 April 1999

\\Poseidon\D_drive\GENhud\Documents\Final _report\Vol_2\Section_2\Fig_3_to_10

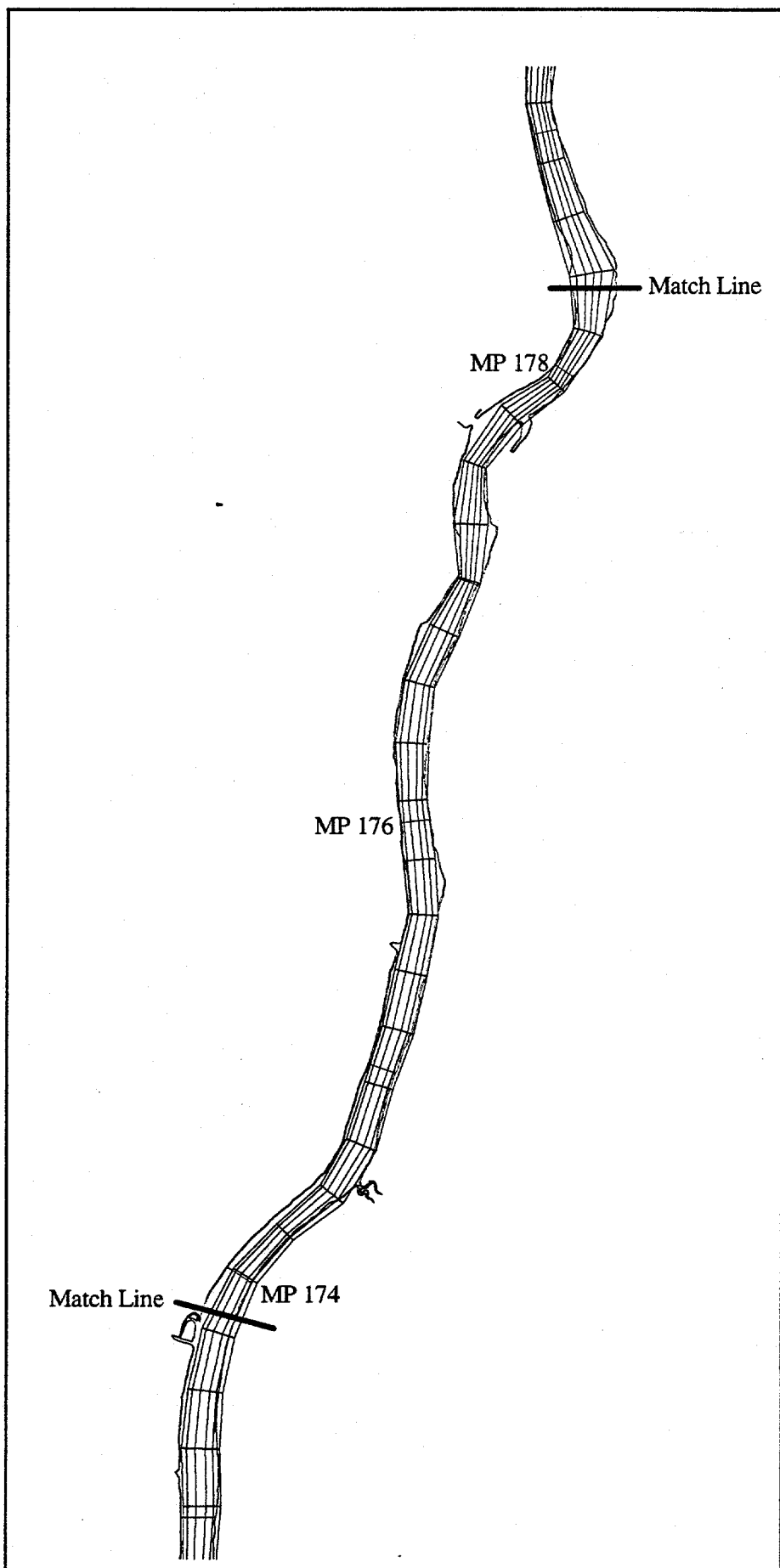

LOCATION MAP OF THE HUDSON RIVER

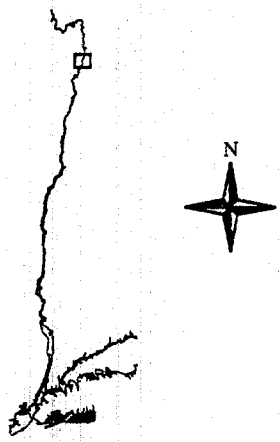

GRAPHIC SCALE

0.4 0 0.4 0.8 Miles

LEGEND

- Shoreline
- Dams and Locks
- Mile Points
- Reach 5 grid

GENERAL ELECTRIC COMPANY
Hudson River Project

PCBs in the Upper Hudson River
Volume 2. A Model of PCB Fate, Transport and Bioaccumulation

Figure 2-6b.

Two-dimensional numerical model for Reach 5.

QEA
Quantitative Environmental Analysis, LLC

Project: Genhud 131 April 1999

\\Poseidon\D_drive\GENhud\Documents\Final _report\Vol_2\Section_2\Fig_3_to_10

313685

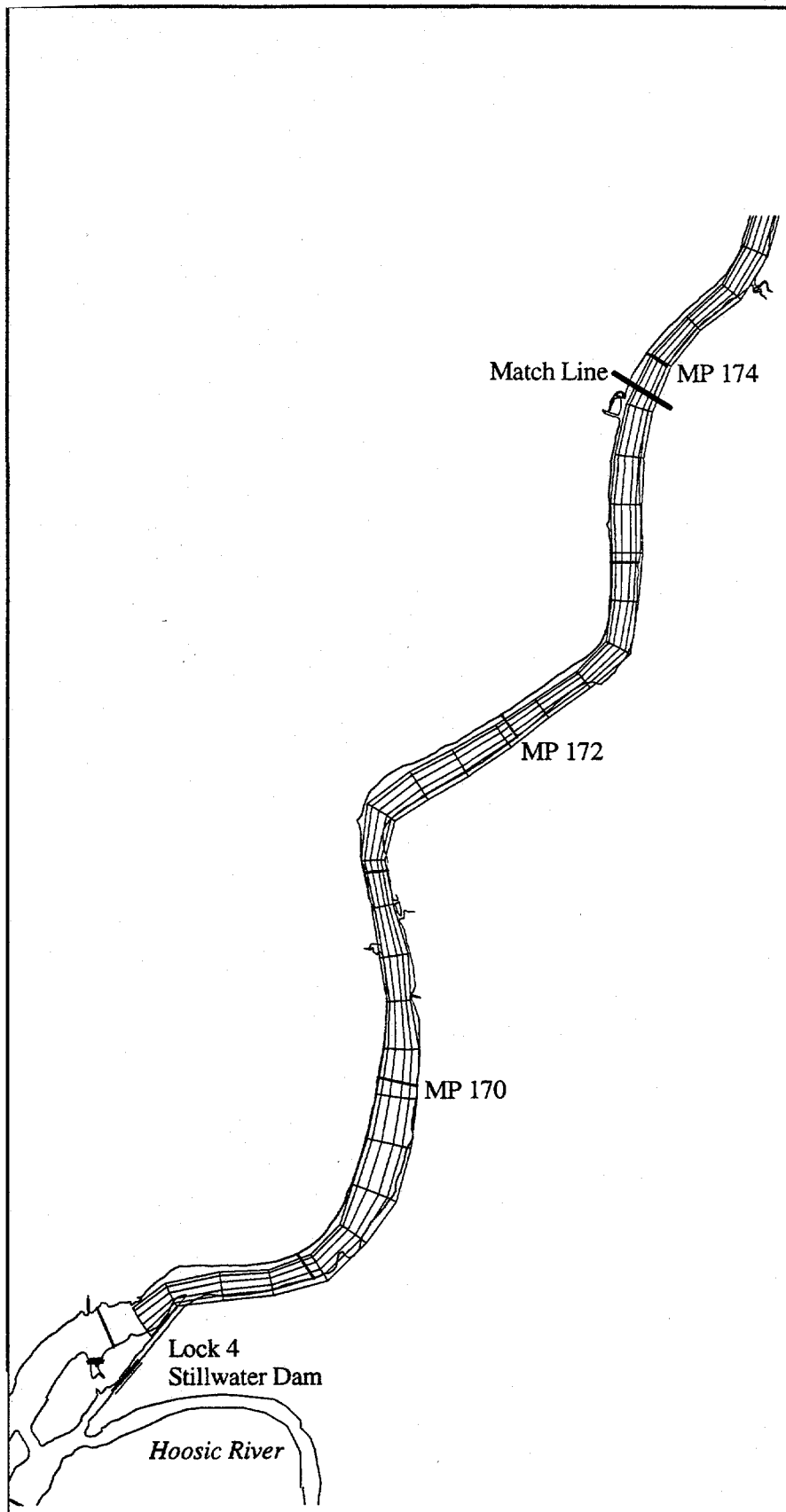

LOCATION MAP OF THE HUDSON RIVER

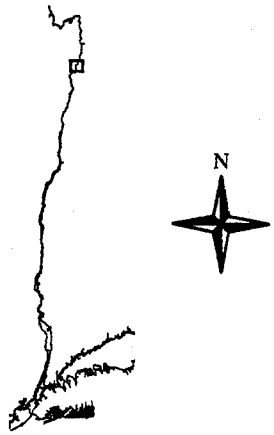

GRAPHIC SCALE

0.5 0 0.5 1 Miles

LEGEND

- Shoreline
- Mile Points
- Dams and Locks
- Reach 5 Grid

GENERAL ELECTRIC COMPANY
Hudson River Project

PCBs in the Upper Hudson River
Volume 2. A Model of PCB Fate, Transport and Bioaccumulation

Figure 2-6c.

Two-dimensional numerical model for Reach 5.

QEA
Quantitative Environmental Analysis, LLC

Project: Genhud 131

April 1999

\\Poseidon\D_drive\GENhud\Documents\Final _report\Vol_2\Section_2\Fig_3_to_10

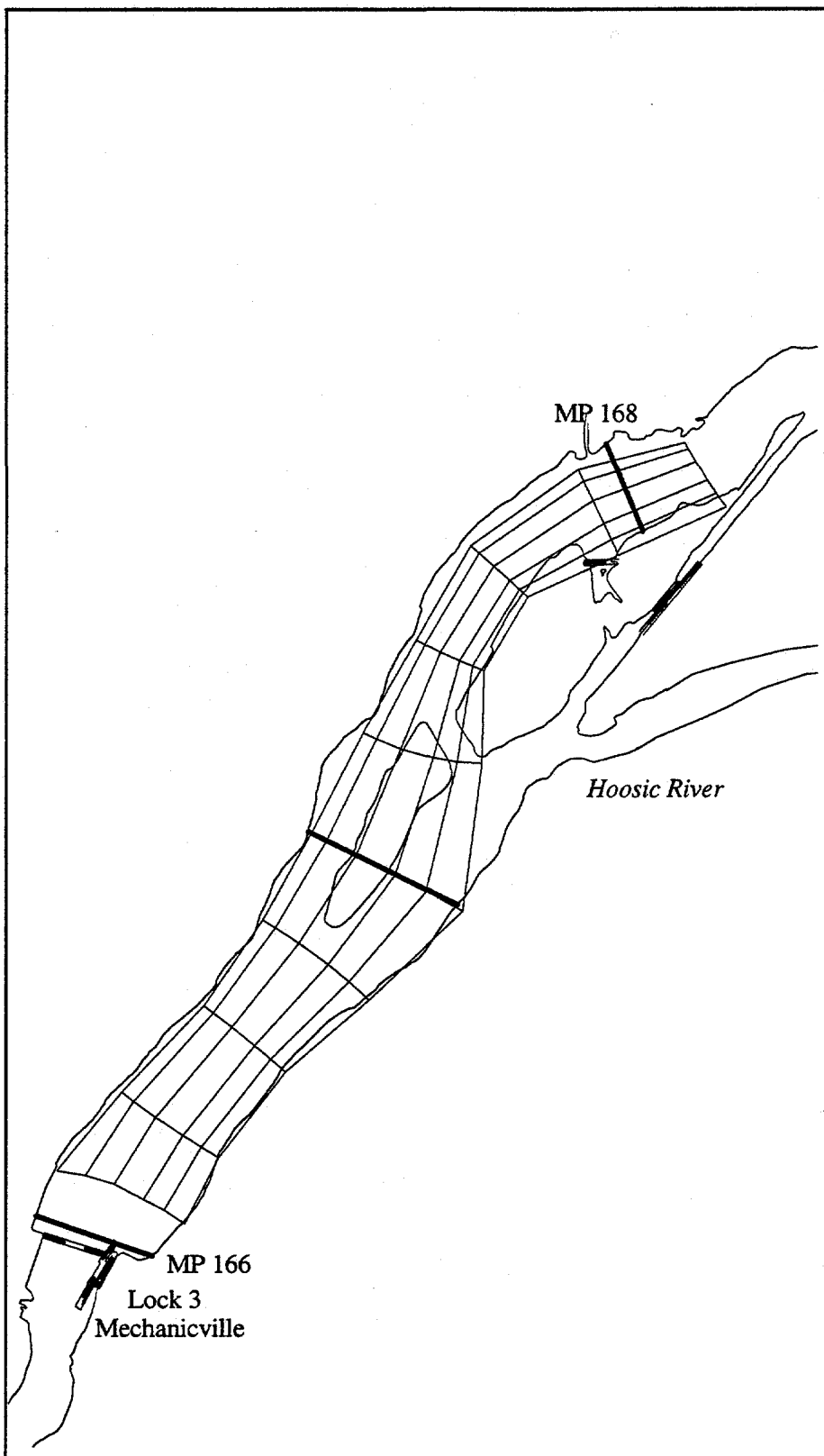

LOCATION MAP OF THE HUDSON RIVER

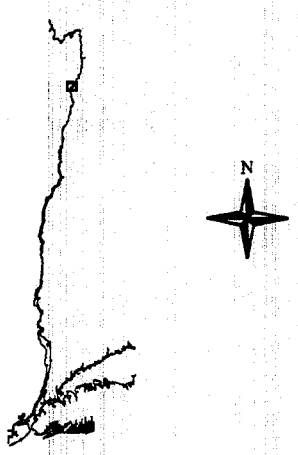

GRAPHIC SCALE

0.2 0 0.2 0.4 Miles

LEGEND

- Shoreline
- Mile Points
- Dams and Locks
- Reach 4 Grid

GENERAL ELECTRIC COMPANY
Hudson River Project

PCBs in the Upper Hudson River
Volume 2. A Model of PCB Fate, Transport and Bioaccumulation

Figure 2-7.

Two-dimensional numerical model for Reach 4.

QEA
Quantitative Environmental Analysis, LLC

Project: Genhud 131

April 1999

313687

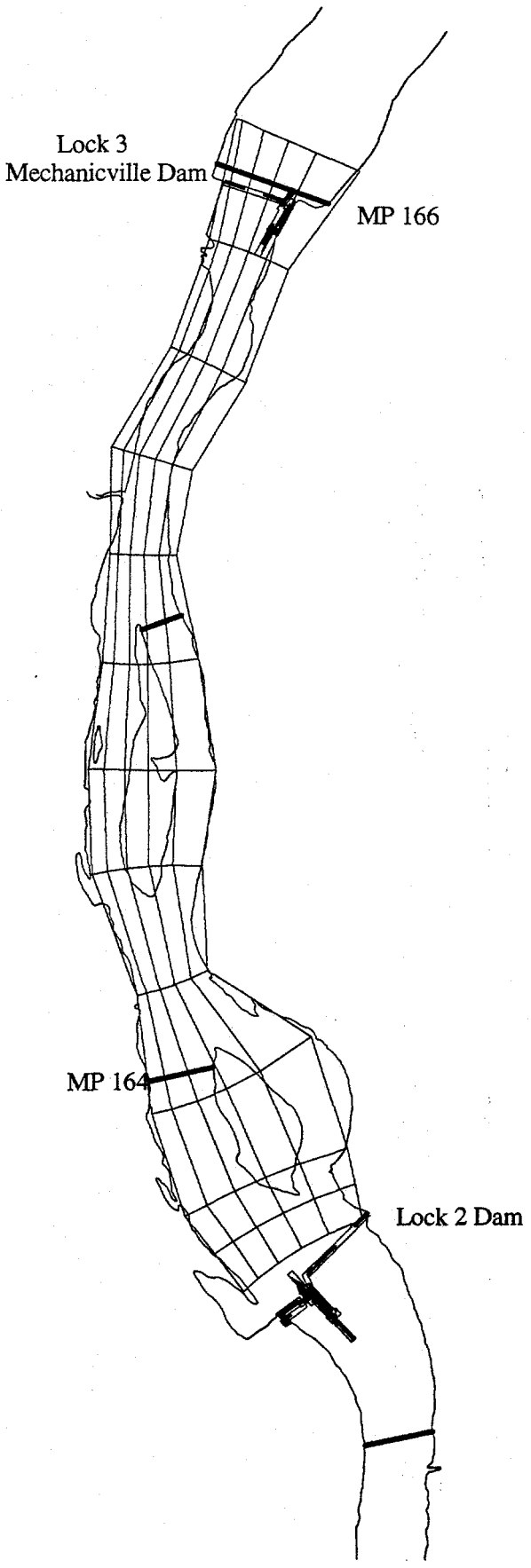

LOCATION MAP OF THE HUDSON RIVER

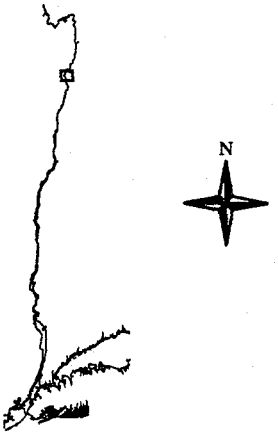

GRAPHIC SCALE

0.2 0 0.2 0.4 Miles

LEGEND

- Shoreline
- Mile Points
- Dams and Locks
- Reach 3 Grid

GENERAL ELECTRIC COMPANY
Hudson River Project

PCBs in the Upper Hudson River
Volume 2. A Model of PCB Fate, Transport and Bioaccumulation

Figure 2-8.

Two-dimensional numerical model for Reach 3.

QEA
Quantitative Environmental Analysis, LLC

d131 April 1999

\\Poseidon\D_drive\GENhud\Documents\Final _report\Vol_2\Section_2\Fig_3_to_10

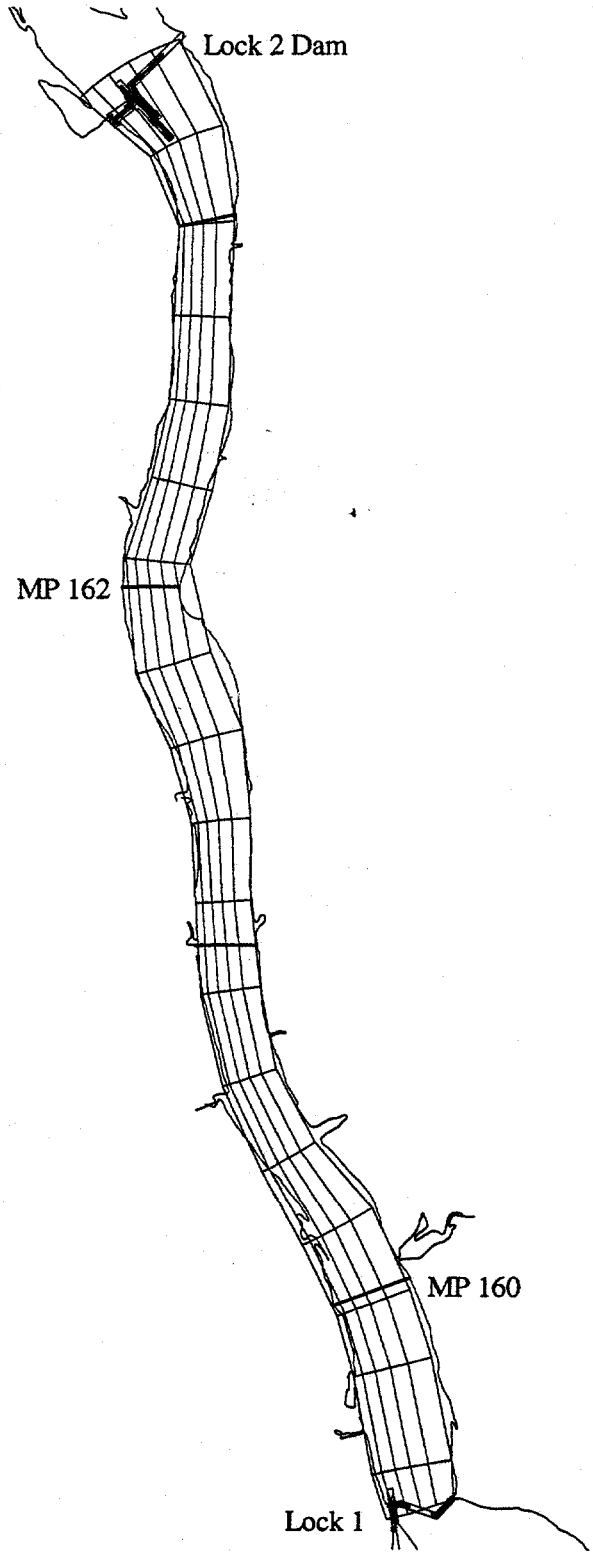

LOCATION MAP OF THE HUDSON RIVER

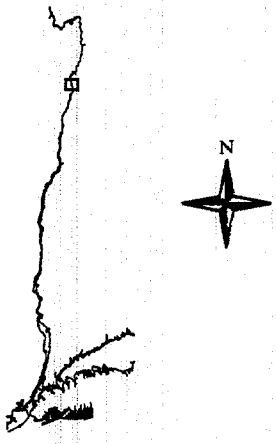

GRAPHIC SCALE

0.3 0 0.3 0.6 Miles

LEGEND

- Shoreline
- Mile Points
- Dams and Locks
- Reach 2 Grid

GENERAL ELECTRIC COMPANY
Hudson River Project

PCBs in the Upper Hudson River
Volume 2. A Model of PCB Fate, Transport and Bioaccumulation

Figure 2-9.

Two-dimensional numerical model for Reach 2.

QEA
Quantitative Environmental Analysis, LLC

Project: Genhud 131 April 1999

313689

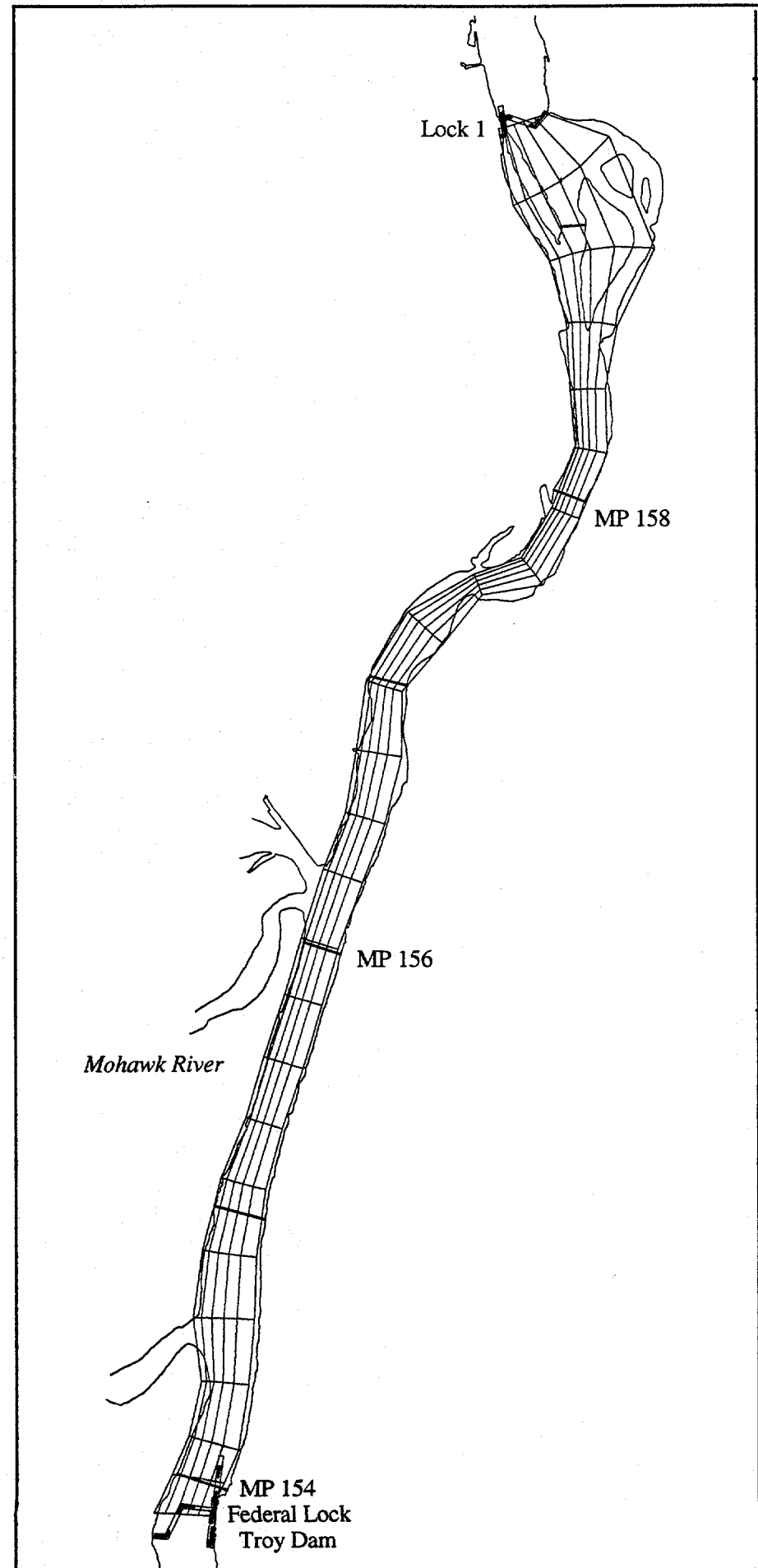

LOCATION MAP OF THE HUDSON RIVER

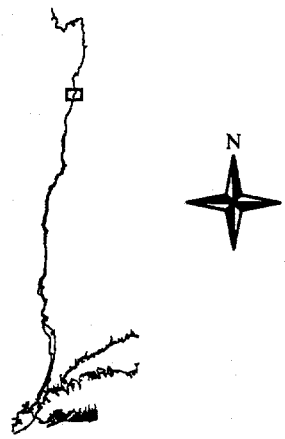

GRAPHIC SCALE

0.4 0 0.4 0.8 Miles

LEGEND

- Shoreline
- Mile Points
- Dams and Locks
- Reach 1 Grid

GENERAL ELECTRIC COMPANY
Hudson River Project

PCBs in the Upper Hudson River
Volume 2. A Model of PCB Fate, Transport and Bioaccumulation

Figure 2-10.

Two-dimensional numerical model for Reach 1.

QEA
Quantitative Environmental Analysis, LLC

Project: Genhud 131 April 1999

\\Poseidon\D_drive\GENhud\Documents\Final _report\Vol_2\Section_2\Fig_3_to_10

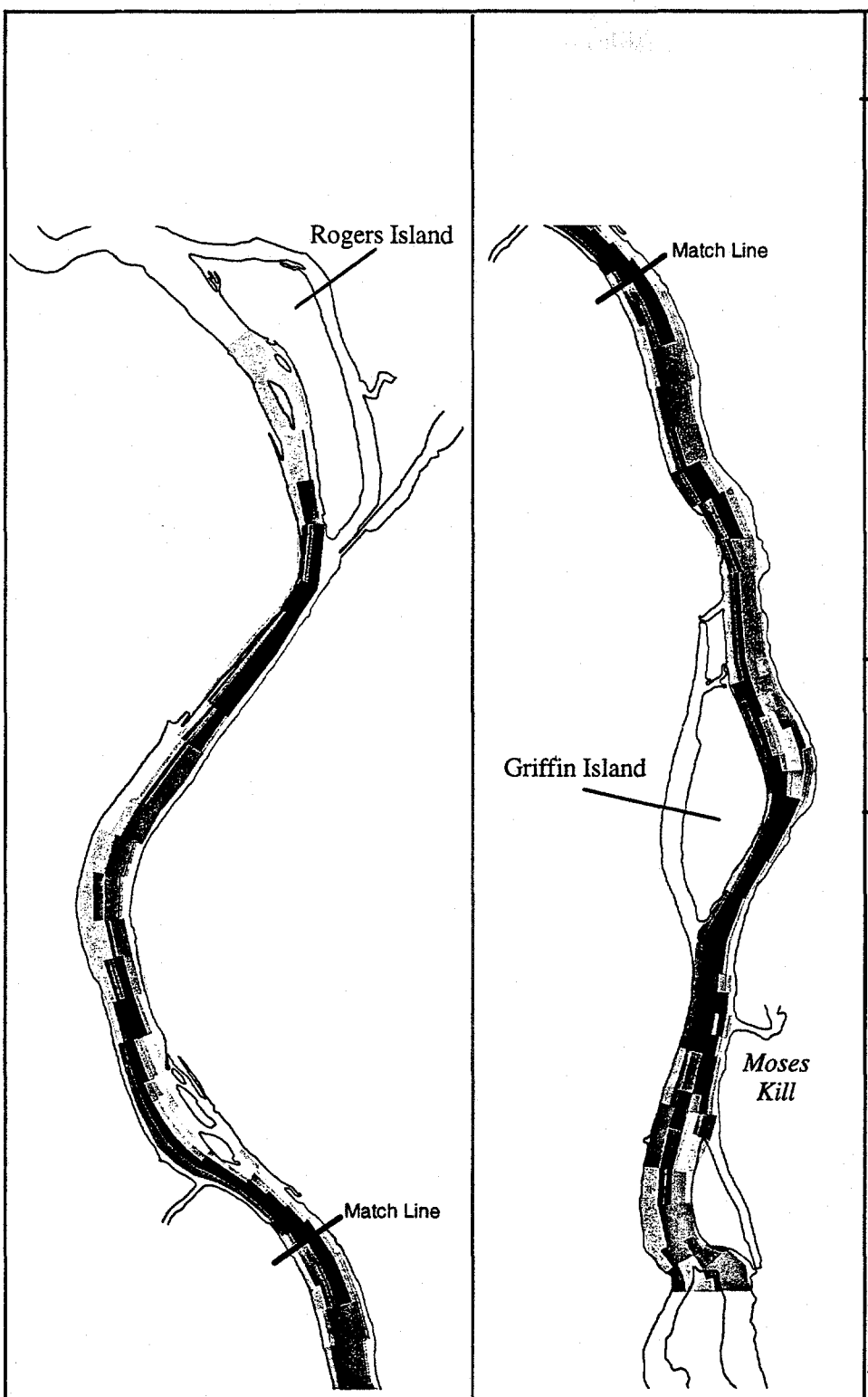

LOCATION MAP OF THE HUDSON RIVER

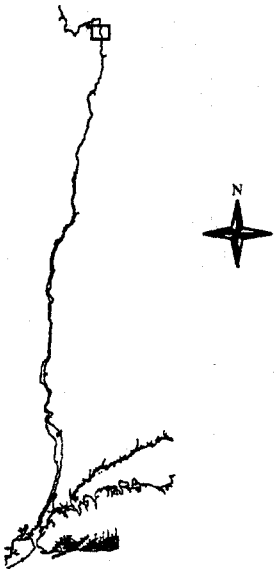

GRAPHIC SCALE

1000 0 1000 2000 Feet

LEGEND

Shoreline
Depth (ft)
< 0
0 - 3
3 - 6
6 - 9
9 - 12
12 - 15
15 - 18
18 - 21

GENERAL ELECTRIC COMPANY
Hudson River Project

PCBs in the Upper Hudson River
Volume 2. A Model of PCB Fate, Transport and Bioaccumulation

Figure 2-11.

Thompson Island Pool bathymetry, depths in feet.

\\poseidon\D_drive\Genhud\Documents\Final_report\vol_2\section_2\bathym_comp_fig_2_11

QEA
Quantitative Environmental Analysis, LLC

Project: Genhud 131 April 1999

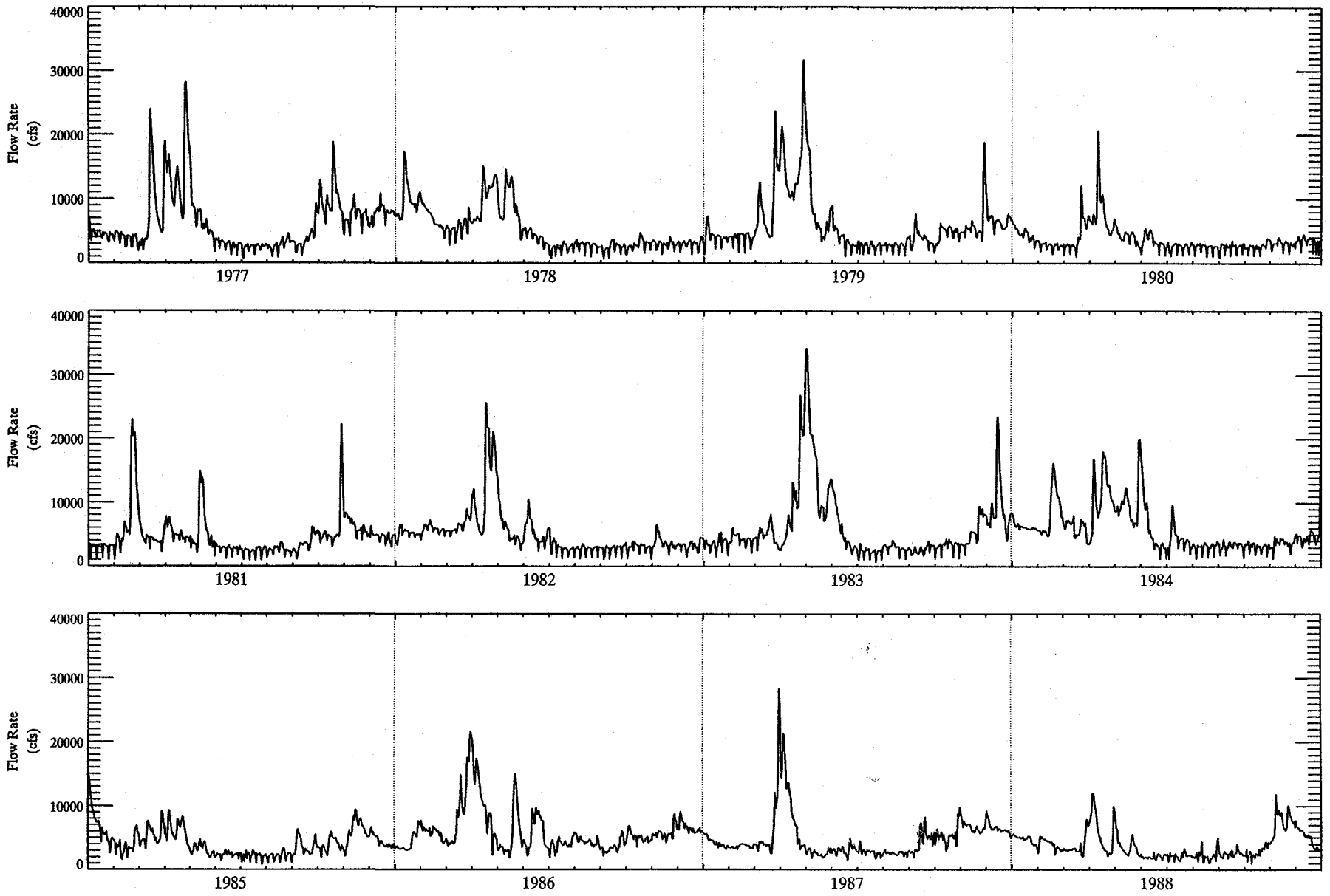

Figure 2-12a. Daily average flow rate at Fort Edward, 1977 to 1988.

Poseidon - S:\GENhud\Documents\Final_report\Vol_2\Section_2\plot_feflow_fig_2_12.pro
Mon Apr 12 15:48:44 199?

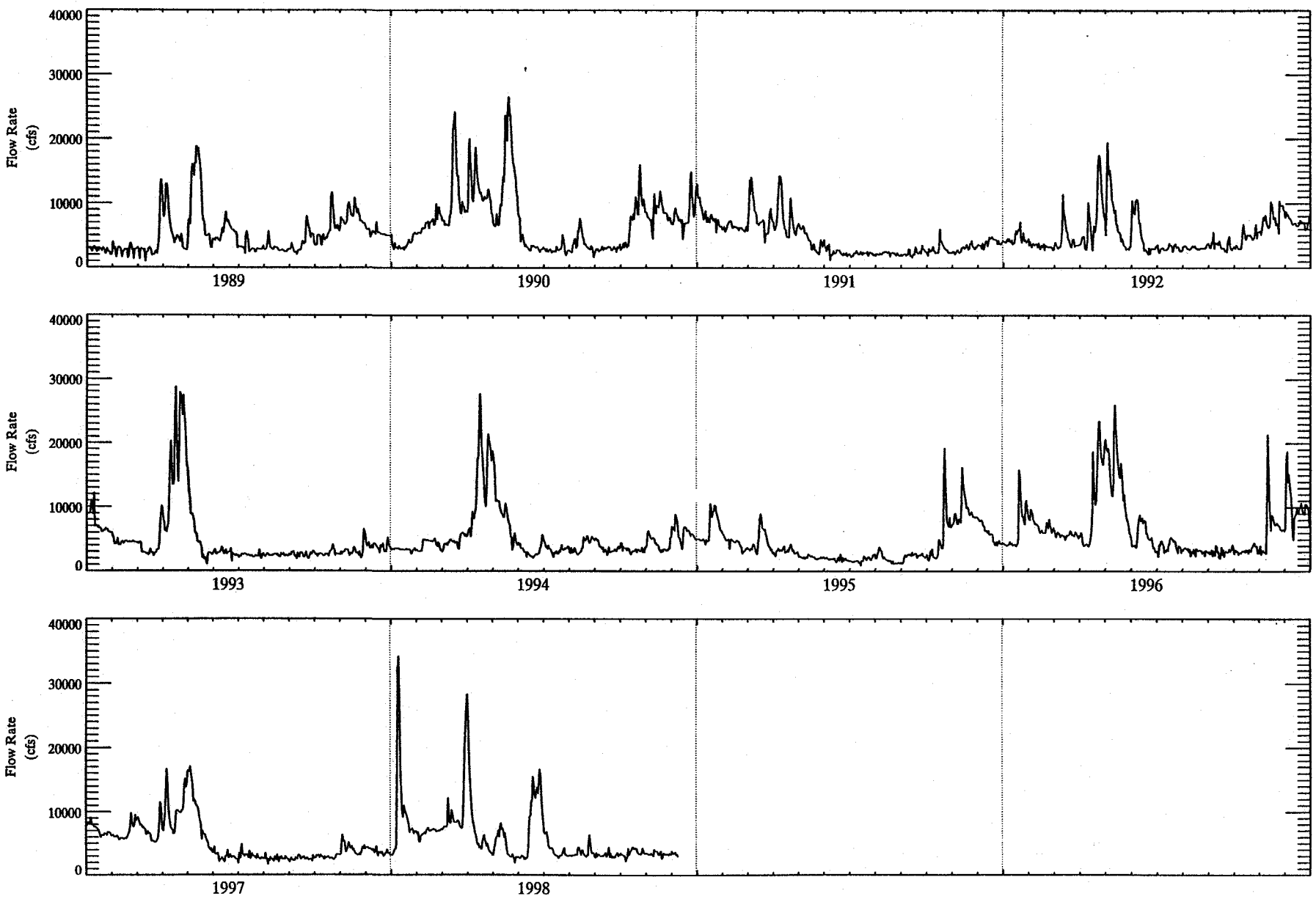

Figure 2-12b. Daily average flow rate at Fort Edward, 1989 to 1998.

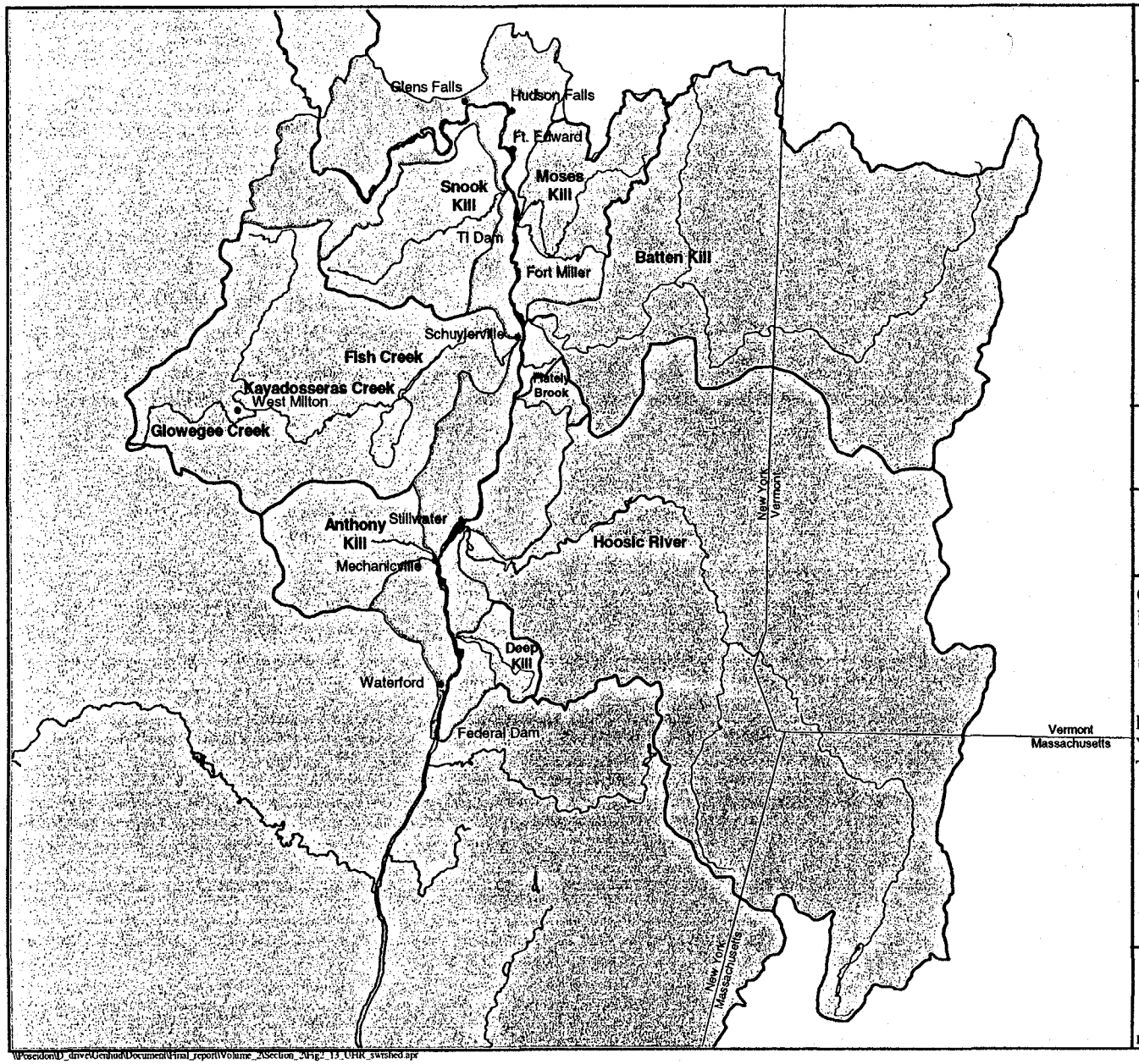

LOCATION MAP OF THE HUDSON RIVER

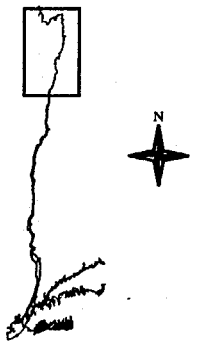

GRAPHIC SCALE

5 0 5 Miles

LEGEND

Direct Drainage
Subwatersheds

GENERAL ELECTRIC COMPANY
Hudson River Project

PCBs in the Upper Hudson River
Volume 2. A Model of PCB Fate, Transport, and Bioaccumulation

Figure 2-13.

Drainage basins for tributaries to the Upper Hudson River.

QEA
Quantitative Environmental Analysis, LLC

Project: Genhud 131 April 1999

\\Poseidon\D_drive\Genhud\Document\Final_report\Volume_2\Section_2\Fig_2_13_UHR_swished.apr

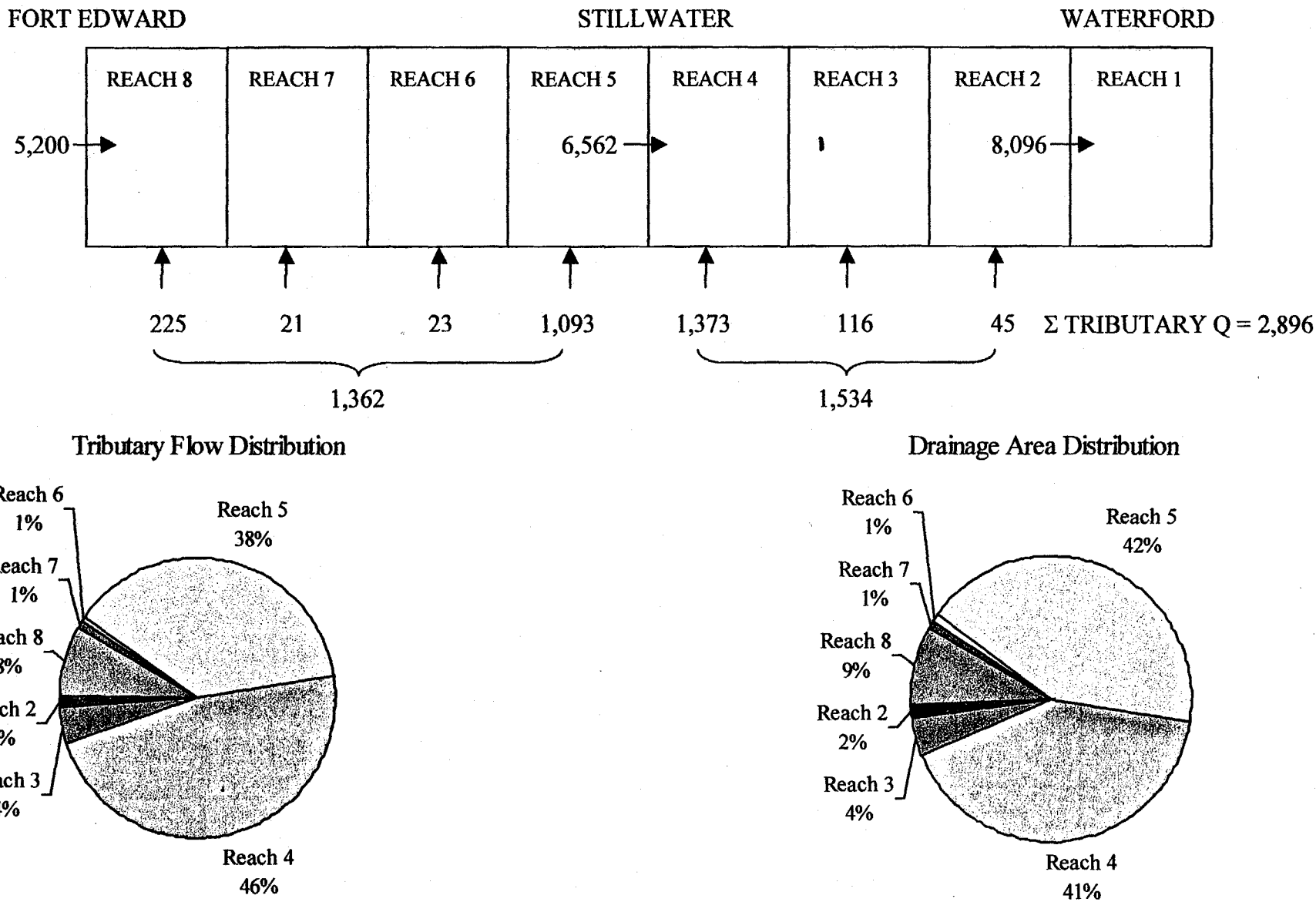

Figure 2-14. Mean flow balance for Upper Hudson River between Fort Edward and Waterford (flow rates are in cfs).

\\Poseidon\D_Drive\GENhud\Documents\Final_report\Vol_2\Section_2\flow_b_fig_2_14.ppt

4/15/99

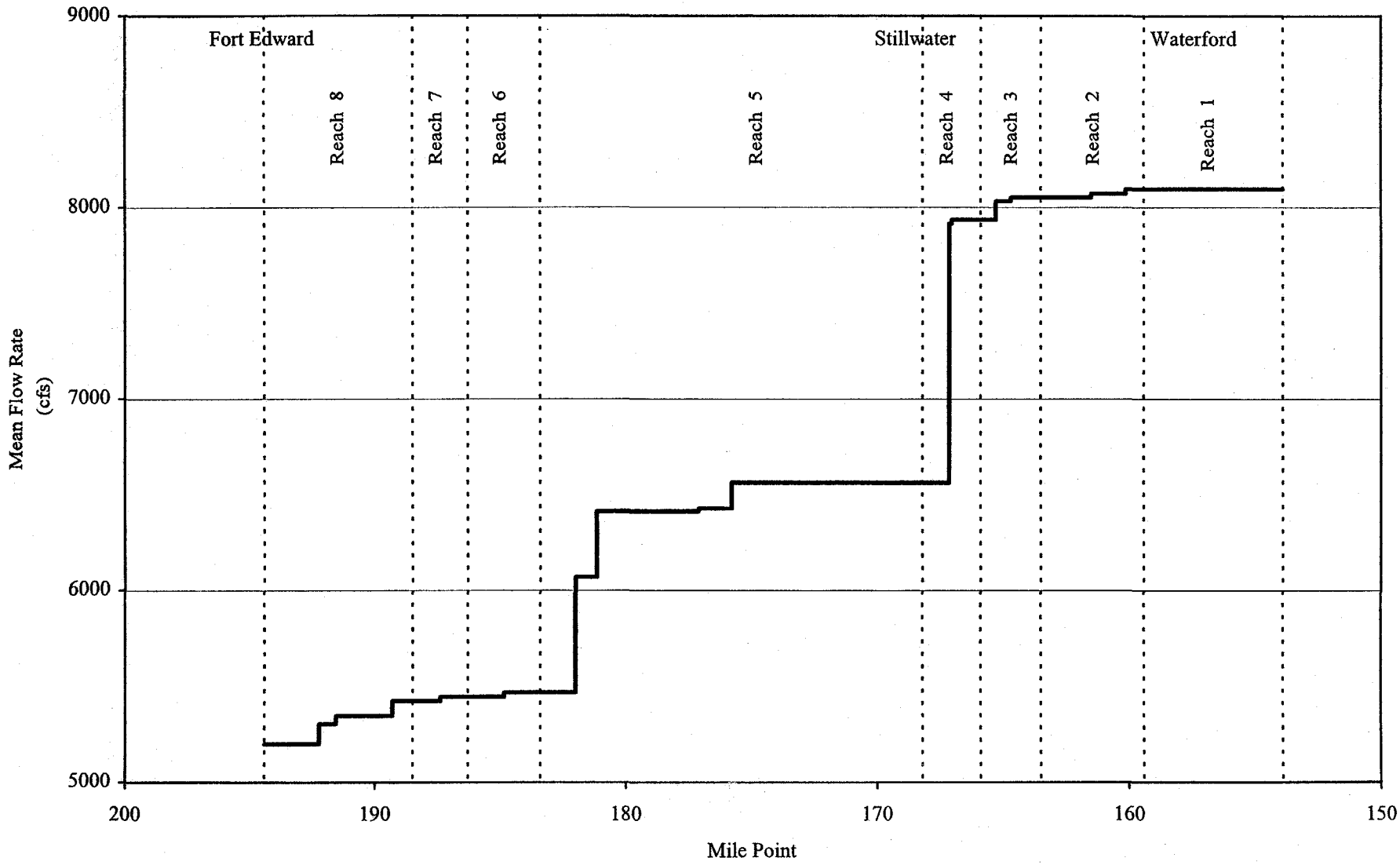

Figure 2-15. Cumulative mean flow rate between Fort Edward and Waterford.

\\poseidon\GENhud\documents\final_report\vol-2\section_2\tribflow_fig_2_15.xls
4/12/99

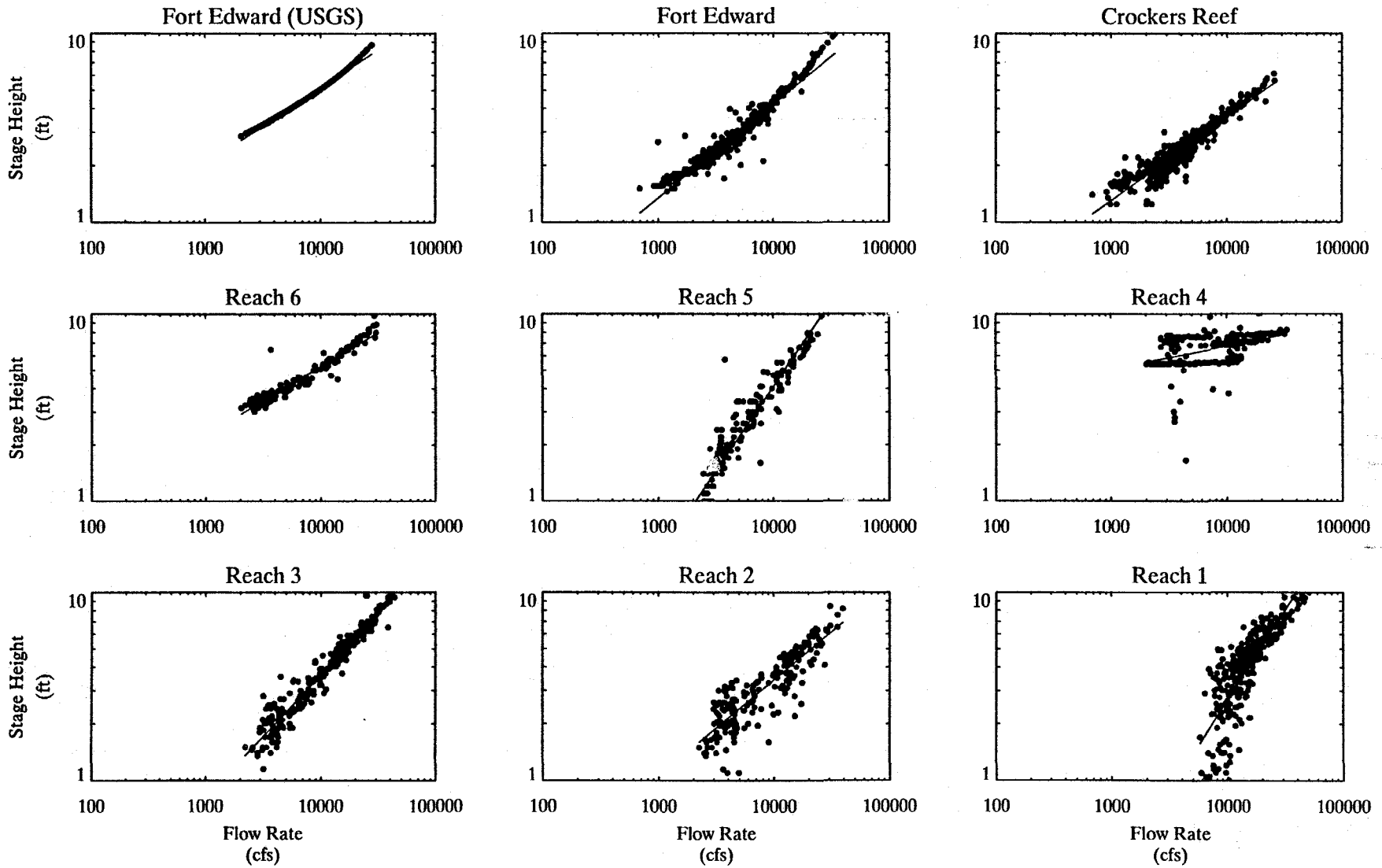

Figure 2-16. Stage height rating curves and data for Reaches 1 to 8. Champlain Canal data displayed at all locations except as noted at Fort Edward.

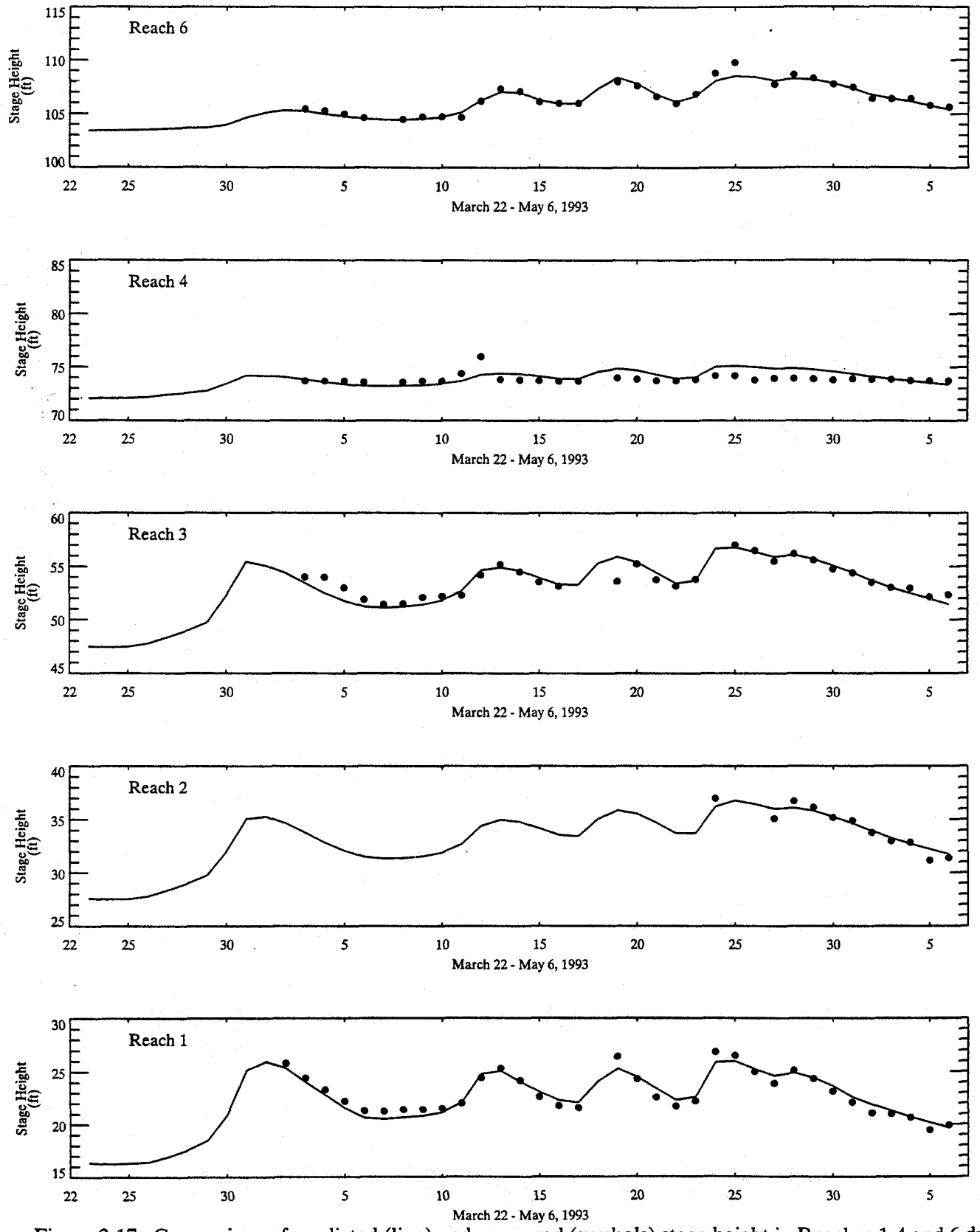

Figure 2-17. Comparison of predicted (line) and measured (symbols) stage height in Reaches 1-4 and 6 during the 1993 spring flood; one-dimensional model results.

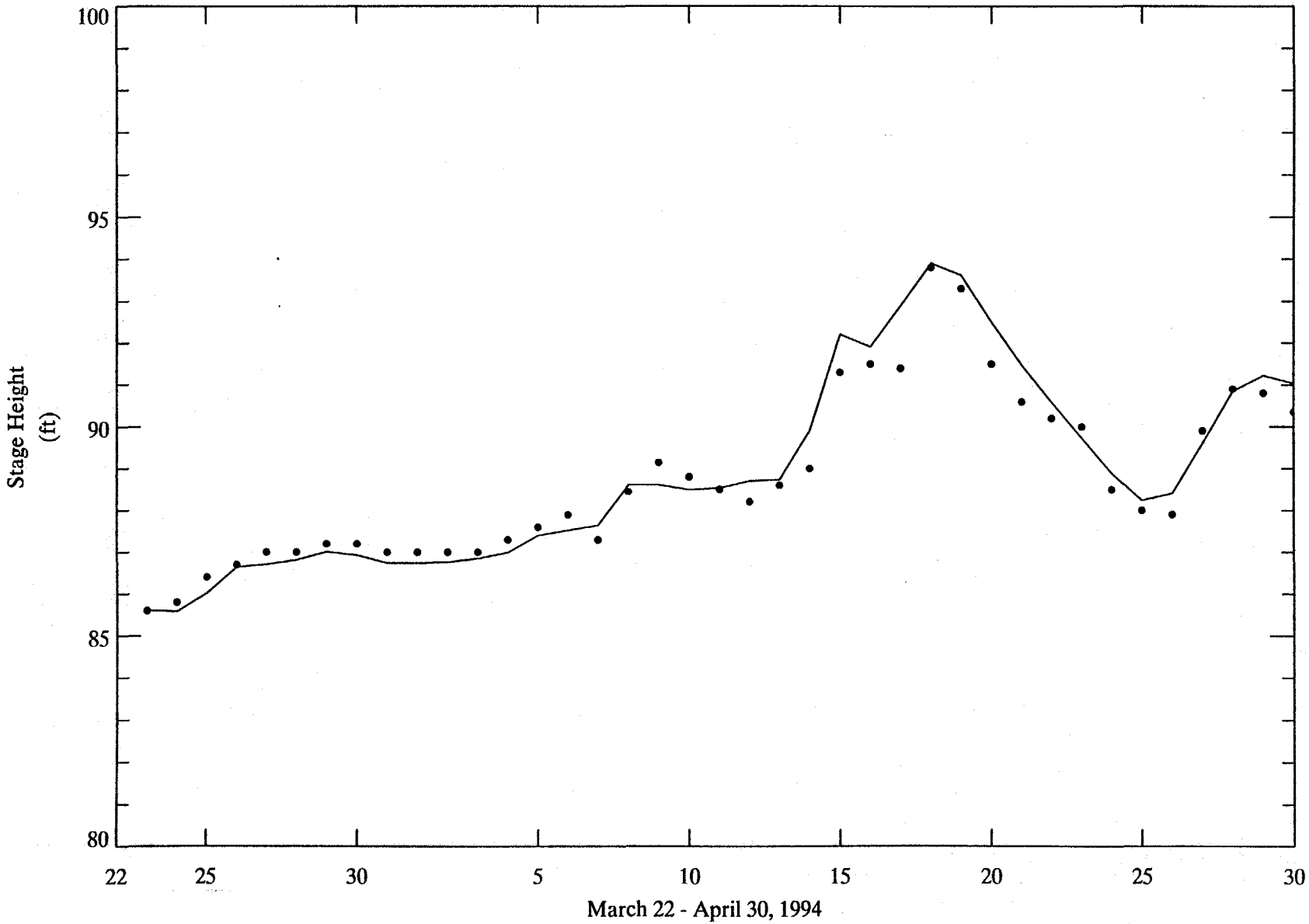

Figure 2-18. Comparison of predicted (line) and measured (symbols) stage height in Reach 5 during the 1994 spring flood; one-dimensional model results.

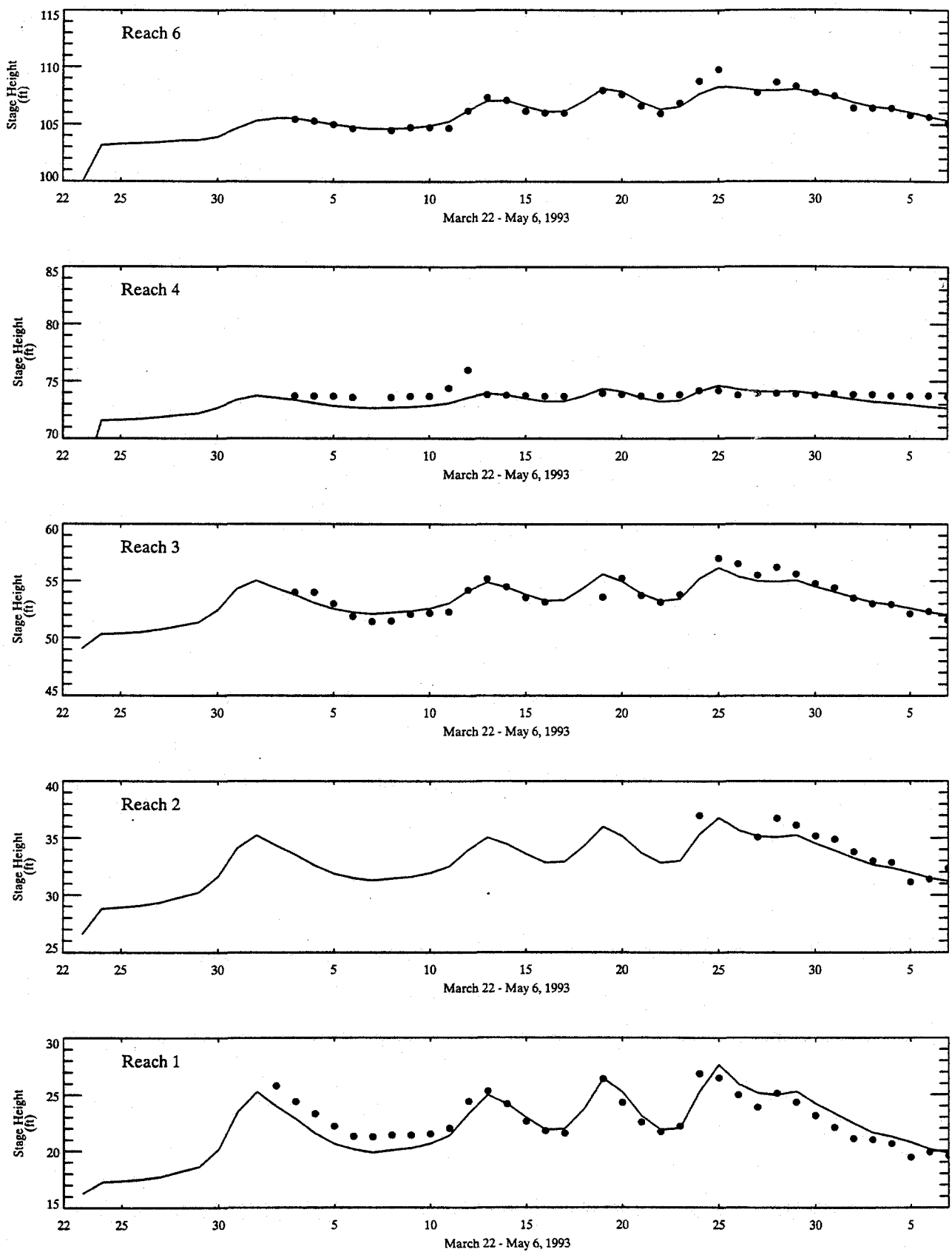

Figure 2-19. Comparison of predicted (solid) and measured (symbols) stage height in Reaches 1-4 and 6 during the 1993 spring flood; two-dimensional model results.

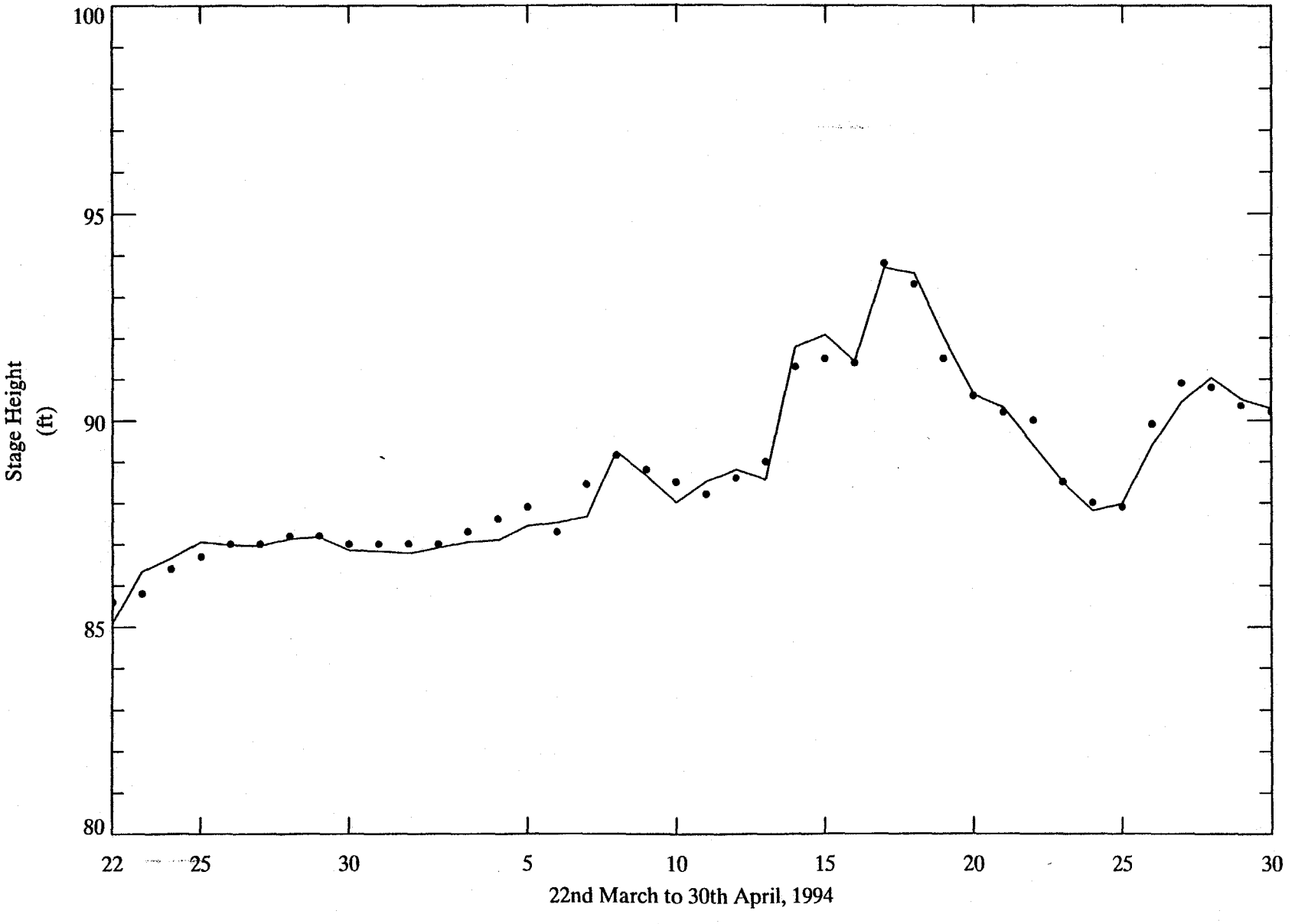

Figure 2-20. Comparison of predicted (solid) and measured (symbols) stage height in Reach 5 during the 1994 spring flood; two-dimensional model results.

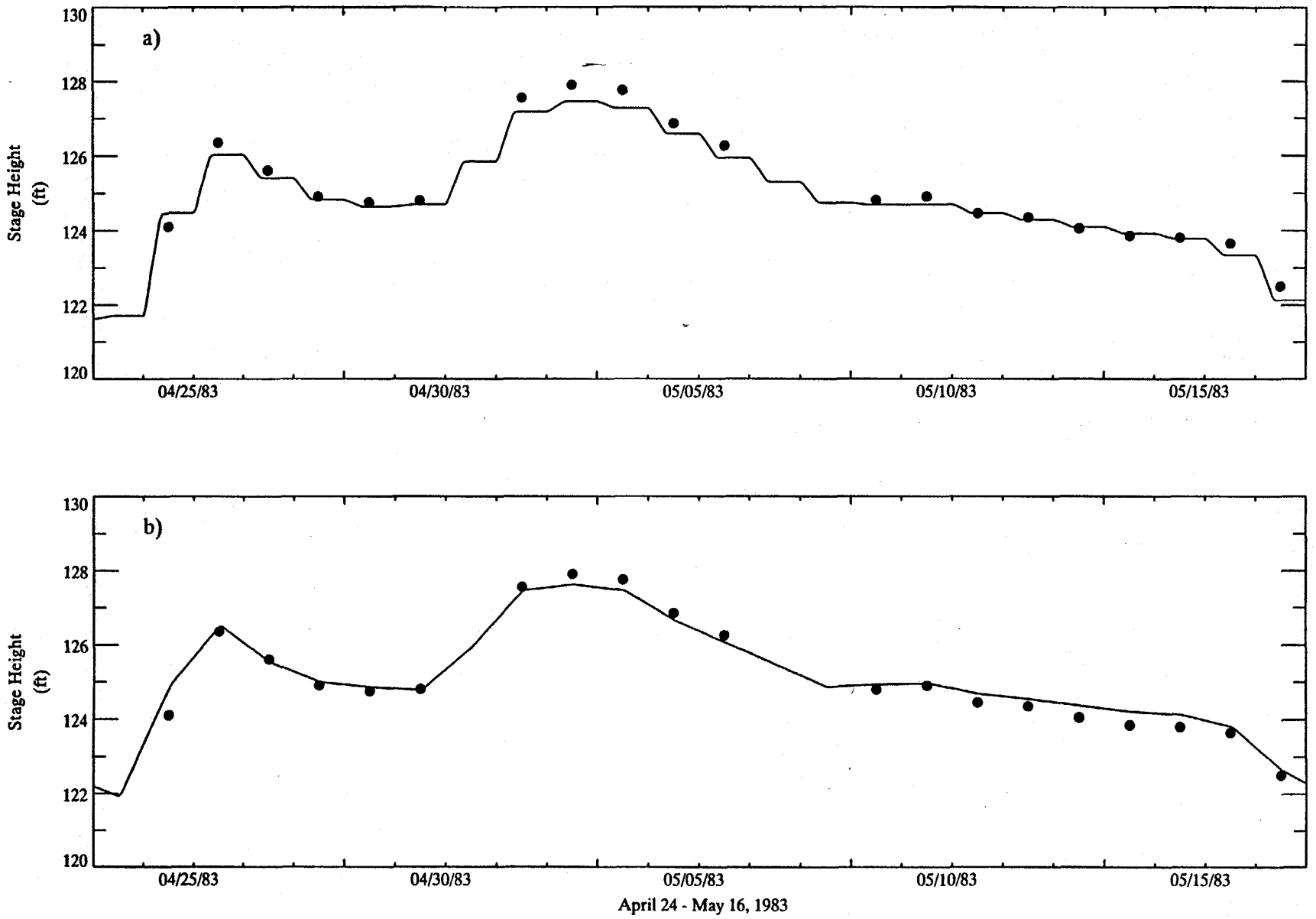

Figure 2-21. Comparison of predicted (line) and measured (symbols) TIP stage heights at guage 119 during 1983 spring flood for (a) one-dimensional and (b) two-dimensional models.

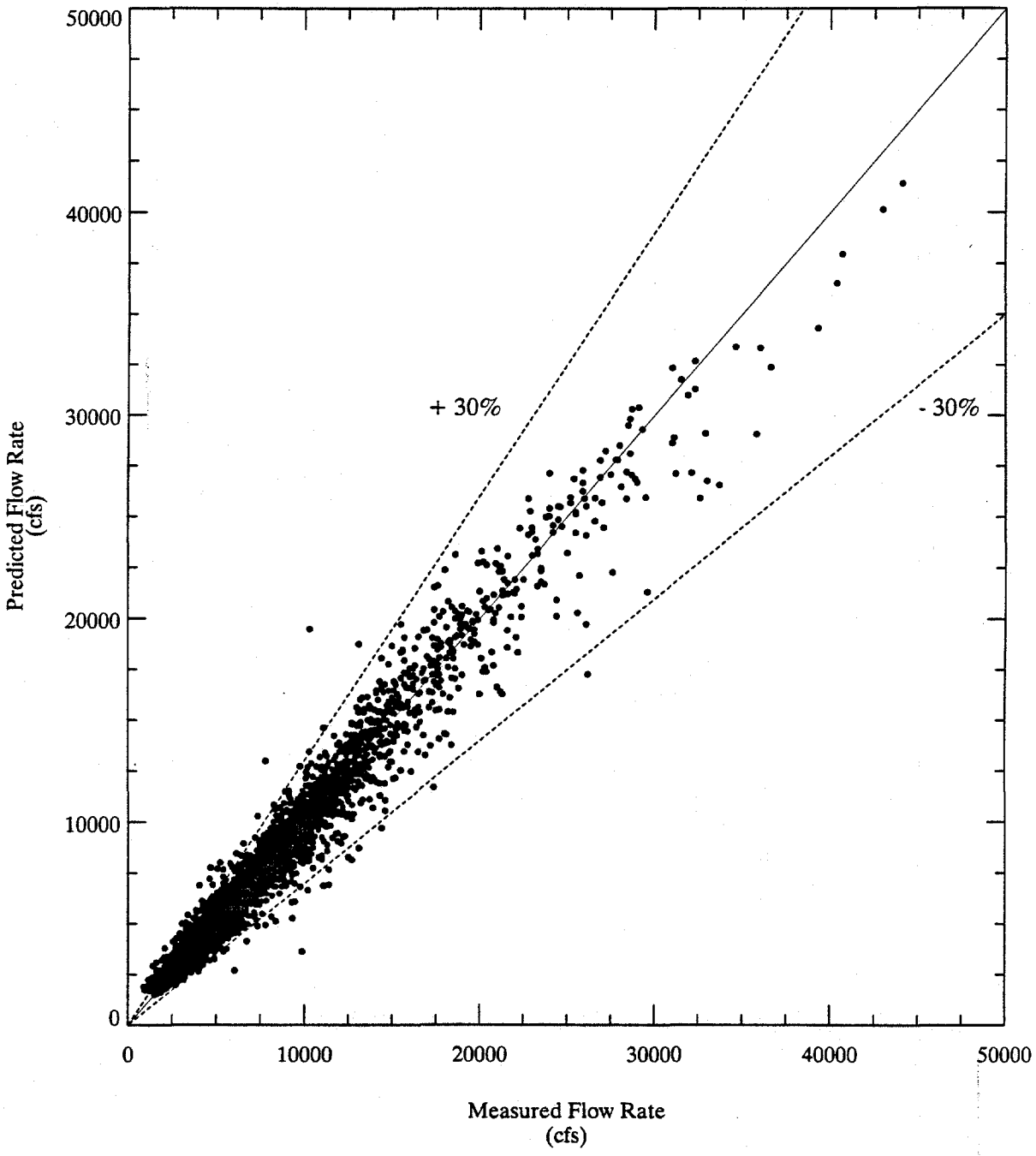

Figure 2-22. Comparison of measured and predicted daily average flow rates at Stillwater, one-dimensional model results.
Dashed lines represent +/- 30% error bounds.

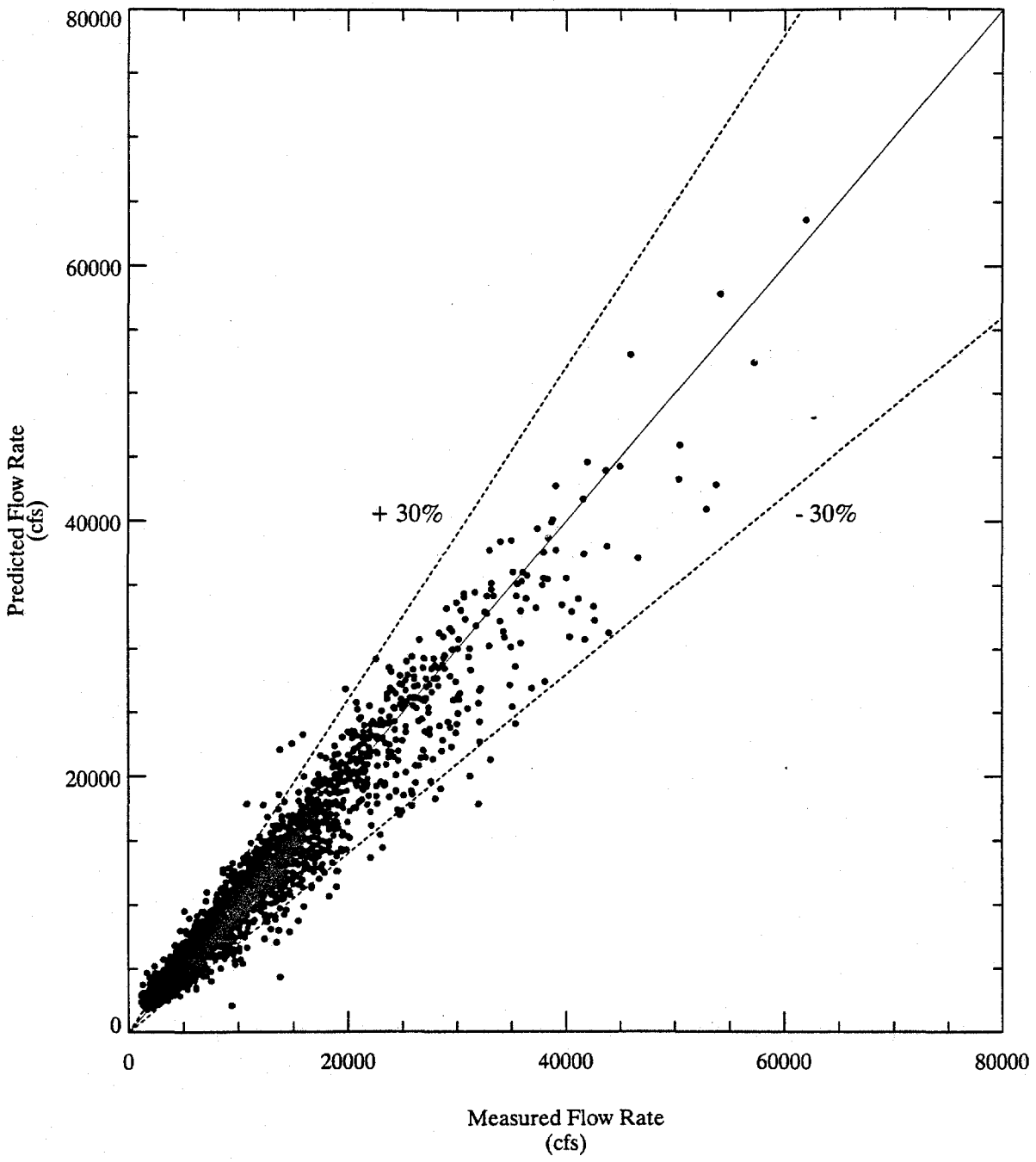

Figure 2-23. Comparison of measured and predicted daily average flow rates at Waterford, one-dimensional model results.
Dashed lines represent +/- 30% error bounds.

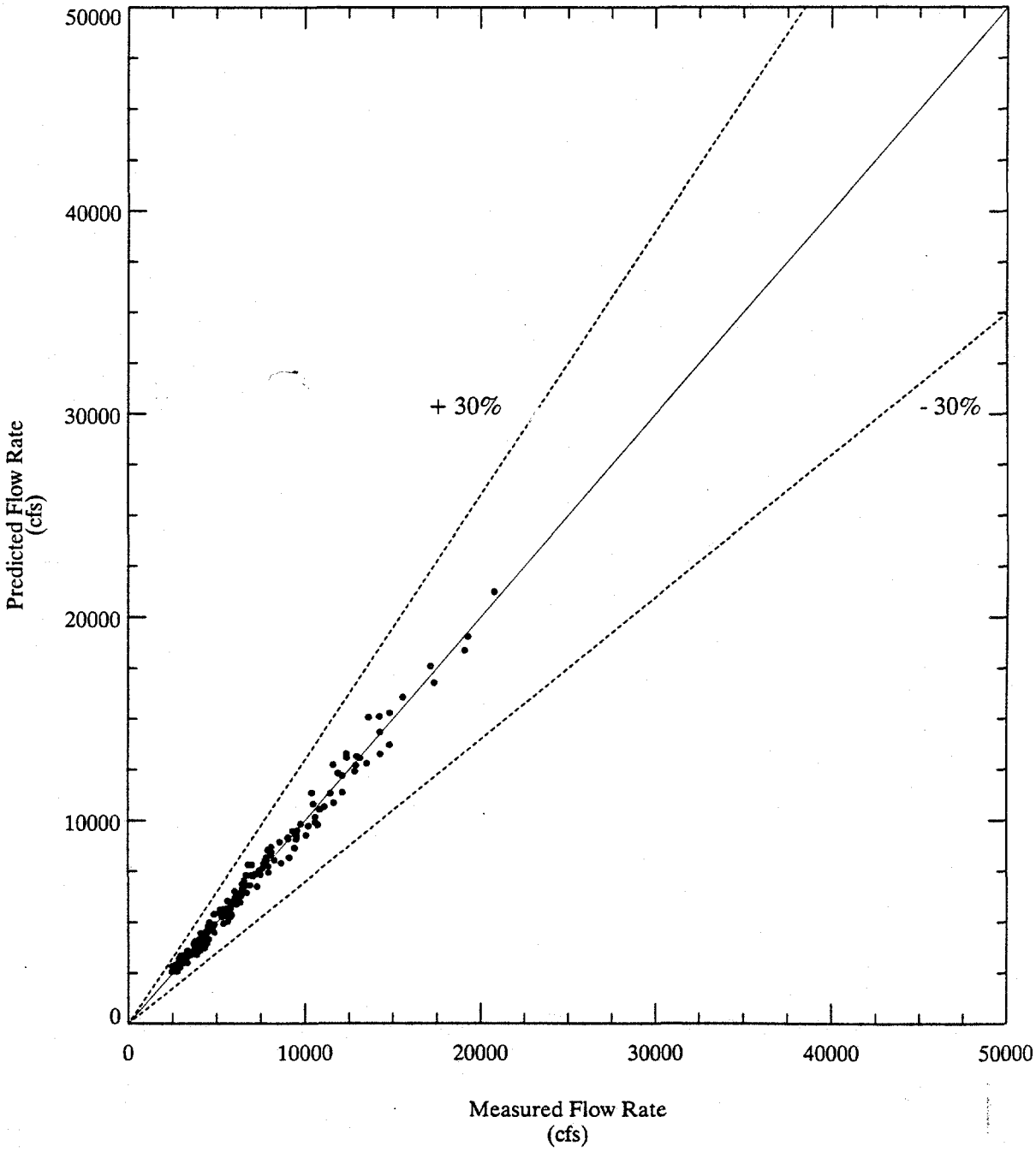

Figure 2-24. Comparison of measured and predicted monthly average flow rates at Stillwater, one-dimensional model results.
Dashed lines represent +/- 30% error bounds.

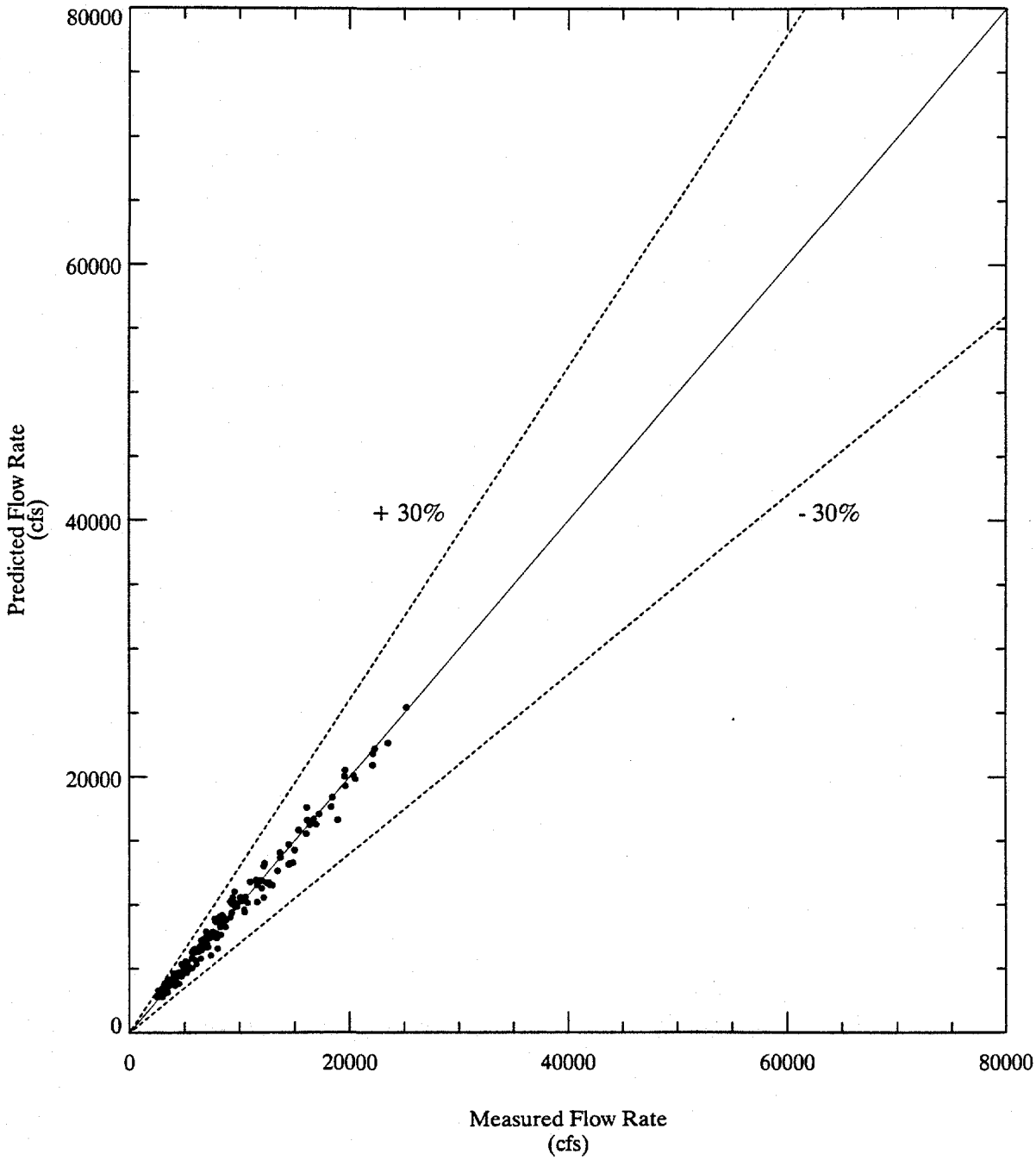

Figure 2-25. Comparison of measured and predicted monthly average flow rates at Waterford, one-dimensional model results.
Dashed lines represent +/- 30% error bounds.

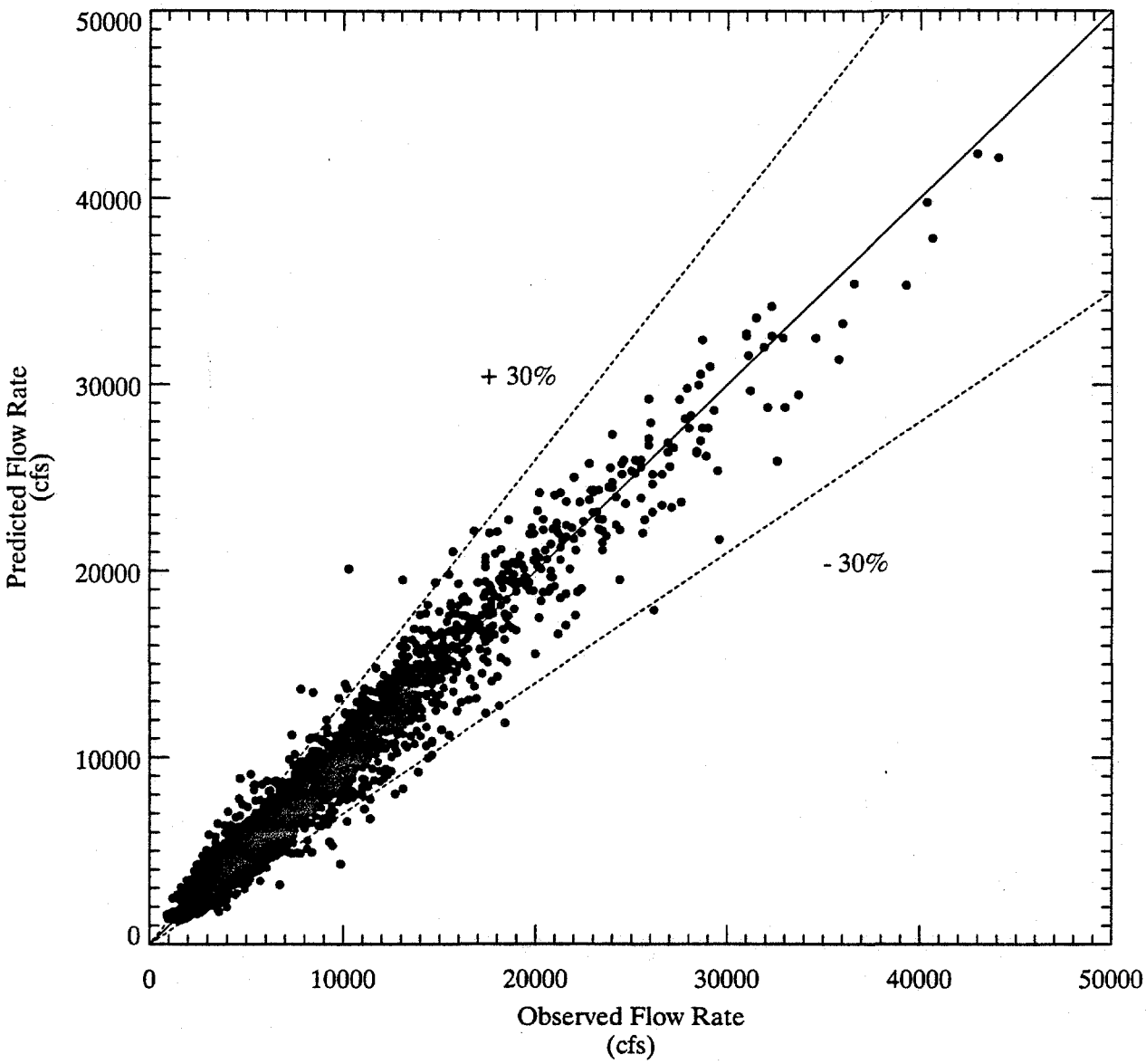

Figure 2-26. Comparison of measured and predicted daily average flow rates at Stillwater, two-dimensional model results.
Dashed lines represent +/-30% error bounds.

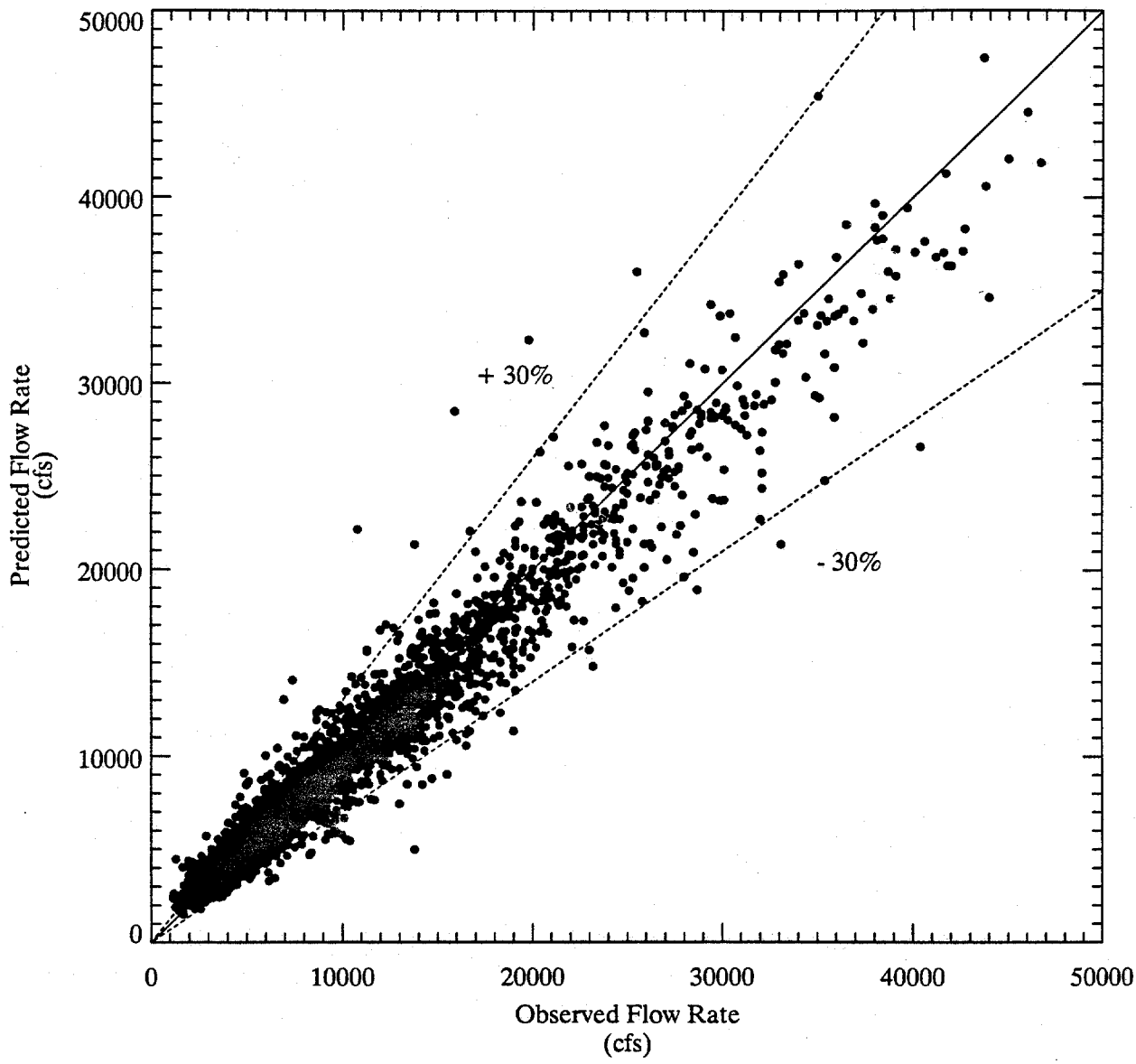

Figure 2-27. Comparison of measured and predicted daily average flow rates at Waterford, two-dimensional model results.
Dashed lines represent +/-30% error bounds.

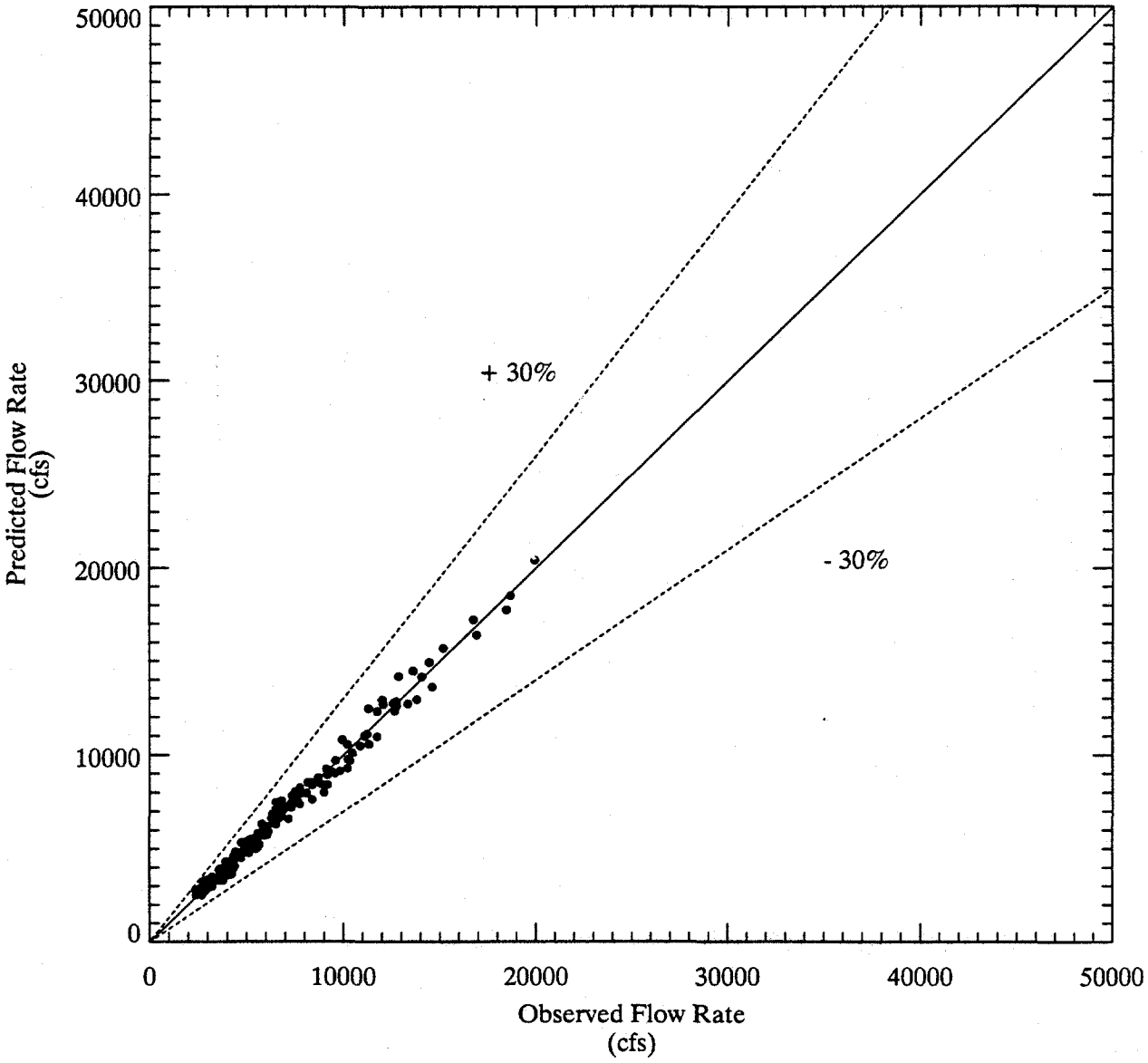

Figure 2-28. Comparison of measured and predicted monthly average flow rates at Stillwater, two-dimensional model results.
Dashed lines represent +/-30% error bounds.

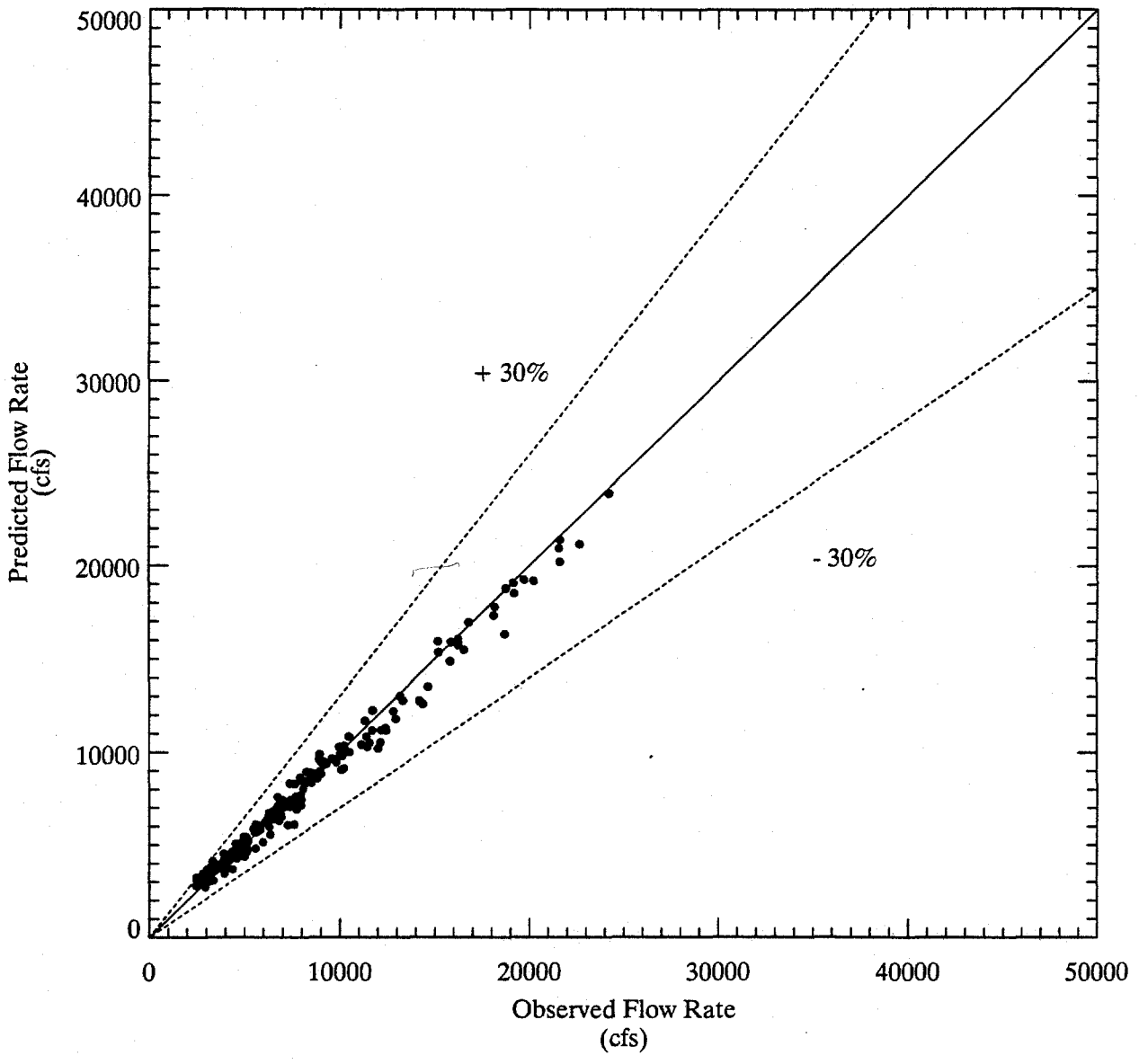

Figure 2-29. Comparison of measured and predicted monthly average flow rates at Waterford, two-dimensional model results.
Dashed lines represent +/-30% error bounds.

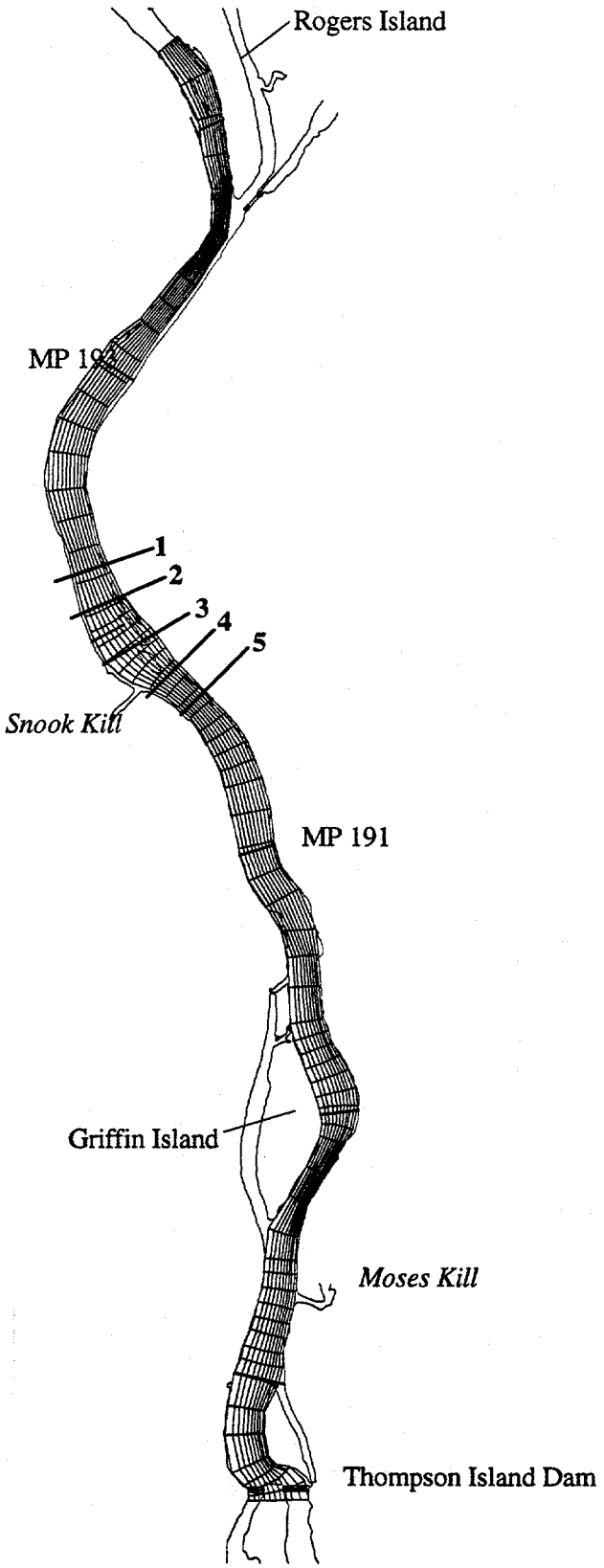

LOCATION MAP OF THE HUDSON RIVER

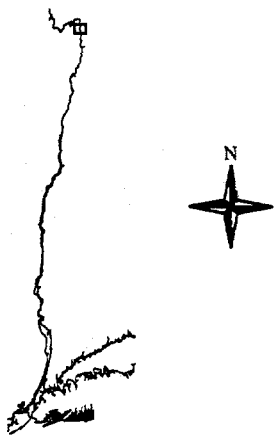

GRAPHIC SCALE

0.3 0 0.3 0.6 Miles

LEGEND

Shoreline
Mile Points
Dams and Locks
Reach 8 Grid

GENERAL ELECTRIC COMPANY
Hudson River Project

PCBs in the Upper Hudson River
Volume 2. A Model of PCB Fate, Transport and Bioaccumulation

Figure 2-30.

Transect locations for 1997 velocity data.

QEA
Quantitative Environmental Analysis, LLC

Project: Genhud 131 April 1999

\\Poseidon\D_drive\GEN\hud\Documents\Final _report\Vol_2\Section_2\Fig_3_to_10

313710

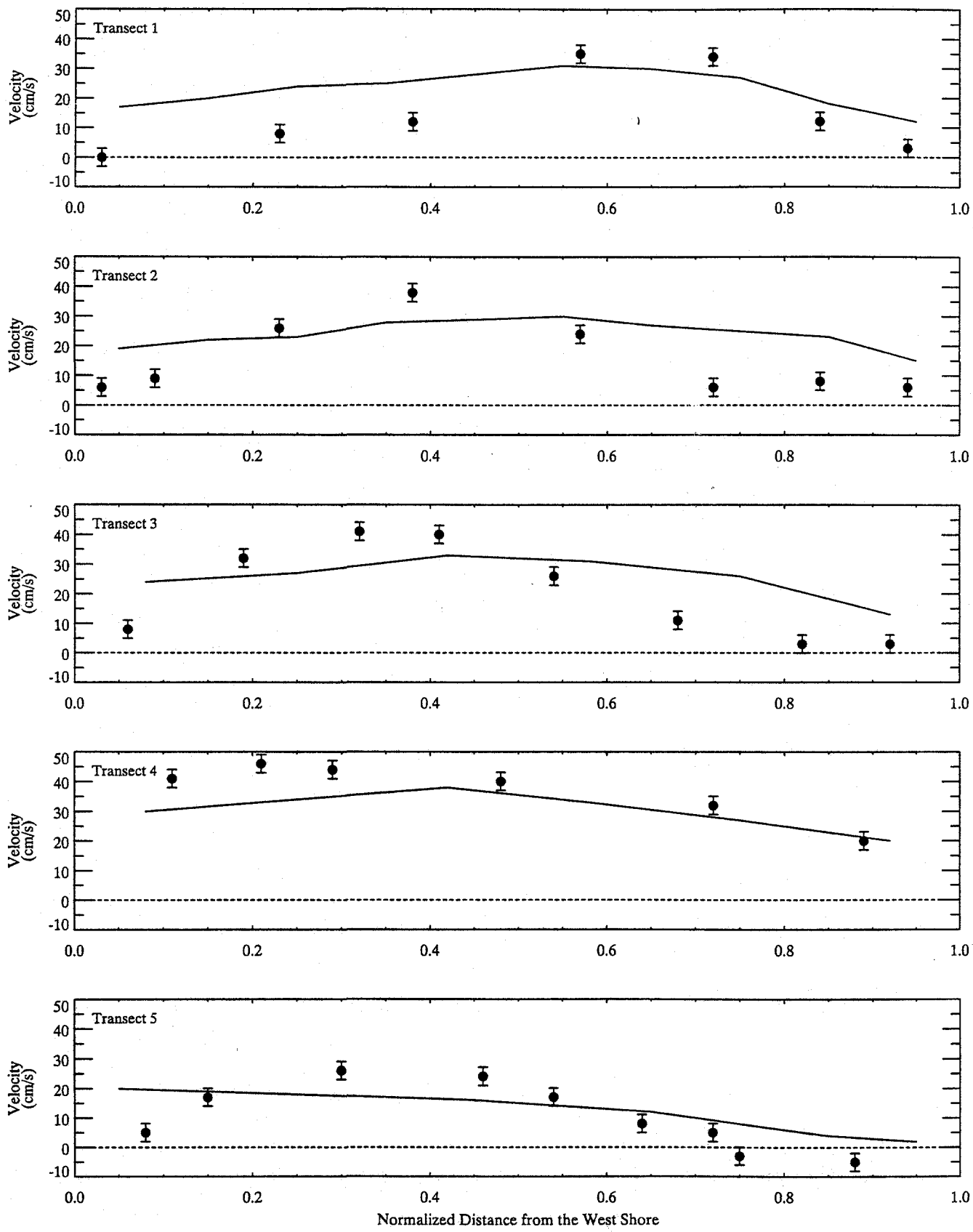

Fig 2-31. Comparisons of predicted (solid) and measured (symbols) current velocities at five transects in the TIP. Positive velocity is in the downstream direction.

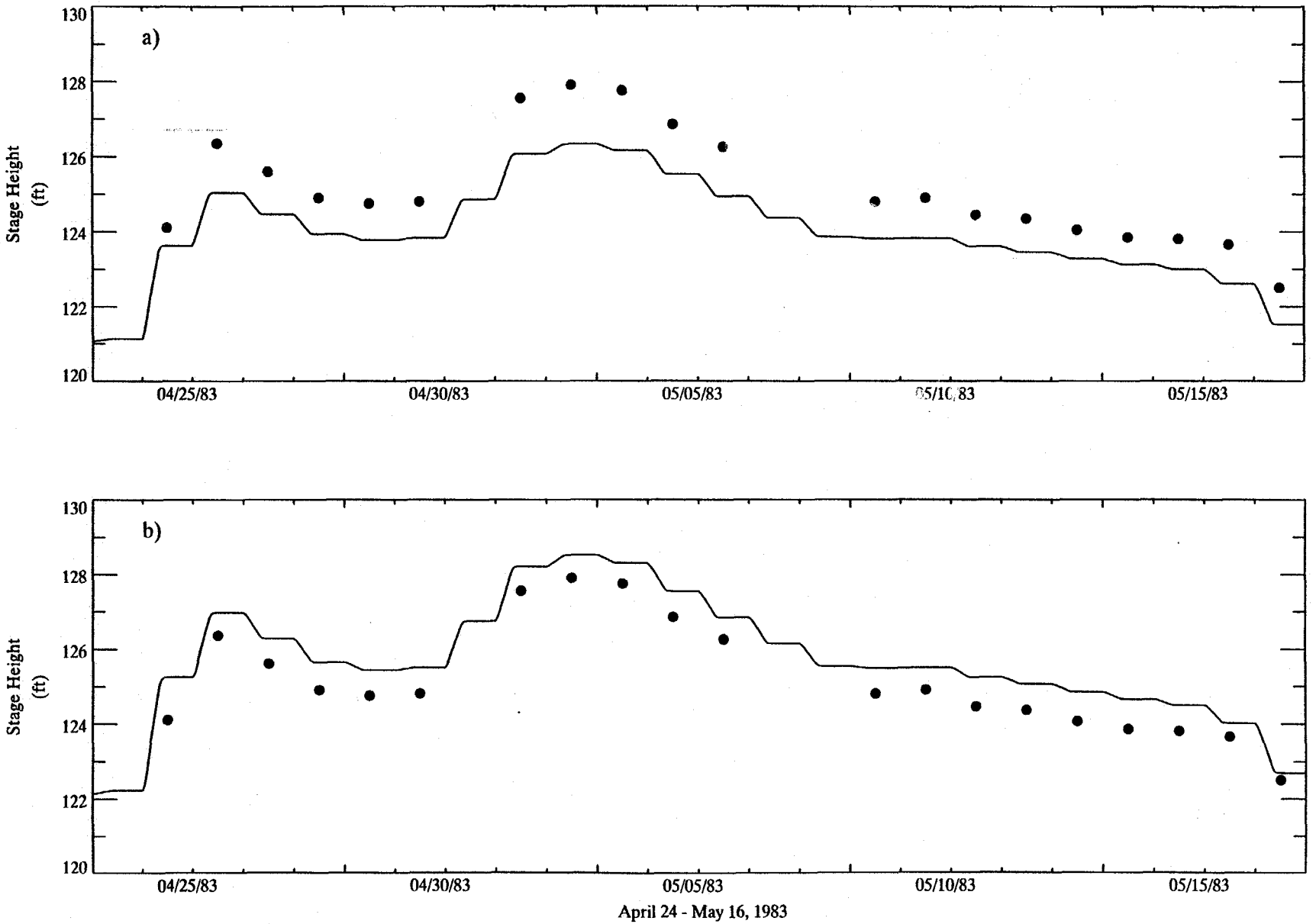

Figure 2-32. Results of one-dimensional model sensitivity analysis during 1983 spring flood, with Manning's n=0.015 (a) and 0.023 (b)

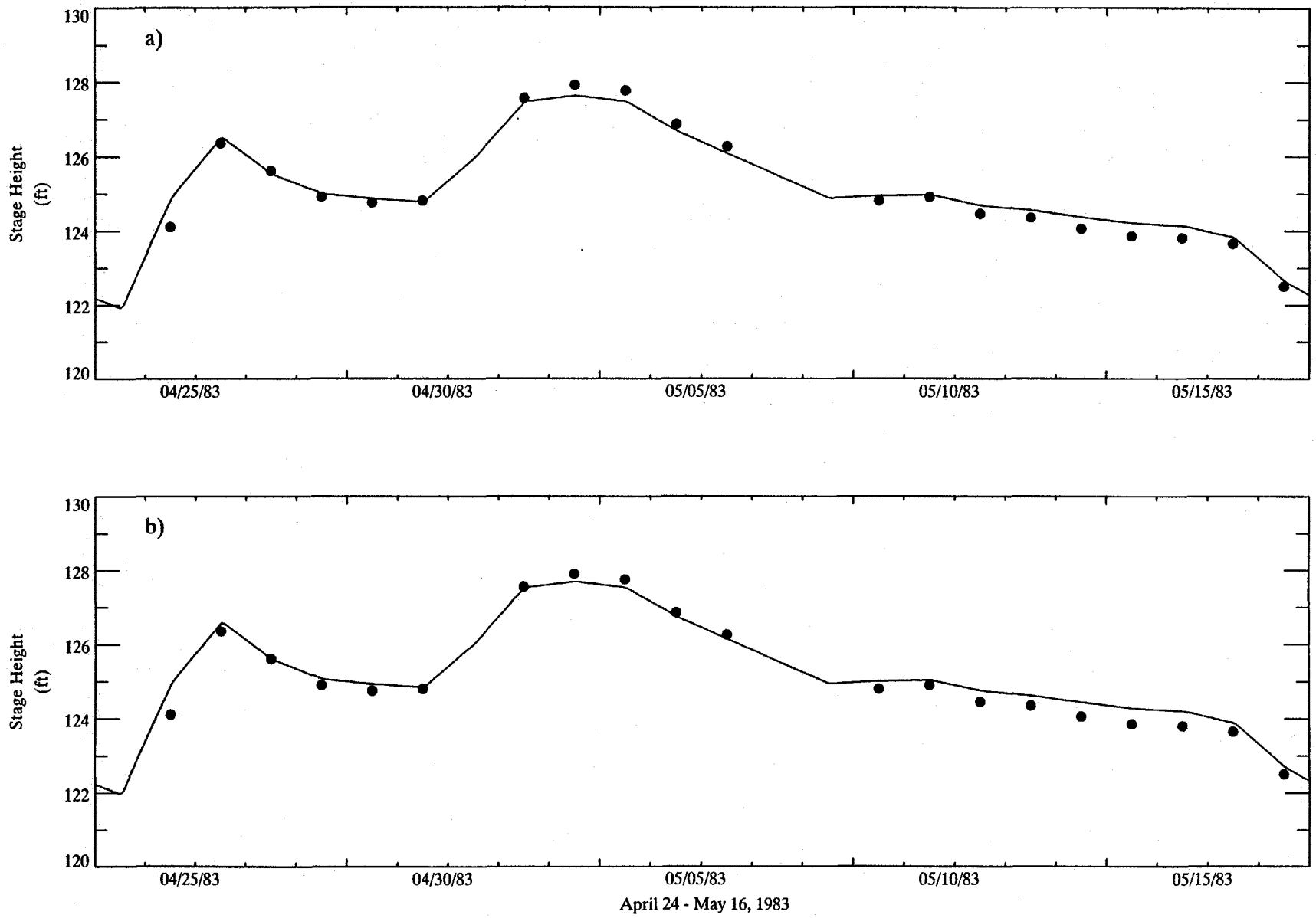

Figure 2-33. Results of two-dimensional model sensitivity analysis during 1983 spring flood, with z_o = 750um (a) and 3,000um (b)

Sediment Transport Model

Section 3

Quantitative Environmental Analysis, LLC

313714

SECTION 3
SEDIMENT TRANSPORT MODEL

3.1 MODEL STRUCTURE AND EQUATIONS

A numerical model called HEC-6 has been widely used for evaluating sediment transport processes in rivers (U.S. Army Corps of Engineers 1976, 1990). This model has proven to be useful in a number of river studies, including previous Upper Hudson River modeling efforts (Zimmie 1985). However, this model does have its limitations. First, HEC-6 is a one-dimensional hydrodynamic model; therefore, lateral variations in the river flow cannot be resolved. This limitation is especially important when studying rivers such as the Upper Hudson River. Second, the original version (1976) of the model did not simulate erosion of fine-grained, cohesive sediments, only deposition of clays and silts was allowed in that version of the model. A new version (1990) of HEC-6 incorporates the work of Partheniades (1965) and Ariathuri and Krone (1976) on cohesive sediment erosion.

Development and application of two-dimensional and three-dimensional cohesive sediment transport models were reviewed by the Task Committee of American Society Civil Engineers on Fine Sediment Processes (1989). Various models were discussed with an emphasis on the STUDH model, a two-dimensional, vertically-averaged model using the sediment dynamics of Ariathuri and Krone (1976). Applications reviewed were primarily limited to cohesive sediment transport in estuaries and coastal waters, with no presentation of studies in rivers. Application of a vertically-averaged, finite element model for cohesive sediment transport, CSTM-H, to simulate sedimentation in a small yacht basin was presented by Hayter and Mehta (1986).

The sediment transport model used in the present study, and discussed here, is a modified version of the SEDZL sediment transport model that was originally developed by Ziegler and Lick (1986). SEDZL has been used in a number of sediment transport studies, including the Fox River in Wisconsin (Gailani *et al.* 1991), Pawtuxet River in Rhode Island (Ziegler and Nisbet

1994), Lake Erie (Lick *et al.* 1994), Saginaw River in Michigan (Cardenas *et al.* 1995), Buffalo River in New York (Gailani *et al.* 1996) and Watts Bar Reservoir in Tennessee (Ziegler and Nisbet 1995).

3.1.1 Suspended Sediment Dynamics

Suspended sediment particles in a river have a large range of sizes, from less than 1 μm clays to medium sands on the order of 400 μm. Simulation of the entire particle size spectrum is impractical. Therefore, particles were broadly segregated into two groups: silts and clays that may interact and form flocs and sands that are transported as discrete particles. The model uses this approach to approximate the particle size spectrum. "Class 1" particles include all the cohesive particles, i.e., clays and silts, with disaggregated particle diameters of less than 62 μm, while the "class 2" particles include coarser, non-cohesive sediments, primarily fine sands with diameters between 62 and 250 μm.

The Upper Hudson River water column is assumed to be well-mixed and suspended fine-grained sediment concentrations are assumed to be uniformly distributed within the water column. For these conditions, a two-dimensional, vertically-averaged sediment transport equation for size-class k (k = 1,2) was applied (Ziegler and Nisbet 1994):

$$\frac{\partial(hC_k)}{\partial t}+\frac{\partial(u_x hC_k)}{\partial x}+\frac{\partial(u_y hC_k)}{\partial y}=\frac{\partial}{\partial x}\left(hE_x\frac{\partial C_k}{\partial x}\right)+\frac{\partial}{\partial y}\left(hE_y\frac{\partial C_k}{\partial y}\right)+R_k-D_k \qquad (3\text{-}1)$$

where:

C_k = concentration of suspended sediment of size-class k (M/L^3)

E_x, E_y = horizontal eddy diffusivities along the x- and y-axes, respectively (L^2/T)

R_k = resuspension (erosion) flux of size-class k (M/L^2-T)

D_k = deposition flux of size-class k (M/L^2-T)

Results from the two-dimensional hydrodynamic model provide information about the transport field in Equation (3-1), i.e., u_x, u_y and h. Similar to the hydrodynamic equations, Equation (3-1) has been transformed into an orthogonal, curvilinear coordinate system and solved numerically.

Long-term sediment transport simulations, i.e., 20 to 30 years, were conducted with this model, making it necessary to account for bathymetric changes due to deposition and erosion. As discussed in Section 2.1.2, sediment bed elevations predicted by the model were used to dynamically adjust reference water depths (h_o) in the two-dimensional hydrodynamic model. This coupling produced a feedback mechanism between the sediment transport and hydrodynamic models.

As mentioned above, cohesive sediments in the water column range from clay particles smaller than 1 μm up to ~62 μm silts. The discrete particles aggregate and form flocs that can vary greatly in size and effective density. Variations in concentration and shear stress affect both floc diameter and settling speed (Burban *et al.* 1990). Modeling the settling characteristics and associated depositional fluxes of cohesive sediments in a natural water system is difficult.

One way to model cohesive sediment deposition is to use multiple size classes to simulate particle/floc heterogeneity in the water column. Difficulties with this approach include: (1) specification of composition of sediment loading from tributaries; (2) obtaining data for model calibration/validation; and (3) computational constraints.

Previous modeling studies (Ziegler and Nisbet 1994, 1995; Gailani *et al.* 1996) have shown that an effective approximation is to treat suspended cohesive sediments as a single class. This approach assumes that the settling and depositional characteristics of cohesive sediments can be represented by average values of a distribution of properties. Using this approximation, the deposition flux of cohesive (class 1) sediments to the sediment bed is expressed as (Ziegler and Nisbet 1994):

$$D_1 = P_1 W_{s,1} C_1 \qquad (3\text{-}2)$$

where:

$W_{s,1}$ = cohesive sediment settling speed (L/T)

P_1 = probability of deposition for cohesive sediments

Settling speeds of cohesive flocs have been measured over a large range of concentrations and shear stresses in freshwater (Burban *et al.* 1990). The Burban settling speed data for cohesive flocs in freshwater were analyzed to develop a formulation to approximate the effects of flocculation on settling speed. This analysis indicated that the settling speed is dependent on the product of the concentration (C_1) and the water column shear stress (G) at which the flocs are formed, resulting in the following relationship:

$$W_{s,1} = 3.3\left(C_1 G\right)^{0.12} \tag{3-3}$$

where the units of $W_{s,1}$, C_1, and G are m/day, mg/l and dynes/cm^2, respectively (Figure 3-1). For a depth-averaged model, as used in this study, the relevant shear stress for use in Equation (3-3) is the bottom shear stress (τ_b), i.e., $G = \tau_b = C_f q^2$.

Modeling suspended cohesive sediments as a single class, with an effective $W_{s,1}$ given by Equation (3-3), makes it necessary to use a probability of deposition (P_1) to parameterize the effects of particle/floc size heterogeneity and near-bed turbulence on the deposition rate. The complex interactions occurring in the vicinity of the sediment-water interface cause only a certain fraction of the settling cohesive sediments, represented by P_1, to become incorporated into the bed (Krone 1962, Partheniades 1992). An experimentally-based formulation that represents the effects of variable floc size on probability of deposition was developed by Partheniades (1992), see Figure 3-2:

$$P_1 = 1 - \left(2\pi\right)^{-1/2} \int_{-\infty}^{Y} e^{-\frac{w^2}{2}} dw \tag{3-4}$$

where:

$$Y = 2.04 \ln\left[0.25\left(\frac{\tau_b}{\tau_{b,\min}} - 1\right)e^{1.27\tau_{b,\min}}\right] \quad (3\text{-}5)$$

and

$\tau_{b,min}$ = bottom shear stress below which $P_1 = 1$ (dynes/cm^2)

Class 2 particles, i.e., non-cohesive fine sands, suspended in the water column are assumed to have an effective settling speed ($W_{s,2}$) that corresponds to an effective particle diameter (d_2). The depositional flux for this sediment class is then:

$$D_2 = P_2 W_{s,2} \Gamma C_2 \quad (3\text{-}6)$$

where:

P_2 = probability of deposition for non-cohesive sediments

Γ = class 2 stratification correction factor

Details concerning methods for calculating Γ, $W_{s,2}$ and P_2 are presented in Appendix A. Significant vertical stratification of class 2 sediment can occur in the water column due to the high settling speeds of fine sands. This characteristic means that accurate calculation of class 2 deposition flux requires use of the near-bed concentration ($C_{a,2}$), where $C_{a,2} = \Gamma C_2$ and $\Gamma > 1$. Note that Γ is dependent upon $W_{s,2}$, τ_b, bottom roughness and local depth (see Appendix A). The relationship between $W_{s,2}$ and d_2, which was developed by Cheng (1997), is presented in Figure 3-3.

3.1.2 Cohesive Sediment Bed Dynamics

Only a finite amount of material can be resuspended from a fine-grained, cohesive sediment bed exposed to a constant bottom shear stress. This phenomenon, referred to as bed armoring, has been observed and quantified in a number of laboratory (Parchure and Mehta 1985, Tsai and Lick 1987, Graham *et al.* 1992) and field studies (Hawley 1991, Amos *et al.*

1992). The amount of fine-grained sediment resuspended from a cohesive deposit is given by (Gailani *et al.* 1991):

$$\epsilon = \frac{a_o}{T_d^N}\left(\frac{\tau_b - \tau_{cr}}{\tau_{cr}}\right)^n \quad , \quad \tau_b \geq \tau_{cr} \tag{3-7}$$

where:

ϵ	=	net mass of resuspended sediment per unit surface area (M/L^2)
a_o	=	site-specific constant
T_d	=	time after deposition in days
N, n	=	exponents dependent upon the deposition environment
τ_{cr}	=	effective critical shear stress (dynes/cm^2)

Note that ϵ is referred to as the resuspension potential.

Experimental results show that cohesive sediment is eroded over a time period on the order of one hour (Tsai and Lick 1987, MacIntyre *et al.* 1990). Thus, the total resuspension rate ($R_{tot,coh}$) is given by:

$$R_{tot,coh} = \frac{\epsilon}{3600} \tag{3-8}$$

where $R_{tot,coh}$ is assumed to be constant until all available sediment is eroded. Once the amount ϵ has been resuspended, $R_{tot,coh}$ is set to zero until additional sediment is deposited and available for resuspension or until the shear stress increases (Gailani *et al.* 1991). The resuspension rate of class k (R_k) sediment from the cohesive bed is then given by:

$$R_k = f_k R_{tot,coh} \tag{3-9}$$

where:

f_k	=	fraction of class k sediment in the surficial layer of the cohesive bed

The present study models two classes of suspendable sediment, with f_1 corresponding to the fraction of cohesive particles (clay and silt) in the bed and f_2 representing the fraction of suspendable non-cohesive particles (fine and medium sand with particle diameters between 62 and 425 μm). The total fraction of suspendable sediment in the bed ($f_{sus} = f_1 + f_2$) is equal to one in the cohesive bed. In non-cohesive bed areas, f_{sus} can be less than or equal to one, depending on local conditions (see Section 3.2.1 for further discussion).

The effects of bed consolidation with depth and horizontal variations in bed composition are simulated using a three-dimensional model of the cohesive sediment bed. The layered bed model conserves mass, with mass flux occurring only at the sediment-water interface due to deposition and resuspension. Vertical variations of sediment bed consolidation, or equivalently porosity, are accounted for by discretizing the bed into seven layers. The time after deposition of the layers increases linearly from one day at the surface, which is composed of freshly deposited sediment, to seven days in the bottom layer. Previous laboratory studies (Tsai and Lick 1987, MacIntyre *et al.* 1990) indicate that consolidation effects on resuspension are minimal after about seven days of consolidation. Therefore, the maximum age of deposited sediments was set at seven days. Consolidation effects on resuspension are accounted for in Equation (3-7) by the $(T_d)^{-N}$ term, which causes the resuspension potential (ϵ) to decrease as the bed consolidates with time. The critical shear stress, τ_{cr}, was assumed to be constant in all layers of the bed. The model accounts for changes in bed composition, i.e., f_1 and f_2, due to resuspension and deposition during the course of a simulation.

3.1.3 Non-Cohesive Sediment Bed Dynamics

The non-cohesive suspended load transport model developed by Ziegler and Nisbet (1994), and applied to the Pawtuxet River (Rhode Island), was modified and enhanced for application to the Upper Hudson River. A complete description of the model is presented in Appendix A but a general overview will be presented here. The resuspension of sediment from the non-cohesive portion of the sediment bed in the Upper Hudson River was calculated using a procedure developed by van Rijn (1984). The van Rijn method has been shown to yield good

results for predicting suspended load transport of sands (van Rijn 1984; Garcia and Parker 1991; van Rijn *et al.* 1993).

Non-cohesive sediment beds that contain a wide range of particle sizes, from clay, silt, fine sand and medium sand (which are suspendable) to coarse sand and gravel (which are only transportable as bed load), will experience the phenomenon known as bed armoring during a resuspension event. Bed armoring occurs when fine-grained sediment is eroded from a heterogeneous sediment bed and the coarser material that cannot be resuspended remains on the bed surface. As the erosion process continues, the suspendable sediment in the near-surface layer, referred to as the active layer, is depleted and a layer of coarse, non-suspendable sediment forms. Continuous depletion of suspendable sediment in the active layer will eventually reduce the erosion rate to zero. At this point, the active layer is composed entirely of non-suspendable sediment, and the sediment bed has become armored (Shen and Lu 1983; Karim and Holly 1986; Jain and Park 1989; Rahuel *et al.* 1989; van Niekerk *et al.* 1992).

Non-cohesive areas of the sediment bed in the Upper Hudson River typically contain a significant fraction of non-suspendable material. For example, on average, coarse sand and gravel comprise approximately 50% of the non-cohesive bed in the TIP. Thus, the effects of bed armoring must be included in a non-cohesive sediment transport model applied to this river. Erosion rates will be significantly over-estimated if bed armoring effects are not considered during a sediment transport simulation of a flood event.

The thickness of the active layer is of critical importance in applying this model. An expression for the active layer thickness, which is a linear function of the local bottom shear stress, was proposed by van Niekerk *et al.* (1992). A modified form of their formulation was used in this study:

$$T_a = \begin{cases} 2d_{50} & , \quad \tau_b < \tau_{c50} \\ 2d_{50}\left[B\left(\dfrac{\tau_b}{\tau_{c50}}\right) + (1-B)\right] & , \quad \tau_b \geq \tau_{c50} \end{cases} \tag{3-10}$$

where:

T_a	=	active layer thickness (L)
d_{50}	=	median particle size of bed sediment (L)
τ_{c50}	=	critical shear stress for initiation of bed load based upon the parent bed d_{50}
B	=	adjustable constant

Note that Equation (3-10) reduces to the original van Niekerk *et al.* (1992) equation when B is equal to 1. Varying hydrodynamic conditions affect the active layer thickness, with T_a increasing as the current velocity (and τ_b) increases, which causes the amount of sediment that is available for resuspension to increase. The dependence of T_a on τ_b is not well known and the constant (B) in Equation (3-10) was adjusted during model calibration to account for local conditions in the Upper Hudson River.

Other expressions have been proposed for the active layer thickness, e.g., Borah *et al.* (1982), Karim and Holly (1986) and Jain and Park (1989). For the bed parameters used in this study, the Borah *et al.* (1982) formulation reduces to:

$$T_a = \frac{d_{non}}{(1-\lambda)(1-\sum f_{a,k})} \qquad (3\text{-}11)$$

where: d_{non}	=	effective particle size of non-suspendable bed material
$(1 - \sum f_{a,k})$	=	fraction of the active layer composed of non-suspendable sediment
$f_{a,k}$	=	fraction of class k sediment that is suspendable in the active layer
λ	=	bed porosity

This active layer thickness equation only depends upon bed properties and it is insensitive to variable hydrodynamic conditions. The Jain and Park (1989) expression is very similar to the Borah *et al.* (1982) equation, with T_a depending upon non-suspendable particle size and fraction of the material in the bed.

The Karim and Holly (1986) relationship depends upon bed properties and bottom shear stress:

$$T_a = \frac{1}{2} H(1 - C_1 \xi) \tag{3-12}$$

where:

H	=	dune height
ξ	=	fraction of area covered with non-moving particles (the bed is armored when $\xi = 1$)
C_1	=	adjustable constant ($0 \rightarrow 1$)

Dune height is given by:

$$H = h(0.08 + 0.75\theta - 2.01\theta^2 + 2.63\theta^3 - 1.09\theta^4) \tag{3-13}$$

and the non-dimensional bottom shear stress (θ) is (with τ_b and d_{50} in cgs units):

$$\theta = (6x10^{-4}) \frac{\tau_b}{d_{50}} \tag{3-14}$$

For $\theta > 1.5$, a plane bed is achieved and H = 0. Thus, this relationship depends on both bed properties and bottom shear stress, as does the formulation used in the Upper Hudson River model.

None of these active layer thickness formulations were developed from laboratory or field data. The relationship between bed properties and/or bottom shear stress in each equation was hypothesized and supported by qualitative, mechanistic arguments, with no data used to support the proposed T_a equations. Hence, active layer thickness formulations used in non-cohesive bed armoring algorithms must be considered to be mathematical constructs that approximate a complicated, and poorly understood, physical process. At present, the available

formulations are based on rational physical arguments. However, the equations are not universally applicable because of their general, qualitative nature. Thus, development of a model for a particular riverine system, such as the Upper Hudson River, will probably require modifications of the active layer thickness formulation to account for system-specific conditions. Better understanding of the bed armoring process, and specification of T_a, will require additional laboratory and field data, and corresponding theoretical development, which are active topics in non-cohesive sediment transport research.

The bed armoring formulations discussed in Appendix A include a hiding factor, H_k, for size-class k sediment that has been used in other studies (Karim and Kennedy 1981, Rahuel *et al.* 1989). For an armoring bed, H_k is less than one, which effectively reduces the resuspension rate (R_k) from the non-cohesive sediment bed. In this study, we found that during initial model calibration efforts the use of a hiding factor was unnecessary. Thus, H_k was set equal to one in all simulations.

Bed load transport of non-cohesive sediments was neglected in this study for several reasons. First, bed load transport involves the near-bed transport of coarse sand and gravel, which means that these coarse sediments do not directly affect water column transport of particle-sorbed PCBs. Therefore, including a bed load model would provide minimal improvement in the predictive capabilities of the PCB fate model. Second, bed load transport within a particular reach is limited to that reach because the dams prevent bed load transport of sediments between reaches. Third, bed load transport is difficult to measure and Upper Hudson River bed load data were either sparse or non-existent in the various reaches of the river. This situation made development and calibration of a credible bed load model difficult to impossible.

3.1.4 Summary

The formulations used in this study to represent resuspension, deposition and transport of fine-grained sediment in the Upper Hudson River yielded a modeling framework that is mechanistic and has a strong experimental foundation. Many of the deposition and resuspension parameters were determined from laboratory or Upper Hudson River data, with a small number

of free parameters available for adjustment during model calibration. Using a minimum number of calibration parameters (only two in the present study) tightly constrains the model and provides, after successful calibration and validation, increased confidence in the model's capabilities and accuracy.

As in the development of any sediment transport model, assumptions and approximations were necessary to make the problem solvable. Use of two sediment classes to approximate the wide distribution of particle sizes in the water column and sediment bed is an obvious (and necessary) simplification; earlier modeling studies have shown this approximation to be effective. Effects of flocculation on cohesive (class 1) sediment settling speed have been approximated using a data-based formulation that was assumed to be applicable to suspended cohesive particles/flocs in the Upper Hudson River. The high settling speed of non-cohesive (class 2) can invalidate the assumption of a well-mixed water column, which was used in the application of Equation (3-1), due to vertical stratification of fine sands. A stratification correction factor (Γ) was introduced to solve this problem.

Simulating the non-cohesive bed armoring process is one of the most critical approximations in this analysis. This complex process was approximated using the concept of an active layer, the thickness of which (T_a) is poorly understood. Various expressions have been proposed for calculating T_a, but only qualitative arguments were used to support the development of those formulations; no experimental data are available to directly support available T_a equations. Uncertainty is thus introduced into simulations due to this approximation. However, successful calibration and validation will provide evidence that the non-cohesive bed armoring, which is represented mechanistically, has been properly parameterized for the Upper Hudson River.

Cohesive and non-cohesive sediment resuspension were assumed to be caused only by bottom shear stresses due to current velocities. Other possible physical mechanisms that generate turbulence at the sediment-water interface include wind waves, boat waves, prop wash and ice scour. All of these processes have minimal effect on sediment resuspension for the temporal and spatial scales of importance when considering PCB fate in the Upper Hudson

River. Therefore, explicit inclusion of these processes in the sediment transport model was not necessary for this study.

3.2 APPLICATION TO THE UPPER HUDSON RIVER

3.2.1 Representation of the River

The sediment transport model used the same numerical grid in each reach of the Upper Hudson River as the two-dimensional hydrodynamic model. Thus, similar to the hydrodynamic model, a separate sediment transport model was developed and calibrated for each reach. This process required that the sediment transport models be run sequentially from Reach 8 to Reach 1, with the temporally variable sediment load predicted at the dam of a reach being used as the upstream boundary condition for the adjacent downstream reach.

Side-scan sonar surveys were conducted by USEPA in Reaches 6, 7 and 8 (Flood 1993). Data from the side-scan sonar surveys were used to determine the distribution of various sediment bed types, e.g., fine, coarse and rock, in these reaches of the Upper Hudson River (Figure 3-4). The sediment transport model required specification of a bed map that distinguishes between three types of sediment: (1) cohesive; (2) non-cohesive; and (3) rock or hard bottom. Bed maps for Reaches 8, 7 and 6, based on side-scan sonar data, are presented in Figures 3-5, 3-6 and 3-7, respectively. A bed map of fine and coarse areas in the TIP was developed by Brown *et al.* (1988) from various bed property data sets (both qualitative and quantitative information). Comparison of the Brown *et al.* (1988) bed map with the TIP bed map (Figure 3-4) showed remarkable consistency, which provided added confidence in the accuracy of the side scan sonar bed map for that reach. Sediment bed maps for Reaches 1 to 5 were developed using bed type information collected by GE in 1997 (QEA 1998a). A summary of bed areas is provided in Table 3-1.

Table 3-1. Cohesive Bed Areas in Reaches 1 to 8			
Reach	Total Bed Area (mi^2)	Cohesive Bed Area (mi^2)	Relative Cohesive Area (%)
8	0.69	0.15	22
7	0.31	0.016	5
6	0.41	0.11	27
5	1.90	0.36	19
4	0.45	0.15	34
3	0.43	0.022	5
2	0.69	0.027	4
1	0.93	0.005	<1

Side-scan sonar data collected in Reaches 6, 7 and 8 provided excellent spatial coverage of surficial bed types in those reaches. However, uncertainty does exist in the bed maps generated from that data because those bed maps were developed from interpretations of the raw side-scan sonar images (Flood 1993). The interpretations were somewhat subjective, even though ground truthing was done to minimize the subjectivity. More uncertainty exists in the bed maps developed for Reaches 1 to 5 because the spatial coverage along this approximately 30-mile long stretch of river was somewhat limited. Bed map sampling was done along 77 transects in these five reaches, which resulted in estimates of bed type being made in grid cells not located along a transect. The uncertainty in model results due to bed mapping uncertainty, for all eight reaches, cannot be easily quantified but it should be acknowledged to exist.

A review of bulk bed property data for cohesive sediments in the TIP indicated no definite spatial trends. Therefore, average values, based on available data, were used to specify the dry density (0.87 g/cm^3) and initial composition (f_1 = 0.32) in the cohesive bed areas. Cohesive sediments in Reaches 1 to 7 were assumed to have the same dry density and initial composition as TIP cohesive sediments. An average dry density of 1.38 g/cm^3 was applied to non-cohesive sediments in all reaches based on bulk property data (Limno-Tech 1997).

A field study was conducted during November 1990 to measure *in situ* resuspension potential of cohesive sediments in the Upper Hudson River (HydroQual 1995a). Analysis of TIP data indicated that an appropriate value for the exponent n in Equation (3-7) is 2.94. The TIP

data also exhibited a spatial variation in the site-specific constant, a_o, with lower a_o upstream of MP 191 (approximately). Thus, $a_o = 0.035$ for cohesive sediments upstream of MP 190.7 and $a_o = 0.107$ for cohesive sediments downstream of that location (Figure 3-8). Cohesive sediments immediately downstream of the jetty at the entrance to the Champlain Canal, at about MP 189, were more easily resuspendable and $a_o = 0.239$ in that small area. Data in Reaches 1 to 7 were insufficient to confidently perform a log-linear regression analysis to determine the exponent n, as was done in the TIP, for each of those reaches. Thus, it was assumed that the exponent n was approximately equal to the value determined from TIP data (2.94) and it was set equal to 3.0 in Reaches 1 to 7. Reach-specific values of a_o were determined from the data collected in Reaches 1 to 7, with these values ranging from 0.067 to 0.340 (HydroQual 1995a)[1]. Values of $\tau_{cr} = 1$ dyne/cm^2, N = 0.5 and $T_{d,max} = 7$ days were used in the calculations of a_o (HydroQual 1995a) and all model simulations.

The non-cohesive suspended load transport model required specification of median particle diameter (d_{50}) and suspendable sediment fractions (i.e., f_1 and f_2) in the non-cohesive bed. As discussed in Section 3.1.2, the non-cohesive bed is composed of suspendable particles (clay, silt, fine and medium sands, with particle diameters < 425 μm) and non-suspendable particles (coarse sand and gravel, with particle diameters > 425 μm, that are only transported as bed load). The total fraction of suspendable sediment in the non-cohesive bed ($f_{sus} = f_1 + f_2$) can be less than or equal to one, depending on local conditions.

The non-cohesive transport model is sensitive to local values of d_{50}, f_1 and f_2. Data for these quantities are highly variable. Hence, it was necessary to develop spatial distributions for d_{50}, f_1 and f_2 to realistically simulate non-cohesive suspended load transport in the Upper Hudson River.

A relationship between median particle diameter (d_{50}) and fraction of suspendable sediment (f_{sus}) in the non-cohesive bed was determined from grain size distribution data collected from the TIP (Figure 3-9):

[1] All a_o values are for ϵ in mg/cm^2.

$$d_{50} = 135\, f_{sus}^{-1.67} \qquad (3\text{-}15)$$

where d_{50} has units of μm.

Spatial distributions for d_{50}, f_1 and f_2 were estimated by assuming that a relationship exists between local bottom shear stress and d_{50}, i.e., $d_{50} = f(\tau_b)$. The hydrodynamic model was used to predict the bottom shear stress distribution for the non-cohesive bed at a given flow rate (30,000 cfs). The functional relationship between d_{50} and τ_b was adjusted until the predicted and measured distributions of d_{50} were in general agreement (Figure 3-10). The resulting function is (for d_{50} in μm):

$$\begin{aligned} d_{50} &= 140\, e^{16.6\tau_n^2} \quad , \quad \tau_n < 0.45 \\ &= 9000\, \tau_n^{1.02} \quad , \quad \tau_n \geq 0.45 \end{aligned} \qquad (3\text{-}16)$$

where:

τ_n = normalized bottom shear stress (τ_b/τ_{max})

τ_{max} = maximum bottom shear stress in non-cohesive bed area at given flow rate (47 dynes/cm^2 at 30,000 cfs)

The predicted spatial distribution of d_{50} is presented in Figure 3-11.

This process was validated as follows. Similar to Equation (3-15), a log-linear correlation between f_2 and d_{50} was observed in the data (R^2= 0.80):

$$f_2 = 22\, d_{50}^{-0.66} \qquad (3\text{-}17)$$

Predicted d_{50} values, from Equation (3-16), were used in Equation (3-17) to generate a predicted distribution of f_2 in the TIP. The resulting comparison with observed f_2 values is presented in Figure 3-10. The average predicted and measured f_2 values in the TIP non-cohesive bed area were 0.29 and 0.34, respectively. The good agreement between predicted and measured f_2 indicates that this procedure yields reasonable spatial distributions of d_{50} and f_2. Non-cohesive

bed data did not indicate a strong relationship between d_{50} and f_1. Thus, an average f_1 value of 0.065 was used throughout the TIP non-cohesive bed.

Initial distributions of d_{50}, f_1 and f_2 in Reaches 1 to 7 were developed using the same procedure applied to the TIP. Due to relatively sparse bed data downstream of the TIP, bed property data and shear stress distributions in these seven reaches were combined to determine a functional relationship between d_{50} and bottom shear stress. Bottom shear stress distributions were predicted in each reach at a given flow rate, with the flow rate in the river being proportionally increased due to tributary inflows (based on a flow rate at Fort Edward of 30,000 cfs). Similar to the relationship developed in the TIP, for Reaches 1 to 7 (Figure 3-12):

$$\begin{aligned} d_{50} &= 190\, e^{15.5\tau_n^2} \quad , \quad \tau_n < 0.45 \\ &= 6000\, \tau_n^2 \quad , \quad \tau_n \geq 0.45 \end{aligned} \tag{3-18}$$

where d_{50} has units of μm and τ_{max} = 114 dynes/cm^2 (in Reach 7). Bed data were insufficient in Reaches 1 to 7 to develop credible relationships between d_{50}, f_1, f_2 and f_{sus} as was done in the TIP. Thus, it was assumed that the TIP relationships between these quantities were applicable to Reaches 1 to 7; for these seven reaches, Equations (3-15) and (3-17) were used and f_1 had an initial value of 0.065.

The spatial distributions of d_{50}, f_1 and f_2 that were estimated using the above procedure are initial conditions for the model. The non-cohesive sediment bed model tracks temporal changes in f_1 and f_2 in each grid cell due to resuspension and deposition. The data-based relationship between d_{50} and f_{sus}, Equation (3-15), was used to dynamically adjust d_{50} during a simulation.

3.2.2 Sediment Transport Model Boundary Conditions

Sediment loading at the upstream boundary of the model (Fort Edward) and from the TIP tributaries was estimated using TSS concentration data collected at those locations. Sediment rating curves, which relate TSS concentration to flow rate, were developed using available data

for the Hudson River at Fort Edward, Snook Kill and Moses Kill. To correct for bias introduced when performing log-linear regression analyses on the data, the minimum variance unbiased estimator (MVUE) method of Cohn *et al.* (1992) was used. The resulting rating curves for Fort Edward, Snook Kill and Moses Kill are shown in Figures 3-13, 3-14 and 3-15, respectively. Sediment loading from TIP direct drainage was estimated using a rating curve that was the average of the rating curves for Snook and Moses Kills. The Fort Edward rating curve is:

$$C_{FE} = 4.5\left(\frac{Q_{FE}}{10{,}000}\right)^{0.29} \quad , \quad Q_{FE} \le 10{,}000$$
$$= 5.4\left(\frac{Q_{FE}}{10{,}000}\right)^{2.02} \quad , \quad Q_{FE} > 10{,}000 \qquad (3\text{-}19)$$

where:

C_{FE} = sediment concentration at Fort Edward (mg/l)

Q_{FE} = Fort Edward flow rate (cfs)

The rating curves for Snook Kill, Moses Kill and TIP direct drainage have the form:

$$C_{trib} = A_{trib} \quad , \quad Q_{trib} \le \overline{Q}_{trib}$$
$$= A_{trib}\left(\frac{Q_{trib}}{\overline{Q}_{trib}}\right)^{N_{trib}} \quad , \quad Q_{trib} > \overline{Q}_{trib} \qquad (3\text{-}20)$$

where:

C_{trib} = tributary sediment concentration (mg/l)

Q_{trib} = tributary flow rate (L^3/T)

$\overline{Q}_{trib}$ = mean flow rate of the tributary (L^3/T)

The coefficient A_{trib} has values of 6.5, 8.0 and 1.9 for Snook Kill, Moses Kill and TIP direct drainage, respectively. The exponent N_{trib} has values of 1.7, 1.5 and 1.6 for Snook Kill, Moses Kill and TIP direct drainage, respectively. The tributary rating curves produced a sediment yield of 53 MT/yr-mi^2 for the TIP drainage basin. Note that the effective direct drainage area for

sediment runoff is only 8 mi^2. The remaining 23 mi^2 of direct drainage do not contribute sediment to the TIP because this area drains into the Champlain Canal.

Specification of the upstream boundary condition for sediment loading at Fort Edward for model calibration and validation simulations used a combination of TSS concentration data and rating curve estimates. Fort Edward solids loads were specified using TSS concentration data when data were available. Equation (3-19) was used to estimate TSS concentration at that location when data were not available.

The potential impact of hysteresis on solids loading at Fort Edward was also investigated. Solids loading hysteresis occurs when TSS concentrations are much higher on the rising limb of a flood hydrograph than TSS concentrations on the falling limb of the hydrograph. This phenomenon occurs in many rivers and has been observed frequently at Fort Edward. Attempts were made to incorporate hysteresis effects into the Fort Edward rating curve. Unfortunately, significant variability in TSS concentrations occurred between individual high flow events. This situation made it difficult to develop a credible method for including hysteresis effects in the Fort Edward rating curve. Thus, hysteresis effects were not included in Fort Edward solids loading estimates.

Tributary TSS concentration data for Reaches 1 to 7 were insufficient to generate rating curves that could adequately specify sediment loading to the Upper Hudson River. Therefore, a procedure was developed to estimate sediment loading from tributaries downstream of the TIP that used data-based mass balances on the Upper Hudson River.

Available TSS concentration data and rating curves were used to determine average annual sediment loads at Fort Edward, Stillwater and Waterford for a 5,592-day period that extended from March 1977 through June 1992. This period was chosen because USGS flow gauges were operable at all three locations. The average annual sediment load increases by at least a factor of five between Fort Edward and Waterford (Figure 3-16), while the mean flow rate only increases by about 60% between those locations. The large increase in sediment load, combined with a proportionately lower discharge increase, between Fort Edward and Waterford

indicates that: (1) tributary sediment loading to the Upper Hudson River is significant and (2) tributary sediment yield increases as one travels downstream from Fort Edward to Waterford.

Minimum tributary loads were determined, using estimated annual average loads at the three main stem locations, by assuming conservative transport, i.e., no net deposition, in the river. The minimum average annual load from tributaries between Fort Edward and Stillwater was thus estimated to be 48,200 metric tons/year (MT/yr). The total TIP tributary load was 7,300 MT/yr, which was estimated using the rating curves discussed above. Hence, the minimum load from tributaries between TID and Stillwater was 40,900 MT/yr. Similarly, the minimum tributary load between Stillwater and Waterford was estimated to be 94,600 MT/yr, which is more than twice that between TI dam and Stillwater.

These minimum load estimates assumed conservative transport. However, on an annual average basis, the Upper Hudson River is a net depositional system due to the dams on the river. Therefore, increasing the minimum tributary sediment loading estimates to account for net deposition required estimates of sediment trapping efficiency in the river. Initial results of the long-term TIP simulation (see Section 3.3.3) indicated a trapping efficiency of 8.5% for the TIP. As a first approximation, it was thus assumed that Reaches 1 to 7 also had average trapping efficiencies of 8.5%. This approximation resulted in tributary sediment loading of 50,100 and 110,800 MT/yr for TID to Stillwater and Stillwater to Waterford, respectively (Figure 3-16).

Sediment yields corresponding to these load estimates are 84 and 132 MT/yr-mi^2 for TID to Stillwater and Stillwater to Waterford, respectively. The tributary sediment yield between TID and Stillwater is about 60% greater than the TIP tributaries. Similarly, the Stillwater to Waterford yield is about 2.5 times higher than sediment yield for tributaries flowing into the TIP. This significant increase in sediment yield between Fort Edward and Waterford is needed to support the observed increase in loading between those two locations.

A check of the tributary sediment loading procedure was accomplished using Upper Hudson River sediment yield estimates made by Phillips and Hanchar (1996). A correlation was found between sediment yield and percent of a watershed basin covered by forest (Figure 33,

Phillips and Hanchar, 1996). Typically, roughly 50% of a tributary drainage basin in the Upper Hudson River is forested (Soil Conservation Service 1974). Using the Phillips and Hanchar (1996) correlation with a 50% forest cover produced a sediment yield of about 100 MT/yr-mi^2, which is consistent with the sediment yield estimates in the present analysis.

The mass balance procedure described above produced credible estimates of annual average tributary sediment loads (Table 3-2). Model inputs required specification of tributary sediment loads on much shorter time scales, e.g., hourly or daily. To estimate sediment loads, or equivalently TSS concentrations, for these shorter time scales, and still input the specified annual average load, tributary rating curves were developed using the following procedure.

Table 3-2. Tributary Sediment Loading Estimation

Tributary	Reach	Mean Annual Load (MT/yr)	N_{trib}
Direct Drainage, R7	7	1,260	1.99
Direct Drainage, R6	6	1,340	2.02
Batten Kill	5	36,100	2.00
Fish Creek	5	4,100	0.91
Flately Brook	5	670	1.66
Direct Drainage, R5	5	6,600	1.63
Hoosic River	4	95,300	1.67
Direct Drainage, R4	4	1,720	1.59
Anthony Kill	3	8,300	1.61
Direct Drainage, R3	3	1,720	1.59
Deep Kill	2	2,120	1.60
Direct Drainage, R2	2	1,720	1.59

Rating curves for tributaries between TID and Waterford were assumed to have the same form as Equation (3-20) that was used for the TIP tributaries. For Reaches 5, 6 and 7, the low flow solids concentration (A_{trib}) was determined using Batten Kill TSS concentration data. Mean TSS concentration in Batten Kill during low flow conditions ($Q_{BK} < \overline{Q}_{BK}$) is 6.1 mg/l (Limno-Tech 1998), therefore, A_{trib} = 6.1 mg/l for Reaches 5, 6 and 7. The exponent (N_{trib}) in the rating curve was determined iteratively for each tributary. For a particular tributary, an initial value of N_{trib} = 2 was chosen and the tributary hydrograph for the 5,592-day period from 1977 to 1992 was used with the rating curve to calculate daily sediment loads for that period. The annual

average sediment load resulting from the first iteration was compared to the desired load (Table 3-2). The exponent (N_{trib}) was adjusted appropriately to start the next iteration and the process was repeated until the difference between calculated and desired load was less than 1%. The values of N_{trib} produced by this procedure ranged from 0.91 to 2.02 in these three reaches (Table 3-2).

Note that the effective drainage area for sediment loading from Fish Creek is only 49 mi^2, which is 20% of the total drainage area for this tributary. The reason for this reduction is that approximately 80% of the Fish Creek drainage area is upstream of Saratoga Lake. It was assumed that all sediment transported into the lake by Fish Creek was deposited; the sediment load out of Saratoga Lake was assumed to be zero.

A similar procedure was used to develop rating curve parameters for Reaches 1 to 4. Mean TSS concentration in the Hoosic River during low flow conditions is 8.1 mg/l (Limno-Tech, 1998). Thus, A_{trib} = 8.1 for tributaries between Stillwater and Waterford. The iteration process was applied to adjust N_{trib} for each tributary in these four reaches until the appropriate annual average sediment loads were achieved for those tributaries. This procedure resulted in N_{trib} ranging between 1.59 and 1.67 (Table 3-2).

As a check on the validity of the rating curve estimation procedure, the Hoosic River rating curve determined from the above analysis was compared to TSS concentration and flow data for that tributary (Figure 3-17). The estimated rating curve agrees very well with the data. This validation of the sediment loading method gives added confidence to the accuracy of the estimation procedure.

Specification of total sediment load at Fort Edward and the tributaries was accomplished using the methods described above. However, model inputs also required specifying the composition of all sediment loads because the transport of two classes of sediment, i.e., fine and coarse, was simulated. Hence, the fractions of class 1 (clay/silt) and class 2 (fine sand) in the input loads had to be determined.

The USGS collected particle size distribution data for suspended sediments at Schuylerville (32 observations), Stillwater (20 observations) and Waterford (80 observations). While these data sets are limited (the number of particle size observations represent a small fraction of the TSS concentration observations at each location), the data were useful for estimating load composition in the Upper Hudson River and its tributaries.

Analysis of the particle size data showed no correlation existed between sand content and flow (or TSS concentration) at the three main stem locations. This finding is consistent with observations from other riverine systems that indicate that, as flow rate increases, sand content can: (1) increase, (2) decrease or (3) remain approximately constant (Walling and Moorehead 1989). The relationship between sediment load composition and flow rate for a particular river is determined by drainage basin characteristics (Walling and Moorehead 1989).

The available sand content data at Schuylerville, Stillwater and Waterford yielded mean (and 95% confidence interval) values of 0.26 ± 0.04, 0.19 ± 0.04 and 0.16 ± 0.03, respectively. This trend of downstream fining, where sand content decreases in the downstream direction, is consistent with observed trends in other rivers (Paola, *et al.* 1992, Paola and Seal 1995).

Based on these data, the assumption was made that the sand content of sediment loads at Fort Edward and all tributaries, except Moses Kill and direct drainage, was 0.25 for all flow rates. The sand content of sediment loads from Moses Kill and direct drainage was assumed to be zero. Initial model testing showed that unrealistic amounts of sediment were predicted to be deposited at the mouth of Moses Kill whenever sand was included in the sediment loading for that tributary. An examination of the geometry/bathymetry of Moses Kill near its confluence with the Hudson River suggests that this portion of the tributary is a depositional zone that would likely trap most suspended sands and significantly reduce the sand load from the tributary to the river. Sediment loading from all direct drainage was assumed to originate from direct runoff and very small streams. The hydraulic characteristics of these sediment sources prevent the transport of significant quantities of sand from the direct drainage area to the Hudson River.

3.2.3 Coupling of Sediment Transport and PCB Fate Models

Accurate and realistic simulations of the Upper Hudson River were realized through coupling the sediment transport and PCB fate models. Coupling the models means that sediment transport model results were aggregated to determine total suspended sediment concentration (m), deposition flux (D_{tot}) and resuspension flux (R_{tot}), i.e., $m = C_1 + C_2$, $D_{tot} = D_1 + D_2$ and $R_{tot} = R_1 + R_2$, in each grid cell of the PCB fate model. Thus, solids transport was not simulated within the PCB fate model. All sediment transport information needed by the PCB fate model, i.e., m, D_{tot} and R_{tot}, was specified, and input to the PCB fate model, using output from the sediment transport model.

Coupling of the two models was accomplished as follows. The sediment transport model was used to simulate the period of interest, e.g., 1977 to 1998. Output from the sediment transport model was temporally averaged on a daily basis to produce daily-average values of m, D_{tot} and R_{tot} for each grid cell in the two-dimensional, sediment transport model. Spatial aggregation of the two-dimensional model output was then necessary to produce sediment transport information for the one-dimensional PCB fate model (see Section 4.3.1 for a description of the one-dimensional numerical grid used by the PCB fate model). Note that the PCB fate model segregated the sediment bed into cohesive and non-cohesive areas. Hence, during spatial aggregation from the two-dimensional grid to the one-dimensional grid, D_{tot} and R_{tot} were separated into cohesive ($D_{tot,coh}$ and $R_{tot,coh}$) and non-cohesive ($D_{tot,non}$ and $R_{tot,non}$) components for each grid cell of the PCB fate model.

Spatial aggregation of the sediment transport model output produced unique values of m, D_{tot} and R_{tot} in a particular grid cell for each day of a simulation. An examination of the relationships between D_{tot} and R_{tot} and flow rate provided insight into Upper Hudson River sediment transport processes. For convenience, D_{tot} was converted to an effective settling speed (W_s):

$$W_s = \frac{D_{tot}}{m} \qquad (3\text{-}21)$$

An approximately 22-year simulation, from 1977 to 1998, was conducted in the TIP (see Section 3.3.3). Results (W_s and R_{tot}) from this simulation were analyzed to better understand sediment transport processes in the TIP. Relationships between W_s and flow rate in the cohesive and non-cohesive bed areas of a particular one-dimensional grid cell, located in the vicinity of Snook Kill, are shown in Figures 3-18 and 3-19, respectively. The settling speed functions in both bed types exhibit an underlying functional form that has a stochastic component. Flow-dependent depositional processes, due to variations in probability of deposition and water column composition, produced the S-shaped curves. In cohesive bed areas, low W_s values (< 1 m/day) occurred for flow rates less than about 5,000 to 7,000 cfs. Effective settling speed increased significantly (> 10 m/day) between 5,000 and 10,000 cfs due to an increase in class 2 sediment in the water column during high flow conditions. For high flow rates, decreasing W_s with increasing flow rate was caused by probability of deposition effects, i.e., P_1 and P_2 decrease as shear stress (flow) increases. Qualitatively, similar depositional processes occurred in the non-cohesive bed area. However, two distinct differences exist between deposition in the cohesive and non-cohesive areas: (1) higher settling speeds at low flow rates in non-cohesive areas and (2) deposition was minimal in non-cohesive areas during high flows. Temporal variations in the magnitude and composition of sediment loads from tributary and upstream sources generated stochastic fluctuations in the settling speed functions.

Resuspension rate, expressed as total mass of sediment resuspended per day, as a function of flow rate for cohesive and non-cohesive bed areas is presented in Figures 3-20 and 3-21, respectively. Model results shown in those figures are from the grid cell near Snook Kill. Cohesive bed resuspension has a definite underlying structure that includes a stochastic component. In this grid cell, resuspension was negligible from the cohesive bed for flows less than about 5,000 cfs. Due to spatial variations in bottom shear stress, the critical flow rate for resuspension, i.e., flow below which resuspension was negligible, varies from about 4,000 to 9,000 cfs in the different grid cells. Generally, the slope of the resuspension function decreased for flow rates greater than about 10,000 cfs. Maximization of the resuspension area in a particular grid cell caused the change in slope. Temporal and spatial variations in cohesive bed properties generated the random fluctuations in the resuspension function.

No correlation existed between resuspension rate and flow in non-cohesive bed areas. This result is somewhat surprising, but it emphasizes the importance of properly accounting for temporal and spatial variations in non-cohesive bed properties. Without implementation of mechanistic formulations to predict non-cohesive resuspension and bed armoring, as has been done in this study, empirical relationships cannot be developed that accurately predict non-cohesive resuspension rate as a function of flow rate in the Upper Hudson River. The non-cohesive resuspension functions also show that negligible resuspension occurred for flow rates between about 2,500 and 5,000 cfs, depending upon grid cell location.

3.2.4 Summary

The sediment transport model required specification of two general types of input: (1) bed properties and (2) sediment loading. A significant amount of Upper Hudson River data were available for determining model input information. However, as in any river, the Upper Hudson River data were insufficient to completely determine all model inputs. Thus, estimation methods were developed, using Upper Hudson River data, to determine model inputs when data were unavailable. These estimation procedures introduce uncertainty into the simulations, even though the methods were data-based.

Bed property data for cohesive sediments in the Upper Hudson River were sufficient to specify erosion and bulk property parameters accurately. Non-cohesive bed property data, while relatively abundant, were insufficient to develop credible spatial distributions of model inputs, e.g., d_{50}, which were determined to be necessary for realistic simulations. A procedure was thus developed for estimating spatial distributions of non-cohesive bed inputs for the Upper Hudson River model. A unique benefit of this analysis was the ability to dynamically adjust d_{50}, due to predicted changes in bed composition, during a simulation.

Sediment loading to the Upper Hudson River is one of the primary factors controlling sedimentation rates (and, hence, temporal variation in surficial PCB bed concentrations) in the river. Therefore, accurate determination of solids loading to the Upper Hudson River is of critical importance to any modeling effort. Fortunately, sufficient data were available to develop

credible sediment rating curves for TIP sediment sources, i.e., Fort Edward and TIP tributaries. However, sediment loading data were insufficient for development of data-based rating curves for tributaries downstream of the TIP. A mass balance approach, using main stem sediment load data, was developed to estimate tributary sediment loading for Reaches 1 to 7.

The procedures developed to specify Upper Hudson River sediment loading, from upstream and tributary sources, provide reasonably accurate estimates of annual average sediment loads. Various assumptions and approximations were necessary to develop the load estimation techniques, which introduced uncertainty into sediment transport simulations. The greatest uncertainty occurs in the specification of sediment loading during individual short-term, high flow events using a rating curve. Magnitude and timing of flood sediment loading from a tributary may not be predicted accurately by a rating curve for individual events. However, the rating curve method will predict annual average sediment loading with reasonable accuracy, which is of primary importance for realistic and accurate simulation of long-term deposition rates.

Specification of solids load composition was estimated using relatively sparse data collected at three main stem locations. The assumption of constant sand content in the sediment load, for all flow rates and all tributaries, is clearly an over simplification of a complex process. Sand content of incoming sediment loads certainly varies between tributaries and it is probably dependent upon flow rate. However, the available data are insufficient for credible specification of variable sand content (between sources or with flow rate). Instead of hypothesizing sand content relationships that depended upon tributary and flow rate, and introducing another free variable that could be adjusted during model calibration, sand content was set based upon the available data and not adjusted during the simulations.

3.3 SEDIMENT TRANSPORT MODEL CALIBRATION AND VALIDATION

3.3.1 Calibration and Validation Strategy

The sediment transport model was calibrated using TSS concentration data collected during the 1994 spring flood. A mass balance assessment and TSS concentration comparisons were used to calibrate the model and to evaluate the resuspension and deposition formulas. Model calibration was achieved by adjusting two model parameters: effective particle diameter of class 2 sediment (d_2) (and, thus, the settling speed of class 2 particles as shown in Figure 3-3) and constant (B) in the non-cohesive active layer thickness formulation (Equation (3-10)). No other parameters were adjusted during model calibration.

Model performance was validated using three simulation periods: (1) 1993 spring flood; (2) 1997 spring flood; and (3) long-term, 1977 to 1998. No adjustment of model parameters was made during these validation simulations, only boundary conditions, e.g., inflows and sediment loads, were changed. The 1993 and 1997 spring flood results provided additional confidence in the capability of the model to simulate short-term, high flow events. The long-term simulation demonstrated that the model accurately predicted sedimentation rates in cohesive bed areas and sediment loads at Stillwater and Waterford.

3.3.2 Calibration Results

The longitudinal eddy diffusivity (E_x) was set equal to the eddy viscosity (B_H) used in the hydrodynamic model (0.5 or 1 m^2/s, depending upon reach). Initial model testing, using data and observations from the 1997 spring flood, indicated that the model produced more realistic results in the TIP when an anisotropic eddy diffusivity was used. The lateral eddy diffusivity (E_y) was reduced to 0.05 m^2/s to better reproduce observed patterns of suspended sediment plumes from Snook and Moses Kills during the 1997 spring flood. Lateral eddy diffusivity in Reaches 1 to 7 was reduced to 0.1 m^2/s.

The TIP sediment transport model was calibrated using TSS concentration data collected during the 1994 spring flood. The 40-day simulation period extended from March 22 to April 30, 1994. The maximum daily average flow rate at Fort Edward during this period was 27,700 cfs (Figure 3-23). This period was unique because TSS concentration data were collected at Fort Edward, Snook Kill, Moses Kill and three locations in the TIP (HydroQual 1997a). The most continuous set of TSS concentration data at these six locations in the TIP was collected during

the 30-day period from March 31 through April 29. Model calibration efforts focussed on this 30-day period.

Model parameters governing cohesive sediment resuspension and deposition were determined using TIP field data and were not adjusted during model calibration. Settling speeds for cohesive (class 1) sediments were calculated using Equation (3-3). The probability of deposition parameter $\tau_{b,min}$ used in Equations (3-4) and (3-5) was set at 0.1 dyne/cm^2 and not adjusted during calibration.

Model calibration involved determining a consistent set of values for the following four parameters: (1) d_2, the effective diameter of suspended class 2 particles; (2) B, the constant in the non-cohesive bed active layer thickness equation; (3) $d_{50}(x,y)$, the spatially variable median diameter of sediment in the non-cohesive bed; and (4) $f_2(x,y)$, the spatially variable fraction of class 2 sediment in the non-cohesive bed. Only d_2 and B were adjusted during model calibration. The model calculated spatial and temporal changes in d_{50}, f_1 and f_2. However, changes in d_2 and B values can affect the predicted distributions of d_{50}, f_1 and f_2.

Because suspended class 2 particles are not likely to be coarser than the largest fine sands, i.e., diameter < 250 μm, values of d_2 were restricted to the range of 62 to 250 μm. Initial values for $d_{50}(x,y)$ and $f_2(x,y)$ were generated using Equations (3-16) and (3-17). Determination of consistent parameter values involved finding values of d_2 and B that produced accurate erosion and deposition fluxes for bed characteristics (d_{50} and f_2) expected to exist at the time of the calibration flood. The following iterative procedure was employed (Figure 3-22):

1. Use the spatial distributions of d_{50} and f_2 that were generated by Equations (3-16) and (3-17) as initial conditions for the non-cohesive bed during the 1994 calibration simulation. Denote these estimated bed property distributions as ${}^0d_{50}(x,y)$ and ${}^0f_2(x,y)$.
2. Adjust d_2 and B to achieve the best agreement between predicted and observed sediment transport information during the 30-day period from March 30 through April 29 (descriptions of model-data comparisons are provided below). Denote parameter values for the first 1994 calibration iteration as ${}^1d_2$ and ${}^1B$.

3. Run a long-term simulation (which extends from 1977 to 1998 and is described in Section 3.3.3) using ${}^{1}d_2$ and ${}^{1}B$. The initial bed property distributions used in the long-term run were ${}^{0}d_{50}(x,y)$ and ${}^{0}f_2(x,y)$.
4. Use Equation (3-15) to dynamically calculate d_{50} as f_{sus} (= f_1 + f_2) changes due to resuspension and deposition during the long-term simulation. The model was then run from 1977 to March 21, 1994 and the predicted non-cohesive bed property distributions at the end of that simulation, i.e., ${}^{94,1}d_{50}(x,y)$ and ${}^{94,1}f_2(x,y)$, were output.
5. Re-calibrate the model using the predicted bed property distributions, ${}^{94,1}d_{50}(x,y)$ and ${}^{94,1}f_2(x,y)$, as initial conditions. Denote the best-fit parameter values determined during the second 1994 calibration iteration as ${}^{2}d_2$ and ${}^{2}B$.
6. Repeat the long-term simulation (1977 to 1994) using ${}^{2}d_2$ and ${}^{2}B$. The initial bed property distributions used in the second long-term run were ${}^{0}d_{50}(x,y)$ and ${}^{0}f_2(x,y)$. Denote the bed property distributions at the end of this simulation (March 21, 1994) as ${}^{94,2}d_{50}(x,y)$ and ${}^{94,2}f_2(x,y)$.
7. Simulate the 1994 spring flood using the parameter values ${}^{2}d_2$ and ${}^{2}B$, with ${}^{94,2}d_{50}(x,y)$ and ${}^{94,2}f_2(x,y)$ as initial conditions. The differences in the model predictions between the second and final iteration were small, indicating that "convergence" had been achieved. The values of ${}^{2}d_2$ and ${}^{2}B$ were 90 μm and 0.016, respectively.

The calibration process involved comparing predicted and observed TSS concentrations at three locations in the TIP: (1) upstream of Snook Kill; (2) McDonald's dock (see Figure 3-4 for location); and (3) TID. Results of the final calibration are presented in Figure 3-23. Generally, the model agreed very well with observed TSS concentration at all three locations in the TIP. The model was about 10 mg/l higher than the data at McDonald's dock (located on the east shore across from Griffin Island) from April 15 to 18, indicating that the model probably under-predicted deposition between Snook Kill and that location. TSS concentrations on April 25 were also over-predicted at the above Snook Kill and McDonald's dock sampling locations, suggesting that deposition was under-predicted between Fort Edward and the above Snook Kill station.

Comparisons between predicted and observed TSS are a standard method of calibrating and validating a sediment transport model (e.g., Gailani *et al.* 1991, Ziegler and Nisbet 1994).

However, this method does not necessarily ensure that the model realistically and accurately simulates resuspension and deposition fluxes in the TIP. The reason for this uncertainty is that external solids loadings, from upstream and tributary sources, may dominate predicted/observed TSS concentrations in the TIP, with deposition and resuspension causing relatively small changes in water column sediment concentrations. Large changes in model parameters, creating large changes in deposition and resuspension, may cause relatively small changes in predicted TSS concentrations.

To reduce the uncertainty in model parameterization of deposition and resuspension processes, and thus to improve the predictive capabilities of the sediment transport model, an additional calibration procedure was developed. This procedure involved constructing a sediment mass balance for the TIP, using the total sediment load input from upstream and tributary sources (L_{in}) and the output sediment load at TID (L_{out}), to calculate the net resuspension/deposition in the TIP. Now, a complete mass balance on the TIP for a particular period would produce $L_{in} - L_{out} = \Delta M_{wc} + M_{dep} - M_{res}$, where ΔM_{wc} = change in total suspended sediment mass, M_{dep} = deposition mass and M_{res} = resuspension mass. Net flux to the sediment bed (M_{bed}) was calculated using: $M_{bed} = L_{in} - L_{out} - \Delta M_{wc} = M_{dep} - M_{res}$. Thus, for a given time period, net deposition occurs if $M_{bed} > 0$ and net resuspension occurs if $M_{bed} < 0$.

Sufficient data were collected during the 30-day period from March 31 to April 29, 1994 to develop estimates of M_{bed} on an hourly basis. Note that it was assumed for data-based mass balances, during calibration and validation simulation periods, that the model was the best estimator of ΔM_{wc}. So, predicted ΔM_{wc} values were used to complete the data-based mass balance. Generally, ΔM_{wc} was small compared to the quantity ($L_{in} - L_{out}$), i.e., less than 5%, so using predicted ΔM_{wc} in the data-based mass balance did not introduce significant error.

The results of this data-based analysis showed that net erosion occurred during this period and that 450 MT of sediment were transported out of the TIP. Further examination of data indicated that the 30-day period under consideration could be separated into two distinct sub-periods: (1) tributary deposition and (2) main stem flood. From March 31 to April 10, flow rates in the Hudson River were non-flooding (< 10,000 cfs) but high flow events occurred in the

tributaries. Snook and Moses Kills transported large quantities of sediment into the TIP during this sub-period and, because flow rates in the Hudson River were relatively low, significant deposition occurred. The mass balance results indicated that 390 MT of sediment were deposited during the tributary deposition sub-period. Net erosion occurred during the main stem flood sub-period, extending from April 11 to 29, with 840 MT of sediment lost from the TIP.

Note that this type of data analysis can only be used to estimate global losses or gains due to net erosion or deposition from the TIP sediment bed. Results from this analysis cannot be used to infer net erosion or deposition in specific bed types, e.g., cohesive or non-cohesive, or areas of the TIP.

Comparisons between predicted and observed cumulative M_{bed} for the final calibration, during the entire 30-day period and the two sub-periods, are presented in Figure 3-24. These results show that the model can predict temporal variations in M_{bed} with good accuracy. The model predicted that a total of 370 MT of sediment were exported from the TIP during the 30-day period, which is 18% lower than the data-based estimate. For this 30-day period, ΔM_{wc} was approximately 10 MT, which corresponds to less than 3% of M_{bed}. During the tributary deposition sub-period, 530 MT of deposited sediment were predicted, corresponding to a 36% over-prediction when compared to the observed value. The model is within 7% (900 MT) of the data-based estimate of net erosion during the main stem flood sub-period.

Very good agreement between predicted and data-based estimates of cumulative M_{bed} during the 1994 spring flood demonstrated that: (1) deposition and resuspension processes were realistically and accurately formulated in the model and (2) the model is an effective diagnostic tool for quantitatively evaluating net deposition and erosion from various areas of the TIP. While the model and data indicate net erosion occurred during this 30-day period, closer examination of the model results showed that erosion did not occur in all areas of the TIP. The model showed non-cohesive portions of the TIP, which are about 80% of the total bed area in this reach, experienced a loss of 1,250 MT corresponding to a decrease in the mean non-cohesive bed elevation of 0.06 cm. Conversely, the model showed 880 MT of deposition occurred in the TIP cohesive bed, which is equivalent to an average increase in the cohesive bed elevation of

0.26 cm. The predicted spatial distribution of sediment deposition for this flood is presented in Figure 3-25. The cohesive bed was primarily depositional, with about 87% of the cohesive bed area experiencing net deposition (Figure 3-26). The non-cohesive bed had net erosion occur in 98% of the area of that bed type (Figure 3-26). Prediction of net deposition in the TIP cohesive bed area during this flood is consistent with observed depositional patterns in fine-grained areas of the Upper Mississippi River during major flooding in 1993 (Barber and Writer 1998).

The predicted sediment mass balance for the TIP during the 1994 spring flood is presented in Figure 3-27. While net erosion occurred during the flood period, the erosional and depositional masses were small fractions (< 9%) of the total sediment load transported out of the TIP. Approximately 6% of the incoming sediment load to the TIP was deposited in the cohesive bed area during the flood.

Calibration of the sediment transport model in Reaches 1 to 7 was accomplished using the same procedure applied to the TIP. A consistent set of values for d_2, B, $d_{50}(x,y)$ and $f_2(x,y)$ in Reaches 1 to 7 was determined using the same iterative procedure applied to the TIP, i.e., Figure 3-23. Initial f_2 and d_{50} distributions were specified using Equations (3-17) and (3-18), respectively. A combination of 1994 spring flood and long-term simulations were then conducted to determine appropriate values for ${}^2d_2$ and ${}^2B$ in these reaches. Model calibration yielded parameter values for d_2 and B of 90 μm and 0.005 for Reaches 1 to 7. Note that the value of d_2 (90 μm) determined during model calibration was constant throughout the Upper Hudson River.

Comparisons between observed and predicted TSS concentrations were made at six locations downstream of TID (Figures 3-28 and 3-29). Model results were good to very good at four locations in Reach 5 during the 1994 spring flood (Figure 3-28). Occasionally, the model would under- or over-predict TSS concentrations at the various locations but, generally, the model was able to reproduce observed spatial and temporal patterns in suspended sediment concentration with good accuracy. At the Mechanicville (Reach 3) and Waterford (Reach 1) stations, very good results were achieved with the model able to reproduce the large temporal variability in TSS concentrations during the flood period (Figure 3-29). The model captured the

significant increase in solids load between Stillwater and Mechanicville, which was primarily due to Hoosic River sediment loading.

As in the TIP calibration, a mass balance approach was used to evaluate model performance in Reaches 1 to 7. Mass balances for the 30-day period from March 31 through April 29 were constructed between the following locations: (1) TID to Stillwater and (2) Stillwater to Waterford. A data-based mass balance for this 30-day period showed that 5,500 MT of sediment were eroded and transported out of the river bed between TID and Stillwater. The model predicted 6,500 MT of net erosion, which corresponds to an 18% error. Between Stillwater and Waterford, the data-based analysis indicated that 14,600 MT of net deposition occurred during this flood. The model predicted that 8,600 MT of sediment were deposited in this reach (41% error). For the entire Upper Hudson River (Reaches 1 to 8), the data-based analysis indicated that 8,700 MT of net deposition occurred during the 30-day high flow period. The model predicted net deposition in the Upper Hudson River (1,700 MT), with most of the error occurring due to under-prediction of deposition in Reaches 1 to 4. A summary of the mass balance results for the 1994 spring flood is presented in Table 3-3.

Table 3-3. Mass Balance Results for 1994 Spring Flood
(deposition is positive, erosion is negative)

	Net Sediment Mass Change (metric tons)		
Reach	Observed	Predicted	Error (%)
TIP	-450	-370	-18
TI Dam to Stillwater	-5,500	-6,500	18
Stillwater to Waterford	14,600	8,600	-41

Predicted and data-based mass balances for the Upper Hudson River during the 1994 spring flood period are illustrated in Figure 3-27. Net erosion occurred in the reaches upstream of Stillwater and net deposition occurred downstream of Stillwater. On a system-wide basis, the Upper Hudson River was net depositional during this high flow period; predicted and observed depositional masses were 2 and 12%, respectively, of the total sediment load input to the system. These results suggest that, generally, sediment was deposited in the non-cohesive areas of Reaches 5 to 8 during low to moderate flow periods prior to the flood. Resuspension of this

sediment from non-cohesive areas upstream of Stillwater during the flood provided an additional source of sediment load to Reach 1 to 4, where most of the deposition in the Upper Hudson River occurred.

The mass balance procedures used to calibrate (and, subsequently, validate) the sediment transport model are of particular importance in this study. The data-based mass balances provided valuable information about sediment transport processes in the Upper Hudson River during high flow events that could not have been otherwise obtained. Successful model calibration and validation, using mass balance results provided significantly more confidence in the capabilities of the model to simulate Upper Hudson River resuspension and deposition processes than could have been realized using TSS concentration comparisons, as has been done in other modeling studies, e.g., Gailani *et al.* (1991) and Ziegler and Nisbet (1994).

The calibration process yielded very good to excellent results for the 1994 spring flood simulation. Calibration of the model was achieved by adjusting only two parameters (d_2 and B) with d_2 being set at 90 μm, which corresponds to very fine sand and is a realistic value of the effective diameter of suspended coarse sediments. Very fine sand with a particle diameter of 90 μm has a settling speed of about 400 m/day. The non-cohesive bed armoring constant (B) was set at 0.016 in the TIP and 0.005 in Reaches 1 to 7. These parameter values have no physical basis but the low B values indicated that the active layer thickness (T_a) was weakly dependent on bottom shear stress in the Upper Hudson River. The model demonstrated that net erosion or deposition could be predicted with a maximum error of 40% in the various reaches of the Upper Hudson River. This level of accuracy in a sediment transport model is excellent; it is well below the generally accepted "factor of two" error that is typically used as a criteria to judge the capabilities of this type of model.

3.3.3 Validation Results

Three simulations were conducted to validate the sediment transport model: (1) 1997 spring flood; (2) 1993 spring flood; and (3) 22-year (1977 to 1998) period. No adjustments of model parameter values were made during the validation simulations. Only model boundary

conditions, e.g., flow rates and sediment loadings, were changed to reflect the time-varying conditions during each validation period.

The spring flood that occurred in early May 1997 had a relatively low peak flow, with a maximum flow rate at Fort Edward of approximately 18,000 cfs, see Figure 3-30. GE collected TSS concentration data at Fort Edward, Snook Kill, Moses Kill and TID between April 25 and May 7, which was the period when a high flow event occurred on Snook and Moses Kills. Comparisons of predicted and observed TSS concentrations at TID during this eleven-day period are shown in Figure 3-30. Model results were in good to very good agreement with measured TSS concentrations on both the western and eastern shores of the dam. The model over-predicted peak TSS concentrations by about 10 mg/l on April 28 on both sides of the river. However, the model did accurately reproduce the relative difference in peak TSS concentration between the east and west shore, with model and data indicating that west shore TSS concentrations were about 8-10 mg/l higher than those found on the east shore. Model simulation of the solids pulse during May 3-4 was very accurate, except for a short transient along the western shore on May 3. The source of this predicted transient is unclear but probably due to simulated erosion along the western portion of the channel.

Similar to the 1994 spring flood, a mass balance approach was applied to the 1997 spring flood to evaluate model performance. A seven-day period, from April 28 to May 4, was used for the mass balance because high frequency data were available during this period. The data-based mass balance indicated that net erosion occurred in the TIP, with 450 MT of sediment transported out of this reach. A comparison between predicted and observed cumulative M_{bed} during the seven-day period is shown in Figure 3-31. The model is in excellent agreement with the observed cumulative M_{bed}, with 470 MT of net erosion being predicted during the mass balance period, which corresponds to a 4% error.

Net erosion from the TIP is shown by the data analysis during the seven-day period from April 28 to May 4. This result is similar to the mass balance results for the 1994 spring flood that also indicated global net erosion. These results cannot be used to infer what occurred in the cohesive and non-cohesive bed areas of the TIP. However, the model is a useful tool for evaluating the impacts of this high flow event on different areas of this reach. Net erosion (560

MT) was predicted to occur in the non-cohesive bed area while net deposition (90 MT) occurred in the cohesive bed. These sediment masses correspond to bed elevation changes of approximately 0.02 and –0.03 cm in the cohesive and non-cohesive bed areas, respectively.

Predicted and data-based mass balances for the TIP during this seven-day period are presented in Figure 3-32. Net erosion from the TIP comprised 23% of the sediment load transport past the TID during this flood. About 6% of the incoming sediment load was deposited in the cohesive bed of the TIP.

Peak flow in the TIP during the 1993 spring flood was comparable to the 1994 flood, with a maximum flow rate at Fort Edward of approximately 29,000 cfs (about 5% higher than the 1994 flood peak). A limited amount of TSS concentration data were collected at Fort Edward and TID between March 22 and May 6, 1993, which was the 45-day period simulated. No TSS concentration data were obtained from the tributaries, so sediment loads from Snook and Moses Kills were estimated using the sediment rating curves discussed in Section 3.2.2. Comparisons between predicted and measured TSS concentrations at the dam are shown in Figure 3-33. The model generally agreed with the limited data collected at TID during this high flow period. Patterns of TSS concentration variation during the TIP flood period, which occurred after April 10, were predicted reasonably well.

A high flow event occurred downstream of Stillwater on March 30, while flow rates upstream of this location were relatively low. This first flood was primarily caused by high discharge in the Hoosic River, which had a daily average flow rate of 14,200 cfs on March 30. Good to very good agreement between measured and predicted TSS concentrations at Stillwater and Waterford during the 1993 spring flood was achieved, see Figure 3-34. Under-prediction of TSS concentrations, by about 100 mg/l, at Stillwater on March 30 was probably due to under-estimation of tributary loading to Reach 5, which was estimated using procedures discussed in Section 3.2.2. The model also under-predicted the peak TSS concentration at Waterford during the high flow event on the lower portion of the Upper Hudson River that occurred on March 30, but by less than 10% (about 30 mg/l). Timing of the solids pulse during the March 30 flood was off by about one day. This discrepancy is probably attributable to uncertainty in tributary flow and solids loading timing, which were both estimated. The model generally predicted with good

accuracy the three solids pulses that occurred after April 10. However, the model did appear to over-predict TSS concentrations slightly during this period, suggesting that deposition may have been under-predicted.

Mass balances were constructed during this 45-day period in 1993 between the following locations: (1) Fort Edward to Stillwater and (2) Stillwater to Waterford. The data-based mass balance showed that 9,600 MT of net deposition occurred between Fort Edward and Stillwater. However, the model predicted net erosion of 5,100 MT between these locations. The cause of this discrepancy between the predicted and data-based mass balances is uncertain. This significant difference in the observed (net deposition) and predicted (net erosion) mass balances for the reach between Fort Edward and Stillwater may have been due to relatively sparse solids loading data for locations upstream of Stillwater during this flood. Data-based and predicted mass balance results indicated that 61,400 and 29,400 MT, respectively, were deposited between Stillwater and Waterford during the 1993 spring flood. The model was thus able to predict net deposition within 52% of the observed amount. The data-based analysis showed that about 33% of the sediment input to the reach between Stillwater and Waterford was deposited, while the model predicted a trapping efficiency of 15% for this reach during the 1993 spring flood.

Predicted and data-based mass balances for the Upper Hudson River during the 1993 spring flood period are presented in Figure 3-35. Comparison of the 1993 and 1994 spring floods (Figures 3-35 and 3-27) indicates that the river tends to be net depositional during floods, with most of the net deposition occurring between Stillwater and Waterford. For these floods, the model predicted that net deposition occurred in cohesive bed areas and, generally, the non-cohesive bed areas were net erosional. These results have important implications concerning sediment transport processes in the Upper Hudson River, see Volume 1, Section 2.4.1 for further discussion.

These results demonstrated that the tributary solids loading estimation method works reasonably well when no tributary TSS concentration data were available. All tributary sediment loads were estimated using rating curves. Uncertainty exists in the timing and magnitude of tributary flows and sediment loads during a flood because of the estimation methods used to

specify these model inputs. Thus, most of the phase error in predicted TSS concentrations (Figure 3-34) around May 30 is probably due to the use of rating curves for specification of tributary loads and the uncertainty associated with those loads.

As discussed in Section 3.3.2, long-term calculations were performed iteratively as part of the model calibration process. A final long-term simulation was conducted to further validate the sediment transport model. This calculation was almost 22 years long, starting on January 1, 1977 and ending on December 9, 1998. The hydrograph at Fort Edward during this period is presented in Figure 2-10.

Sediment loading to the Upper Hudson River was determined using a combination of data and sediment rating curves. At Fort Edward, TSS concentration data were used on all days for which data were available, which comprised about 9% of the time during the long-term simulation. On days that data were not collected at Fort Edward, TSS concentration was estimated using Equation (3-19). Tributary sediment loads were estimated using rating curves, i.e., Equation (3-20) and Table 3-2.

This estimation method produced the annual sediment loads to the TIP from upstream and tributary sources, for 1977 to 1998, shown in Figure 3-36. For this period, maximum flow rates at Fort Edward exceeded 25,000 cfs during ten years and 30,000 cfs during five years. Annual sediment loads to the TIP had a mean value of about 38,000 MT/yr, with a range of 16,300 to 69,700 MT/yr. The total sediment load varied, on a yearly basis, between about 40% and 180% of the mean load.

Predicted areas of TIP erosion and deposition at the end of the long-term simulation are shown in Figure 3-37. Deposition rate distributions for this approximate 22-year period in the TIP are presented in Figure 3-38. Net erosion depth patterns are displayed in Figure 3-39. Distributions of deposition rates and net erosion depths in cohesive and non-cohesive bed areas of the TIP are presented in Figure 3-40. These results show that net deposition occurred in over 92% of the cohesive bed areas of the TIP during this 22-year period, with 66% of the cohesive bed having deposition rates of 1 cm/yr or less. In the non-cohesive bed, the areas upstream of Snook Kill were generally net depositional and net erosion typically occurred downstream of

Snook Kill. Approximately 36% of the non-cohesive bed area in the TIP was net depositional, with 34% of the non-cohesive bed having deposition rates of 0.5 cm/yr or less. About 52% of the non-cohesive bed experienced net erosion depths of 2 cm or less.

Performing a sediment mass balance on the TIP, i.e., calculating M_{bed} for the long-term simulation period, showed that the model predicted 69,600 MT of sediment were deposited during the period from May 1, 1977 through December 9, 1998 (Figure 3-41). This 21.6-year period corresponds to the calibration period for the PCB fate model. This depositional mass corresponds to a long-term trapping efficiency of 8.8% for the TIP. Most of the deposition occurred in the cohesive bed areas of the pool, with 87% (nearly 60,200 MT) being deposited in those areas. This amount of deposition translates to an average sedimentation rate of 0.81 cm/yr for the cohesive bed in the TIP. This sedimentation rate equates to an average deposition of about 18 cm (7 inches) over the 22-year period simulated. Even though net deposition occurred in only 36% of the non-cohesive bed area, average net deposition, at the relatively low rate of 0.027 cm/yr, was predicted over this area.

Mass balances in Reaches 1 to 7 for the May 1977 to December 1998 period yielded trapping efficiencies ranging from <0.1 to 11% (Figure 3-41 and Table 3-4). Reaches 4 and 5 have significantly higher trapping efficiencies (> 9%) than Reaches 1, 2, 3, 6 and 7 (< 3%). About 90% of the tributary sediment loading to Reaches 1 to 7 is delivered to Reaches 4 and 5 (from Batten Kill and Hoosic River), with the combination of high sediment loading and hydrodynamic/geometry conditions being the primary causes of the relatively high trapping efficiencies in those two reaches. Similar to the TIP, most of the deposition occurred in the cohesive bed areas of Reaches 1 to 7. Average deposition rates in the cohesive bed areas ranged from 0.02 cm/yr in Reach 1 to 3.8 cm/yr in Reach 4 (Table 3-4). Mean deposition rates in the non-cohesive bed areas of these reaches varied between 0.01 cm/yr (Reach 5) to 1.0 cm/yr (Reach 4). Note that small amounts of net erosion were predicted in the non-cohesive bed in Reaches 2, 6 and 7.

Table 3-4. Mass Balance Results for Long-Term Simulation in Reaches 1 to 8			
		Mean Deposition Rate (cm/yr)	
Reach	Trapping Efficiency (%)	Cohesive Bed	Non-Cohesive Bed
8	8.8	0.81	0.03
7	0.8	0.76	0*
6	2.3	0.38	0*
5	11	1.1	0.01
4	10	3.8	1.0
3	1.8	2.3	0.30
2	< 0.1	0.33	0*
1	< 0.1	0.02	0.02
*Net erosion was predicted			

Daily sediment loading was estimated or measured by USGS at Stillwater and Waterford between 1977 and 1992. Predicted daily sediment loads at these two locations were compared to the USGS data-based loads during this period, see Figures 3-42 and 3-43 and Table 3-5. While significant differences between the predicted and observed daily load could occur on a particular day, primarily due to uncertainty in the timing and magnitude of tributary sediment loading on a daily basis, the mean predicted sediment loads at Stillwater and Waterford are about 7% below the mean data-based loads at those locations. These results suggest that tributary sediment loading to the Upper Hudson River has been under-estimated by about 10 to 15%.

Table 3-5. Comparison of Predicted and Observed Mean Daily Sediment Loads at Stillwater and Waterford				
Location	Number of Observations	Mean Observed Load (MT/day)	Mean Predicted Load (MT/day)	Error (%)
Stillwater	3,908	250	235	-7
Waterford	4,387	540	505	-7

Comparisons of predicted and measured TSS concentrations at various locations during several floods have been used to qualitatively evaluate model performance. Typically, these results have been described as "good" to "excellent." However, differences between predicted and observed TSS concentration values at specific times, either on an absolute or relative basis,

can be significant due to uncertainties in boundary condition timing, e.g., tributary flow rates and sediment loading. Thus, calculating the mean error in predicted TSS concentration at a particular location during a high flow event may produce a result that does not truly represent model accuracy. In addition, quantitatively evaluating model performance using mass balances over specific time periods, as has been done in this study, is more informative than an error analysis of predicted TSS concentrations.

Another way to view model accuracy is to compare the probability distributions of predicted and observed TSS concentrations at various locations in the Upper Hudson River. This method allows a more quantitative evaluation of the predictive capability of the model than the simple visual comparison of simulated and measured TSS concentration time-series. Comparison of TSS concentration distributions demonstrates how well the model can predict both the median concentration and the variability in suspended sediment concentration at a particular location.

Results of the long-term simulation were used to construct distributions of predicted TSS concentrations at TID, Stillwater and Waterford, i.e., predicted daily average concentrations for each day of the 22-year simulation. All available TSS concentration data collected at these three locations were used to generate the data-based distributions. Comparisons of the predicted and observed probability distributions at TID, Stillwater and Waterford are presented on Figures 3-44 to 3-46, respectively. These results demonstrate that the probability distributions of predicted and observed TSS concentrations agree reasonably well at all three locations. The model is able to predict the median concentration at each location within 3 mg/l. Variability in TSS concentration at all locations was also predicted accurately, with the model producing TSS concentration distributions at the three locations that are very similar to the data-based distributions. The model under-predicts TSS concentrations at Stillwater and Waterford, which is consistent with under-prediction of mean sediment loading at those locations (Table 3-5).

As discussed in Section 3.2.2, downstream fining of the suspended sediment load occurs between Schuylerville and Waterford, with data indicating a decrease in mean sand content of 26% to 16% between those locations (Figure 3-47). Predicted spatial changes in sand content

(average values during the 22-year simulation) between Schuylerville and Waterford agree qualitatively with the observed changes (Figure 3-47). The model under-predicts mean sand content at all three locations but the spatial pattern is simulated correctly, indicating consistency between the model and observed downstream fining in the Upper Hudson River, as well as other rivers (Paola, *et al.* 1992, Paola and Seal 1995). Under-prediction of mean sand content at the three main stem locations suggests that the sand content of tributary sediment loads may have been under-estimated.

Comparisons of observed and predicted sedimentation rates in Reaches 1 to 8 were made as another evaluation of long-term model performance. Eight high-resolution sediment cores were collected in 1992 by USEPA in the Upper Hudson River. Geochronologic dating of those cores indicated average sedimentation rates that ranged between 0.8 and 1.8 cm/yr (Table 3-6). Predicted sedimentation rates at those locations compare reasonably well, with predicted-observed errors ranging from -44 to 355% (Table 3-6). Core HR-15 in Reach 1 was not used in this analysis because there were no cohesive sediment grid cells in Reach 1 where this core was obtained. Three cores were collected in the TIP, with model-to-data comparisons at these locations being 0.5 to 0.9, 1.1 to 1.2 and 1.7 to 0.9 cm/yr. The last comparison was between the sampled location and the model grid cell just upstream of that location. The grid cell at the matching location exhibited net erosion, with this difference being attributed to uncertainty in bed mapping. The model-data comparison at the first location improves to 0.95 to 0.9 cm/yr if the grid cell just upstream of the core location is used. In Reach 6, the model-to-data comparison was excellent (0.73 to 0.8 cm/yr). Two cores (HR-21 and HR-22) were located in the same non-cohesive grid cell in Reach 5, which was predicted to be net erosional. Model-to-data comparisons between these two cores and the grid cell immediately upstream of their location, which was a cohesive bed cell, yielded results of 1.1 to 1.2 and 1.1 to 1.8 cm/yr. In Reach 4, near the mouth of the Hoosic River, the highest error occurred (355%), the model-to-data comparison being 4.1 to 0.9 cm/yr.

Table 3-6. Predicted and Observed Average Sedimentation Rates in Reaches 1 to 8				
Reach and Location	Core	Observed Rate (cm/yr)	Predicted Rate (cm/yr)	Error (%)
8 (MP 191.2)	HR-20	0.9	0.5 to 0.95	-44 to 6
8 (MP 189.3)	HR-23	1.2	1.1	-8
8 (MP 188.5)	HR-19	0.9	1.7*	89
6 (MP185.8)	HR-18	0.8	0.73	-9
5 (MP 177.8)	HR-21	1.2	1.1*	-8
5 (MP 177.8)	HR-22	1.8	1.1*	-39
4 (MP 166.3)	HR-16	0.9	4.1	355
*In grid cell immediately upstream of core location				

Comparison of predicted and observed sedimentation rates at all core locations provided additional insight regarding model accuracy (Figure 3-48). The model predicted deposition rates within a factor of two of the measured value, with the exception of the Reach 4 core. These results demonstrate that the model is not biased low or high, but that the results are relatively evenly distributed about the line of perfect agreement. Thus, the overall results provide added confidence that the sediment transport model can simulate long-term deposition processes in the Upper Hudson River.

Predicted deposition rates in Reach 4, into which the Hoosic River flows, are relatively high and do not compare well to the observed sedimentation rate at HR-16 (355% error). High deposition rates are predicted in this reach due to the deposition of fine sand (class 2 sediment), primarily from the Hoosic River, in the relatively quiescent water behind Mechanicville Dam, which is the highest dam on the Upper Hudson River. Even though model results for the long-term simulation are inconsistent with the observed sedimentation rate in Reach 4, mass balance results between Stillwater and Waterford indicated that the model under-predicted deposition in Reaches 1 to 4 during the 1993 and 1994 spring floods by about 40 to 50%. These results suggest that the model probably under-predicted the average deposition rate in the reaches between Stillwater and Waterford during the long-term simulation. In addition, the spatial distribution of deposition in Reaches 1 to 4 is probably not highly accurate, i.e., too high in Reach 4 (9% trapping efficiency) and too low in Reaches 1 to 3 (trapping efficiencies of 0.1 to

2%). These discrepancies are due to the following factors: (1) relatively low grid cell resolution; (2) uncertainty in sediment bed mapping; and (3) uncertainty in the composition of Hoosic River sediment loads.

Additional validation of the long-term model results through comparison with bed elevation changes, based on historical bathymetric analysis, was also attempted. Widespread bathymetric data were collected in the TIP in 1977, 1982 and 1991. The 1977 survey was carried out by Normandeau Associates with bed elevations measured along 165 transects between Fort Edward and Troy, with about 40 transects in the TIP. Depth soundings were made at approximately 44,000 locations in the TIP during a 1982 survey run by Raytheon. General Electric conducted two bathymetric surveys in 1991. One survey collected depth soundings at about 107,000 points in the TIP, while the other survey measured bed elevations along the same transects used in the 1977 survey.

Analysis of bed elevation data to estimate net deposition or erosion at a particular location, or in a localized area, in the TIP involved calculating differences in bed elevations collected at different times, e.g., difference between 1991 and 1982 data. Achieving reliable results from this analysis required accurate determination of horizontal and vertical datums so that bed elevation differences could be accurately calculated. Numerous attempts were made to determine common reference points between the three data sets. Unfortunately, common horizontal and vertical datums could not be established with sufficient precision to produce bed elevation change calculations that were reliable and accurate enough to use for model validation.

3.3.4 Summary

Successful completion of a rigorous calibration and validation process, which was comprised of three floods and a 22-year simulation, yielded a high level of confidence in the predictive capabilities of the Upper Hudson River sediment transport model. Use of mass balance comparisons, combined with conventional comparisons of predicted and observed TSS concentrations, during calibration and validation provided strong evidence that the model can accurately and realistically simulate resuspension, deposition and transport processes in the

Upper Hudson River. Numerous independent data sets were used to evaluate model accuracy during short-term, high flow events and long-term simulations.

Model calibration was achieved by adjusting only two parameters: effective particle size of coarse (class 2) sediment (d_2) and adjustable active layer constant (B). The value of d_2 determined during calibration was 90 μm, which is a very fine sand and corresponds to a realistic effective particle size for suspended coarse sediments in the Upper Hudson River. Using the same value of d_2 (90 μm) in all eight reaches suggests consistency in the effective settling characteristics of non-cohesive suspended sediment throughout the river. The active layer constant (B) ranged between 0.005 and 0.016, indicating that the active layer thickness is weakly dependent on bottom shear stress. The value of this parameter has no physical justification, which may introduce uncertainty into the simulations. Sensitivity of model results to variation of d_2 and B was investigated and is discussed in the next section. Use of only two adjustable parameters for model calibration demonstrates the validity, and importance, of the data-based, mechanistic approach used to develop and parameterize the deposition and resuspension formulations incorporated into the model.

Generally, calibration and validation results demonstrated that the model accurately and realistically simulates sediment transport processes in the Upper Hudson River. Simulations in the TIP produced the highest level of confidence in model predictive capabilities, which is due to model resolution and an abundance of data. The TIP is of primary importance when considering PCB fate and transport in the Upper Hudson River, so it was necessary to focus sediment transport efforts on that reach. Between Stillwater and Waterford, model resolution was lower and data available for model input were sparser. These factors contributed to uncertainty in model results in Reaches 1 to 4; the model tended to under-predict deposition between Stillwater and Waterford and the spatial distribution of deposition in those four reaches may not be highly accurate.

3.4 MODEL SENSITIVITY AND UNCERTAINTY

Sensitivity of the sediment transport model to various parameters and inputs was evaluated using simulations during four periods: (1) 1994 spring flood; (2) 1983; (3) 1988; and (4) 1977 to 1998. All sensitivity runs were done using the TIP model. The one-year runs were conducted to investigate the effects of flow rate and sediment load, with 1983 and 1988 representing high and low flow years, respectively. The impact of non-cohesive suspended load transport was studied by setting the non-cohesive bed as hard bottom and repeating the 1994 spring flood and 22-year simulations. The long-term simulation was also used to determine the impact of sediment loading on mean deposition rates.

Sensitivity of the 1994 spring flood, 1983 and 1988 simulations to variations in the following parameters was determined: (1) cohesive resuspension constant, a_o; (2) sand fraction of incoming sediment load; (3) effective particle diameter of class 2 sediment, d_2; (4) non-cohesive bottom roughness, z_o; and (5) non-cohesive bed armoring constant, B. These five parameters were chosen because these inputs are primary factors that control model predictions. Note that the mean annual flow rates at Fort Edward during 1983 and 1988 were 5,980 and 3,900 cfs, respectively. The maximum daily average flow rates during 1983 and 1988 were 34,100 and 13,100, respectively.

The first two parameters, a_o and sand fraction, were determined from data and not adjusted during model calibration. The available data were used to determine 95% confidence intervals for these parameters and the model was run at the high and low limits of this range. Upstream of MP 190.7, the 95% confidence interval for a_o ranged from 0.025 to 0.045, while downstream of this mile point, a_o had high and low values of 0.126 and 0.088. The 95% confidence interval for sand content ranged from 21 to 29%. The two calibration parameters, d_2 and B, were adjusted as follows. Class 2 particle diameter (d_2) was varied by $\pm$ 20 μm, i.e., 70 and 110 μm. The bed armoring constant, B, was increased and decreased by a factor of two, i.e., 0.008 and 0.032. Effective bottom roughness in the non-cohesive bed areas (z_o) was varied from 750 to 3,000 μm, which corresponds to the same range used in the sensitivity analysis of the two-dimensional hydrodynamic model.

Summaries of sensitivity results for the 1994 spring flood, 1983 and 1988 simulations are presented in Tables 3-7 to 3-9, respectively. Model sensitivity was quantified by comparing net

mass changes, with respect to the original run, for each simulation in three areas of the TIP: (1) entire reach; (2) cohesive bed; and (3) non-cohesive bed. The model was most sensitive to d_2 and B during the 1994 spring flood simulation, with total mass changes ranging from –84 to 132% (with respect to the original run) and most of the impact was in the cohesive bed areas. Variation of non-cohesive bottom roughness (z_o) caused negligible changes in sediment transport results, which indicated that variation in bottom shear stress is not highly dependent upon bottom roughness. These results show that the model is sensitive to input parameter variation during the calibration period and that the parameter values determined during calibration are relatively precise.

Evaluating the validity of the parameter ranges used in the sensitivity analysis required comparison of these results to the data, i.e., net erosion of 450 MT during the 1994 spring flood. A sensitivity simulation would be regarded as valid only if the predicted net erosion were within a factor of two of the data-based value, i.e., within the range of 225 to 900 MT of net erosion. Two sensitivity simulations were outside of this range: high d_2 (60 MT of net erosion) and low B (190 MT of net erosion). Thus, these two parameter values should be considered to be outside the valid range.

The model was less sensitive during the 1983 and 1988 simulations, with the maximum total mass change being about –3% (with respect to the original run). Thus, variation in the primary model parameters, within reasonable limits, that affect calibration results has minor impact on long-term average deposition rates predicted by the model.

The bed armoring constant (B) is the adjustable parameter that controls simulation of the non-cohesive bed armoring process. This parameter has no physical basis; B is a free parameter that was determined during model calibration. Analysis of the sensitivity results, combined with calibration results, showed that predicted net erosion from the TIP during the 1994 spring flood is a linear function of B. A valid calibration, i.e., predicted net erosion between 225 and 900 MT, would thus be produced for B values ranging between 0.0097 and 0.039. Therefore, the calibration value of B (0.016) in the TIP model is known to within approximately a factor of two,

which is reasonably precise for a lumped parameter that approximates a complex physical process in an environmental system model.

Table 3-7. Sensitivity Analysis Results for 1994 Spring Flood.
Negative Mass Change Values Indicate Erosion and Positive Values Indicate Deposition.

		Mass Change (MT)			Difference with respect to Original Run (%)		
Parameter	Value	Fine	Coarse	Total	Fine	Coarse	Total
Cohesive erosion, a_o	Low	970	-1,270	-300	10	2	-19
Cohesive erosion, a_o	High	790	-1,260	-470	-10	0.8	-27
Sand content	Low	990	-1,230	-240	13	-2	-35
Sand content	High	770	-1,300	-530	-12	4	43
Class 2 particle size, d_2	Low	530	-1,390	-860	-40	11	132
Class 2 particle size, d_2	High	1,120	-1,180	-60	27	-6	-84
Bed armoring constant, B	Low	830	-1,020	-190	-6	-18	51
Bed armoring constant, B	High	980	-1,740	-760	12	39	105
Non-cohesive bottom roughness, z_o	Low	880	-1,260	-380	0	0.8	3
Non-cohesive bottom roughness, z_o	High	860	-1,250	-390	-2	0	5

Table 3-8. Sensitivity Analysis Results for 1983, High Flow Year.
Negative Mass Change Values Indicate Erosion and Positive Values Indicate Deposition.

		Mass Change (MT)			Difference with respect to Original Run (%)		
Parameter	Value	Fine	Coarse	Total	Fine	Coarse	Total
Cohesive erosion, a_o	Low	2,070	1,700	3,770	0.0	-0.6	0.0
Cohesive erosion, a_o	High	2,070	1,700	3,770	0.0	-0.6	0.0
Sand content	Low	2,080	1,810	3,890	0.5	6	3
Sand content	High	2,060	1,610	3,670	-0.5	-6	-3
Class 2 particle size, d_2	Low	2,130	1,610	3,740	3	-6	-0.8
Class 2 particle size, d_2	High	2,040	1,750	3,790	-1	2	0.5
Bed armoring constant, B	Low	2,070	1,710	3,780	0.0	0.0	0.3
Bed armoring constant, B	High	2,070	1,700	3,770	0.0	-0.6	0.0
Non-cohesive bottom roughness, z_o	Low	2,060	1,730	3,790	-0.5	1	0.5
Non-cohesive bottom roughness, z_o	High	2,140	1,590	3,730	3	-7	-1

Table 3-9. Sensitivity Analysis Results for 1988, Low Flow Year.
Negative Mass Change Values Indicate Erosion and Positive Values Indicate Deposition.

		Mass Change (MT)			Difference with respect to Original Run (%)		
Parameter	Value	Fine	Coarse	Total	Fine	Coarse	Total
Cohesive erosion, a_o	Low	2,990	670	3,660	0.0	0.0	0.0
Cohesive erosion, a_o	High	2,990	670	3,660	0.0	0.0	0.0
Sand content	Low	3,000	790	3,790	0.3	18	4
Sand content	High	2,990	560	3,550	0.0	-16	-3
Class 2 particle size, d_2	Low	3,060	590	3,650	2	-12	-0.3
Class 2 particle size, d_2	High	2,980	690	3,670	-0.3	3	0.3
Bed armoring constant, B	Low	2,990	670	3,660	0.0	0.0	0.0
Bed armoring constant, B	High	3,000	670	3,670	0.3	0.0	0.3
Non-cohesive bottom roughness, z_o	Low	2,990	690	3,680	0.0	3	0.5
Non-cohesive bottom roughness, z_o	High	3,060	590	3,650	2	-12	-0.3

The impact of treating the non-cohesive bed in the TIP as a hard bottom was examined using the 1994 spring flood and 21-year simulation. Net deposition in the cohesive bed during the 1994 spring flood decreased by 28% when non-cohesive suspended load transport was neglected. The reason for this decrease in net deposition was that the non-cohesive bed served as a reservoir of class 2 sediment that can be resuspended during a flood, transported downstream and enhance cohesive bed deposition. In contrast, net cohesive deposition increased by 37% during the long-term simulation; the average sedimentation rate in the cohesive bed areas increased from 0.8 cm/yr to 1.1 cm/yr. The increase in cohesive deposition rate during the long-term simulation was due to an increase in suspended class 2 sediment throughout most of the TIP; additional suspended class 2 sediment, which was previously deposited in non-cohesive bed areas, was transported to and deposited in the cohesive bed areas.

The potential impact of the initial non-cohesive bed distribution on model results was investigated by repeating the 1994 spring flood run with the initial bed distributions ${}^0d_{50}(x,y)$ and ${}^0f_2(x,y)$. The results of this simulation are presented in Figure 3-49. Using ${}^0d_{50}(x,y)$ and ${}^0f_2(x,y)$ primarily affected the main stem flood sub-period, with erosion increasing from 900 to 1,215

MT (35% increase). Net erosion increased during this sensitivity simulation because additional sediment in the non-cohesive bed was available for resuspension; temporal and spatial bed armoring effects, which were included in ${}^{2}d_{50}(x,y)$ and ${}^{2}f_{2}(x,y)$, are not included in ${}^{0}d_{50}(x,y)$ and ${}^{0}f_{2}(x,y)$, which increased resuspension.

As discussed in Section 3.2.2, upstream and tributary sediment loadings to the Upper Hudson River were estimated using rating curves during simulation periods when no data were available. The loading estimation procedure introduced uncertainty into the long-term simulation results, i.e., mean deposition rates, which may affect predictions of the PCB fate model. To better understand the impacts of sediment loading uncertainty on long-term burial rates, long-term TIP simulations were conducted using low and high sediment loading, with respect to the original TIP loading of 37,900 MT/yr (total).

Limits of the low and high sediment loading simulations were determined by adjusting the exponents in the rating curves for Fort Edward, Snook Kill and Moses Kill, i.e., Equations (3-19) and (3-20). The exponents for the high-flow portion of the rating curves were adjusted such that the resulting high and low rating curves used in the sensitivity analysis were consistent with TSS concentration data for each location. A listing of the adjusted exponents, compared to the original exponent for each location, is given in Table 3-10. Use of these adjusted rating curves to calculate solids loading to the TIP for the long-term simulation resulted in load changes of –10% and 26%, with respect to the original average solids loading of 37,900 MT/yr (Table 3-10). Increasing solids loading by 26% caused increases in mean deposition rates of 15 and 32% in the fine and coarse bed areas, respectively. Conversely, decreasing solids loading by 10% resulted in the mean deposition rates in the fine and coarse bed areas to decrease by 5 and 9%, respectively (Table 3-10). The impacts of these solids loading changes on PCB fate in the TIP were also investigated and those results are presented in Section 4.6.

Table 3-10. Solids Loading Sensitivity Analysis Results

Case	Rating Curve Exponent			TIP Loading (MT/yr)	Mean Deposition Rate (cm/yr)	
	Ft. Edward	Snook Kill	Moses Kill		Fine	Coarse
Original	2.02	1.7	1.5	37,900	0.82	0.022

High load	2.6	2.0	1.8	47,600	0.94	0.029
Low load	1.9	1.6	1.2	34,200	0.78	0.020

3.5 IMPACTS OF A RARE FLOOD EVENT

The impacts of a 100-year flood on sediment transport processes in the Upper Hudson River were investigated using the calibrated and validated sediment transport model. No model parameters were adjusted during this simulation. All parameters were set at the values determined during calibration.

The rare flood event typically referred to as the 100-year flood is defined statistically as a discharge that has a 1% chance of occurring in any given year. This probability means that there are 26, 63 and 87% chances that a 100-year flood will occur in any 30-, 100- and 200-year period, respectively. This rare flood event will generate high current velocities in the Upper Hudson River, resulting in erosion at various locations, but it will also cause large quantities of sediment to be transported into the river from tributaries. High sediment loads in the river will make it possible for net deposition to occur at some locations during a 100-year flood. A rare flood event does not necessarily cause erosion to occur throughout the entire river.

3.5.1 Development of Model Inputs

Model input parameters developed and used during the calibration process were not adjusted for the 100-year flood simulation. Boundary conditions, e.g., flow rates and sediment loading, were specified as discussed below. Selection of appropriate initial conditions for non-cohesive bed properties was made using an objective process.

The peak flow rate for a 100-year flood at Fort Edward has been estimated to be 47,330 cfs, on a daily-average basis (USEPA 1996). This discharge is compared to the mean flow rate and peak daily-average flow rates during historical floods at Fort Edward in Figure 3-50. The 1993 and 1994 spring floods, which were used for model calibration and validation, had peak flows that were about 60% of the 100-year peak flow. Similarly, 10-year floods that occurred in

1983 and 1998 had peak discharge that was only 28% lower than the 100-year flood. Note that the effects of both of these floods were included in the long-term validation simulation. Thus, the 100-year flood is a rare high flow event but the peak flow rate expected during such a flood is no more than 40% greater than discharge during the calibration and validation flood simulations. This characteristic of the Upper Hudson River means that the 100-year flood simulation does not represent an extreme extrapolation beyond conditions that occurred during model calibration and validation.

Flood hydrographs in the Upper Hudson River are variable, making it necessary to construct upstream and tributary hydrographs for the 100-year flood that are representative of average flood conditions. Between 1977 and 1997, nine floods occurred at Fort Edward that were used for construction of the 100-year flood hydrograph at the upstream boundary of the hydrodynamic models (one- and two-dimensional). Peak daily-average flow rates for these floods ranged from 21,400 to 34,100 cfs (Table 3-11).

Table 3-11. Fort Edward Floods Used to Construct 100-Year Flood Hydrograph

Date of Peak Flow	Peak Daily Average Flow Rate (cfs)
April 29, 1979	31,700
April 19, 1982	25,600
May 3, 1983	34,100
April 6, 1987	21,400
May 18, 1990	23,700
April 18, 1993	28,800
April 23, 1993	27,900
April 17, 1994	27,700
May 13, 1996	26,000

The rising and falling limb of the flood hydrograph was assumed to extend four days before and after the peak flow rate, resulting in a nine-day flood hydrograph for each of the nine floods listed in Table 3-10. The flow rates for each of the nine flood hydrographs were normalized with respect to the maximum flow rate that occurred during a particular flood. This process generated nine normalized flood hydrographs (Figure 3-51). A representative flood hydrograph was created by averaging the nine normalized flow rates on each day of the flood (Figure 3-52). The flood hydrograph used for model input was generated by multiplying the

normalized flow rates on Figure 3-52 by the maximum daily-average flow rate for the 100-year flood (47,330 cfs). Adjustment of the peak flow rate used for model input (49,700 cfs) was necessary to ensure that a peak daily average of 47,330 cfs was achieved during the simulation. This adjustment was necessary because the hydrodynamic models linearly interpolate boundary inflows in time.

An Upper Hudson River flood that occurred in early April 1976 has been characterized as being equivalent to a 50-year to 100-year flood. This flood occurred prior to establishment of the USGS gauging station at Fort Edward and the magnitude of this flood can only be estimated from discharge data at upstream gauging stations, e.g., at Hadley. However, since this flood was obviously a major high flow event on the Upper Hudson River, the 1976 flood hydrograph at Hadley, normalized with respect to the maximum flow rate that occurred on April 2, was compared to the synthetic hydrograph developed above (Figure 3-52). The normalized 1976 flood hydrograph closely approximates the lower 95% confidence interval hydrograph that resulted from the analysis. Hence, the synthetic flood hydrograph used in evaluating the impacts of a 100-year flood is consistent with the hydrograph of a major flood on the Upper Hudson River.

Synthetic flood hydrographs for Upper Hudson River tributaries were generated by analyzing the hydrographs of Kayaderosseras Creek and Hoosic River during the nine floods listed in Table 3-10. Normalized flood hydrographs for Kayaderosseras Creek were created for each of the nine floods (Figure 3-53). An average flood hydrograph for Kayaderosseras Creek was then calculated (Figure 3-54). Note that the peak flow in Kayaderosseras Creek typically occurred one day before the peak flow at Fort Edward. The same procedure was used to generate a synthetic flood hydrograph for Hoosic River, which was very similar to the Kayaderosseras Creek hydrograph shown in Figure 3-54.

Peak daily-average flow rates in the tributaries during the 100-year flood were estimated using results of flood insurance studies conducted by FEMA (1995). The FEMA studies indicated that daily-average runoff rate during a 100-year flood on the Upper Hudson River ranges from about 17 to 19 cfs/mi^2. A runoff rate of 18.5 cfs/mi^2 was thus applied to all

tributaries on the day of peak flow at Fort Edward during the 100-year flood; tributary flow rates on day 5 of the flood were specified by multiplying the runoff rate by the tributary drainage area. Tributary hydrographs used for model input were calculated by scaling the normalized flood hydrograph to the flow rate specified on day 5 for each tributary. Maximum tributary flow rates ranged from 180 cfs (Flately Brook) to 16,100 cfs (Hoosic River).

Sediment loadings from upstream and tributary sources were specified using the rating curves developed in Section 3.2.2. Total sediment loading to the TIP during the 100-year flood was 71,400 MT. This load corresponds to approximately 190% of the estimated average annual TIP sediment load of 37,900 MT/yr. Tributaries in Reaches 1 to 7 contributed about 164,300 MT of sediment to the river during the flood.

Initial non-cohesive bed property distributions, e.g., $d_{50}(x,y)$ and $f_2(x,y)$, used in the 100-year flood simulation were determined as follows. Predicted non-cohesive bed property distributions at the end of each year, i.e. December 31, were extracted from the TIP long-term simulation results. Twenty-one simulations of the 100-year flood in the TIP were conducted, with the initial non-cohesive bed property distributions of each run corresponding to the predicted distributions at the end of 1977 to 1997. Net erosion from the cohesive bed for the 21 simulations varied within 1% of the average value. For the non-cohesive bed, the range of predicted net erosion ranged from 7% below to 4% above the mean value of the 21 simulations. These results show that 100-year flood results were relatively insensitive to initial non-cohesive bed property distributions.

3.5.2 100-Year Flood Simulation Results

The 100-year flood simulation was conducted using the non-cohesive bed property distributions predicted at the end of 1987, which produced results approximately equal to the average of the twenty-one 100-year flood simulations. The model predicted mean erosional depths of 0.84 and 0.14 cm for the cohesive and non-cohesive bed in the TIP, respectively. Maximum erosional depths for the cohesive and non-cohesive bed were approximately 9 and 8 cm, respectively.

The spatial distribution of predicted erosional depths in the TIP at the end of the 100-year flood is presented in Figure 3-55. Erosion occurred in approximately 94% of the cohesive bed area, with net deposition in the remaining area. In the eroded portions of the TIP cohesive bed, erosional depths of 2 cm or less were predicted for 78% of the total cohesive area and about 4% of the area had erosional depths greater than 5 cm (Figure 3-56). Scour depths of 1 cm or less were predicted in approximately 97% of the non-cohesive bed area (Figure 3-56).

The model predicted that a total of 5,100 MT of sediment would be transported out of the TIP during the 100-year flood (Figure 3-57). This mass corresponds to about 7% of the total sediment load input to the TIP during the flood. Of the total amount of net erosion, 2,850 and 2,250 MT of net erosion occurred in the cohesive and non-cohesive bed areas of the TIP, respectively. For comparison, net deposition was predicted in the cohesive bed areas during the 1993 and 1994 spring floods (1,360 and 880 MT of net deposition, respectively). In the non-cohesive bed areas, 1,330 and 1,250 MT of net erosion were predicted during the 1993 and 1994 floods, respectively.

In Reaches 1 to 7, the model predicted that 2,600 MT of sediment were deposited, which means that 2,500 MT of sediment were eroded from the Upper Hudson River and transported to the Lower Hudson River during the flood (Figure 3-57). This amount of sediment corresponds to approximately 1% of the average annual sediment load at Waterford. For comparison, 24,300 and 1,700 MT of net deposition were predicted in the Upper Hudson River during the 1993 and 1994 spring floods, respectively. This large difference in predicted net deposition between the 1993 and 1994 spring floods was consistent with data-based analyses of those floods, which indicated that 71,000 and 8,700 MT of net deposition occurred in the Upper Hudson River during the 1993 and 1994 floods, respectively. These results show the importance of tributary sediment loading during a flood and the impact that tributary loads have on sediment transport processes in the Upper Hudson River. Net erosion was predicted for the 100-year flood in Reaches 2, 4, 6 and 7, with net deposition being simulated in Reaches 1, 3 and 5. Mass balances and average bed elevation changes for each reach are summarized in Table 3-12.

Table 3-12. Impacts of 100-Year Flood on Bed Elevations in the Upper Hudson River. Negative Values Indicate Erosion and Positive Values Indicate Deposition.					
	Cohesive Bed Changes		Non-Cohesive Bed Changes		Total Net Mass Change (MT)
Reach	Net Mass (MT)	Mean Bed Elevation (cm)	Net Mass (MT)	Bed Elevation (cm)	
8	-2,850	-0.84	-2,250	-0.14	-5,100
7	-1,500	-4.1	200	0.03	-1,300
6	-2,200	-0.90	-400	-0.05	-2,600
5	-2,800	-0.36	-3,900	0.09	1,100
4	-3,500	-1.0	2,200	0.95	-1,300
3	-1,660	-0.33	8,960	0.18	7,300
2	-2,100	-0.35	-200	-0.05	-2,300
1	-100	-0.10	1,800	0.02	1,700

The 100-year flood simulation represents an extrapolation beyond the range of Upper Hudson River conditions included in calibration and validation simulations. This extrapolation creates uncertainty in the 100-year results and brings into question the accuracy of the predictions. Therefore, the validity of these results was investigated by comparing 100-year flood results to calibration and validation results in order to evaluate the significance of extrapolating beyond data-based simulations.

Predicted flow rates at Stillwater and Waterford during the 100-year flood are compared to the Fort Edward hydrograph on Figure 3-58. Peak flow rates at Stillwater during the 1993 and 1994 spring floods were about 33,000 cfs. Peak flow at Stillwater during the simulated 100-year flood was predicted to be about 65,000 cfs, which is approximately twice as high as the 1993-94 floods. Similarly, Waterford peak flow during the simulated 100-year flood was nearly 80,000 cfs, corresponding to an increase of about 70% when compared to the 1993-94 flood peaks at that location. These proportional flow increases are similar to the relative increase at Fort Edward.

Probability distributions of maximum current velocities predicted during the 1993, 1994, 1997 and 100-year floods in cohesive and non-cohesive bed areas are given in Figure 3-59. In cohesive areas, maximum velocities during the 100-year flood were typically about 47% higher

than maximum velocities during the 1993-94 floods, with the median difference being about 40 cm/s (1.3 ft/s). Similarly, in non-cohesive bed areas, 100-year flood maximum velocities were predicted to be about 43% higher than 1993-94 flood velocities, with the median difference being about 45 cm/s (1.5 ft/s).

Of particular importance to sediment transport processes is bottom shear stress (τ_b), with probability distributions of maximum τ_b during the four floods being compared on Figure 3-60. The median value of the maximum bottom shear stress during the 100-year flood was about double that found during the 1993-4 floods in both the cohesive and non-cohesive bed areas.

The 100-year flood required extrapolation of erosion calculations beyond the upper limit of 9 dynes/cm^2 used in the reach-specific resuspension potential studies conducted in the Upper Hudson River (Appendix B). Distributions of maximum bottom shear stress, normalized with respect to 9 dynes/cm^2, in the TIP cohesive bed areas during the 1994 spring flood and the 100-year flood are presented in Figure 3-61. Approximately 80% of the cohesive bed area had maximum shear stresses exceeding 9 dynes/cm^2 during the 1994 flood (the 1993 spring flood had very similar results). Thus, the calibration and validation simulations produced satisfactory results even though the resuspension flux calculations required extrapolation beyond the upper limit of the data range for a large portion of the cohesive bed area. For comparison, the 100-year flood produced maximum shear stresses greater than 9 dynes/cm^2 over 96% of the cohesive bed.

These results make it necessary to discuss the validity of extrapolating resuspension potential data beyond the 9 dynes/cm^2 limit. Investigation of cohesive sediment resuspension properties at high shear stresses, up to 100 dynes/cm^2, has been made possible by a new type of flume, called Sedflume, developed by Prof. Wilber Lick at the University of California, Santa Barbara. Lick and co-workers have been studying the effects of various sediment properties, e.g., bulk density and grain size distribution, on cohesive sediment erosion rates over a wide range of applied shear stresses (Jepsen *et al.* 1997, Roberts *et al.* 1998). Results of a series of erosion rate experiments by Jepsen *et al.* (1997) on cohesive sediments collected from the Detroit River in Michigan are presented in Figure 3-62. The experimental data ranged from 2 to 64 dynes/cm^2 and the main purpose of the study was to investigate the effects of bulk density on

erosion over this range. To eliminate the effects of bulk density and standardize the data, erosion rate values presented in Jepsen *et al.* (1997) have been normalized with respect to the reported bulk densities. Normalization of the data shows that erosion rate is a continuous function over the range of shear stresses used in this study. This result indicates that extrapolation of resuspension potential data beyond the 9 dynes/cm^2 limit is valid and applicable to maximum bottom shear stresses predicted in the Upper Hudson River during the 100-year flood simulation.

Comparisons of probability distributions of TIP bed elevation changes during the simulated 1993, 1994, 1997 and 100-year floods in cohesive and non-cohesive bed areas, are shown in Figure 3-63. The major impact of the 100-year flood is widespread erosion in cohesive areas, where net deposition was generally predicted during the smaller, historical floods. Non-cohesive erosional depths during the 100-year flood were greater than during the other three floods, with about 10% of that bed area experiencing significantly greater erosion.

Maximum active layer thickness (T_a) during the 100-year flood ranged from less than 0.1 cm to about 1.3 cm in the TIP. These values were not significantly higher than the maximum T_a values predicted during the 1993, 1994 and 1997 floods. This result would be expected, however, because T_a is weakly dependent upon bottom shear stress.

Time-series of predicted 100-year flood suspended sediment concentrations at Stillwater and Waterford are compared to the specified values at Fort Edward in Figure 3-64. Significant increases in TSS concentration, and sediment load, were predicted to occur between Fort Edward and Waterford, with maximum concentrations increasing from about 150 to over 900 mg/l along the Upper Hudson River. The largest increase in TSS concentration occurred between TID and Stillwater (~300 to 800 mg/l).

Maximum TSS concentrations during the 100-year flood at TID, Stillwater and Waterford are compared with maximum values during the 1993, 1994 and 1997 spring floods in Figure 3-65. Generally, the relative difference between the floods tends to decrease as one travels downstream from the TIP. Tributary sediment loading has a significant impact on the observed increase in solids loading, as would be expected.

The above results strongly indicate that the 100-year flood, while certainly an extrapolation beyond calibration and validation simulations, is not an extreme extrapolation. Conditions during the 100-year flood are generally within a factor of two of hydrodynamic and sediment transport conditions experienced during the historical flood simulations. Extrapolation of the cohesive resuspension formulation beyond the experimental limit, i.e., 9 dynes/cm^2, appears to be valid based upon erosion rate data presented in Jepsen *et al.* (1997). In addition, bottom shear stresses exceeded this limit in 80% of the cohesive bed area of the TIP during the 1994 spring flood simulation. Therefore, the 100-year flood results can be considered a realistic and valid extrapolation beyond calibration and validation conditions.

3.5.3 Comparison to Zimmie Model Predictions

A one-dimensional sediment transport model (HEC-6) was applied to the TIP by Zimmie (1985). This model only considered non-cohesive sediment transport; cohesive sediment resuspension and deposition were neglected. TIP bed property data were used to develop site-specific model inputs for HEC-6. The sediment transport model was not rigorously calibrated, so model predictions are uncertain. However, comparisons of Zimmie (1985) predictions to the results presented above are informative.

The 100-year flood that Zimmie (1985) simulated used a flow rate of 63,700 cfs, which is nearly 50% greater than the flow rate accepted as the 100-year flood at present time. Zimmie (1985) also simulated another flood, referred to as the 10-year flood in his report, which had a flow rate of 46,600 cfs and is only 2% (730 cfs) lower than the 100-year flood flow rate used in this study. Thus, Zimmie's (1985) 10-year flood results are comparable to the 100-year flood projections made in the present study. For the 46,600 cfs flood, Zimmie (1985) predicted the maximum erosion depth to be about 5 cm (0.15 ft), with the average bed elevation change in the TIP being –0.5 cm (-0.02 ft), i.e., net erosion. While these results indicate a slightly greater average erosional depth than the present model (about 0.35 cm deeper mean erosion in non-cohesive bed areas), the two models yield the same basic conclusion: the 100-year flood causes relatively minor erosion in the TIP.

3.5.4 Sensitivity Analysis

Sensitivity of the 100-year flood simulation to input parameters was investigated using the procedure applied in Section 3.4. The same five parameters were varied (as discussed in that section): (1) cohesive resuspension constant, a_o; (2) sand fraction of incoming sediment load; (3) effective particle diameter of class 2 sediment, d_2; (4) non-cohesive bottom roughness, z_o; and (5) non-cohesive bed armoring constant, B. A summary of the results is presented in Table 3-13. Varying a_o to the 95% confidence interval limits caused cohesive bed erosion changes of about $\pm$ 26%. Total erosional masses were changed by 10% or less due to changes in sand content of incoming sediment load, d_2 and z_o. As might be expected, non-cohesive bed erosion was sensitive to variations in the bed armoring constant (B), with changes in net erosion of –47 and +82% from that portion of the TIP sediment bed. Consistent with the 1994 flood sensitivity analysis, non-cohesive bed erosion varies approximately linearly with B, so changing B by a factor of two generates about the same change in non-cohesive bed erosion. However, note that reasonable calibration results could only be achieved using a factor of two range for B; varying B by more than a factor of two produces an inadequately calibrated model. Thus, a factor of two variation in non-cohesive bed erosion during the 100-year flood is the maximum range that can be attributed to uncertainty in B.

Table 3-13. Sensitivity Analysis Results for 100-Year Flood in the TIP. Negative Mass Change Values Indicate Erosion and Positive Values Indicate Deposition.

		Mass Change (MT)			Difference with respect to Original Run (%)		
Parameter	Value	Fine	Coarse	Total	Fine	Coarse	Total
Cohesive erosion, a_o	Low	-2,120	-2,250	-4,370	-26	0.0	-14
Cohesive erosion, a_o	High	-3,610	-2,260	-5,870	27	0.4	15
Sand content	Low	-2,730	-2,170	-4,900	-4	-4	-4
Sand content	High	-3,010	-2,330	-5,340	6	4	5
Class 2 particle size, d_2	Low	-3,240	-2,330	-5,570	14	4	9
Class 2 particle size, d_2	High	-2,520	-2,140	-4,660	-12	-5	-9
Bed armoring constant, B	Low	-2,900	-1,200	-4,100	2	-47	-20
Bed armoring constant, B	High	-2,900	-4,090	-5,140	2	82	37
Non-cohesive bottom roughness, z_o	Low	-2,870	-2,260	-5,190	0.7	0.4	0.6
Non-cohesive bottom roughness, z_o	High	-2,780	-2,280	-1,600	-2	1	-0.8
Hydrograph	Low	-3,240	-1,900	-5,140	14	-16	0.8
Hydrograph	High	-2,370	-2,820	-5,190	-17	25	2
Flood Plains		-1,290	-310	-1,600	-55	-86	-69

Sediment loading, at Fort Edward and from TIP tributaries, for the 100-year flood simulation was estimated using rating curves, which introduces uncertainty into the results. As a bounding calculation to estimate the effects of solids loading, the 100-year flood simulation was repeated with zero sediment loading from upstream and tributary sources. The impacts of solids loading on predicted TSS concentrations at TID, Stillwater and Waterford are shown in Figures 3-64 and 3-65. These results indicate a large fraction of the predicted increase in TSS concentration between Fort Edward and Waterford was caused by tributary solids loading, as might be expected. However, sediment loading has minimal impact on erosional depths (Figure 3-66).

Variability in the nine flood hydrographs (Figures 3-51 and 3-53) used to construct the synthetic flood hydrograph introduced uncertainty into the 100-year flood simulation. Uncertainty in the synthetic flood hydrograph can be estimated by calculating 95% confidence intervals about the mean normalized flow rate for each day of the flood and constructing the corresponding high and low flood hydrographs shown in Figures 3-52 and 3-54. The 100-year flood simulation was conducted using both the high and low hydrographs (Table 3-13). Variation

in the hydrograph was found to have minor impacts on total erosion in the TIP, with total erosional mass changing by 1% or less. The high flood hydrograph caused net erosion changes of –17 and +25% in the cohesive and non-cohesive bed areas, respectively. This hydrograph caused more resuspension from the non-cohesive bed, which provided additional suspended sediment that was transported downstream and re-deposited in depositional areas of the cohesive bed (causing a decrease in net erosion). Conversely, the low flood hydrograph produced 16% less non-cohesive bed erosion, which caused a 13% increase in net erosion from the cohesive bed of the TIP because less eroded sediment was available for re-deposition at downstream locations.

The simulations presented above used the numerical grids shown in Figures 2-1 to 2-8. These numerical grids assume that the flow is confined to the main channel of the river and overbank flow is not simulated during a major flood. The river will overflow its banks during a major flood and flow onto the flood plains adjacent to the main channel. Current velocity distributions, and bottom shear stress distributions, in the river will be affected when flow occurs in the flood plains during the 100-year flood. This occurrence may also affect sediment transport processes in the river.

The impacts of flood plain inundation on sediment transport processes in the TIP during the 100-year flood were investigated using a modified numerical grid. This grid extended from the main channel into the flood plains along the east and west shores of the TIP (Figure 3-67). Topography in the flood plain grid cells was determined from flood plain topography information utilized in the USEPA hydrodynamic model that was applied to the TIP for calculating 100-year flood scour depths (M. Erickson, *personal communication 1998*).

Vegetation can significantly affect flow in the flood plains due to an increased effective bottom roughness, $z_{o,fp}$ (Darby and Thorne 1996). A formulation was developed by Darby and Thorne (1996) that estimates the effective bottom roughness for a vegetated flood plain ($z_{o,fp}$ in meters):

$$z_{o,fp} = 1.3 H_{veg}^{-0.59} \left(\frac{mei}{\tau_b} \right)^{0.40} \qquad (3\text{-}22)$$

where:

H_{veg}	=	vegetation height (m)
mei	=	vegetation stiffness
τ_b	=	bottom shear stress (dynes/cm^2)

It has been assumed in this simulation that the100-year flood occurred during the early spring and the flood plain was covered with dead/dormant grass, for which:

$$mei = 25.4\ H_{veg}^{2.26} \tag{3-23}$$

Calculation of $z_{o,fp}$ in Equation (3-22) required an estimation of τ_b to avoid having to solve for $z_{o,fp}$ iteratively. In the simulation, τ_b calculated at the previous timestep was used to determine $z_{o,fp}$ in a flood plain grid cell.

For the 100-year flood simulation with flood plains, it was assumed that all flood plain grid cells were vegetated and H_{veg} was set equal to 0.1 m. The assumption was also made that no erosion occurred in the flood plains; only deposition was allowed in the flood plain grid cells. Thus, inclusion of flood plains in the 100-year flood simulation will not only affect TIP hydrodynamics, but also serve as a way to increase the trapping efficiency of the TIP.

The hydrodynamic model, using the flood plain numerical grid, predicted that overbank flow began in a few small areas in the TIP between 25,000 and 30,000 cfs. However, significant overbank flow in the TIP was initiated between 30,000 and 35,000 cfs. These results are qualitatively consistent with anecdotal evidence concerning flood plain activity in the TIP.

The primary impact of allowing overbank flow during the 100-year flood simulation was to significantly reduce erosion in the main channel of the TIP. This reduction was due to overbank flow creating lower current velocities, and τ_b, in the main channel. The model predicted that the total net mass of sediment eroded from the main channel was 69% lower, with respect to the original run, with the inclusion of flood plains (Table 3-13). Mean erosional

depths in the cohesive and non-cohesive bed areas of the main channel were 0.37 and 0.019 cm, respectively, which correspond to 55 and 86% reductions when compared to the non-flood plain simulation. Maximum erosional depths were about 5 and 2 cm in the cohesive and non-cohesive bed, respectively. Thus, the original calculation, which neglected flood plain effects, produced conservative results; inclusion of flood plain effects in a 100-year flood simulation, which is more realistic, reduced net erosion from the TIP.

3.5.5 Summary

The 100-year flood results indicated that relatively minor erosion, in both cohesive and non-cohesive bed areas, will occur in the TIP, with mean erosion depths of less than 1 cm and maximum scour depths of about 9 cm. The present TIP results for this flood were of the same order of magnitude as predictions made by Zimmie (1985) for a similar high flow event. Comparison of the 100-year flood to historical flood results, i.e., 1993, 1994 and 1997 floods, showed that simulation of this rare flood event is not an extreme extrapolation from the calibration and validation simulations. Therefore, the 100-year flood results can be considered realistic and a valid extrapolation beyond calibration and validation conditions. Sensitivity analyses indicated that uncertainty in the 100-year projections, due to parameter and boundary condition variation, is less than 82%, with variation in the bed armoring constant (B) causing the greatest uncertainty. Inclusion of flood plain effects caused a significant decrease in TIP erosion, due to lower velocities in the main channel when the river goes overbank. Thus, the 100-year flood simulation, with flood plains being ignored, produced conservative results and should be viewed as an upper bound calculation.

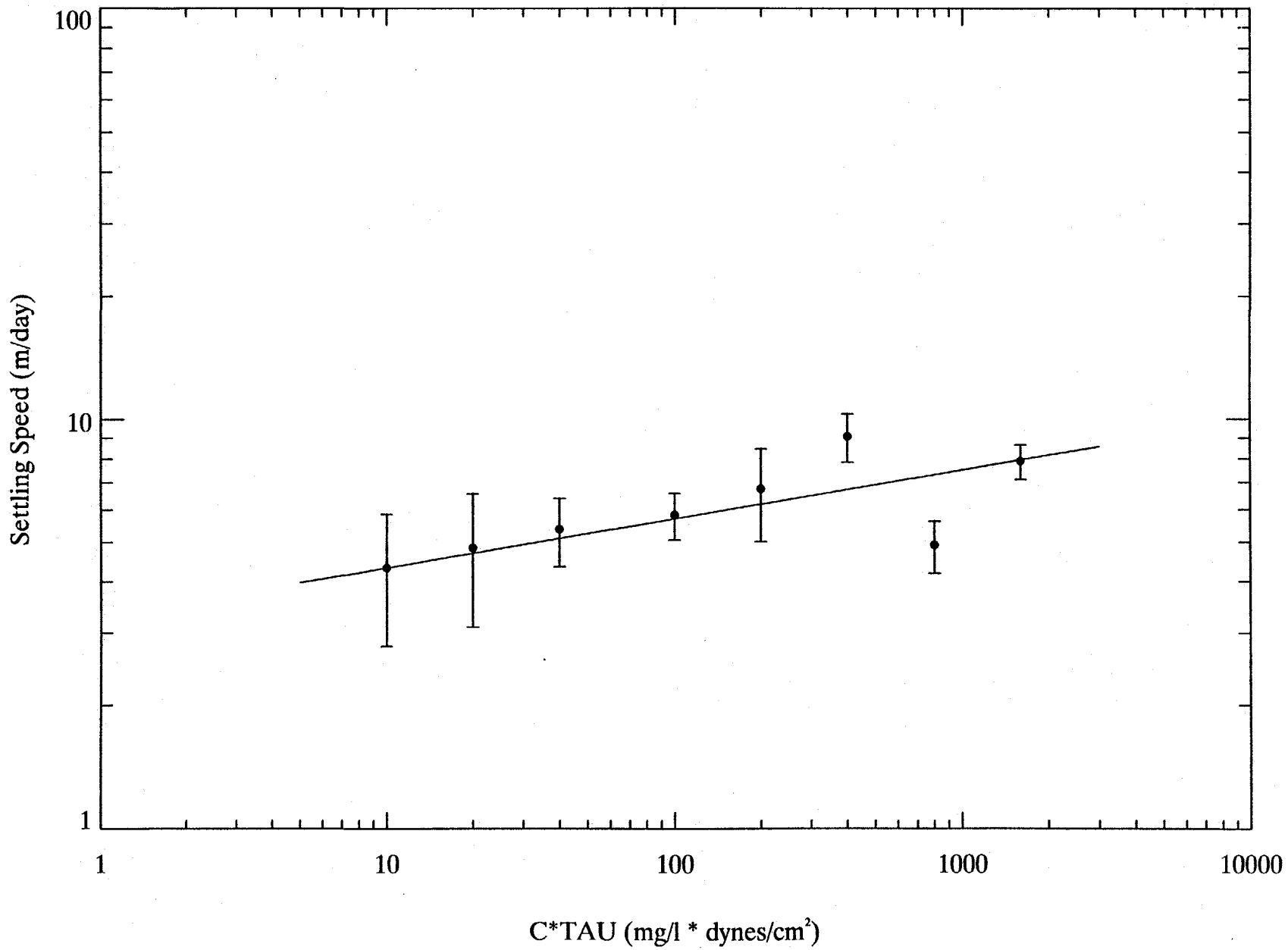

Figure 3-1. Settling speed function for cohesive (class 1) sediments (solid line) and floc settling speed data (mean +/- 95% confidence interval, Burban et al., 1990) used to construct function.

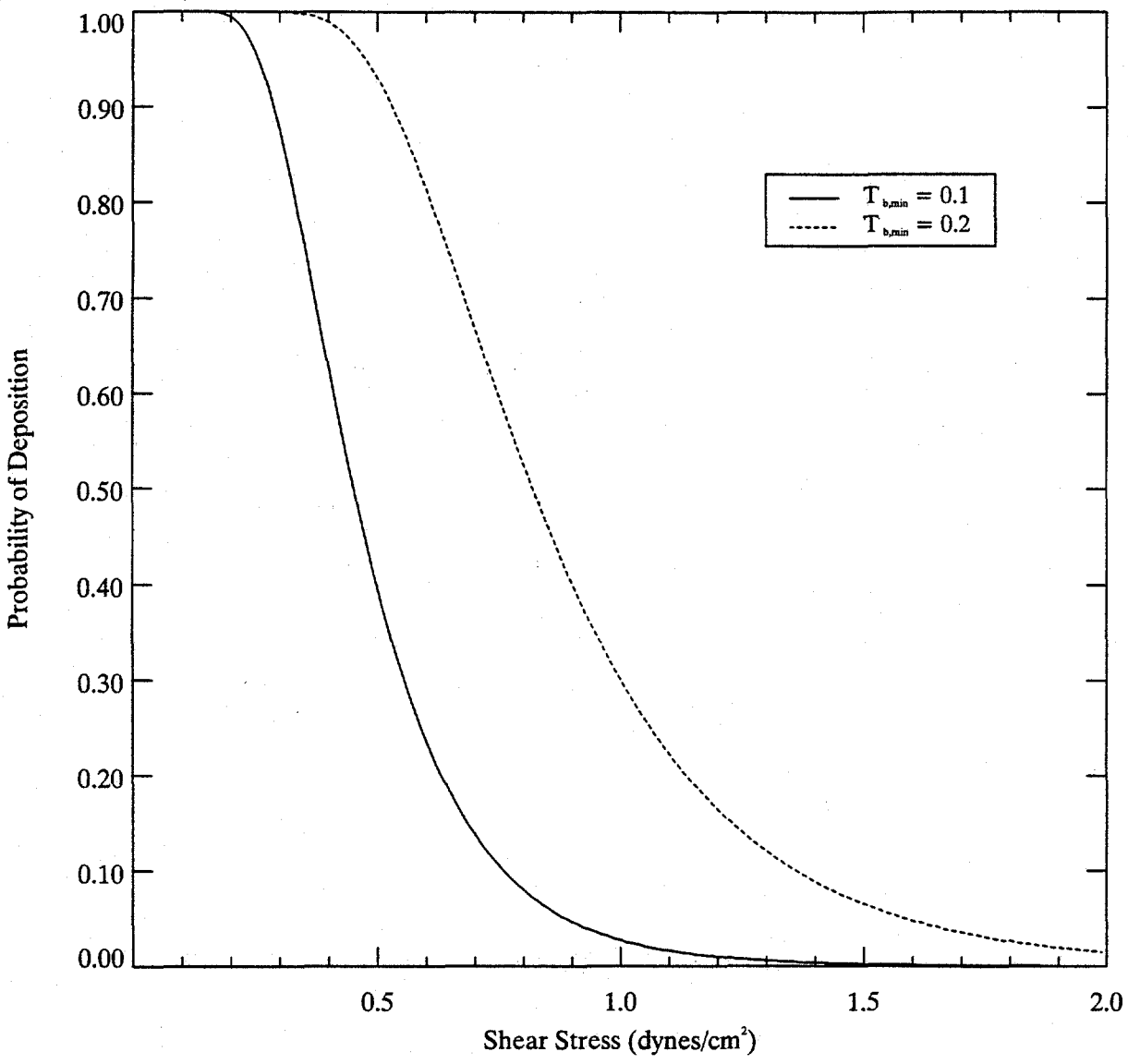

Figure 3-2. Probability of deposition function for cohesive (class 1) sediments. $T_{b,min}$ has units of dynes/cm^2.

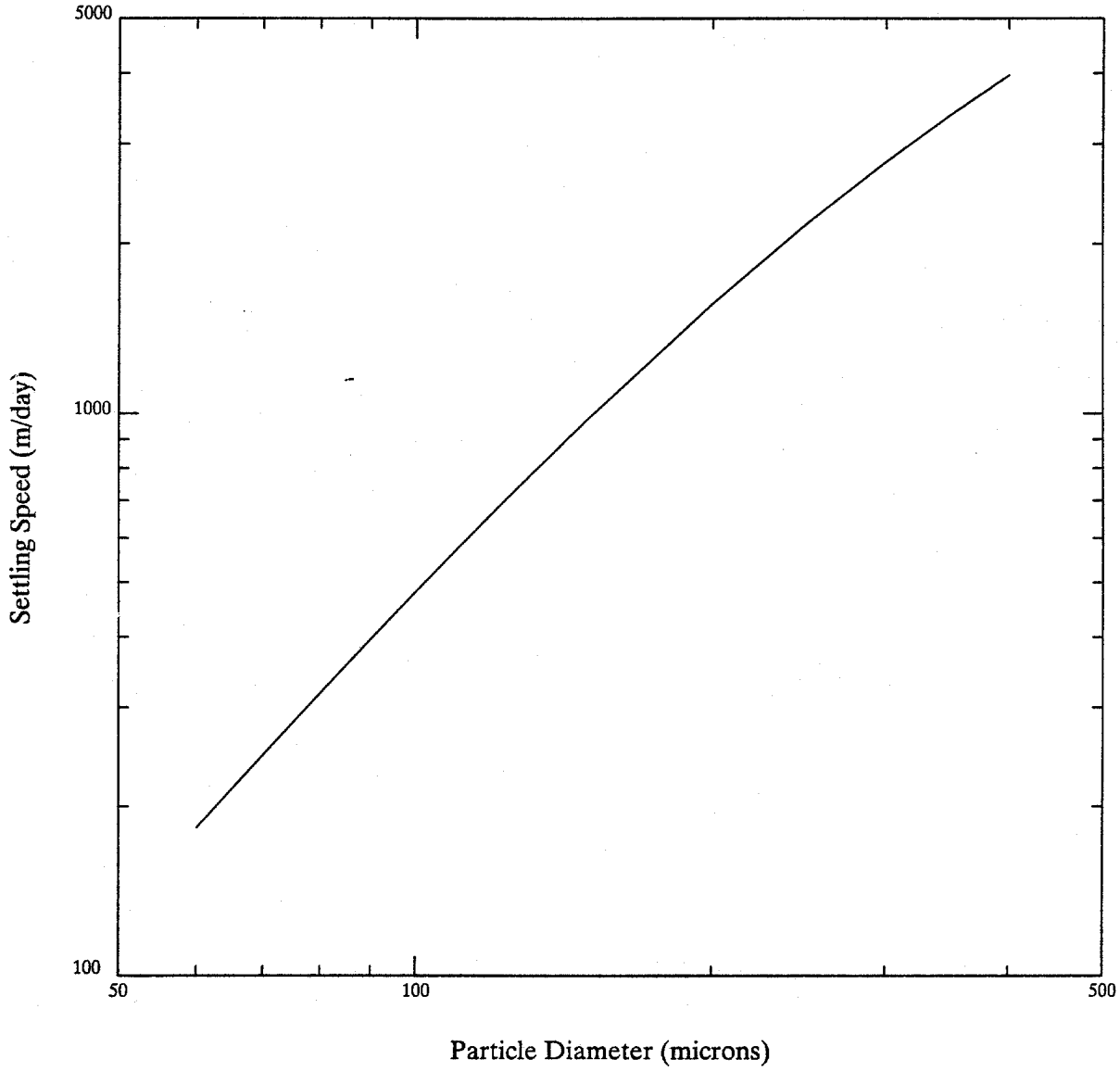

Figure 3-3. Settling speed of sand particles (class 2) as a function of particle diameter (Cheng, 1997).

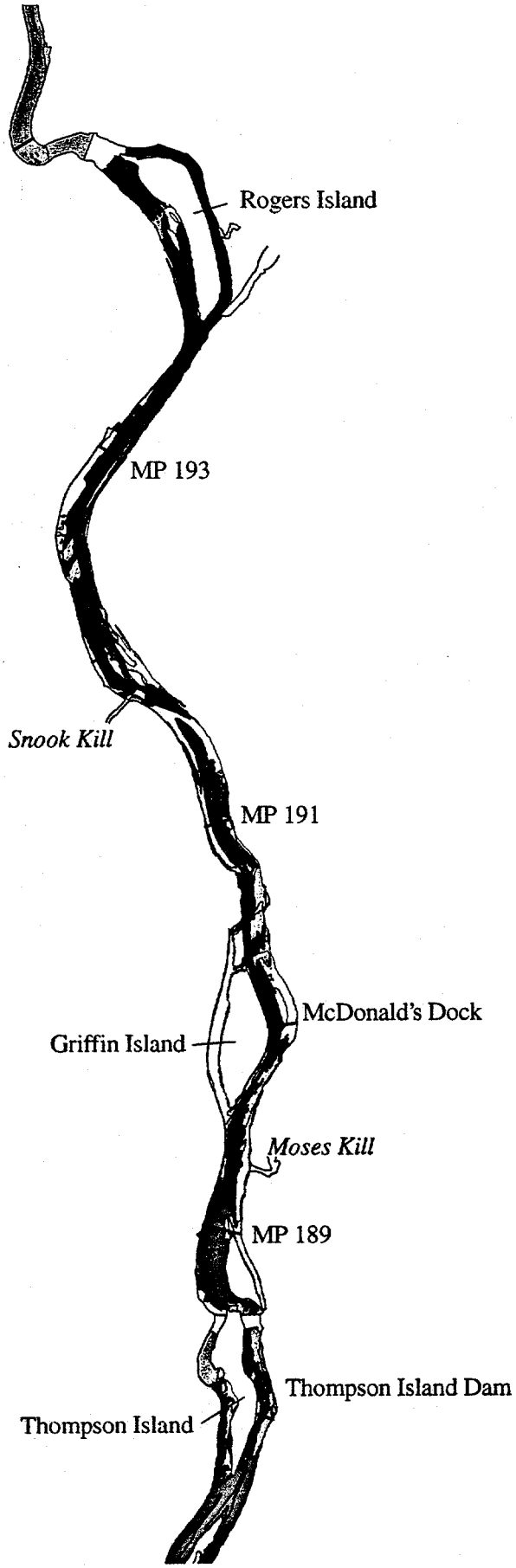

LOCATION MAP OF THE HUDSON RIVER

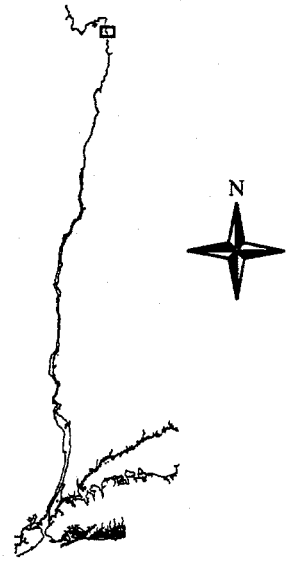

GRAPHIC SCALE

0.4 0 0.4 0.8 Miles

LEGEND

- Shoreline
- Mile Points
- Dams & Locks

Side Scan Sonar

- COARSE
- FINER
- ROCKY

GENERAL ELECTRIC COMPANY
Hudson River Project

PCBs in the Upper Hudson River
Volume 2. A Model of PCB Fate, Transport and Bioaccumulation

Figure 3-4.

Thompson Island Pool bed map based on side scan sonar information.

QEA
Quantitative Environmental Analysis, LLC

Project: GENhud 131 April 1999

313783

\\Poseidon\D_drive\genhud\Documents\Final_report\Vol_2\Section_3\Uhr_sss_fig_3_4.apr

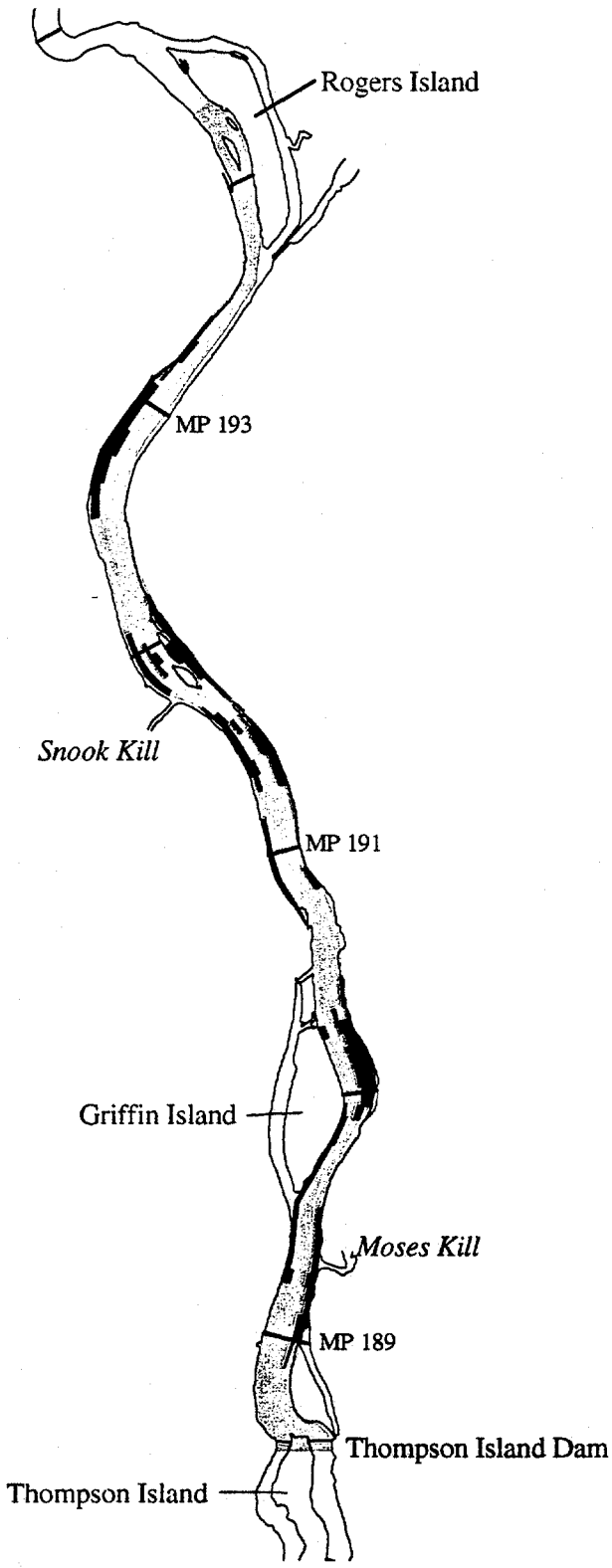

LOCATION MAP OF THE HUDSON RIVER

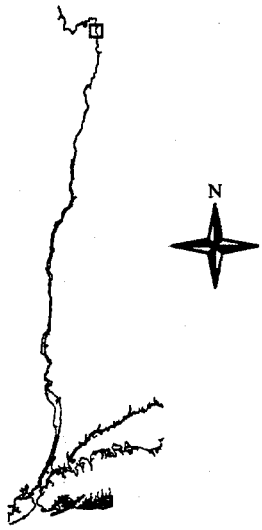

GRAPHIC SCALE

0.3 0 0.3 0.6 Miles

LEGEND

- Shoreline
- Mile Points
- Dams and Locks
- Hard Bottom
- Non-Cohesive
- Cohesive

GENERAL ELECTRIC COMPANY
Hudson River Project

PCBs in the Upper Hudson River
Volume 2. A Model of PCB Fate, Transport and Bioaccumulation

Figure 3-5.

Thompson Island Pool bed map used for model input.

QEA
Quantitative Environmental Analysis, LLC

Project: Genhud 131 April 1999

\\poseidon\d_drive\Genhud\documents\final_report\Vol_2\Section_3\whreach_fig_3_7

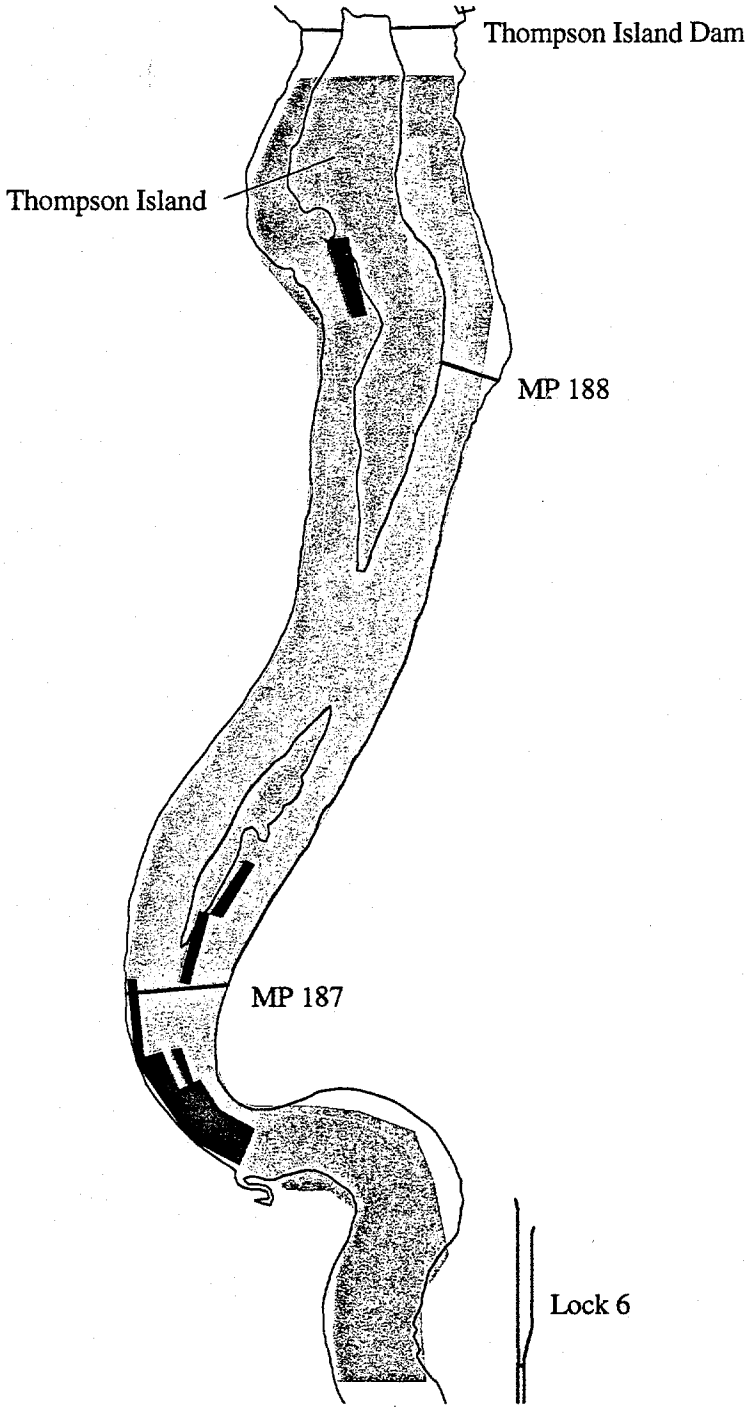

LOCATION MAP OF THE HUDSON RIVER

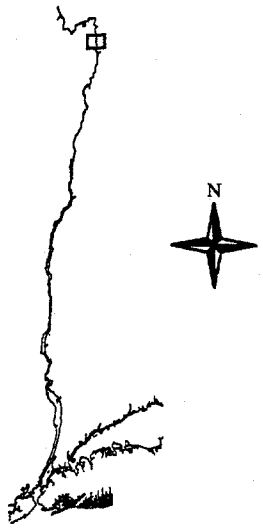

GRAPHIC SCALE

0.1 0 0.1 0.2 Miles

LEGEND

Shoreline
Mile Markers
Dams and Locks
Sediment Bed Map
Hard Bottom
Non-cohesive
Cohesive

GENERAL ELECTRIC COMPANY
Hudson River Project

PCBs in the Upper Hudson River
Volume 2. A Model of PCB Fate, Transport and Bioaccumulation

Figure 3-6.

Reach 7 bed map used for model input.

QEA
Quantitative Environmental Analysis, LLC

Project: Genhud 131 April 1999

313785

\\poseidon\d_drive\Genhud\documents\final_report\Vol_2\Section_3\uhrreach_fig_5_7

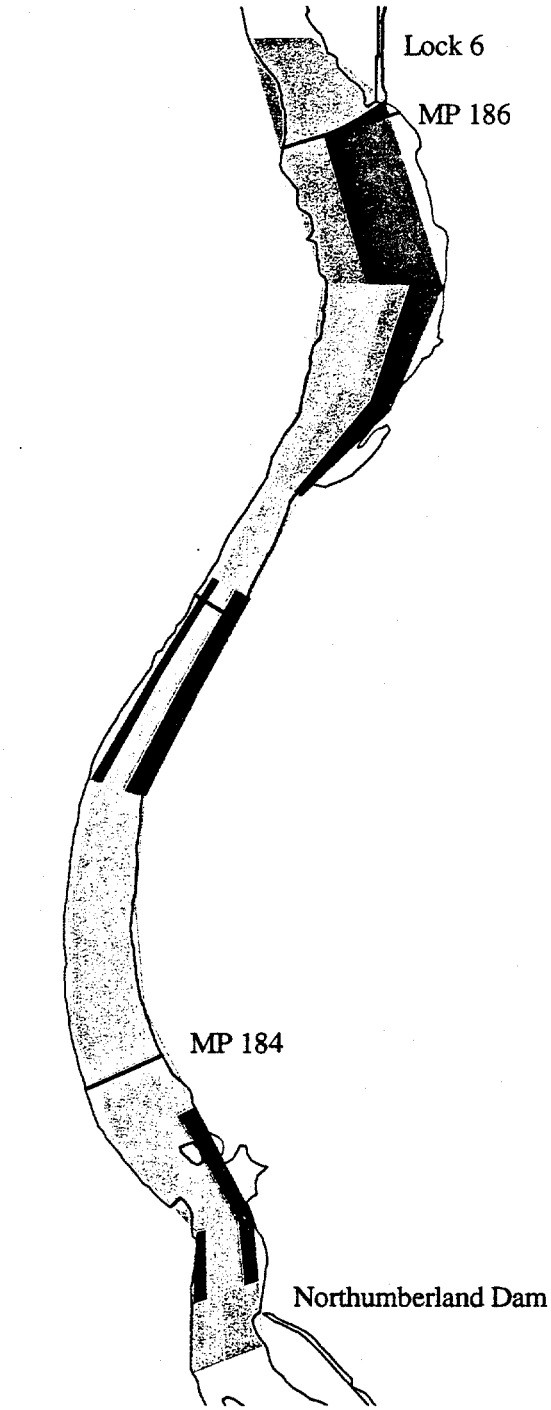

LOCATION MAP OF THE HUDSON RIVER

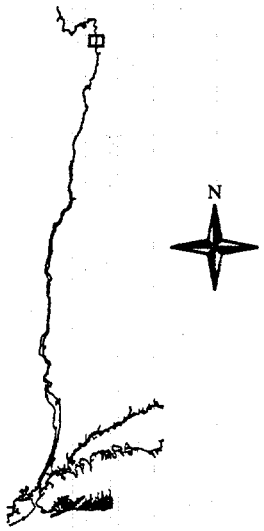

GRAPHIC SCALE

0.2 0 0.2 0.4 Miles

LEGEND

Shoreline
Mile Markers
Dams and Locks
Sediment Bed Map
Hard Bottom
Non-Cohesive
Cohesive

GENERAL ELECTRIC COMPANY
Hudson River Project

PCBs in the Upper Hudson River
Volume 2. A Model of PCB Fate, Transport and Bioaccumulation

Figure 3-7

Reach 6 bed map used for model input.

QEA
Quantitative Environmental Analysis, LLC

Project: Genhud 131 April 1999

\\Poseidon\D_drive\Genhud\Documents\Final_report\vol_2\Section_3\uhrreach_fig_5_to_7

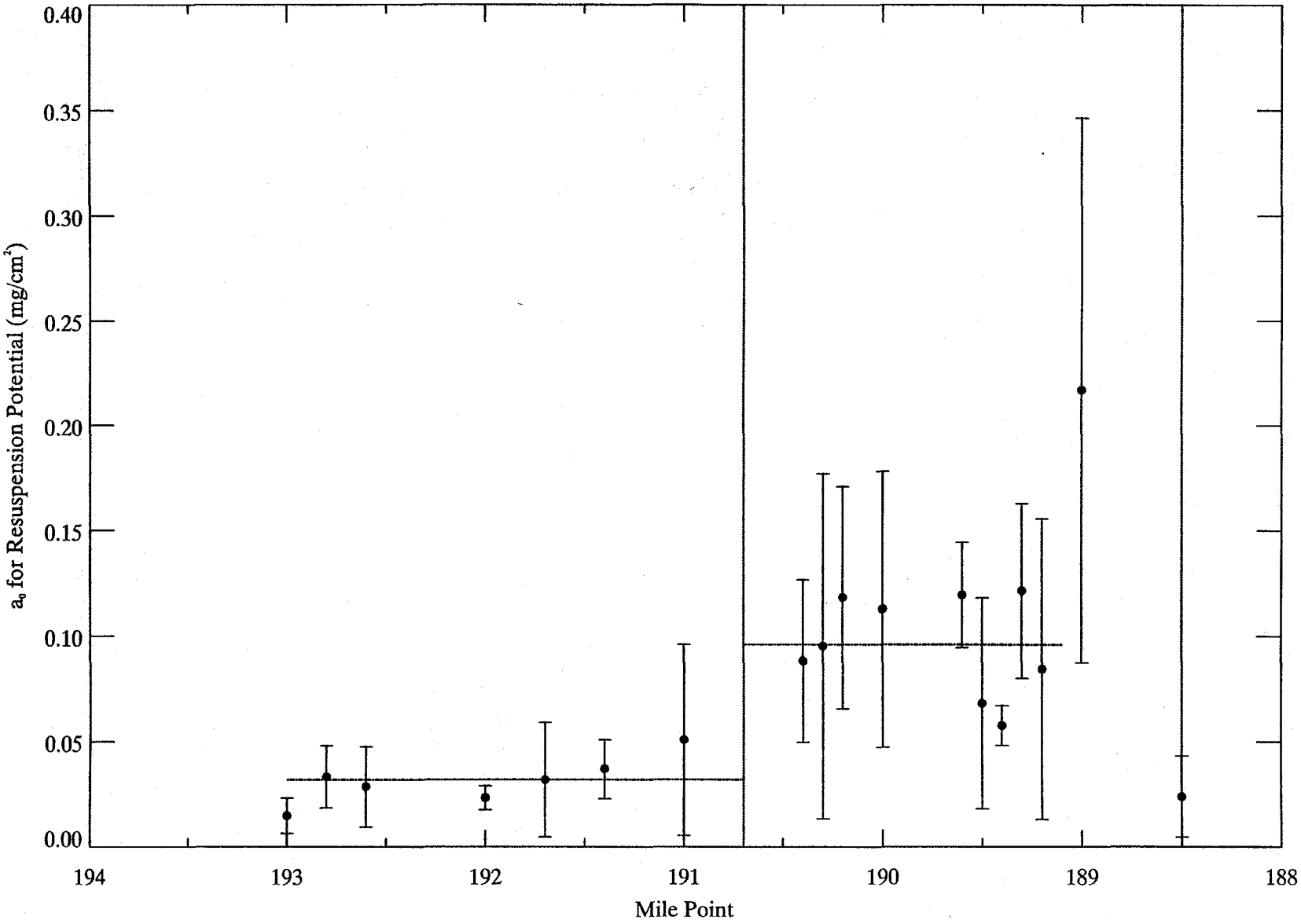

Figure 3-8. Spatial distribution of resuspension potential parameter (a_o) used as model input.
TIP shaker data (mean +/- 95% confidence interval) used to determine model input are also shown.

Poseidon - S:\GENhud\Documents\Final_report\Vol_2\Section_3\a0spat_fig_3_8.pro
Tue Apr 13 11:59:15 1999

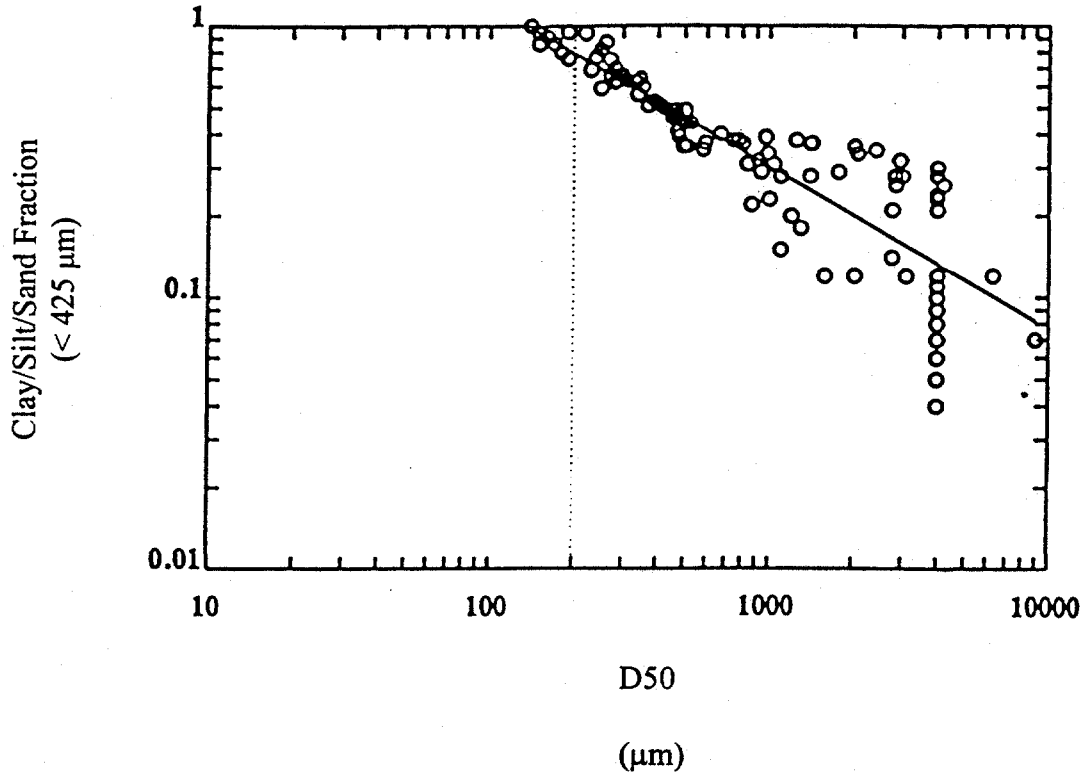

Figure 3-9. Relationship between fraction suspendable sediment ($d_2 < 425$ μm) and median particle diameter (d_{50} in μm) for the non-cohesive sediment bed in the Thompson Island Pool.

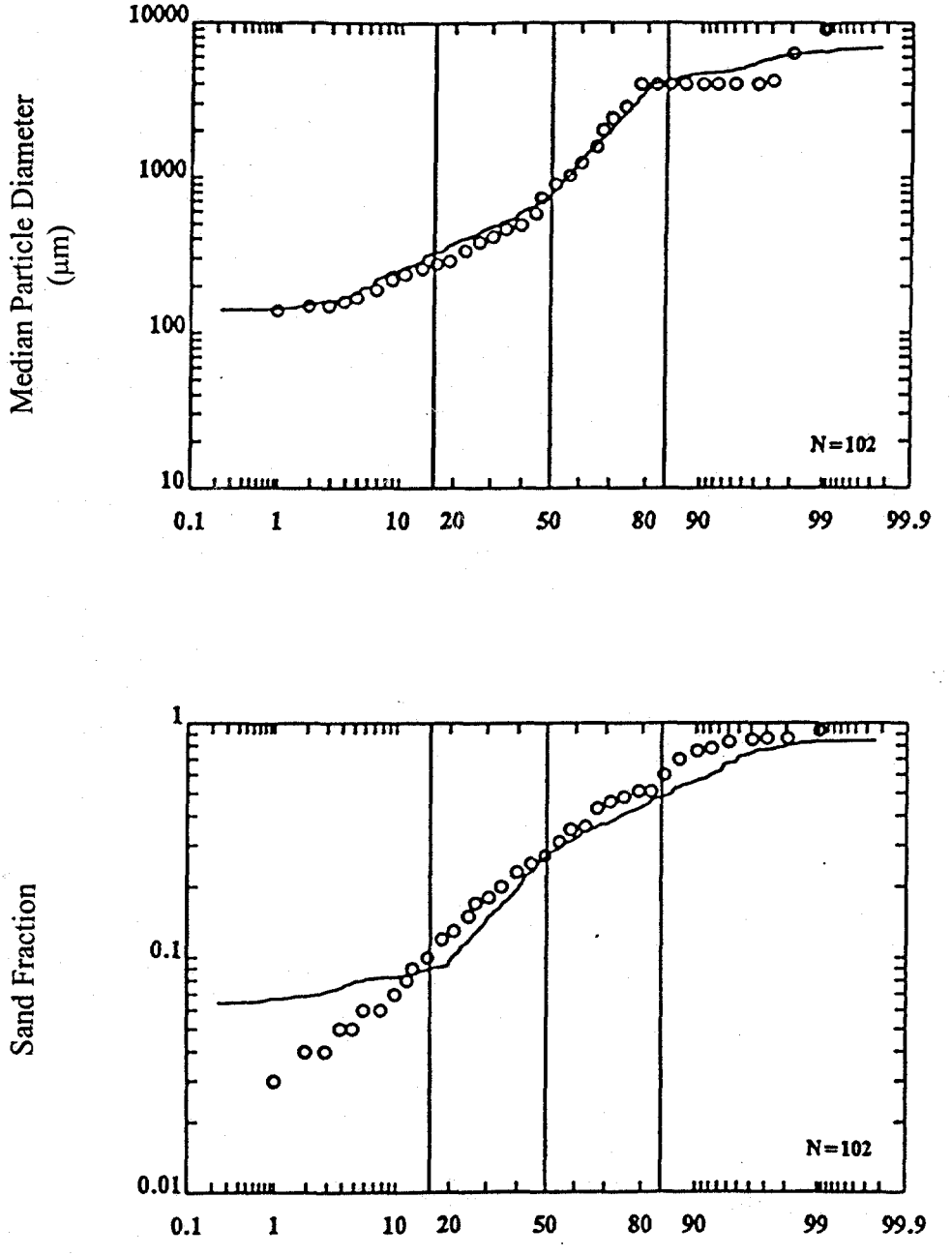

Figure 3-10. Comparison of predicted (solid line) and measured distributions of the median particle diameter (d_{50} in μm) and sand fraction for the non-cohesive sediment bed in the Thompson Island Pool.

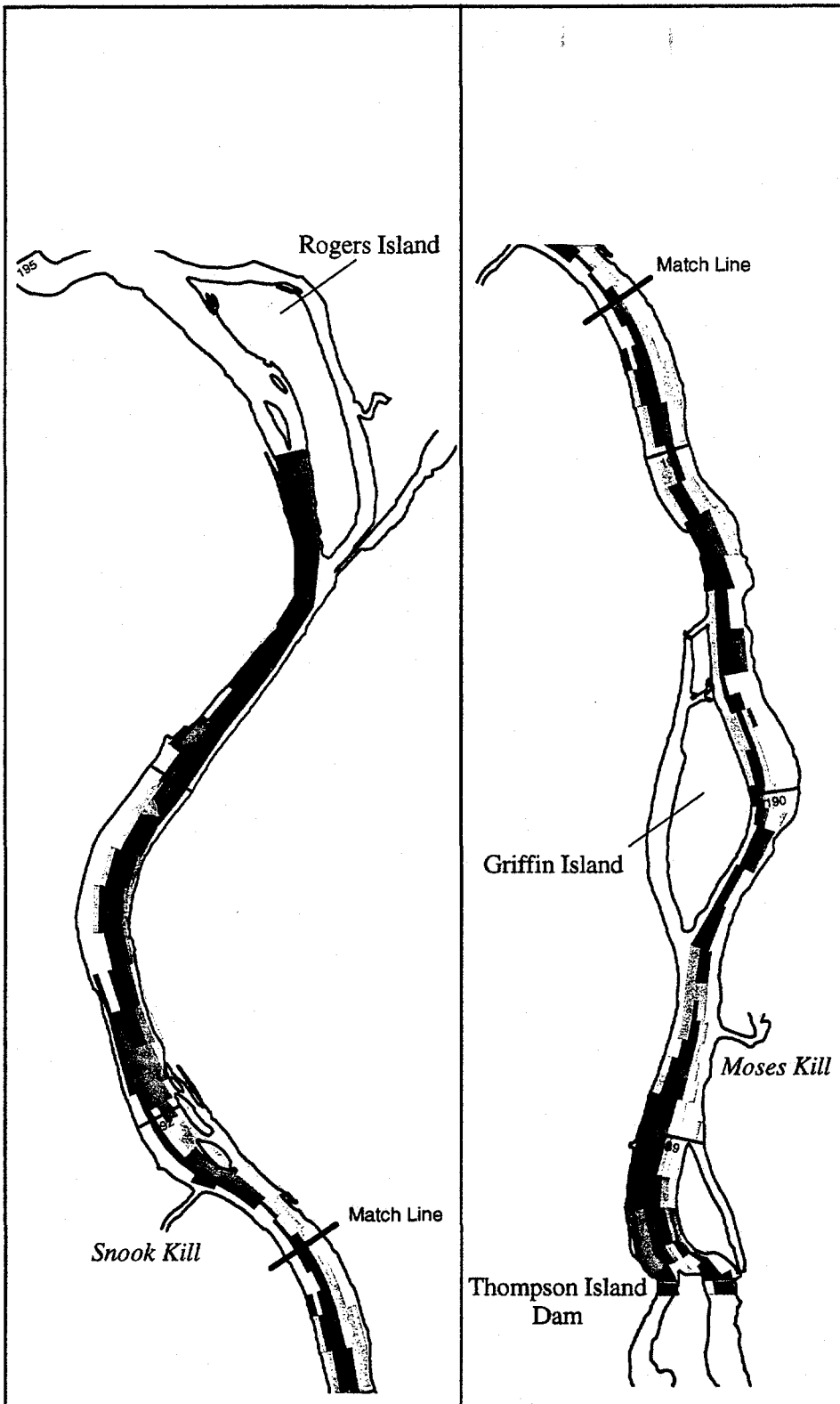

LOCATION MAP OF THE HUDSON RIVER

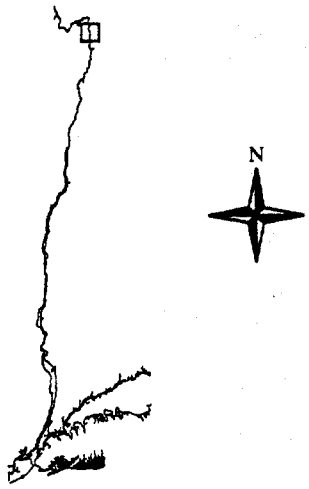

GRAPHIC SCALE

0.2 0 0.2 0.4 Miles

LEGEND

- Shoreline
- Mile Points
- Dams & Locks

Non Cohesive Bed D50

- Fine Sands
- Medium Sands
- Coarse Sand
- Very Coarse Sand
- Gravel

GENERAL ELECTRIC COMPANY
Hudson River Project

PCBs in the Upper Hudson River
Volume 2. A Model of PCB Fate, Transport and Bioaccumulation

Figure 3-11.

Estimated median particle diameter (d50) used as model initial conditions for the non-cohesive sediment bed in the Thompson Island Pool.

QEA
Quantitative Environmental Analysis, LLC

Project: Genhud 131 April 1999

\\Poseidon\D_drive\genhud\documents\final_report\vol_2\section_3\spatial_d50_fig_3_11

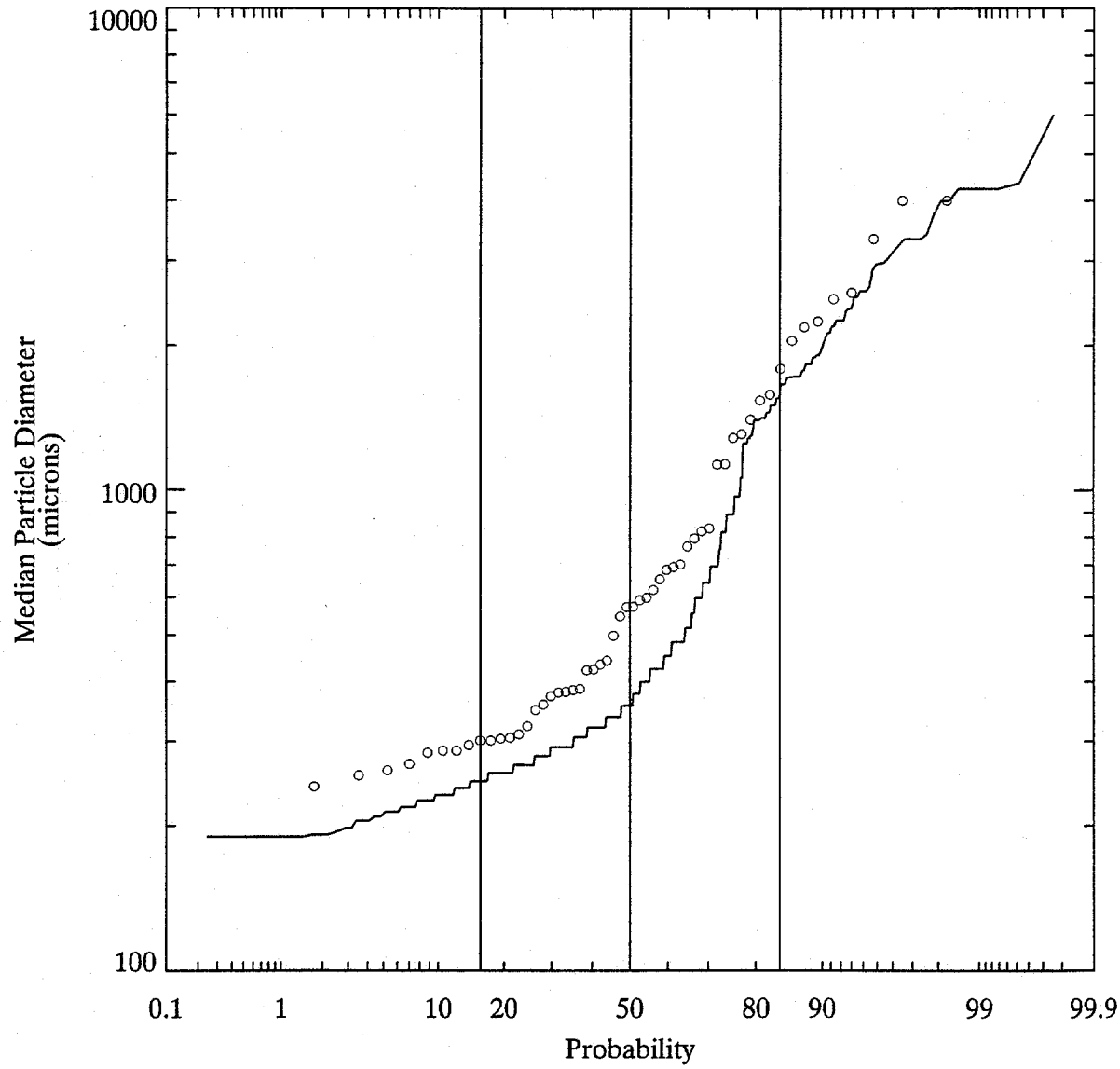

Figure 3-12. Comparison of predicted (solid line) and measured distributions of median particle diameter (d_{50}) for non-cohesive sediment bed in Reaches 1 to 7.

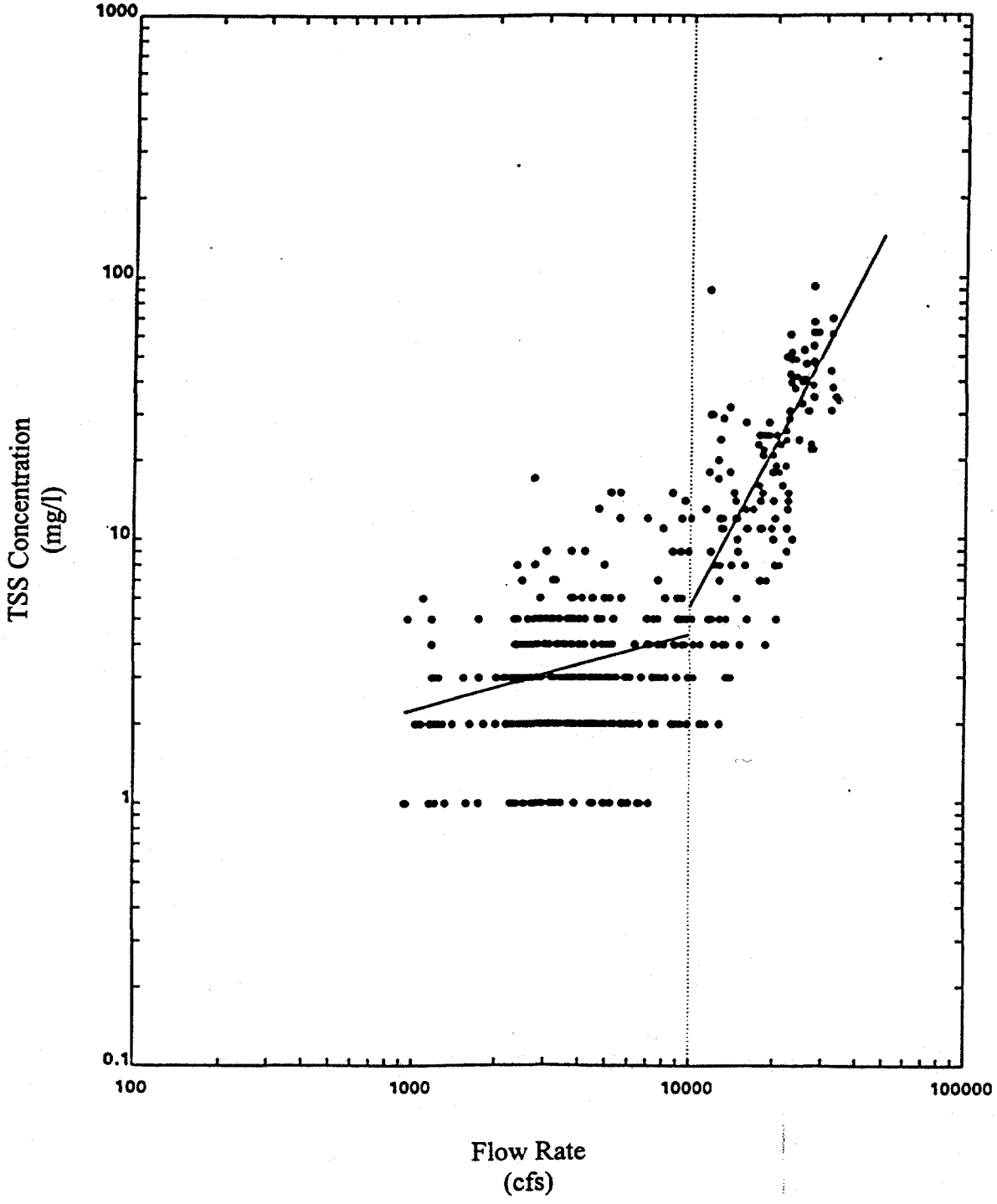

Figure 3-13. Sediment rating curve (solid line) for upstream boundary at Fort Edward.

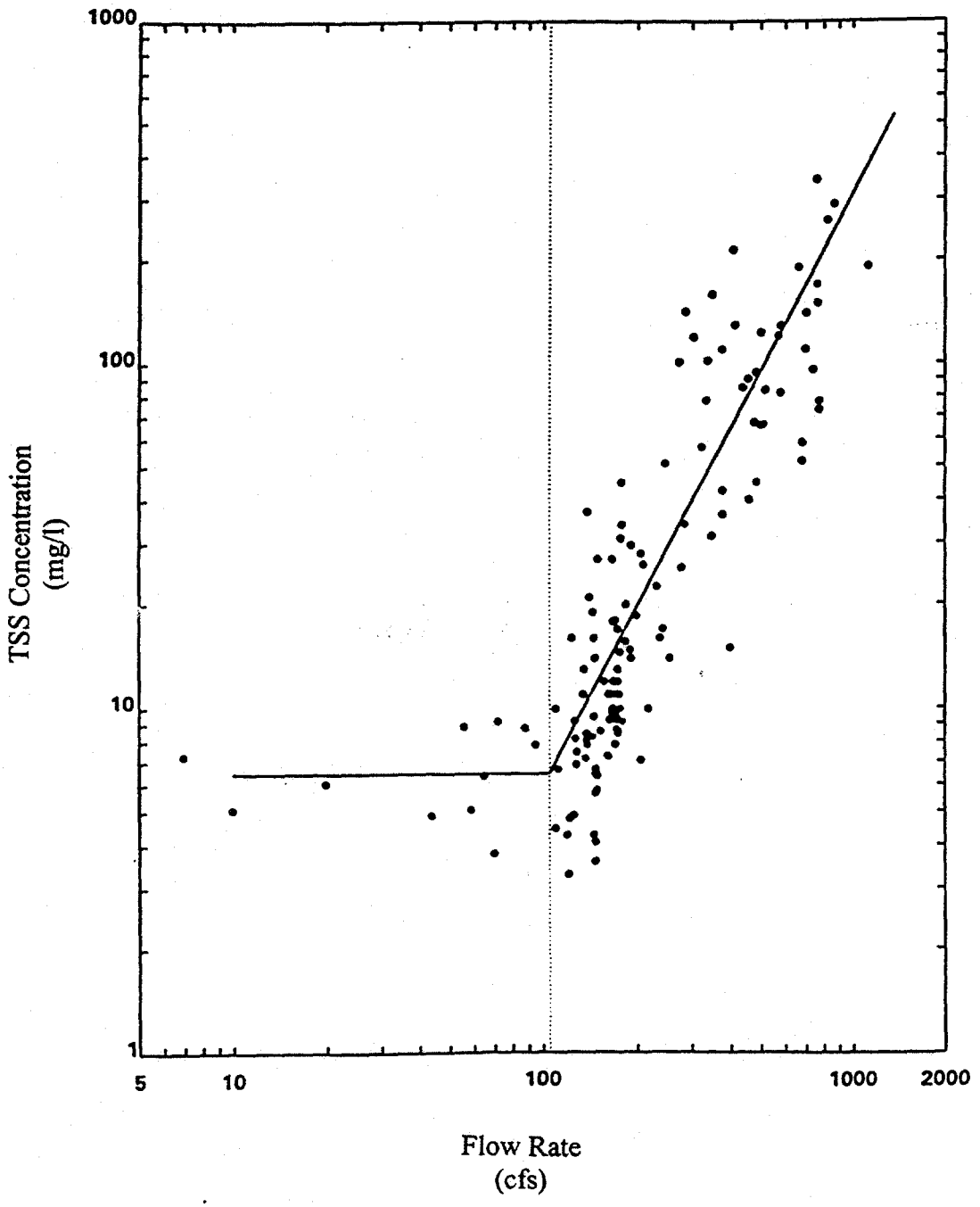

Figure 3-14. Sediment rating curve (solid line) for Snook Kill.

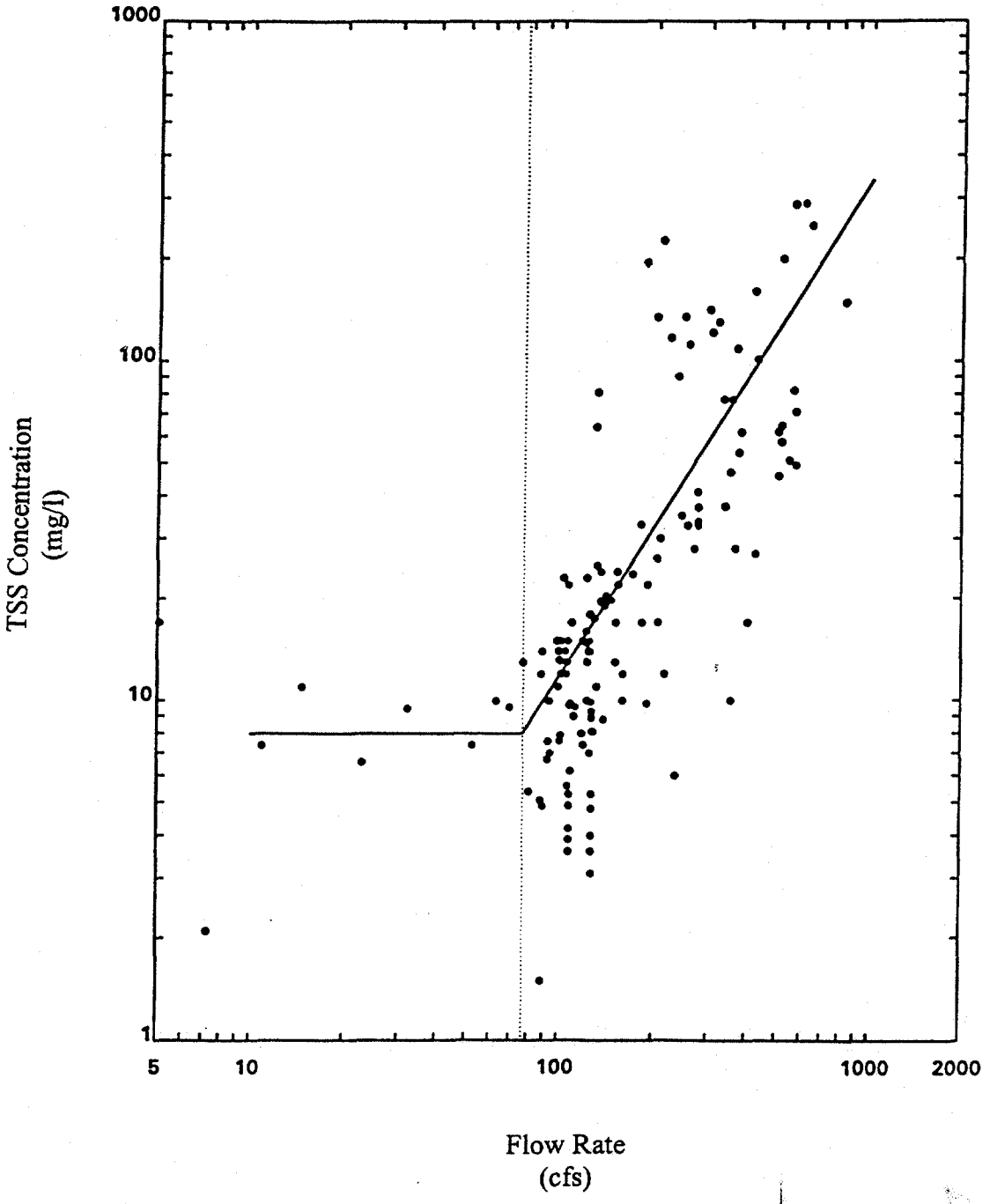

Figure 3-15. Sediment rating curve (solid line) for Moses Kill.

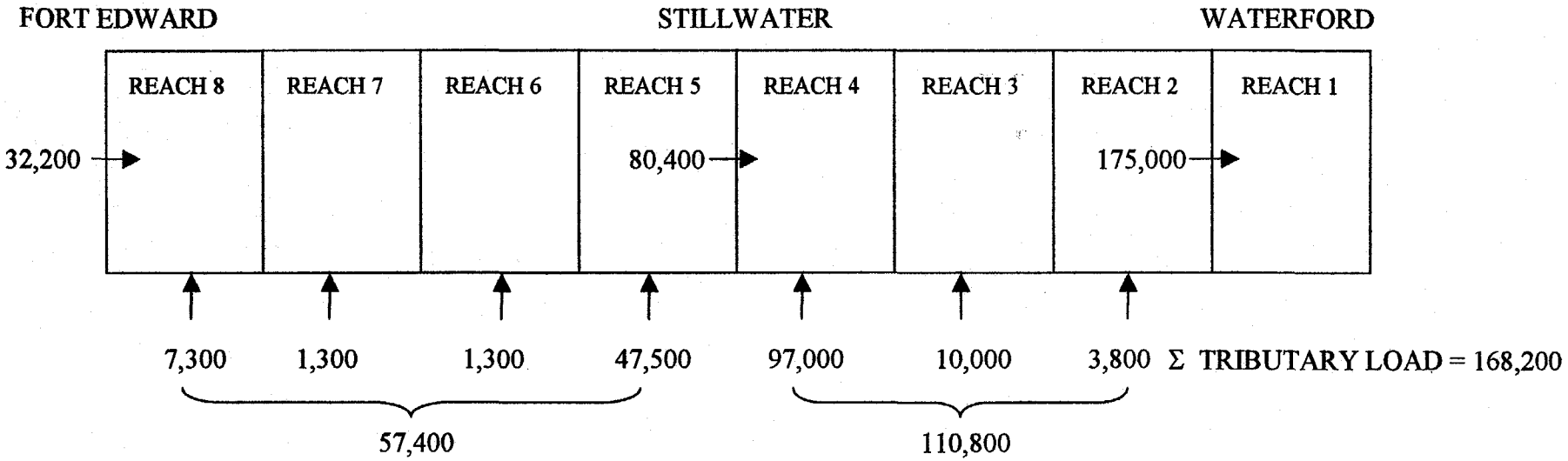

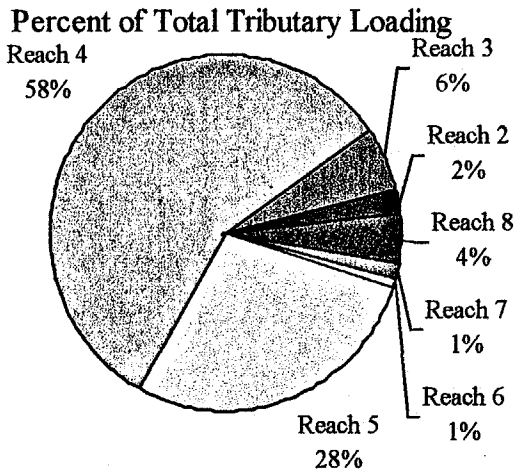

3-16. Sediment mass balance and estimated tributary loading for the UHR (March 1977 through June 1992 period). Sediment loadings are in MT.

\\Poseidon\D_Drive\GENhud\Documents\Final_report\Vol_2\Section_3\SOLIDS_MB_fig_3_16.ppt

4/14/99

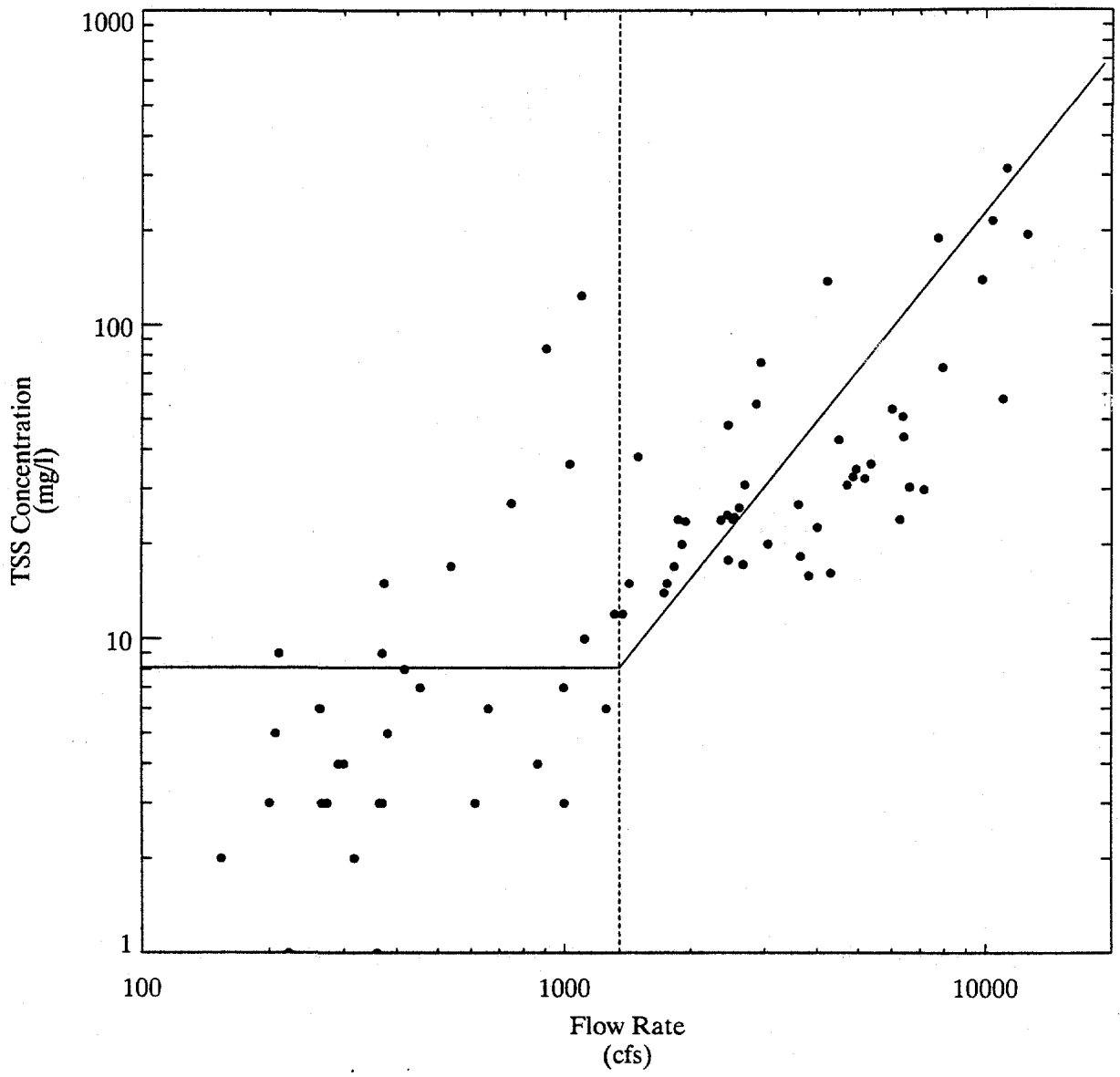

Figure 3-17. Comparison of Hoosic River rating curve (solid line), developed from sediment loading analysis, to TSS concentration data collected at Eagle Bridge gauging station on the Hoosic.

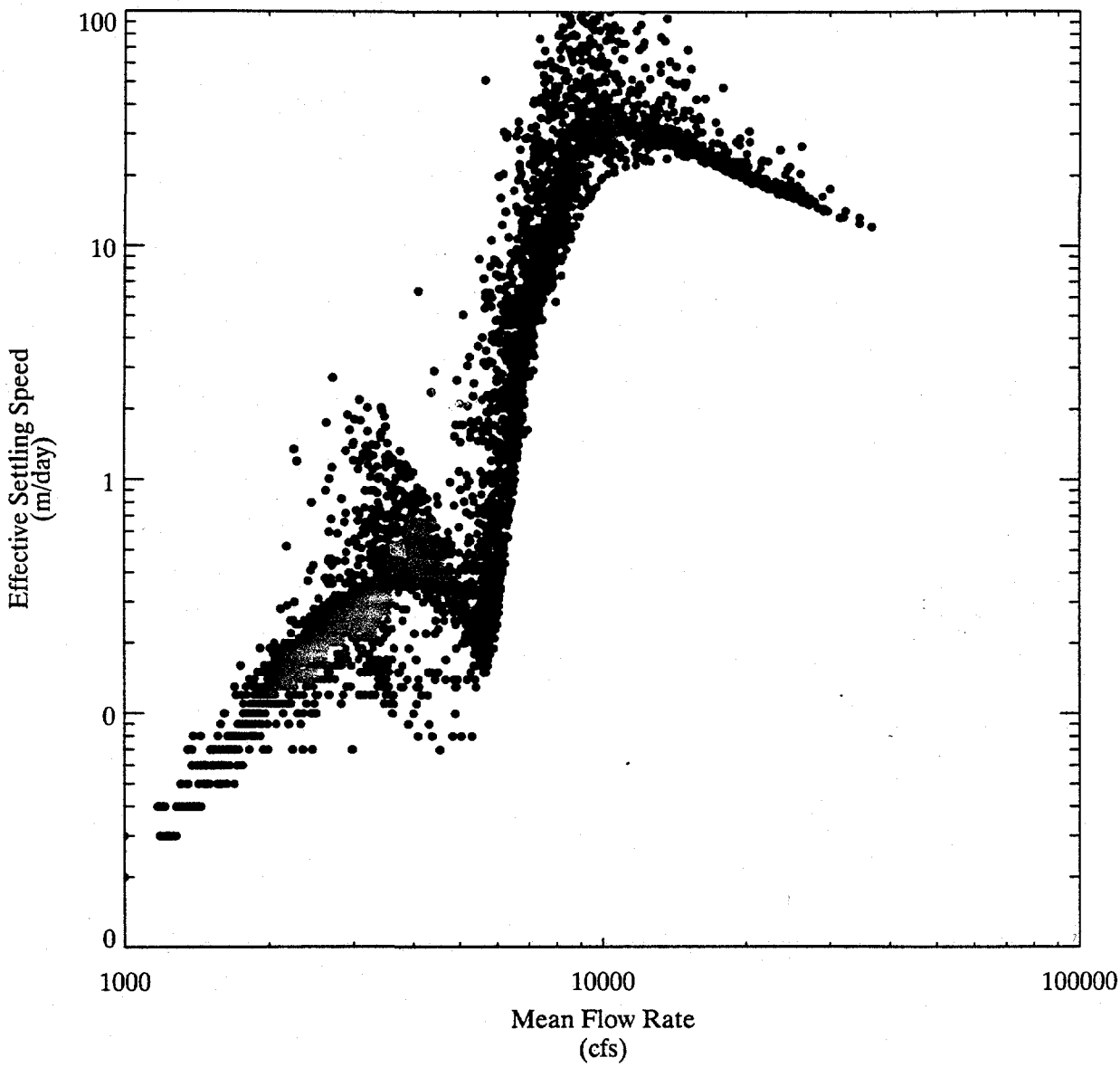

Figure 3-18. Relationship between effective settling speed and flow rate for the cohesive bed in a one-dimensional model grid element in the vicinity of Snook Kill.

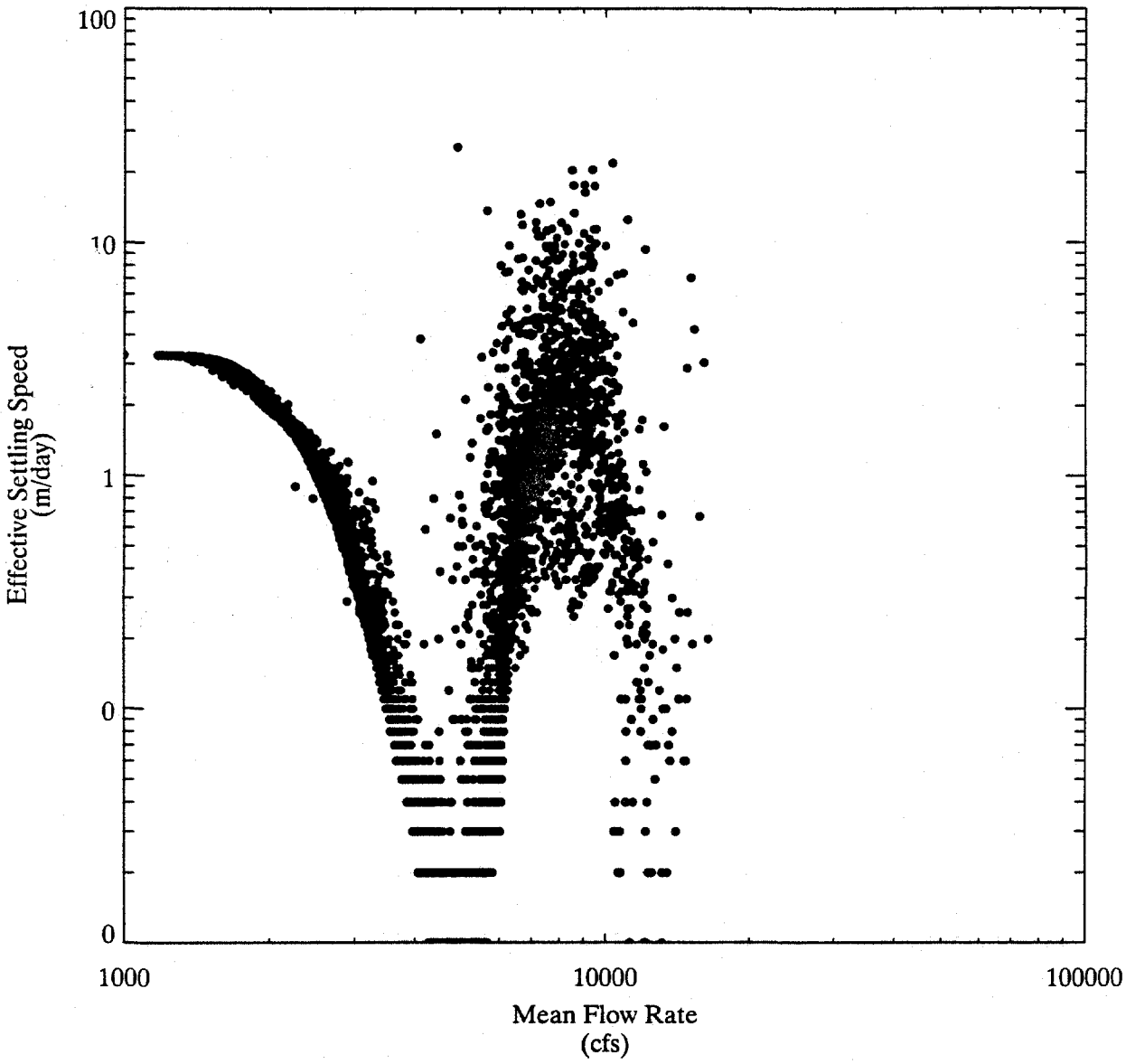

Figure 3-19. Relationship between effective settling speed and flow rate for the non-cohesive bed in a one-dimensional model grid element in the vicinity of Snook Kill.

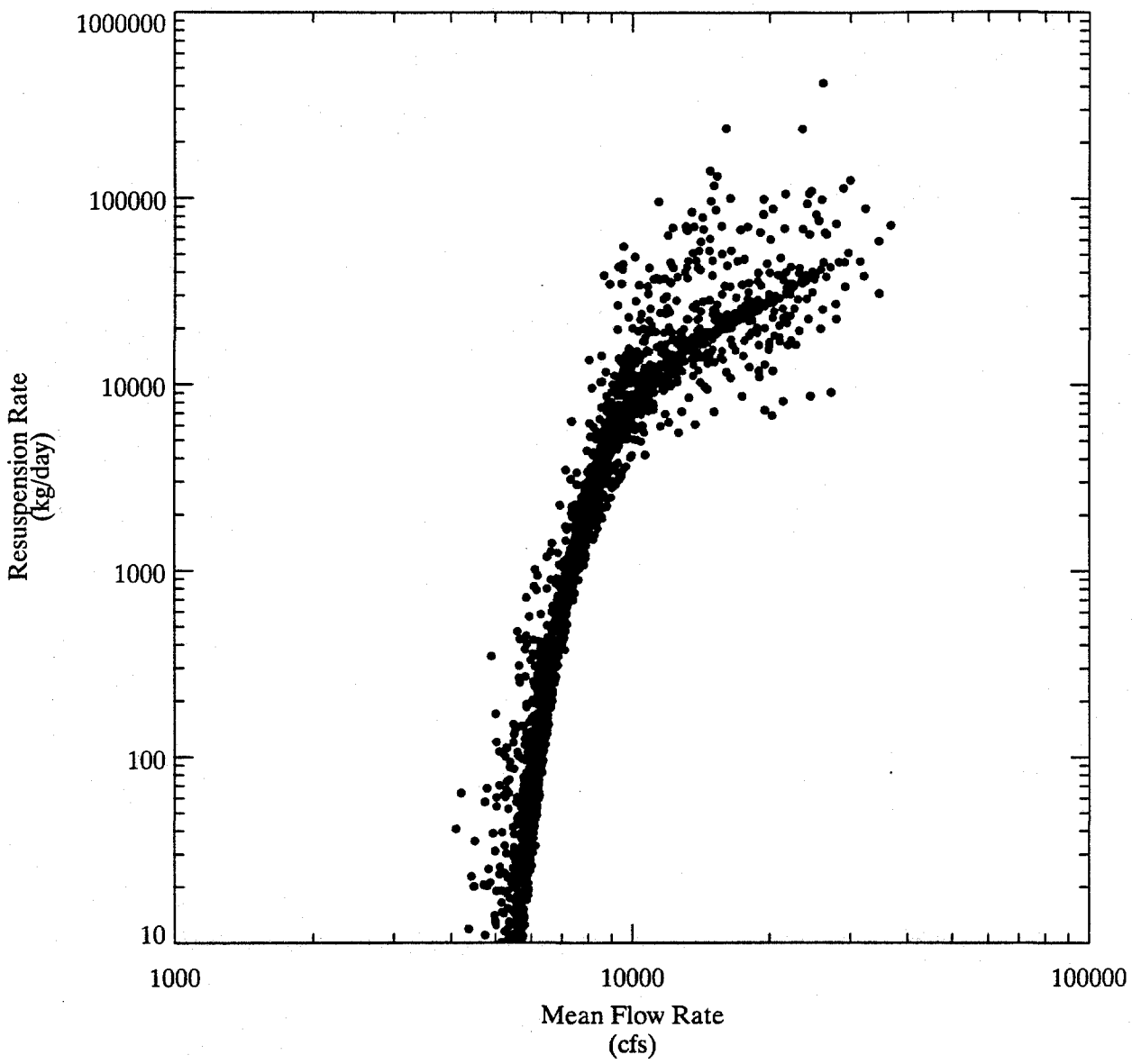

Figure 3-20. Relationship between resuspension rate and flow rate for the cohesive bed in a one-dimensional model grid element in the vicinity of Snook Kill.

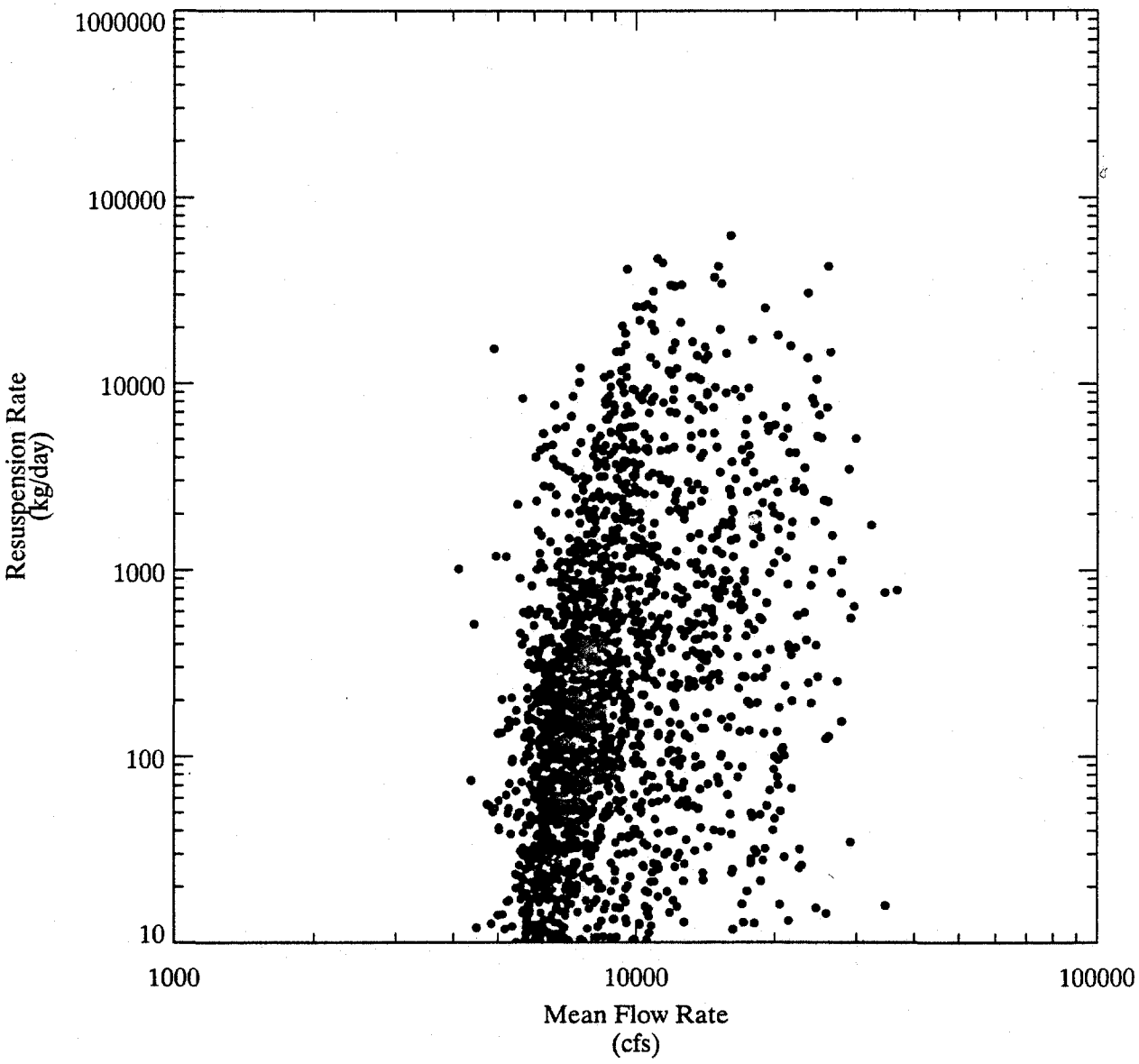

Figure 3-21. Relationship between resuspension rate and flow rate for the non-cohesive bed in a one-dimensional model grid element in the vicinity of Snook Kill.

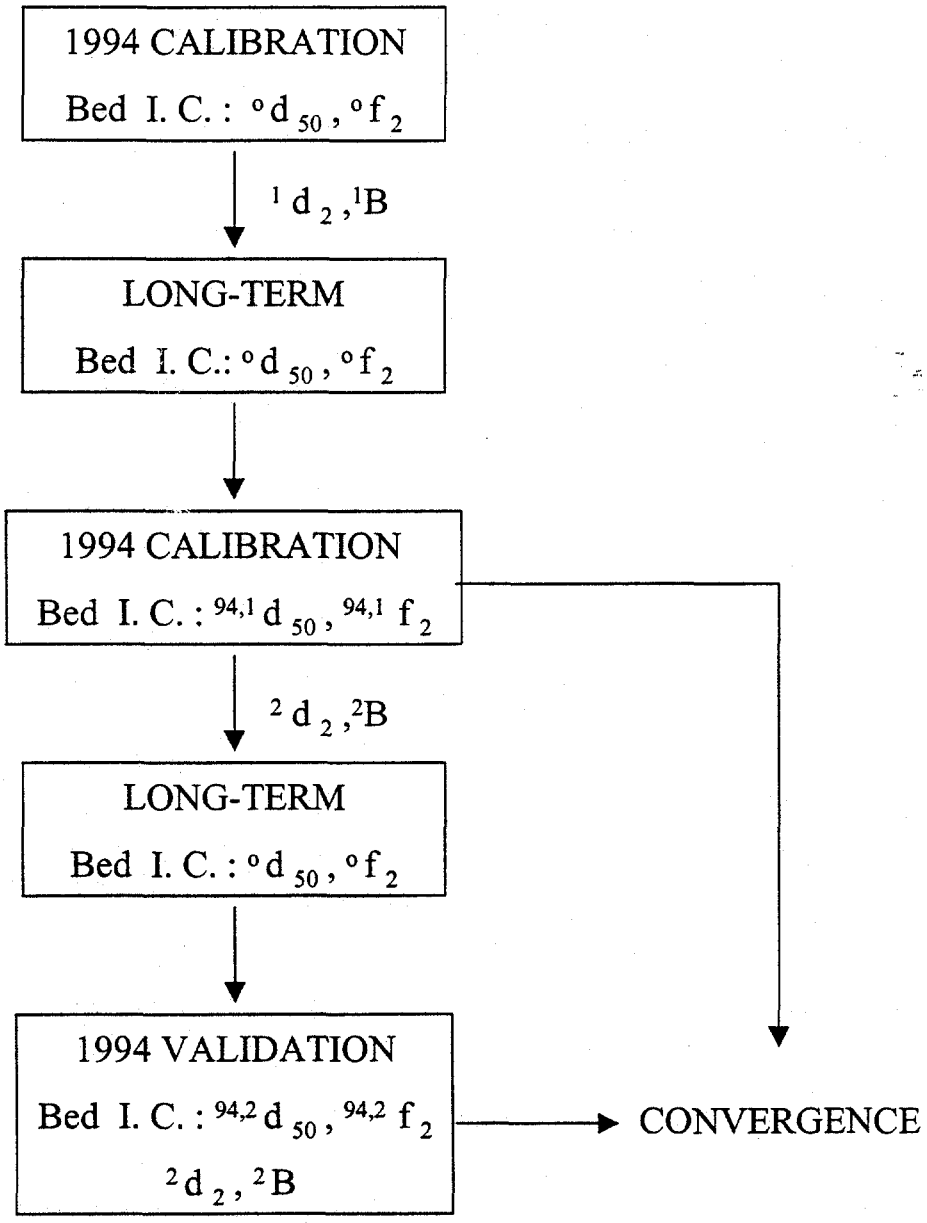

Figure 3-22. Schematic of iterative procedure used to calibrate model.

\\Poseidon\D_Drive\GENhud\Documents\Final_report\Vol_2\Section_3\flwchrt_fig_3_22.ppt

4/14/99

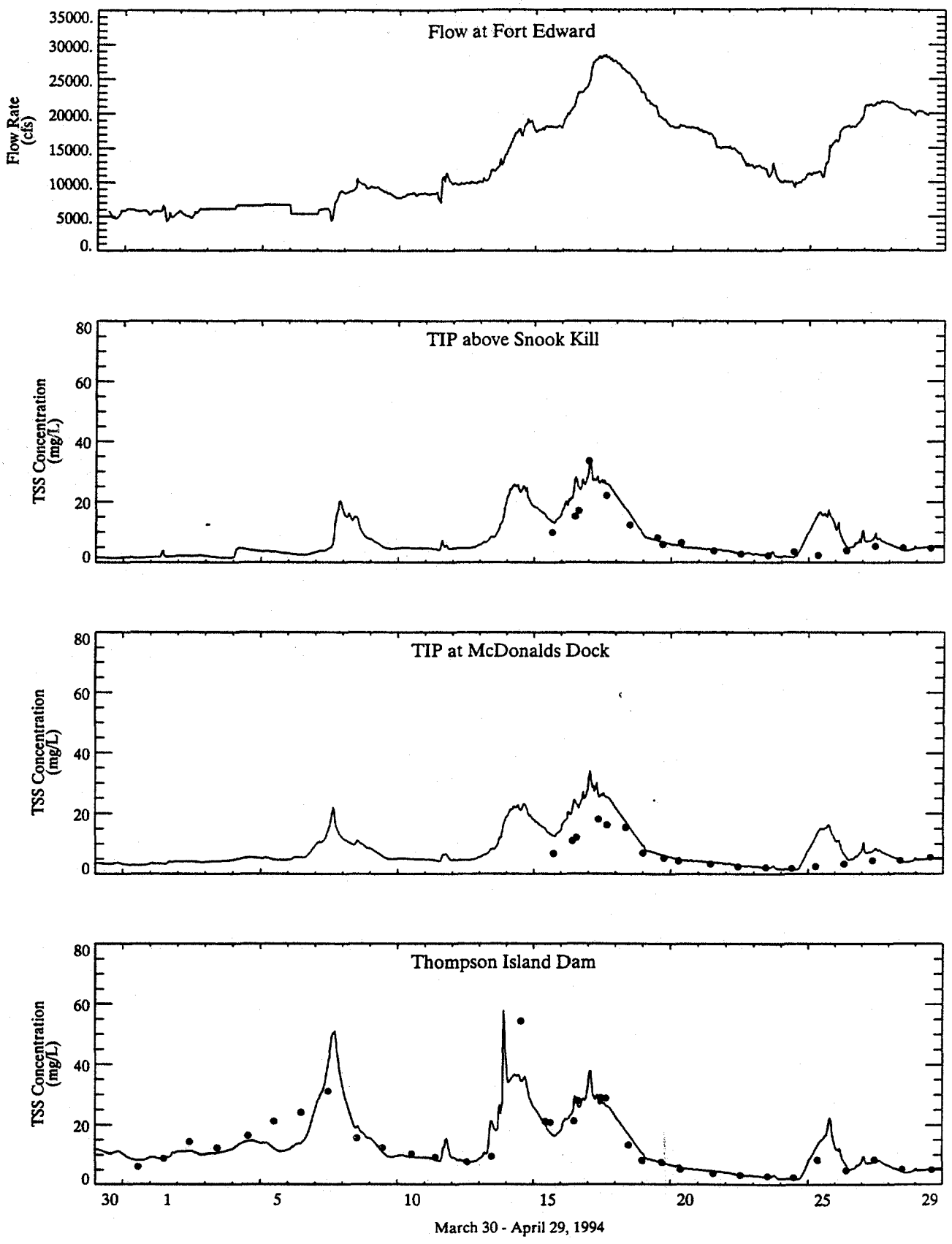

Figure 3-23. Comparison of predicted (line) and measured (symbols) suspended sediment concentrations at three locations in the TIP during the 1994 flood. Top panel shows measured flow at Fort Edward.

Poseidon - S:\GENhud\Documents\Final_report\Vol_2\Section_3\tsr_plot_Flood94_long_fig_3_23.pro
Fri Apr 30 10:22:05 1999

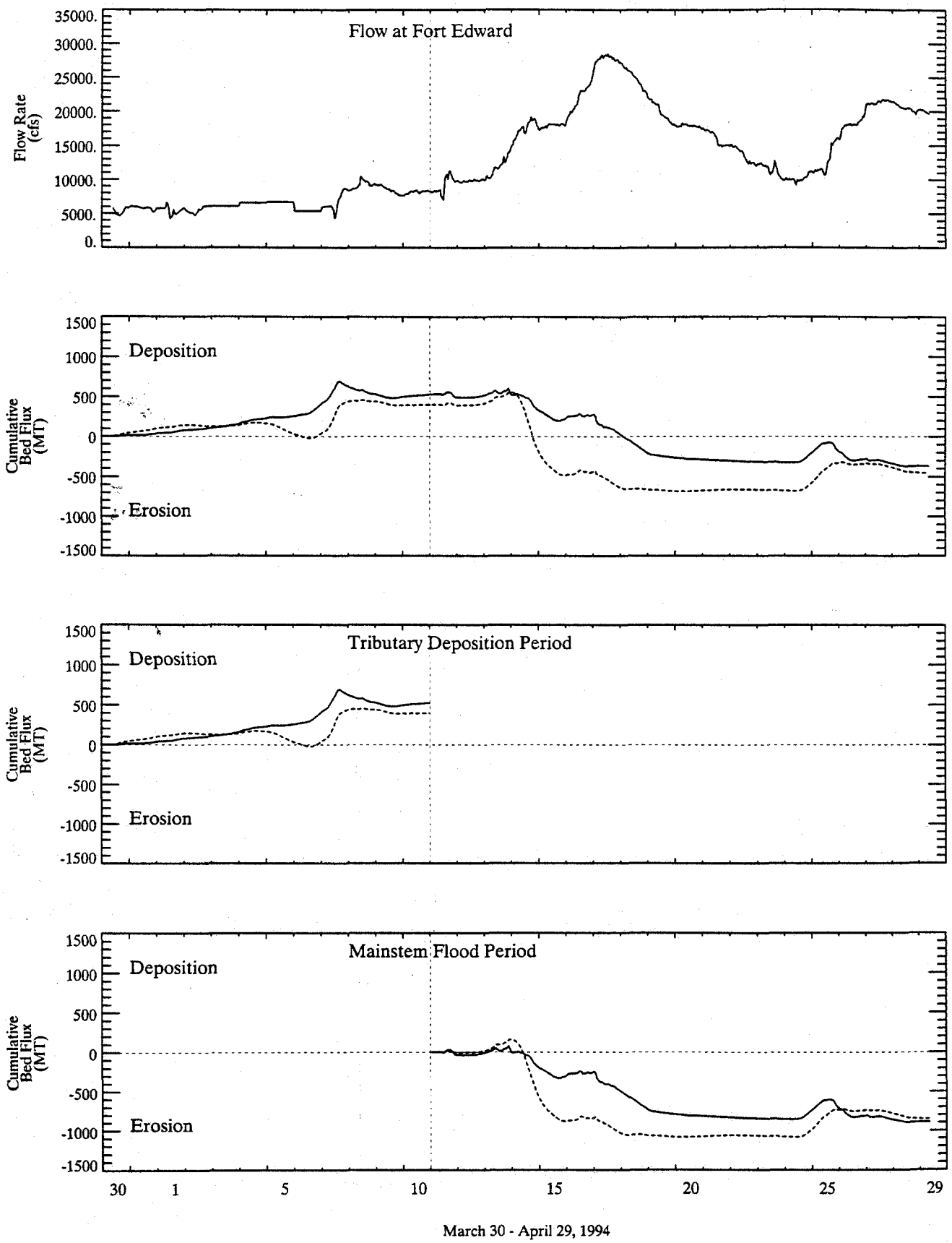

Figure 3-24. Comparison of predicted (solid line) and data-based (dashed line) changes in TIP sediment bed mass during the 1994 spring flood. Initial condition for non-cohesive bed properties calculated during long-term simulation.

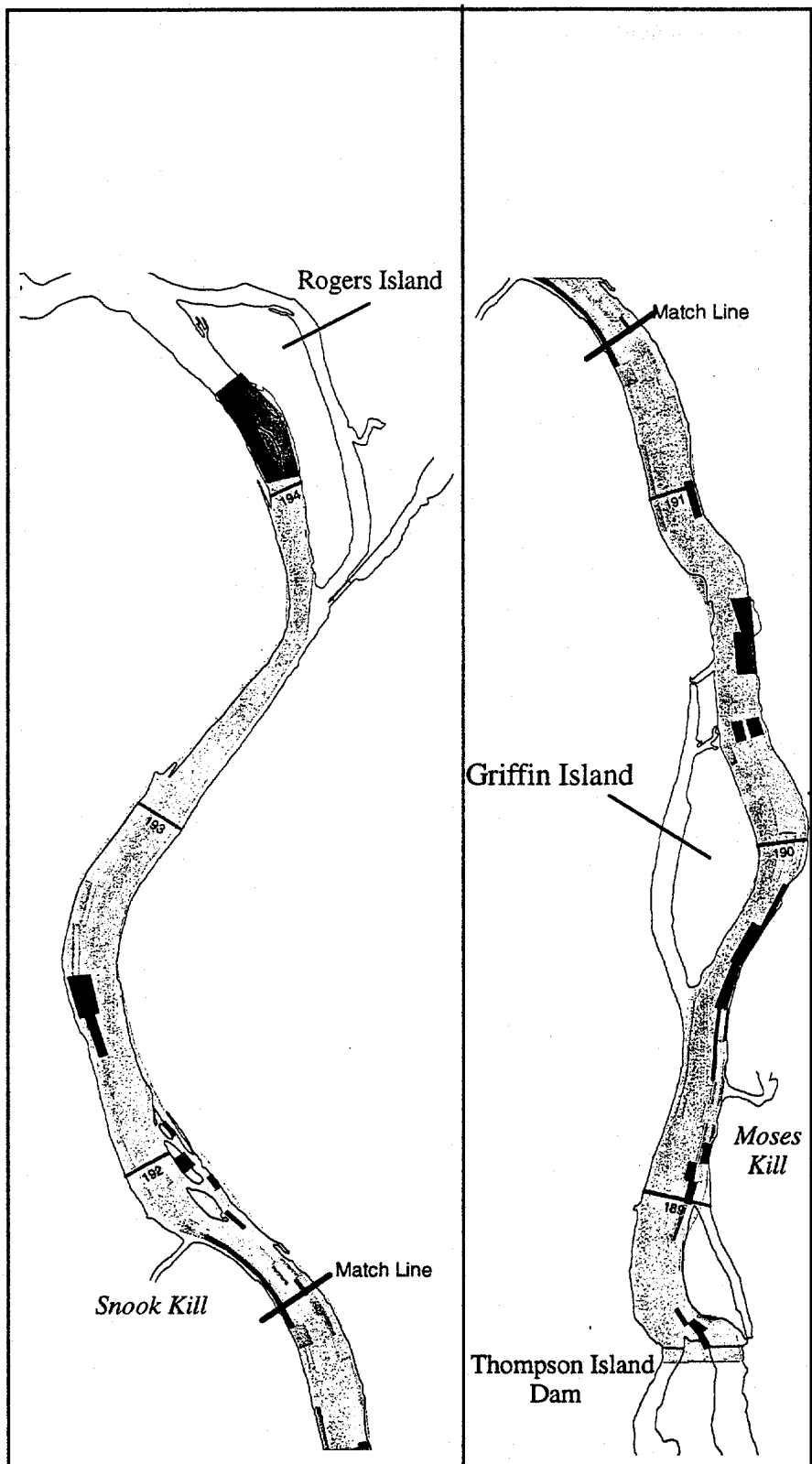

LOCATION MAP OF THE HUDSON RIVER

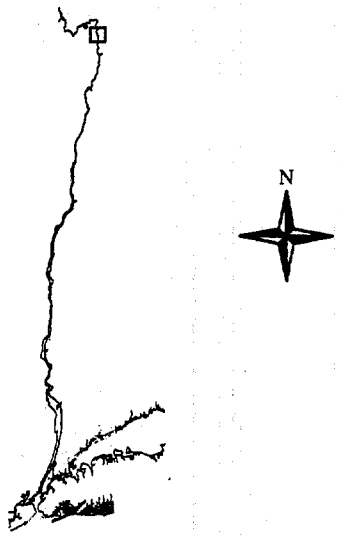

GRAPHIC SCALE

0.2 0 0.2 0.4 Miles

LEGEND

- Shoreline
- Mile Markers
- Dams & Locks
- Rocky Areas

Bed Elevation Change (mm)

- Erosion
- 0 - 5
- 5 - 10
- 10 - 15
- 15 - 20
- > 20

GENERAL ELECTRIC COMPANY
Hudson River Project

PCBs in the Upper Hudson River
Volume 2. A Model of PCB Fate, Transport and Bioaccumulation

Figure 3-25.

Predicted deposition (in mm) that occurred during the 1994 spring flood.

QEA
Quantitative Environmental Analysis, LLC

Project: Genhud 131 April 1999

\\Poseidon\d_drive\genhud\documents\final_report\vol_2\section_3\flood94results_fig_3_25.apr

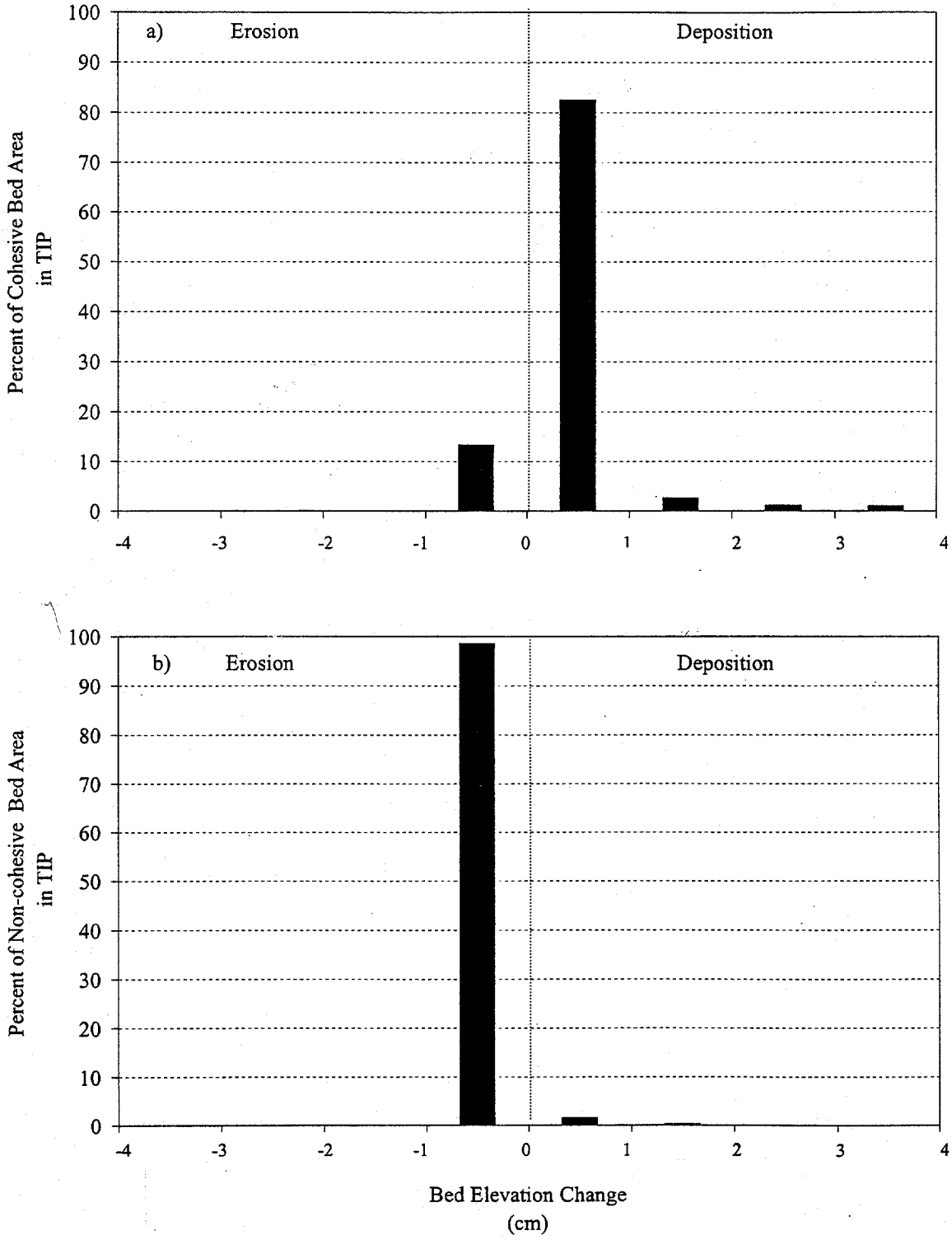

Figure 3-26. Distributions of (a) cohesive and (b) non-cohesive bed elevation changes in the TIP due to the 1994 spring flood.

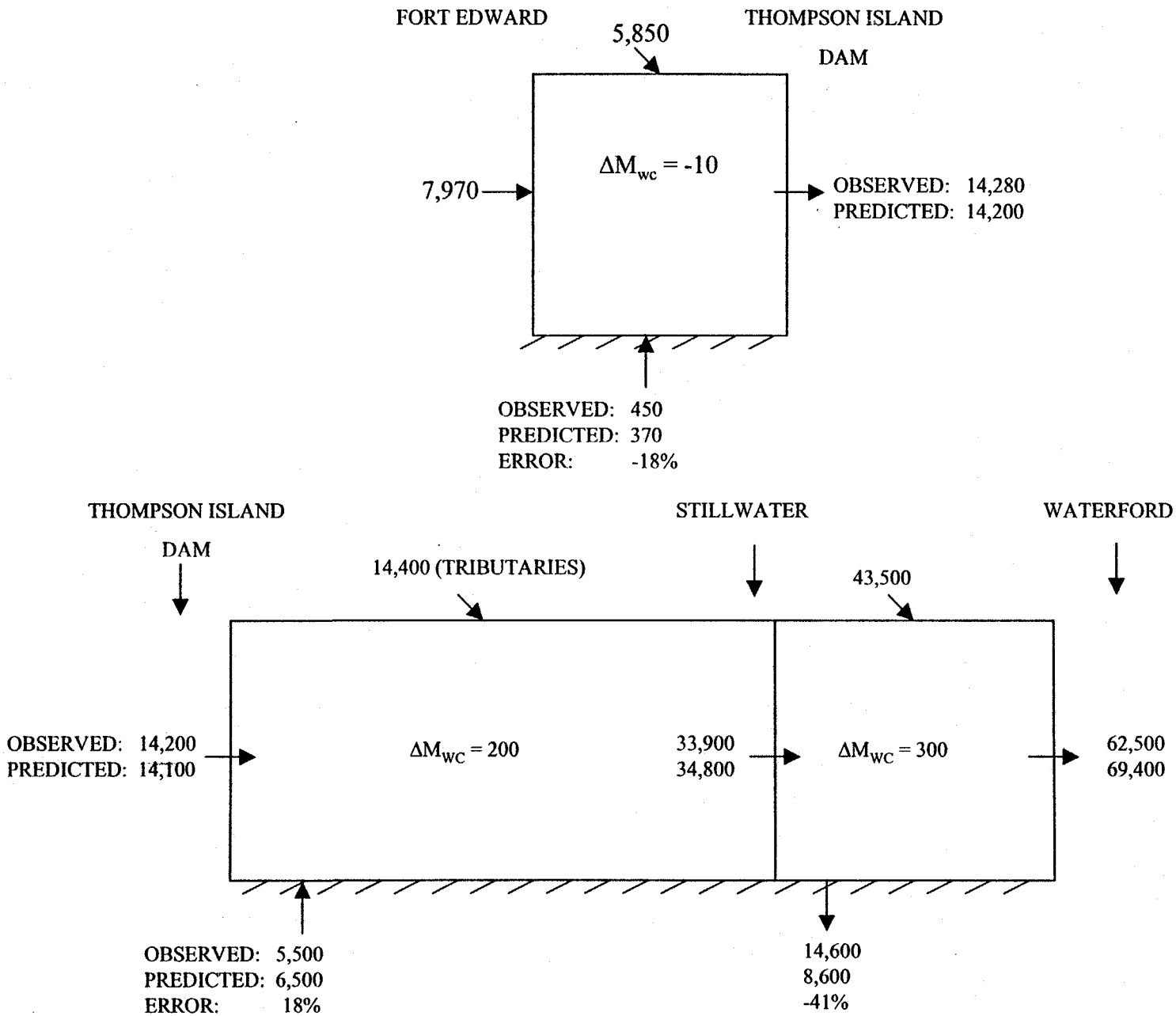

Figure 3-27. Sediment mass balance for 1994 spring flood, Reaches 1 to 8. Note that slightly different time periods were used for mass balances in the two regions. Sediment masses are in MT.

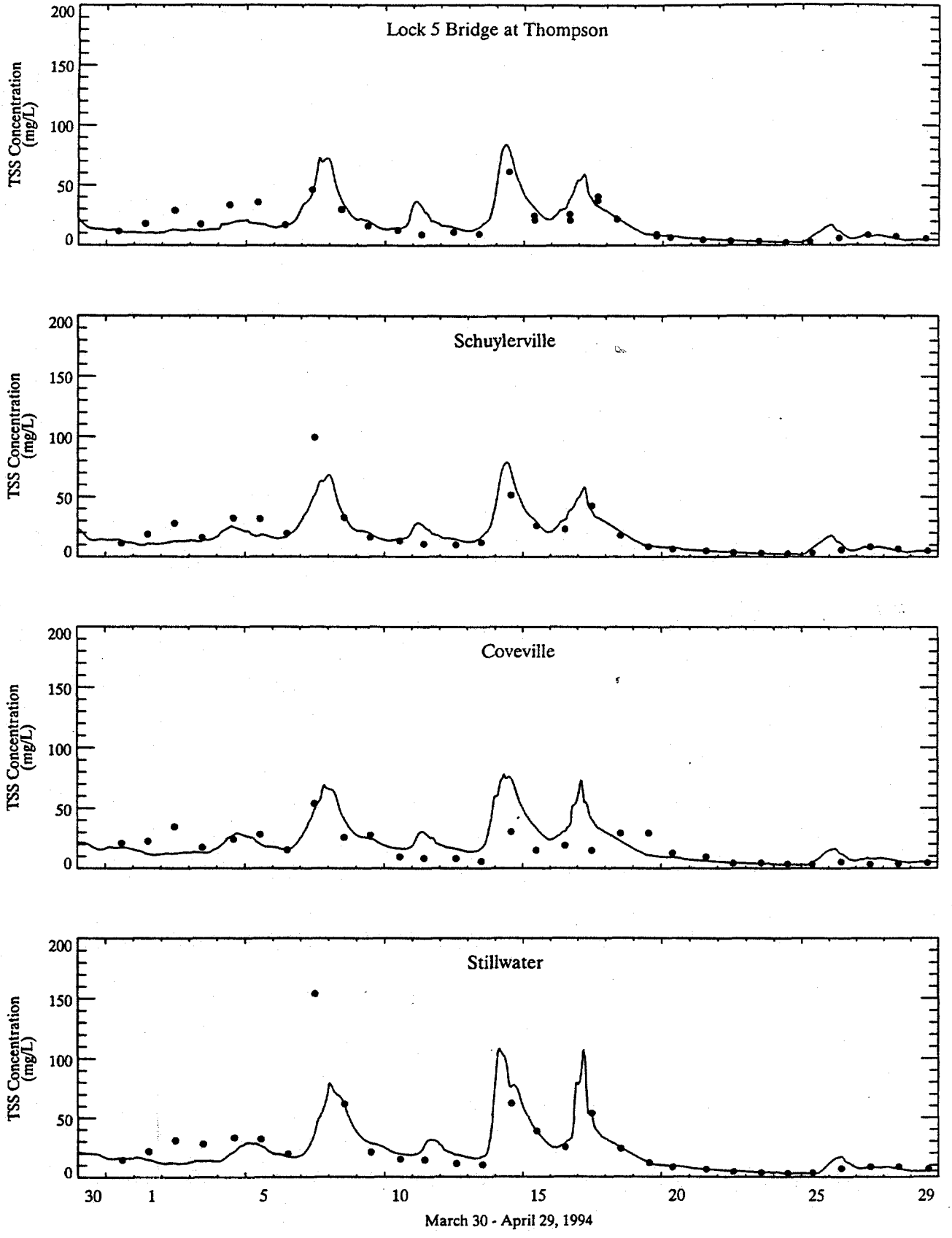

Figure 3-28. Comparison of predicted (solid) and measured (symbols) suspended sediment concentrations at four locations in Reach 5 during the 1994 spring flood.

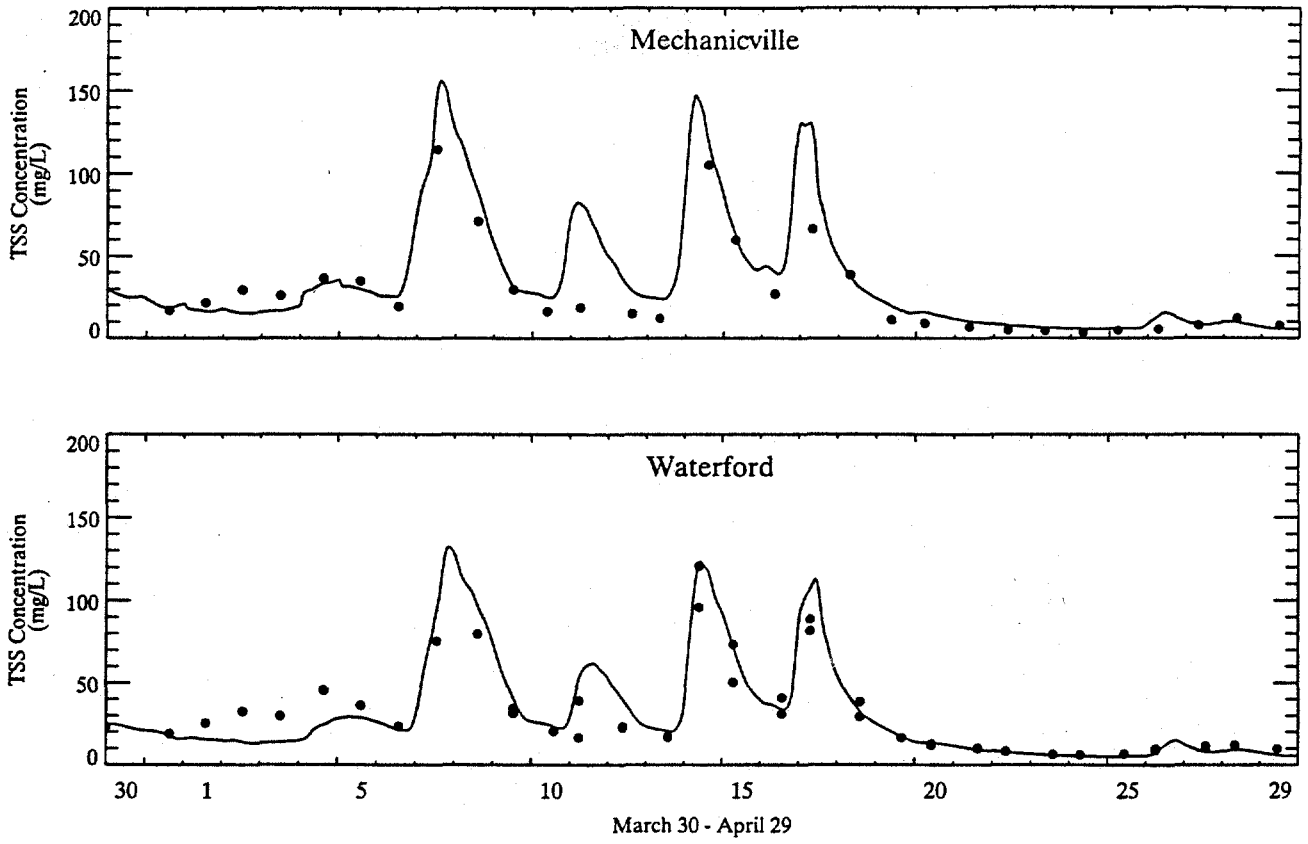

Figure 3-29. Comparison of predicted (solid) and measured (symbols) suspended sediment concentrations at Mechanicville and Waterford during the 1994 spring flood.

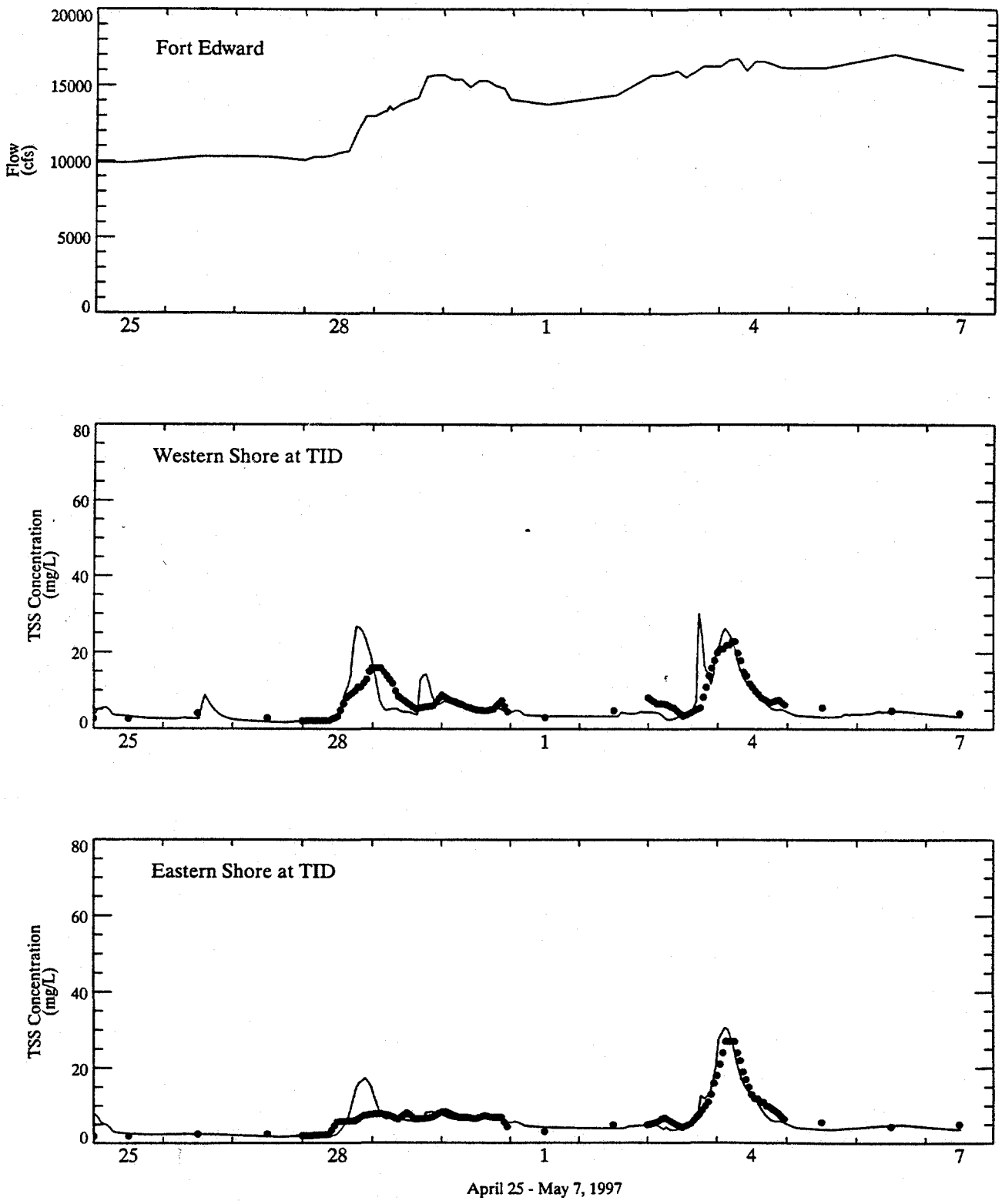

Figure 3-30. Comparison of predicted (solid) and measured (symbols) suspended sediment concentrations at the TID during the 1997 spring flood (April 25 to May 7).

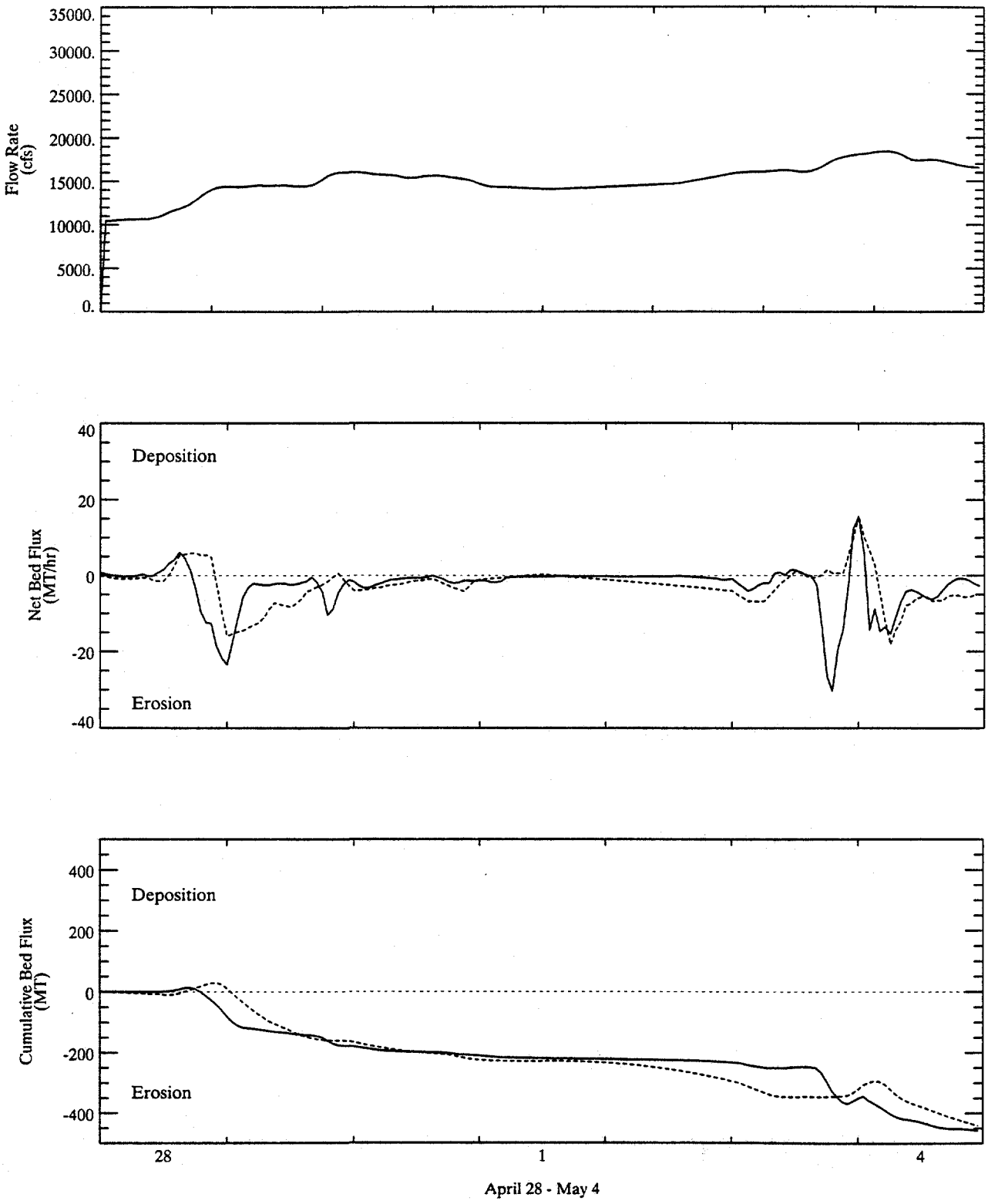

Figure 3-31. Comparison of predicted (solid line) and data-based (dashed line) changes in TIP sediment bed mass during the 1997 spring flood. Initial conditions for non-cohesive bed properties calculated during long-term simulation

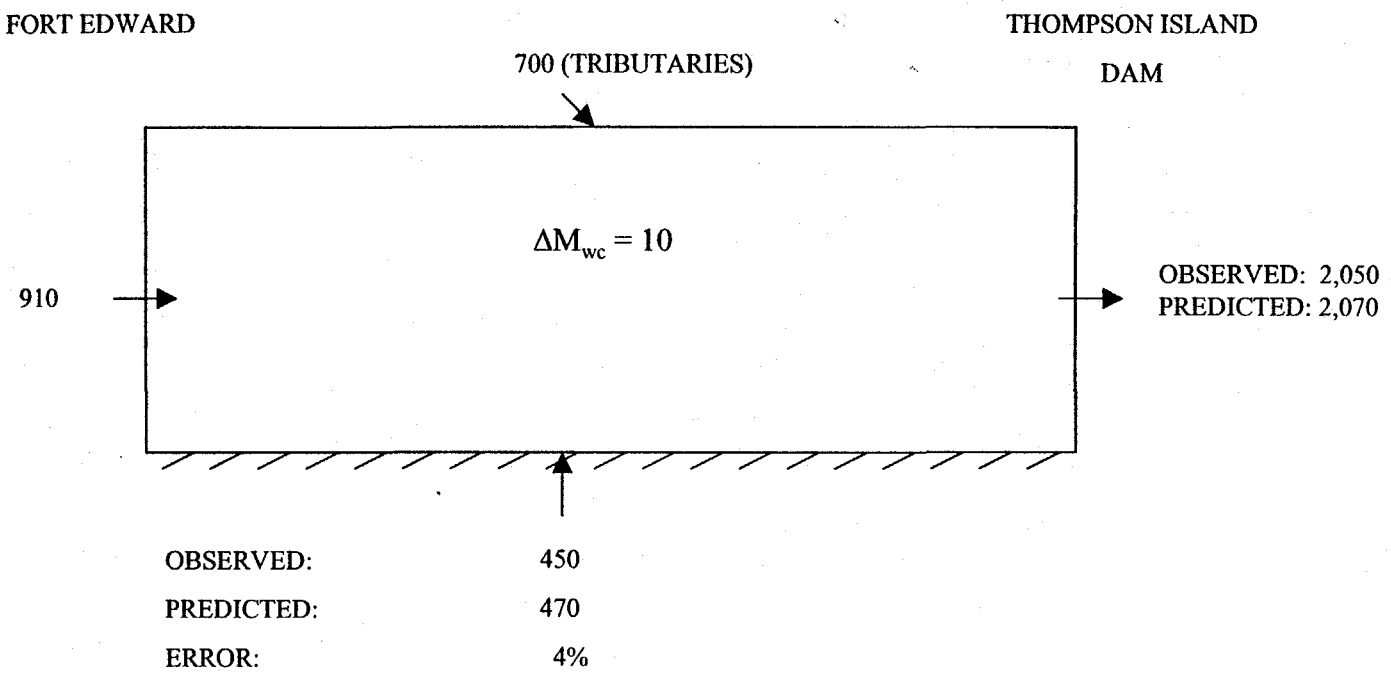

Figure 3-32. Sediment mass balance for 1997 spring flood, TIP. Sediment masses are in MT.

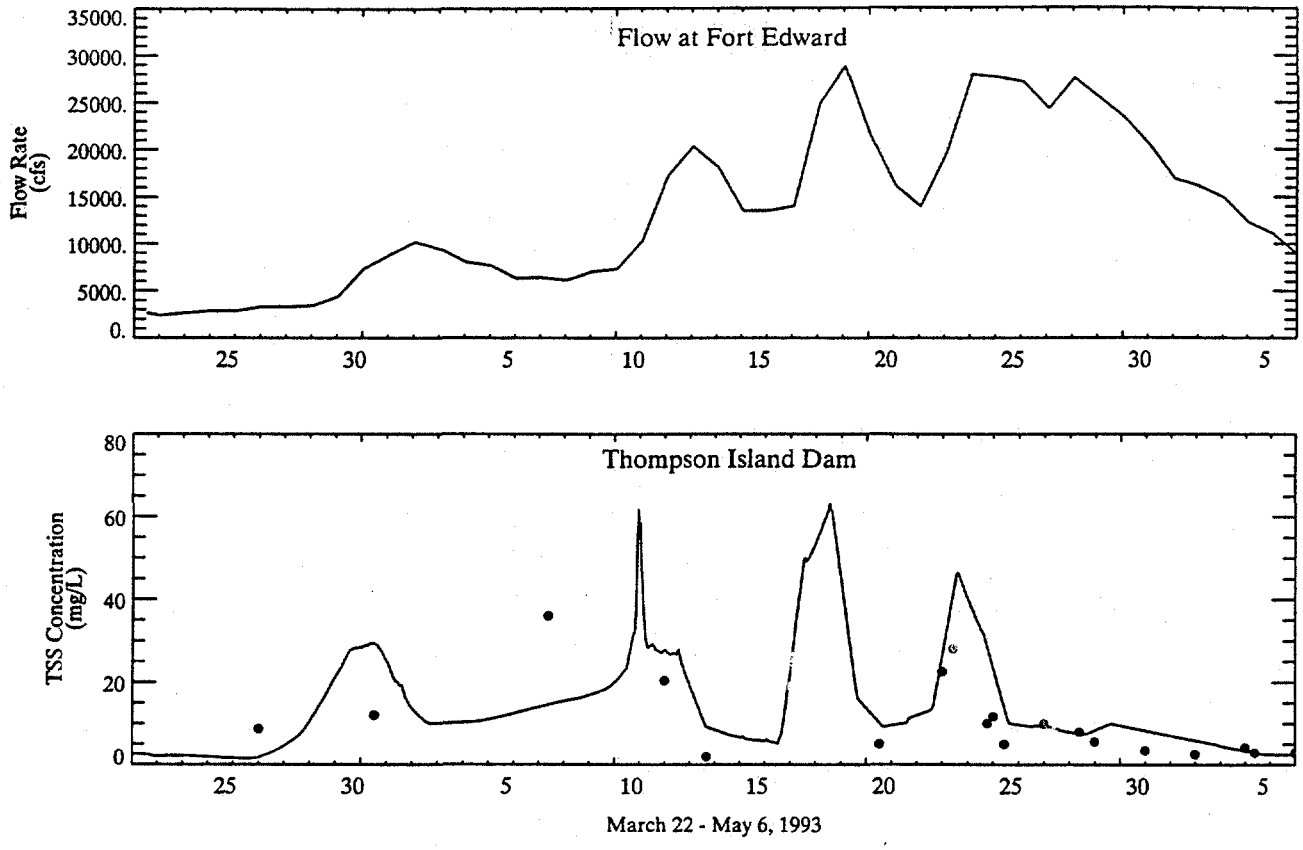

Figure 3-33. Comparison of predicted (solid) and measured (symbols) suspended sediment concentrations at the TID during the 1993 spring flood (April 25 to May 7).

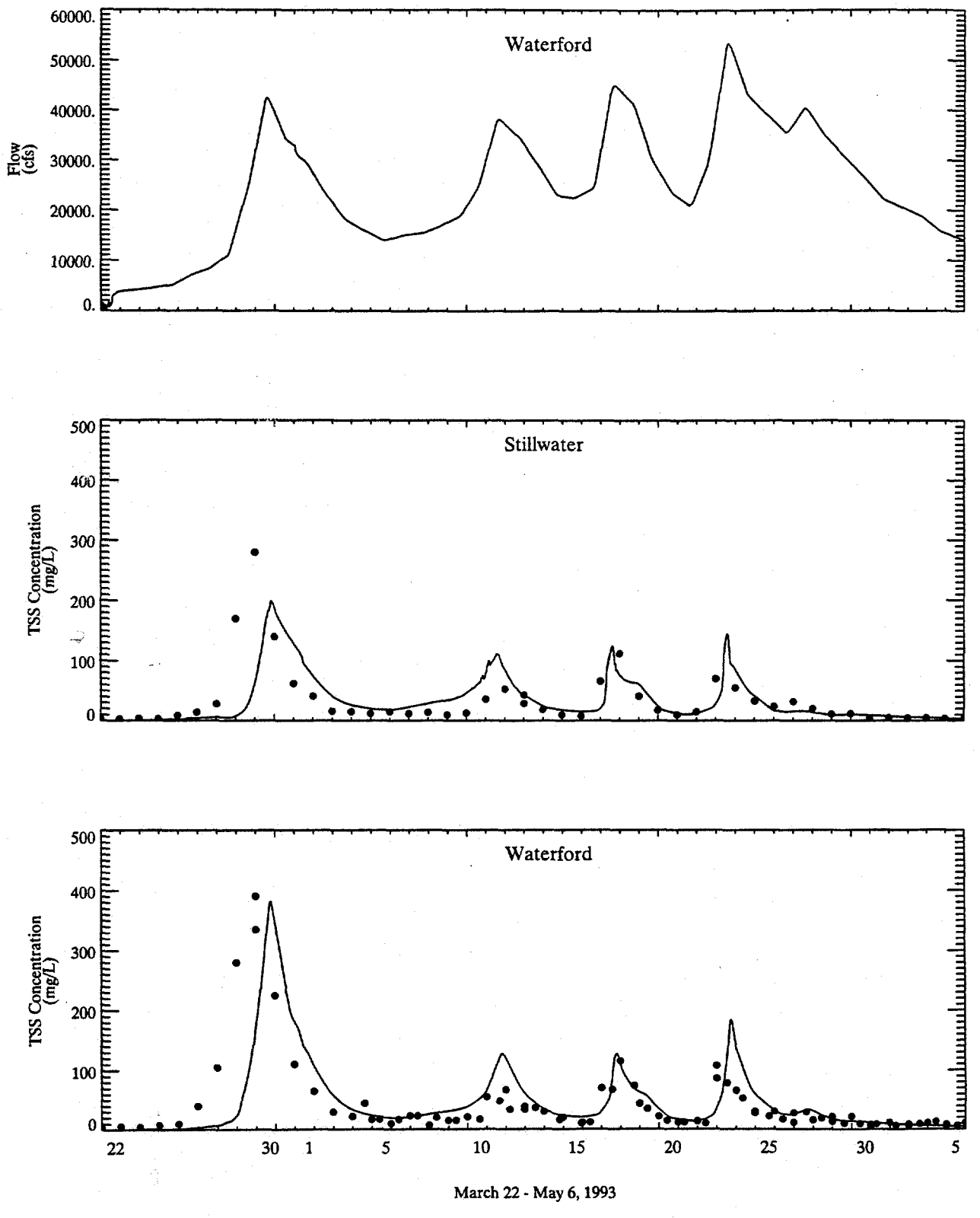

Figure 3-34. Comparison of predicted (solid) and measured (symbols) suspended sediment concentration at Stillwater and Waterford during the 1993 spring flood. Top panel shows measured flow at Waterford.

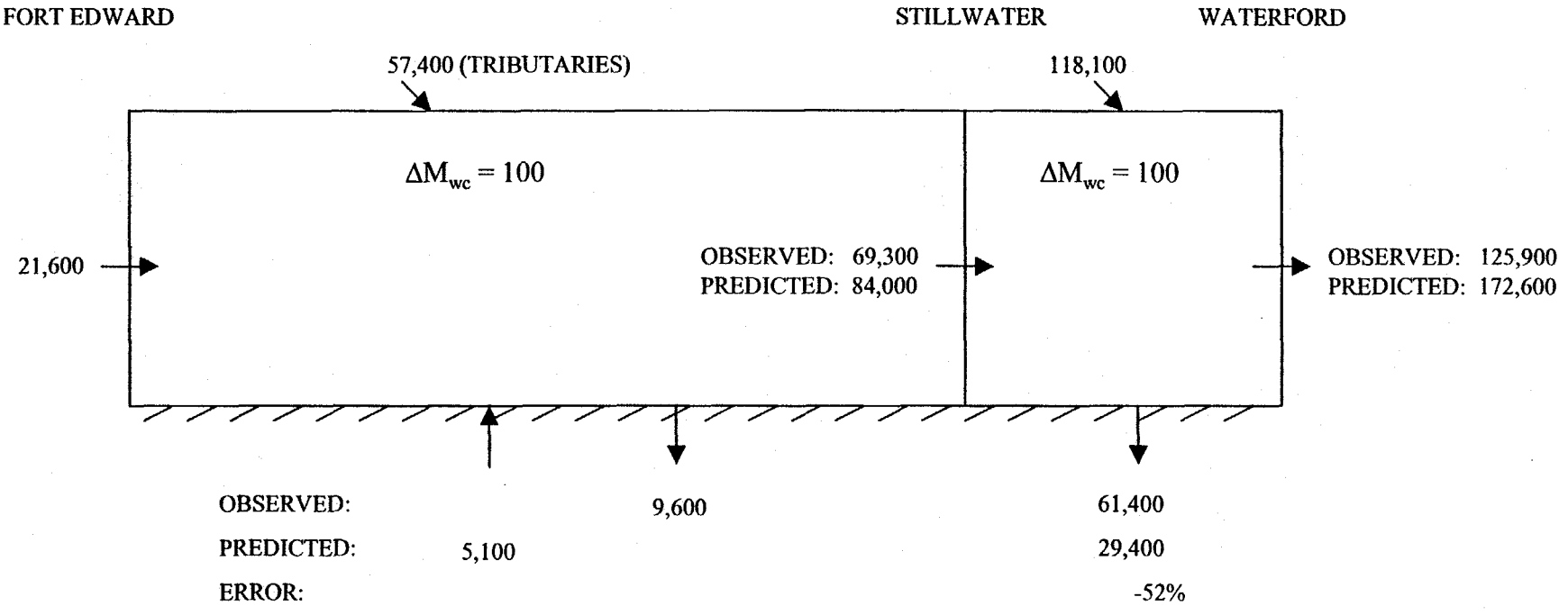

313814

Figure 3-35. Sediment mass balance for 1993 flood, Reaches 1 to 8. Sediment masses are in MT.

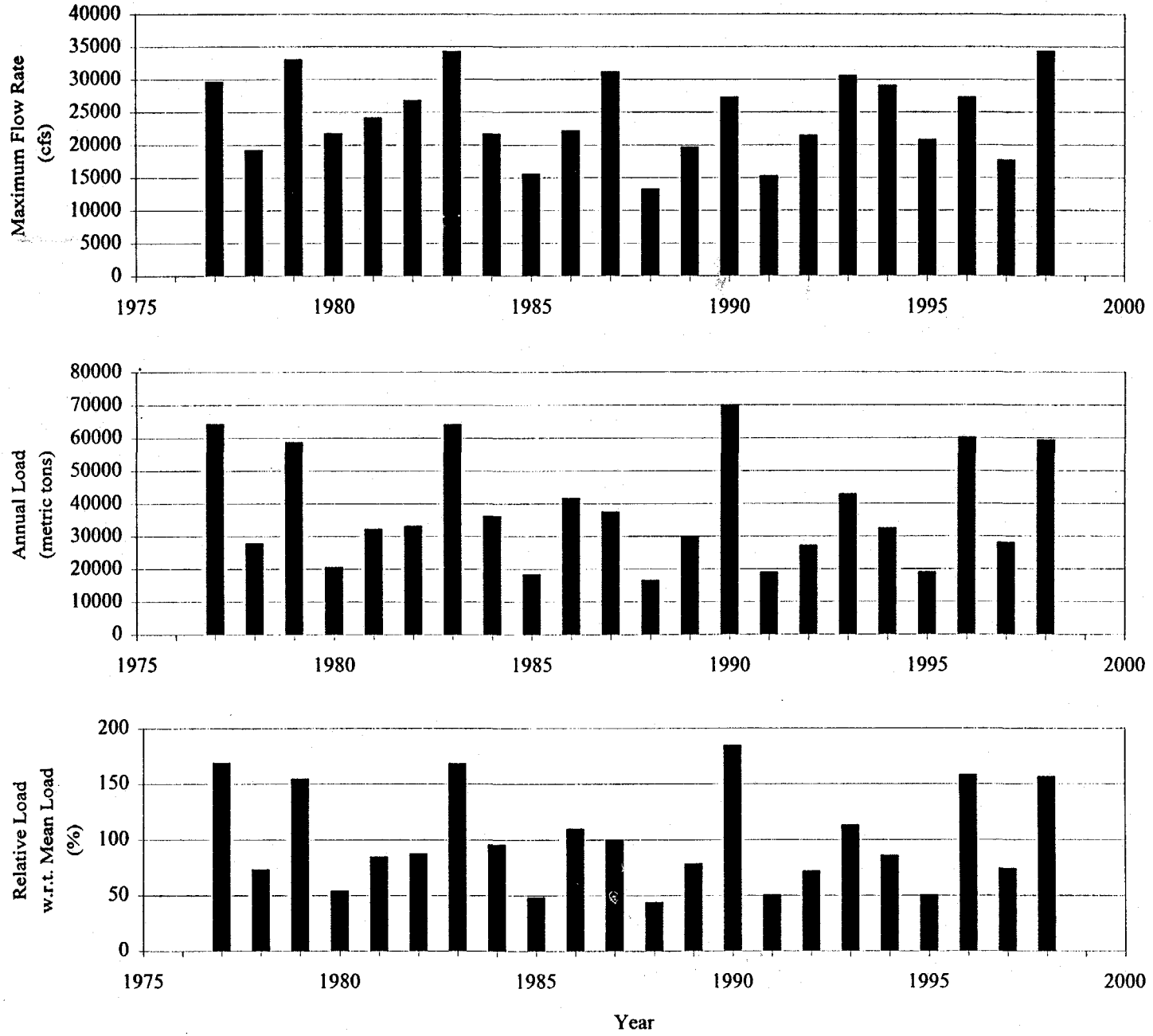

Figure 3-36. Maximum annual flow rate at Fort Edward, total TIP annual sediment load and relative annual sediment load for 1977 to 1998. Note that 1998 values are for January 1 to December 9.

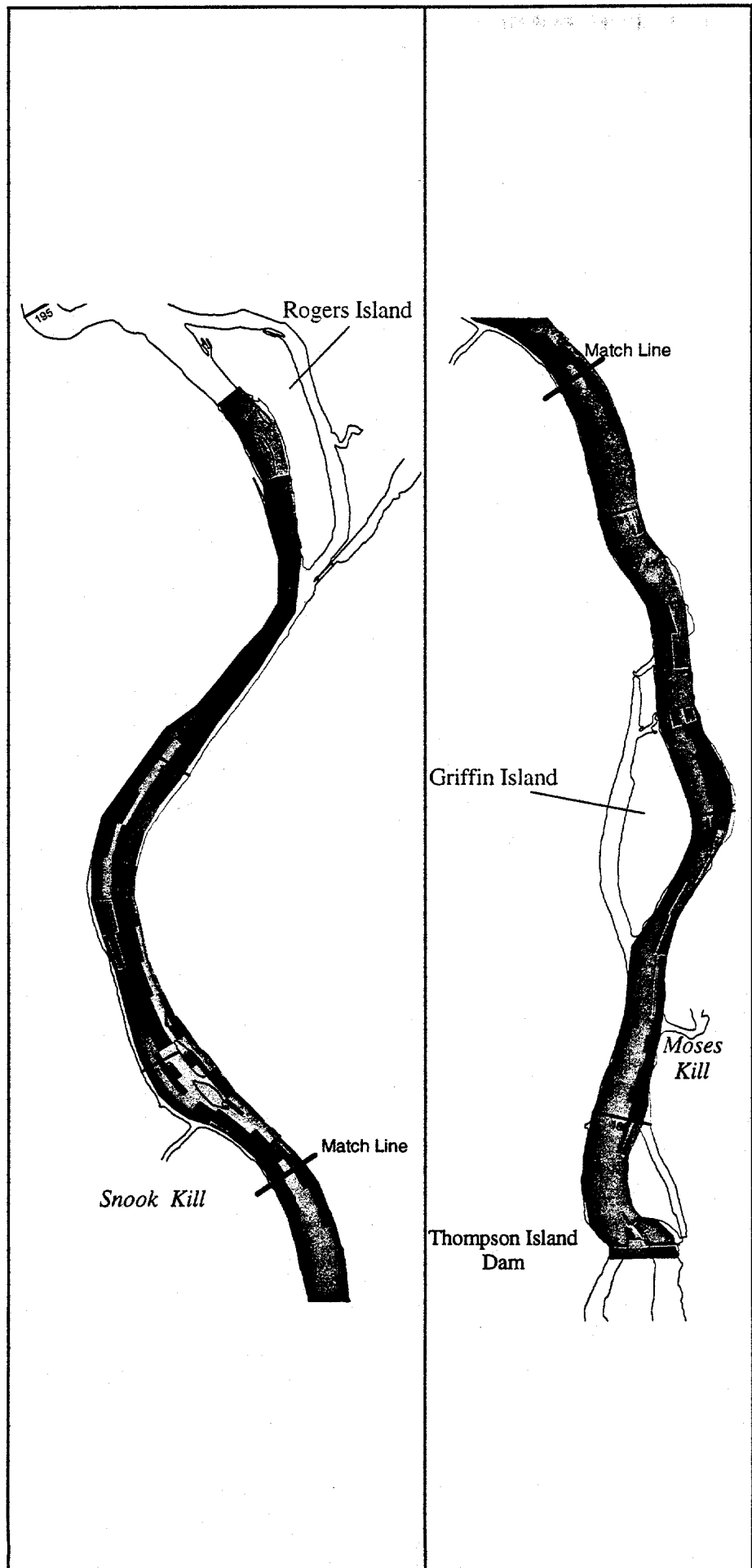

LOCATION MAP OF THE HUDSON RIVER

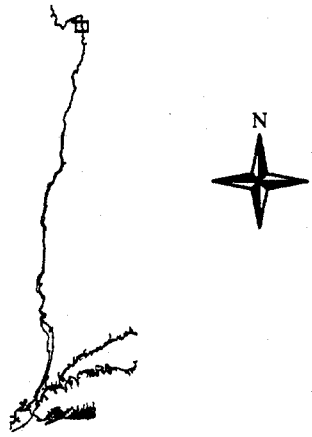

GRAPHIC SCALE

0.2 0 0.2 0.4 Miles

LEGEND

- Shoreline
- Mile Points
- Dams & Locks
- Rocky Areas

Bed Elevation Change

- Erosion
- Deposition

GENERAL ELECTRIC COMPANY
Hudson River Project

PCBs in the Upper Hudson River
Volume 2. A Model of PCB Fate, Transport and Bioaccumulation

Figure 3-37.

Predicted TIP deposition and erosion areas at end of long-term simulation (1977 to 1998).

QEA da/a
Quantitative Environmental Analysis, LLC

Project: Genhud 131 April 1999

\\Poseidon\D_drive\GENhud\Documents\Final_report\Vol_2\Section_3\longterm_results_fig_37_to_39

313817

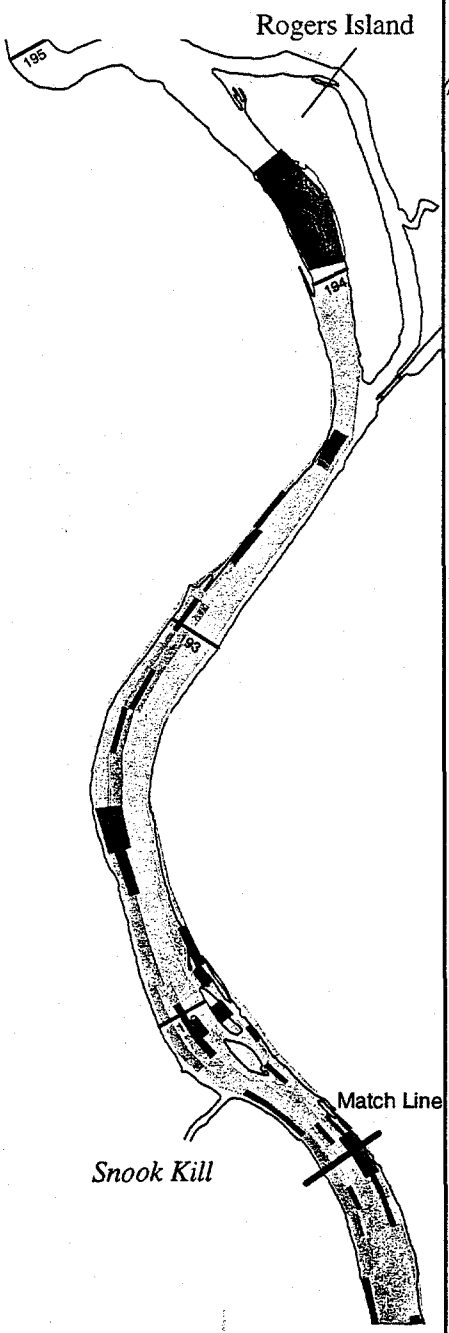

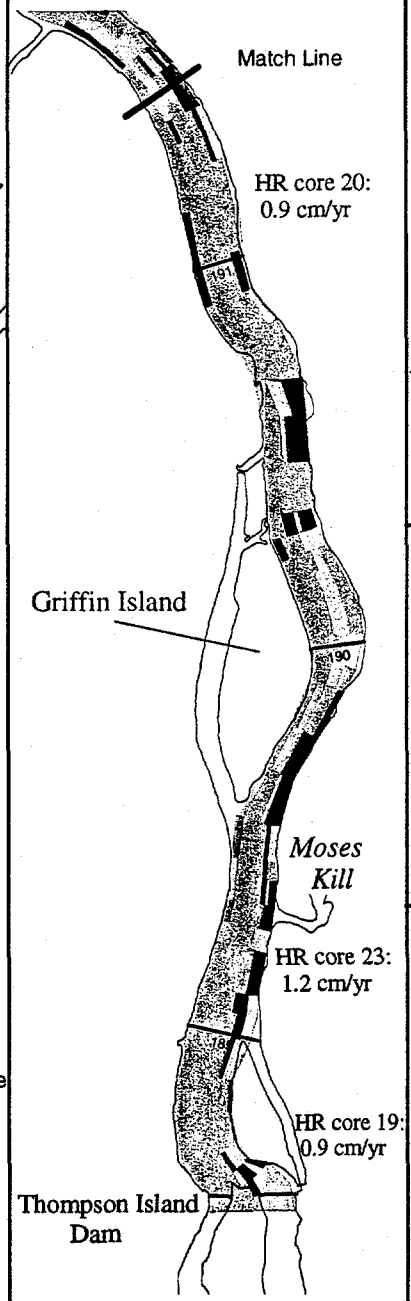

LOCATION MAP OF THE HUDSON RIVER

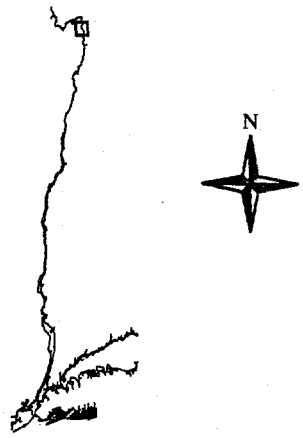

GRAPHIC SCALE

0.2 0 0.2 0.4 Miles

LEGEND

- Shoreline
- Mile Points
- Dams & Locks
- Rocky Areas

Deposition Rate (cm/yr)

- Erosion
- 0.0 - 0.5
- 0.5 - 1.0
- 1.0 - 1.5
- 1.5 - 2.0
- > 2.0

GENERAL ELECTRIC COMPANY
Hudson River Project

PCBs in the Upper Hudson River
Volume 2. A Model of PCB Fate, Transport and Bioaccumulation

Figure 3-38.

Predicted average TIP deposition rates (cm/yr) for 22-year period (January 1977 to March 1998). Measured deposition rates at three high resolution cores are also shown.

QEA
Quantitative Environmental Analysis, LLC

Project: Genhud 131 April 1999

\\Poseidon\D_drive\GENhud\Documents\Final_report\Vol_2\Section_3\longterm_results_fig_37_to_39

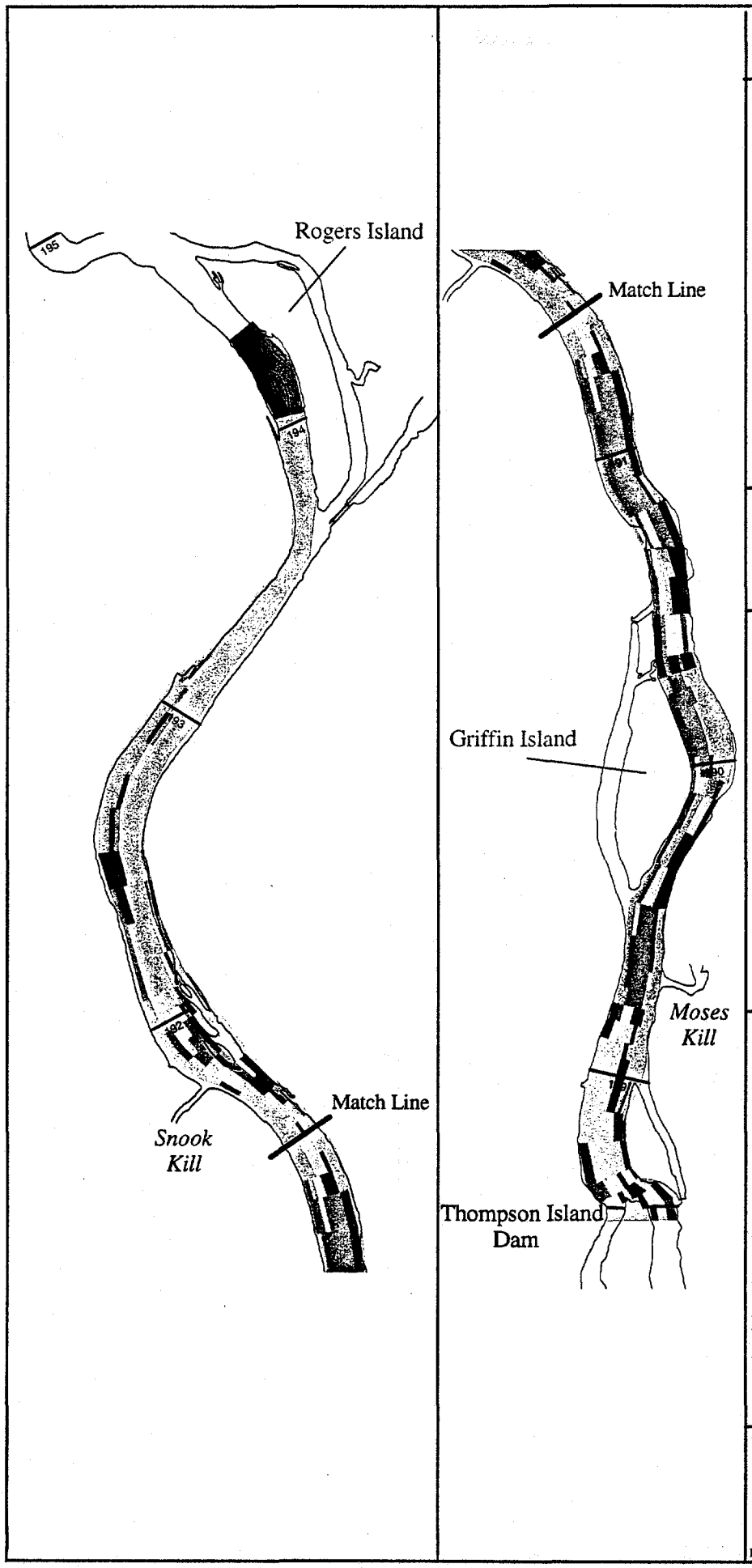

LOCATION MAP OF THE HUDSON RIVER

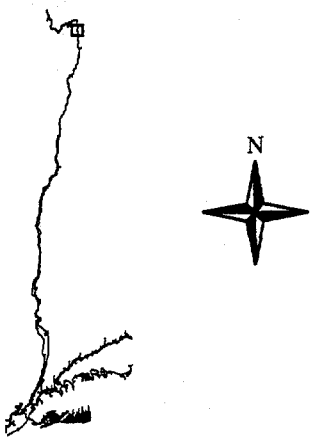

GRAPHIC SCALE

0.2 0 0.2 0.4 Miles

LEGEND

- Shoreline
- Mile Points
- Dams & Locks
- Rocky Areas

Bed Elevation Change (cm)

- < -5
- -5 - -4
- -4 - -3
- -3 - -2
- -2 - -1
- -1 - 0
- Deposition

GENERAL ELECTRIC COMPANY
Hudson River Project

PCBs in the Upper Hudson River
Volume 2. A Model of PCB Fate, Transport and Bioaccumulation

Figure 3-39.

Predicted erosion depths (cm) for 22-year period (January 1977 to March 1998).

QEA
Quantitative Environmental Analysis, LLC

Project: Genhud 131 April 1999

\\Poseidon\D_drive\GENhud\Documents\Final_report\Vol_2\Section_3\longterm_results_fig_37_to_39

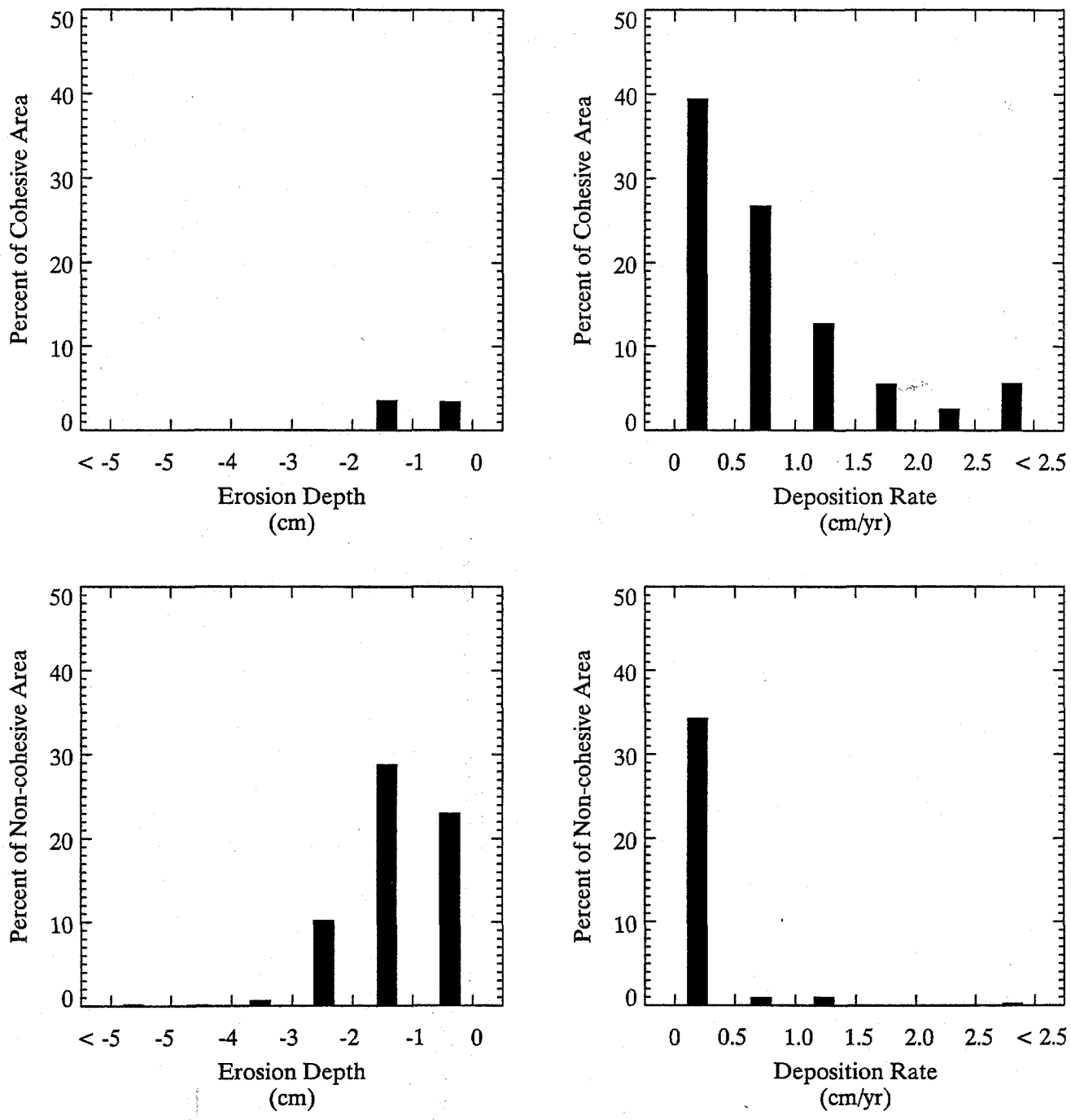

Figure 3-40. Distributions of cohesive and non-cohesive bed elevation changes in the TIP at the end of the 22-year (1977-1998) simulation.

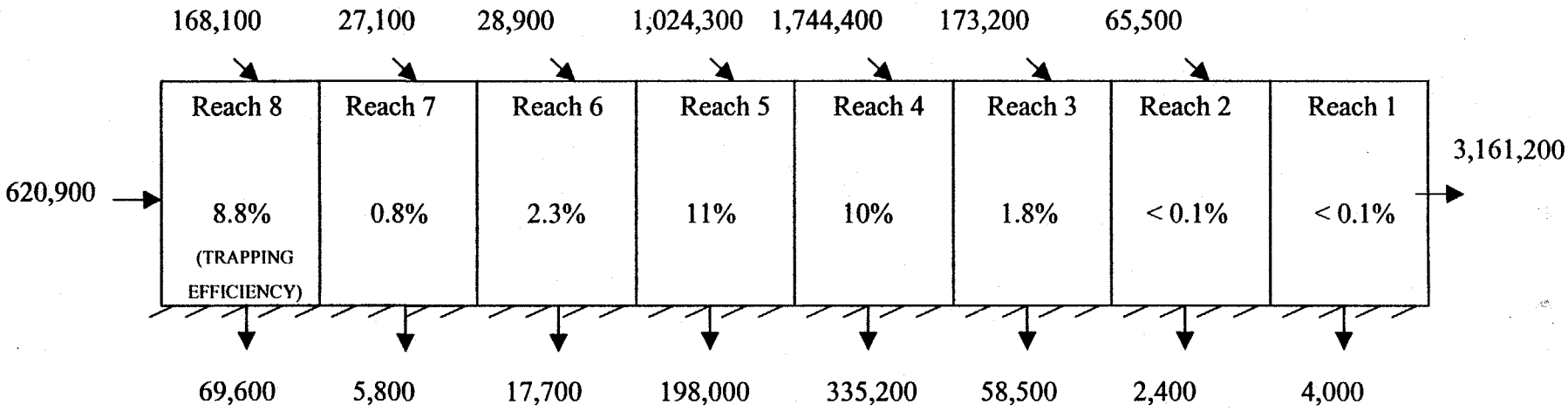

Figure 3-41. Sediment mass balance for the 22-year (May 1977 - December 1998) simulation, Reaches 1-8. Sediment masses are in MT.

313820

\\Poseidon\D_Drive\GENhud\Documents\Final_report\Vol_2\Section_3\LT_SED_MB_fig_3_41.ppt

4/14/99

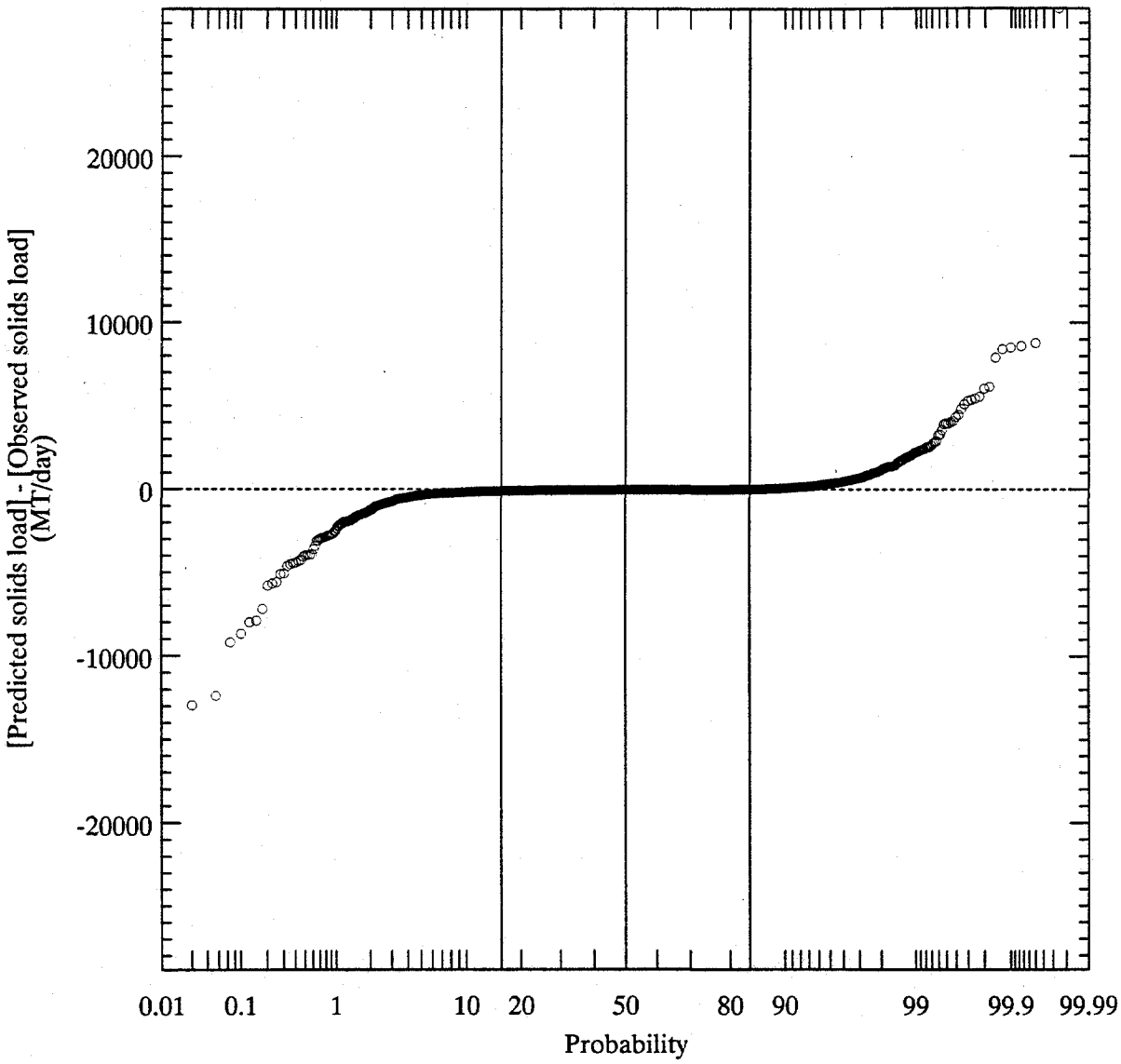

Figure 3-42. Probability distribution of error in predicted daily sediment load at Stillwater (error = predicted - observed) during the long-term simulation.

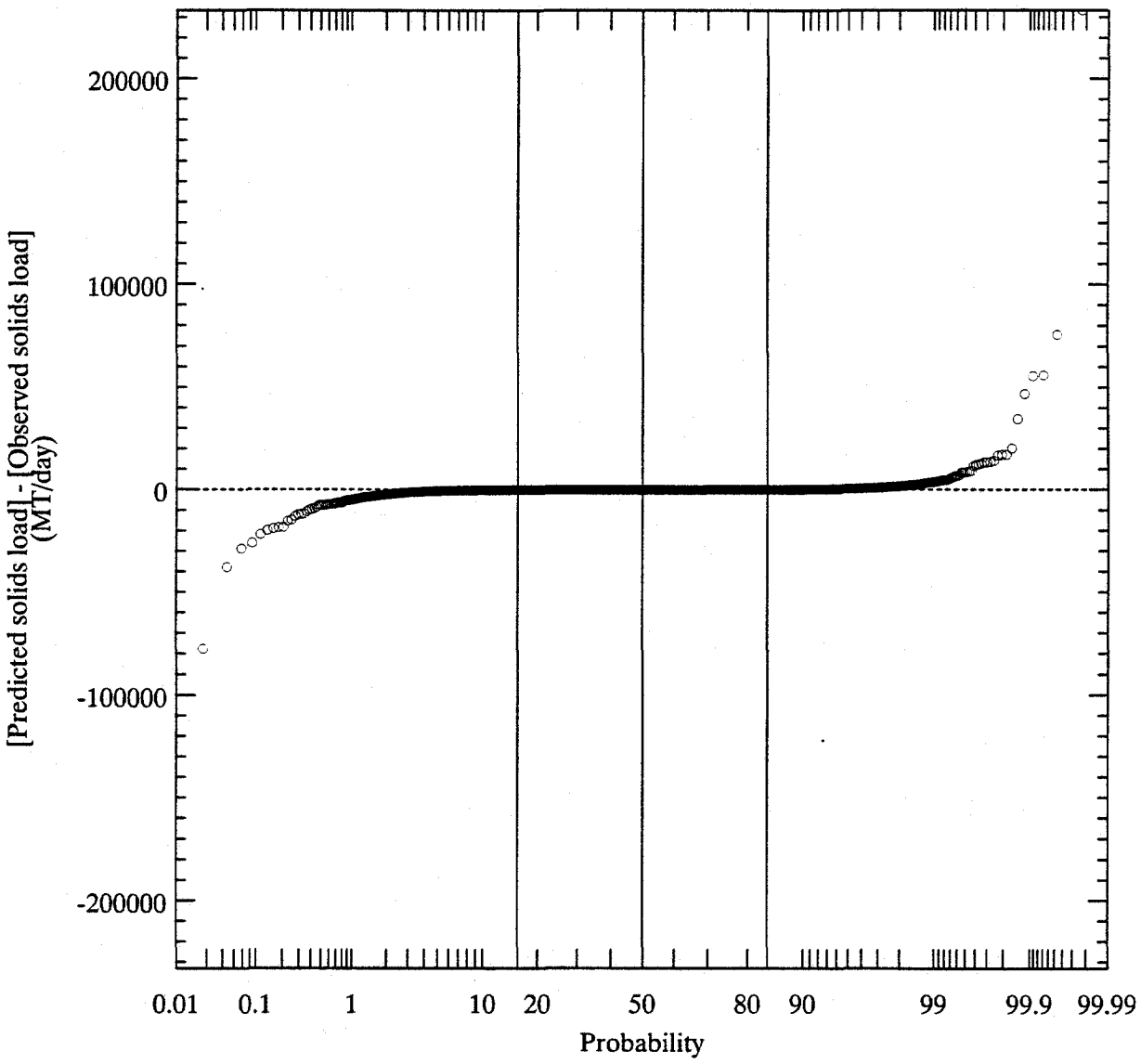

Figure 3-43. Probability distribution of error in predicted daily sediment load at Waterford (error = predicted - observed) during the long-term simulation.

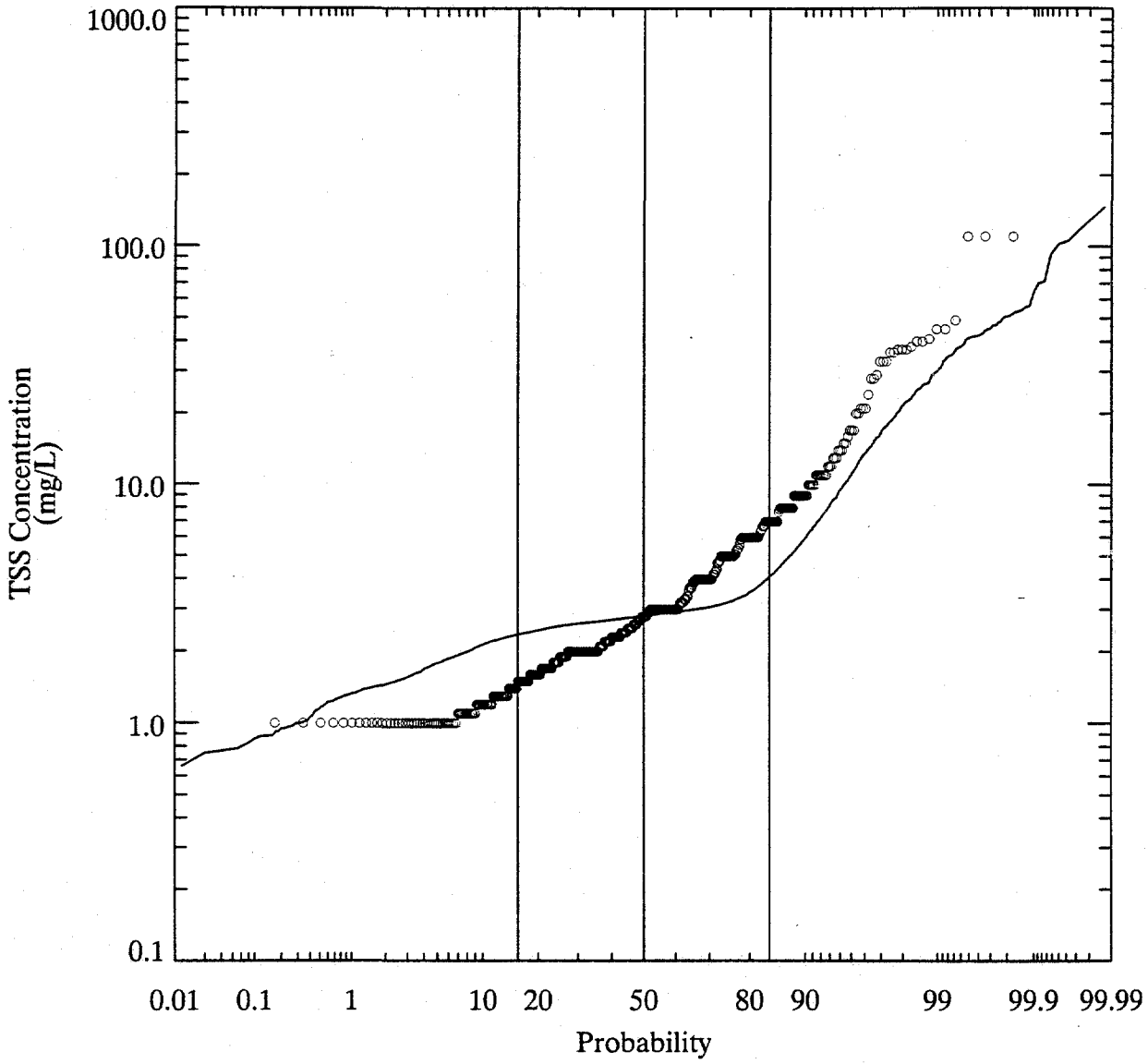

Figure 3-44. Comparison of predicted (solid line) and observed TSS concentration probability distributions at TID.

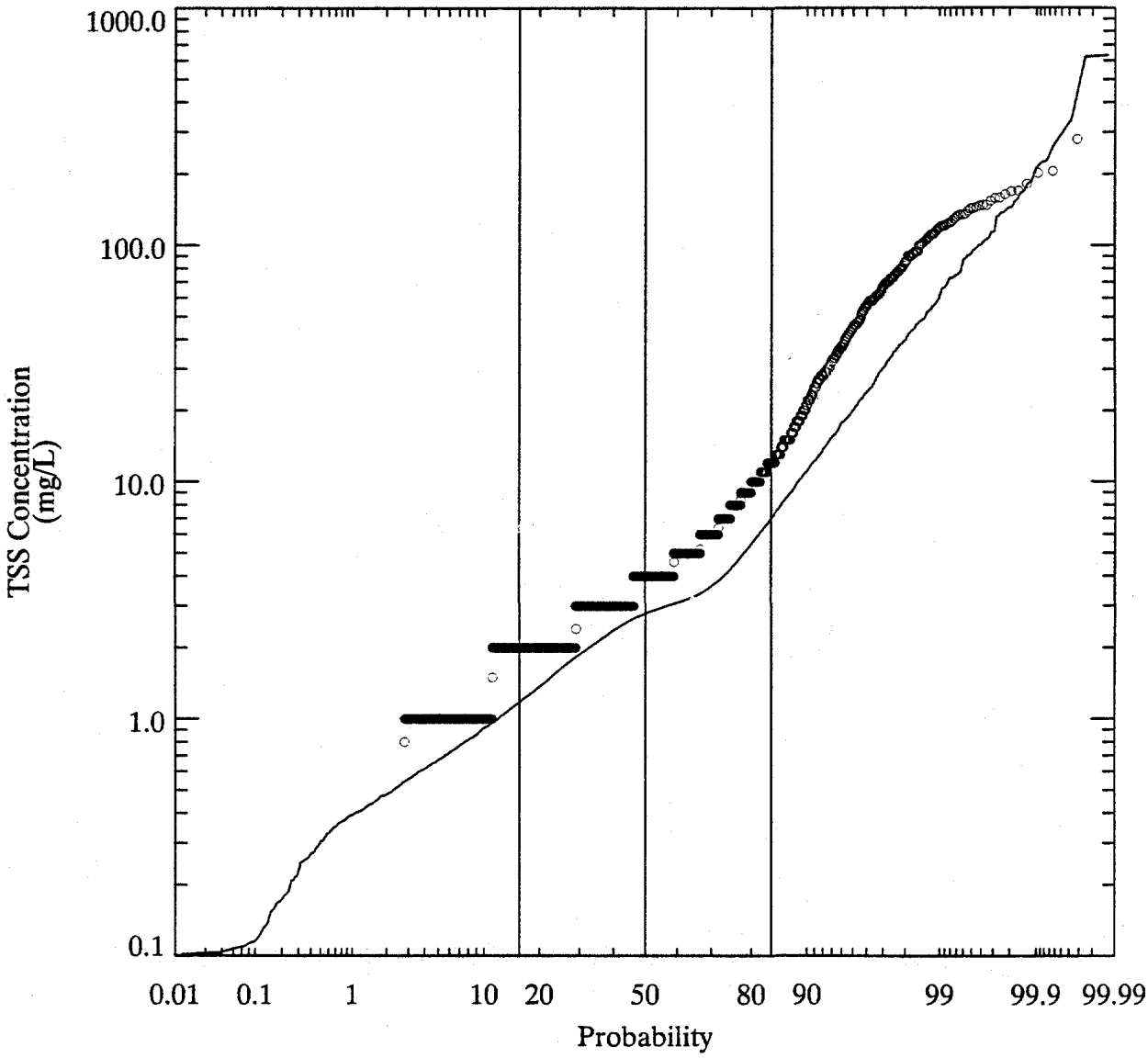

Figure 3-45. Comparison of predicted (solid line) and observed TSS concentration probability distributions at Stillwater.

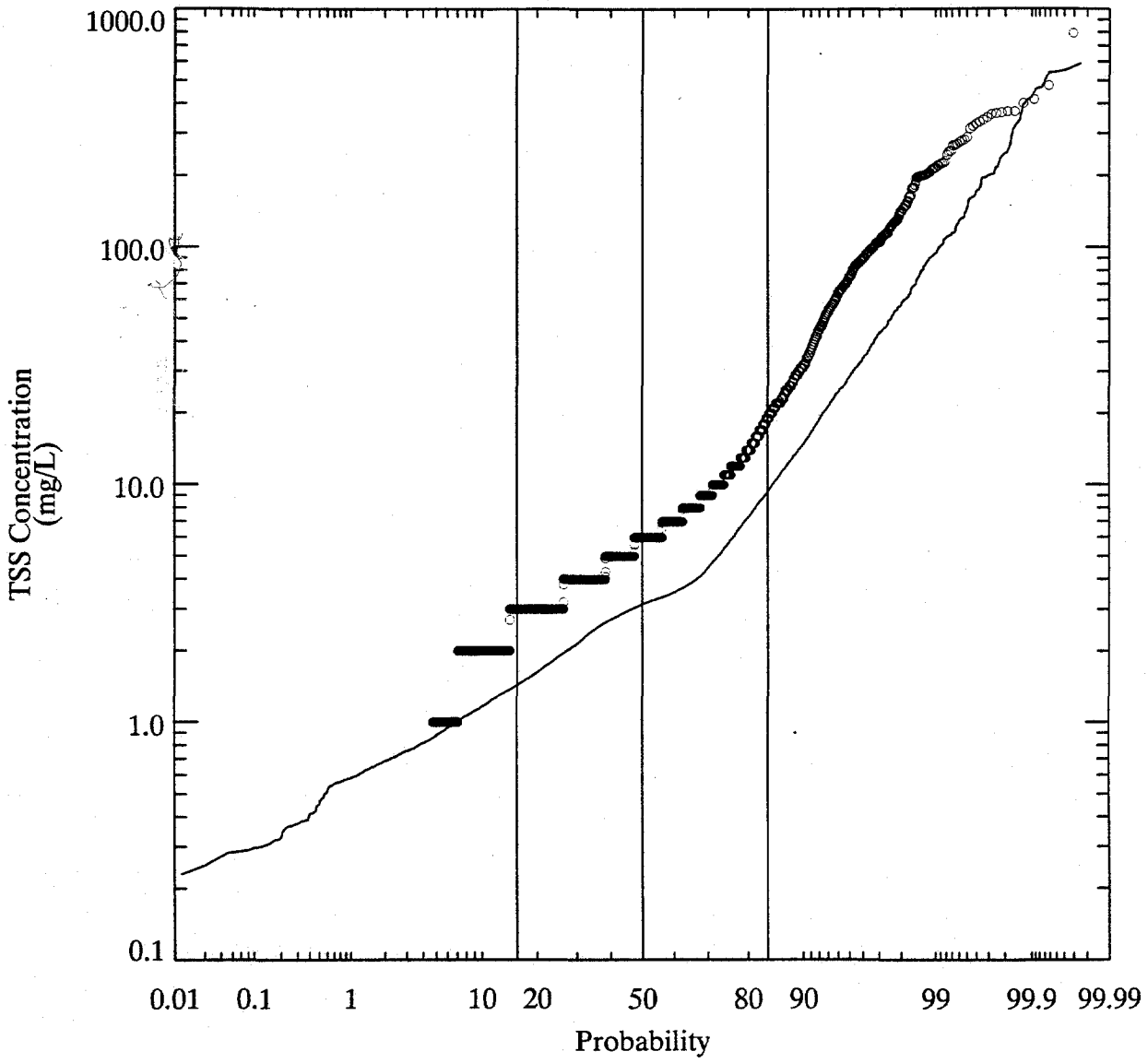

Figure 3-46. Comparison of predicted (solid line) and observed TSS concentration probability distributions at Waterford.

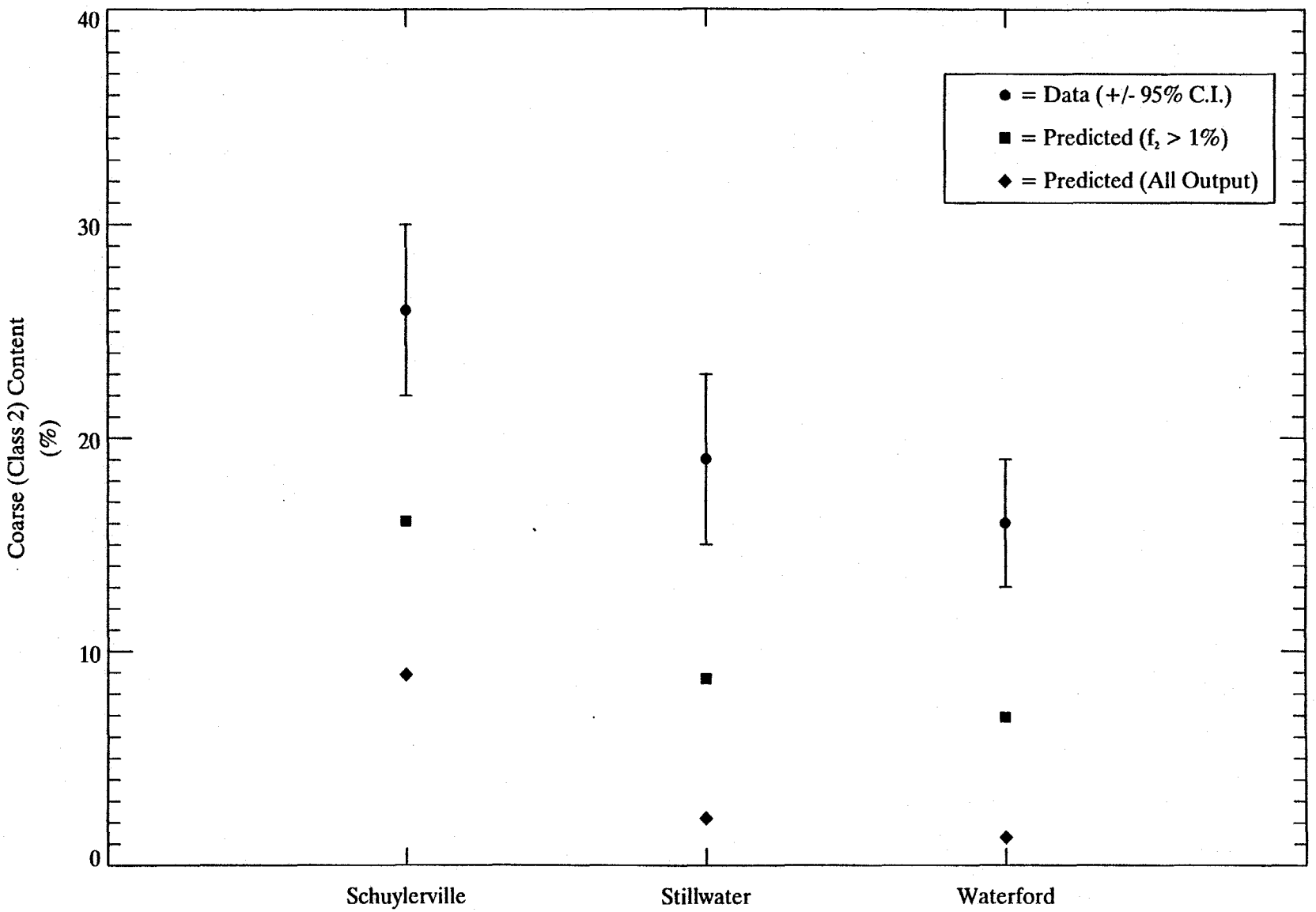

Figure 3-47. Predicted and observed spatial trends in sand content at three UHR locations.
Average values for model output for days when predicted sand content was greater than 1% are shown as squares

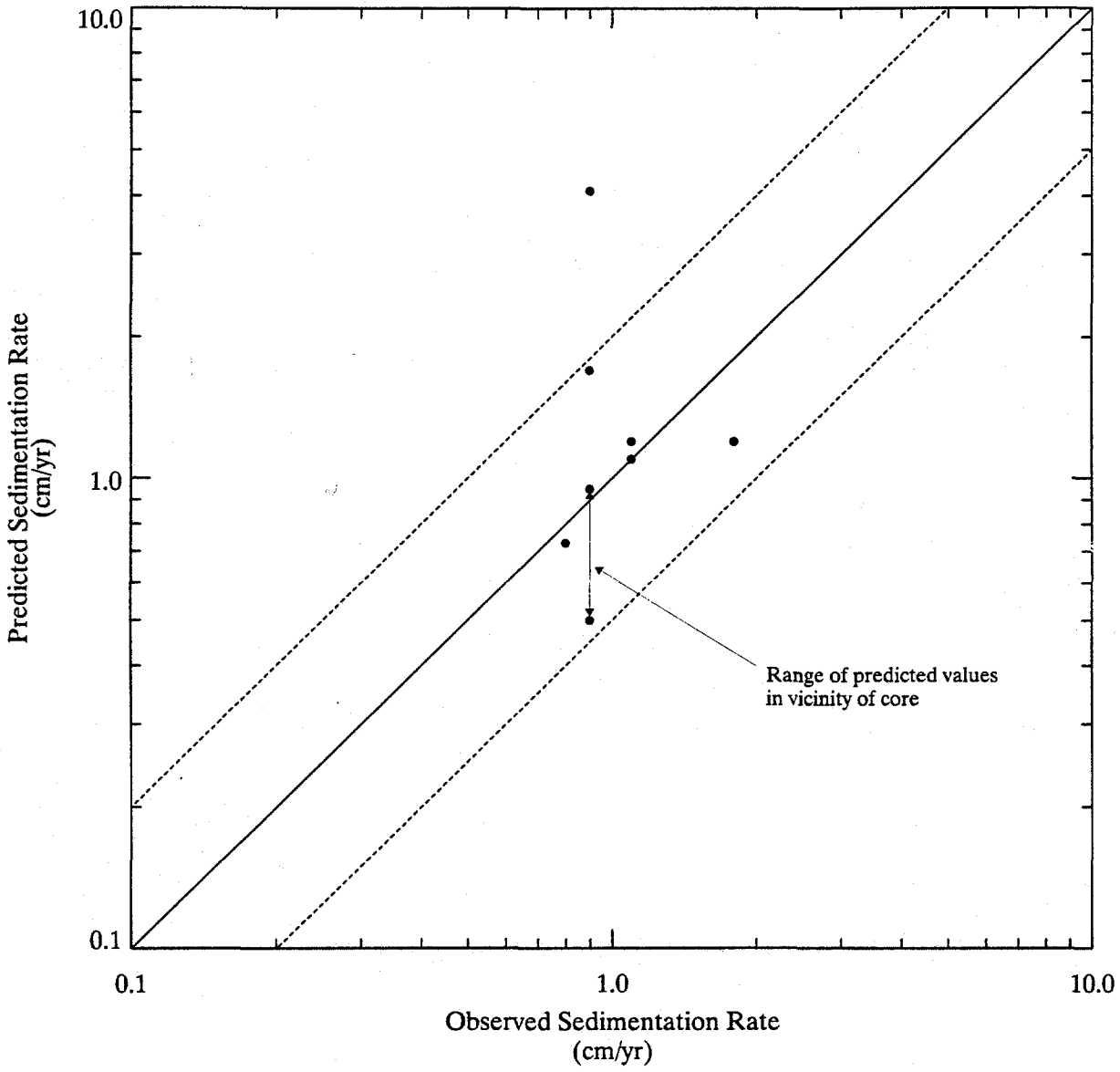

Figure 3-48. Comparison of predicted and observed sedimentation of rates at various UHR locations Dashed lines represent factor of two error limits, with repect to line of perfect agreement

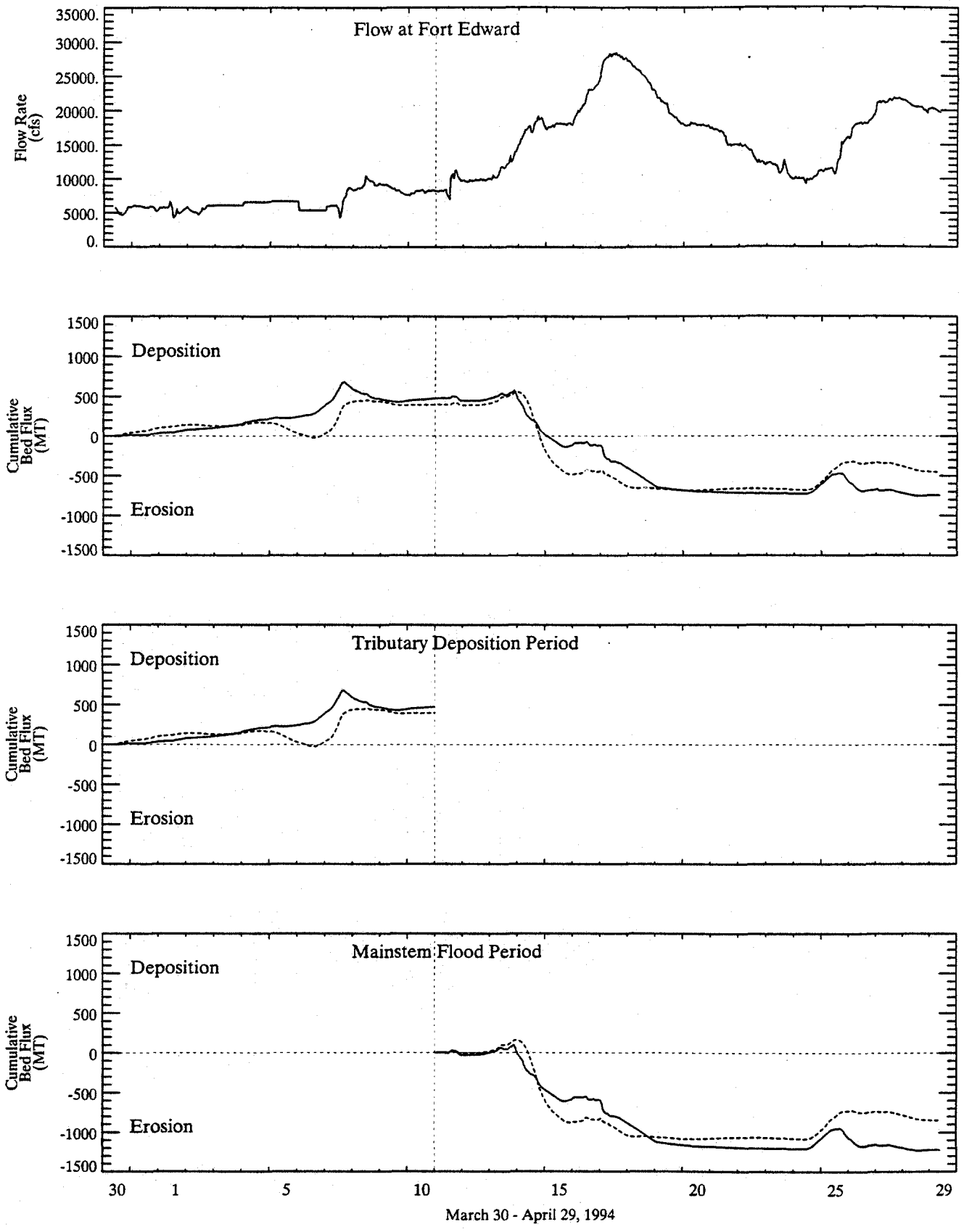

Figure 3-49. Comparison of predicted (solid line) and data-based (dashed line) changes in TIP sediment bed mass during the 1994 spring flood. Initial condition for non-cohesive bed properties estimated as shown on Figures 3-10 and 3-11.

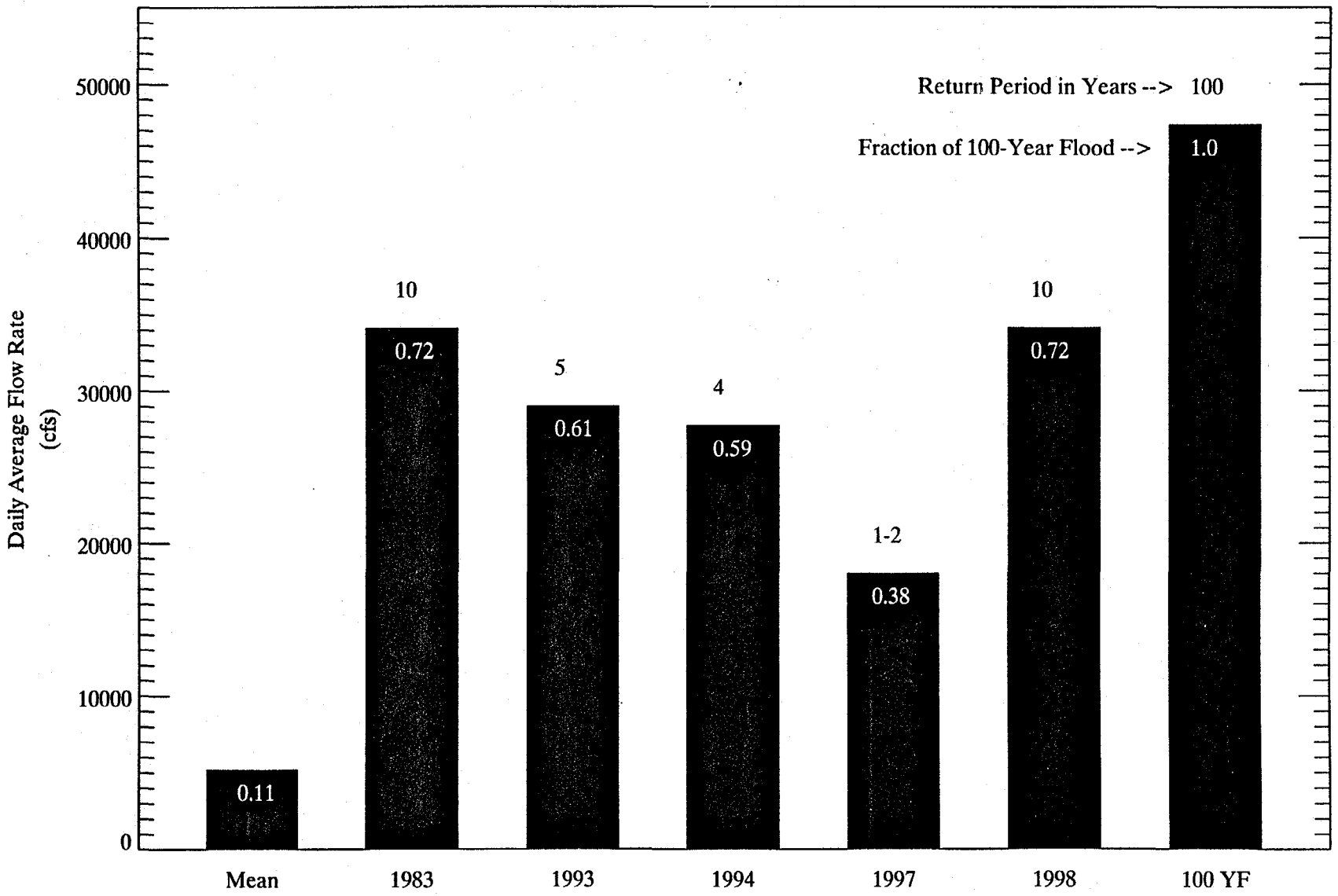

Figure 3-50. Comparison of peak daily average flow rates at Fort Edward during various historical floods to 100-year flood peak discharge. Mean flow rate represents long-term average at that gauging station.

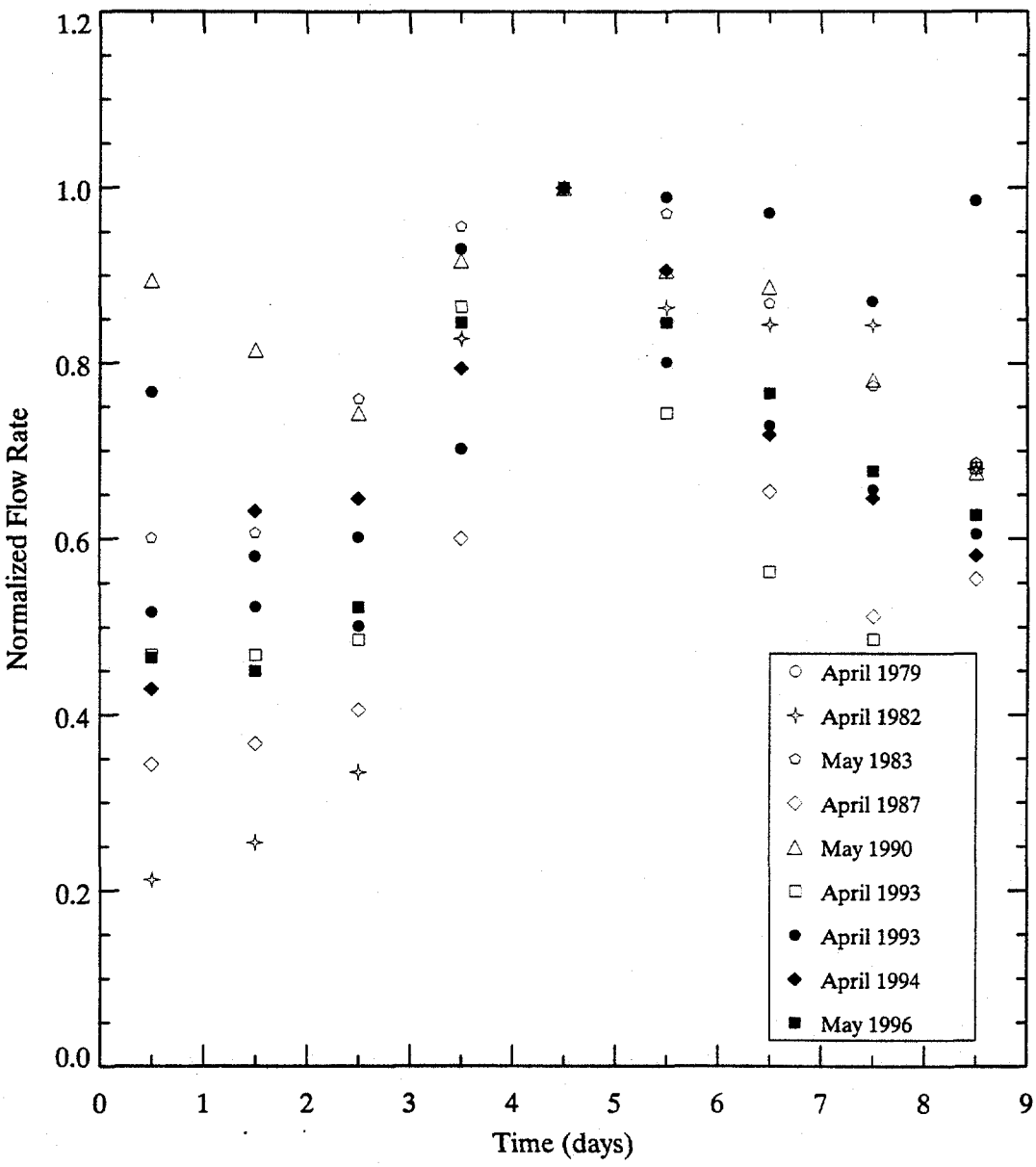

Figure 3-51. Normalized Fort Edward flood hydrographs for nine floods that occurred between 1977 and 1997.

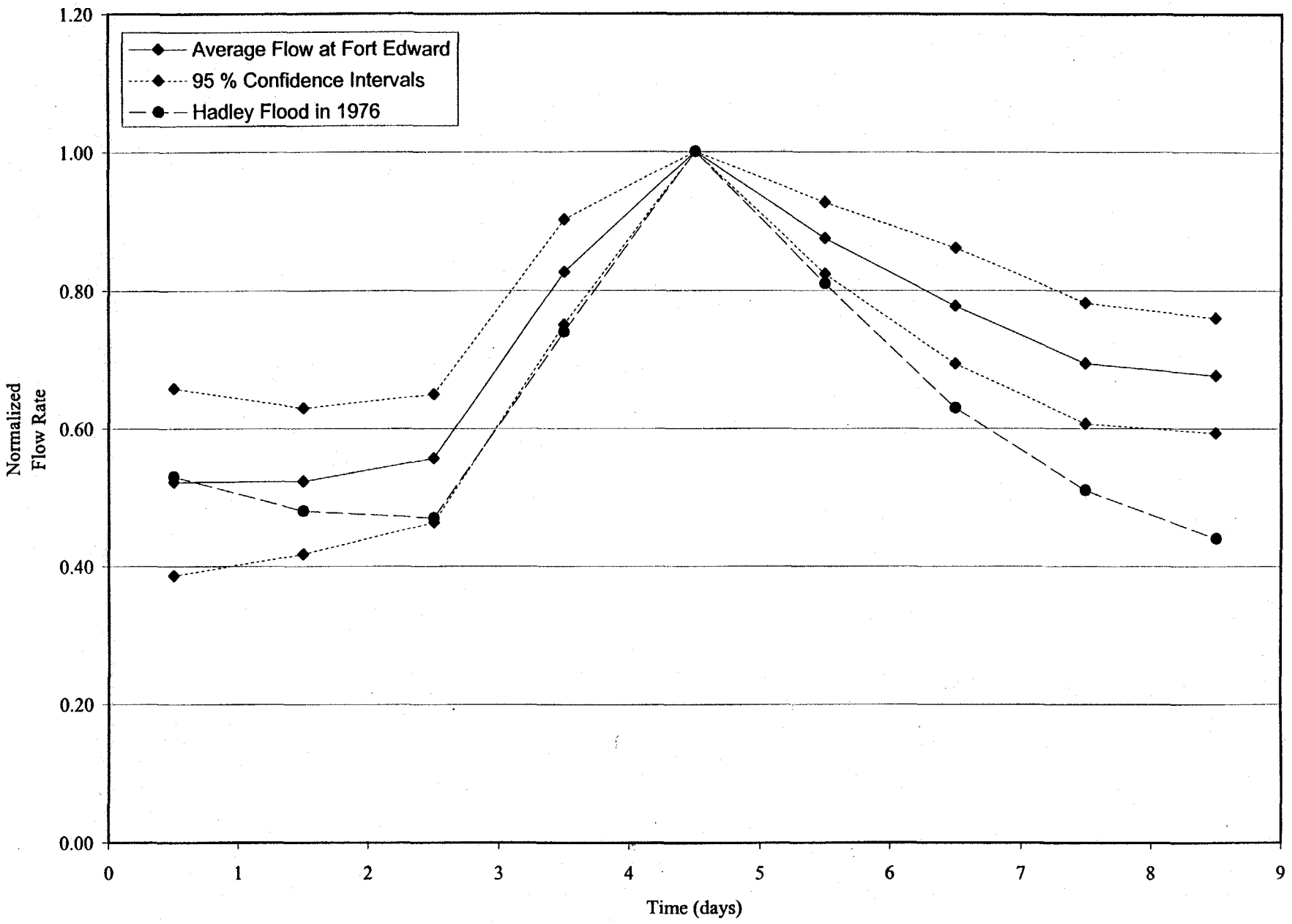

Figure 3-52. Normalized synthetic hydrograph at Fort Edward used for the 100-year flood simulation.

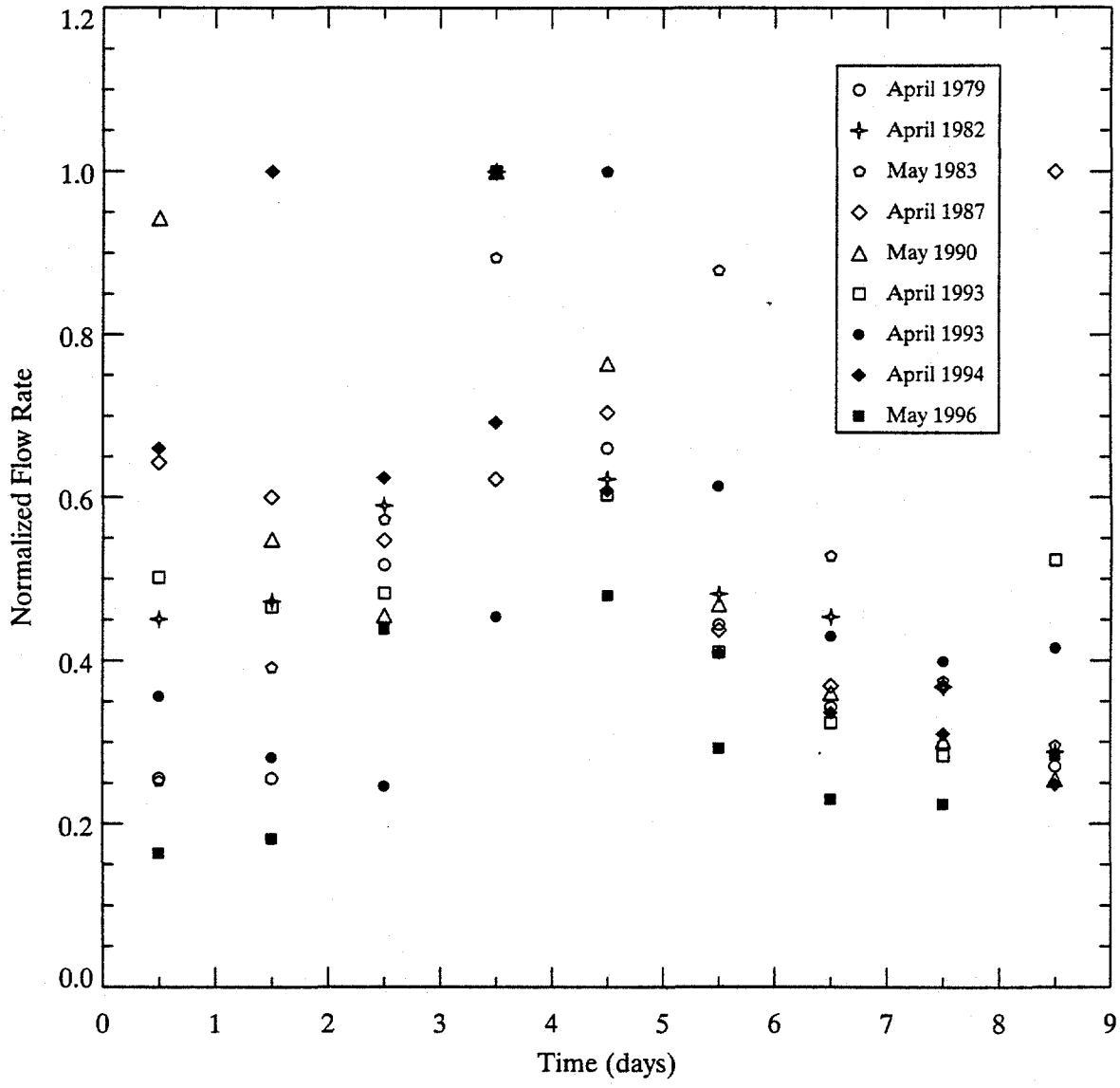

Figure 3-53. Normalized Kayaderosseras Creek flood hydrographs for nine floods that occurred between 1977 and 1997.

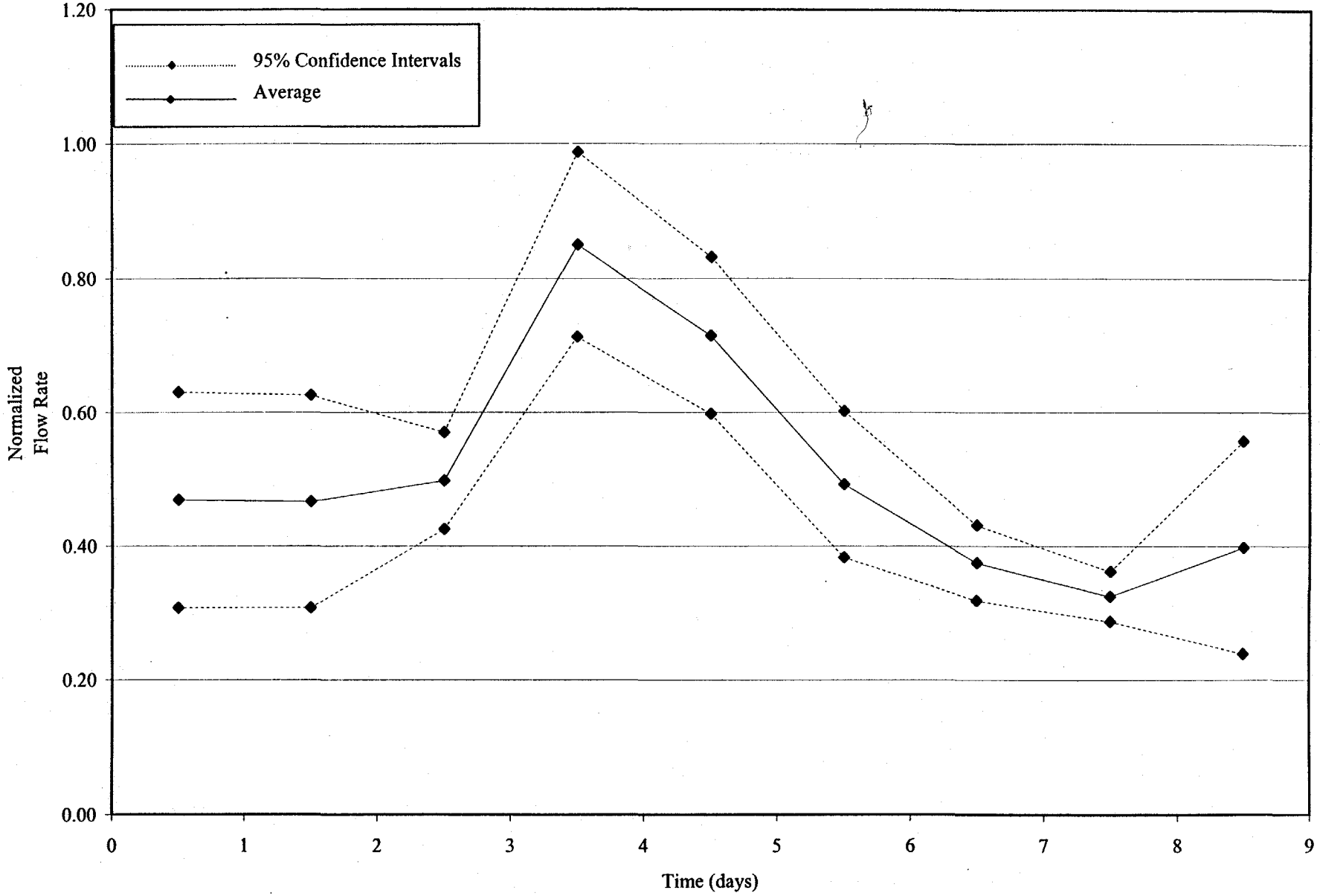

Figure 3-54. Normalized synthetic hydrograph used to specify Kayaderosseras Creek discharge during the 100-year flood simulation.

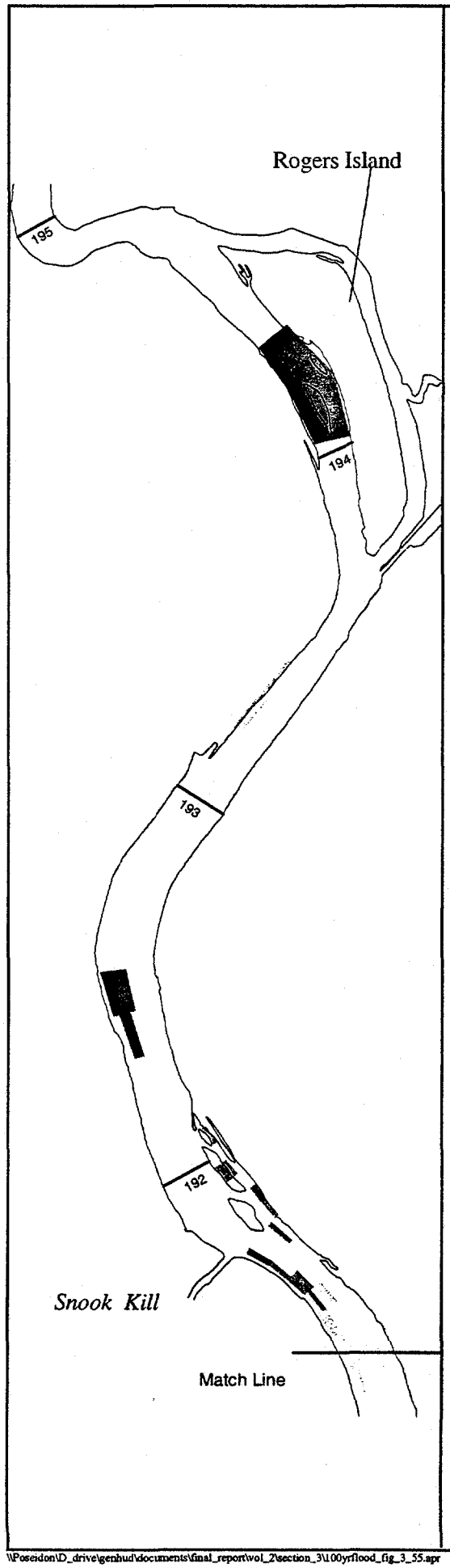

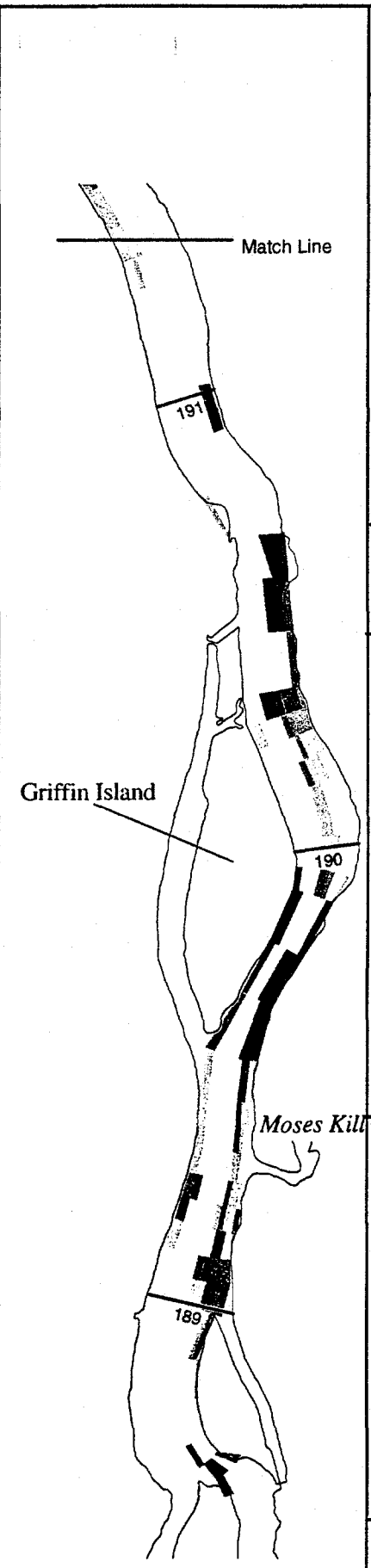

LOCATION MAP OF THE HUDSON RIVER

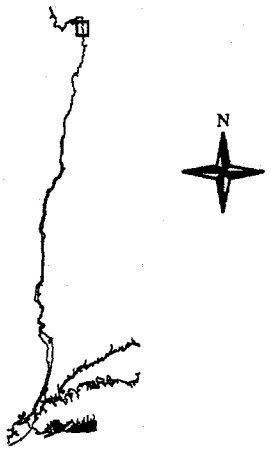

GRAPHIC SCALE

0.2 0 0.2 Miles

LEGEND

- Uppershore
- Mile Points
- Rocky Areas
- Rocky Areas

Bed Elevation Changes (cm)

- > -5
- -5 - -4
- -4 - -3
- -3 - -2
- -2 - -1
- -1 - 0
- Deposition

GENERAL ELECTRIC COMPANY
Hudson River Project

PCBs in the Upper Hudson River
Volume 2. A Model of PCB Fate, Transport and Bioaccumulation

Figure 3-55.

Predicted erosion depths (cm) for 100 year flood.

QEA
Quantitative Environmental Analysis, LLC

Project: Genhud 131 April 1999

\\Poseidon\D_drive\genhud\documents\final_report\vol_2\section_3\100yrflood_fig_3_55.apr

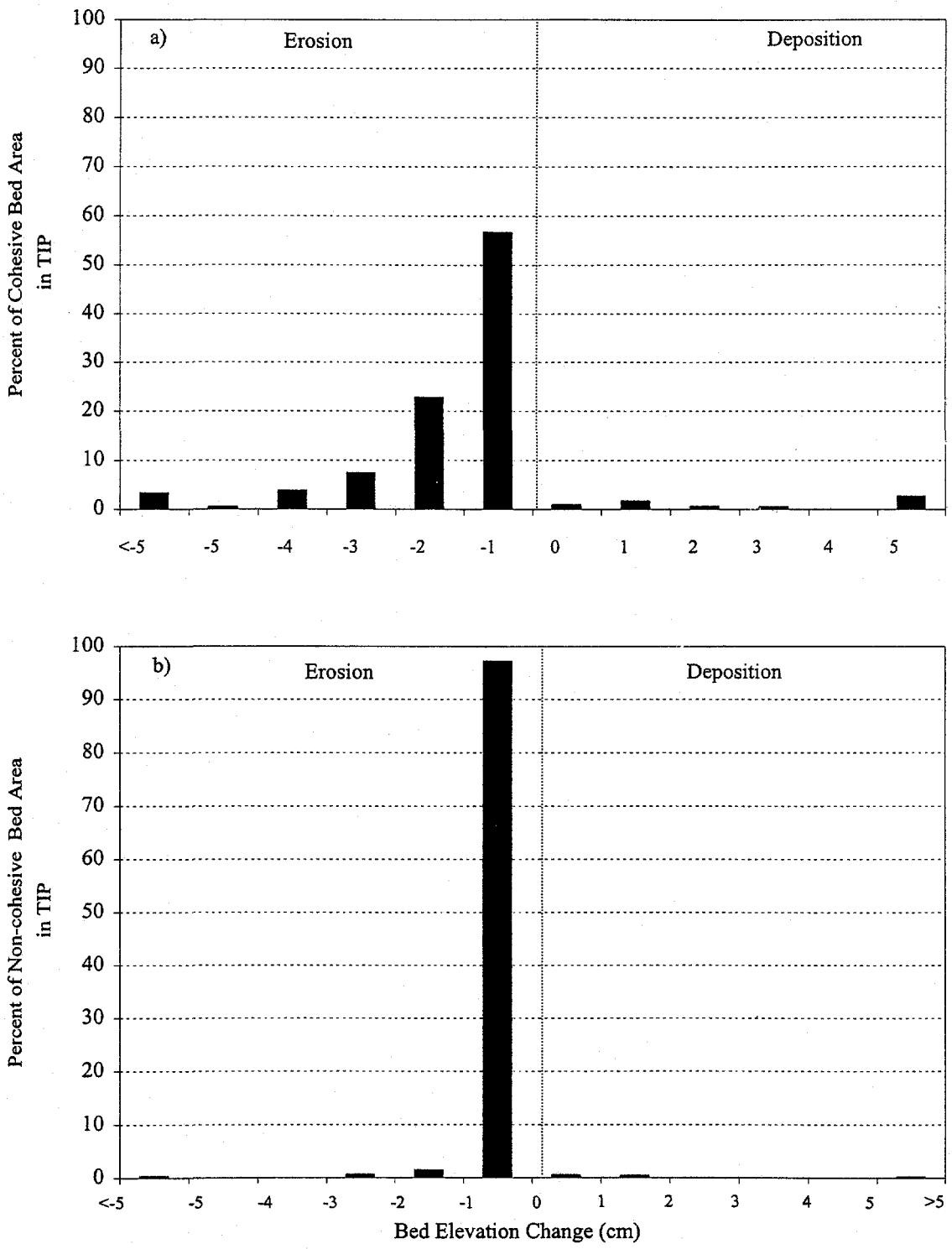

Figure 3-56. Predicted distributions of (a) cohesive and (b) non-cohesive bed elevation changes in the TIP at the end of the 100-year flood.

poseidon\d_drive\GENhud\documents\final_report\vol_2\section_3\flood_elev_100yf_fig_3_56.xls
4/14/99

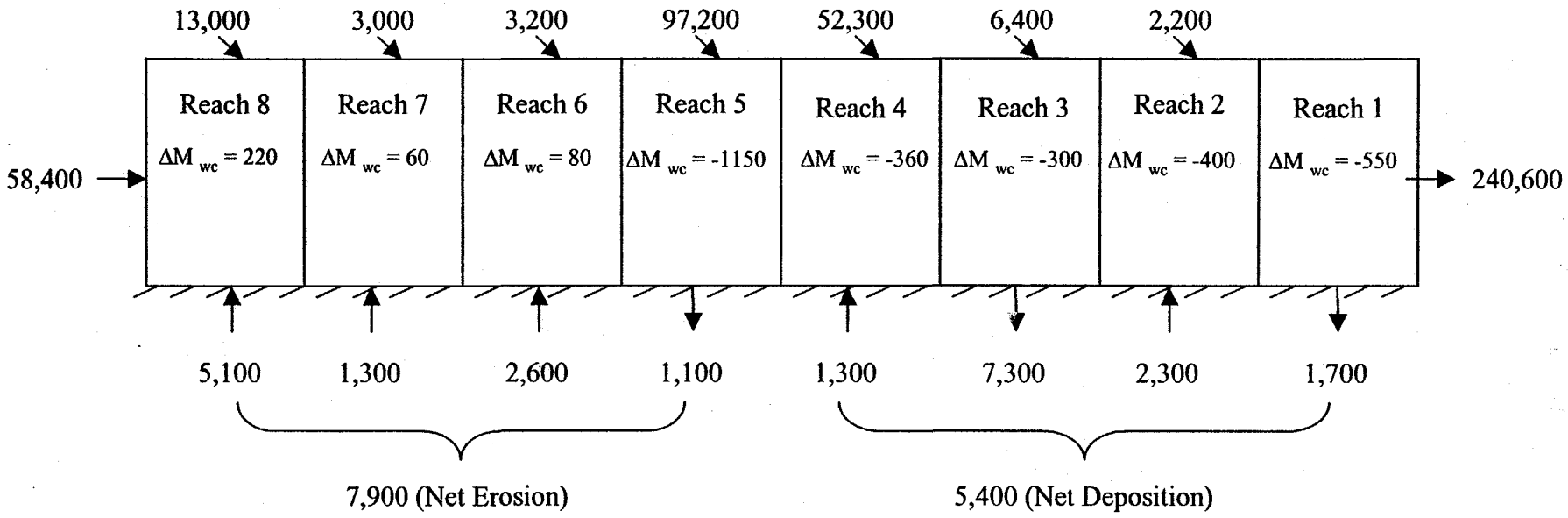

313835A

Figure 3-57. Sediment mass balance for the 100-year flood simulation, Reaches 1 to 8. Sediment masses are in MT.

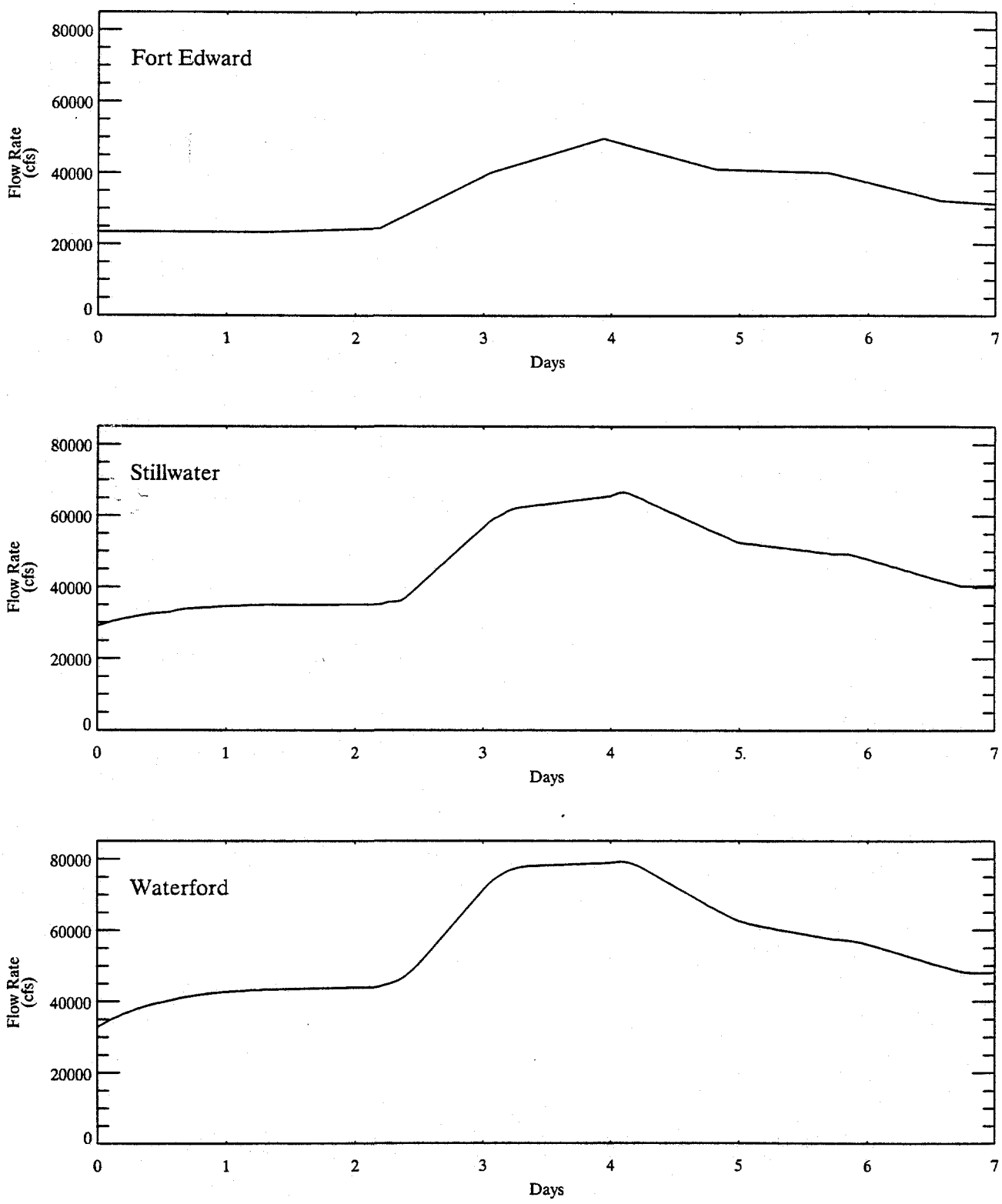

Figure 3-58. Flow rate time-series during the 100-year flood at Fort Edward, Stillwater and Waterford

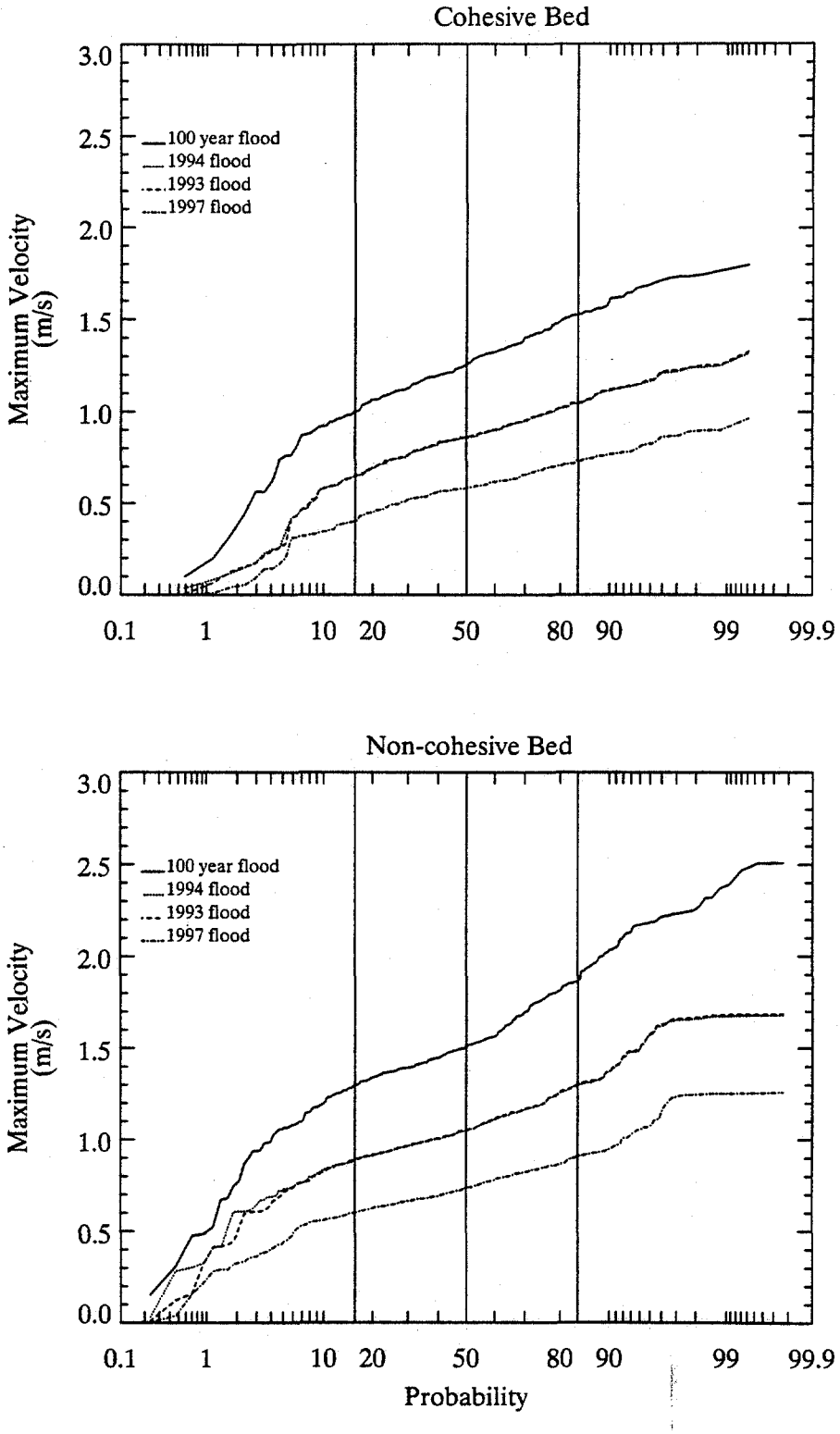

Figure 3-59. Probability distributions of TIP current velocity during 1993, 1994, 1997 and 100-year floods.

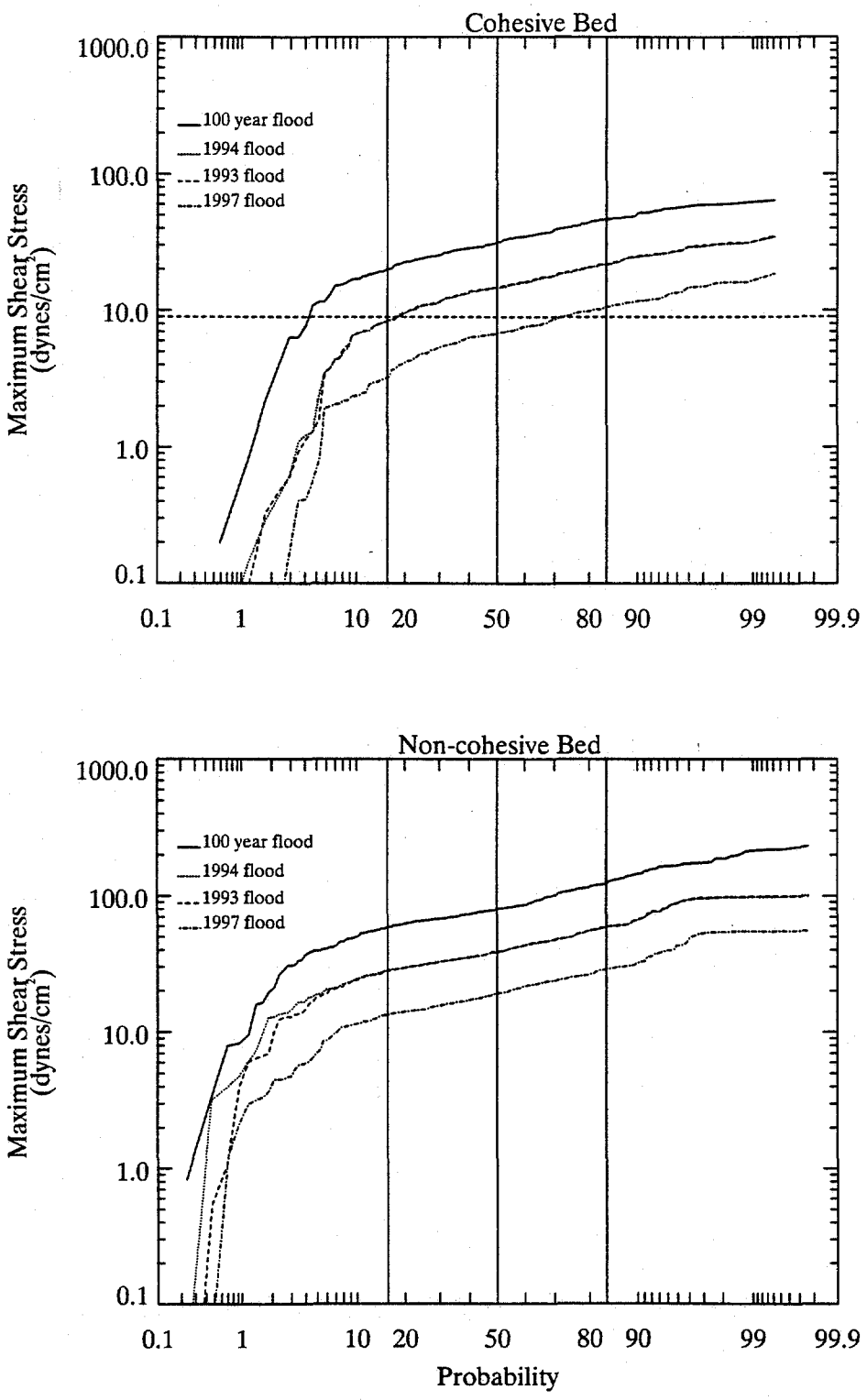

Figure 3-60. Probability distributions of TIP bottom shear stress during 1993, 1994, 1997 and 100-year floods.

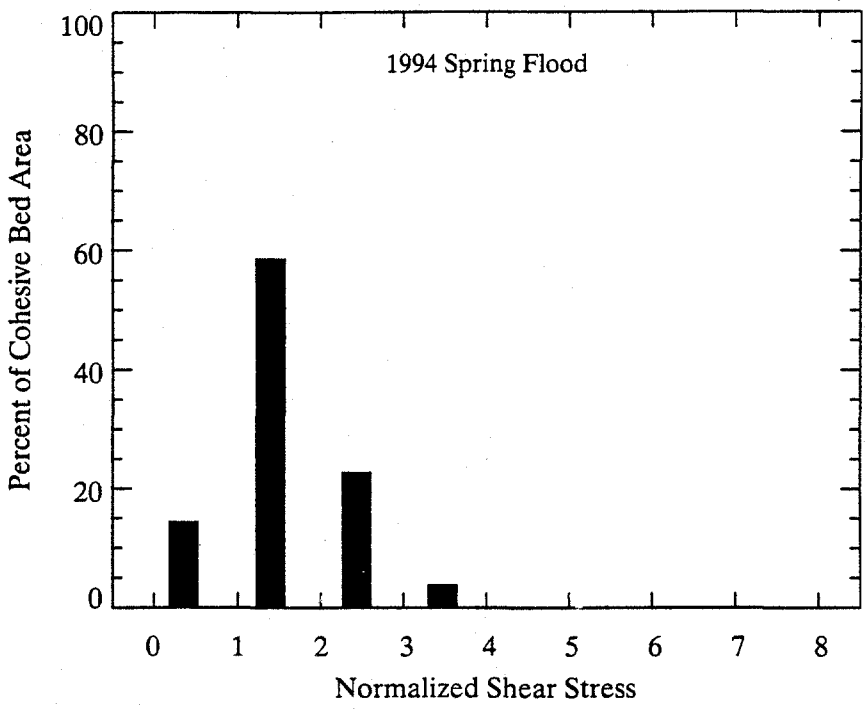

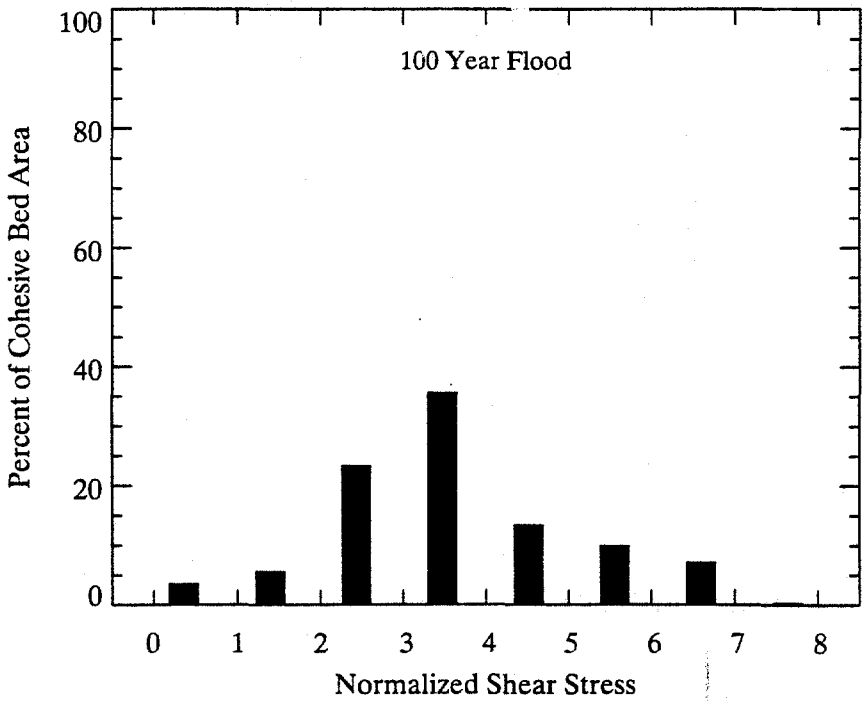

Figure 3-61. Distribution of maximum bottom shear stresses (normalized with respect to 9 dynes/cm^2) during the 1994 spring flood and the 100 year flood.

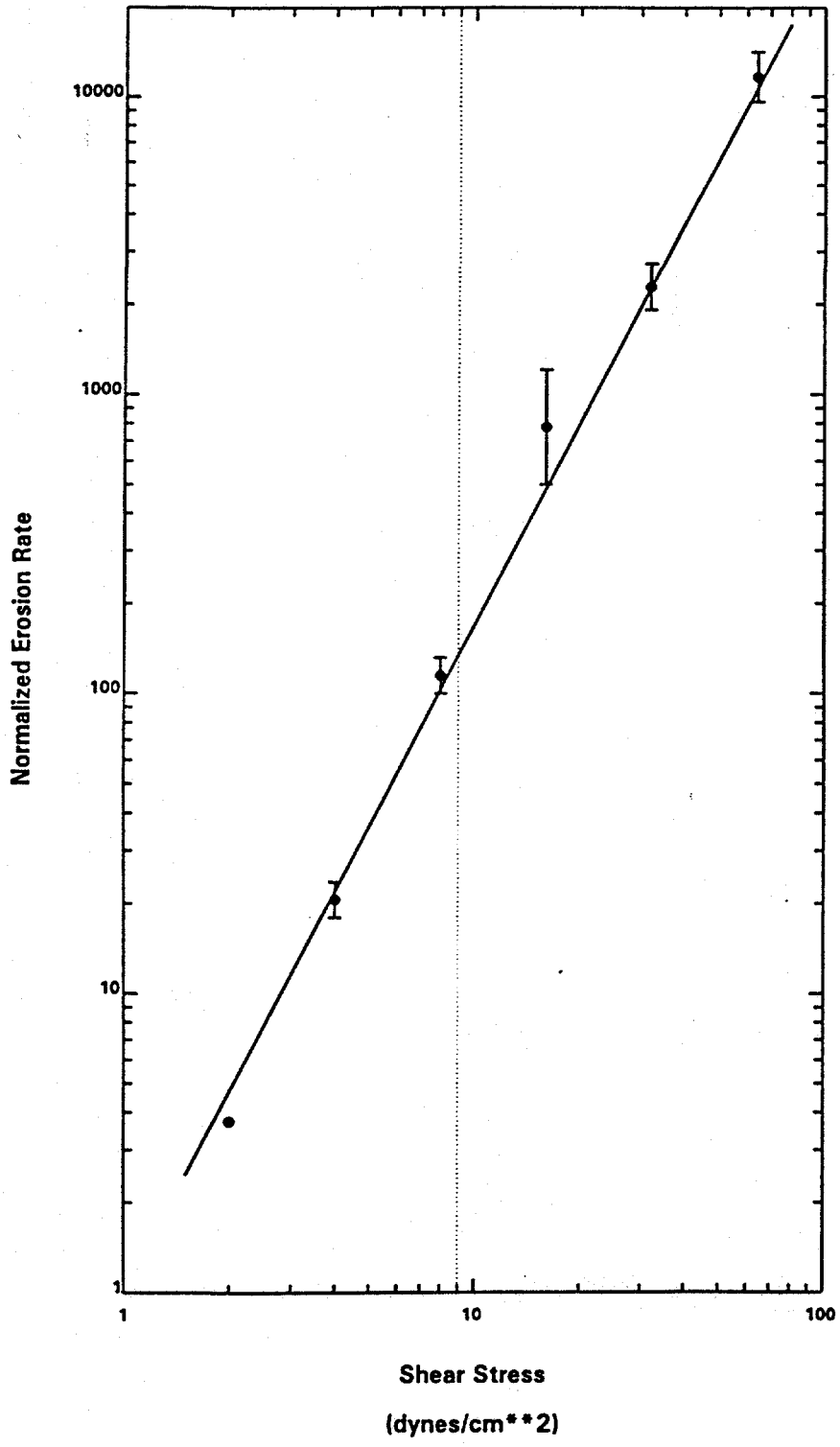

Figure 3-62. Results of cohesive erosion rate experiments conducted by Jepsen et al. (1997). Measured erosion rates were normalized with respect to bed bulk density.

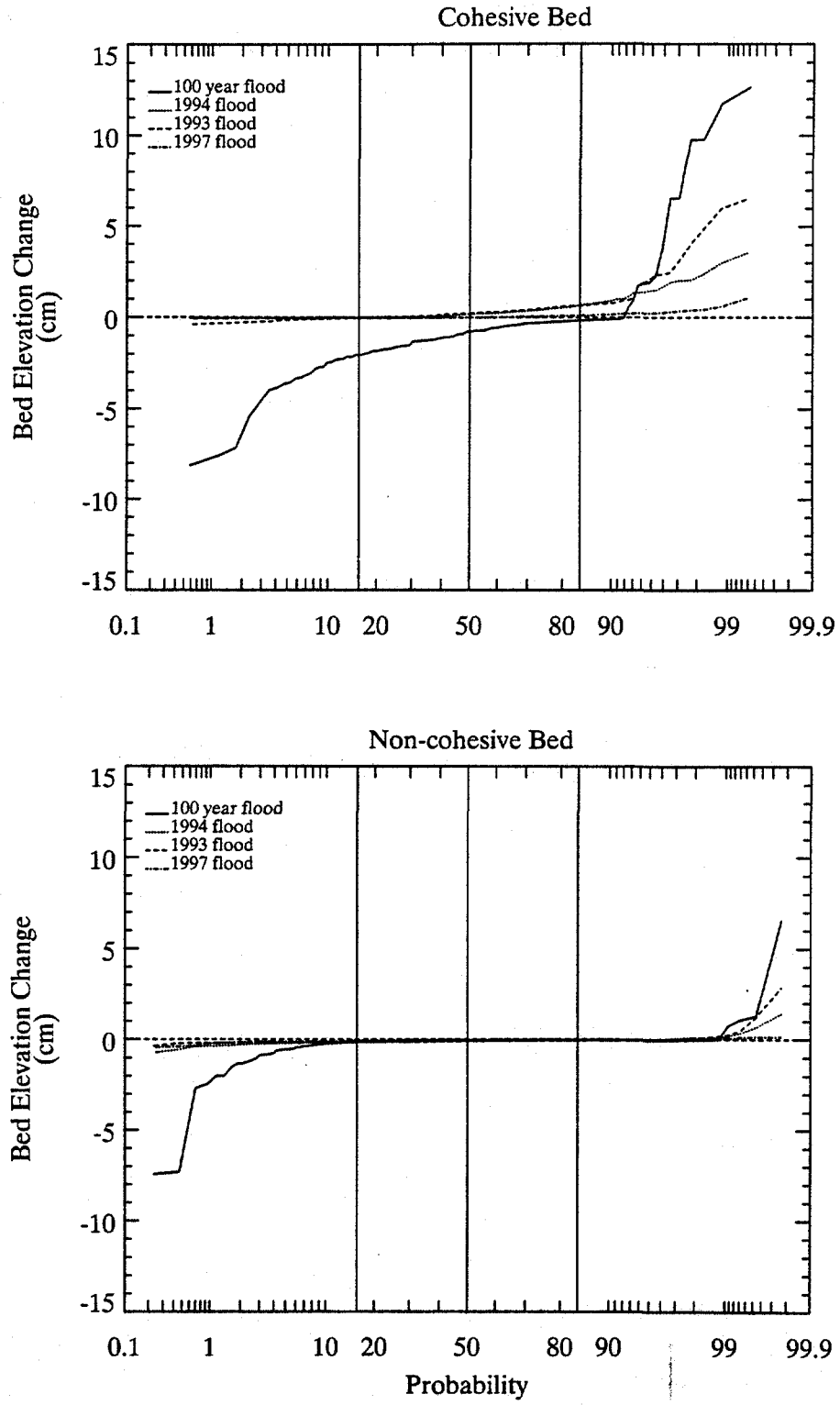

Figure 3-63. Probability distributions of TIP bed elevation change during 1993, 1994, 1997 and 100-year floods.

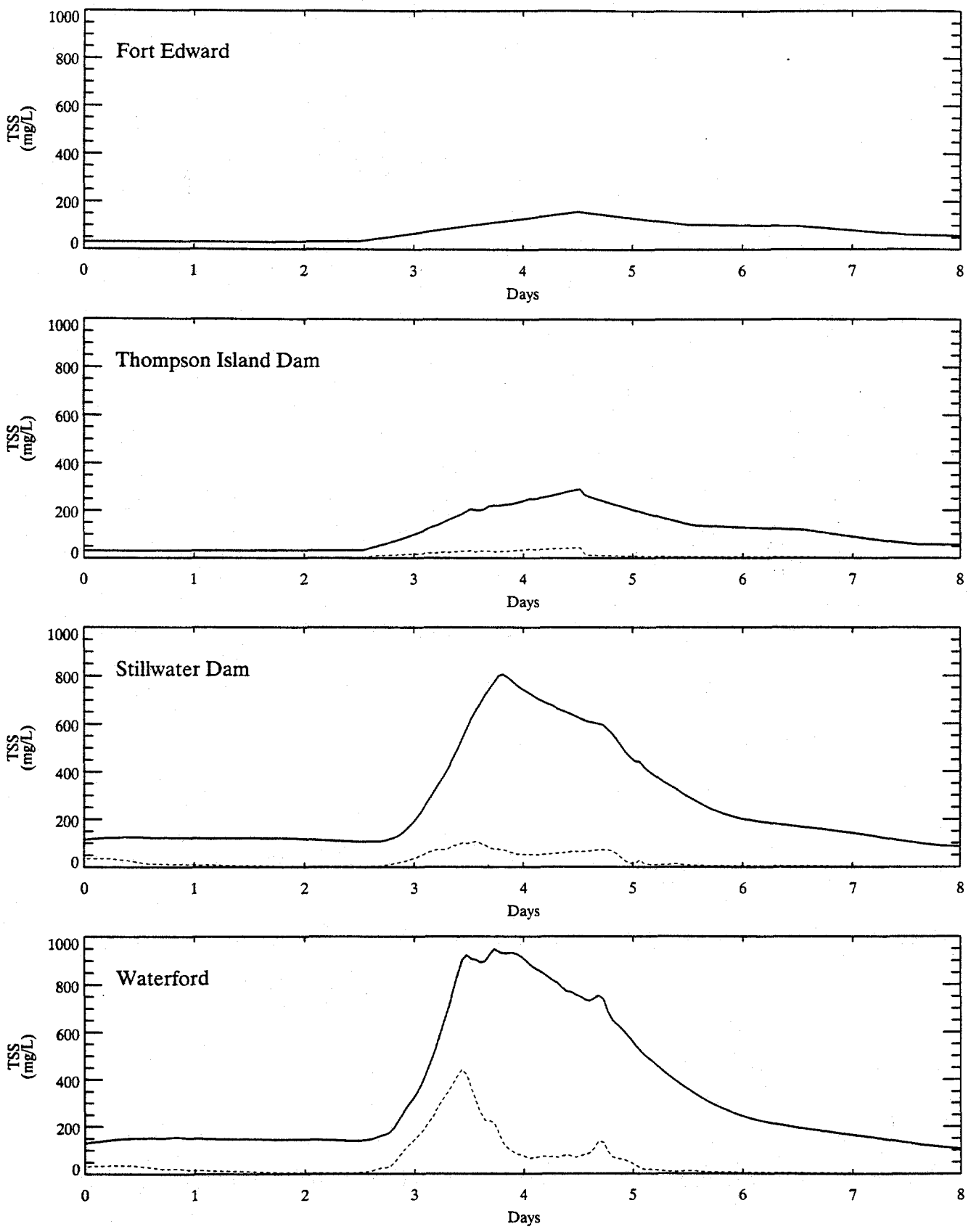

Figure 3-64. Sediment concentration time series during the 100 year flood at Fort Edward, Stillwater, and Waterford. Zero sediment load results shown as dashed line.

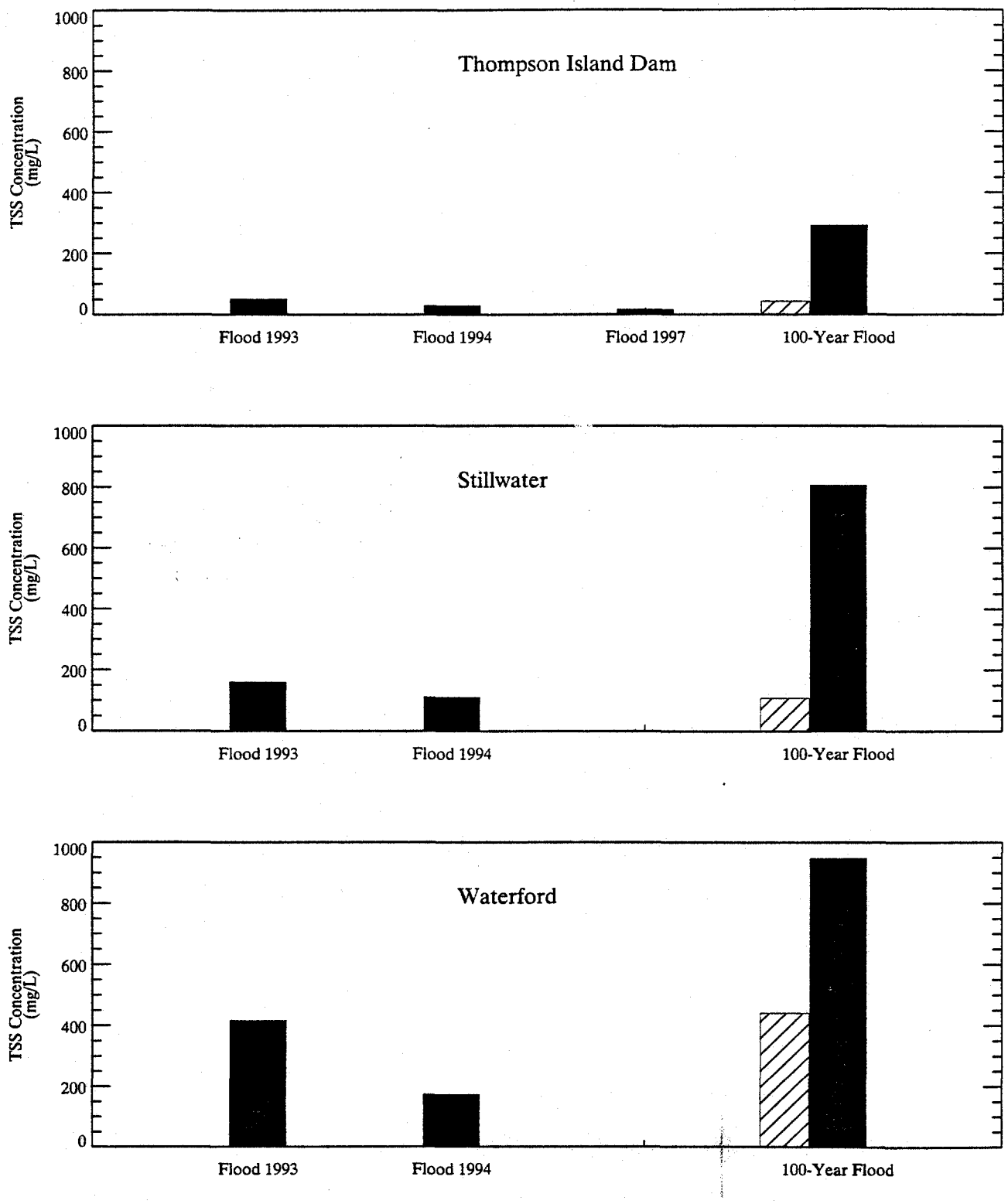

Figure 3-65. Comparison of maximum tss concentration predicted during historical and 100-year flood simulations at TID, Stillwater and Waterford. Zero sediment load simulation results for the 100-year flood are shown as cross-hatched bar.

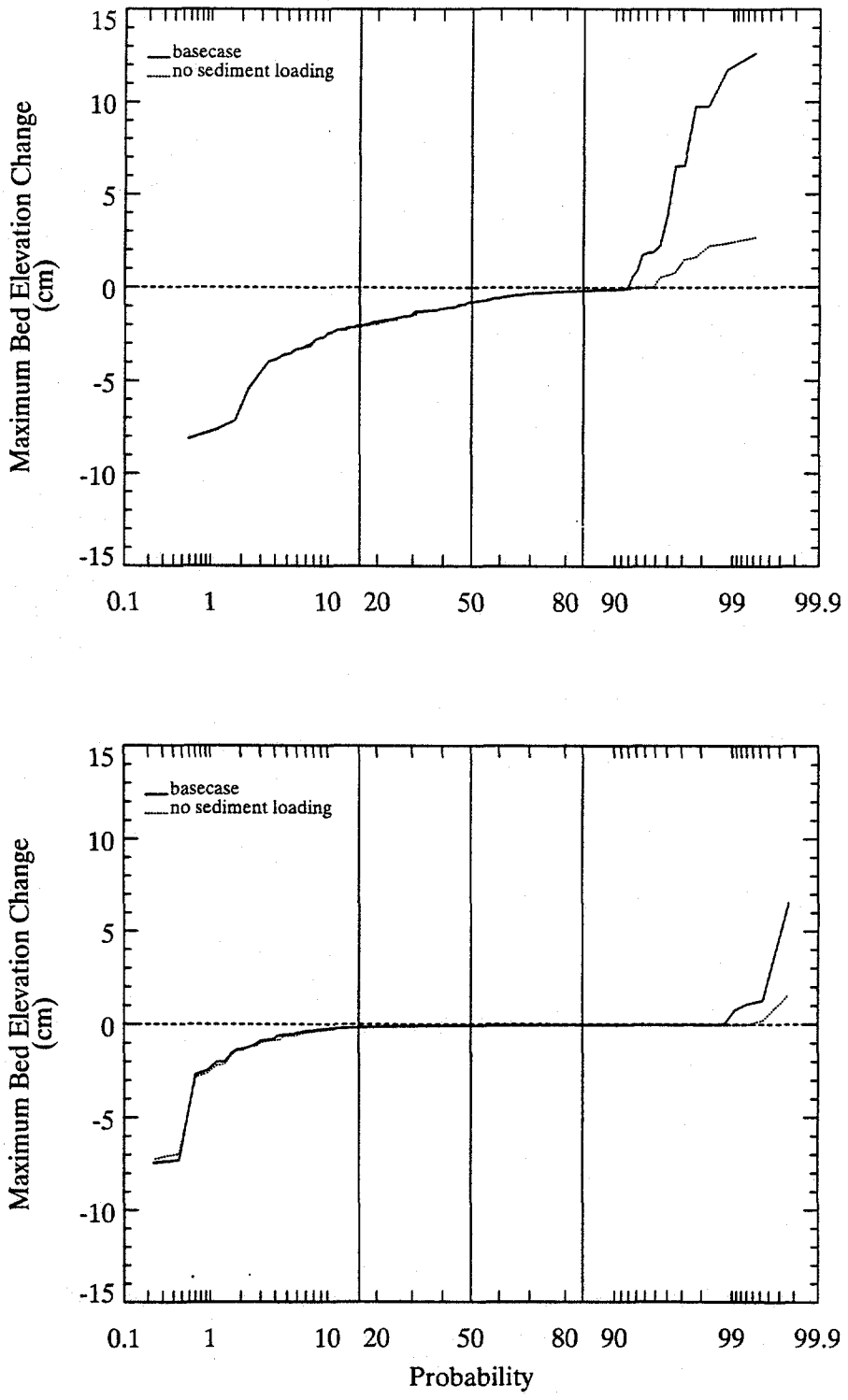

Figure 3-66. Probability distributions of maximum TIP bed elevation change during basecase and no sediment loading 100-year floods.

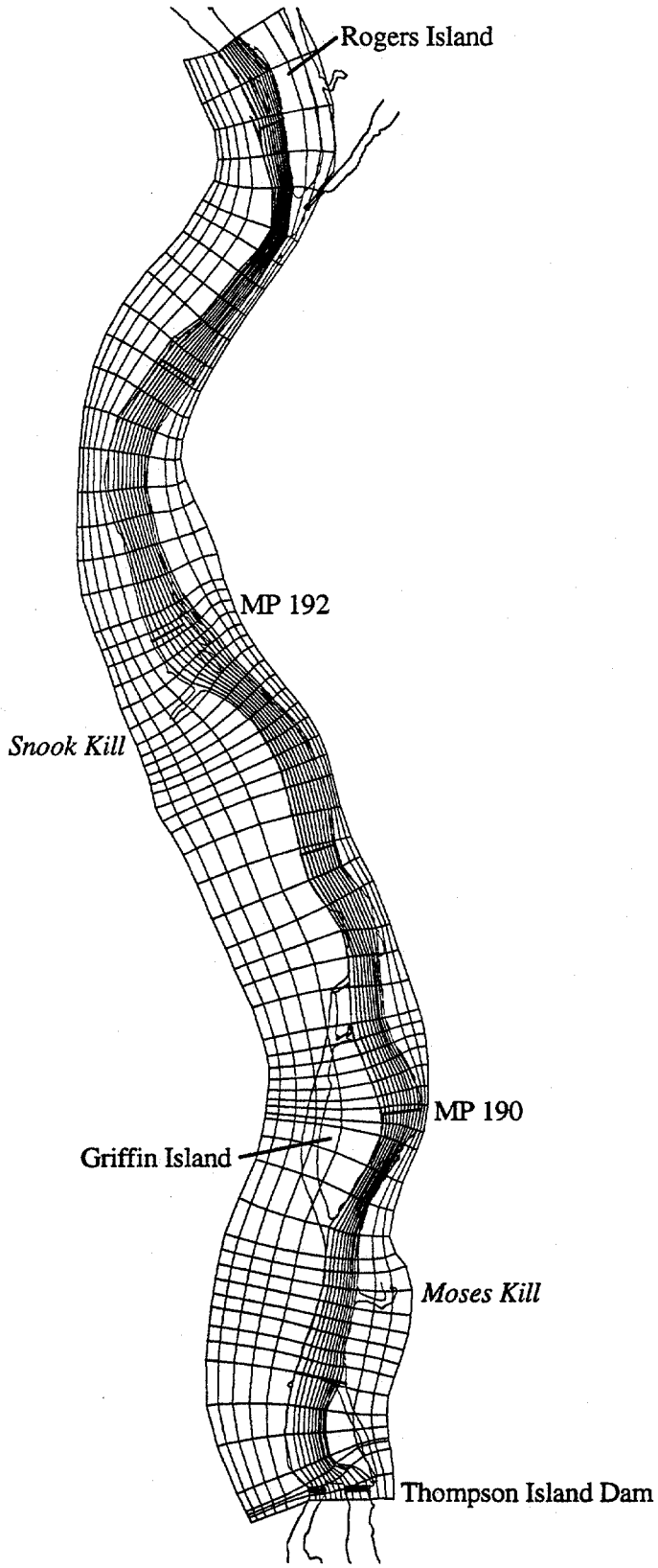

LOCATION MAP OF THE HUDSON RIVER

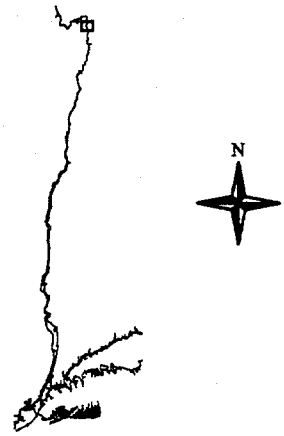

GRAPHIC SCALE

0.3 0 0.3 0.6 Miles

LEGEND

- Shoreline
- Mile Points
- Dams and Locks
- Reach 8 Grid
- Flood Plain Grid

GENERAL ELECTRIC COMPANY
Hudson River Project

PCBs in the Upper Hudson River
Volume 2. A Model of PCB Fate, Transport and Bioaccumulation

Figure 3-67.

Two-dimensional TIP numerical grid with flood plain grid elements.

QEA
Quantitative Environmental Analysis, LLC

Project: Genhud 131 April 1999

\\Poseidon\d_drive\genhud\documents\final_report\vol_2\section_3\2dnumerical_grid_fig_3_67.apr

PCB Fate Model

Section 4

Quantitative Environmental Analysis, LLC

313846

SECTION 4
PCB FATE MODEL

4.1 BASIC EQUATIONS

The processes that determine the fate of PCBs in the Upper Hudson River may be divided into two classes; (a) transport and (b) transfer and reaction. Transport is the physical movement of PCBs caused by the net advective movement of water, mixing, and resuspension/deposition of solids to which PCBs are adsorbed. It is specified by the flow and dispersion characteristics in the water column and the settling velocity and resuspension rate of the solids. Transfer and reaction include movement of PCBs among the air, water, and solid phases of the system and biological [or biochemical] transformation or degradation of the compound. The processes involved in transfer and reaction are volatilization, adsorption, dechlorination and biodegradation.

A conceptual model of PCB fate is presented pictorially in Figure 4-1. PCBs are present in three interacting phases: 1) freely dissolved; 2) sorbed to particulate matter or solids; and 3) sorbed or complexed with dissolved or colloidal organic matter (DOM). PCB concentration is affected by the various transport, transfer and reaction processes as well as external loadings from the upstream plant site areas. A mathematical model of the system was developed from the conceptual model by application of the principal of conservation of mass. Using this principal, mechanistic descriptions of the various processes were combined to form the basic mass balance equations that constitute the model. The external loadings were incorporated as forcing functions in the solution of the equations.

Consider the concentration, c, to be the freely dissolved component of PCBs in water. It interacts with the particulate component (i.e., the component sorbed to particulate matter) at concentration p, through an adsorption-desorption reaction. The particulate PCB concentration is expressed as:

$$p = rm \tag{4-1}$$

where:

p	=	particulate PCB concentration (M/L^3)
r	=	mass of chemical/unit mass of solids (M/M)
m	=	concentration of the solids (M/L^3)

Initially ignoring the component sorbed to DOM, the equations governing the distribution of the dissolved and particulate components in any surface water system may be written as follows (Connolly and Winfield 1984):

$$\frac{\partial c}{\partial t} = \frac{\partial}{\partial x}\left(E_x \frac{\partial c}{\partial x}\right) + \frac{\partial}{\partial y}\left(E_y \frac{\partial c}{\partial y}\right) + \frac{\partial}{\partial z}\left(E_z \frac{\partial c}{\partial z}\right) - \frac{\partial}{\partial x}u_x c - \frac{\partial}{\partial y}u_y c - \frac{\partial}{\partial z}u_z c - K_o mc + K_2 p \pm S_1(s,y,z,t) \tag{4-2}$$

$$\frac{\partial p}{\partial t} = \frac{\partial}{\partial x}\left(E_x \frac{\partial p}{\partial x}\right) + \frac{\partial}{\partial y}\left(E_y \frac{\partial p}{\partial y}\right) + \frac{\partial}{\partial z}\left(E_z \frac{\partial p}{\partial z}\right) - \frac{\partial}{\partial x}u_x p - \frac{\partial}{\partial y}u_y p - \frac{\partial}{\partial z}u_z p + \frac{\partial}{\partial z}w_s p + K_o mc - K_2 p \pm S_2(s,y,z,t) \tag{4-3}$$

where:

E	=	dispersion coefficient (L^2/T)
u	=	velocity (L/T)
w_s	=	settling velocity of the particulates (L/T)
K_o	=	adsorption coefficient ($L^3/(M \cdot T)$)
K_2	=	desorption coefficient (1/T)
x,y,z	=	coordinate directions (L)
t	=	time (T)
S_i	=	sources and sinks of the component due to reactions, phase transfers and resuspension of contaminated bed sediment

The first three terms in each equation represent dispersion or mixing due to temporal and spatial velocity gradients and density differences within the river. The next three terms represent longitudinal, lateral and vertical advection, respectively. The seventh term in Equation (4-3) accounts for the vertical advection of the particulate component due to settling. The following two terms (and the seventh and eighth terms in Equation (4-2)) define the rate of adsorption and desorption, respectively. The last term in both equations accounts for the chemical and biological reactions and volatilization (water column only) that may produce or degrade the component.

Adsorption is generally treated as a rapid process relative to other processes affecting PCBs. Following the conventional assumption, local instantaneous equilibrium is assumed. Further, since vertical concentration gradients are small in the water column of a riverine system such as the Hudson, the problem may be reduced to the longitudinal and lateral dimensions. This permits the reduction of the equations for dissolved and particulate chemical (Equations 4-2 and 4-3) to the following single equation for total chemical concentration, c_T:

$$\frac{\partial c_T}{\partial t} = \frac{\partial}{\partial x}\left(E_x \frac{\partial c_T}{\partial x}\right) + \frac{\partial}{\partial y}\left(E_y \frac{\partial c_T}{\partial y}\right) - \frac{\partial u_x c_T}{\partial x} - \frac{\partial u_y c_T}{\partial y} - \frac{D_{iot}}{hm}\left(f_p c_T\right) \pm S \qquad (4\text{-}4)$$

where:

S	=	$S_1 + S_2$
D_{tot}	=	depositional flux of solids calculated by the sediment transport model ($M/(L^2 \cdot T)$)
h	=	depth of the water column (L)

and

$$c = f_d c_T \qquad (4\text{-}5)$$

$$p = f_p c_T \qquad (4\text{-}6)$$

where:

f_d = fraction dissolved

f_p = fraction particulate

The expressions for fraction dissolved and fraction particulate are derived from the relationship defining equilibrium adsorption. For organic chemicals whose adsorption is classified as hydrophobic bonding, equilibrium adsorption at environmentally relevant concentrations (i.e., less than 10^{-5}M or one-half water solubility) is linearly related to dissolved chemical concentration (Karickhoff 1984) and may be written as:

$$r = K_p c \tag{4-7}$$

where K_p is the adsorption partition coefficient. Using Equation (4-7), the resulting expressions for fraction dissolved and fraction particulate are:

$$f_d = \frac{\theta}{\theta + K_p m} \tag{4-8}$$

$$f_p = \frac{K_p m}{\theta + K_p m} \tag{4-9}$$

where θ is the porosity (water volume/total volume) and m is the concentration of suspended or bed solids.

Inclusion of the component sorbed to DOM alters Equation (4-4) by changing the definitions of f_d and f_p and adding a third component equation for the fraction sorbed to DOM (f_{dom}). Applying the local instantaneous equilibrium assumption and expressing the DOM concentration as mass of organic carbon per unit volume, the expressions for fraction dissolved, fraction particulate and fraction sorbed to DOM become:

$$f_d = \frac{\theta}{\theta + K_p m + K_{doc} m_{doc}} \quad (4\text{-}10)$$

$$f_p = \frac{K_p m}{\theta + K_p m + K_{doc} m_{doc}} \quad (4\text{-}11)$$

$$f_{dom} = \frac{K_{doc} m_{doc}}{\theta + K_p m + K_{doc} m_{doc}} \quad (4\text{-}12)$$

where:

K_{doc} = the partition coefficient between PCBs sorbed to DOM and freely dissolved (liters/kg organic carbon)

m_{doc} = concentration of dissolved organic matter expressed in terms of organic carbon (kg organic carbon/liter)

The component fractions are applied to the various processes included in the source/sink term (S) in Equation (4-4). The descriptions of these processes are presented in Section 4.2.

A number of the terms in Equations (4-4) to (4-12) are supplied by the coupled hydrodynamic and sediment transport models. The one-dimensional hydrodynamic model provides longitudinal velocities (u_x) and water depths (h) using the method outlined in Section 2. Sediment transport information, (i.e., suspended solids concentration (m) and deposition and resuspension fluxes) is transferred to the PCB fate model via the direct and indirect coupling procedures discussed in Section 3.

The equation governing the distribution of PCBs within the sediment is similar to Equation (4-4), however, advection and dispersion are defined differently and only vertical transport is considered. Advection within the sediment applies only to the fraction of the PCBs in the pore water (i.e., the freely dissolved and DOM bound fractions). Dispersion is applied separately to the particulate fraction and the fraction in the pore water. The particulate fraction in surface sediments is subject to mixing due to biological activity and the propagation of water

turbulence into the bed. The fraction in the pore water is subject to molecular diffusion and dispersion associated with advection. This mixing is parameterized by the dispersion coefficient E_d. The bed equation is as follows:

$$\frac{\partial c_T}{\partial t} = \frac{\partial}{\partial z}\left(E_p \frac{\partial p}{\partial z}\right) + \frac{\partial}{\partial z}\left[E_d \frac{\partial (c + c_{dom})}{\partial z}\right] - \frac{\partial u_z (c + c_{dom})}{\partial z} \pm S_b \qquad (4\text{-}13)$$

where c_{dom} is the concentration of PCBs bound to DOM. The source/sink term (S_b) includes dechlorination and biodegradation. In solving the equation, the component concentrations are expressed as the product of the component fraction and the total chemical concentration (e.g., $c = f_i c_T$).

The sediment and water column equations are linked by fluxes at the water-bed interface. The equations are solved using finite difference numerical approximations with the interface fluxes (settling, resuspension, diffusion and advection) specified as boundary conditions. The settling and resuspension fluxes of PCBs are derived from the solids settling and resuspension fluxes provided by the linked sediment transport model (Section 3). The equation defining the diffusion boundary fluxes is presented in Section 4.2.1.

4.2 PROCESS DESCRIPTIONS

4.2.1 PCB Flux between Sediment Pore Water and the Water Column

The transfer of PCBs between sediment pore water and the water column occurs via some combination of diffusion and advection. Because advection is not significant (see Volume 1 of this report, Section 5.2.2.2), the total transfer is expressed as a diffusive process in which the flux is dependent on the concentration gradient between the water column and the surface sediment:

$$J_D = k_f \left[(c + c_{dom})_s - (c + c_{dom})_w \right] \qquad (4\text{-}14)$$

where J_D is an areal flux rate [i.e., the units are $M/(L^2T)$], k_f is the diffusive mass transfer coefficient (L/T), and the subscripts s and w refer to the sediment bed and water column, respectively. The areal flux is converted to a volumetric flux by dividing by depth of the water column. Thus, the term describing PCB flux between sediment pore water and the water column in Equation (4-14) is written as follows:

$$S_D = \frac{J_D}{h} \tag{4-15}$$

The mass transfer coefficient (k_f) is an empirical parameter that incorporates a number of processes occurring in the surface sediments, including molecular diffusion, turbulence, bioirrigation, bioturbation and advection. As such, its value is best determined through the analysis of field data.

4.2.2 Vertical Diffusion within the Bed

Vertical pore water diffusive transport within the sediment is mathematically described as a Fickian process, in which the diffusive flux is expressed as the product of the vertical gradient of dissolved plus DOM bound pore water concentration and a diffusion coefficient (D_s).

$$J_{i,j} = \frac{D_s}{l_{i,j}}\left[\left(c + c_{dom}\right)_i - \left(c + c_{dom}\right)_j\right] \tag{4-16}$$

The mixing length between adjacent bed segments i and j ($l_{i,j}$) is set at the distance between segment midpoints. The pore water diffusion coefficient is based on the molecular diffusion coefficient for PCB_{3+} in aqueous solution, adjusted for the tortuosity of the sediment bed. The effect of tortuosity is to decrease the rate of diffusion, as the solid matrix impedes the Brownian motion of dissolved PCB_{3+} molecules. Experimental data have shown that the effect of tortuosity can be expressed by multiplying the molecular diffusion coefficient in solution by the bed porosity raised to an exponent of approximately 2 (Lerman 1978).

4.2.3 Sorption

PCBs sorb to inorganic and detrital organic particulate material, microorganisms and "dissolved" humic material. For uncharged organic chemicals of limited water solubility such as PCBs, organic matter is the predominant sorptive component of the sorbant (Karickoff 1984). Generally, the sorptive tendency of such chemicals is described by a carbon-referenced sorption partition coefficient, K_{oc}. This partition coefficient describes the ratio of sorbed chemical concentration (mass of chemical sorbed per unit mass of organic carbon) to dissolved chemical concentration after the sorption reaction has attained equilibrium. K_{oc} is typically treated as a basic property of an organic chemical that is independent of the sorbant material. Since the sorption of uncharged organic chemicals is essentially a physical association between the chemical and the sorbant resulting from the hydrophobic nature of the chemical, the value of K_{oc} is proportional to other properties of the chemical that are related to hydrophobicity. By convention, the partitioning of an organic chemical between the hydrophobic organic solvent octanol and water is used as a measure of the chemical's hydrophobicity. The octanol/water partition coefficient, K_{ow}, has been shown to be approximately linearly related to laboratory determined K_{oc} values (Karickoff 1981, 1984; Baker *et al.* 1997) and it is common to assume that K_{oc} is equal to K_{ow}. Since K_{ow} values of PCBs range over 3 orders of magnitude, increasing with increasing chlorination, the appropriate K_{oc} value to describe partitioning of PCBs as a group (PCB_{3+} in the model) will depend on congener composition.

The use of an equilibrium partition coefficient to describe PCB sorption (see Equations (4-7) to (4-9)) requires the assumption that the kinetics of adsorption and desorption are much faster than other processes affecting PCBs. Sorption has fast and slow stages (Pignatello and Xing 1996). The fast stage has a time scale of minutes to hours, whereas the slow stage's time scale is weeks to months. This biphasic process may be caused by a number of phenomena, including: 1) rate limiting intra-particle and/or intra-organic matter diffusion; 2) different extents of sorption among the multiple types of organic matter present on the particle; and 3) rearrangement of the organic matter matrix after the chemical is sorbed. The conventional conceptual model of biphasic sorption includes a reversibly sorbing component with fast stage kinetics and a resistantly bound component with slow stage kinetics. Reversible sorption is

adequately described by the equilibrium partitioning model (DiToro and Horzempa 1982), resistant sorption is not. However, the resistant component is sometimes small and can be neglected. For example, McGroddy *et al.* (1996) found that equilibrium partitioning accurately described the partitioning of PCB congeners in Boston Harbor sediments and their desorption from those sediments in laboratory experiments.

It appears that sediments have a limited capacity for resistant sorption. Studies with field contaminated Hudson River sediments (Carroll *et al.* 1994) and laboratory-contaminated sediments (Kan *et al.* 1997) indicate a saturation of the resistant compartment at environmentally relevant concentrations of sorbed contaminant. Carroll *et al.* (1994) found that about 1000 μg total PCB/g organic carbon was resistantly bound in Hudson River sediments with total sorbed PCB concentrations ranging from 2500 to 8700 μg total PCB/g organic carbon. Kan *et al.* (1997) found that the resistant component on a river sediment saturated at about 2400 μg naphthalene/g organic carbon and about 70 μg 2,2',5,5' tetrachlorobiphenyl/g organic carbon.

Ignoring biphasic sorption by assuming instantaneous equilibrium introduces error in the PCB fate model. The model over-estimates desorption of PCBs from resuspended sediment and may over-estimate desorption of PCBs from sediments into pore water, depending on the time scales of diffusion and the slow stage of desorption. Use of field derived relationships between pore water and sediment PCB concentration minimizes any error due to slow desorption into pore water. Over-estimation of desorption from resuspended sediments results in over-estimation of PCB flux from sediments and downstream transport of PCBs. The significance of this over-estimation depends on the relative contributions of intermittent resuspension events and continuous flux from pore water to downstream PCB transport and the fraction of the sediment PCB that is resistantly sorbed. Sensitivity analyses were used to explore this issue (Section 4.6).

PCBs are known to partition to dissolved and colloidal organic matter in both the water column and sediment. This phenomena affects the distribution of PCBs between the aqueous and particulate phases. Sorption of PCBs within the aqueous phase reduces bioavailability, because only freely dissolved chemical can be taken up through the respiratory surfaces of aquatic animals (Landrum *et al.* 1985 and 1987).

The partition coefficient describing the equilibrium sorption of PCBs to dissolved/colloidal organic matter typically is expressed on an organic carbon basis, and is termed K_{doc}. The value of K_{doc} typically is less than that of K_{oc}. For example, Evans (1988) found that K_{doc} values for three PCB congeners sorbing to natural dissolved/colloidal organic matter from ten lakes and two streams in south-central Ontario were 0.2 to 4% of their K_{ow} values. The difference is likely a consequence of differences in size, complexity and polarity of dissolved/colloidal and particulate organic matter.

4.2.3.1 Temperature Effects on PCB Partitioning

For equilibrium partitioning reactions, basic thermodynamics states that the equilibrium constant (K_p) will be a function of temperature (T) and pressure (P):

$$R\,d\ln K_p = \frac{\Delta H^\circ}{T^2}dT - \frac{\Delta V^\circ}{T}dP \qquad (4\text{-}17)$$

where:

ΔH° = net change in entropy (heat content) of the reaction

ΔV° = net change in volume of the system

R = universal gas constant

Taking the partial derivatives of Equation (4-17), assuming no change in pressure produces:

$$\left(\frac{\partial \ln K_p}{\partial T}\right) = \frac{\Delta H^\circ}{RT^2} \qquad (4\text{-}18)$$

Since:

$$d\left(\frac{1}{T}\right) = -\frac{dT}{T^2} \tag{4-19}$$

then Equation (4-18) can be converted to:

$$\frac{\partial \ln K_p}{\partial\left(\frac{1}{T}\right)} = \frac{\Delta H^\circ}{R} \tag{4-20}$$

Assuming that ΔH° is reasonably constant over environmentally significant temperature ranges (273-293° Kelvin), then Equation (4-20) can be integrated to yield:

$$\ln\frac{K_{p2}}{K_{p1}} = -\frac{\Delta H^\circ}{R}\left(\frac{1}{T_2} - \frac{1}{T_1}\right) \tag{4-21}$$

where:

K_{p2} = partition coefficient at temperature T_2

K_{p1} = partition coefficient at temperature T_1

By rearranging Equation (4-21) an expression for the equilibrium partition coefficient at temperature T_2 can be obtained knowing K_{p1}, T_1, and ΔH°. For large non-polar compounds such as PCBs, ΔH° is negative (exothermic). This indicates that PCB adsorption to natural particles will decrease as temperature increases.

Knowing the equilibrium partition coefficient at more than one temperature allows the solution of Equation (4-21) for the constant $\frac{-\Delta H^\circ}{R}$:

$$A = \frac{-\Delta H^\circ}{R} = \frac{\ln\frac{K_{p2}}{K_{p1}}}{\left(\frac{1}{T_2} - \frac{1}{T_1}\right)} \tag{4-22}$$

The constant A was developed for individual congeners and used in Equation (4-21) to describe the temperature effect on equilibrium partitioning during the model simulations.

4.2.4 Volatilization

Volatilization is the process by which PCBs are transported across the air-water interface. A chemical's tendency to volatilize is determined by the ratio of its equilibrium activities in air and water (Henry's Constant). This ratio is a fundamental property of the chemical that is defined by Henry's Law. The value of Henry's Constant may be calculated from the vapor pressure of the chemical and its solubility in water (i.e., Henry's Constant equals the vapor pressure divided by the solubility) or it may be calculated from the equilibrium ratio of gas phase and water phase concentrations in a laboratory experiment. A high Henry's Constant is indicative of a volatile chemical that preferentially accumulates in the air phase. A low Henry's Constant is indicative of a non-volatile chemical that preferentially accumulates in the water phase. Values of Henry's Constant are presented either in units of partial pressure per unit aqueous concentration (e.g., atm-m^3/mol) or as a dimensionless ratio of concentrations (e.g., (mol/m^3)/(mol/m^3)). The dimensionless ratio is derived from the dimensioned ratio by dividing by the product of the universal gas constant and absolute temperature, i.e., RT, thus converting pressure into concentration using the ideal gas law.

Volatile chemicals have dimensionless Henry's Constants greater than about 0.1 (0.0025 atm-m^3/mol). As points of references, the highly volatile chemicals vinyl chloride and oxygen have Henry's Constants at 20°C of about 4 and 21 (0.1 and 0.5 atm-m^3/mol), respectively. Numerous experimental determinations of Henry's Constants for PCBs have been published (e.g., Bopp 1983, Burkhard *et al.* 1985, Murphy *et al.* 1987, Dunnivant and Elzerman 1988, Brunner *et al.* 1990). These studies have used various methodologies that have yielded differing estimates. Several of these results, aggregated by homolog group and adjusted to a temperature of 20°C, are shown in Figure 4-2. Values range from about 0.05 to 0.0005. They are highest for the lowest chlorinated congeners and decrease as chlorination increases. Values for Aroclors 1242 and 1254, as reported by Murphy *et al.* (1987) and indicated in Figure 4-2, are about 0.01

and 0.008, respectively. While all of the reported PCB Henry's Constants are below the level of volatile chemicals, they are of sufficient magnitude to make volatilization a significant process, particularly in systems with large surface areas and long residence times.

The PCB Henry's Constants have a positive dependency on temperature that conforms to Equation (4-21). Laboratory data indicate an approximate doubling of the Henry's Constant for every 10°C temperature increase (Tateya *et al.* 1988, ten Hulscher *et al.* 1992).

The rate at which volatilization occurs is dependent on the mass transfer coefficient at the air-water interface and the concentration of PCBs in the water column. Only freely-dissolved PCB can be transported across the interface and sorption to particulate or dissolved organic carbon reduces volatilization. The equation used to describe PCB flux due to volatilization is as follows:

$$S_v = \frac{k_L}{h}\left(c - \frac{c_{air}}{H}\right) \qquad (4\text{-}23)$$

where:

k_L = volatilization mass transfer coefficient (L/T)

c_{air} = vapor phase PCB concentration in air (M/L^3)

H = dimensionless Henry's Constant

The mass transfer coefficient is dependent on the rates of mass transfer through relatively thin layers of water and air at the interface, which are in turn dependent on the concentration gradients in the layers, and the diffusivity of PCBs in the layers (O'Connor 1983, 1984).

$$k_L = \frac{k_g k_l}{k_g + \frac{k_l}{H}} \qquad (4\text{-}24)$$

where:

k_g = vapor phase mass transfer constant (L/T)

k_l = water phase mass transfer constant (L/T)

Volatilization also occurs at each of the waterfalls at the dams on a river. Nearly all of the mass transfer associated with the waterfall occurs in the plunge pool between the water and entrained air bubbles (McLachlan *et al.* 1990, Cirpka *et al.* 1993). The mass flux is dependent on the relative flow rates of entrained air and water, the Henry's Constant of the chemical, the rate of mass transfer between the bubble and the water and the residence time of the rising air bubble (Cirpka *et al.* 1993). At small Henry's Constants, the bubbles equilibrate with the water and the downstream dissolved chemical concentration (c_d) may be computed from the upstream concentration (c_u) by the following formula:

$$c_d = \left(\frac{1}{1 + \frac{GH}{Q}} \right) c_u + \left(\frac{\frac{GH}{Q}}{1 + \frac{GH}{Q}} \right) \frac{c_{air}}{H} \qquad (4\text{-}25)$$

where:

G = entrained air flow rate

Q = river flow rate

The flow rate ratio (G/Q) depends on the speed of the falling water and the volume of air trapped within that water. Cirpka *et al.* (1993) estimated ratios of about 0.03 to 0.07 from field studies with chemicals volatilizing at river cascades 1 to 2 meters in height. On the other hand, McLachlan *et al.* (1990) estimated a value of 20 for Niagara Falls.

4.2.5 Dechlorination

Numerous studies in the laboratory and the field have identified anaerobic PCB dechlorination as important biotransformation processes (see Bedard and Quensen 1995 for a review). The process depends on the chlorine substitution pattern of the PCB and site-specific environmental factors. In general, only *meta* and *para* chlorine can be removed and their removal depends on the total number and position of the chlorine atoms on the molecule (Brown

et al. 1987a&b, Sokol *et al.* 1998a). The rate of dechlorination increases with PCB concentration and may plateau at PCB concentrations of several hundred ppm (Abromowicz *et al.* 1993, Sokol *et al.* 1998b). A threshold PCB concentration necessary for dechlorination has been observed in some studies, but not in others. Sokol *et al.* (1998b) found that dechlorination did not occur below Aroclor 1248 concentrations of about 30 ppm that were added experimentally to St. Lawrence River, New York sediments. Similarly, the USEPA concluded from an analysis of PCB congener composition in Upper Hudson River sediments that dechlorination did not occur in any predictable manner below a sediment PCB concentration of about 30 ppm (USEPA 1997). However, this conclusion was contested by the independent panel of peers selected by EPA to review their Data Evaluation and Interpretation Report and Low Resolution Sediment Coring Report (Albany Marriott, Albany, New York, March 16-18, 1999). In addition, alternate analyses of the Upper Hudson River data indicated that dechlorination occurred at concentrations as low as 1 ppm (Schweiger *et al.* 1997). Consistent with these analyses, experiments using Upper Hudson River sediments spiked with PCBs found no evidence of a threshold (Abromowicz *et al.* 1993, Fish 1996).

Laboratory experiments indicate that dechlorination is accomplished over a period of several months to a year. A lag is sometimes observed, followed by a rapid phase and then a slow phase to completion (Abromowicz *et al.* 1993, Fish 1996, Sokol *et al.* 1998b). *In situ* dechlorination rates may be lower than those observed in the laboratory. Sokol *et al.* (1998a) found that PCBs in St. Lawrence River sediment at a concentration of about 300 ppm had undergone a reduction in the average number of chlorine atoms per biphenyl from a presumed starting level of 3.9 to 3.2. During incubation in the lab, the average chlorine content declined to 2.5 chlorine atoms per biphenyl in less than four months, a period much shorter than the likely incubation time in the river. A further suggestion that *in situ* rates are slow is provided by the dechlorination status of Upper Hudson River sediments. Sediments with lower PCB concentrations generally exhibit less dechlorination (USEPA 1997, Schweiger *et al.* 1997) and a congener makeup consistent with ongoing dechlorination (Schweiger *et al.* 1997). Further, dated sediments show continual dechlorination over decade-long time scales (McNulty 1997).

Dechlorination is not a major mass loss mechanism for total PCBs. The USEPA has estimated that it accounts for about a 10% loss in the Upper Hudson River (USEPA 1997). As such, it may not be an important factor in a total PCB model. However, it could be significant to the modeling of PCB_{3+} because dechlorination involves the transformation of PCBs from the PCB_{3+} fraction to mono- and dechlorinated PCBs.

The laboratory and field data suggest a model for dechlorination of PCB_{3+} in which the PCBs are divided into dechlorinateable and non-dechlorinateable fractions. The kinetics are complex because the loss of chlorine atoms equates to a loss of PCB_{3+} only for tri-chlorinated congeners. Thus, an accurate model requires consideration of the dechlorination pathways of individual congeners as well as their dechlorination rates. Such quantification is a formidable task and was beyond the scope of this modeling effort. However, a simple approximation was made by grouping PCB_{3+} congeners into those that can and can not be dechlorinated and treating the loss of the dechlorination susceptible fraction as a first-order kinetic process:

$$\frac{dc_{dc_{3+}}}{dt} = -k_{dc} c_{dc_{3+}} \qquad (4\text{-}26)$$

where:

$c_{dc_{3+}}$ = concentration of dechlorination susceptible PCB_{3+}

k_{dc} = first-order rate constant (1/T)

4.3 APPLICATION TO THE UPPER HUDSON RIVER

Application of the PCB fate modeling framework to the Upper Hudson River involves a finite difference numerical approximation of the spatial derivatives in Equation (4-4) and specification of the coefficients and parameters that define the hydrodynamic, sediment transport and PCB fate processes described previously. The numerical approximation of the spatial derivatives is, in essence, the division of the river into discrete grid cells or segments within which concentration is constant. The hydrodynamic and sediment transport coefficients and parameters are passed to the fate model from the hydrodynamic and sediment transport models. These include water surface elevation, flow, suspended solids concentration, depositional solids

flux and resuspension solids flux. The coefficients and parameters describing the PCB fate processes were estimated from site-specific data and/or theory as described below.

4.3.1 Segmentation of the Water Column

Division of the river into grid cells or segments for solution of the mass balance equations was based on data availability and the desired spatial resolution. In general, the water column is well-mixed over the cross-section such that a one-dimensional representation of the water column captures its major characteristics. Longitudinal changes in the water column tend to be gradual, as evidenced by the differences in PCB and TSS levels at the four USGS sampling stations between Fort Edward and Waterford. The greatest change in PCBs occurs across the TIP. In consideration of these patterns, the water column was segmented more finely within the TIP than in reaches downstream of the TIP. The TIP is represented by twelve grid cells; each approximately 0.5 miles in length (Figure 4-3). The 34-miles from the TID to Troy is divided into fourteen grid cells (Figure 4-4) that vary in length from about 2 to 3 miles.

Lateral concentration gradients exist at locations with backwater areas along the shoreline (QEA 1998b). The one-dimensional segmentation does not resolve these gradients. A separate model of the TIP is being developed to investigate the two-dimensional aspects of water column PCB levels in the TIP. This model will be reported on at a later date.

Cross-sectional geometry, temperature and suspended solids organic carbon content were specified for each segment. The geometric analysis conducted for the hydrodynamic models was used to specify the average width of each segment. Segment depth varies with river flow and the depths calculated by the hydrodynamic model were used in the PCB fate model. Because of the difference in resolution between the models, the hydrodynamic results were manipulated as discussed in Section 2.2.4 to provide flows, volumes, and depths to the fate model. An annual temperature cycle was estimated from the temperature data collected at TID as part of the weekly monitoring conducted by GE (Figure 4-5). This temperature cycle was assigned to each of the water column segments.

Suspended solids organic carbon (OC) contents were estimated from USEPA Phase 2 weight-loss-on-ignition (WLOI) measurements conducted at 375°C and 450°C using the relationships, (USEPA 1997):

$$\%OC = 0.611 * WLOI_{375}$$
$$\%OC = 0.528 * WLOI_{450} \quad (4\text{-}27)$$

These relationships were developed from paired measurements of organic carbon and WLOI on sediment samples from the USEPA High Resolution Core Study (USEPA 1997). Thus, their application to WLOI measurements for suspended solids represents extrapolation. The validity of this extrapolation is supported by the observation that surface sediment samples (i.e., sediments most recently deposited from the water column) exhibit a relationship consistent with the overall data set (Figure 4-6).

Figure 4-7 shows the estimated %OC at five stations from Fort Edward to Waterford. The data exhibit a strong seasonal variation at all stations with Spring OC dipping to about 1/3 of the Summer and Autumn levels. A strong correlation of OC with location also exists, with the highest values occurring at the upstream stations and decreasing with distance downstream.

The seasonal variation appears to be caused by a dependency of %OC on river flow. At the stations with sufficient data to examine this dependency (Fort Edward, TIP and Waterford), a consistent pattern was observed (Figure 4-8). Values exhibit little dependency on flow at flows less than about the annual average value. A decline occurs as flow increases to about double the average flow, after which values are again relatively independent of flow. The low flow %OC was about 32 at Fort Edward, 29 at TID and 17 at Waterford. The high flow %OC was about 14 at Fort Edward, 13 at TID and 8 at Waterford. Thus, at all three stations, the average at low flow was about twice the average at high flow. The relatively high %OC calculated from the WLOI data are supported by direct measurements of %OC on particulate matter captured from the water column at Rogers Island at a river flow of about 2,900 cfs as part of the GE DNAPL study (HydroQual 1997b). Six measurements on particulate matter from the surface, mid-depth and bottom waters ranged from 22% to 32% with a mean of 26%.

The %OC data at Waterford were grouped into normalized flow intervals and averaged. The mean of these averages at river flows less than the annual average flow (Q_{avg}) was used to estimate low flow %OC at 17.3%, and the mean at flows greater than $2Q_{avg}$ was used to estimate high flow %OC at 8.2%. The %OC in the transitional flow region between Q_{avg} and $2Q_{avg}$ was assumed to decline as a simple power function of order n=-1.08. This functional relationship also describes the Fort Edward and TID %OC data using scale factors of 1.80 and 1.63, respectively. Distance based linear interpolation was used to estimate the %OC for model segments locations between Fort Edward, TID and Waterford.

4.3.2 Segmentation of the Sediment

The sediment transport model divides the riverbed into areas of cohesive or fine sediments, areas of non-cohesive or coarse sediments and hard bottom (see Figures 3-5, 3-6 and 3-7 and Table 3-1). The PCB model uses the same differentiation, but with a coarser segmentation. All of the sediment transport grid cells were aggregated by type of sediment. In this way, the PCB model has single cohesive and non-cohesive sediment cells under each water column cell.

The cohesive and non-cohesive sediments associated with each water column grid cell are vertically segmented at one-centimeter intervals. The cohesive sediment is 25 centimeters deep and thus has 25 grid cells for each water column cell. The non-cohesive sediment is 5 centimeters deep and thus has 5 grid cells for each water column cell. A shallower depth is accounted for in non-cohesive sediments because data for these coarse sediments generally is limited to surface sediment grab samples. The non-cohesive sediments of the Upper Hudson River have a median particle diameter of about 800 μm, corresponding to a coarse sand and a gravel content of about 20 to 40%. This type of sediment resists penetration by grab sampling devices and the sampling depth of grab samples was presumed to be less than the average of 5 inches indicated by Tofflemire *et al.* (1979) for all grab samples collected in the 1977 survey. Further, the sediment transport model confirms that the non-cohesive sediments are non-depositional and are not likely to have accumulated PCBs at significant depths.

Surface area, dry bulk density, particle density and solids organic matter content were specified for each sediment segment. Surface area was determined from the cohesive and non-cohesive bed areas developed for the sediment transport model (see Section 4.2.1). From data analyses conducted for the sediment transport model, dry bulk densities of 0.87 g/cm^3 and 1.38 g/cm^3 were assigned to the cohesive and non-cohesive segments, respectively.

The solids organic matter content was calculated from the 1991 GE sediment survey. Average values of surface OC content of non-cohesive sediments were calculated for each reach individually and are given in Table 4-1. These values range from 0.55% to 1.04% with the highest OC at the TIP. Since no non-cohesive samples were taken in reach 7, adjacent reach OC values were interpolated by distance to estimate reach 7 OC. These OC values were applied to all model 0-5cm non-cohesive sediment segments within each respective reach. Surface and sub-surface cohesive sediment OC were analyzed by reach and it was found that surface and sub-surface samples were not statistically different from each other. Accordingly, cohesive sediment OC values at all depths were averaged by reach to generate the cohesive OC values in Table 4-1. These values range from 0.72% to 3.18%, being generally 2-3 times higher than non-cohesive OC. Reach average values were applied to all cohesive sediment segments within the reach. The 1991 sediment OC distributions were compared to sediment OC (estimated using volatile solids) from other sediment surveys. The estimated OC content in both cohesive and non-cohesive sediment from 1977 and 1984 were generally more than a factor of two higher than 1991. This higher OC content may be associated with the presence of organic debris, including wood chips, that was deposited following the removal of the Fort Edward Dam. Sediment OC distribution from the 1998 survey is generally the same as 1991.

Table 4-1. Sediment Organic Carbon Content (%)

Reach	Non-cohesive	Cohesive
1	0.72	1.44
2	0.62	0.72
3	0.55	1.78
4	0.57	2.68
5	0.62	1.59
6	0.81	2.56
7	0.93	3.18

8	1.04	2.08

4.3.3 Diffusion Mass Transfer Coefficients within the Bed and at the Water-Bed Interface

Pore water mass transport within the sediment bed and at the sediment/water interface consists of diffusive and advective mechanisms. Pore water diffusion is driven by a vertical concentration gradient, while advection within the bed and between the bed and water column results from vertical hydraulic gradients. Pore water mass transport in the model is represented as two separate processes: 1) vertical diffusion between sediment bed layers, and 2) exchange with the water column at the sediment/water interface. These processes are parameterized differently in the model, as described below.

4.3.3.1 Vertical Diffusion within the Bed

The vertical pore water diffusion coefficient used in the Hudson River model was based on the molecular diffusion coefficient for PCB_{3+} (Section 4.3.7) and sediment bed porosity. Porosity was calculated from measurements of sediment dry bulk density (see Section 4.3.2) and an assumed particle density of 2.6 g/cc. Calculated values of porosity are 0.67 for cohesive sediments and 0.47 for non-cohesive sediments. Based on these values and the expression discussed in Section 4.2.2 ($D_s = D_w\theta^2$), the vertical pore water diffusion coefficient at 20°C was estimated at 0.2 cm^2/d for cohesive sediments and 0.1 cm^2/d for non-cohesive sediments.

4.3.3.2 PCB Exchange at the Sediment Water Interface

Mechanisms of sediment-water exchange

PCB exchange across the sediment-water interface occurs as a result of numerous physical, chemical, and biological mechanisms. Hydrodynamically induced resuspension, described in Sections 2 and 3, dominates sediment-water exchange during periods of elevated flow. During low flow periods, a number of possible mechanism contribute to sediment-water exchange, including:

- molecular diffusion of PCBs contained within sediment pore waters,
- transport of natural colloids to which PCBs have sorbed,
- groundwater advection of contaminated pore water, and
- bioturbation induced pore water and particulate transport.

Molecular diffusion occurs as a result of the random molecular motion which transports dissolved PCB molecules from the region of high concentration within surface sediment pore waters to the lower concentration region of the overlying water column. Molecular diffusion, the most ubiquitous mechanism of PCB transport across the sediment-water interface, occurs wherever a concentration gradient exists between sediment pore water and the overlying water column.

Decomposition of natural organic matter and subsequent sediment diagenesis processes form stable colloidal-sized particle suspensions within sediment pore waters. Due to their organic content, these suspended colloidal particles preferentially sorb PCBs. Transport of these sorbed PCBs across the sediment-water interface occurs as a result of diffusion of the colloids across a concentration gradient that exists at the sediment-water interface.

The advection of groundwater across the sediment-water interface occurs due to hydraulic gradients that may exist between the adjacent groundwater aquifer and the river. The upward flow of groundwater through surface sediments and into the overlying water column results in water column PCB loading since groundwater traveling through sediments will accumulate PCBs as a result of partitioning between groundwater and the contaminated sediment particles. This process is regulated by the hydraulic conductivity of the sediment, which varies by sediment type.

Bioturbation is a general term describing the transport of pore waters and surface sediment particles by the activities of benthic organisms such as macroinvertebrates. Benthic macroinvertebrates process sediment during burrowing, sediment ingestion, sediment defecation, and tube building activities. The net result of bioturbation is that surface sediments are mixed.

This mixing activity enhances the exchange of contaminants between the sediments and overlying water column by transporting materials across the interface.

While the processes controlling sediment-water exchange are generally understood, a mechanistic representation of each of these processes with appropriate Hudson River-specific parameterization is not feasible because data do not exist to support such representations in the model. Therefore, the combined effect of these sediment-water exchange processes was modeled empirically by a lumped sediment-water exchange coefficient that is calibrated to seasonal sediment PCB loadings under low flow conditions, as described in detail below.

Seasonality and Source of Observed PCB_{3+} Loadings

PCB_{3+} loading observed between the Rogers Island station at the headwaters of the TIP and the TID follows a seasonal pattern (Figure 4-9). Typically, lowest daily loads occurred during the winter low-flow period and maximum daily loads occurred immediately following the spring high flow period. Although a sampling bias was discovered for the TID-west station used to calculate these loadings (QEA 1998b), simultaneous monitoring from this station and an unbiased station in 1998 indicate that, while the absolute magnitude of the loading differs, the seasonal loading patterns generally track each other (Figure 4-10). These data indicate that seasonally varying low flow sediment-water exchange, attributable to a number of possible mechanisms, is a characteristic of the upper Hudson River.

The composition of summer low-flow PCB loadings from the TIP was used to infer the nature of PCB sources to the water column. The composition of the summer low-flow (June - August 1998) average TIP load was calculated as the difference in water column derived PCB congener peak loading across the TIP using data collected from Fort Edward and the unbiased station at the TID (QEA 1998b). The source of this loading was assessed by: 1) calculating the required composition of a particulate-phase sediment source under the assumption of equilibrium

partitioning between sediments and pore waters[2], and 2) comparing the "required" sediment source with sediment obtained from different depths within the TIP.

The sediment source required to produce the PCB congener loadings observed from the TIP in 1998 best matches the surface sediment PCB composition as represented by the 0-2 cm sections of the cores collected from the TIP in 1998 (Figure 4-11a). In contrast, the source of the TIP load does not appear to match the composition of PCBs found at depths greater than 9 inches (Figure 4-11b). This analysis indicates that the source of the TIP PCB load is surface sediments as expressed through desorption and transport mechanisms. These could include a direct pore water exchange process (e.g., diffusion, bioturbation, or groundwater advection) and/or surface sediment resuspension and subsequent PCB desorption (e.g. biologically-induced particle resuspension) each of which can be described as a Fickian mixing process occurring across the concentration gradient that exists at the sediment-water interface. Regardless of the mechanism, the source of the PCB loadings observed from the TIP appear to be derived from surface sediment sources (i.e., 0-2 cm).

Representation in the model

Mass transport at the sediment-water interface by mechanisms other than hydrodynamic resuspension, as presented above, is represented in the model as a Fickian process (Equation 4-14). The concentration gradient is expressed as the difference between the pore water concentration in the surficial bed layer (top 1 cm in the model) and the dissolved phase concentration in the overlying water column segment. An overall mass transfer coefficient, k_f, that combines the effects of the various physical, biological, and chemical mass transfer mechanisms was used to represent non-hydrodynamically induced PCB_{3+} exchange across the sediment-water interface.

Parameterization of k_f in the Hudson River model was empirically derived based upon 1998 water column and sediment data collected from TIP[3]. To account for the observed

[2] Equilibrium partition coefficients were derived from USEPA water column particulate and aqueous phase PCB data and were adjusted for temperature effects (USEPA, 1997).

seasonality in low flow sediment-water exchange, a low flow mass balance calculation was developed for the entire pool. The PCB_{3+} loading to the water column (i.e., gain across the pool) observed in 1998 (Figure 4-12) was set equal to the 1998 surface sediment pore water diffusive loading. Mathematically, this was accomplished by rearranging the mass balance Equation (4-14) to solve for k_f as follows:

$$k_f = \frac{Q_{FE}\left(c_{T_{TID}} - c_{T_{RI}}\right)}{A_S\left(c + c_{dom}\right)_s} \qquad (4\text{-}28)$$

where:

Q_{FE} = the average daily flow at the USGS gage in Fort Edward, New York,

c_{TTID} = the PCB_{3+} concentration at TID (TID-PRW2 station),

c_{TRI} = the PCB_{3+} at Rogers Island (R[3].197Br. station),

A_s = the sediment surface area in TIP, and

$(c+c_{dom})_s$ = the average surface sediment pore water dissolved + DOM bound PCB_{3+} concentration in TIP (calculated from sediment-pore water equilibrium partitioning)

The value of $(c + c_{dom})_s$ in Equation (4-28) was calculated from the observed surface sediment PCB_{3+} concentration and the sediment partition coefficient used in the model (see Section 4.3.5). An observed K_{oc} of $10^{5.61}$ L/kg was used to calculate sediment-pore water partitioning. Temperature effects on sediment-pore water partitioning in the TIP k_f calculation were based on Equation 4-21 and parameterized from water column partitioning studies conducted by the USEPA (USEPA 1997).

The average surface sediment PCB_{3+} concentration in TIP was calculated from 1998 surface sediment data (0-2 cm; QEA 1998c). The averaging procedure for the 1998 data was similar to that used to develop initial conditions for the model (Section 4.4.3.1):

---

[3]Data for 1998 collected from the station located within the center channel immediately downstream of the dam was used because of a sampling bias that exists for data collected from the shore-based sampling station prior to this time (QEA, 1998).

1. Each sample was classified as cohesive or non-cohesive, based on sediment description information provided in field logs,
2. Average cohesive and non-cohesive concentrations for each model segment within TIP were developed based on an arithmetic mean (non-cohesive) or an area-weighted mean (cohesive)[4], and
3. Cohesive and non-cohesive areas (Plate 4-1) and average PCB_{3+} concentrations for each model segment within TIP were used to develop an area-weighted mean concentration for the entire TIP.

Using this procedure and organic carbon values from the model (Section 4.3.2) produced an average organic carbon-normalized PCB_{3+} concentration for TIP surface sediments (0-2 cm) of 706 mg/kg OC. Based on this value and the observed partitioning coefficient discussed above, a 20°C average $(c_d + c_{dom})_s$ of 1.7 µg/L was used for the TIP k_f calculation.

Equation (4-28) was solved for all low-flow sampling events between October 1997 and September 1998 for which unbiased samples from the TID region of the river were available. A temporal plot of the flow at Fort Edward, water column PCB_{3+} concentrations, the PCB_{3+} load gain across TIP, and the k_f calculated by Equation (4-28) is shown in Figure 4-13. As this plot demonstrates, the calculated exchange coefficient within TIP appears to vary seasonally. During the winter months (November to March), k_f is on the order of 3 cm/day. The calculated k_f increases in early spring and peaks between 10 and 14 cm/d in late spring/early summer. The value of k_f remains higher than 4 cm/day throughout the summer and decreases in late summer/autumn. Although the precise mechanism(s) responsible for the seasonality in sediment-water exchange are unknown, the timing of the peak and subsequent decline suggests that k_f may be linked to biologically mediated mixing in the surface sediments.

Specification of k_f seasonality in the model was based upon a visual inspection of the values calculated by the TIP low-flow mass balance analysis (i.e., Figure 4-13, panel d). The general trend of the fit was based upon an early summer peak, a tail-off in the autumn, and a sustained low value throughout the winter months. The function used to describe the yearly fluctuation of k_f is shown in Figure 4-14. This function was based upon average calculated

[4] Means were weighted by the number of cores in each sample so that composite samples (i.e., from the Broad-Scale Program) were given more weight than individual cores (i.e., from the Focused Sediment and Cesium Coring Programs) in the averaging (QEA, 1998b).

values with occasional anomalous high values omitted. Uncertainty associated with non-detect PCB values at Fort Edward was accounted for by calculating k_f values with assumed concentrations of both the total PCB detection limit (11 ng/L) and zero. Greater confidence was given to values at intermediate flows (i.e., 3500-10,000 cfs) since the long TIP residence times at low flows likely degrade the assumption that the Fort Edward and TID samples are paired. The yearly k_f pattern exhibited in Figure 4-14 was used to describe non-hydrodynamically-induced sediment-water exchange throughout the model domain.

4.3.4 Particulate Mixing within the Bed

The varied feeding and burrowing activities of the Upper Hudson River benthic invertebrate community result in the random movement of sediment particles and entrained sediment pore waters. This process of bioturbation is mathematically described as a "particle diffusion" process (first term of Equation (4-13)). The parameterization of this process in the model (depth and intensity of surface sediment mixing) was inferred from the observed surface sediment gradients in PCB concentration and composition, the structure and abundance of the benthic macroinvertebrate community, and the relationship between biota and surficial sediment PCB composition.

The gradients in surface sediment PCB_{3+} concentrations and composition observed in finely sectioned sediment cores collected in 1998 were used to qualitatively assess the depth of surface sediment mixing. Although highly variable, PCB_{3+} concentration and composition (molar chlorine per biphenyl) profiles typically showed little gradient within the surface 2 to 5 cm (Figures 4-15a-c and 4-16a-c). This lack of structure within the sediment profiles indicates that there is some degree of biological mixing within the top 5 cm of the fine sediments in which the cores were taken. This conclusion is supported by the detection of ^{7}Be in the 2-4 cm layer of most of the high-resolution cores collected in 1992 as part of the USEPA Phase 2 sampling program (USEPA 1995). ^{7}Be is a cosmogenic radionuclide that decays with a half-life of 53 days. Its presence in the 2-4 cm layer indicates that particle mixing has occurred to at least a depth somewhat greater than 2 cm.

The invertebrate fauna of the Upper Hudson River sediment bed is dominated by chironomids and oligochaetes (see Section 5.2.1). In a recent Upper Hudson River survey, Exponent (1998a,b&c) measured the abundance of benthic macroinvertebrates within a number of Upper Hudson River habitats. The mean total abundance of benthic macroinvertebrates occupying the surface sediments ranged between approximately 10,000 to 35,000 individuals/m^2 depending on the substrate and vegetation type (Figure 4-17). Generally, the chironomid midges were the most abundant taxon, ranging from 1600 individuals/m^2 to over 16,000/m^2 depending upon the habitat (Figure 4-18).

The depth to which chironomids and oligochaetes burrow is species-, substrate- and environment-specific. Most of the available studies of the effects of these organisms on sediment bed mixing have been conducted in lake sediments. These studies indicate that chironomids and oligochaetes are generally found at depths of 8 to 10 cm (McCall and Tevesz 1982, Ford 1962). Based upon these data, some mixing is likely to be occurring within the Upper Hudson River to a depth of approximately 10 cm. However, the majority of the feeding activity and, therefore, particle mixing is likely to be at a shallower depth. In the Upper Hudson River, analysis of PCB composition fish and sediments suggests that PCB exposure to the benthic fauna is limited to the top 2 cm of the sediment (see Section 5.2.3).

Based upon the results of the benthic macroinvertebrate survey, the 1998 surface sediment coring program, the 1992 sediment coring program, analysis of PCB composition in sediments and fish, and model calibration a partially mixed surficial sediment layer depth of 10 cm was chosen to represent conditions within the Upper Hudson River cohesive sediment.

Because non-cohesive sediment has a high solids content and little or no net deposition of particulate matter, it seems logical that the depth of particle-mixing would be lower than that of the cohesive sediment. On the basis of model calibration, a depth of 3 cm was chosen for these sediments.

The magnitude of the particle-mixing coefficient is uncertain. Values have been estimated at numerous sites by fitting the diffusion model to the measured vertical profiles of

natural or introduced tracers. Thoms *et al.* (1995) presented a compilation of the available data that indicate that the mixing process varies seasonally and from site-to-site. Values of the particle diffusion coefficient range from about 10^{-9} to 10^{-6} cm^2/s. Olsen *et al.* (1981) calculated surface values of about 10^{-8} cm^2/s in Foundry Cove and Lents Cove in the Lower Hudson River. The ^7Be data from the high resolution cores, although noisy, suggest a high particle mixing intensity because mean levels in the 2-4 cm layer were typically within a factor of 2 to 3 of levels in the 0-2 cm layer. A value of 10^{-7} cm^2/s was used in the model for both cohesive and non-cohesive sediments.

4.3.5 Sorption Partition Coefficients

Sorption of PCBs to water column suspended particulate matter was analyzed using USEPA Phase 2 water column data (USEPA 1995). Partition coefficients calculated from Phase 2 Transect Survey data (Figure 4-19) generally fall into two spatial categories, those samples above Fort Edward show about an order of magnitude higher partition coefficients than those below Fort Edward. The average partition coefficient below Fort Edward remains relatively constant from TID to Green Island Bridge. Differences in suspended organic matter above and below Fort Edward (Section 4.3.1) are not sufficient to account for the order of magnitude partitioning differences.

Partition coefficients on an organic carbon basis (K_{oc}) were calculated using organic carbon contents of solids (%OC) estimated using $WLOI_{375}$ and Equation (4-27). Measured apparent organic carbon partition coefficients for each congener were evaluated in relation to octanol-water partition coefficients (K_{ow}) as reported by Hawker and Connell (1988) (Figure 4-20a-b). Measured values for K_{oc} approximately equal K_{ow} in summer (Transects 005-006) and are higher in winter and spring (Transects 001-004). This is most likely the consequence of the temperature dependency of partitioning. It is notable that in all samples the relationship between K_{oc} and K_{ow} is approximately linear. A linear relationship indicates that sorption was not appreciably impacted by the presence of DOM. If a significant fraction of the PCBs in the filtered water samples had been sorbed to DOM, the K_{oc}-K_{ow} relationship would deviate from linearity in the manner illustrated in Figure 4-21. Consistent with the work cited in Section

4.2.3, the partitioning to particulate organic matter apparently is much greater than the partitioning to DOM. For this reason, competitive sorption to DOM was not considered in the model.

Dissolved and particulate PCB_{3+} data for Transects 001 to 006 were analyzed in order to estimate K_{oc}. Because of anticipated temperature effects, data from different transects were grouped based upon in situ temperature: Transects 001 and 002 at about 1°C, Transects 003 and 004 at about 3°C, and Transects 005 and 006 at about 20°C. Data at Fort Edward were analyzed separate from data at stations between TID and Waterford due to the observed partitioning differences cited above. Figure 4-22a shows particulate (on organic carbon basis) versus dissolved PCB_{3+} for samples taken at Fort Edward. Regression at each temperature yields K_{oc} values that increase from $10^{6.26}$ at 20°C to $10^{6.75}$ at 1°C. Similar regressions of TID through Waterford data (Figure 4-22b) yield K_{oc} values that range from $10^{5.62}$ to $10^{5.93}$. A K_{oc} at 20°C value of $10^{5.6}$ was used for model segments representing TID through Waterford, a value of $10^{6.3}$ was used for Fort Edward, and distance based linear interpolation was used to estimate K_{oc} at 20°C values from Fort Edward to TID. In order to determine the temperature correction coefficient [$\Delta H°/R$ in Equation (4-21)], K_{oc} values at each temperature were normalized to the corresponding 20°C value and regressed against 1/T (Figure 4-23) to produce a coefficient of 1375K. With this correction, K_{oc} more than doubles as temperature decreases from 20°C to 0°C.

The sorption of PCBs within the sediments was examined using measurements of sediment and pore water PCBs taken as part of the GE 1991 sampling program (O'Brien and Gere 1993a). K_{oc} values calculated from these data range over two orders of magnitude and tend to be higher than the K_{oc} values calculated from the USEPA Phase 2 water column data. Lower values tend to be associated with samples having relatively high concentrations of organic carbon in the pore water, but the relationship between K_{oc} and pore water organic carbon concentration is weak (Figure 4-24). A stronger relationship exists between K_{oc} and the pore water PCB concentration (Figure 4-25). The highest K_{oc} values occur at the lowest pore water concentrations. A relationship also exists between K_{oc} and the percent of the pore water PCBs that have 3 or more chlorine atoms (Figure 4-26). High K_{oc} values tend to be associated with sediments in which PCBs have undergone extensive dechlorination (low % of PCB_{3+}). This suggests that the K_{oc} values are related to PCB dechlorination status. It is possible that

dechlorination has eliminated much of the reversibly sorbed PCB_{3+} and the remaining PCB_{3+} is resistantly sorbed.

An isotherm plot of the sediment and pore water data suggests that the data fall into two groupings (Figure 4-27). One portion of the data (indicated by filled symbols) falls about a line that represents a K_{oc} of about 350,000 l/kg. The remainder of the data (represented by open symbols) forms an almost vertical line, indicating that a partition coefficient is not applicable to this data. This observation supports the hypothesis that a fraction of the sediment PCBs are resistantly sorbed, an apparent consequence of the removal of reversibly bound PCBs by dechlorination. Regression of the portion of the data that represents reversibly sorbed PCB_{3+}, shown as closed symbols on Figure 4-27, yields a K_{oc} value of $10^{5.6}$. This result is the same as the value generated from the water K_{oc} analysis for TID through Waterford. This suggests equality between water column and sediment K_{oc} with no evident influence of dissolved organic matter.

Sediment partitioning has its greatest impact on PCB fate in surface sediments where it modifies the diffusive flux between the buried sediments and the surface mixed layer. These sediments tend to be the least dechlorinated. For this reason, the 2-phase partition coefficients developed from the USEPA Phase 2 water column data for stations between TID and Waterford are applied to sediments throughout the model domain (USEPA 1997). Partitioning to the sediment pore water dissolved organic matter was not modeled because the data indicated that it did not have a significant affect on PCB distribution in the sediment.

It is important to note that any error that may exist in the calculated pore water concentration does not introduce error in the PCB mass transfer from sediment to water. The portion of the mass transfer due to hydrodynamic resuspension is unaffected because the pore water constitutes such a small fraction of the PCB mass that large changes in concentration have insignificant affect on the sediment PCB concentration. The portion of mass transfer due to all other processes, although appearing to depend on the pore water PCB concentration (see Section 4.3.3.2), actually depends on the sediment PCB concentration. This is evident by examination

of the flux calculation. The flux at a time designated as t may be written from Equation (4-14), ignoring the water column concentration and dropping the DOM component for convenience:

$$J_{D_t} = k_f c_{s_t} \tag{4-29}$$

The mass transfer coefficient was empirically defined from the 1998 sediment PCB data and the measured increase in PCB flux across the TIP in 1998 using Equation (4-28). Substituting Equation (4-28) into Equation (4-29), again dropping the DOM component, yields the following expression:

$$J_{D_t} = \frac{\left|Q_{FE}(c_{T_{TID}} - c_{T_{RI}})\right|_{1998}}{A_s} \frac{c_{s_t}}{c_{s_{1998}}} \tag{4-30}$$

The ratio of pore water concentrations in Equation (4-30) may be expressed in terms of sediment concentrations by using Equation (4-5):

$$\frac{c_{s_t}}{c_{s_{1998}}} = \frac{f_d c_{T_{s_t}}}{f_d c_{T_{s_{1998}}}} \tag{4-31}$$

The fraction dissolved term, f_d, is not a function of time and therefore cancels out. Therefore, Equation (4-30) may be rewritten in terms of the sediment concentrations:

$$J_{D_t} = \frac{\left|Q_{FE}(c_{T_{TID}} - c_{T_{RI}})\right|_{1998}}{A_s} \frac{c_{T_{s_t}}}{c_{T_{s_{1998}}}} \tag{4-32}$$

4.3.6 Dechlorination

Loss of PCB_{3+} in Upper Hudson River sediments was assessed by examination of the USEPA Phase 2 High Resolution sediment cores. Cores used in this analysis were those characterized by continual deposition and minimal vertical mixing of sediments as defined by the

profile of ^{137}Cs (Table 4-2). High resolution core HR-020 from the TIP was excluded because the ^{137}Cs data suggested that significant mixing had occurred over the upper 20 cm of the core.

Table 4-2. USEPA Phase 2 High Resolution Cores Used for Analysis of Dechlorination

Core Number	Location	Reach	River Mile
HR-026	East side of Rogers Island	8	194.1
HR-023	Thompson Island Pool	8	189.3
HR-019	Thompson Island Pool	8	188.5
HR-018	Above Lock #5	7	185.8
HR-021	Stillwater Pool	5	177.8
HR-022	Stillwater Pool	5	177.8
HR-016	Above Lock #1	2	166.3
HR-015	Below Lock #1	1	159.0

The relationships between the weight percent of PCB as PCB_{3+} (f_{3+}) and time of deposition exhibited two general patterns. Cores from the northern section of the river (i.e., Reaches 8 and 6) exhibited a continual decline in f_{3+} with sediment age (Figure 4-28a). Cores from further downstream (i.e., Reaches 5, 2 and 1) exhibited no decline in f_{3+} in core sections deposited between the mid-1970s and 1991 (Figure 4-28b). These data suggest that dechlorination is most significant in Reaches 8 and 6. It is possible that the lack of dechlorination in the lower reaches is attributable to the existence of a threshold concentration for dechlorination that was not exceeded in the downstream reaches except in sediments deposited before the mid-1970s.

To determine whether the loss of PCB_{3+} by dechlorination is concentration dependent, the data from the older sediments (1963-1975) were examined. Presumably, these sediments have been in place long enough to allow dechlorination to be near, if not at, completion. Thus, interpretation of the data should be minimally confounded by a concentration dependent dechlorination rate. The data indicate that concentration has a substantial impact on the extent of PCB_{3+} mass loss (Figure 4-29). At ΣPCB concentration greater than about 100 ppm, f_{3+} is at its lowest levels (ca. 0.2) and is independent of concentration, apparently indicative of the maximum loss attainable by dechlorination. Between ΣPCB levels of 10 and 100 ppm, f_{3+} is an inverse function of ΣPCB concentration declining from about 0.75 at 10 ppm to about 0.2 at 100 ppm. Below 10 ppm, f_{3+} is approximately constant at about 0.75, which is similar to its value in

Aroclor 1242. These data indicate that dechlorination does not significantly reduce PCB_{3+} mass at ΣPCB concentrations below 10 ppm.

Between ΣPCB concentrations of 10 and 100 ppm the reduction in f_{3+} could signal a dependency of the rate or extent of dechlorination on ΣPCB concentration. If the relationship is the result of a concentration dependent dechlorination rate, the relationship should be time-dependent and more recently deposited sediments should exhibit less reduction in f_{3+}. Although considerable variability exists, the relationship for more recently deposited sediment layers is consistent with the relationship for the oldest sediments (Figure 4-30). This suggests that, in Upper Hudson River sediments, the mass loss of PCB_{3+} occurs rapidly and that the magnitude of the loss is dependent on ΣPCB concentration.

In contrast to the conclusions indicated by the USEPA data, comparison of high-resolution cores taken in close proximity within the TIP in 1983 and 1991 suggests a relatively slow *in situ* dechlorination rate (McNulty 1997). Cross sections were matched using ^{137}Cs dating so that sediments deposited at the same time could be compared between the two cores. Congener PCB data were then used to evaluate composition changes over the 1983-1991 period. PCB_{3+} dechlorination mass loss from the McNulty data was calculated for sediments deposited in approximately 1968, having total PCB concentration in excess of 500 ppm. The homolog compositions of this sediment layer, as measured in 1983 and 1991, are plotted in Figure 4-31. Also plotted is the change in the homolog weight percent. Decreases in di-, tri-, and tetrachlorinated biphenyls are accompanied by a large increase in monochlorinated biphenyls. Over this eight-year period, the PCB_{3+} weight fraction dropped from about 59% to 49%, corresponding to a first-order loss rate of 0.023 yr^{-1}. Assuming that the PCBs deposited in 1968 had the composition of Aroclor 1242 and thus contained about 86% PCB_{3+} by weight, the loss rate constant for the earlier period (1968 to 1983) is 0.038 yr^{-1}. However, this analysis is based upon data from two cores collected from different locations in the River approximately eight years apart. Therefore, the differences in PCB dechlorination patterns and rates derived from these data are subject to considerable uncertainty related to differences in the microbiological community and environmental condition of the sediment.

Consistent with the interpretations of the high resolution coring data, there is evidence that PCB dechlorination within the Hudson River was well underway by the 1977 survey conducted by NYSDEC. Brown *et al.* (1987a) examined 100 of the original 2000 packed column GC chromatograms of sediment samples collected from the Upper Hudson River. All chromatograms of sediment samples containing appreciable PCB concentrations contained evidence of PCB dechlorination (Brown *et al.* 1987a). Based on this evidence, the authors concluded that PCB dechlorination was well established within Hudson River sediments by 1977. Moreover, the chemist interpreting the 1977 sediment chromatograms identified significant deviations from established Aroclor patterns, providing independent evidence that sediment PCBs were likely altered by reductive dechlorination mechanism by 1977 (O'Brien & Gere 1978).

The dechlorination patterns described by Brown *et al.* (1987a) can be generally characterized as a loss of PCB_{3+} with a concomitant increase in mono- and dichlorinated PCBs. Therefore, post 1977 dechlorination is likely to have an insignificant impact on the concentration of PCB_{3+} within sediments deposited prior to 1977. As the concentrations of PCB deposited after this period are generally within the range of 1-50 ppm, little dechlorination is expected based upon the relationship between the extent of dechlorination and total PCB concentration established from the high resolution coring data. For these reasons, the loss of PCB_{3+} due to dechlorination was not simulated in the model.

4.3.7 Volatilization Mass Transfer Coefficients

The overall volatilization mass transfer coefficient was calculated from water phase and vapor phase mass transfer coefficients and from Henry's Constant as indicated in Equation (4-24).

Henry's Constant for PCB_{3+} was estimated from congener-specific Henry's Constants and measurements of PCB composition in thirteen water samples from the USEPA Phase 2 investigation of the Hudson River taken at TID. Congener fractions of PCB_{3+} for each of these samples were calculated and then averaged to yield an estimate of average congener

composition. These average congener fractions were applied to experimentally determined values[5] of congener-specific Henry's Constants (Brunner *et al.* 1990) to calculate a mass-weighted average 20°C Henry's Constant. The result was a dimensionless value of 0.0078 (19.04 Pa*m^3/mol)[6]. The variation of Henry's Constant with temperature was calculated using Equation (4-21). The terms in the equation were determined from the 20°C value and the observation that Henry's Constant doubles from 10°C to 20°C:

$$\ln(H_T) = 22.57 - \frac{5753}{T} \qquad (4\text{-}33)$$

where:

H_T = Henry's Constant at temperature T (Pa*m^3/mol)

T = temperature (°K)

The water phase mass transfer coefficient was calculated from the O'Connor-Dobbins equation (O'Connor and Dobbins 1958):

$$k_l = \sqrt{\frac{D_w u}{h}} \qquad (4\text{-}34)$$

where:

D_w = molecular diffusivity of the PCBs in water (L^2/T)

u = depth-average water velocity (L/T)

The molecular diffusivity was calculated using the equation presented by Hayduk and Laudie (1974):

[5] Henry's constants for congeners lacking experimentally determined values were estimated using the chlorine-atom QSPR method (Brunner *et al.* 1990)

[6] Only detected congeners were included in the calculation. Inclusion of non-detects at the detection limit changes the result to 0.0070 (17.09 Pa*m^3/mol).

$$D_w = \frac{13.26x10^{-5}}{\mu^{1.14}(\overline{V})^{0.589}} \quad (4\text{-}35)$$

where:

μ = viscosity of the water (centipoise, 10^{-2} g/cm-s)

$\overline{V}$ = the molar volume of the PCB (cm^3/mol)

The molar volume was assigned a value of 247.3 cm^3/mol which is representative of a trichlorobiphenyl (Mackay *et al.* 1992). The viscosity of water was calculated from the following equation:

$$\mu = 100\left[10^{\frac{1.301x10^3}{998.333+8.1855(T-20)+0.00585(T-20)^2}-3.30233}\right] \quad (4\text{-}36)$$

where:

T = water temperature (°C)

At 20°C and average conditions in the TIP (h = 2.5 m; u = 0.2 m/s), Equations (4-22) through (4-24) yield a k_l value of 0.56 m/d.

The vapor phase mass transfer constant was assigned a constant value of 100 m/d. A constant of this magnitude is a reasonable approximation because of the limited impact of air motion (winds) on transfer in streams and rivers (O'Connor 1983).

The overall mass transfer constant (k_L) at the average depth and velocity in the TIP is about 0.31 m/d. This equates to a volatilization loss rate constant of 0.12/d. At this rate, about 6% of the PCBs would be lost to volatilization during the 0.5 day travel time through the TIP (assuming all of the PCBs in the water column were dissolved).

The temporal variation in volatilization due to variation in river velocity, water column depth and temperature is described by Equations (4-33) to (4-36). Additional variation occurs as a result of seasonal freezing of the river which reduces the air-water interfacial area through which volatilization occurs. Based on anecdotal information, the river typically begins to ice over in December. Maximum ice cover is reached by early January when about 80% of the river surface is covered. Ice breaks up in early March. This information is roughly consistent with the long-term (1973-1993) daily average air temperature record in the vicinity of the river which indicates below freezing levels from the beginning of December to mid-March (Figure 4-32). To simulate the seasonal effect of ice cover on volatilization, the air-water interfacial area was reduced by 80% from December 1 to March 1 of each year. This reduction is equivalent to an 80% reduction of k_L.

The vapor phase concentration of PCBs in air, c_{air} of Equation (4-23), was assumed to be zero in volatilization calculations. Using Equation (4-23) one can show what levels of atmospheric PCBs are required to significantly impact the calculations. We have defined "significant" in this case to mean that the volatilization flux will change by more than 10%. At a dissolved water concentration of 10 ng/L (i.e., the detection limit) and a dimensionless Henry's Constant of 0.0078, the air concentration would have to be 7800 pg/m^3 to affect the flux calculation by 10%. The dissolved water concentration of 10 ng/L is conservative since PCB levels in the Upper Hudson River are routinely measured at much higher concentrations.

Measurements of atmospheric PCB concentrations are well below the 7800 pg/m^3 threshold above which volatilization fluxes would be significantly impacted. Hoff *et al.* (1992) measured 91 vapor phase congeners of IUPAC no.16 and higher at Egbert, Ontario from July 1988 to September 1989. The mean annual total PCB concentration (calculated by summing the annual mean concentrations for each congener) is approximately 192 pg/m^3. Hillary *et al.* (1997) reported mean yearly average vapor phase total PCB concentrations of 89 to 370 pg/m^3 at three sites near the Great Lakes. Eisenreich's laboratory (Steven Eisenreich, Rutgers University, New Brunswick, NJ, *personal communication* 1998) has measured atmospheric PCB concentrations on a regular basis in New Brunswick, NJ for the past year and at Sandy Hook beginning in February, 1998. Preliminary results indicate that vapor phase total PCB concentrations range

from approximately 200 to 3000 and 100 to 500 pg/m^3 at the New Brunswick site and the Sandy Hook site, respectively. Total PCB vapor phase concentrations in the Upper Hudson River are expected to be in the range of the Sandy Hook site which is probably indicative of background levels and probably less than values measured at the New Brunswick site given that New Brunswick is a highly urbanized/industrialized area. Therefore, the assumption of an atmospheric concentration of zero is reasonable. Even under the conservative assumptions of low dissolved water PCB and high vapor phase PCB concentrations, the atmospheric PCB concentrations cited above would impact the volatilization flux by no more than 4%.

The PCB loss due to volatilization at each of the dams depends on the ratio of entrained air flow to river flow. Using the estimates cited in Section 4.2.3, the ratio probably is on the order of 0.1 for the dams between Rogers Island and Stillwater (heights of about 2-3 m). It is probably somewhat higher for the dams below Stillwater which range in height from about 4 m to 6 m. Applying Equation (4-25) with the conservative assumptions that all of the PCBs are dissolved and the air concentration is zero, about 0.1% of the PCBs would be volatilized at each of the smaller dams. Assuming a ratio of 1 as an upper bound estimate for the larger dams, about 0.7% of the PCBs would be volatilized at each of these dams. Thus, the loss of PCBs due to volatilization at the dams is small. The total loss from all of the dams is likely to be less than 3% and volatilization of PCBs at the dams was not included in the model.

4.4 CALIBRATION/VALIDATION STRATEGY

Calibration/validation of the PCB fate model was accomplished by comparing predicted and observed PCB_{3+} concentrations in the water column and sediment of the river. Water column concentrations vary on daily, seasonal and annual time scales. Sediment concentrations vary slowly and significant changes occur on an annual to decade-long time scale. Thus, an evaluation of the accuracy of the model must include model-data comparisons at multiple time scales. These key comparisons included the following:

- water column PCB_{3+} levels during storm events,
- seasonal variation in water column PCB_{3+} levels during low river flows,

- decade scale trends in water column PCB_{3+} levels due to declines in surface sediment PCB_{3+} levels and upstream water column concentrations, and
- decade scale trends in sediment PCB_{3+} levels.

To evaluate the model on these different scales, the model calibration extended over a decades-long time scale. This was accomplished by simulating the time period from 1977, the time of the first comprehensive survey of sediment PCB levels, to 1998.

4.4.1 Overall Approach

The calibration approach minimized the number of parameters and coefficients that had to be defined by model calibration. Efforts were taken to determine values from independent analysis of data and theory as discussed in Section 4.3. The only significant parameters whose values were not tightly constrained by data or theory were the depth and extent of particle mixing in the surface sediments. These parameters were calibrated based on the vertical gradients in PCB_{3+} concentration and the depth of ^{7}Be penetration observed in high resolution sediment cores as discussed in Section 4.3.4. The choice of the maximum depth of particle mixing was also guided by data on composition of the benthic community.

The major uncertainty in model calibration was the magnitude of pulse PCB loadings entering from upstream. Unusually high PCB loadings were periodically observed at Rogers Island. Typically, these loadings were associated with high river flow, but not necessarily with high suspended solids. It is likely that these loadings were the result of PCB oils entering the river from the vicinity of the GE Hudson Falls Plant. The frequency of sampling at Rogers Island was inadequate to accurately quantify the total loading associated with the pulse events. A strategy for estimating the loading was developed and is discussed in detail in Section 4.4.3.2. The loading was finalized by adjusting it based on the temporal profile of surface sediment PCBs in the TIP.

4.4.2 Calibration/Validation Data Sets

The fate and transport model was calibrated against multiple data sets generated by GE, USEPA, USGS, and NYSDEC (Table 4-3). The water column data consisted of two data sets: The first is composed of approximately 2000 PCB and TSS measurements from water samples collected by the USGS at Fort Edward, Schuylerville, Stillwater, and Waterford from 1975 to 1995 (Figure 1-4). The second includes approximately 3000 PCB and TSS measurements from water samples collected about once a week by GE from 1991 to present at Bakers Falls, Fort Edward and TID. GE sampled additional stations during portions of this time period, including Schuylerville (1991-1992, 1997 - present), Stillwater (1991-1992), and Waterford (1991-1992). Because the fate and transport model simulates PCB_{3+}, the data were adjusted to this basis. For the GE data, the calculation of PCB_{3+} involved a subtraction of the measured mono and di weight percent from the total PCB value provided in the database. Obtaining PCB_{3+} for the historical USGS data required more rigorous analyses and calculations based upon a re-analysis of some of the original USGS chromatograms (QEA 1999). A summary of the method applied to calculate PCB_{3+} is provided in Section 1.4.6 and by QEA (1999). A third data set existed that was used in data analysis but not for direct model-to-data comparison. This data set, the USEPA Phase 2 water column survey, consists of about 100 samples taken at transects throughout the Upper Hudson River in 1993. Although these data were useful in determining and verifying model parameters, due to its limited temporal scale, it was not compared directly to the model results.

The sediment data are also composed of multiple data sets. Two surveys were conducted by NYSDEC in the mid 1970s (1976 to 1978) and mid 1980s (1984 to 1985). More recent surveys consist of the 1991 GE Composite Samples, the 1992 USEPA High Resolution Cores, the 1994 USEPA Low Resolution Cores, and the 1998 GE TIP Sediment Survey.

Table 4-3. Hudson River Data Sets Used for Model-Data Comparison

Sampling Program	Media/Type	Agency/Consultant	Stations*	Period of Record
USGS Water Quality	Water	USGS	FE	~1975-1995
			SCH	~1975-1995
			STWR	~1975-1995
			WTFRD	~1975-1995
Routine Sampling	Water	GE	BF	1991-present
			FE	1991-present
			TID	1991-present
			SCH	1991-1992,1997-present
			STWR	1991-1992
			WTFRD	1991-1992
Phase 2 Transect Survey	Water	USEPA	UHR	1993
1977 Sampling Program	Sediment (260 cores, 700 grabs)	NYSDEC	UHR	1976-1978
1984 Sampling Program	Sediment (~550 locations)	NYSDEC	TIP	1984-1985
Composite Survey	Sediment (161 Cores, 46 Grabs)	GE	UHR	1991
High Resolution Survey	Sediment (28 Cores)	USEPA	UHR	1992
Low Resolution Survey	Sediment (171 Cores)	USEPA	UHR	1994
TIP Sediment Survey	Sediment (70 Cores, 3 Grabs)	GE	TIP	1998

*Stations: BF Bakers Falls; FE Fort Edward; SCH Schuylerville; STW Stillwater; TID Thompson Island Dam; TIP Thompson Island Pool; UHR Upper Hudson River; WTFRD Waterford

Note: Composite stations counted as one.

The 1970s data were used as sediment initial conditions for the fate and transport model (Section 4.4.3.1). The 1984 (TIP only), 1991, and 1998 data were used in model calibration/validation. Various graphical comparisons between model and measured sediment PCB_{3+} concentrations were used in the calibration/validation process. These included spatial profiles in the years in which data were collected and temporal profiles at the locations of selected model segments. For several of these comparisons the data within model segments or river reaches were averaged. Because the sampling programs varied in each year, a different approach was used when developing averages for each data set.

1984 - Cores and grabs collected by NYSDEC

The 1984 sampling survey was primarily used in the spatial comparison within the TIP. Because of the large sampling intervals for the cores, a direct comparison to the 0-25 cm layer was most accurate. As a result, an estimate of the cohesive average for each segment was calculated as a straight average of the available cohesive cores and grabs in that segment. Samples were classified as cohesive or non-cohesive based upon a methodology outlined in Erickson (1998) and Section 4.4.3.2 (Table 4-4).

Table 4-4. Criteria Applied to Determine Fine/Coarse Designation for 1984 Data

Criteria / Result	Applied to Reach*	Side Scan Sonar Designation (Reaches 6-8)	Principle Fraction	Other
Cohesive	8	Fine	<400	
Non-cohesive	8	Fine	≥400	
Non-cohesive	8	Coarse	>200 or n. avail.	
Cohesive	8	Coarse	≤200	
Cohesive	8	Either	n. avail.	FOC ≥5%
Cohesive	8	n. avail.	n. avail.	PCB_{3+} ≥50 ppm
Non-cohesive	8	n. avail.	n. avail.	PCB_{3+} < 50ppm

* 1984 survey only sampled the TIP

**Principle Fraction from USEPA v4.1 CD Rom

100	Principle fraction is clay.	400	Principle fraction is medium sand.
200	Principle fraction is silt.	500	Principle fraction is coarse sand.
300	Principle fraction is fine sand.	600	Principle fraction is gravel.

1991 - Composite cores and grabs collected by O'Brien & Gere

These data, located by averaging the location coordinates of their discrete samples, were used in both temporal and spatial comparisons. In the spatial analysis, samples were classified as fine (cohesive) or coarse (non-cohesive) based upon a data analysis report (O'Brien & Gere 1993a). Averages were calculated in half-mile intervals for sediment depth intervals of 0-5 cm, 5-10 cm and 10-25 cm. Cohesive and non-cohesive averages were then calculated for each segment and the entire TIP. Because these averages crossed model segment boundaries, careful consideration was taken when developing an average for a given segment. The non-cohesive average was found by weighting the half-mile average by the number of discrete samples located

within the segment. The cohesive average was found by first developing an average for each cohesive area within a given segment (see Plate 4-1), using the same sample weighting as applied to the non-cohesive data. The overall cohesive average for a segment was calculated by weighting the individual cohesive zone averages by area.

1998 - Composite and individual cores and grabs collected by QEA

The 1998 survey attempted to 'repeat' portions of the 1991 O'Brien & Gere and 1994 USEPA sediment surveys (QEA 1998c). The spatial comparison was performed using the 0-5 cm average for each core or grab, located by mile point. For the temporal plots, an average was developed for each segment and the entire TIP. The 0-5 cm cohesive and non-cohesive averages were calculated using the same averaging method as 1991. The classification of the samples as cohesive or non-cohesive was determined from field notes and sample locations.

4.4.3 External Forcing Functions

4.4.3.1 Sediment Initial Conditions

NYSDEC conducted PCB sediment surveys from 1976 through 1978 that were used to determine the initial PCB_{3+} concentrations for each sediment segment of the fate and transport model. These concentrations were established by grouping the available data to within cohesive and non-cohesive areas of the Upper Hudson River (from Fort Edward to Troy, New York) and averaging the data in each group.

Data Overview

The 1976-78 sediment sampling program (referred to as "1977 sampling program") consisted of both cores and grabs taken at locations from the beginning of Reach 1 (Troy, New York) to Reach 8 (TIP), with the highest density of sampling occurring in Reach 8 (Plate 4-1). Data are available from approximately 700 grabs and 260 cores resulting in a total of 1766 samples with measured Aroclor PCB concentrations. Most of the grab samples were taken along

transects, which are more concentrated in areas of suspected PCB sources. These samples were estimated to represent the top 13 cm (approx. 5 inches) of sediment (Tofflemire *et al.* 1979). The core locations are concentrated on the banks of the river and the sampling depth intervals varied considerably from location to location.

PCBs were quantified as Aroclors using the Webb and McCall method and the Aroclor standards 1221, 1016, and 1254; however, these measurements have been found to contain an analytical bias. A detailed discussion of this bias can be found in a technical memorandum written by Tetra Tech, Inc. (Butcher 1998b). Using suggestions from this document, PCB_{3+} was calculated using the following equation:

$$PCB_{3+} = 1.113*(Aroclor_{1016} + Aroclor_{1254}) \quad (4\text{-}37)$$

Other non-chemical data measured during the survey were also used in the data averaging method. The physical properties of principal fraction-phi and sediment texture number were used to assist in designating the sample as cohesive or non-cohesive. Principle fraction-phi is supplied for approximately 23% of the 1976-78 samples while texture numbers, which are based on visual inspection, are available for about 83% of the samples. The organic carbon content of the sediment samples was estimated from measured volatile suspended solids and used to classify the sediment and convert concentration from units of mg/kg dry to mg/kg oc. Organic carbon concentration was assumed to be 40% of the volatile suspended solids value.

Designation of Samples as Cohesive or Non-Cohesive

Because the PCB fate model separates the riverbed into cohesive and non-cohesive areas, it was necessary to develop averages that represented these two different sediment types (Plate 4-1). In order to do this, each sediment sample had to be classified as cohesive or non-cohesive. The scheme used to assign the classification involved consideration of the USEPA side scan sonar interpretation (Flood 1993), sediment bed map (see Section 3.2.1) and the sample physical properties. The 1977 sediment sampling locations were projected onto the USEPA side scan sonar and lower reach bed map. Within Geographic Information Systems (GIS), each sample

was assigned a model segment number and a cohesive zone (see Plate 4-1). If the sample did not lie within a cohesive zone, the closest cohesive area was noted, along with the distance from the sample location to the area. Once mapped, the associated physical characteristics of each sample were analyzed to determine if the sample should have a final designation of fine (cohesive) or coarse (non-cohesive). The methodology employed for this analysis is similar to that developed by LimnoTech, Inc. (Erickson 1998) and is presented in Table 4-5. All samples from a core were given the same classification as that of the surface sample. In addition, a sample location that initially was not indexed to a cohesive area, but had a fine classification according to the physical criteria, was assigned to the closest cohesive area. However, if the closest cohesive area was greater than 1000 ft away, the sample remained non-cohesive.

Table 4-5. Criteria Applied to Determine Fine/Coarse Designation for 1977 Sediment Data

Criteria / Result	Applied to Reaches	Side Scan Sonar Designation (Reaches 6-8)	Sediment Transport Bed Mask Designation (Reaches 1-5)	Texture Class*	Principle Fraction**	Other
Cohesive	All	Fine	Cohesive	< 8 or n.avail.	n.appl.	
Non-cohesive	All	Fine	Cohesive	≥ 8	n.appl.	
Non-cohesive	6-8	Coarse	n.appl.	n.appl.	> 200 or n.avail.	
Cohesive	6-8	Coarse	n.appl.	n.appl.	≤ 200	
Cohesive	1-5	n.appl.	Non-Cohesive	n.appl.	≤ 200	
Cohesive	1-5	n.appl.	Non-Cohesive	n.appl	=300	%clay + %silt >25
Non-cohesive	1-5	n.appl.	Non-Cohesive	n.appl.	=300	%clay + %silt ≤25
Non-cohesive	1-5	n.appl.	Non-Cohesive	n.appl.	≥ 400	
Cohesive	1-5	n.appl.	Non-Cohesive	≥ 0 and < 6	n.avail.	
Non-cohesive	1-5	n.appl.	Non-Cohesive	≥ 6 and <10	n.avail.	
Cohesive	All	Either	Either	n.appl.	n.avail.	FOC ≥ 10%
Cohesive	All	n.avail.	Non-Cohesive	n.avail.	n.avail.	PCB_{3+} ≥50ppm
Non-cohesive	All	n.avail.	Non-Cohesive	n.avail.	n.avail.	PCB_{3+} <50ppm

n.appl. = not applicable n.avail. = data not available

*Texture Classes (from Tofflemire and Quinn, April 1979)

0 Clay	5 Fine Sand and Wood Chips
1 Silt	6 Sand
2 Muck	7 Sand and Wood Chips
3 Muck and Wood Chips	8 Coarse Sand
4 Fine Sand	9 Coarse Sand and Wood Chips

**Principle Fraction from USEPA v4.1 CD Rom

100	Principle fraction is clay.
200	Principle fraction is silt.
300	Principle fraction is fine sand.
400	Principle fraction is medium sand.
500	Principle fraction is coarse sand.
600	Principle fraction is gravel.

Methodology for Data Averaging

Cohesive sediments to a depth of 25 cm and non-cohesive sediments to a depth of 5 cm are included in the model. Both sediment types are divided into 1-cm layers. Thus, it was necessary to compute averages at 1-cm depth increments within cohesive and non-cohesive zones. Computation of averages was complicated by the fact that the depth intervals for the cores varied from sample to sample. Figure 4-33, which shows a probability plot of the lower depths for each surface layer of the cores, illustrates the variability of segmentation and indicates that the depth intervals at the surface range from 1.5 cm to 46 cm. Consequently, simple averaging of core data is not appropriate. Instead, a concentration was assigned to each centimeter in the core using the available data and applying a weighting factor to each concentration, determined by the sample's depth interval (Figure 4-34). For example, the 1977 core number 31420 has a total PCB concentration of 88 mg/kg in 0 to 2.5 cm and 38 mg/kg in the 2.5 to 5 cm layer. For the averaging, the top two centimeters were assigned the value of 88 mg/kg and a weighting factor of 1 cm each. The third centimeter for this core, though, was assigned two concentrations, each weighted by the data layer located within the third centimeter. In this example, the 88 mg/kg would be assigned a weighting factor, or thickness, of 0.54 cm, while the 38 mg/kg has a weighting factor of 0.46 cm. For the grabs, a constant concentration was assigned for the top 13 cm (~5 in) – corresponding to the estimated depth of a grab sample in the 1977 sampling survey (Tofflemire *et al.* 1979).

In four instances, samples were dropped from the non-cohesive area average in segments 9, 11, and 26. The first 2 data points (id numbers 31169 and 30291), although deemed non-cohesive by the criteria stated in Table 4-5, existed in transitional areas (i.e. near cohesive zones, but not inside) and had unusually high PCB_{3+} measurements. As a result, these high values were controlling the non-cohesive average for the segments and causing unrepresentative results. Not enough additional information was known about these samples to place them into a cohesive area with confidence; therefore, they were dropped from the average. The third outlier was a group of grabs placed into segment 11 by their designated mile point (no available location coordinates). These grabs all occurred on December 27, 1977 and according to the database, were located at mile point 189.2. However, these samples had extremely high PCB_{3+} concentrations (overall

average of ~300 ppm) and their locations were suspect. Because of the extremely high concentrations and the fact that no documentation could be found supporting this December 1977 sampling effort, this group of grabs was dropped from the segment average. The fourth set of data was similar to the December 27 survey in that no location coordinates were designated for these samples. However, these data were given a mile point of 156.5, which placed them into segment 26. As before, this location was suspect, especially due to the high number of samples located at this mile point and the anomalously high concentrations – therefore, these data were also dropped.

Once concentrations were assigned for the entire available depth, the average concentration in each centimeter for each cohesive or non-cohesive area was determined from all cores and grabs in a given area, using the following equation:

$$C_{avg_j} = \frac{\sum c_i l_i}{\sum l_i} \qquad (4\text{-}38)$$

where:

C_{avgj} = average concentration of layer j (non-cohesive or cohesive) within a cohesive or non-cohesive area

c_i = concentration of sample i located within layer j

l_i = weight assigned to sample i, indicating the fraction of sample within layer j

Using this method, averages for 80 different areas were calculated (28 non-cohesive areas and 52 cohesive areas).

Because the delineation of the cohesive areas did not conform to the boundaries of the model segments, it was necessary to estimate the average PCB_{3+} concentration within the cohesive area of each segment. In order to develop this average, the fractional contribution of each cohesive zone to the total cohesive area for each water quality segment was determined using GIS (Table 4-6). The average of each centimeter layer was then calculated with the equation below:

$$C_{avg_j} = \sum f_i c_i \qquad (4\text{-}39)$$

Table 4-6. Cohesive Sediment Distribution in Relation to Water Quality Segmentation

Fine Zone	Water Quality Segment	Reach	Area (ft^2)	Fraction of Total	Fine Zone	Water Quality Segment	Reach	Area (ft^2)	Fraction of Total
56	1	8	13,658	1.00	26	14	6	1,270,735	0.26
1	2	8	66,824	0.35	27	14	6	38,195	0.01
2	2	8	101,213	0.53	28	14	6	248,009	0.05
56	2	8	22,923	0.12	29	14	6	2,068,454	0.42
2	3	8	684,187	0.83	30	14	6	827,919	0.17
2	4	8	97,400	0.12	31	14	6	275,335	0.06
3	4	8	40,397	0.05	32	14	6	171,149	0.03
4	4	8	1	0.00	33	16	5	324,001	0.38
3	5	8	345,932	0.53	34	16	5	171,469	0.20
4	5	8	298,953	0.46	35	16	5	194,478	0.23
5	5	8	3,627	0.01	36	16	5	163,563	0.19
3	6	8	4,628	0.01	37	17	5	660,589	0.59
5	6	8	683,828	0.99	38	17	5	383,299	0.34
5	7	8	353,080	0.90	39	17	5	74,327	0.07
6	7	8	37,467	0.10	20	18	5	742,745	0.42
6	8	8	14,439	0.09	40	18	5	179,275	0.10
7	8	8	51,537	0.34	41	18	5	522,307	0.30
9	8	8	87,638	0.57	42	18	5	303,680	0.17
9	9	8	667,279	0.93	20	19	5	333,820	0.16
10	9	8	26,172	0.04	43	19	5	862,360	0.41
11	9	8	23,464	0.03	44	19	5	64,311	0.03
11	10	8	201,854	0.67	45	19	5	143,485	0.07
12	10	8	98,032	0.33	46	19	5	699,677	0.33
11	11	8	67,168	0.14	47	20	5	2,755,229	0.78
12	11	8	314,973	0.66	49	20	5	797,970	0.22
13	11	8	98,407	0.20	49	21	4	54,979	0.01
13	12	8	46	0.00	50	21	4	3,511,287	0.82
14	12	8	40,876	1.00	51	21	4	705,411	0.17
16	13	7	53,854	0.06	51	22	3	377,843	1.00
17	13	7	31,725	0.04	51	23	2	173,770	0.86
18	13	7	19,374	0.02	52	23	2	27,712	0.14
19	13	7	157,294	0.19	53	24	2	188,653	0.26
21	13	7	16,462	0.02	54	24	2	524,876	0.74
22	13	7	15,711	0.02	55	26	1	135,200	1.00
23	13	7	152,575	0.18					
24	13	7	373,119	0.44					
25	13	7	23,342	0.03					

where:

$C_{avg,j}$ = average cohesive concentration in a given water quality segment, j, for a given layer

f_i = fraction of cohesive zone i relative to total cohesive area within segment j

c_i = concentration of cohesive zone i, for a given layer.

In this manner, each model segment was assigned corresponding sediment averages for each centimeter in non-cohesive areas and, if applicable, cohesive areas. The final averages are shown in Figures 4-35a-c.

4.4.3.2 Upstream PCB Input

PCB_{3+} flux across the upstream boundary of the model at Fort Edward (upstream PCB_{3+} loading) was estimated using two different methods, depending on the period of record. The 1977 to March 1991 loadings were developed using USGS data from the Rogers Island monitoring station (approximate MP 194.4) and an analysis framework based on the concept that the PCB_{3+} loading from upstream of Fort Edward consisted of multiple components. Daily loadings from April 1991 to March 1998 were estimated from weekly monitoring data obtained by GE at Rogers Island. Linear interpolation was used to estimate loadings for periods between the monitoring times.

The USGS data are erratic, limited by frequency of sampling and the large variations in observed loading. In an effort to make maximum use of the data, a phenomenological approach was developed. The loading was presumed to be divisible into three components. The first is a base load that is the result of diffusive and advective flux of PCB from surface sediment into the water column. The second is the resuspension of contaminated surface sediments into the water column during high flow events. The combination of these components produces the 'normal' daily loading. Periodically during high flow conditions, a third component was observed in the data. Although this third phenomenon produced unusually high PCB measurements and generally corresponded to high flow conditions, it was not always associated with elevated suspended solids. It is likely these PCB concentrations were the result of PCB oils entering the

river from the GE Hudson Falls site area (see Section 1.2.1.1). The total estimated PCB loading at Fort Edward was calculated as a combination of the three components of the load as follows:

$$W(t)_{total} = W(t)_{base} + W(t)_{resuspension} + W(t)_{pulse} \quad (4\text{-}40)$$

where:

$W(t)_{total}$	=	total load at Fort Edward (M/T) for the given time period,
$W(t)_{base}$	=	average base load for a given year (M/T)
$W(t)_{resuspension}$	=	$r_{avg} \cdot TSS \cdot Q$; r_{avg} is average PCB_{3+} particulate concentrations (M/M) for a given year during high flow events, TSS is the total suspended solids during the high flow event (M/L^3), and Q is the flow during the event (L^3/T)
$W(t)_{pulse}$	=	estimated pulse load for the given time period

Historical Data Overview

The data used for historical loading were the USGS water quality samples retrieved from USEPA's database (version 4.1). These data fell into three different categories: samples which represented a composite of the east and west channels around Rogers Island, individual samples taken within the east and west channels on the same day, and samples with no qualifiers to indicate a composite or individual channel samples. Composite samples were taken as is and unqualified samples taken on the same day were averaged. The east/west channel samples taken on the same day were averaged to produce a composite result. It should be noted that the majority of the high PCB concentrations, i.e., those which fall into the third loading component described above, occurred within the east channel around Rogers Island. PCB_{3+} concentrations were calculated from the reported Aroclor or total PCB data using the methodology outlined in Section 1.4.6. Once the concentrations were determined, the load was calculated by using the instantaneous river flow measured at the USGS flow gauge at Fort Edward. In a few incidences, daily average river flow was used when instantaneous measurements were not available.

As a means to differentiate base load and resuspension load, the relationship between PCB loading and TSS was examined. The loading was independent of TSS until TSS values exceeded about 10 mg/L (Figures 4-36a-b). On the basis of this result, PCB data from samples with TSS less than or equal to 10 mg/L were presumed to be representative of the base load. Statistical analysis was performed on the loading that occurred within each year at TSS value less than a equal to 10 mg/L to determine outliers. Data points that fell outside the 95% confidence interval around a given mean were dropped from the base load average. This analysis is summarized in Table 4-7. Because the loading displayed a seasonal variation, estimates derived from these PCB data and associated flows were averaged in 3 month intervals to provide quarterly average estimates of the base loading. These loads decline from 2.5 to 3 lb/d in the late 1970s to about 0.6 lb/d by the late 1980s (Figure 4-37).

Table 4-7. Summary of Statistical Analysis on PCB_{3+} Loading to Determine Base Load Outliers

Year	Number of Samples	Median PCB Load lb/day	Lower 95% Confidence Limit	Upper 95% Confidence Limit	Number of Outliers Declared
1979	17	2.16	0.63	7.33	3
1980	22	1.52	0.52	4.44	0
1981	21	0.75	0.13	4.38	1
1982	20	1.83	0.86	3.88	4
1983	23	3.18	0.82	12.38	1
1984	16	0.99	0.17	5.94	3
1985	12	0.88	0.08	9.25	0
1986	15	1.04	0.08	12.91	0
1987	4	0.45	0.11	1.78	0
1988	14	0.39	0.09	1.65	3
1989	7	0.54	0.26	1.11	2
1990	14	2.43	0.22	26.75	0
1991	15	0.439	0.24	0.80	3

A fraction of the PCB measurements were below the method detection limit and are reported at the detection limit value in the database with a qualifier indicating that the value is a "non-detect". In the loading analysis, the detection limit was assumed to be the concentration for

non-detects. This assumption did not have a large impact on the annual base loads where the percentage of non-detects in the data set was below 50% (Table 4-8). However, in 1983, 74% of the samples measured were non-detect, while 92% of the available 1990 data was marked as non-detect. This high percentage of non-detects resulted in a significant impact on the base loading depending on whether the non-detects were set to detection limit or zero (see Table 4-8). For this reason, the values for the previous years were applied in each of these cases.

Table 4-8. Percentage of Base Load Data Flagged at Non-Detect

Year	Base Load with ND=DL	Base Load with ND=0	% of Data Flagged as Non-Detect
1978	2.0	1.9	33
1979	2.5	2.4	36
1980	1.7	1.7	5
1981	1.0	0.9	33
1982	1.9	1.3	40
1983	3.9	1.3	78
1984	1.3	1.3	0
1985	1.4	1.4	17
1986	1.9	1.9	13
1987	0.5	0.5	0
1988	0.8	0.8	6
1989	0.6	0.6	0
1990	4.3	0.1	92

Estimation of the resuspension component of load recognized that at high TSS most of the PCB loading is associated with particulate matter. Thus, at high TSS the PCB concentration per unit TSS is an estimate of the PCB concentration on the particulate matter. At TSS greater than 20 mg/L, the PCB loading and TSS were directly correlated. In fact, the PCB concentration per unit TSS (i.e., mg PCB/kg dry solids) was relatively constant at TSS values greater than 20 mg/L (Figures 4-38a-b). This characteristic of the data supports the use of PCB concentration per unit TSS at high TSS values as an estimate of resuspension-associated particulate phase PCB concentration. Calculated particulate phase PCB_{3+} concentrations at TSS greater than 20 mg/L were averaged in annual increments to provide annual average estimates of resuspension-associated PCB_{3+}. Visual inspection of Figures 4-38a-b suggested that concentrations higher than 20 mg/kg PCB_{3+} in 1979 and 1983 were outliers and these samples were excluded from the annual average calculation. A log-linear regression of the annually-

averaged data was used to interpolate values for each year from 1977 to 1991 (Figure 4-39). PCB loading due to resuspension was computed by multiplying the particulate phase PCB_{3+} concentration by TSS and flow entering Fort Edward provided by the sediment transport and hydrodynamic models.

As mentioned above, the USGS water column PCB data include occasional outliers: anomalously high concentrations that are inconsistent with the base and resuspension loadings. As a result, these high outliers were excluded from the loading components. They are evident in the distribution of residual differences between the observed PCB loading and the loading calculated from the sum of the annual base loading and the resuspension loading (Figures 4-40a-b). The residuals are distributed around zero and cross zero near the middle of the distribution, indicating that the loading estimation method is unbiased and, for the most part, accurately reproduces loading entering from upstream. In several years, high residuals exist that deviate from the distribution formed by the bulk of the points. These high residuals indicate a sampling event in which the observed loading is considerably higher than that predicted from base loading and resuspension. Considering what is currently known about PCB DNAPL sources upstream of Fort Edward (see Volume 1) these anomalous high loadings are likely associated with PCB oil transport from the Hudson Falls plant site to Fort Edward. Moreover, studies have indicated that dense oil phase material may be sequestered upstream of Rogers Island under low river flow and mobilized and transported downstream under higher flows (QEA 1998b). The PCB loading associated with pulse transport of PCB oil cannot be accurately determined from the monitoring data. However, the monitoring data can be used to develop some insights about this loading. The distribution and chronology of the anomalously high residual loadings (Figure 4-41) provide a basis for estimating the frequency and magnitude of the pulse loads. Values range from approximately 20 lb/d to about 200 lb/d. In addition, a composited value in 1983 (~39 ppb) yields a value of greater than 4,900 lb/d (Table 4-9).

Table 4-9. Ranking of High Residual Loads at Fort Edward

Month	Day	Year	Observed Load (lb/day)	Expected Load (lb/day)	Residual Load (lb/day)	TSS (mg/L)	Flow (cfs)
12	15	1983	4939.50	10.24	4929.26	19.5	23800
8	31	1984	196.95	1.33	195.62	8.0	4060
3	15	1977	168.17	2.01	166.16	N/A	24000
4	28	1979	189.73	37.19	152.53	37.5	32000
4	25	1983	138.04	8.81	129.23	19.5	19700
3	27	1979	142.24	14.21	128.03	20.0	20300
5	3	1983	128.66	22.68	105.98	34.0	34100
4	30	1979	80.34	20.11	60.23	22.5	27100
10	24	1990	50.13	4.17	45.96	25.0	18600
5	1	1983	44.79	12.84	31.95	22.0	27700
4	1	1987	48.90	20.55	28.35	65.0	27806
3	14	1977	24.36	2.01	22.35	N/A	22600
3	22	1980	26.82	6.24	20.58	11.0	16050

N/A = data not available

Given the frequency of sampling and the frequency at which pulse loading events were sampled, an estimate of the frequency at which pulse loads occurred was developed. The population size (i.e., number of days), a sample size (i.e., number of days in which PCB concentration was measured) and the fraction of samples exhibiting pulse loads, were used to estimate the frequency of pulse loads. In general, pulses appear to occur at flows greater than about 15,000 cfs. Examination of the timing of pulse loads in relation to flood hydrographs did not reveal an association with particular stages of the flood such as the rising limb. Thus, the population size was defined simply as the number of days during each year when flow exceeded 15,000 cfs (Table 4-10).

Table 4-10. Frequency Analysis for Flow and PCB Data at Fort Edward			
Year	Total Number of Flow Data Points	Number of Data Points with Average Q > 15,000 cfs	Number of Data Points with Average Q > 15,000 cfs with PCB Data
1977	365	21	2
1978	365	4	1
1979	365	23	6
1980	366	2	2
1981	365	9	6
1982	365	12	5
1983	365	26	10
1984	366	13	7
1985	365	0	0
1986	365	13	1
1987	365	9	3
1988	366	0	0
1989	365	10	2
1990	365	25	3
1991	365	0	0
Total	5478	167	48

Over the 14 year period from 1977 to 1990 the flow exceeded 15,000 cfs on 167 days. Samples were taken on 48 of those days and pulse loads were observed in 13 of those samples resulting in a pulse load frequency of 0.27 (i.e., 13/48) or 3.2 days per year (i.e., 0.27 x 167 days/14 yrs). The average magnitude of the pulse loads (Table 4-9) is about 460 lb/d corresponding to approximately 1470 lb/yr. This value is greatly influenced by the greater than 4,900 lb/d loading observed in 1983. To the extent that this loading is not representative of loads over the 14-year period, the average load is over-estimated. In applying these loads in the model, the value of 1470 lb/yr was viewed as an upper bound. Through model calibration we revised the pulse loading to a value of 300 lb/yr or 100 lb/d for 3 days per year. This value corresponds to the median pulse loading observed in the data set.

The timing of the pulse load is uncertain. However, we believe the pulses are related to the migration of PCB oil from the Hudson Falls plant site areas. Field studies indicate that such loadings would be trapped within the TIP (QEA 1998b). The pulse loads were invoked during periods of maximum solids deposition as defined by the sediment transport modeling. In this manner, approximately 40% of the load was predicted to be trapped within the TIP.

With the exception of days that had anomalously high residual loads (Table 4-9), actual monitoring data was used with daily average flow to generate a daily average PCB_{3+} loading for that day. Equation (4-40) was used to generate daily average PCB_{3+} loads for all days lacking PCB_{3+} measurements.

Recent Loadings

GE began to monitor water quality weekly in April 1991. In September 1991, the gate failure in the Allen Mill resulted in a prolonged period of elevated PCB discharge to the river (QEA 1998b). The elevated loads and their variation in time invalidate the three component conceptual model used to estimate the historical loads. Thus, weekly measurements were used directly with linear interpolation to estimate concentration between the days of sampling. Using the interpolated concentrations and daily average flows, a load at Rogers Island was calculated for each day. Figure 4-42 shows the final results of this process.

4.5 CALIBRATION RESULTS

The calibration exercise revealed that the fate model was tightly constrained by the solids fluxes provided by the sediment transport model. These fluxes dominate PCB movement between the sediment and the water column and within the sediment. As a result, the model was only sensitive to a small subset of its remaining parameters: the partition coefficient in the water column; the depth and intensity of particle mixing; and, the depth of contamination in non-cohesive sediments (see Section 4.6).

Initial efforts at calibration were conducted with the depth of particle mixing in cohesive sediments specified as 5 cm and the depth of contamination in non-cohesive sediments specified as 13 cm. This model over-predicted the rate of decline of PCBs in surface cohesive sediments and under-predicted the rate of decline in non-cohesive sediments. Attempts to eliminate the bias by varying the intensity of mixing in both sediments and the depth of mixing in non-cohesive sediments within reasonable ranges were unsuccessful. Thus, any error in these parameters was not responsible for the bias. Only by reducing the depth of contamination in

non-cohesive sediments to 5 cm and increasing the depth of particle mixing in cohesive sediments to 10 cm, was the bias eliminated. For this reason, the values of these parameters are tightly constrained and calibration is viewed as support that the chosen values for these parameters are accurate.

4.5.1 Sediment PCB_{3+} Calibration

Several model-data comparisons were conducted for purposes of calibration and validation. Most of these were for the TIP because this region is the primary focus of remediation and contains the highest density of data. Comparisons of temporal profiles for the 0-5 cm layers of cohesive and non-cohesive sediments were conducted for TIP-wide and segment average concentrations. Comparisons of spatial profiles were conducted for the entire Upper Hudson River.

The long-term trends in the average surface sediment (0-5 cm) PCB_{3+} concentration in the TIP indicated by data and by the model are shown in Figure 4-43. Cohesive sediment PCB_{3+} levels declined from about 105 ppm in 1977 to about 20 ppm in 1991 and to about 14 ppm in 1998, declines of about 80 and 87%, respectively. The model closely reproduces this trend, predicting about 18 ppm in 1991 and about 10 ppm in 1998, declines of about 83 and 90%, respectively. The concentrations computed by the model lie within the uncertainty bars shown on the plot, which indicate ± two standard errors of the mean. Thus, there is no statistically significant difference between the model and the data.

The non-cohesive sediment PCB_{3+} levels declined from about 40 ppm in 1977 to about 12 ppm in 1991 and 7 ppm in 1998, declines of about 70 and 83%, respectively. This downward trend is slightly slower than that of the cohesive sediments. The model accurately reproduces the trend, computing concentrations of about 11 ppm in 1991 and 8 ppm in 1998. Thus, the model accounts for the difference in the trend between the cohesive and non-cohesive sediments, as well as the absolute concentration drops between 1977 and 1998.

Closer examination of the model predictions in the TIP was conducted by comparing concentrations computed for each model segment with average concentrations calculated from the 1991 and 1998 measurements for each river segment. Comparisons for cohesive sediments in nine segments are shown in Figure 4-44. The model reproduces the trends in most segments, including substantial differences in trends among the segments. For example, concentrations drop in Segment 10 (North of Griffin Island) from about 140 ppm in 1977 to about 35 ppm in 1998, whereas concentrations in Segment 13 (At Moses Kill) decline from about 240 ppm in 1977 to about 5 ppm in 1998. The model predicts this difference almost exactly. In other segments, the model sometimes over-predicts or under-predicts the trend, but the deviations are never large. In some cases the 1998 data point represents a single sample (indicated by symbols without error bars) and the deviations between model and data may reflect uncertainty in the actual average sediment concentrations.

The results for the non-cohesive sediments are similar to those of the cohesive sediments (Figure 4-45). Again the model generally predicts the differences in trends among the segments. For example, in Segment 5 (at Snook Kill) concentrations decline from about 40 ppm in 1977 to about 14 ppm in 1998, whereas in Segment 8 (North of Griffin Island) a smaller decline from about 17 ppm to about 8 ppm occurs over this period. The model predicts this difference as well as most of the other differences among the locations. The only segments in which the predicted 1998 concentrations do not fall within the confidence limits of the data mean are ones in which the data is from a single sample.

The ability of the model to reproduce the average trend in TIP sediments and the major features of the spatial variation of that trend within the TIP provides strong evidence of its predictive capabilities. We are unaware of any other model of a contaminated sediment site that has demonstrated this degree of accuracy.

The spatial patterns of sediment PCB_{3+} concentration computed by the model were also compared to data. The 1984 data set for cohesive sediments in the TIP consists mostly of cores sectioned from 0-23 cm and grabs. Segment averages of the core samples and the grab samples are compared to model results in Figure 4-46. Solid horizontal lines terminating at the

boundaries of the segments indict the 0-25 cm average concentrations computed by the model. The shaded region above and below the line indicates the range of computed concentrations over the 25 cm sediment column. Dashed horizontal lines are also shown indicating the 1977 segment mean concentrations used as the initial conditions for the model. In most of the segments the means of the core and grab samples are similar. The model mean values results fall within the uncertainty of the data means except for two segments in the middle of the TIP between mile points 190.6 and 191.6. These deviations appear to be a result of the 1977 initial conditions. In both segments the 1977 data mean is significantly lower than the 1984 data mean. Thus, the model is initialized with a PCB inventory in these segments that is considerably lower than the inventory indicated by the 1984 data. The general concordance between the model and data over an approximate 25 cm sediment column indicates that the model is properly accounting for the fate of the PCB inventory in the cohesive sediments in the period between 1977 and 1984.

The capability of the model to capture the PCB trends throughout the Upper Hudson River was examined using the 1991 individual composite core data and model segment concentrations. As with the 1984 model-data comparison, the segment mean calculated concentrations are indicated by a solid horizontal line and the concentration range is indicated by the shaded region. The horizontal dashed lines show the 1977 initial conditions. The model reproduces the large-scale spatial trend in the cohesive surface sediment (0-5 cm) data (Figure 4-47a), capturing both the decline from levels of tens of ppm above mile point 185 to a few ppm below mile point 180 and the lack of trend from mile point 180 to mile point 155. The model over-predicts concentration in the most-downstream segment between mile points 154 and 156. The single composite core in this region yielded a concentration of about 2 ppm, whereas the model computes a concentration of about 4 ppm. This difference may be partially due to a poorly specified initial condition. No 1977 data were available for this region of the river, and the value from the closest upstream segment was used. It may also reflect an under-prediction of burial in this region. As discussed in Section 3, the sediment transport model under-predicts deposition in this part of the river. The model under-predicts concentrations in the two segments between mile points 164 and 168. The data in this region range from about 1.8 to 6 ppm, whereas the model computes concentrations of about 1.5 ppm. This difference appears to be due to an over-estimation of burial in this region. The causes of errors in burial rate in the lower

reaches of the river are discussed in Section 3. Briefly, it appears that our poor knowledge of sediment bed conditions and bathymetry and the crude resolution of the model in the lower reaches are the primary causative factors.

The model is in general agreement with the data in the subsurface sediments (Figure 4-47b and c). Significant declines are predicted between 1977 (dashed lines) and 1991 in the 5-10 cm layer (Figure 4-47b). These declines yield concentrations that fall within the measurements in this depth range. As in the top 5 cm of sediment, the model over-predicts the decline in the segments between mile points 164 and 168 and under-predicts the decline in the most downstream segment. Again, these differences likely are due to a combination of errors in predicted burial rates and errors in the estimated 1977 concentrations.

In contrast to the 0-5 and 5-10 cm layers, the model predicts little change in concentration in the 10-25 cm layer (Figure 4-47c). In some segments a small decline is predicted, in others a small increase is predicted. The lack of substantial change is in general agreement with the observations, which fall around the predicted concentrations. The lack of large changes in this layer, which contains the largest portion of the sediment PCB mass included in the model, indicates that most of the PCB inventory has remained in the sediment.

Comparison of the 1991 model results and data in the non-cohesive sediments is presented in Figure 4-48. The model reproduces the general features of the data; however, the model tends to over-predict concentrations downstream of mile point 173. The model computes concentrations of about 1 to 3 ppm, whereas the data indicate concentrations in the range of 0.2 to 2 ppm. We are uncertain of the cause of this bias. It could be due to over-estimation of the 1977 concentrations or an over-estimation of the depth of contamination in the coarse sediments in this area of the river. From a practical standpoint, the over-estimation is not significant to the overall modeling because of the relatively low PCB concentrations in this area of the river.

4.5.2 Water Column PCB_{3+} Calibration

Data collected by the USGS and by GE are compared to the model predictions. The USGS data are the more temporally extensive data set, extending from the mid-1970s to the mid-1990s, whereas the GE data extend from 1991 to the present. However, the USGS data are less reliable than the GE data because PCBs were quantified as Aroclor concentrations, and because of an absence of documentation necessary for comprehensive quality assurance checks. In addition, the USGS concentrations were many times reported with only single digit accuracy and some uncertainty exists about the appropriate detection limit (Butcher, 1997b). Work done by GE to reanalyze a limited number of chromatograms indicates the presence of apparent transcription errors in the database (QEA, 1999). Also, during the period of overlap between the GE and USGS, the USGS measurements indicate lower PCB concentrations (Figure 4-49), suggesting the possibility of a low bias.

In addition to the water samples collected at Fort Edward that were cited above, GE collected water samples at the TID, Schuylerville, Stillwater and Waterford from April 1991 through June 1992. From this time until October 1997, samples were collected only at the TID. Beginning in October 1997, and extending to the present, samples were collected at the TID and Schuylerville. The TID samples collected prior to October 1997 were obtained from a shoreline location not representative of the cross-sectional average (QEA 1998b) and cannot be used for comparison to model predictions.

The comparison of predicted and GE measured water column PCB_{3+} concentrations at Schuylerville, Stillwater and Waterford in 1991 and 1992 is presented in Figure 4-50. From April to September 1991, the model predicts concentrations that closely match the measured values at each of the stations. The large concentration increase in September is associated with the Allen Mill event. Following this event, the model under-predicts water column concentrations for a period of about 1 month. Apparently the event had a residual effect that the model did not capture. However, the bias disappears after a month and the predicted concentrations are similar to the measured values.

The comparison of predicted and GE measured water column PCB_{3+} concentrations at the TID and Schuylerville in 1997 and 1998 is presented in Figure 4-51. A seasonal cycle in

concentration, interrupted by occasional spikes associated with high flow events or inputs from above Fort Edward, is evident at both stations. Concentrations are minimum in winter and maximum in early summer. The model generally reproduces the seasonal trend and the absolute concentrations at both stations. The large concentration spike in January 1998 that the model accurately predicts is associated with a high flow event with a peak flow of about 34,000 cfs at Fort Edward. This event equates to about a 1-in-10 year flood in the river. The data were collected at the peak of the flood and the beginning of the falling limb of the hydrograph. The ability of the model to reproduce the concentration increase is evidence that it has accurately represented the resuspension processes occurring during such a rare event.

The ability of the model to accurately predict water column PCB concentrations in 1991, 1997 and 1998, coupled with the accurate prediction of the surface sediment concentration change between 1977 and 1991, indicates that it properly represents the movement of PCBs between the sediment and the water column. These results provide evidence that the model has accurately described the principal processes affecting PCB fate in the Upper Hudson River. They support the use of the model to predict the potential impacts of remedial scenarios on downstream PCB transport and on concentrations of PCBs in the sediment and water column. The models ability to predict increases in water column PCBs associated with a substantial high flow event supports the use of the model to predict sediment processes during rare events.

Further evaluation of the model was conducted using the USGS measured water column PCB_{3+} concentrations at Schuylerville, Stillwater and Waterford. Because of the lower reliability of these data due to limitations of the PCB measurement method, evaluations conducted with them are viewed as supplementary to those discussed above. Comparisons of the long-term temporal pattern of water column PCB concentrations computed by the model at Schuylerville, Stillwater and Waterford with the USGS data are presented in Figure 4-52. The data indicate a decline in concentration from the late-1970s to the mid-1990s by about a factor of ten. In any year, considerable variability is evident with some suggestion of a seasonal cycle. The decline in concentrations computed by the model is shallower than the decline indicated by the data. In the late-1970s the computed concentrations tend to be lower than the measured values. This difference appears to be greatest at Schuylerville, where the model computed concentrations

ranging from about 50 ng/L to about 800 ng/L, whereas the data range from non-detect at 100 ng/L to more than 2,000 ng/L. The bias disappears by the early 1980s. From about 1981 to 1983, the model and data indicate similar concentrations. After this time, a bias is again evident. From about 1984 to 1990, the model computes concentrations that tend to be higher than the measured values by about a factor of two. This bias continues into the 1990s, although the magnitude appears to be lower.

The cause for the differences between the model and the USGS data set are not known. Because the model accurately predicts the changes in PCB_{3+} concentrations in the sediments and the water column concentrations measured by GE between 1991 and 1998, we do not believe the model has misrepresented any major fate process. It is possible that the low bias in the late-1970s is due to the presence of undocumented PCB sources. Sediment and debris dredged from the river after the removal of the Fort Edward Dam and the 1976 flood were placed in close proximity to the river (i.e., on Rogers Island and in landfills along the shore) and could have been a continuing source of PCBs to the river. It is also possible that some of the material left in the river channel after dredging was unconsolidated and easily mobilized into the water column, providing a temporary additional in-river source. The apparent high bias of the model in the later years likely is due to errors in measurement. As discussed above, comparison between the GE and USGS data suggest that the USGS data may have a low bias and the model is not biased to the GE data.

4.5.3 High Flow Model Evaluation

In addition to evaluation of the January 1998 flood discussed above, the ability of the model to describe the water column PCB_{3+} dynamics during high flow events was evaluated for events in 1982, 1983 and 1993 that had peak flows at Fort Edward of about 26,000, 34,000 and 29,000 cfs, respectively.

In 1982, the model reproduces the general features of both the spatial and temporal water column PCB_{3+} concentration patterns observed in the data. During this event, PCB_{3+} concentrations increased rapidly from about 100 ng/L, or less at Schuylerville, Stillwater and

Waterford to maximums of about 800 ng/L prior to peak flow and then decreased to levels of about 200 ng/L immediately following peak flow (Figure 4-53).

The 1983 high flow period was composed of three events, with the last event being the largest (i.e., a peak flow of 34,000 cfs). The concentration increases predicted by the model for the first two events are similar to those observed at Schuylerville, Stillwater and Waterford (Figure 4-53). In the last event the measured concentrations increase to a much greater extent than predicted by the model because the two earlier events reduced the quantity of resuspendable material in the non-cohesive sediment. The TSS data are consistent with this prediction: predicted TSS maximum values are less than those measured in the earlier events that had lower peak flows. For example, the peak PCB_{3+} level at Stillwater in the second event (ca. 400 ng/L) occurred at a TSS of slightly more than 100 mg/L, whereas the peak PCB_{3+} level in the third event (ca., 3000 ng/L) occurred at a TSS of about 70 mg/L. The peak TSS computed by the model at Stillwater for the last event is also about 70 mg/L. Therefore, the observed large increase in PCB_{3+} concentration is anomalous and may be the result of a pulse loading from upstream rather than resuspension.

In 1993, the high flow period occurred in April and, similar to 1983, was composed of three consecutive events with peak flows of about 20,000, 29,000 and 28,000 cfs. The model reproduces the concentrations at the TID during this period as they vary between about 40 and 300 ng/L (Figure 4-53). After the high flow period ends, the model calculates an extended period of high concentrations over which little data exist for comparison. These high concentrations are caused by the propagation of interpolated high concentrations at Fort Edward apparently related to upstream sources. With the exception of a single measured value at Stillwater during the second event, the model also accurately predicts the PCB_{3+} dynamics at Stillwater and Waterford during the three high flow events.

The demonstrated ability of the model to reproduce the general features of PCB_{3+} dynamics during high flow events is further verification that sediment transport processes are accurately represented in the model.

4.5.4 Conclusions Regarding PCB Fate

The calibrated PCB_{3+} fate model was used to examine the various mechanisms by which PCBs were lost from the water and sediment (top 10 cm in cohesive sediments; top 3 cm in non-cohesive sediments) in the Upper Hudson River. Overall, PCB loss varied from year-to-year with a general downward trend from 1978 to 1998 (Figure 4-54). Much of the year-to-year variation around the long-term trend is attributable to variations in burial below the top 10 cm of cohesive sediment. Burial variations are attributed to the fluctuations in the hydrograph and associated solids loading.

In the late-1970s about 2,000 to 2,500 pounds of PCB_{3+} were being transported annually to the Lower Hudson River. This declined steadily to about 700 pounds by the late-1980s. The releases from the area of the GE facility in Hudsons Falls increased the flux to the Lower Hudson River to about 1,200 pounds in 1992 and 1993. Remediation at Hudsons Falls reduced this flux to about 500 pounds by the mid-1990s. The lowest flux occurred in 1997, when about 300 pounds were transported. This increased to about 500 pounds in 1998, apparently due to releases to the river at Hudsons Falls during remedial activities in the river. These releases are evident in the occasional concentration spikes measured at Fort Edward (Figure 4-42).

Burial, which occurs almost exclusively in the cohesive sediments, removed varying amounts of PCB_{3+} from the upper 10 cm of sediment. Between 1978 and 1984, the annual flux ranged from about 900 to 3,500 pounds. After this time, a general decline is evident, although the year-to-year variation is large. Since 1991, burial has removed between about 200 and 300 pounds annually from the upper 10 cm of sediment.

Volatilization of PCBs has been a minor loss mechanism. In the late-1970s, about 250 pounds of PCB_{3+} were volatilized annually from the Upper Hudson River. By the late-1980s this flux had declined to about 100 pounds. It increased in the early 1990s due to the higher water

column concentrations resulting from the Hudson Falls source. Since 1996, the annual flux has been about 50 pounds.

The sources and sinks of PCBs in the water column of the Upper Hudson River include upstream sources, resuspension, non-resuspension flux from sediment, settling, volatilization and advection to the Lower Hudson River. Their relative importance is indicated in Figure 4-55. Resuspension has typically been the largest source of PCB_{3+} to the water column, although its contribution varies greatly from year-to-year due to hydrologic variations. Non-resuspension flux from sediment (i.e., exchange with sediment) is also significant and the two sediment source pathways together exceed the advection in from upstream sources in all years except the early 1990s. Advection to the Lower Hudson River and settling have been the dominant loss mechanisms from the water column. These two mechanisms are of similar magnitude, with advection losses slightly higher than settling. Volatilization has been a minor sink.

Overall, the sources and sinks to the water column are highly correlated, as evidenced by comparison of the two panels of Figure 4-55. This correlation results from the interaction of the dissolved and particulate phases within the water column. The sources and sinks have been closely balanced and the net source or sink has been small. However, the absolute fluxes have been large. For example, in the late 1970s, 4,000 to 5,000 pounds of PCB_{3+} entered and left the water column each year. The flux declined over time to about 500 to 900 pounds in 1997 and 1998.

In contrast to the water column, the sources and sinks of PCB_{3+} in the modeled sediment have not been balanced (Figure 4-56). The sinks have outweighed the sources, accounting for the decline in concentration between 1977 and 1998. Settling provides the only significant source to the sediment. Burial, resuspension and non-resuspension flux to the water column are sinks. Of these, burial and resuspension have been of most importance. They are correlated because both are due to sediment transport processes. In the period from about 1978 to 1985, these processes were of similar magnitude. After 1985, resuspension began to become a more important loss mechanism. From 1992 to 1998, resuspension was about 2 times burial, with 300 to 700 pounds per year being resuspended and 100 to 400 pounds per year being buried. In

terms of net flux from the modeled sediment, the importance of burial is greater. For the 1994 to 1997 period, burial was of similar magnitude as net flux to the water column, which was between about 200 and 400 pounds. As discuss in Section 5 of Volume 1, the differences between net burial and net flux to the water derives from the different behaviors of cohesive versus non-cohesive sediments. All of the net burial of PCB_{3+} in the Upper Hudson River sediments is directly attributable to the burial of cohesive sediments. In contrast, the non-cohesive sediments account for almost all of the net flux of PCB_{3+} to the water.

4.6 MODEL SENSITIVITY AND UNCERTAINTY

The approach taken to reflect model uncertainty in future predictions was to develop a bounding calibration of the model, subject to two constraints: alternative values of key parameters were held within the uncertainty bounds defined by experimental and field evidence; and the bounding calibration reproduced the data, but with a lower estimate of concentration decline rate. The goal was to develop a minimum or lower bound estimate of natural recovery rate so that both best and bounding estimates of the time to recovery could be calculated.

The analysis proceeded in four steps. First, a subset of parameters was chosen for sensitivity analysis, based on the anticipation that reasonable alternative values of those parameters would impact key processes in the model. The key processes in the model include the burial rate, which determines the long-term recovery rate of the system, and the rate at which PCBs are transferred from the sediment to the water column, which determines both the release of PCBs to the water column as well as the recovery rate of the fish. Experience gained in the development of the model facilitated the choice the parameter subset for analysis.

Second, parameter ranges were established for the examination of model sensitivity based upon a combination of the available data and professional judgement.

Third, the sensitivity of the model to changes in these parameters was evaluated by examining changes in calculated TIP surface sediment (0-5 cm) PCB_{3+} concentrations and in the annual flux of PCBs past Waterford. These metrics were used because they have the most

relevance to the questions the model must answer. Surface sediments are the major PCB_{3+} source to the fish and the PCB_{3+} flux past Waterford defines PCB_{3+} loadings to the Lower Hudson River. The impacts of parameter variation were used to define a candidate parameter set that would yield the lower bound decline rate.

Fourth, a simulation was performed using the combined set of alternative parameter values. This simulation resulted in model calibration that reproduced the data and was accepted for use in model projections. This bounding model is viewed as a less likely representation of PCB fate because the parameters have been adjusted away from their maximum likelihood estimates.

Ten parameters were chosen for sensitivity examination because their values were poorly constrained by site data:

- magnitude of the 1977 to 1990 pulse loading,
- depth of particle mixing in cohesive sediment,
- depth of particle mixing in non-cohesive sediment,
- magnitude of particle mixing in cohesive sediment,
- magnitude of particle mixing in non-cohesive sediments,
- sediment partition coefficient,
- water column partition coefficient
- duration and extent of ice cover,
- sediment-water non-particulate mass transfer coefficient, and
- solids loading.

4.6.1 Magnitude of the 1977 to 1990 Pulse Loading

The historical water column sampling at Rogers Island clearly identified a component of the PCB_{3+} load entering the modeled portion of the Upper Hudson River from upstream that is associated with pulses. However, the magnitude of the pulse loading was not well specified by the data, with values ranging from about 20 lb/d to over 4,900 lb/d. The median of the observed

values (100 lb/d occurring at a frequency of 3 days per year) was used in the calibration. Excluding the value of 4,900 lb/d, the highest observed value occurred in 1984 and was about 200 lb/d (Figure 4-41). This value corresponds to the 90th percentile of the distribution of values (Figure 4-41). Based on the shape of the probability distribution (Figure 4-41), the 10th percentile value is less than 10 lb/d. On the basis of these data, sensitivity analyses were conducted with pulse loadings of zero and 600 lb/yr (200 lb/d for 3 days).

The results of the sensitivity analysis show that the magnitude of the pulse loading has a variable impact on surface sediment PCB_{3+} levels and the loading passing Waterford. The maximum impact on cohesive sediments occurs in the late 1980s (Figure 4-57a). The impact declines after 1990 to insignificant levels by 1998. Non-cohesive sediments exhibit similar behavior, although some impact does remain in 1998 (Figure 4-57b). The impact on loading past Waterford is relatively constant through the period of pulse loading, increasing or decreasing the loading by about 200 lb/yr (Figure 4-57c). The impact declines after 1990 and is insignificant by 1998.

The declining impact of pulse loading uncertainty after 1990 indicates that this uncertainty will not propagate into future predictions. For this reason, it will not be included in the future predictions.

4.6.2 Depth of Particle Mixing in the Sediment

The depth of particle mixing was bounded from the composition of the benthic community and the vertical concentration profiles of ^{7}Be and PCBs observed in high resolution sediment cores (Section 4.3.4). These data suggest that the depth of mixing in fine (cohesive) sediments exceeded 2 cm and could be as deep as about 10 cm. The value of 10 cm used in the calibration was determined by calibration. The depth of mixing in coarse (non-cohesive) sediments is also uncertain, although the nature of these sediments (lower organism density; presence of coarse sands and gravel) probably precludes significant mixing to depths greater than a few centimeters. The sensitivity of the model to sediment mixing-depth was examined using values of 5 and 15 cm in cohesive sediments and 2 cm in non-cohesive sediments.

The PCB_{3+} concentration trend in cohesive surface (0-5 cm) sediments is inversely related to the depth of particle mixing (Figure 4-58a). Halving the depth of mixing (i.e., 10 cm → 5 cm) increases the rate of PCB decline such that predicted concentrations in 1991 and 1998 are significantly lower than the mean observed values. Increasing the depth of mixing by 50% (i.e., 10 cm → 15 cm) decreases the rate of decline, resulting in predicted concentrations in 1991 and 1998 that are slightly closer to the mean observed values than in the calibration. The relationship between the concentration trend and the depth of mixing is non-linear; the model is more sensitive to a reduction in mixing depth than to an increase in mixing depth. This is due to the log-linear relationship between the volume of the surface mixed layer and the rate of dilution with less contaminated solids entering from the water column. PCB_{3+} concentration in the non-cohesive sediments is insensitive to mixing depth in the cohesive sediments (Figure 4-58b). The PCB load passing Waterford is impacted only slightly by changes in the mixing depth (Figure 4-58c).

The relationship of PCB_{3+} concentration trend and mixing depth in non-cohesive sediments is opposite that in cohesive sediments. Decreasing the mixing depth decreases the rate of concentration decline (Figure 4-59b). The difference in behavior between the sediment types is a consequence of differences in controlling mechanisms. The trend in cohesive sediments is controlled by burial. Reducing mixing depth increases the rate of dilution within the surface mixed layer. The trend in non-cohesive sediments is controlled by resuspension and non-resuspension mass transfer to the water column. Reducing mixing depth decreases the rate of PCB migration to the sediment surface. The reduction of 33% (i.e., 3 cm → 2 cm) results in a favorable comparison to the 1991 mean observed PCB_{3+} concentration, but an over-estimation of the 1998 mean. It has no significant impact on cohesive sediments (Figure 4-59a) or on the loading passing Waterford (Figure 4-59c).

4.6.3 Magnitude of Particle Mixing in the Sediment

The magnitude of particle mixing was a calibration parameter. The mixing coefficient in cohesive sediments was set at 10^{-7} cm^2/s to produce a vertical concentration gradient over the top

5 cm of about a factor of two. The same value was used in non-cohesive sediments even though the mechanisms responsible for mixing may differ between the sediments. To reflect the paucity of independent data for quantifying the particle mixing coefficient, the sensitivity analysis examined factor of ten changes in the mixing coefficients.

The intensity of particle mixing in cohesive sediments principally impacts the computed cohesive surface (0-5 cm) sediment concentrations early in the calibration period (Figure 4-60a). The higher intensity of mixing brings the more highly contaminated sediments at depth into the surface sediment, resulting in significantly higher concentrations from about 1979 to 1983. Because the vertical concentration gradients evident in the 1977 sediment data are not preserved and the concentration profile becomes essentially uniform (results not shown), the higher intensity is considered to be unrealistic. The lower intensity of mixing results in slightly lower concentrations in the surface sediments. By about 1991, the concentration in surface sediment is relatively insensitive to the mixing intensity. This occurs because burial has removed the historical high concentration sediments from the mixed layer and the vertical concentration gradients are small. The mixing intensity does have some impact on the PCB_{3+} load passing Waterford (Figure 4-60c). The loading is positively related to the mixing intensity because the PCB_{3+} concentration in the 0-1 cm layer is directly related to the mixing intensity. The loading changes are relatively small in the 1990s, varying by about 15% for a factor of ten change in mixing intensity.

The non-cohesive sediment particle mixing intensity affects the concentration trend in these sediments differently than the cohesive sediment particle mixing intensity affects the concentration trend in those sediments. Increasing the mixing intensity increases the rate at which PCB_{3+} concentration declines (Figure 4-61b). This difference occurs for the same reason that the depth of mixing had opposite effects on the two sediments: the fate of the surface sediment PCBs is controlled by burial in cohesive sediments and flux to the water column in non-cohesive sediments. The lower mixing (i.e., 10^{-8} cm^2/s) results in a predicted 1998 concentration that over-predicts the mean observed concentration. The higher mixing (i.e., 10^{-6} cm/s) results in a minor reduction in concentration that has little impact on the comparison to data. The PCB_{3+} load passing Waterford is only slightly affected by the non-cohesive sediment

mixing intensity (Figure 4-61c). This is due to the compensation between the decline rate in the 0-5 cm layer and the concentration in the 0-1 cm layer. Lower mixing results in higher concentration in the 0-5 cm layer, but also a larger concentration gradient over this layer.

4.6.4 Sediment Partition Coefficient

The data used to establish a partition coefficient for the sediments were noisy (see Section 4.3.5). The assigned partition coefficient equaled that of the water column because some of the sediment data were consistent with such an assumption. However, a few of the data points suggested a lower value and a much higher value was indicated for heavily dechlorinated sediments. The importance of this uncertainty was evaluated by examining the impact of changing the K_{oc} value from $10^{5.6}$ to $10^{5.1}$ or $10^{6.1}$. These changes are equivalent to varying the pore water PCB_{3+} concentration over one order of magnitude.

The results of the analysis indicate that the model is insensitive to sediment partition coefficient uncertainty (Figure 4-62). The variation of the partition coefficient impacts only the vertical migration of PCBs within the sediment due to diffusion. The non-resuspension flux of PCBs between the sediment and the water column is independent of partition coefficient variation because it was established on the basis of sediment PCB_{3+} concentration, not pore water concentration (see Section 4.3.5). Diffusive transport of PCBs within the sediment is slow, on the order of millimeters per year or less. As such, it contributes little to the overall mass balance and even order of magnitude changes have little affect on overall PCB_{3+} fate.

4.6.5 Water Column Partition Coefficient

The uncertainty of the water column partition coefficient is due to uncertainty in both the organic carbon content (f_{oc}) of the TSS and the organic carbon based partition coefficient (K_{oc}). The mean f_{oc} values have small uncertainty because of the large data sets. For example, the low flow f_{oc} data at Waterford have a ratio of standard error to mean of about 0.01. Given this, the uncertainty of the water column partition coefficient was defined by the 95% confidence limits

of K_{oc} at a temperature of 20° C: $10^{5.47}$ to $10^{5.74}$. Using these values had little impact on the model results. Cohesive and non-cohesive surface sediment PCB_{3+} concentrations were directly related to the partition coefficient value because of the proportionality between PCB_{3+} concentration on depositing particles and the partition coefficient (Figure 4-xxa & b). However, the changes were small and did not impact the calibration.

The changes in partition coefficient had the opposite effect in the water column. Increasing the partition coefficient decreased the PCB_{3+} load passing Waterford because of the greater loss from the water column due to deposition. Again, the effect was minor.

4.6.6 Duration and Extent of Ice Cover

The surface of the Upper Hudson River freezes each winter. The duration and extent of ice cover were established on the basis of air temperature data and anecdotal information. The assumption of a three-month duration and 80% coverage is probably an upper end estimate, particularly for recent years where atmospheric temperatures have exceeded long-term averages. For this reason, the sensitivity to ice cover was examined by comparing the calibration to a model in which ice cover is assumed not to exist.

Changing the ice cover assumption had no observable effect on the model (Figure 4-64). This lack of sensitivity is due to the small overall contribution of volatilization to the PCB_{3+} mass balance and the fact that volatilization is minimum in the winter due to temperature effects on Henry's Constant and the water phase mass transfer coefficient.

4.6.7 Sediment-Water Non-Particulate Mass Transfer Coefficient

The mass transfer coefficient defining the rate at which PCBs move between the surface sediment and the water column *via* mechanisms other than resuspension (k_f)was empirically defined. Because the data were noisy and impact by non-detect measurements, the coefficient is somewhat uncertain. This uncertainty was quantified by visual estimation of lower and upper

bound relationships between the coefficient and time of year (Figure 4-65). The bounding relationships yielded little change in cohesive surface sediment PCBs (Figure 4-65a). This insensitivity is due to the relative insignificance of non-particulate transfer to the water column as a loss mechanism in comparison to burial. The non-cohesive surface sediment PCB_{3+} concentration exhibited greater sensitivity (Figure 4-65b) because flux to the water column is the dominant loss mechanism from these sediments. The lower bound relationship resulted in predicted 1998 concentrations that were not consistent with the data.

The PCB load passing Waterford was not significantly affected by the changes in k_f. This is due to the fact that these changes are offset by changes in resuspension flux to the water column. For example, if k_f is reduced the non-particulate flux to the water column decreases, but the surface sediment PCB_{3+} concentration increases, and therefore the resuspension flux increases.

4.6.8 Solids Loading

The uncertainty in solids loading resulting from the variability of the data used to establish tributary rating curves is discussed in Section 3.4. This uncertainty did not degrade the sediment transport calibration. Its impact on the PCB_{3+} fate calibration was examined by altering the TSS, and deposition and resuspension fluxes in the PCB_{3+} model to those calculated by the sediment transport model under the altered solids loading.

The uncertainty in solids loading has little effect on the PCB_{3+} calibration (Figure 4-66). Higher solids loading results is slightly lower sediment PCB_{3+} concentrations, while lower solids loading results in slightly higher sediment PCB_{3+} concentrations. The impact on PCB_{3+} flux passing Waterford is insignificant. Thus, this uncertainty is within the bounds of a reasonable calibration.

4.6.9 Development of a Bounding Calibration

The sensitivity analysis indicates that variations in the tested parameters alter the principal results of the model: the rates at which PCB_{3+} concentrations decline in surface sediments and the magnitude of the PCB_{3+} loading passing Waterford. Variations in the sediment partition coefficient, the duration and extent of ice cover and the depth of particle mixing in cohesive sediments have negligible effects on these rates and are not likely to affect future projections. Although uncertainty in the magnitude of the 1977 to 1990 pulse loading does impact these rates, the impact declines quickly through the 1990s and it will also not cause significant uncertainty in future projections. In contrast, uncertainties in the depths and magnitudes of particle mixing in cohesive and non-cohesive sediments, the water column partition coefficient, the sediment-water non-particulate mass transfer coefficient and solids loading all impact the model. However, in all cases these impacts do not alter the principal fate pathways. Rather, they have minor effects on the rates at which PCB_{3+} concentration declines. The absence of major effects is attributable to the small uncertainty ranges for some of the parameters (e.g., solids loading and water column partition coefficient) and the dominant role of sediment transport processes in controlling PCB fate.

On the basis of the sensitivity analysis, a bounding parameter set was chosen so that the rate of decline would be reduced relative to the base calibration, but would still reproduce the major features of the observed data. Three parameters were altered. The water column partition coefficient was set to the upper 95% confidence limit of the mean, the solids loading was set at the lower bound estimate from the solids rating curve and the depth of particle mixing in cohesive sediments was set at 15 cm. These values differ from the best estimates for the parameters and the resulting calibration is considered to be a less likely model of PCB fate.

The bounding model accurately reproduces the changes in average 0-5 cm cohesive and non-cohesive sediment PCB_{3+} concentrations observed in the TIP (Figure 4-67). The rates of decline between 1977 and 1998 are slightly lower than predicted by the base model. In addition, the bounding model predicts slightly higher water column PCB_{3+} concentrations (Figure 4-68). Thus, the bounding model will predict a slightly lower recovery rate into the future.

4.7 IMPACTS OF RARE FLOOD EVENT

The effect of a 100-year flood on Hudson River PCB_{3+} fate was assessed using the calibrated PCB_{3+} fate model. The results of the hydrodynamic and sediment transport model were used to determine flows, volumes, depths, deposition rates, and resuspension rates in the same manner used for the long-term calibration. The flood was assumed to occur immediately after the calibration (3/23/98) and the river PCB_{3+} levels at the end of calibration were used as the initial conditions for the flood. All model parameters were as determined by calibration.

During the 8-day flood period, the model predicts that 411 lbs of PCB_{3+} would be eroded from Upper Hudson River sediments. Of the eroded mass, 289 lbs (70%) are transported to the lower river and 122 lbs (30%) are redistributed within the riverbed. The calculated PCB_{3+} mass eroded from the TIP is 161 lbs. Of the 161 lbs of PCB_{3+} eroded, 6 lbs settle back in the TIP, 31 lbs settle back in reaches 1-7, and 124 lbs are transported to the lower river. Sediment-water diffusive exchange is small (2 lbs) and volatilization losses are negligible. TIP sediments account for 43% of the 289 lbs of PCB_{3+} transported to the lower river.

The 1997 EPA DEIR estimated 1984 TIP PCB_{3+} inventory. The lowest estimate of total PCB_{3+} mass in the TIP was 14.5 MT. Assuming comparable PCB_{3+} mass inventories in 1998, the 100-year flood would only erode about 0.5% of the total TIP PCB_{3+}, and about 0.4% would be transported to the lower river.

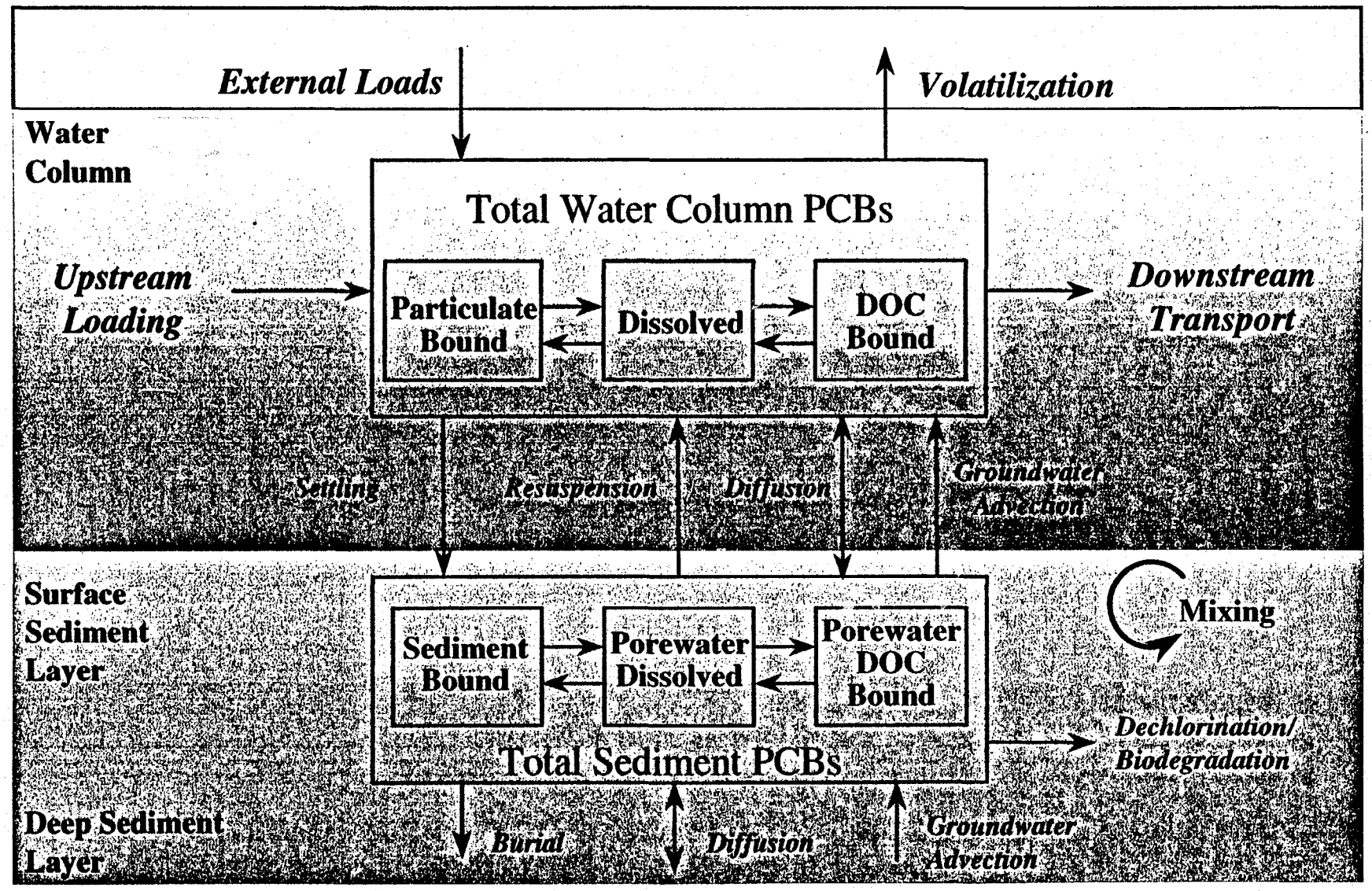

Figure 4-1. Conceptual model of PCB dynamics within the Upper Hudson River.

\\Poseidon\D_drive\Genhud\Documents\Model_report\Vol_2\Section_4\fig4_1.ppt

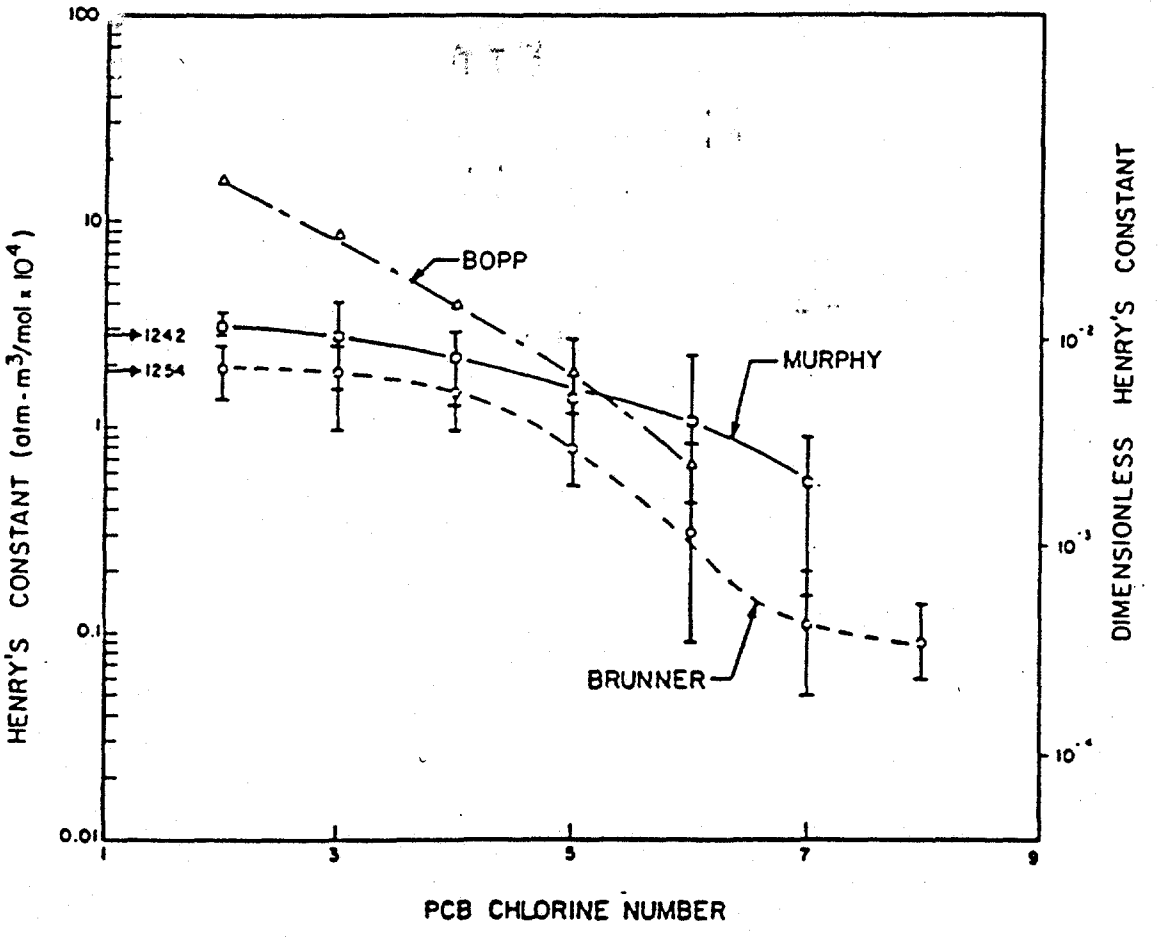

Figure 4-2. Henry's constants for PCBs in relation to chlorine number. Labels indicate references cited in report text.

313926

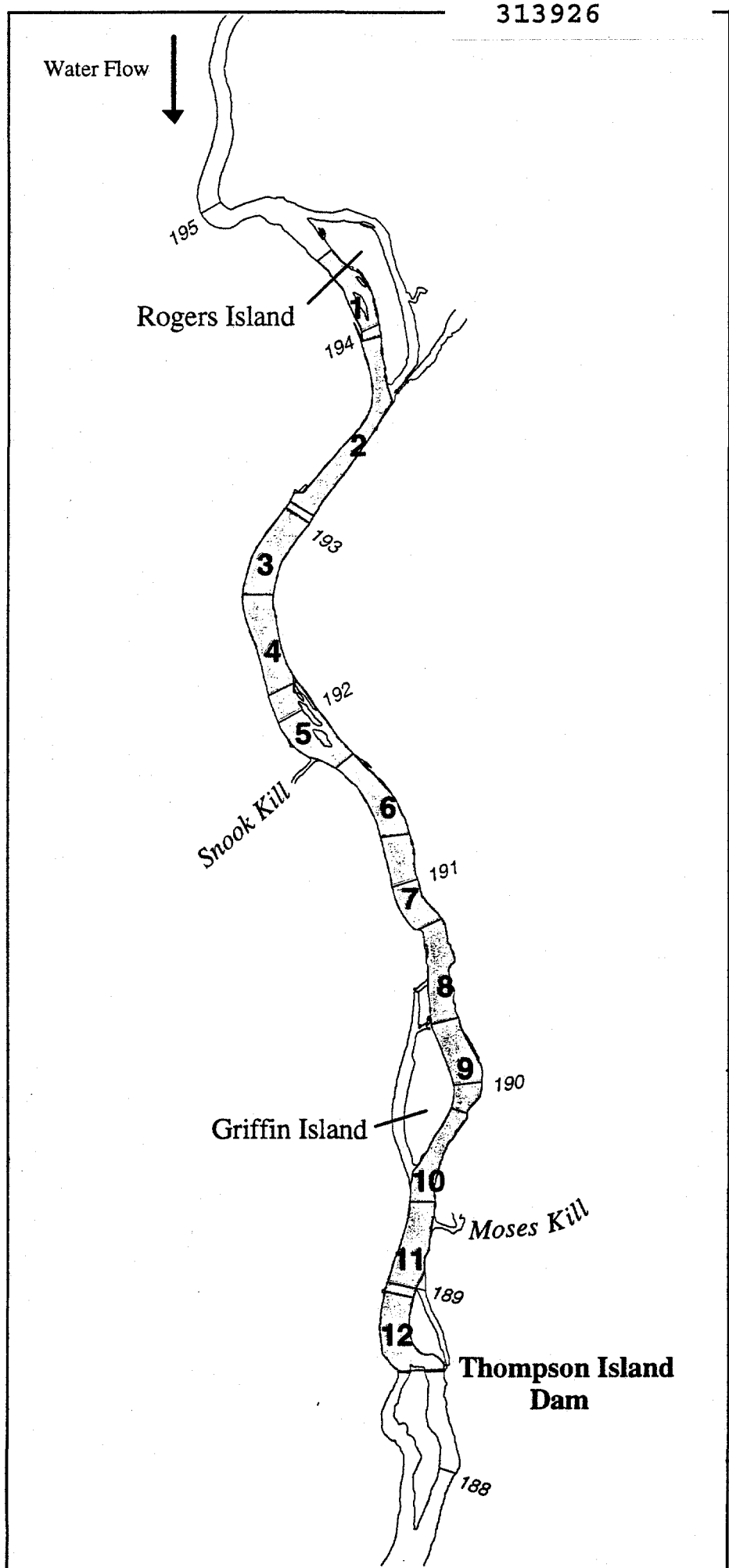

LOCATION MAP OF THE HUDSON RIVER

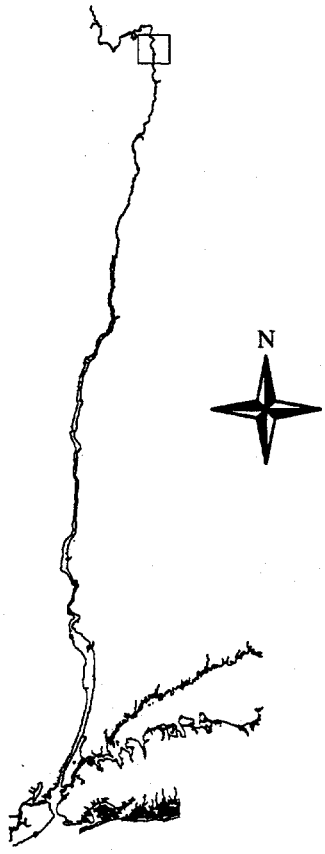

GRAPHIC SCALE

0.4 0 0.4 0.8 Miles

LEGEND

Mile Point above Battery
Water Quality Segments

GENERAL ELECTRIC COMPANY
Hudson River Project

PCBs in the Upper Hudson River
Volume 2. A Model of PCB Fate, Transport, and Bioaccumulation

Figure 4-3.

Fate and Transport Water Quality Segmentation for Thompson Island Pool.

QEA
Quantitative Environmental Analysis, LLC

Project: GENhud 131 April 1999

\\Poseidon\D_drive\Genhud\Documents\Final_report\TIPwqseg_Fig4_3.apr

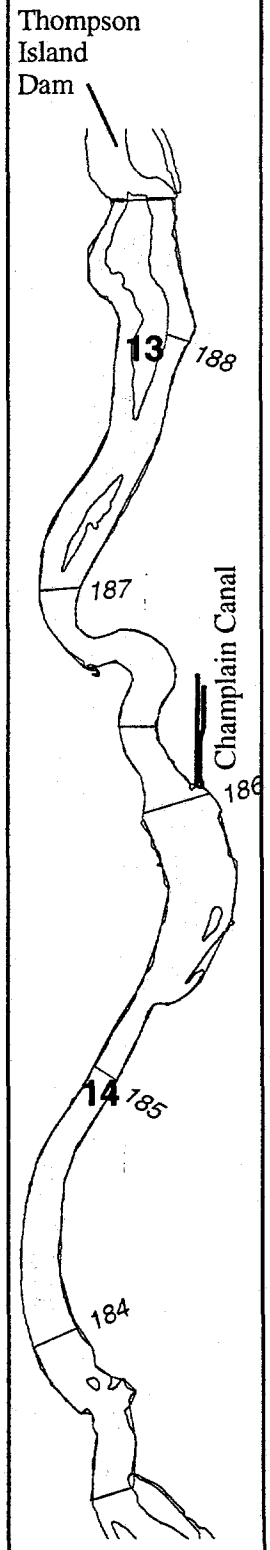

Reach 6-7

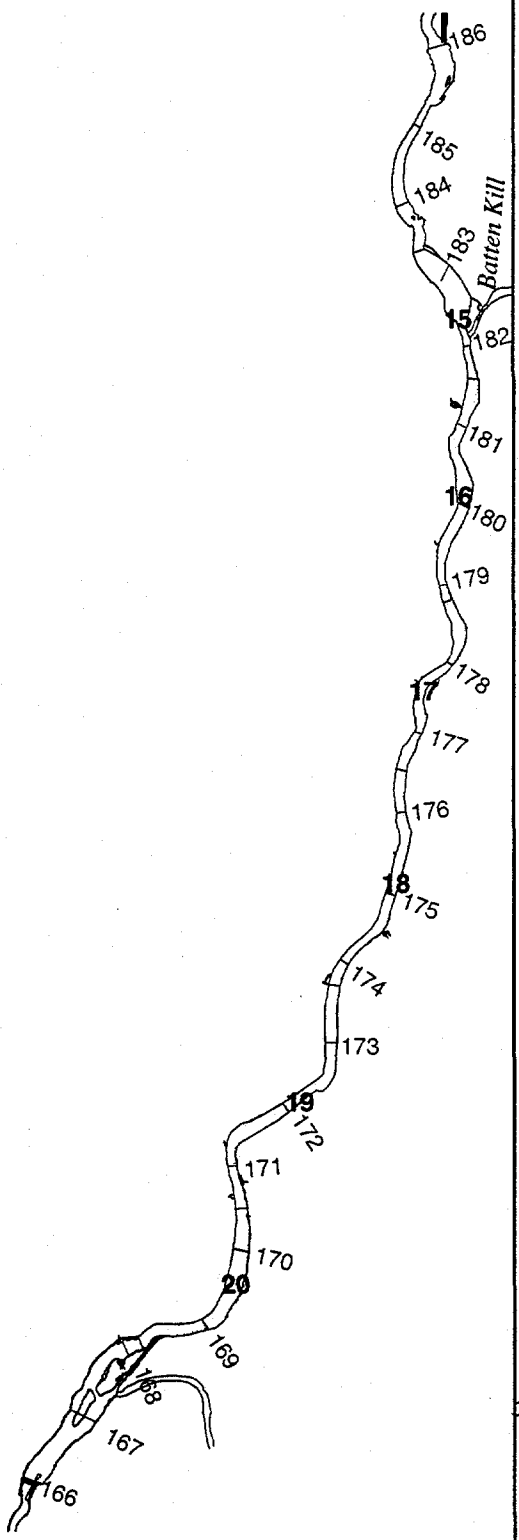

Reach 5

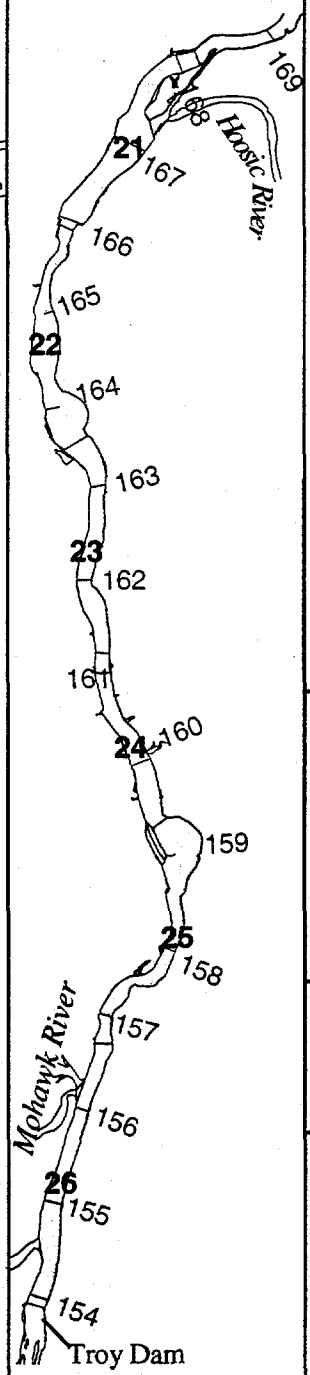

Reach 1-4

LOCATION MAP OF THE HUDSON RIVER

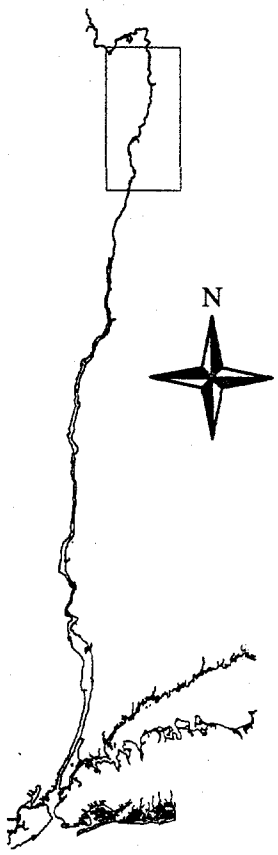

GRAPHIC SCALE

Reach 6-7

0.2 0 0.2 0.4 Miles

Reach 1-5

0.6 0 0.6 1.2 Miles

LEGEND

Mile Point above Battery
Water Quality Segments

GENERAL ELECTRIC COMPANY
Hudson River Project

PCBs in the Upper Hudson River
Volume 2. A Model of PCB Fate,
Transport, and Bioaccumulation

Figure 4-4.

Fate and Transport Water Quality Segmentation for Reaches 1-7 of the Upper Hudson River.

QEA
Quantitative Environmental Analysis, LLC

Project: GENhud 131 April 1999

\\Poseidon\D_drive\Genhud\Documents\Final_report\Vol_2\Section_4\Reach1_7_Fig4_4.apr

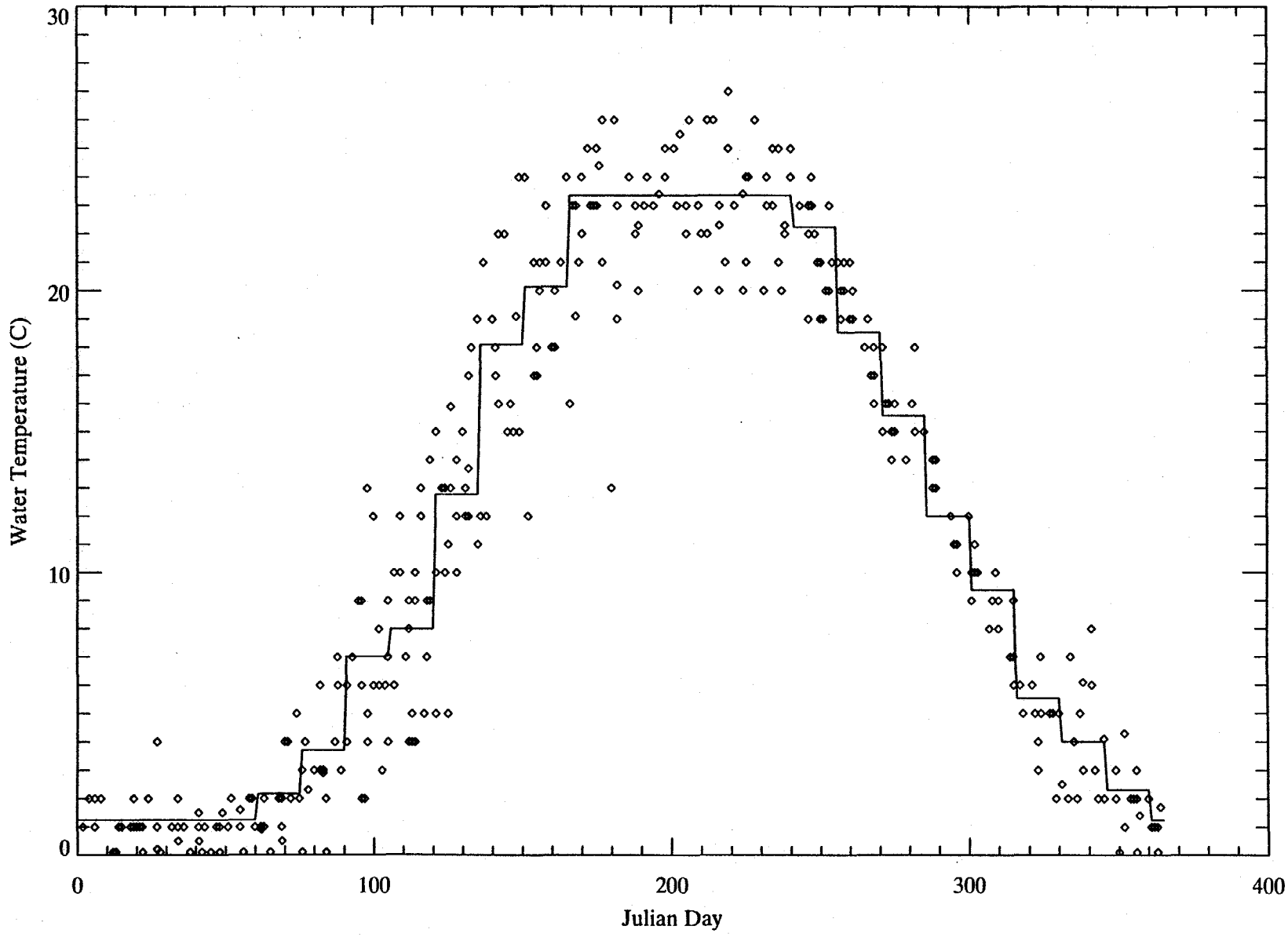

Figure 4-5. Comparison of observed annual water temperature (symbols) cycle at Thompson Island Dam with functional representation used in the model (line).

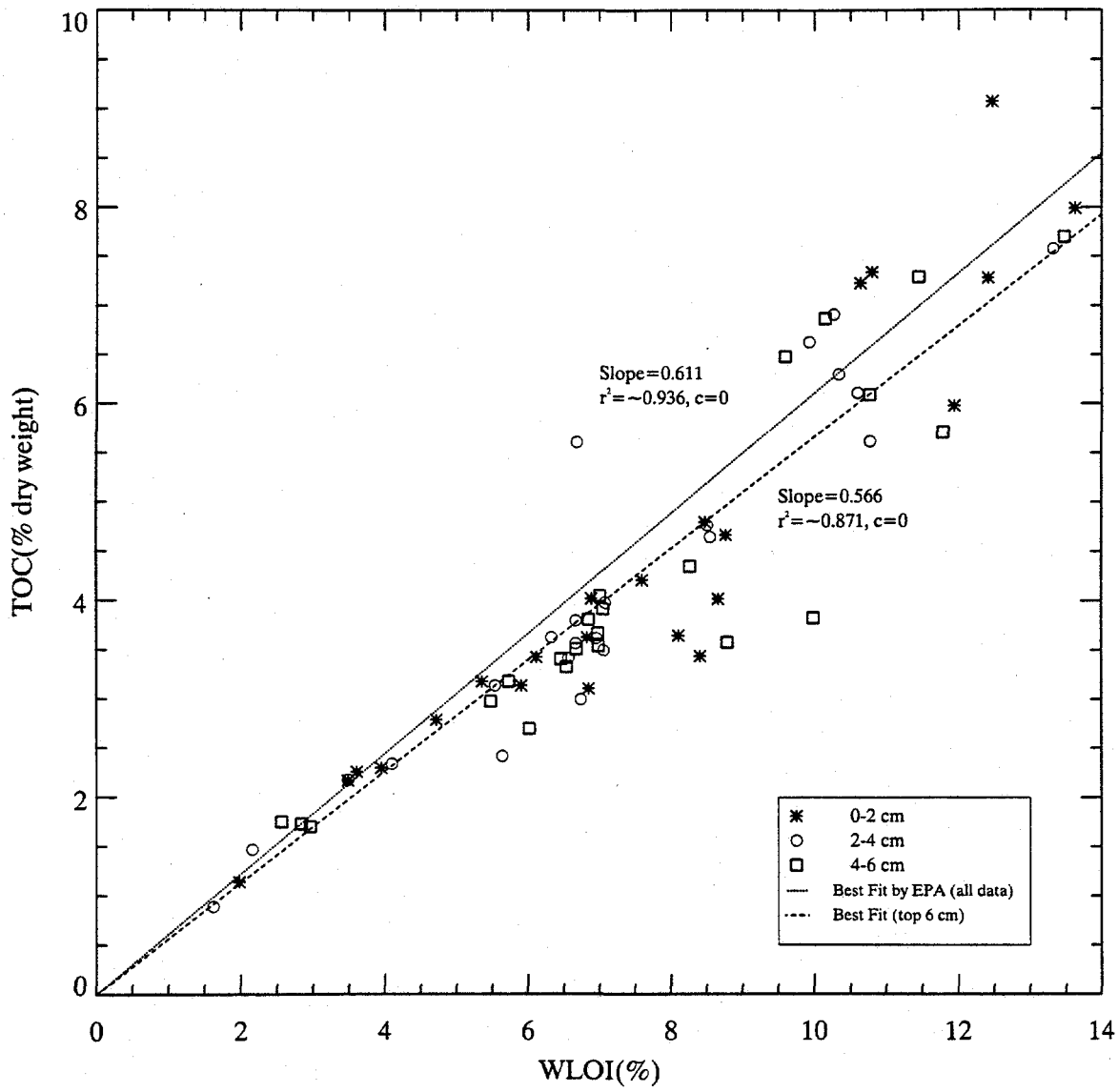

Figure 4-6. Relationship between weight loss on ignition and sediment TOC for EPA High Resolution core samples.

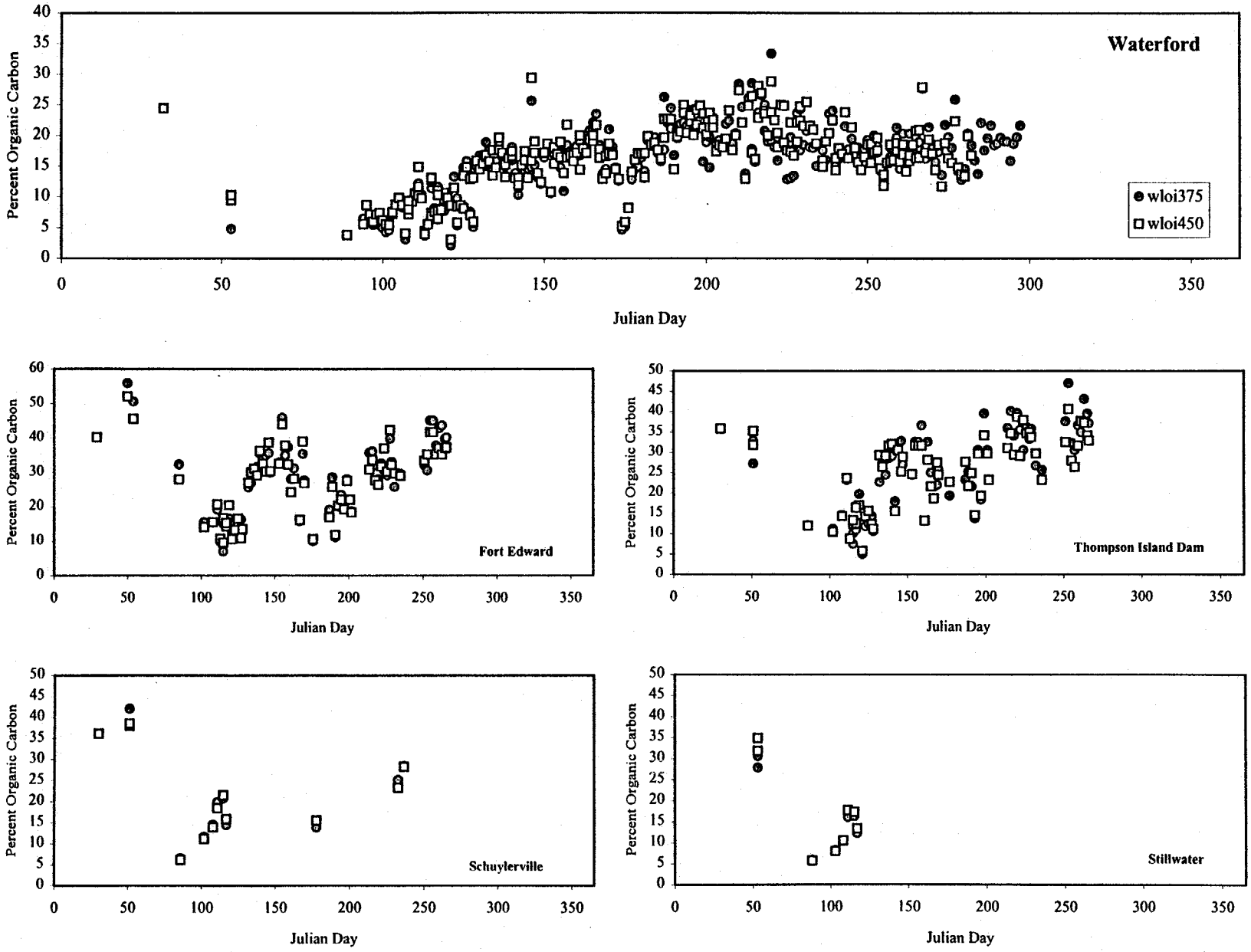

Figure 4-7. Temporal profile of percent organic carbon of water column TSS for 1993 USEPA Phase 2 surveys.

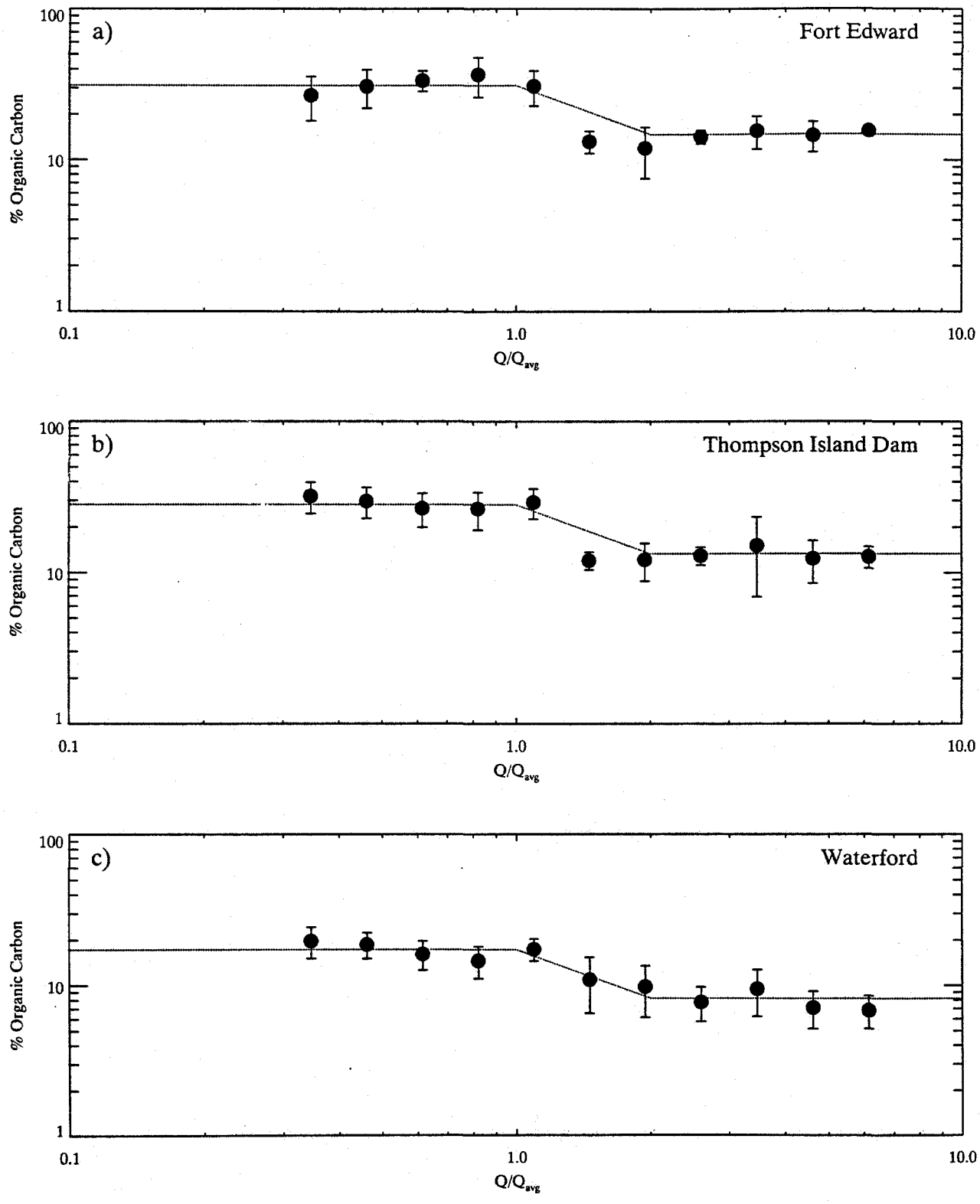

Figure 4-8. USEPA Phase 2 suspended solids organic carbon content versus normalized daily average USGS flow at Waterford. Symbols represent binned averages based on WLOI data (+/- 2 standard errors) and lines represent functional relationships used in model.

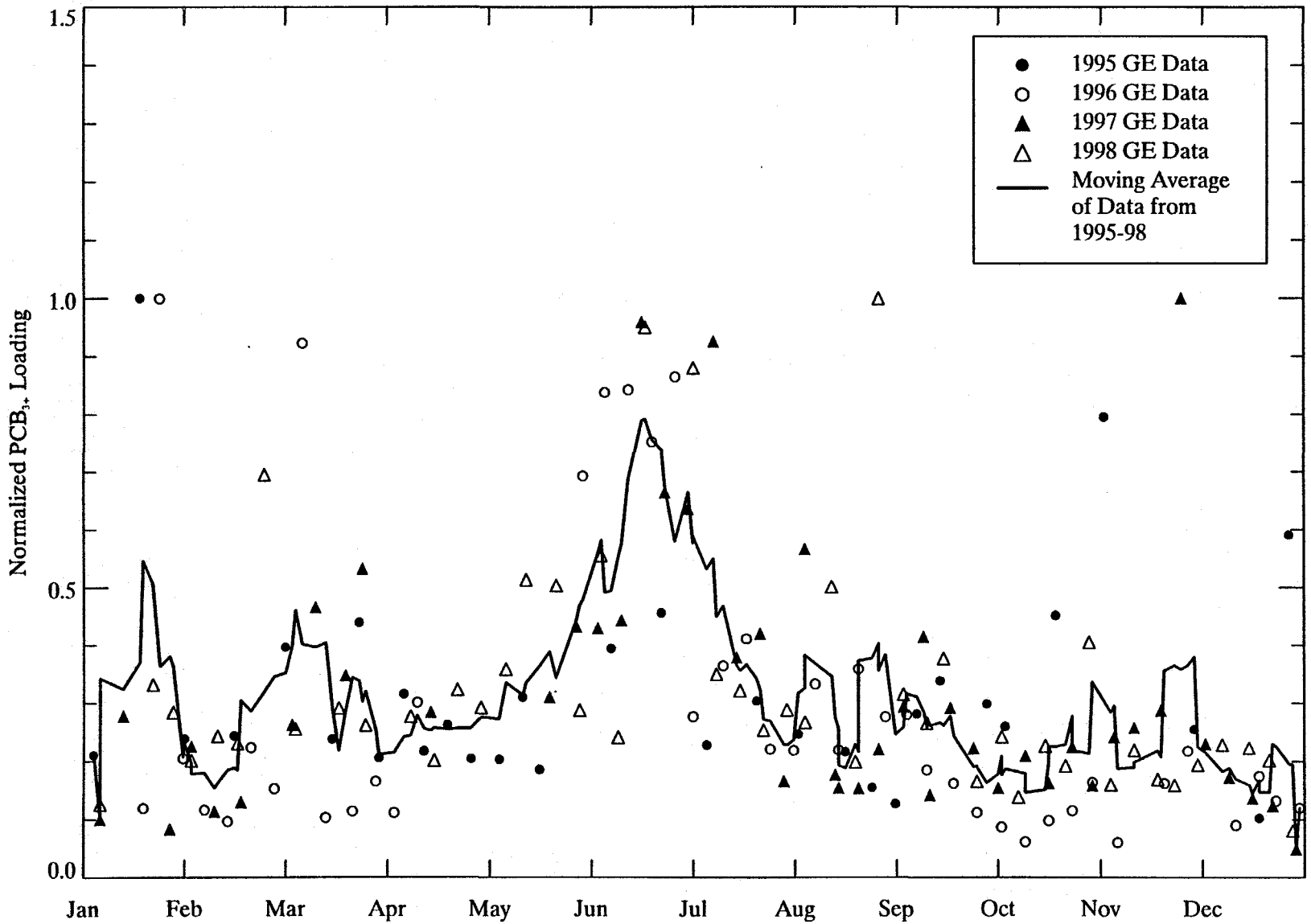

Notes: Loading normalized to the highest observed for a single calendar year. Low flow defined as less than 10,000 cfs at Fort Edward.

Figure 4-9. Seasonal trends in low flow PCB_{3+} loading observed at Thompson Island Dam.

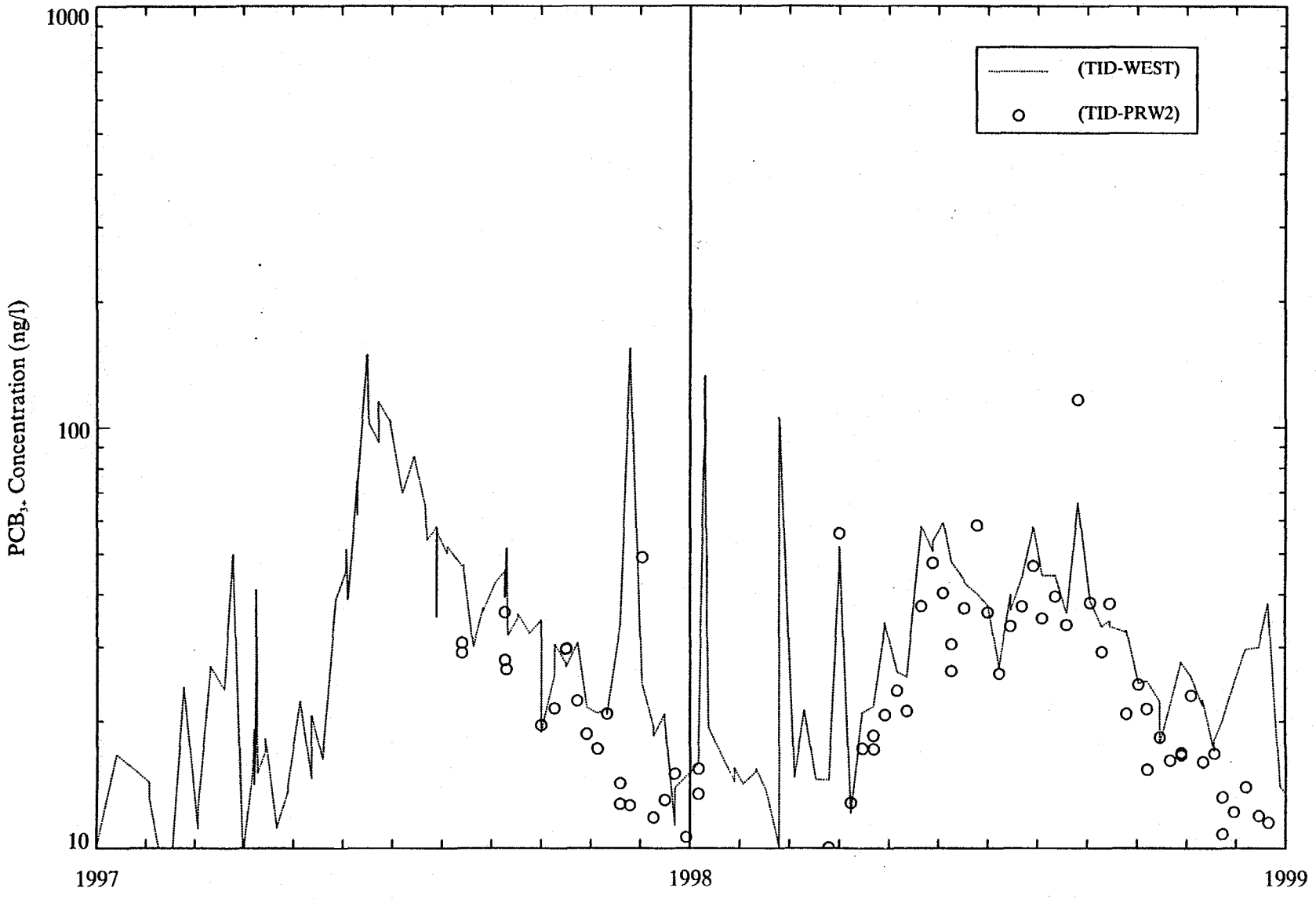

Figure 4-10. PCB_{3+} concentrations observed at biased (TID-WEST) and unbiased (TID-PRW2) sampling stations located near the Thompson Island Dam.

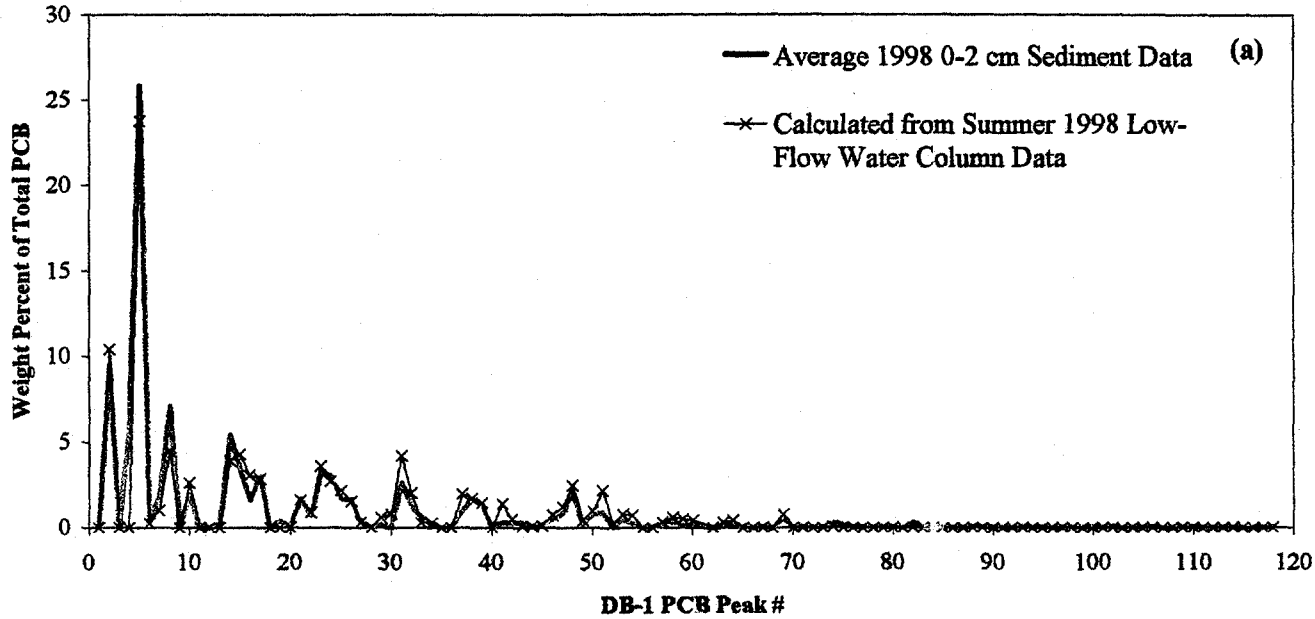

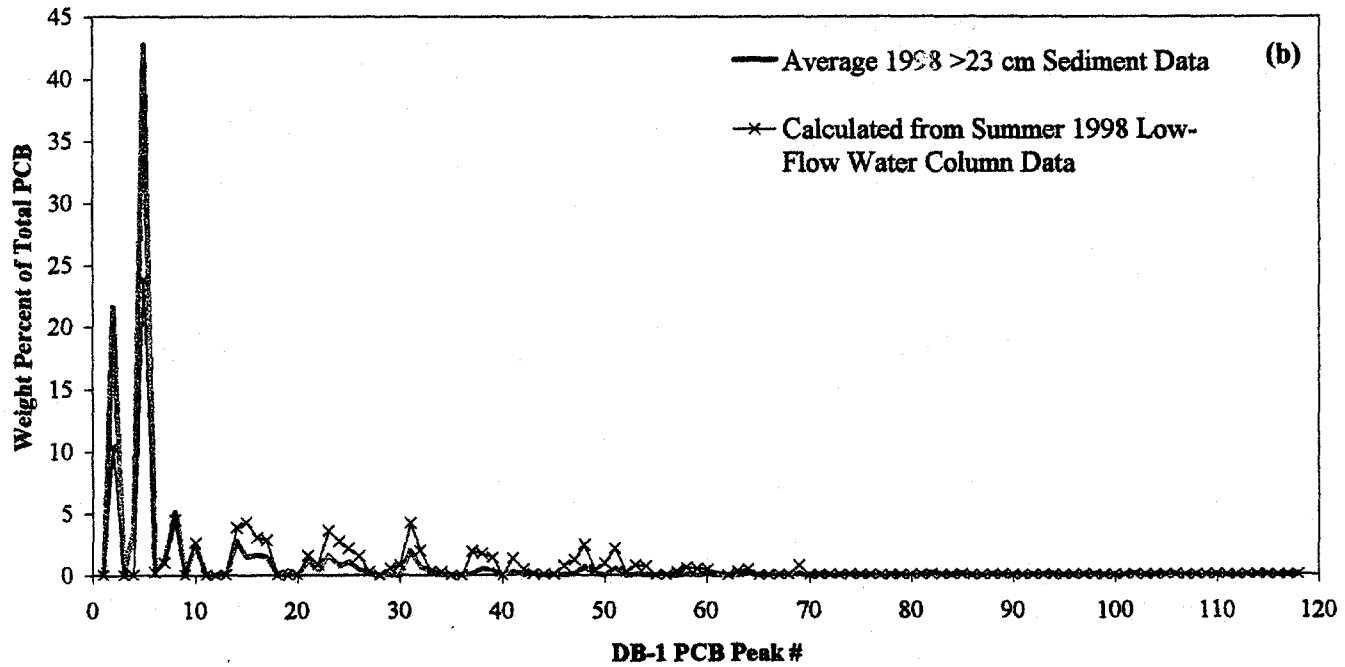

Notes: DB-1 Peaks are groupings of 1-3 PCB congeners, with chlorine level generally increasing with increasing DB-1 Peak #. Sediment data with concentrations less than 5 ppm were excluded from the > 23 cm average.

Figure 4-11. Comparison of the PCB congener composition of the particulate phase sediment source required to produce observed water column PCB loadings across the TIP with (a) surface sediment (0-2 cm) and (b) deep sediment (>23 cm) PCB congener composition.

mjw - v1fig4-11_wscomp.xls - low flow - cong
4/15/99 - 2:50 AM

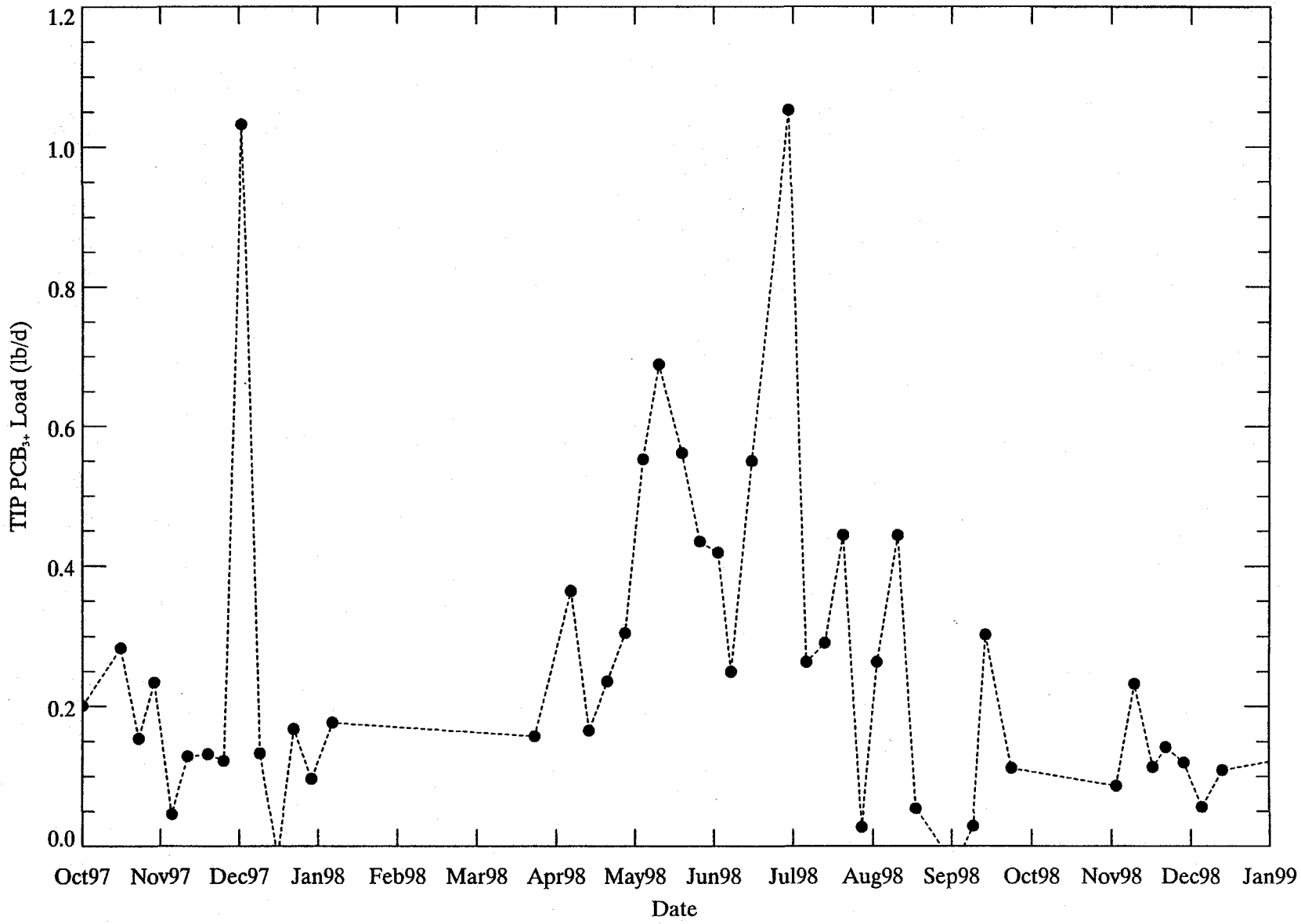

Notes: TIP loading is calculated as the difference between the loadings at Fort Edward and Thompson Island Dam. Low flow (< 10,000 cfs) data only. August, 1998 outlier removed (~3 lb/day).

Figure 4-12. Seasonal trends in PCB_{3+} loading for the Thompson Island Pool region of the Upper Hudson River.

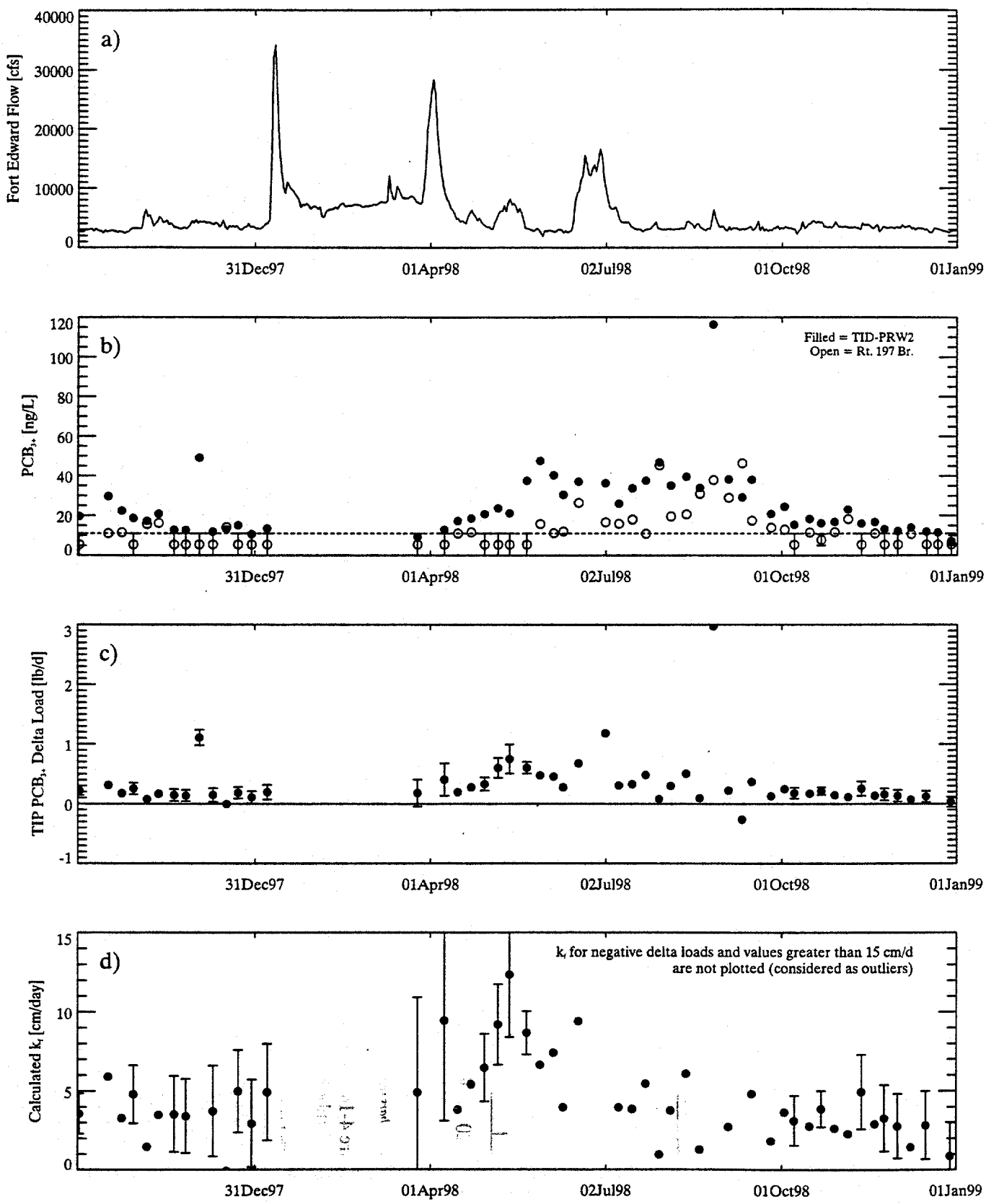

*Note: Error bars represent alternative values for non-detects at Fort Edward ranging from 0 to MDL of 11 ng/L. TID Flow = FE Flow * 1.067*

Figure 4-13. Temporal patterns in a) Hudson River flow at Fort Edward, b) water column PCB_{3+} concentration, c) PCB_{3+} loading increase across TIP, and d) calculated TIP sediment-water exchange coefficients.

ktr - H:\GENhud\analysis\sediment\diffflux\congflux\loaddiff\kf_calc\error_kfcalc98.pro
Thu Apr 15 03:00:21 1999

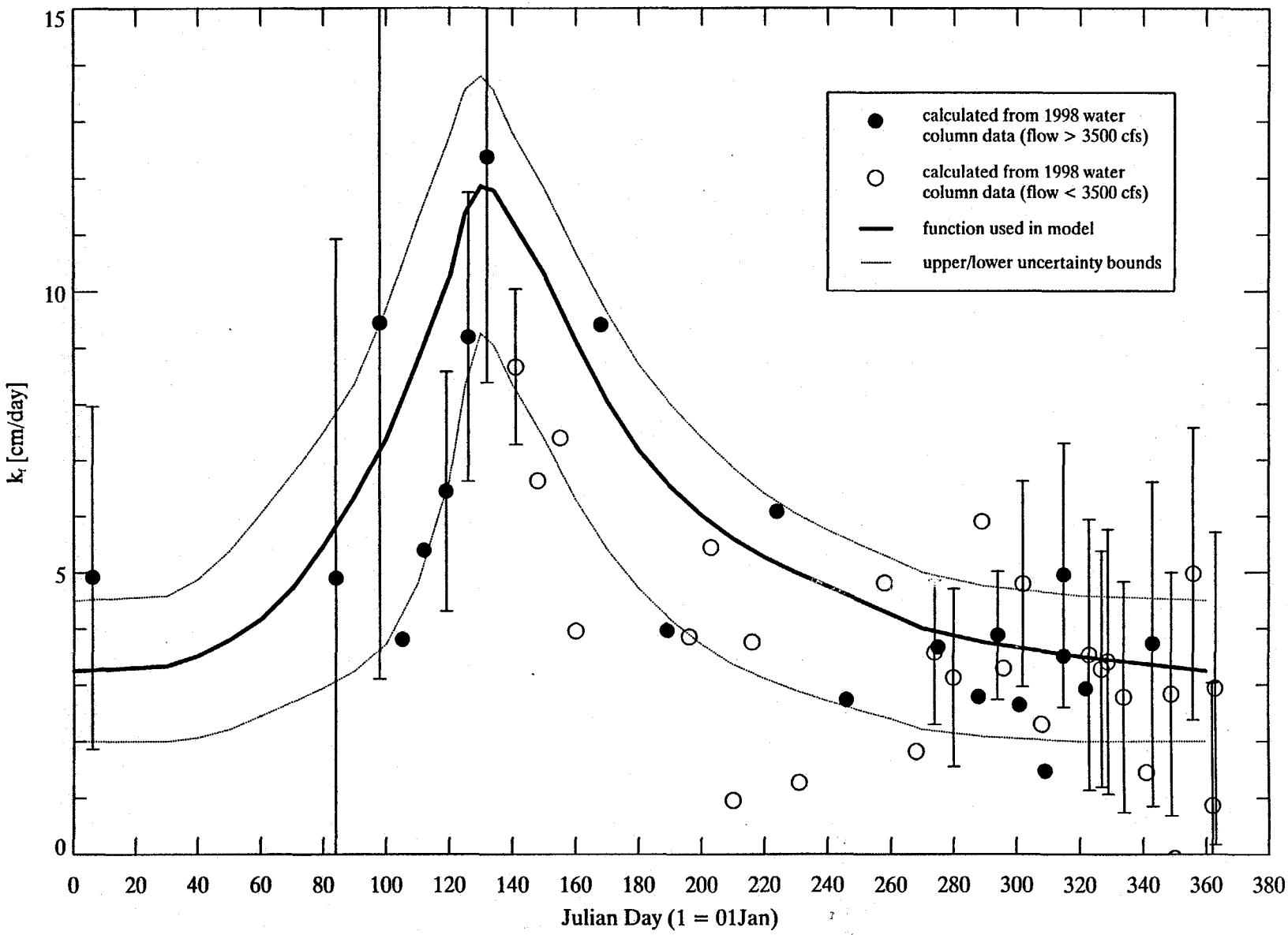

Note: Error bars represent alternative values for non-detects at Fort Edward ranging from 0 to MDL of 11 ng/L

Figure 4-14. Comparison of low flow (<10,000 cfs) sediment-water column PCB_{3+} mass transfer coefficient calculated from data (symbols) and functional relationship used in the model (solid line).

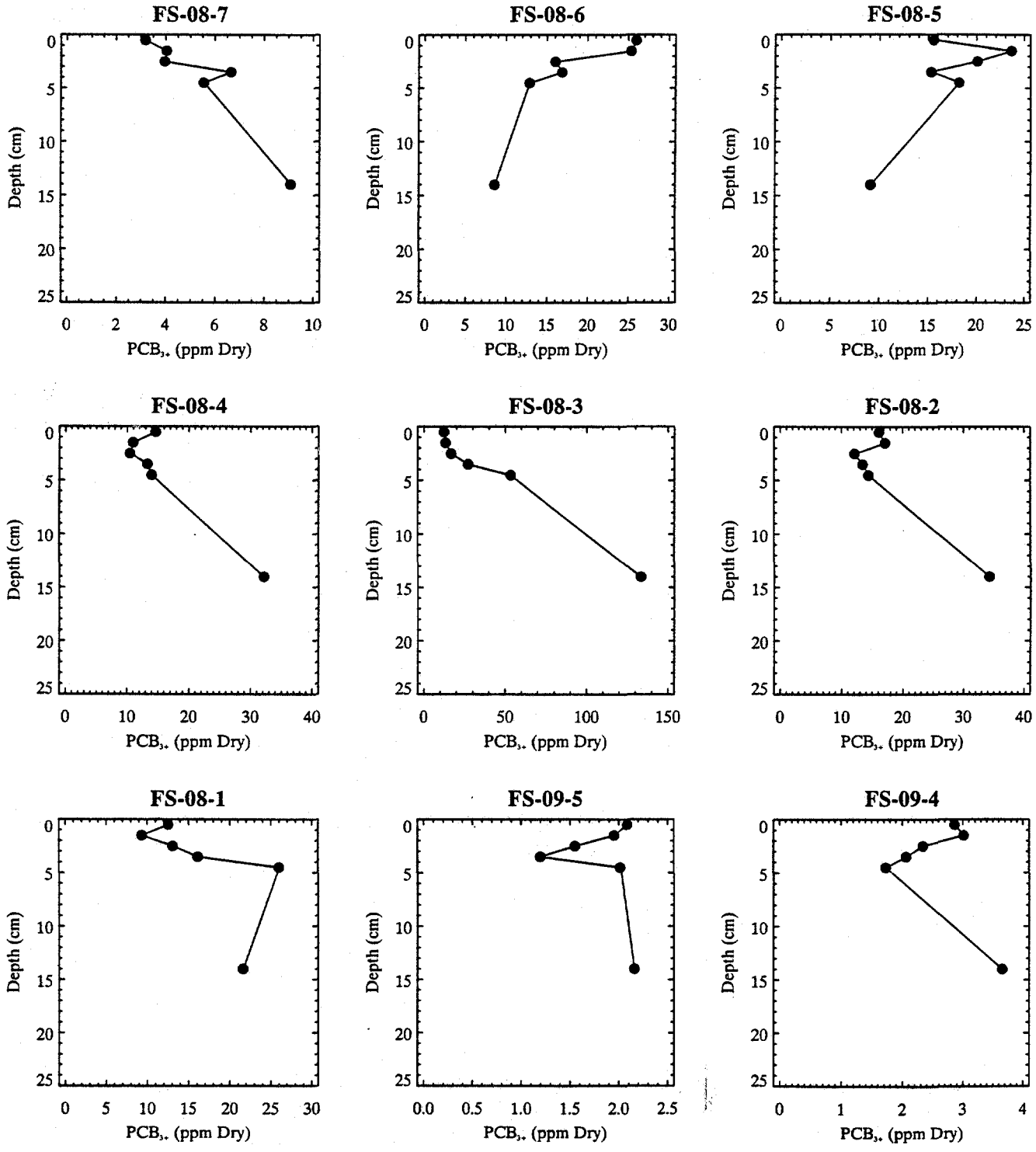

Note: Core sections shown are the top 23 cm of each core, plotted at segment midpoint.

Figure 4-15a. Vertical profiles of PCB_{3+} within finely segmented sediment cores collected from the Upper Hudson River.

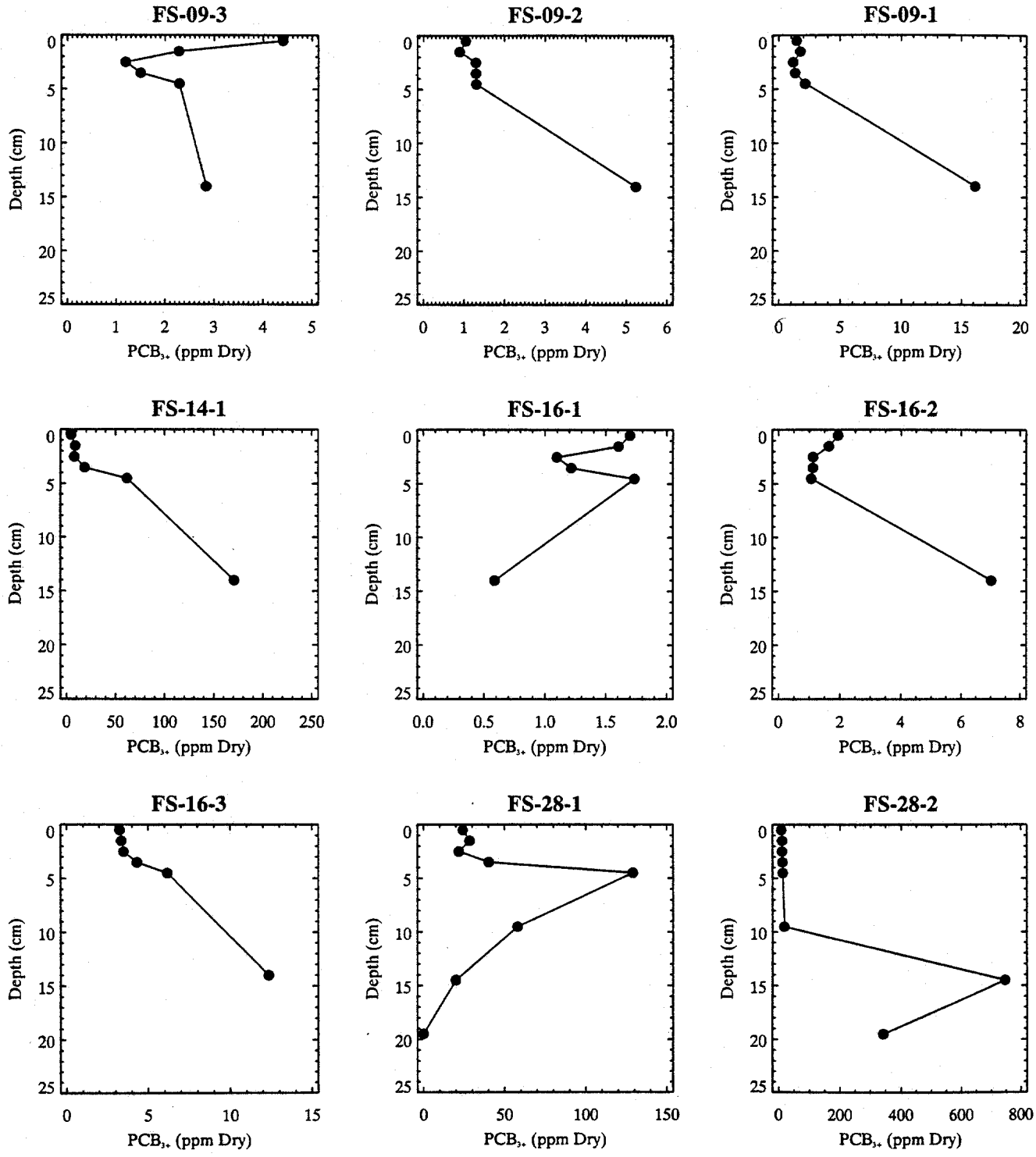

Note: Core sections shown are the top 23 cm of each core, plotted at segment midpoint.

Figure 4-15b. Vertical profiles of PCB_{3+} within finely segmented sediment cores collected from the Upper Hudson River.

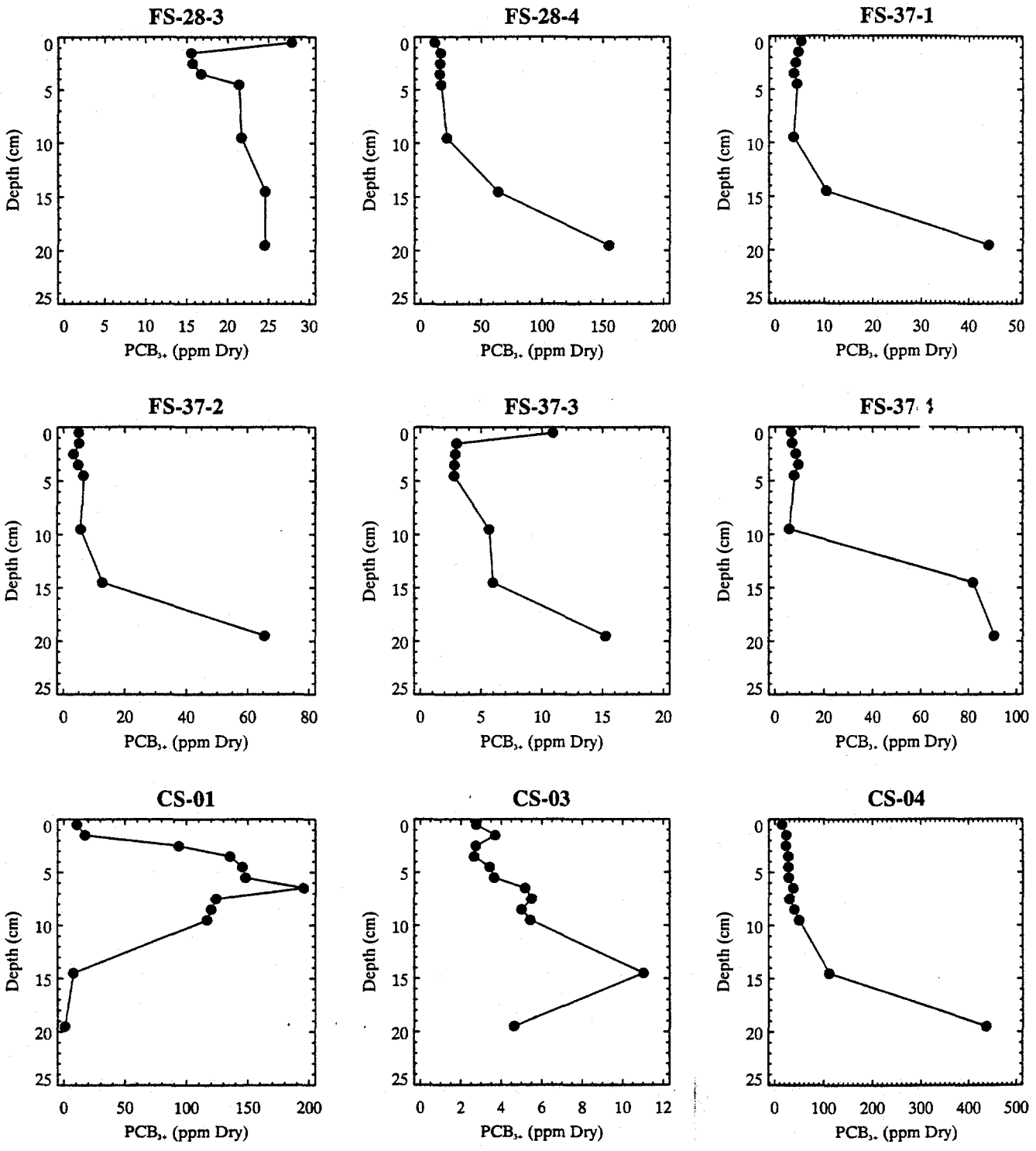

Note: Core sections shown are the top 23 cm of each core, plotted at segment midpoint.

Figure 4-15c. Vertical profiles of PCB_{3+} within finely segmented sediment cores collected from the Upper Hudson River.

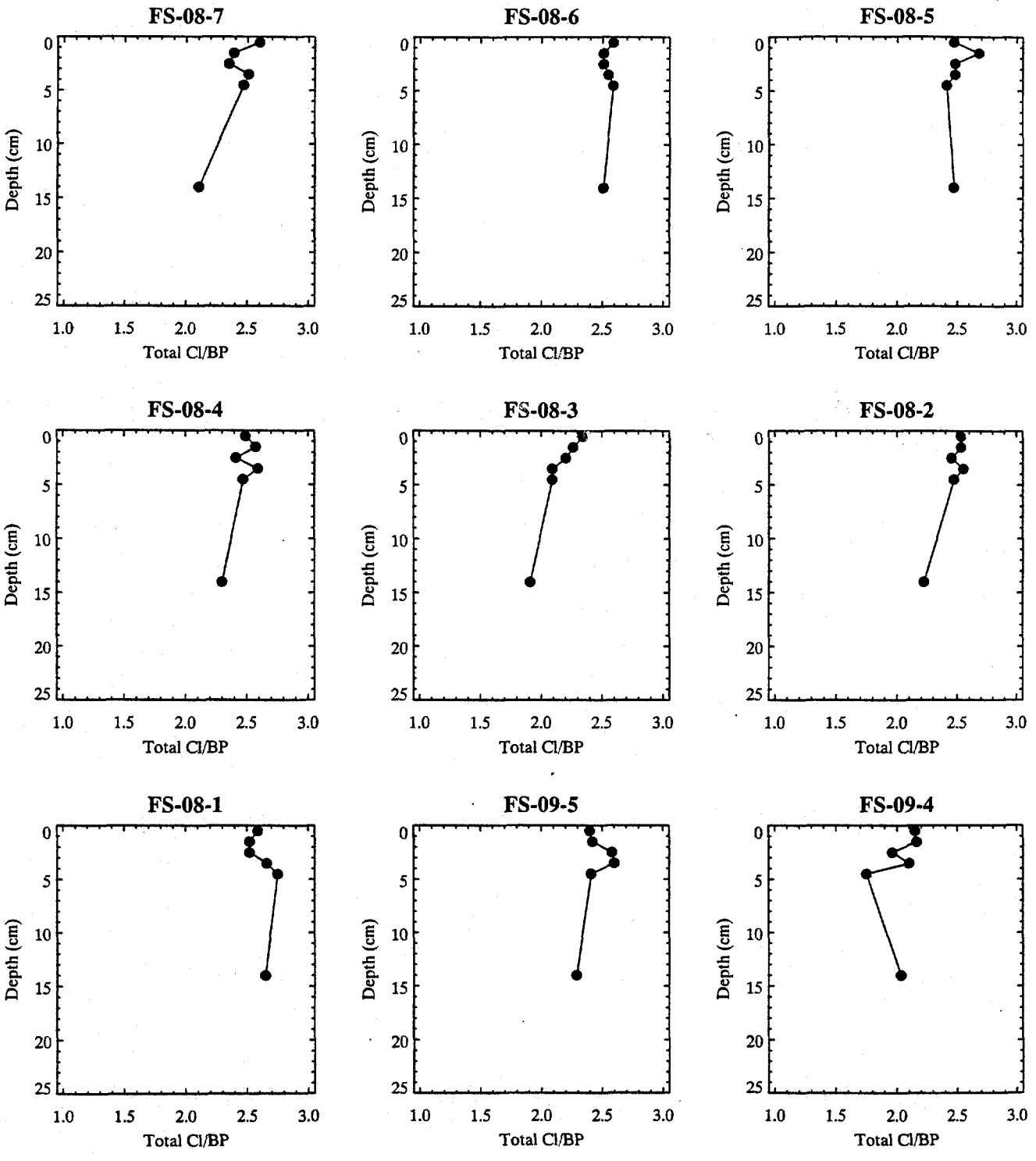

Note: Core sections shown are the top 23 cm of each core, plotted at segment midpoint.

Figure 4-16a. Vertical profiles of total chlorines per biphenyl within finely segmented sediment cores collected from the Upper Hudson River.

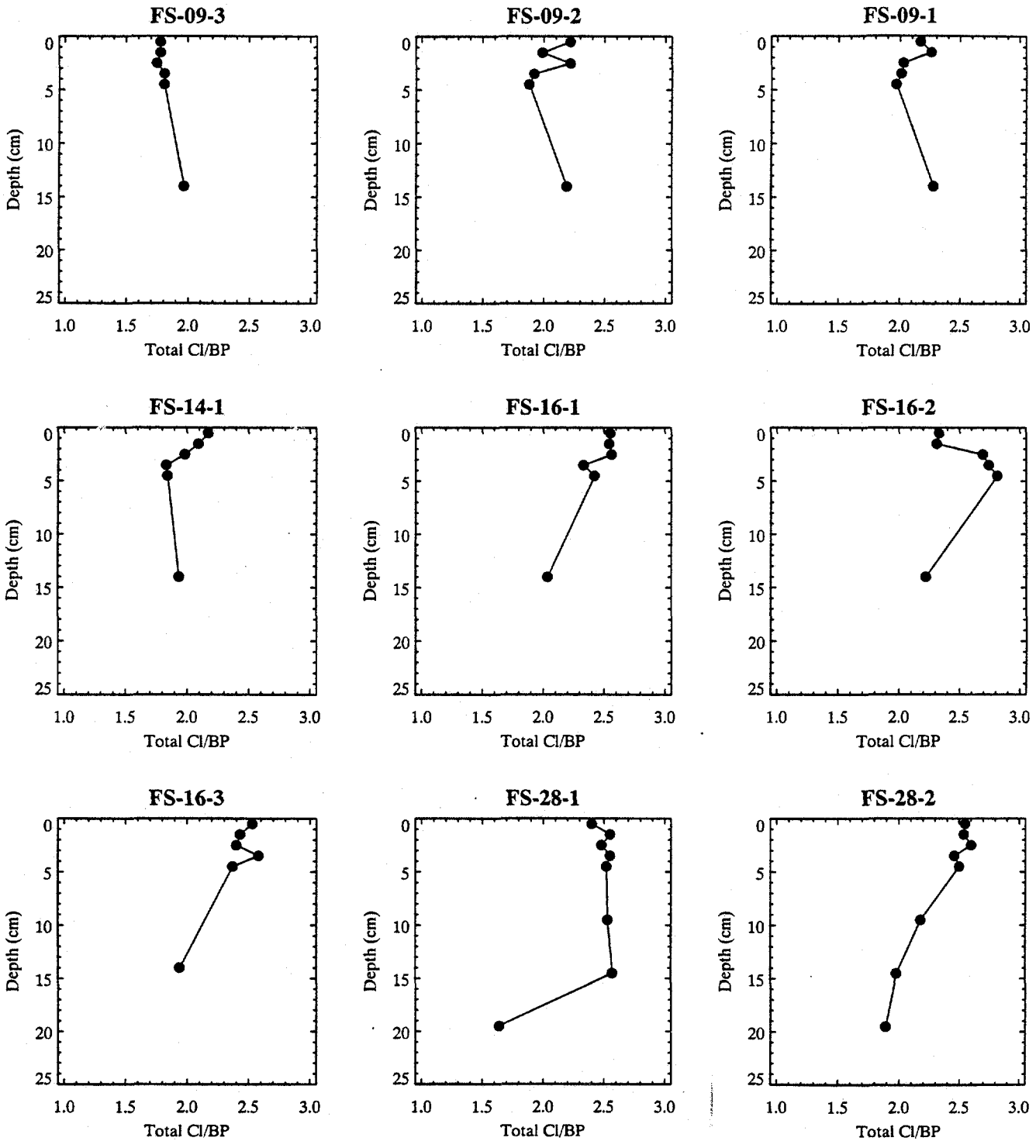

Note: Core sections shown are the top 23 cm of each core, plotted at segment midpoint.

Figure 4-16b. Vertical profiles of total chlorines per biphenyl within finely segmented sediment cores collected from the Upper Hudson River.

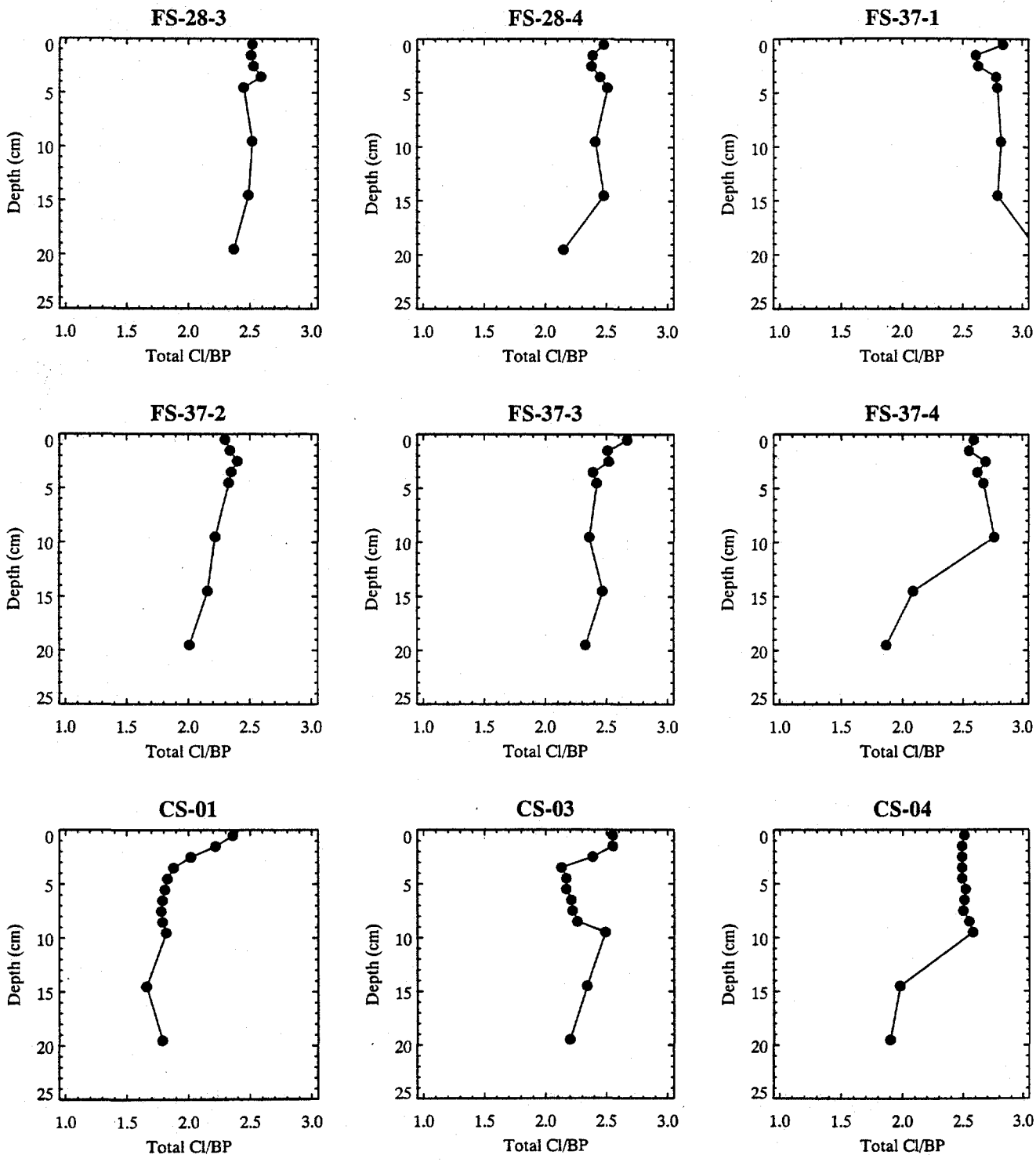

Note: Core sections shown are the top 23 cm of each core, plotted at segment midpoint.

Figure 4-16c. Vertical profiles of total chlorines per biphenyl within finely segmented sediment cores collected from the Upper Hudson River.

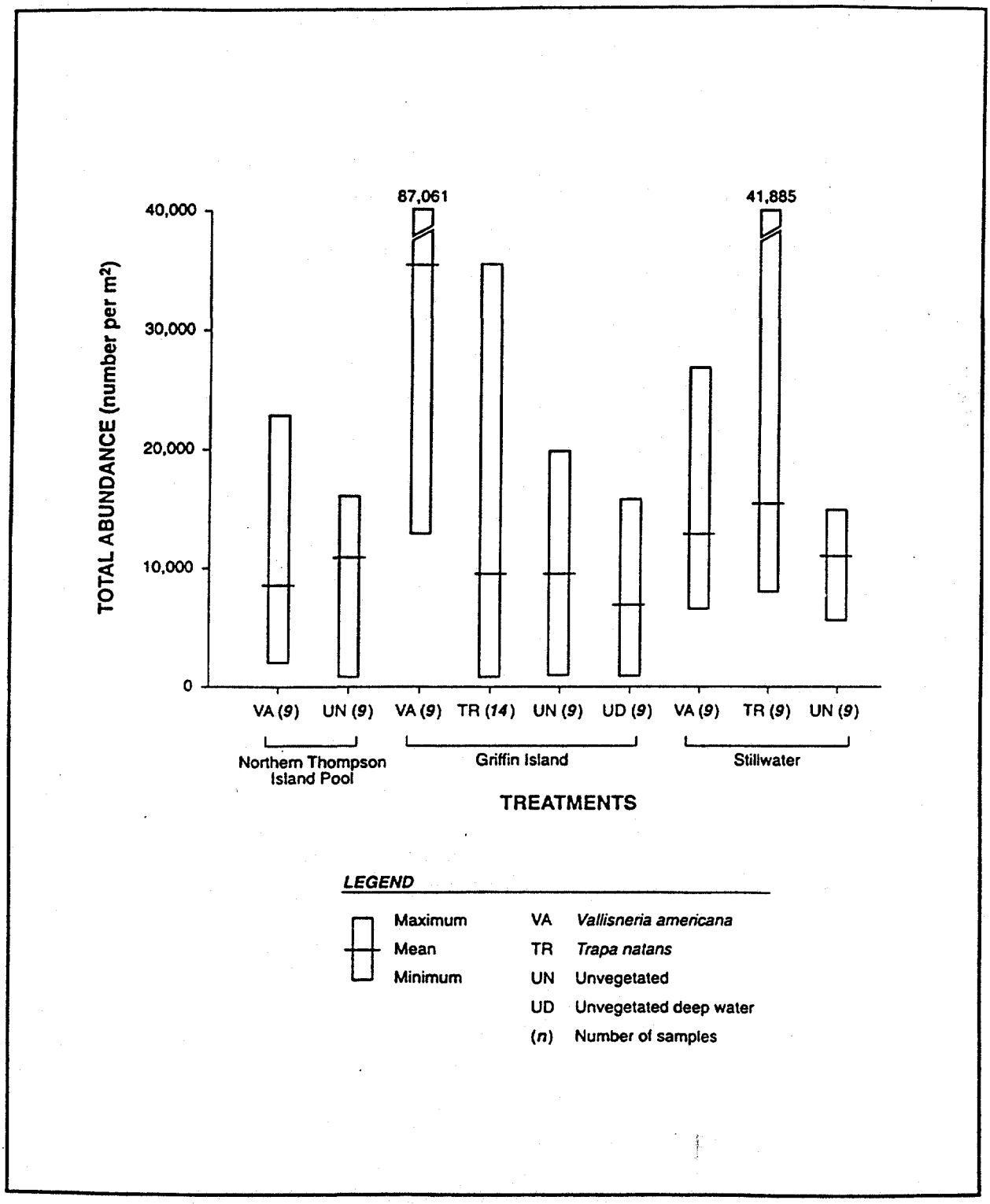

Figure 4-17. Total abundance of benthic macro-invertebrates within different habitats of the Upper Hudson River (from Exponent, 1998).

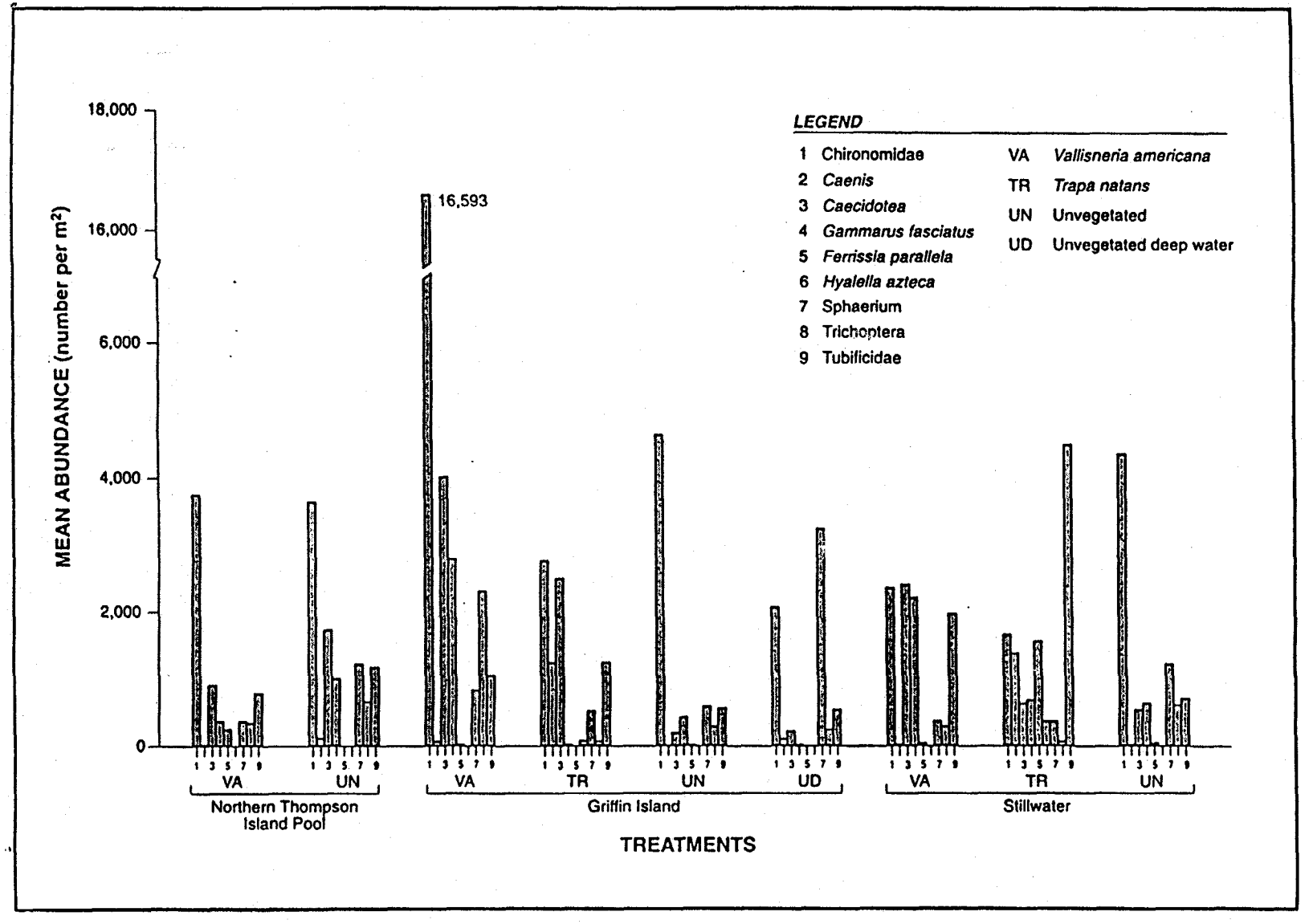

Figure 4-18. Mean abundance of benthic macro-invertebrate taxa within different habitats of the Upper Hudson River (from Exponent, 1998).

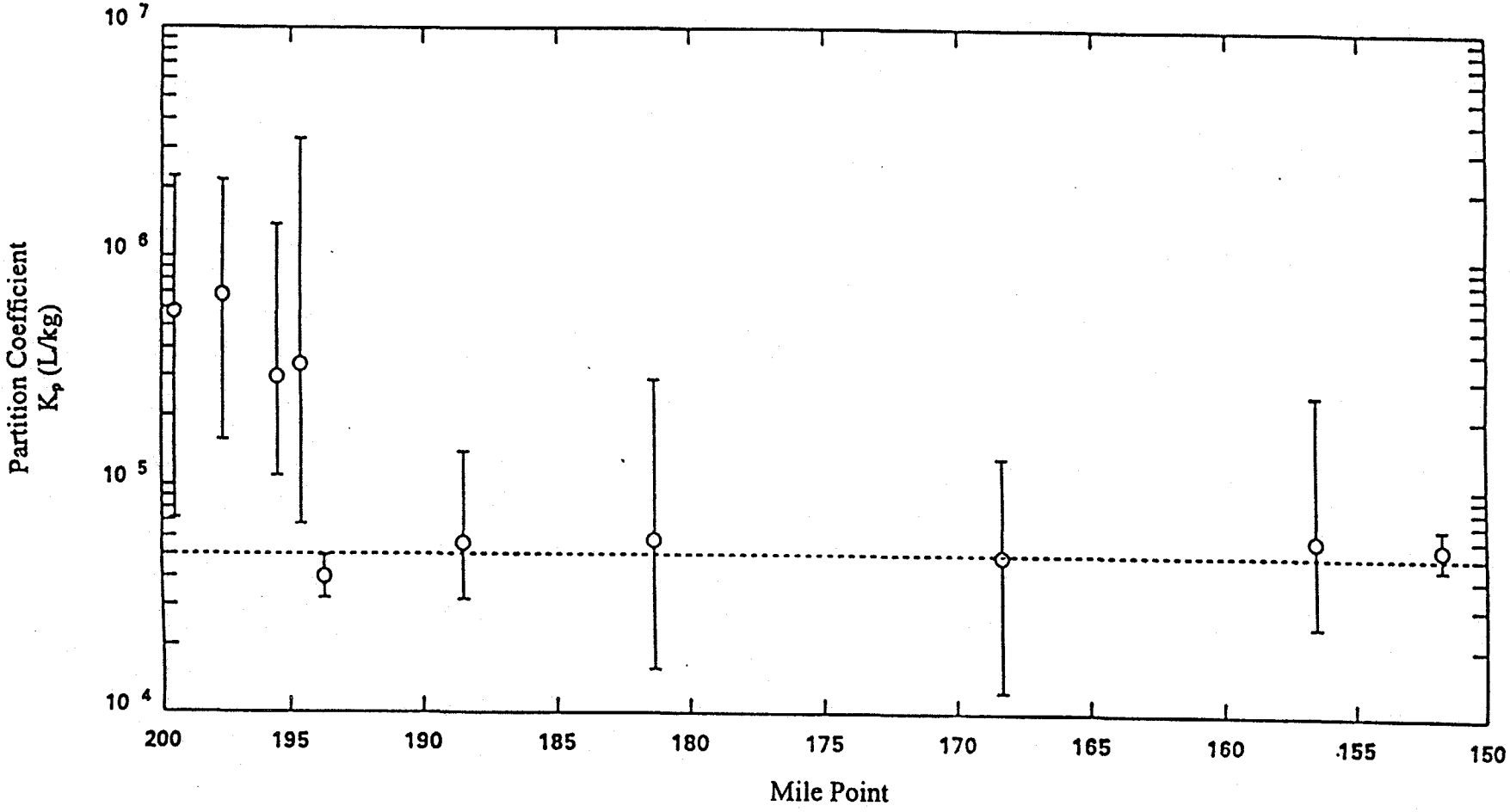

Figure 4-19. Spatial profile of mean (± data range) partition coefficients of total PCB calculated from USEPA Phase 2 water column monitoring transect studies.

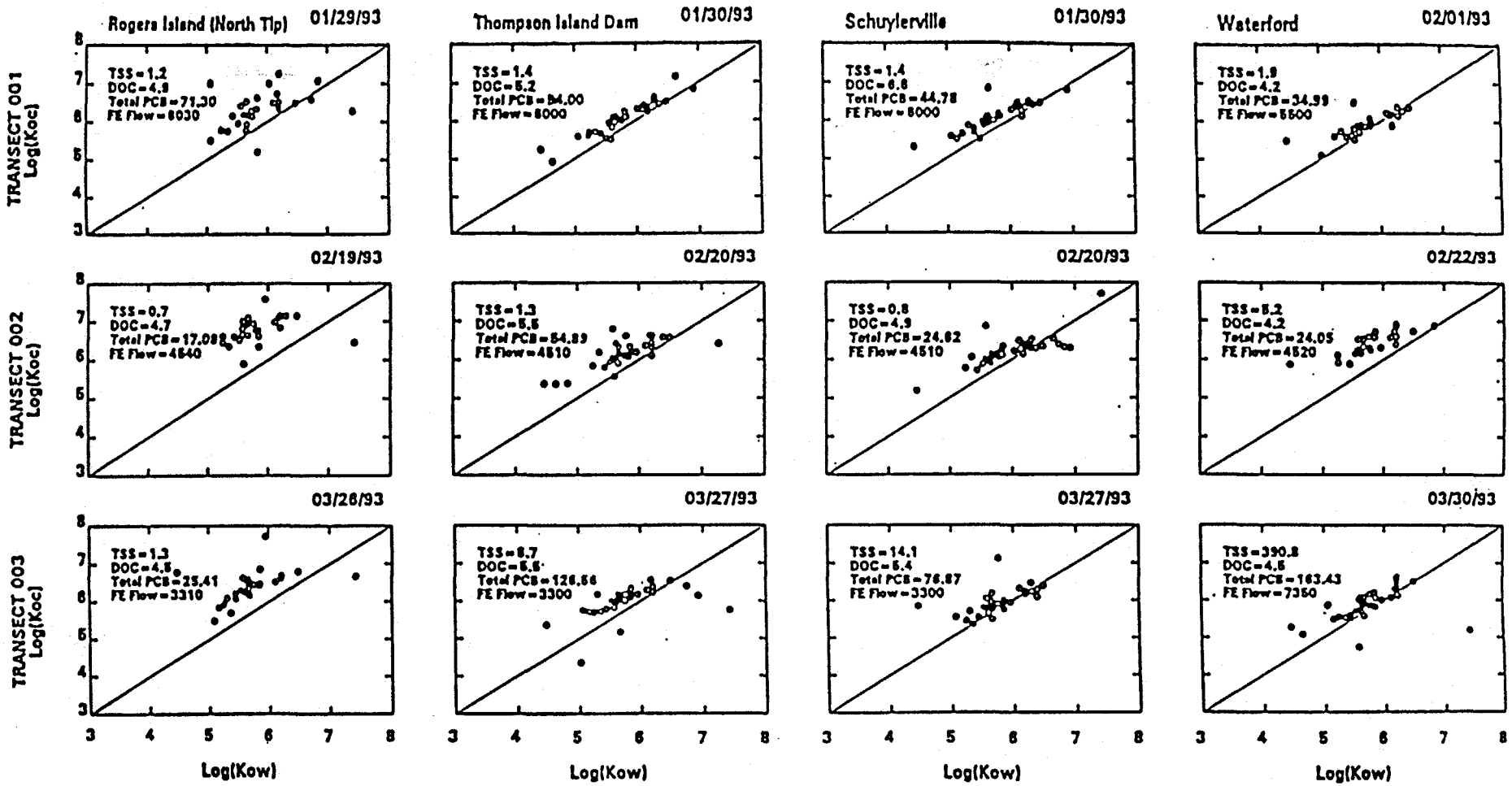

Figure 4-20a. K_{oc} vs. K_{ow} at Rogers Island, the Thompson Island Dam, Schuylerville and Waterford from USEPA Phase 2 transects 001-003 (TSS in mg/L, total PCBs in mg/L and Fort Edward flow in cfs).

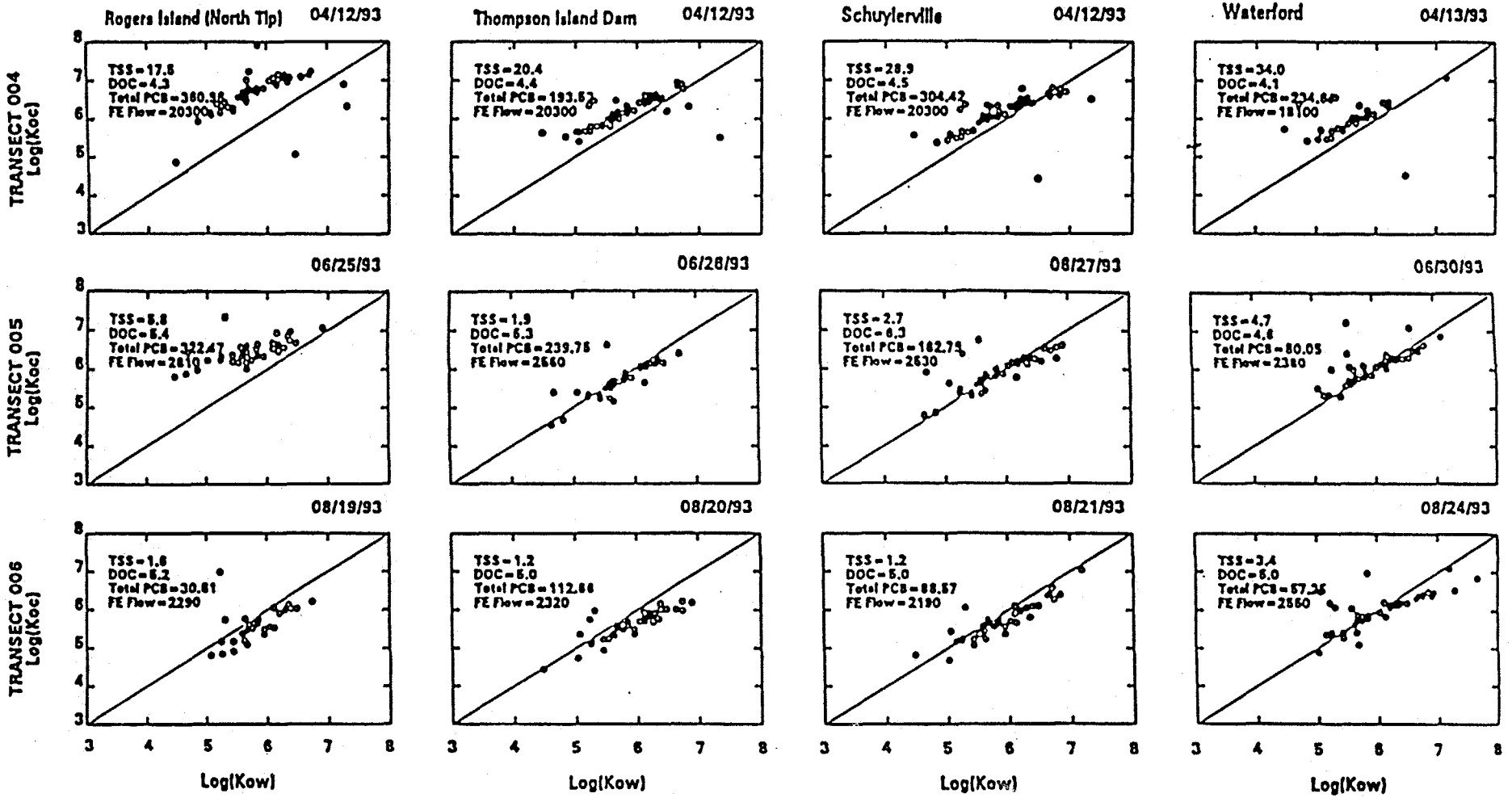

Figure 4-20b. K_{oc} vs. K_{ow} at Rogers Island, the Thompson Island Dam, Schuylerville and Waterford from USEPA Phase 2 transects 004-006 (TSS in mg/L, total PCBs in mg/L and Fort Edward flow in cfs).

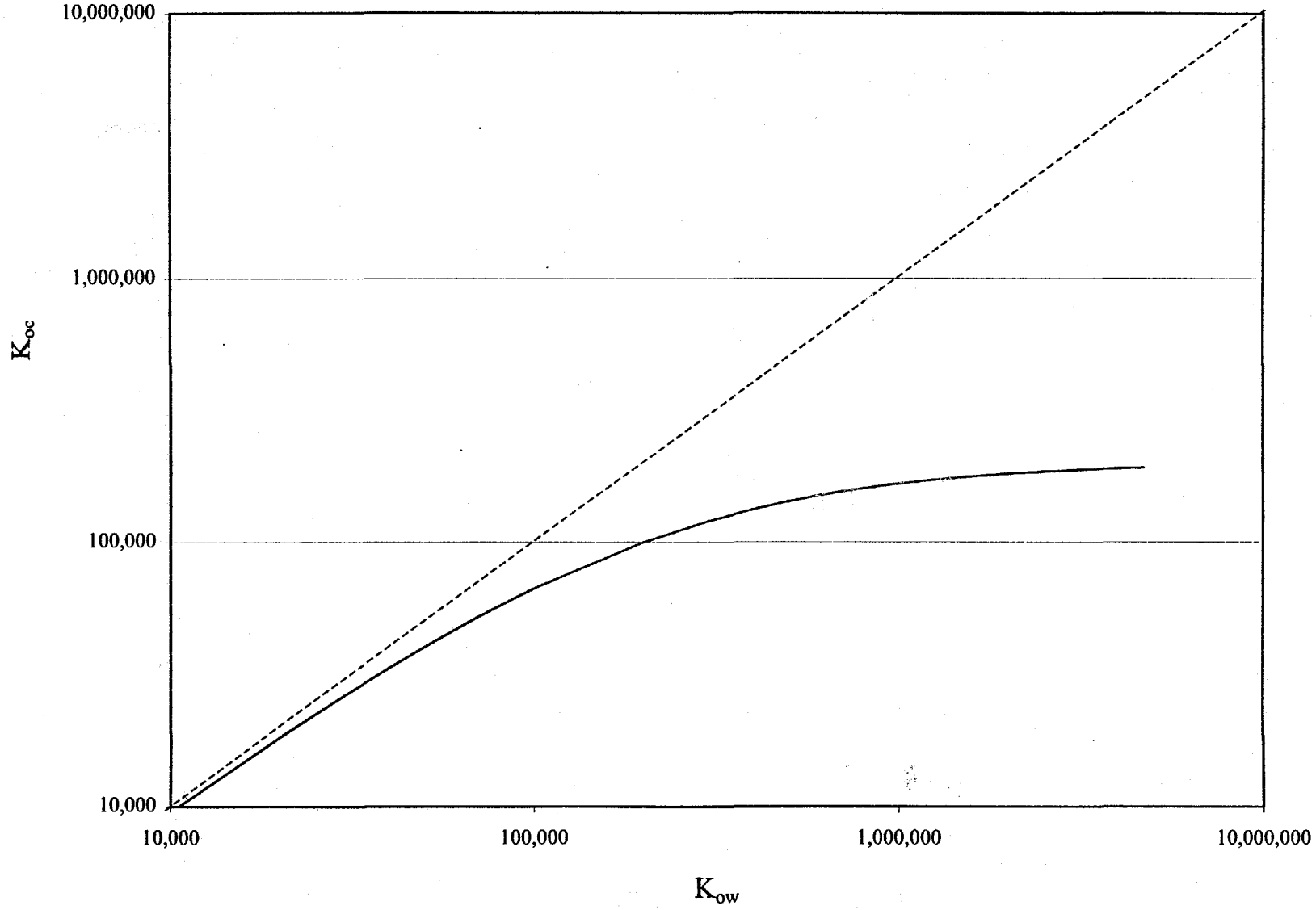

Figure 4-21. Illustration of the impact of third phase (DOM) sorption on the relationship between K_{oc} and K_{ow}.

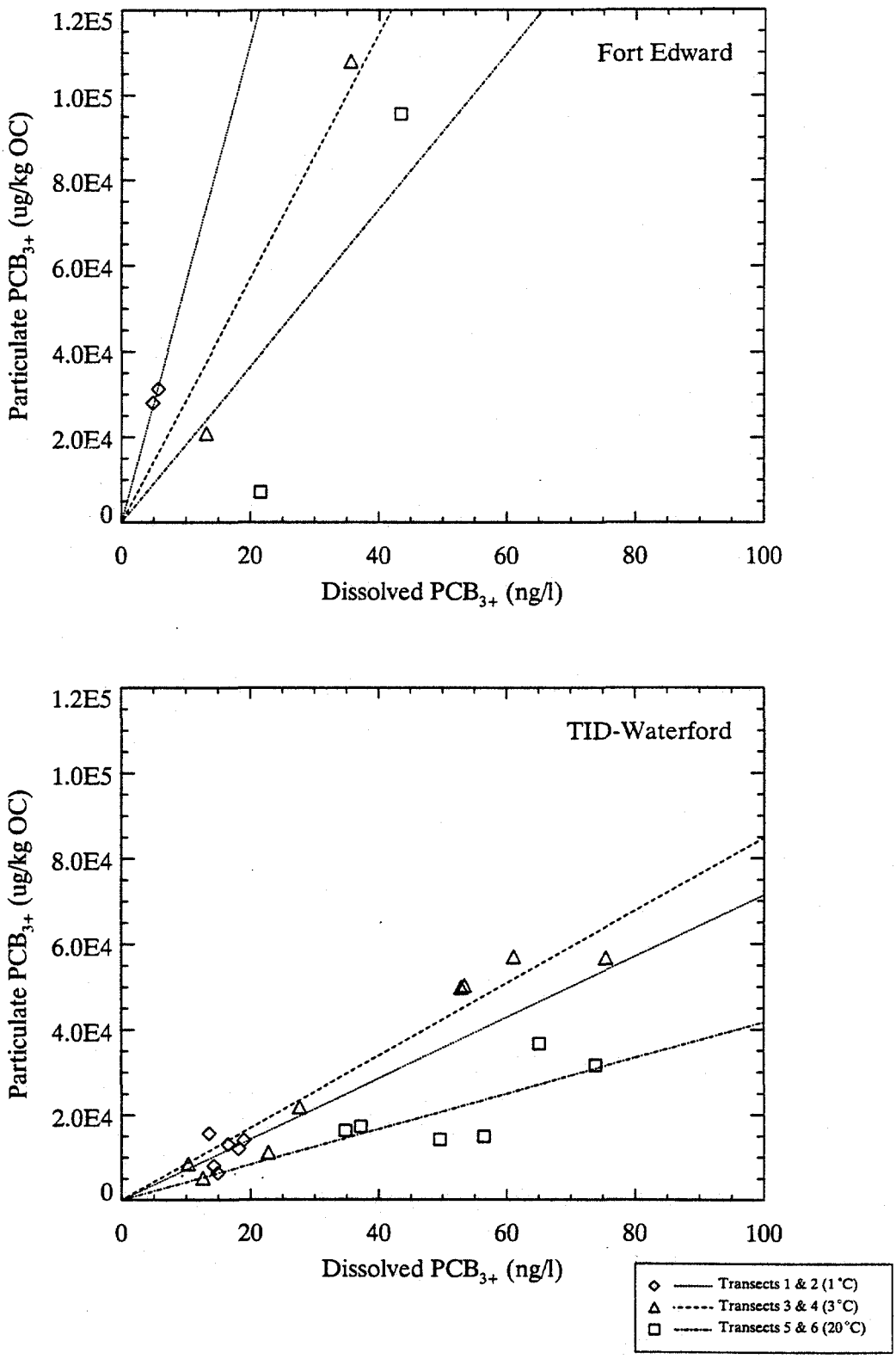

Figure 4-22. USEPA Phase 2 transect study; particulate versus dissolved PCB_{3+} comparisons with isothermal regressions.

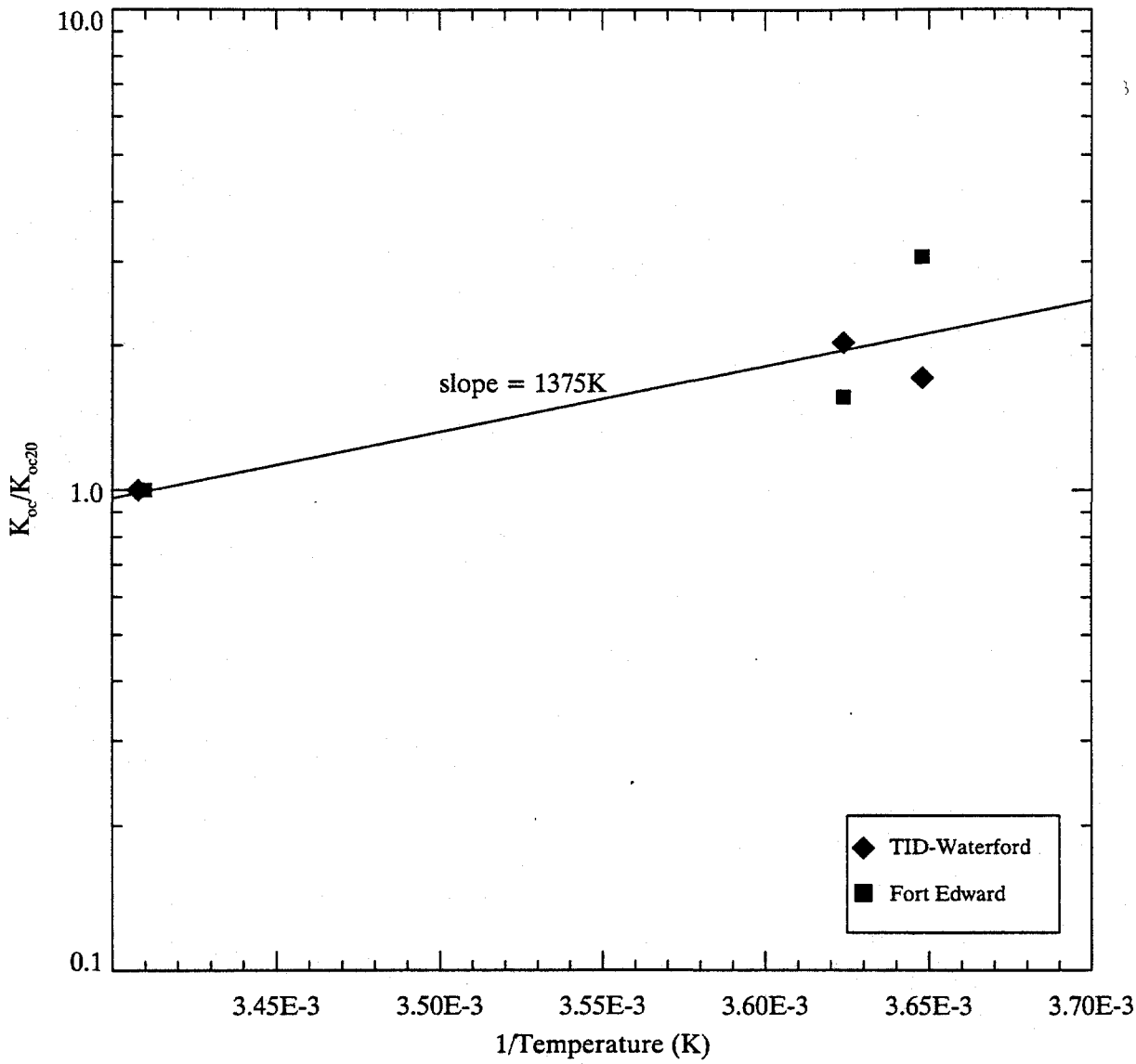

Figure 4-23. Normalized K_{oc} values versus inverse temperature with regression line.

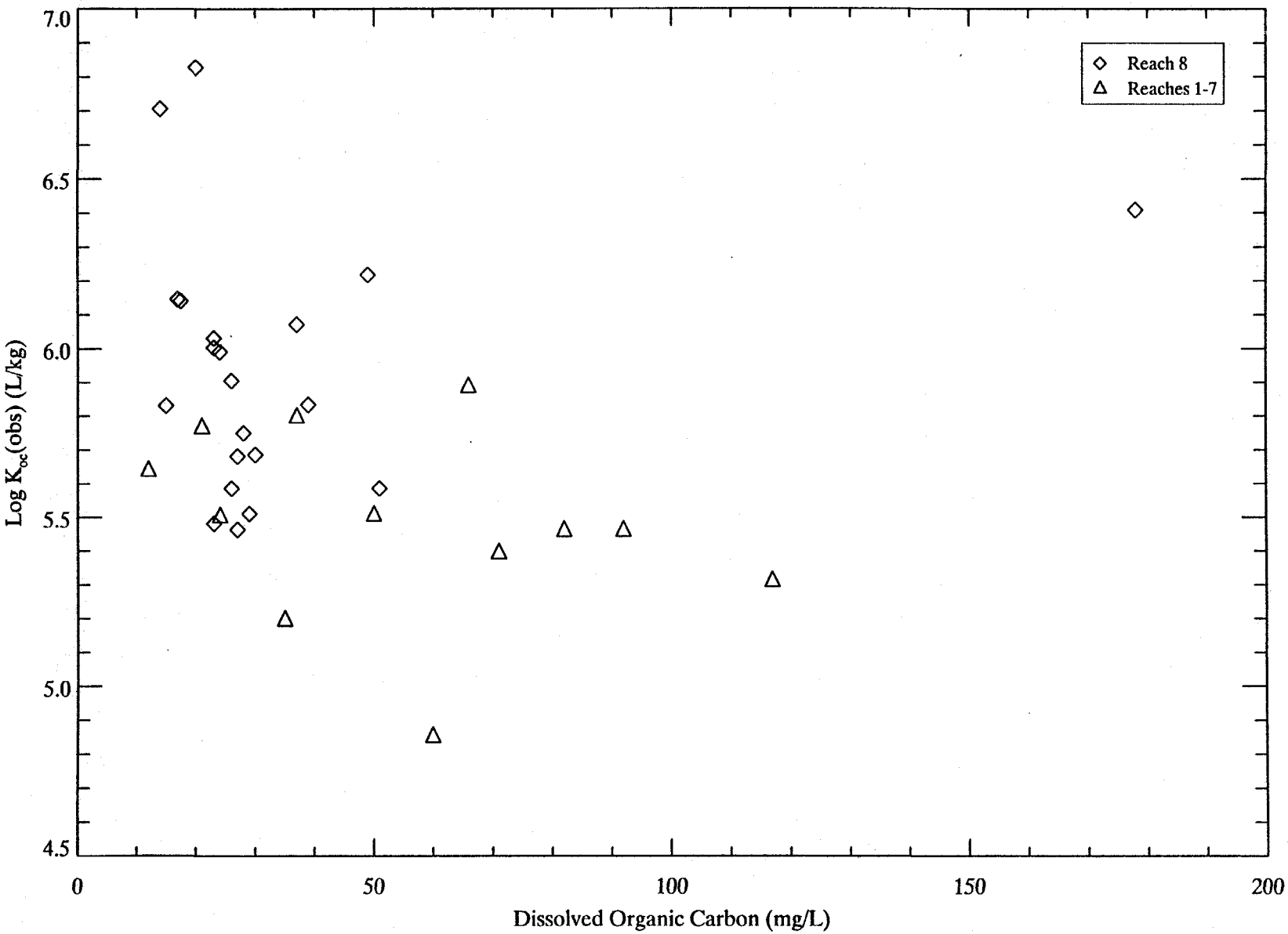

Note: 0-5cm layers sampled in 1991 by GE.

Figure 4-24. Relationship between PCB_{3+} partition coefficients (K_{oc}) calculated from sediment and porewater measurements and porewater dissolved organic carbon (0-5cm).

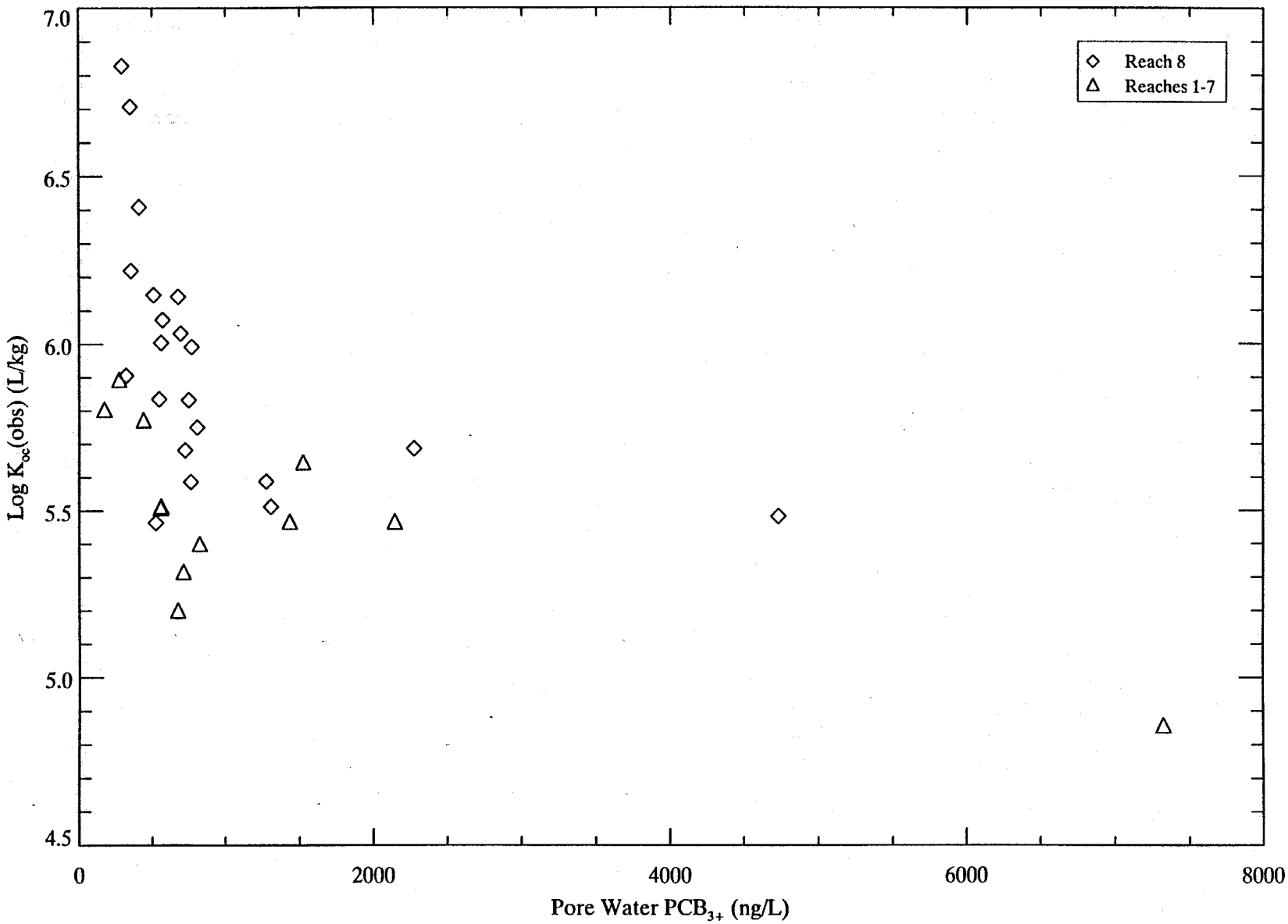

Note: 0-5cm layers sampled in 1991 by GE.

Figure 4-25. Relationship between PCB_{3+} partition coefficients (K_{oc}) calculated from sediment and porewater measurements and porewater PCB_{3+} (0-5cm).

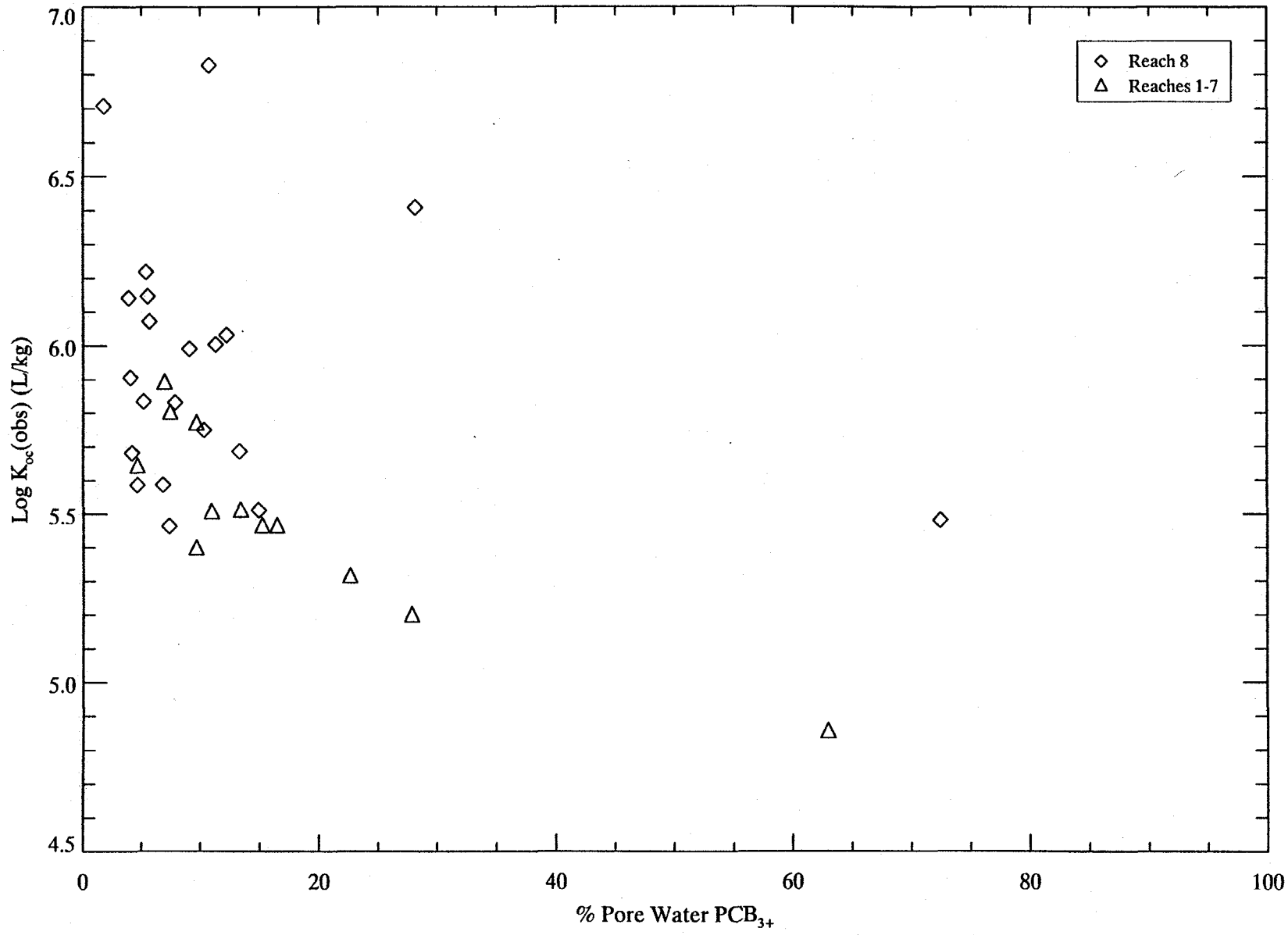

Note: 0-5cm layers sampled in 1991 by GE.

Figure 4-26. Relationship between PCB_{3+} partition coefficients (K_{oc}) calculated from sediment and porewater measurements and porewater fraction PCB_{3+} (0-5cm).

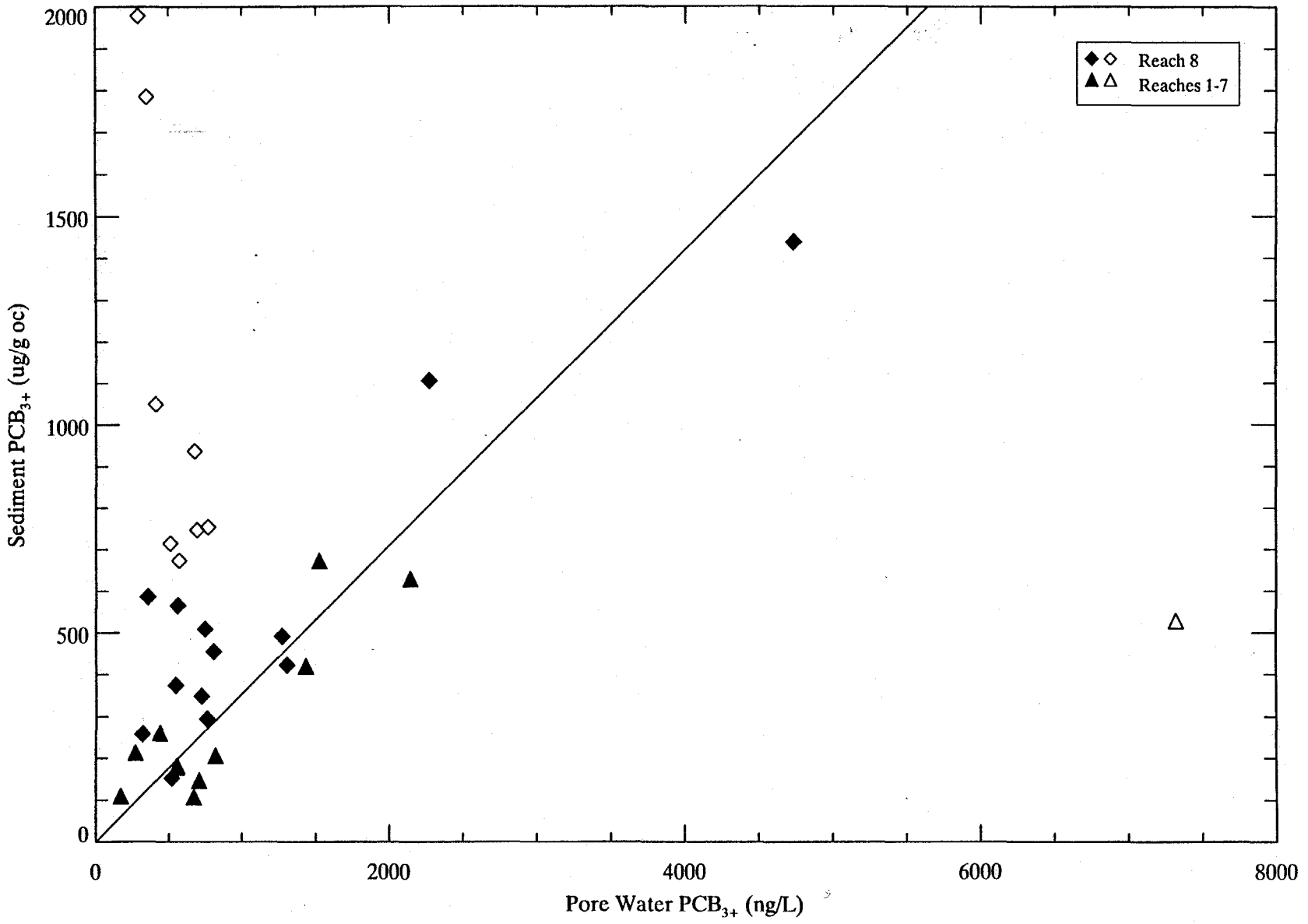

Figure 4-27. Relationship between sediment and porewater PCB_{3+} concentrations. Line conforms to regression of filled symbols ($K_{oc}=10^{5.55}$)

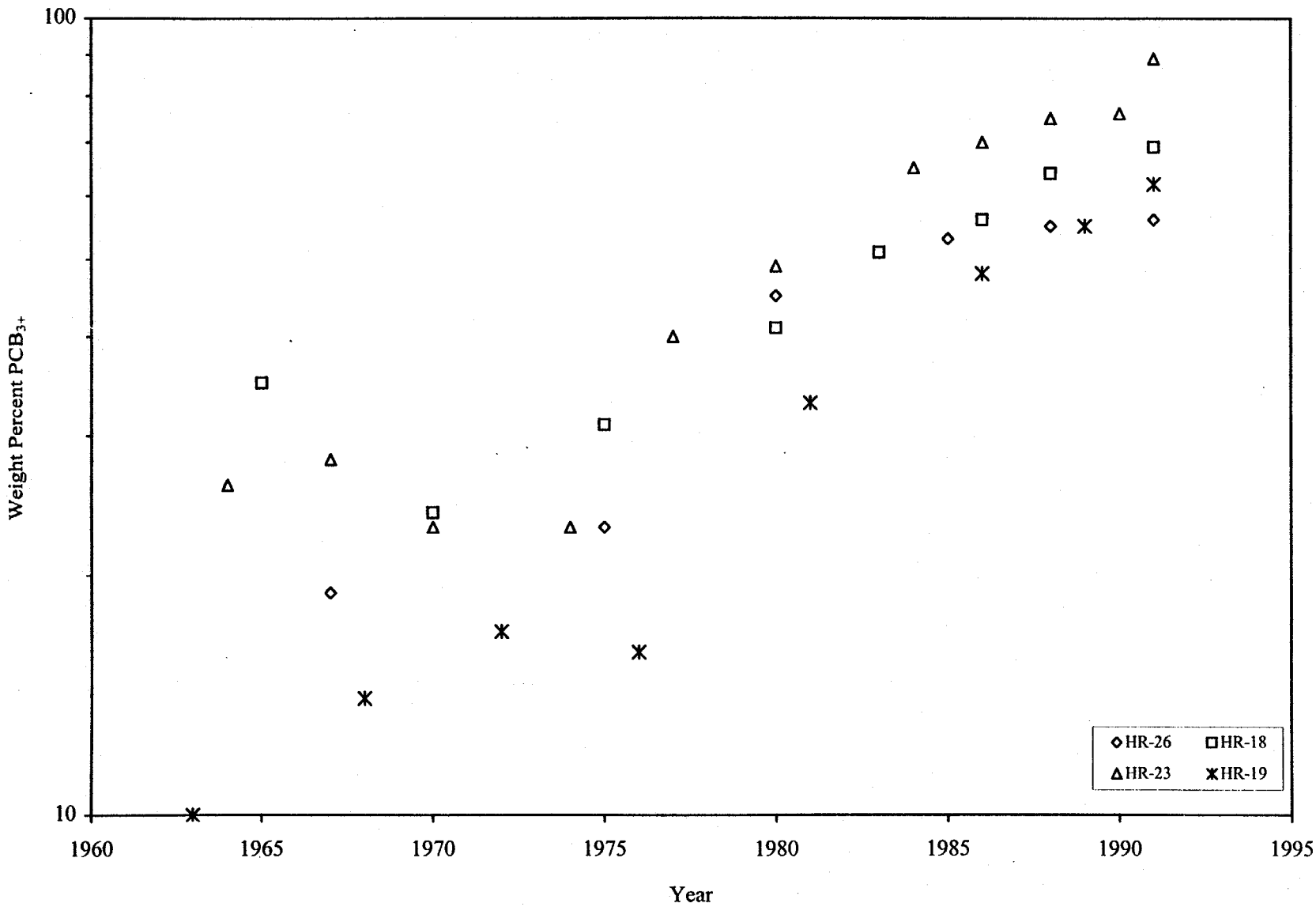

Figure 4-28a. Percent contribution of PCB_{3+} to total PCBs as a function of sediment age for four USEPA high resolution cores collected in Reaches 6 and 8.

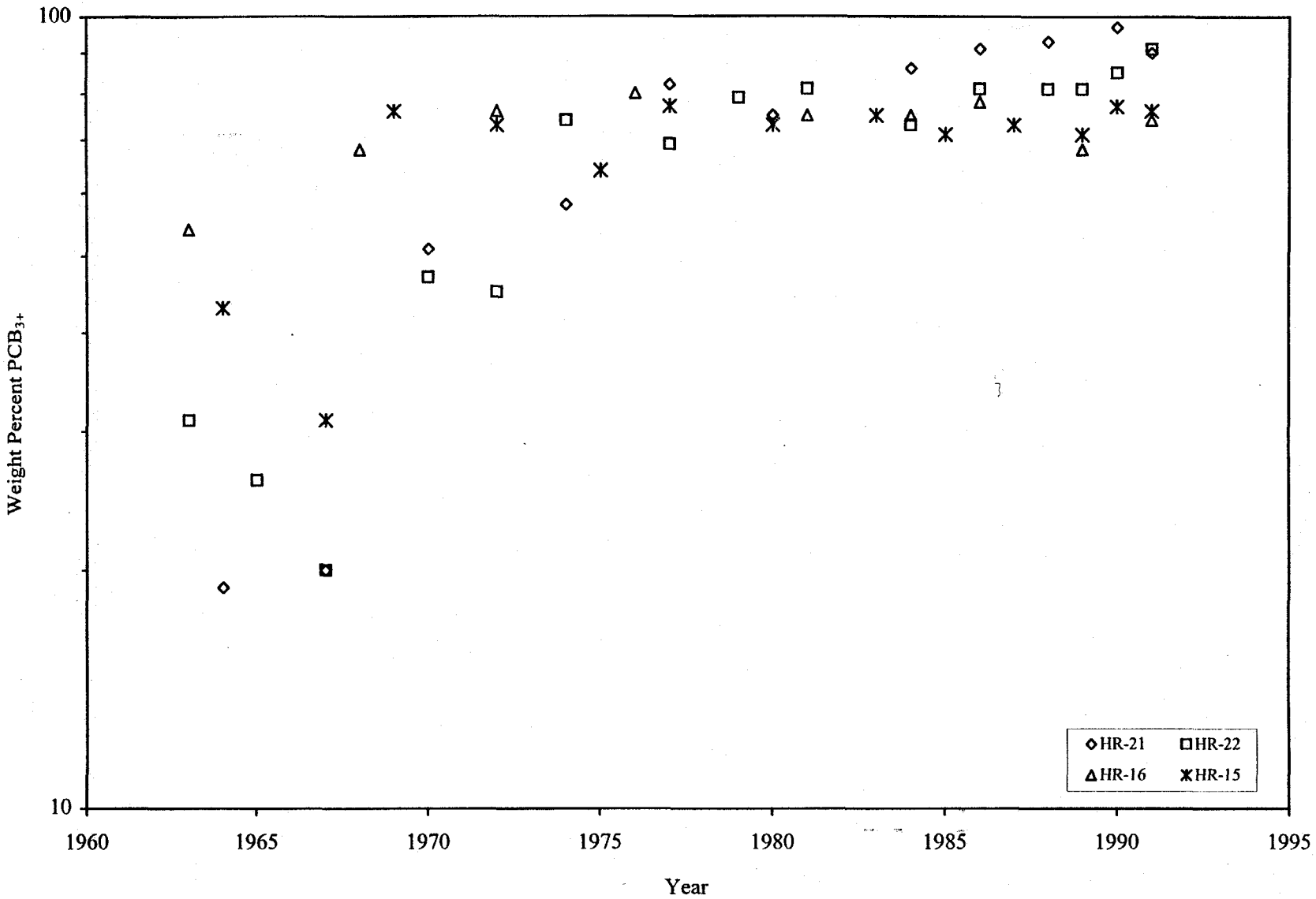

Figure 4-28b. Percent contribution of PCB_{3+} to total PCBs as a function of sediment age for four USEPA high resolution cores collected downstream of Reaches 6 and 8.

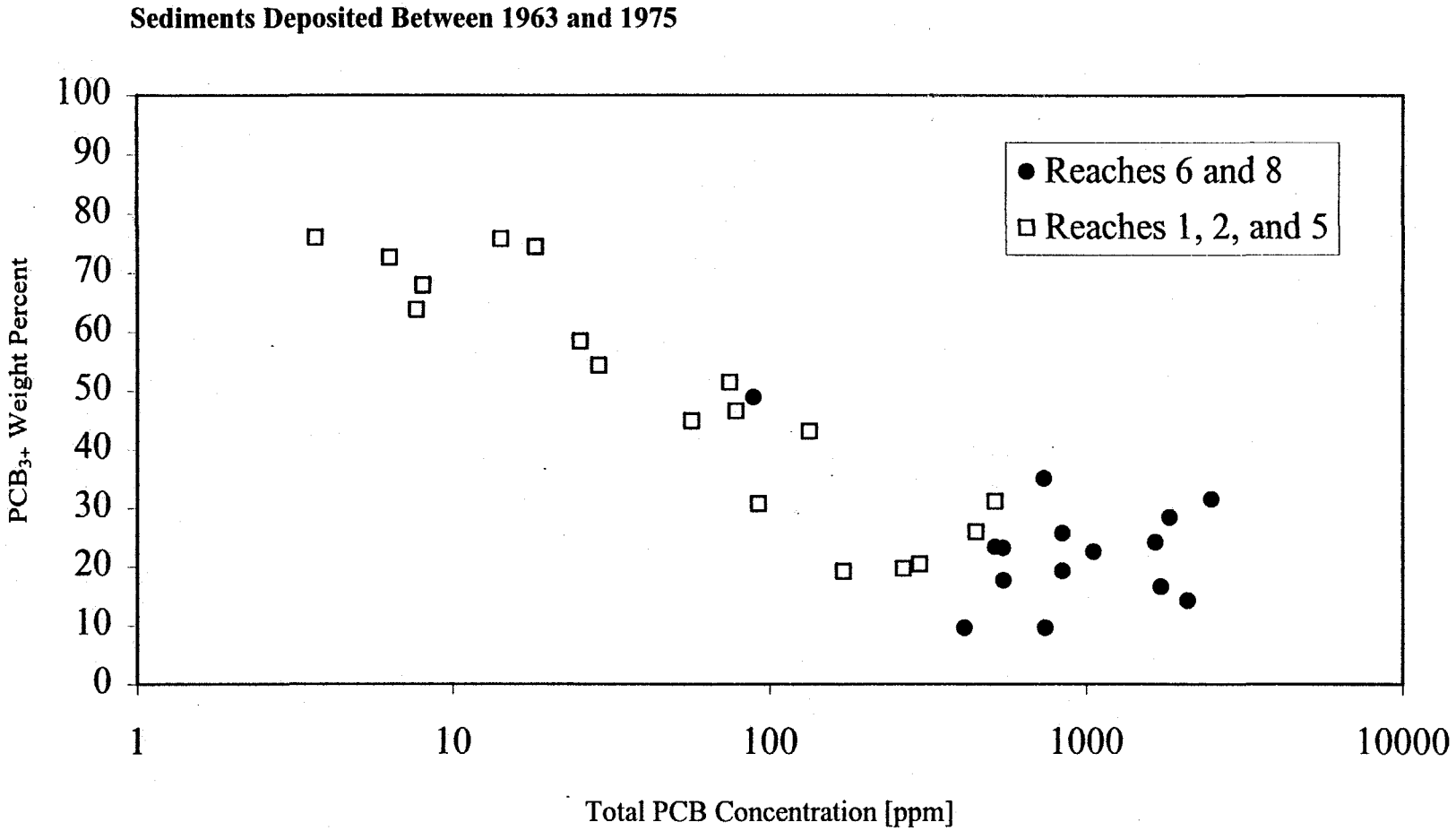

Figure 4-29. Comparison between total PCB concentration and PCB_{3+} weight percent for USEPA high resolution core sections for sediments deposited between 1963 and 1975.

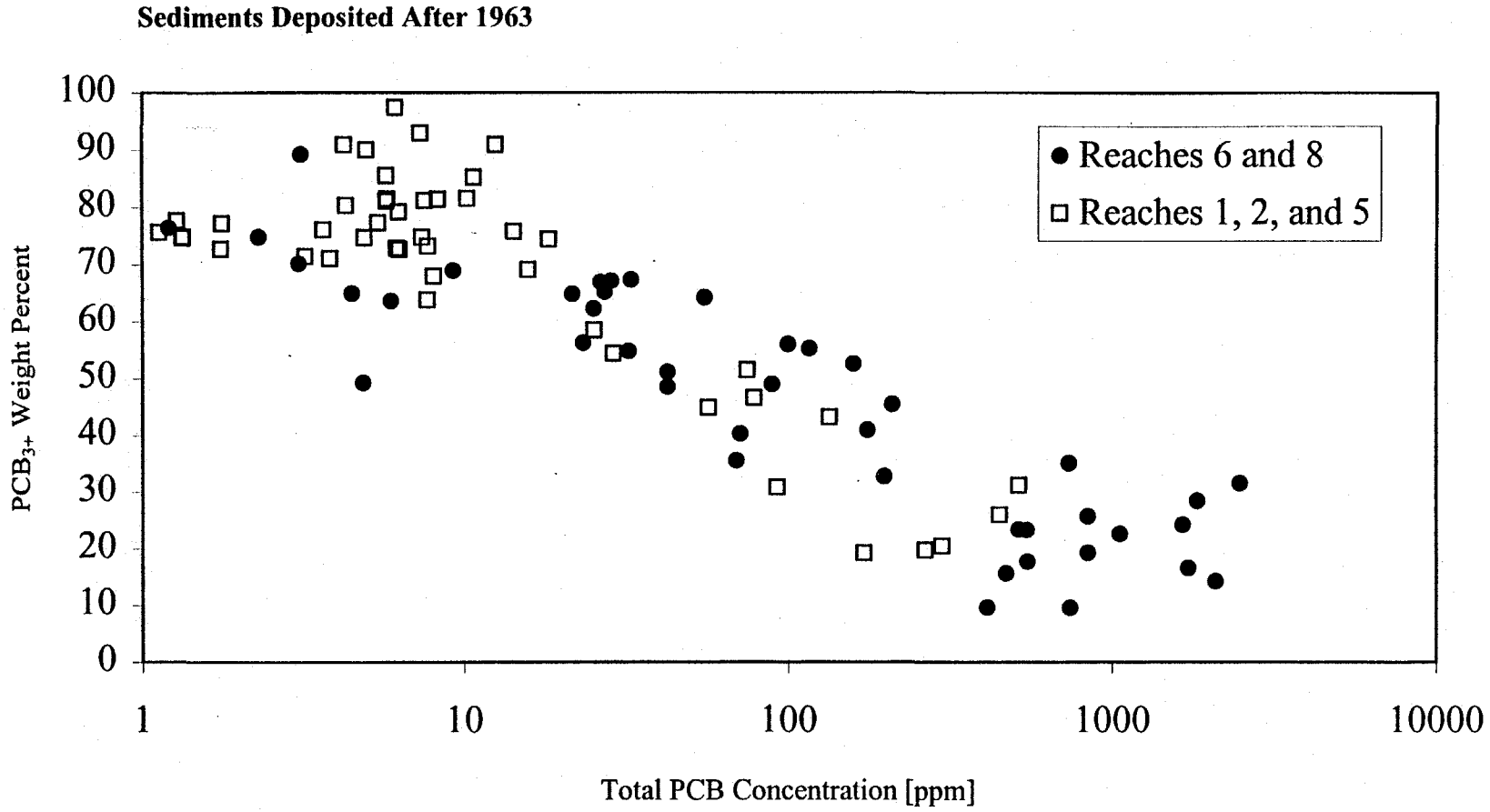

Figure 4-30. Comparison between total PCB concentration and PCB_{3+} weight percent for USEPA high resolution core sections for sediments deposited after 1963.

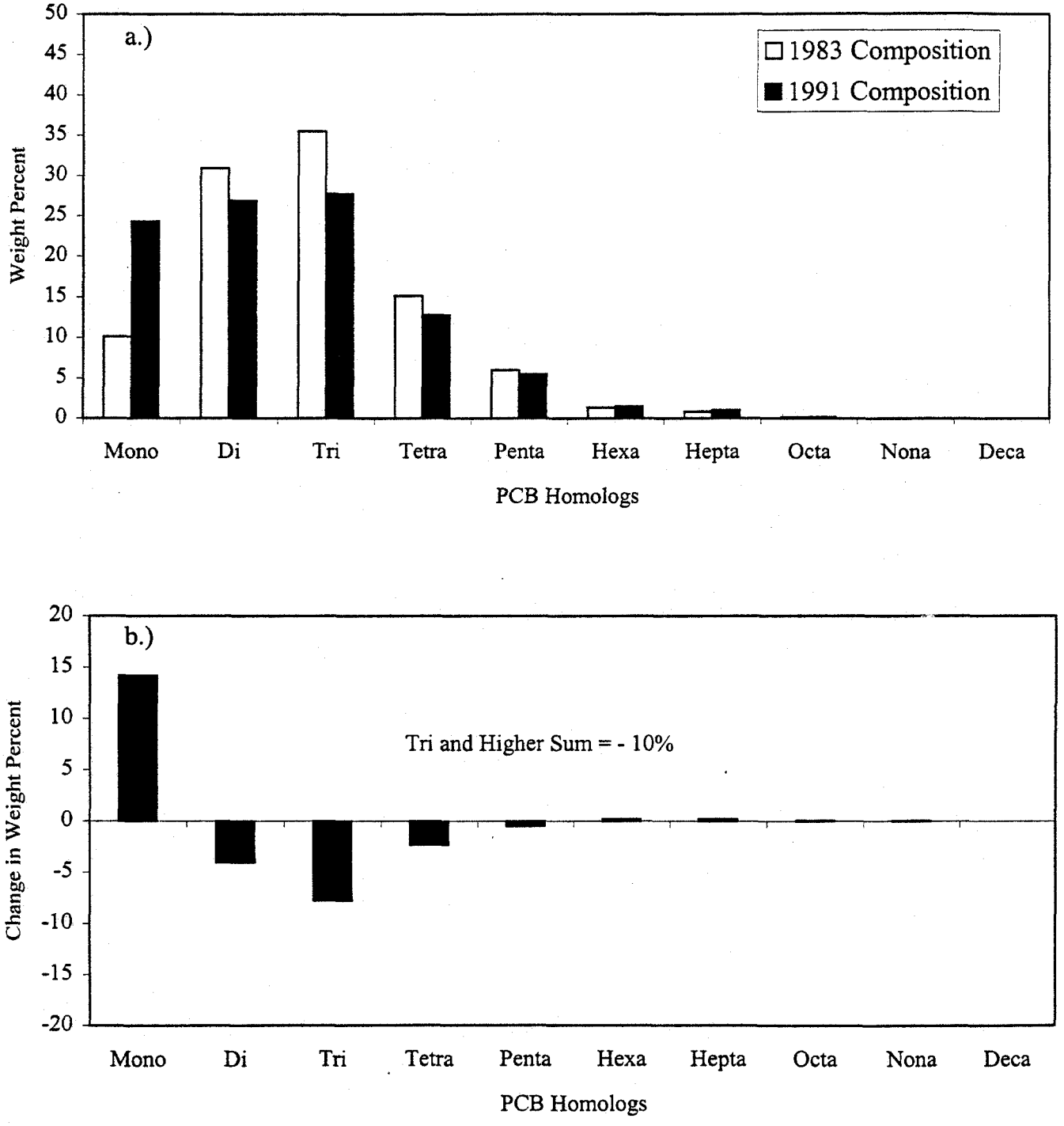

Figure 4-31. PCB composition of TIP sediment deposited in approximately 1968, assessed from core sections collected in 1983 and 1991 (total concentration > 500 ppm). *McNulty 1997.*

KTR - mcnulty.xls - homolog plot
4/15/99 - 3:22 AM

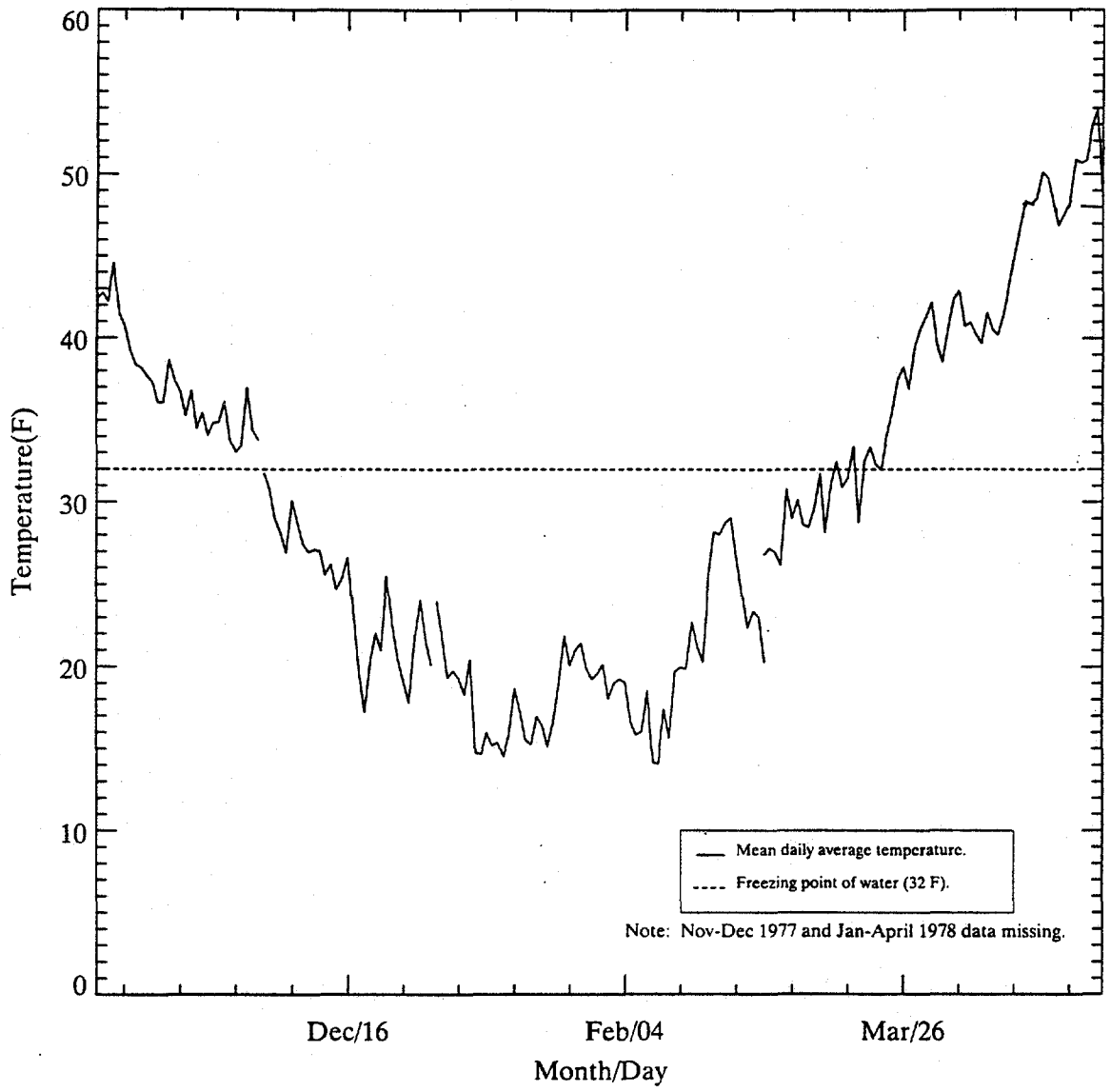

Figure 4-32. Mean daily average temperatures at the Glens Falls Airport measured by NOAA (1973-1993).

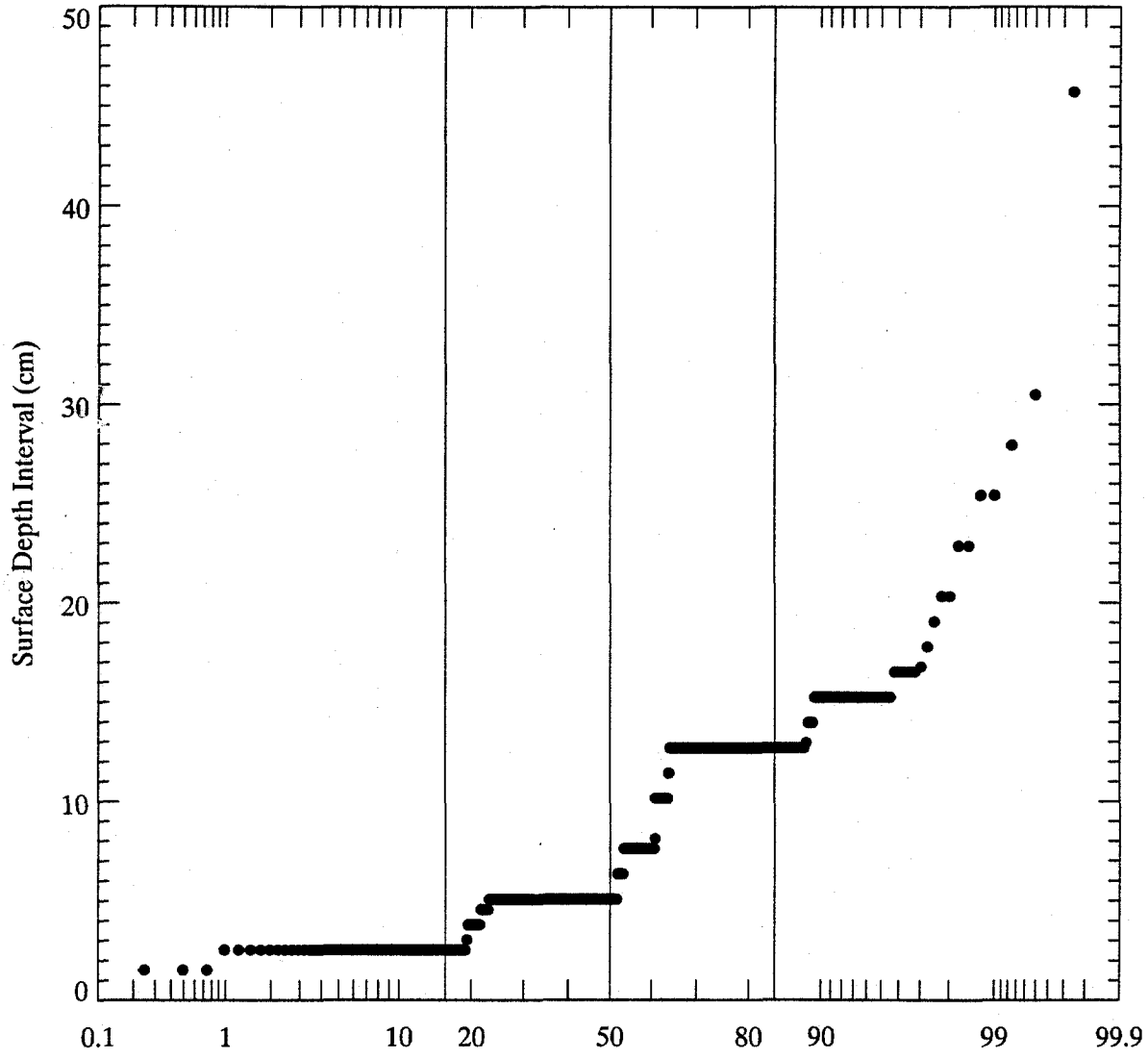

Figure 4-33. Probability distribution of surface sediment sampling intervals for 1976-1978 NYSDEC cores.

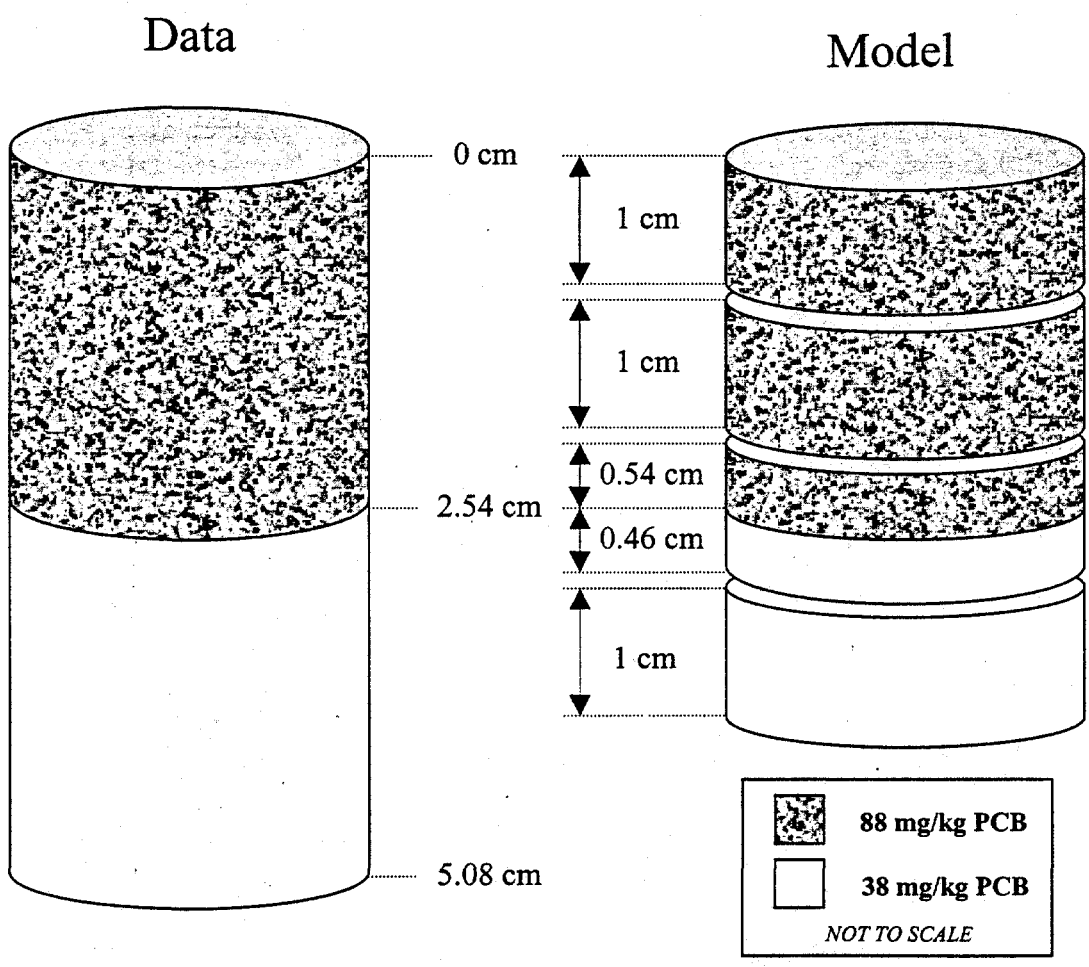

Figure 4-34. Illustration of sediment PCB depth-weighted averaging.

\\Poseidon\D_drive\Genhud\Documents\Final_Report\ Vol_2\Section_4\figure4_34.ppt

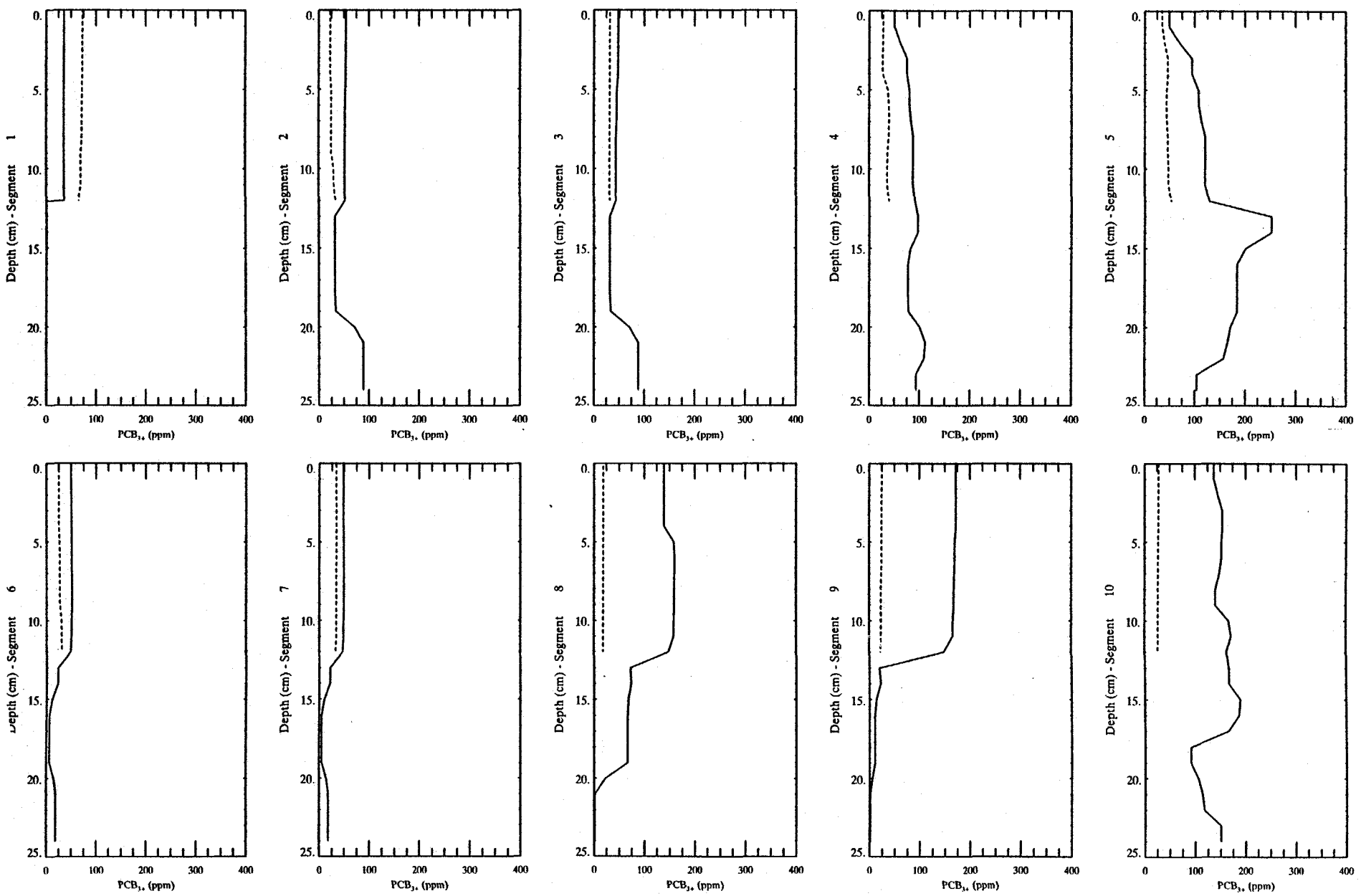

Figure 4-35a. Initial conditions for fate/transport model derived from 1976-78 NYSDEC data.

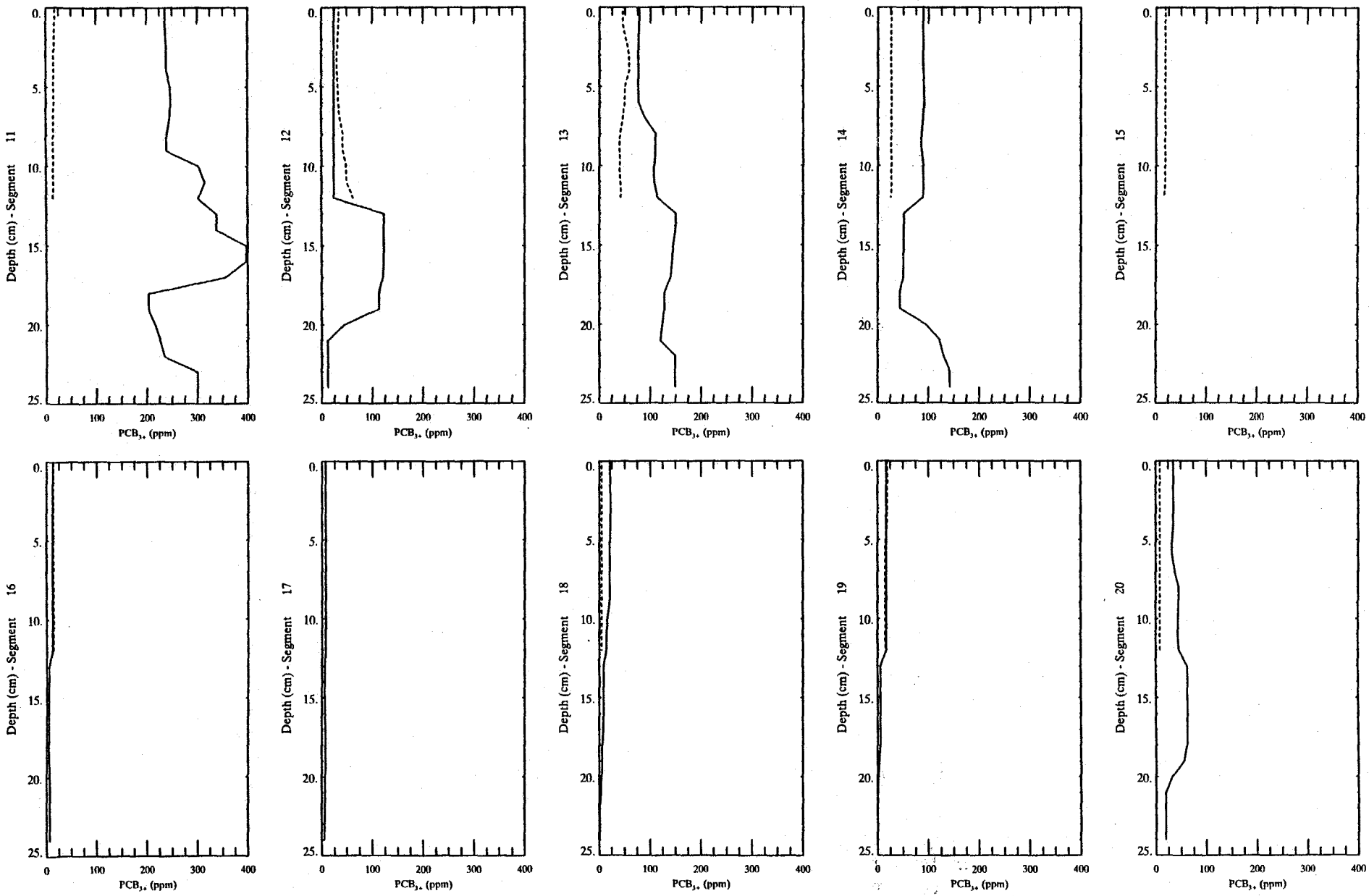

Figure 4-35b. Initial conditions for fate/transport model derived from 1976-78 NYSDEC data.

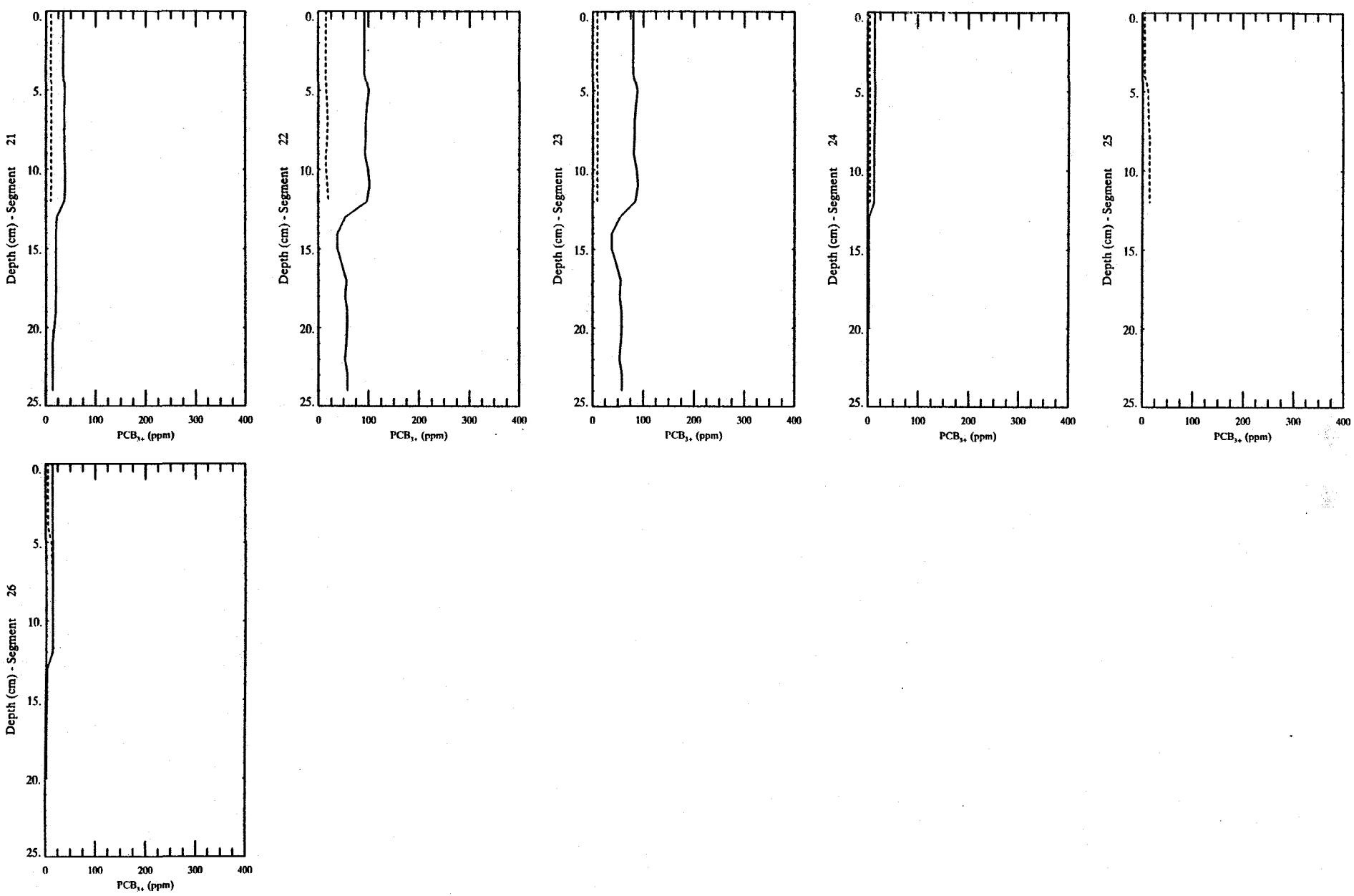

Figure 4-35c. Initial conditions for fate/transport model derived from 1976-78 NYSDEC data.

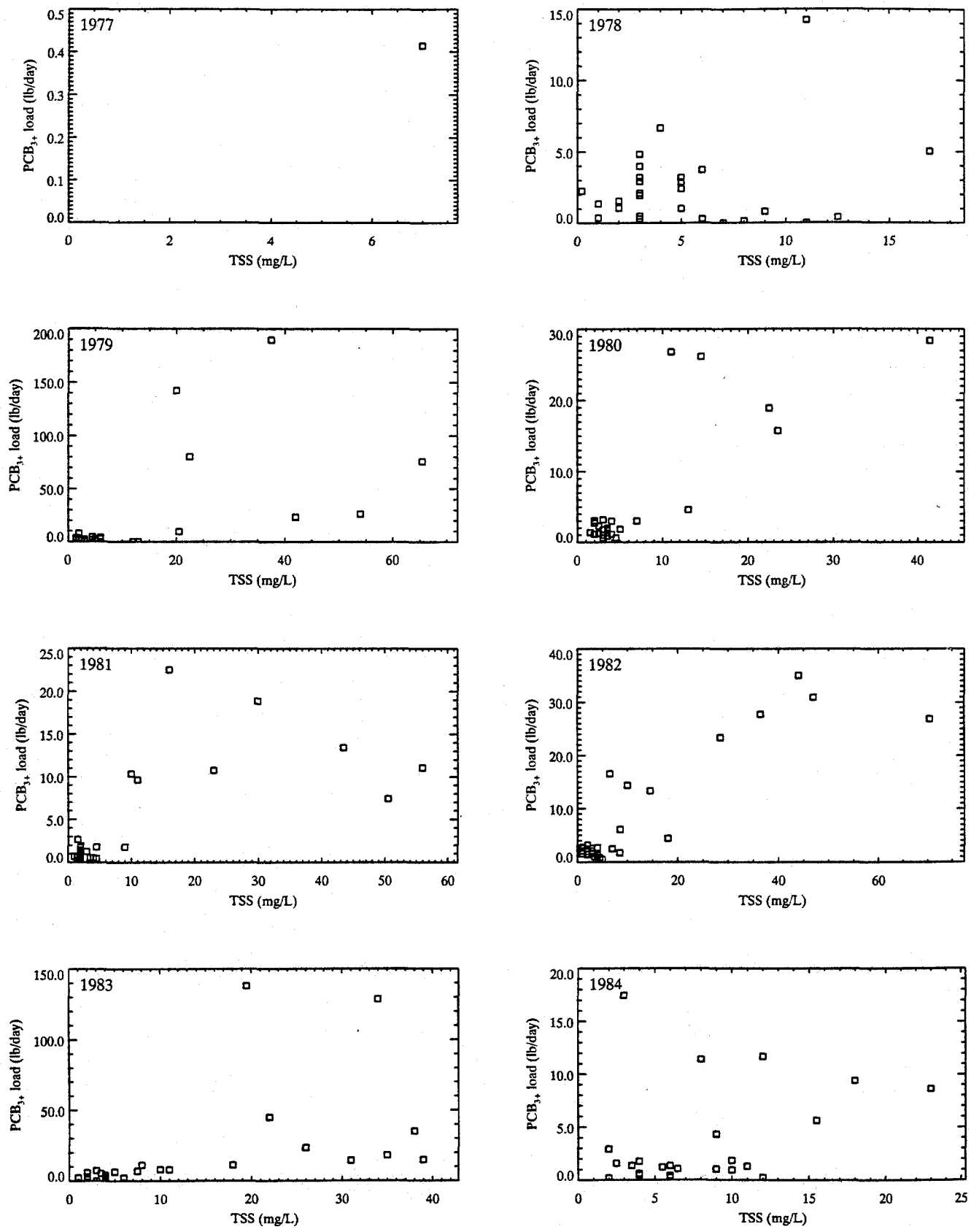

Figure 4-36a. PCB_{3+} load in relation to TSS at Fort Edward.

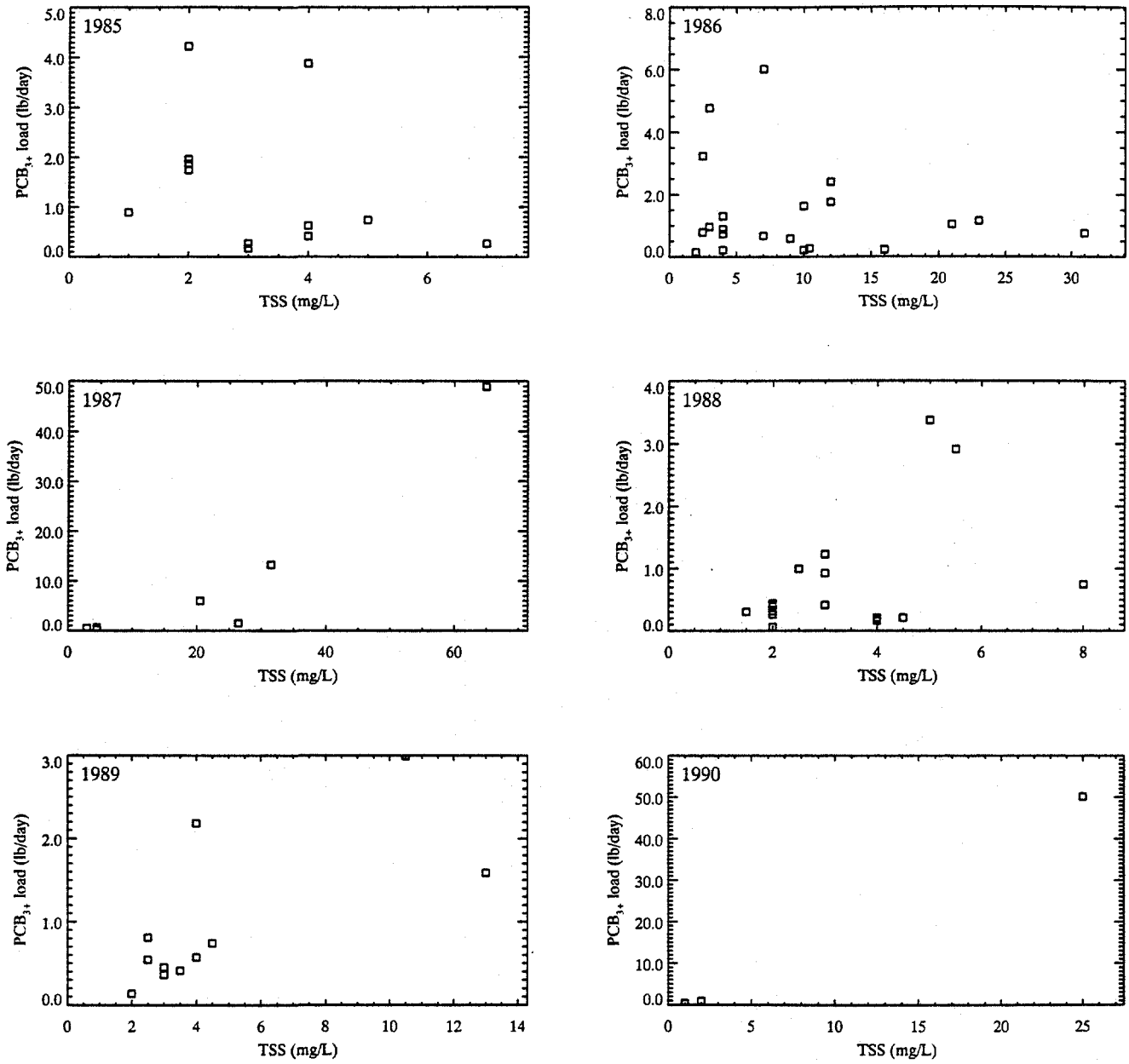

Figure 4-36b. PCB_{3+} load in relation to TSS at Fort Edward.

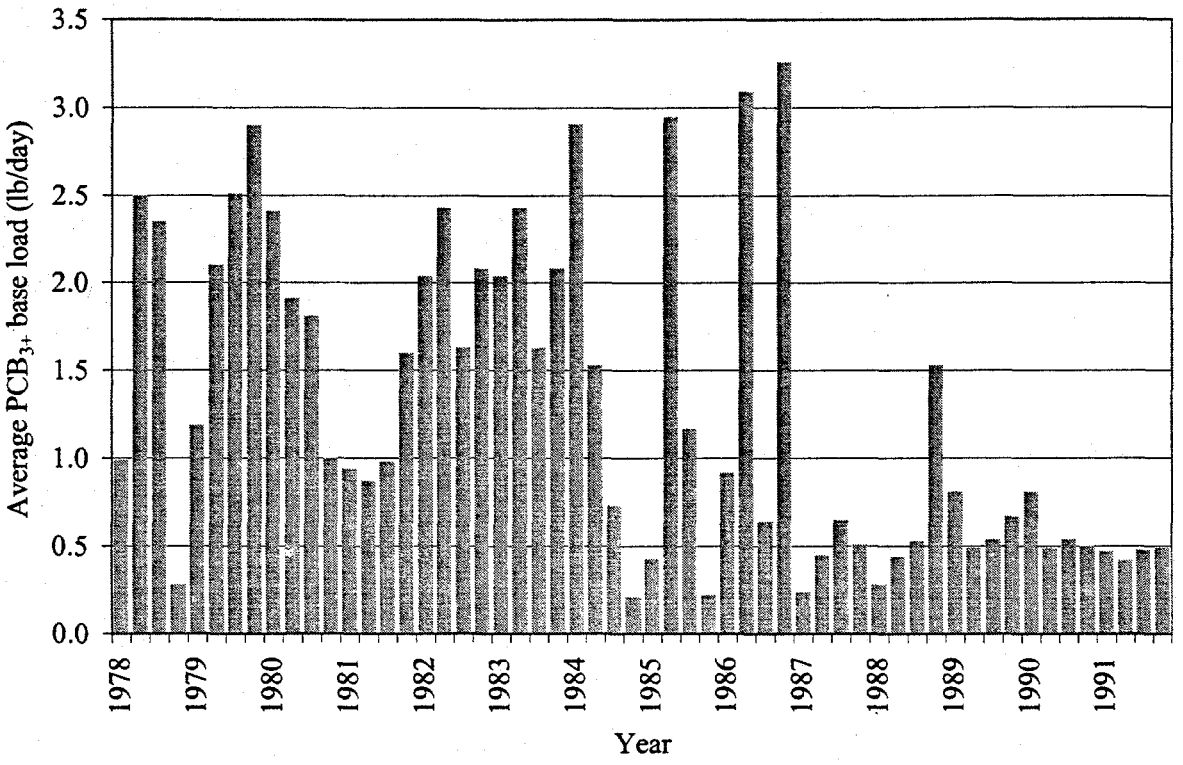

Note: Due to a high percentage of below detection limit values in 1983 and 1990, loads from 1982 and 1989 , respectively, were used in calculating averages.

Figure 4-37. Annual average base PCB_{3+} load (TSS ≤10 mg/L) passing Fort Edward.

\\poseidon\d_drive\genhud\documents\final_report\vol_2\section_4\fig4_37fe_quarter.xls

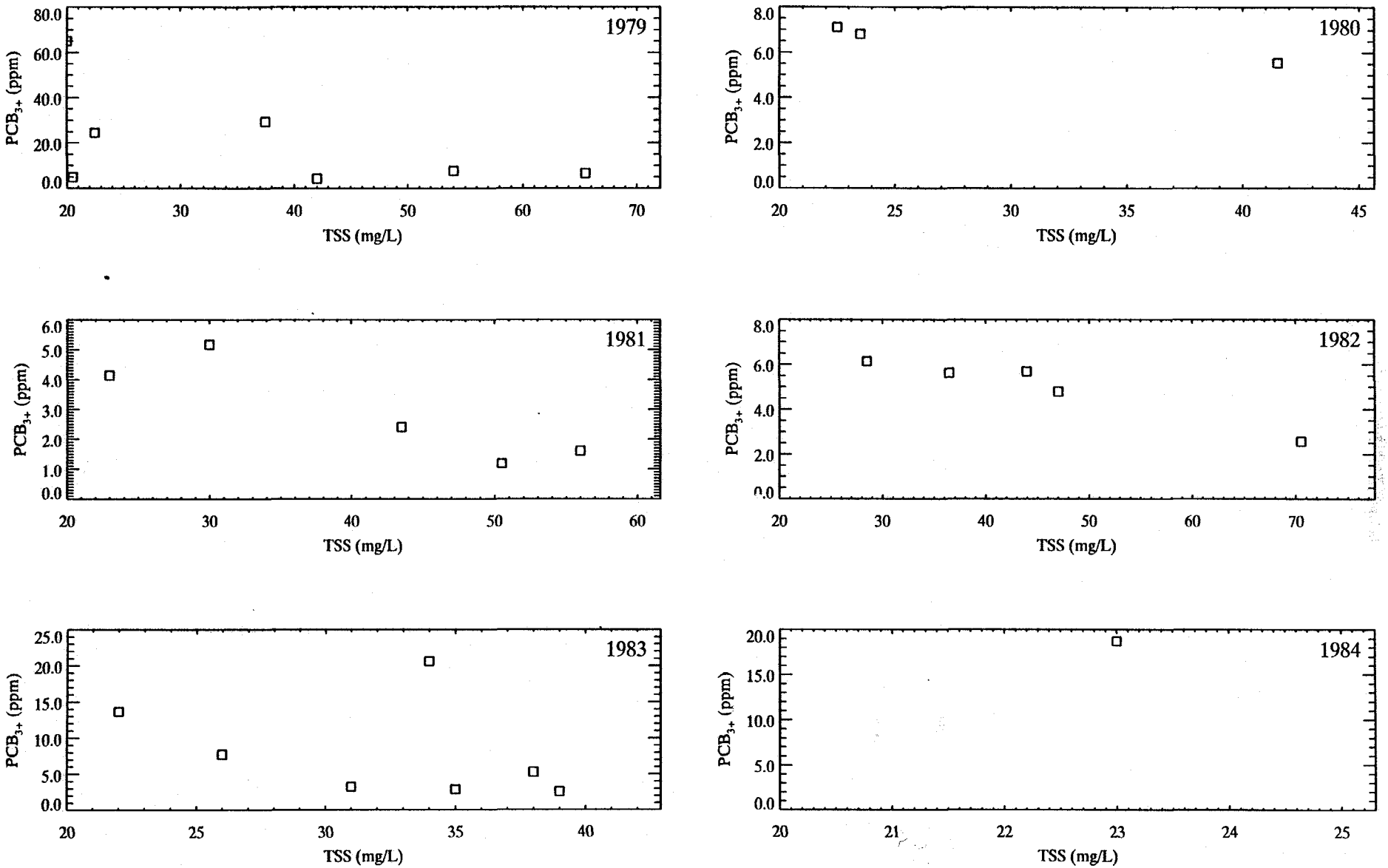

Figure 4-38a. PCB_{3+} concentration per unit TSS at Fort Edward in relation to TSS @ TSS > 20 mg/L.

313970

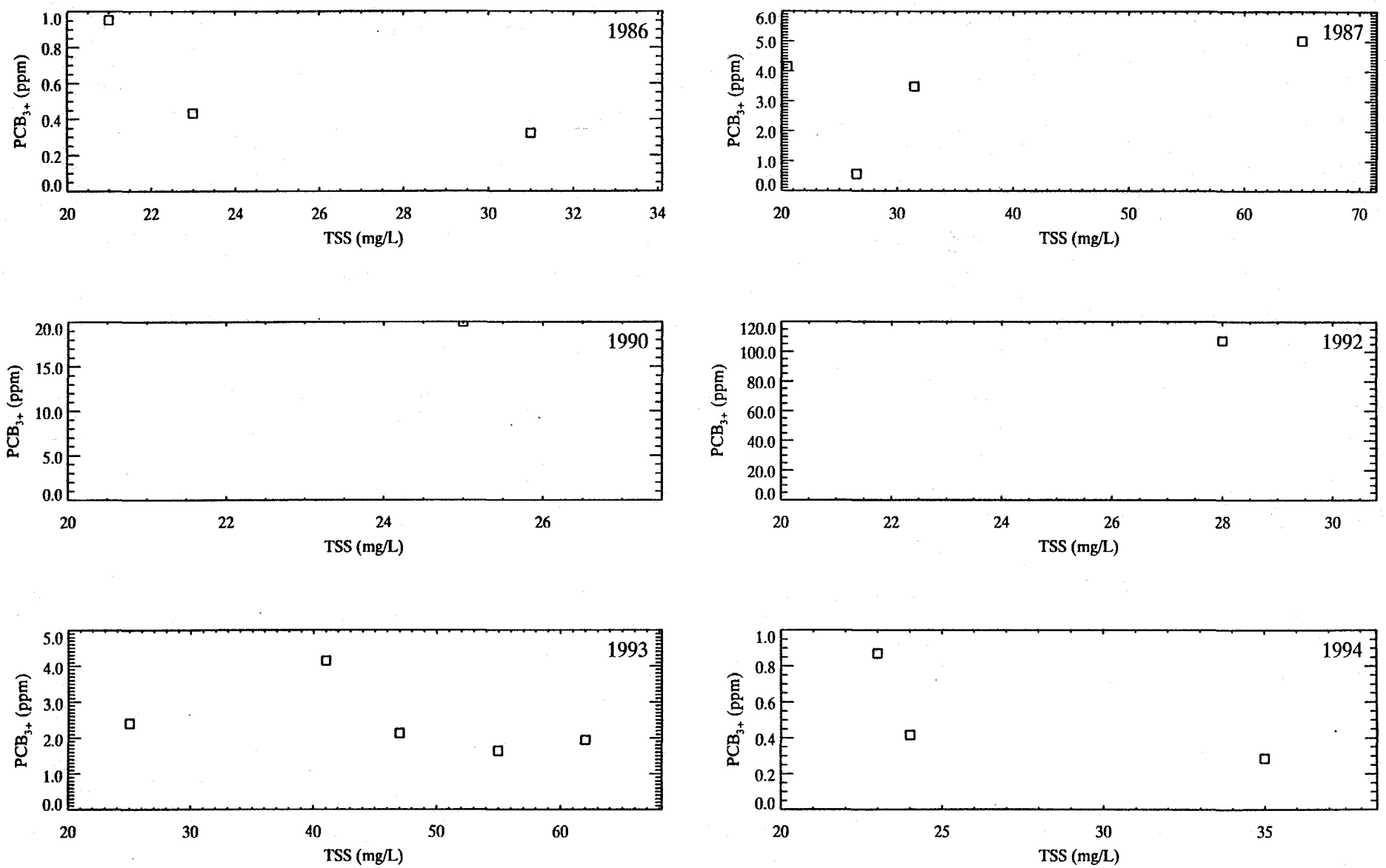

Figure 4-38b. PCB_{3+} concentration per unit TSS at Fort Edward in relation to TSS @ TSS > 20 mg/L.

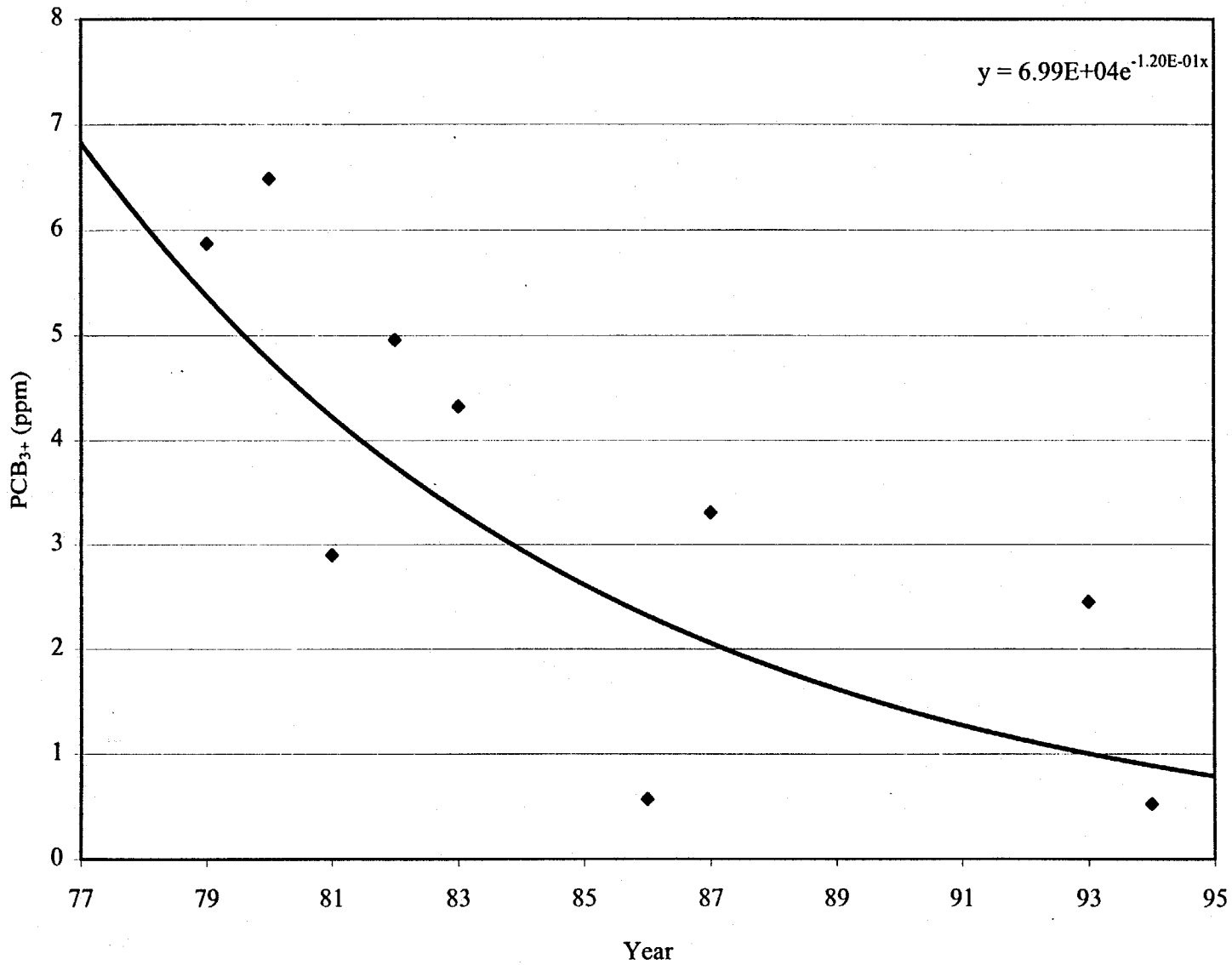

Figure 4-39. Annual average PCB_{3+} concentration per unit TSS. Regression equation used to determine estimated r for 1977-1989.

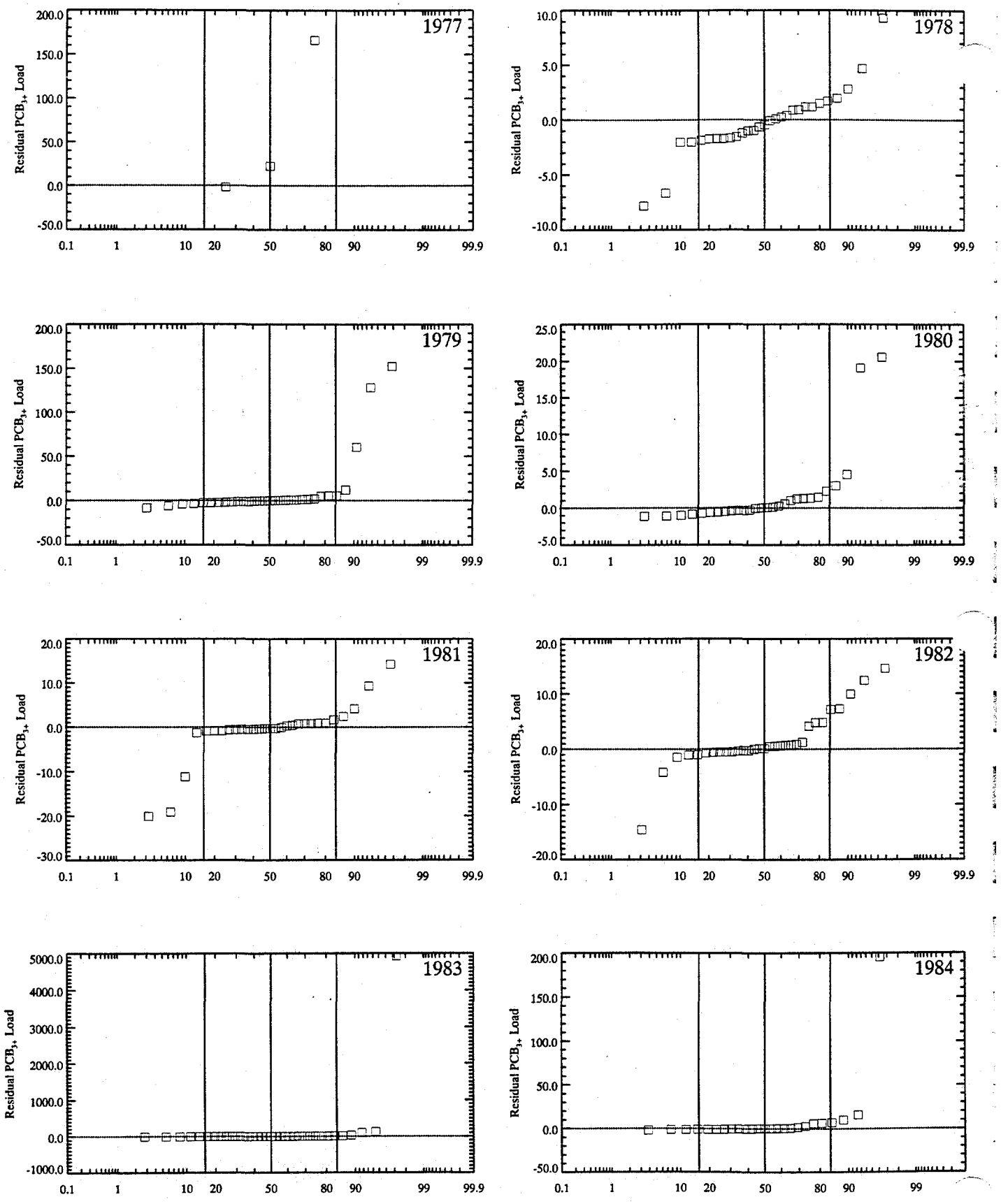

Figure 4-40a. Probability distributions of residual PCB_{3+} load at Fort Edward.

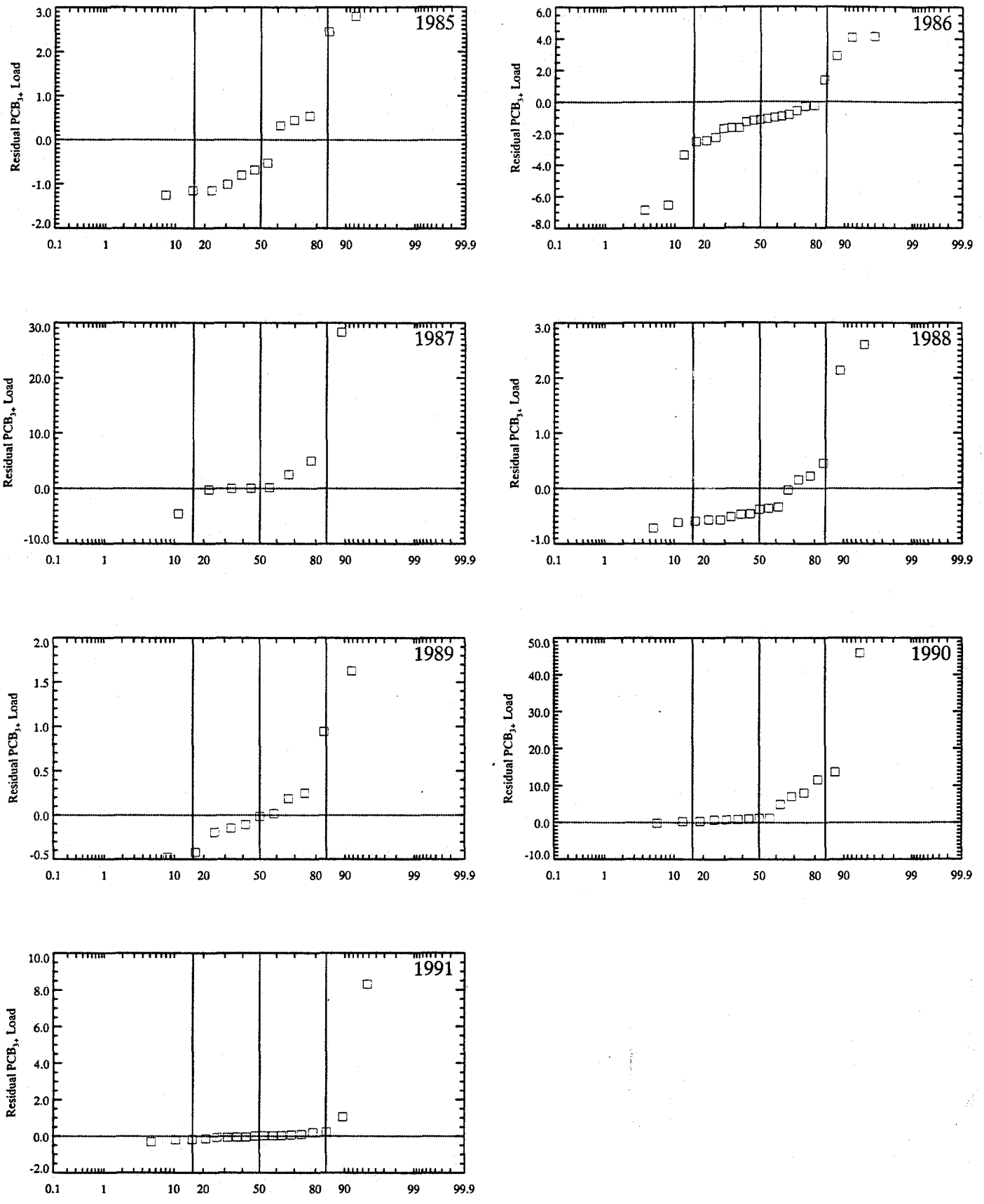

Figure 4-40b. Probability distributions of residual PCB_{3+} load at Fort Edward.

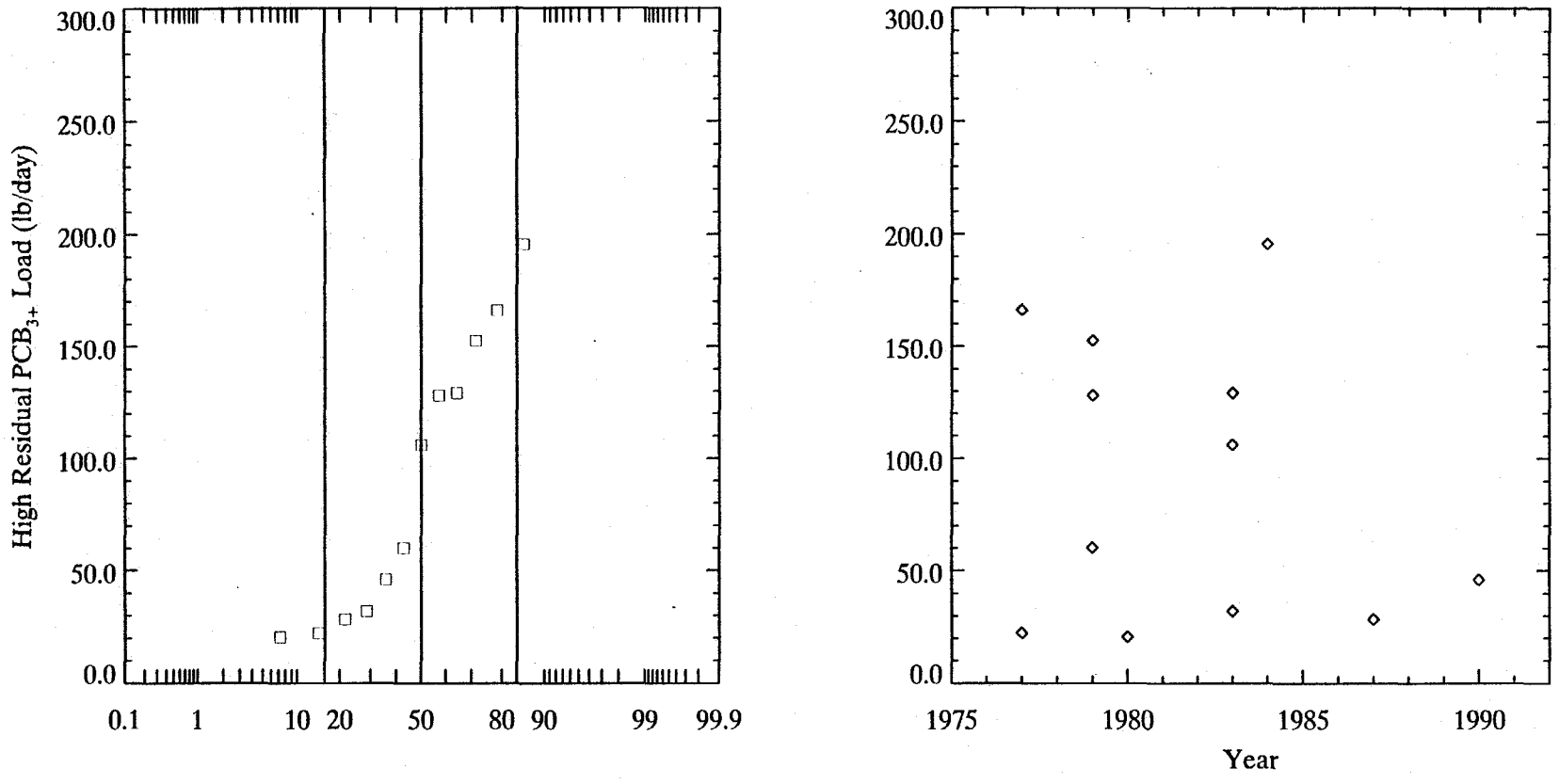

Note: High residual load of ~4900 lb/day not shown on these plots.

Figure 4-41. Probability distribution and chronological plot of anomalously high PCB_{3+} loadings at Fort Edward.

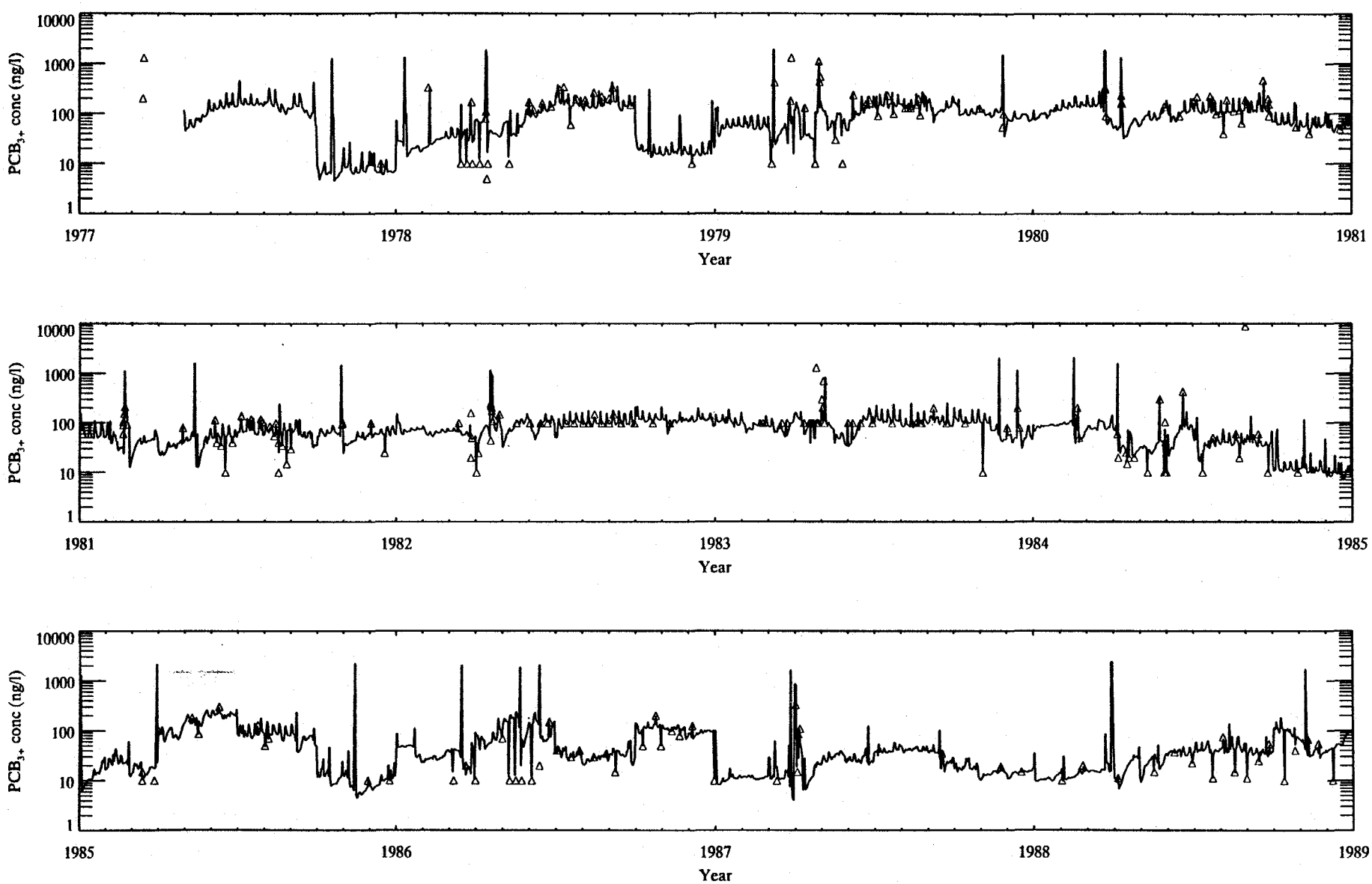

Figure 4-42a. Water column PCB_{3+} concentrations measured (symbols) at the upstream boundary of the model (line) at Fort Edward and the continuous concentration function used in the model.

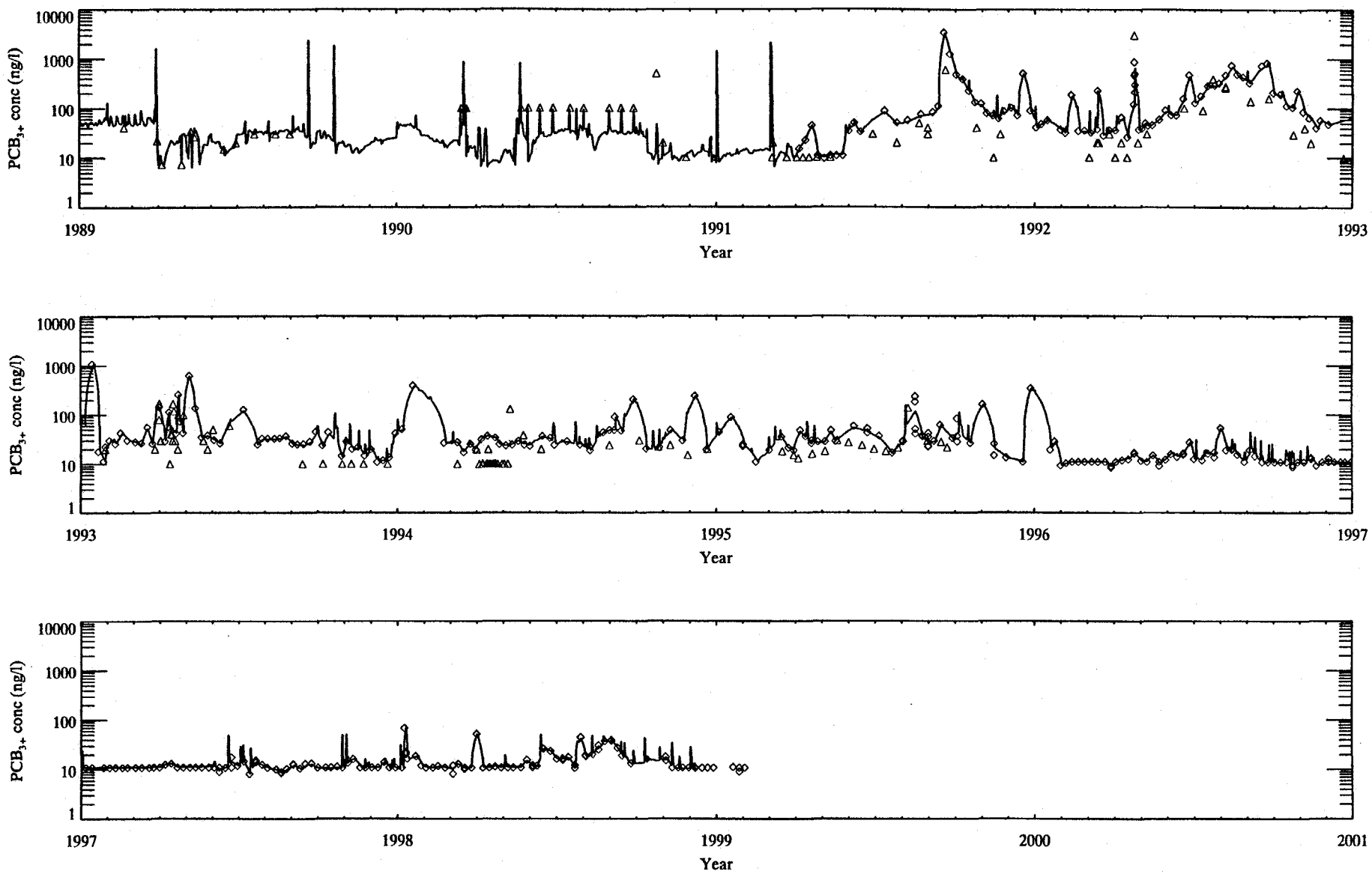

Figure 4-42b. Water column PCB_{3+} concentrations measured (symbols) at the upstream boundary of the model (line) at Fort Edward and the continuous concentration function used in the model.

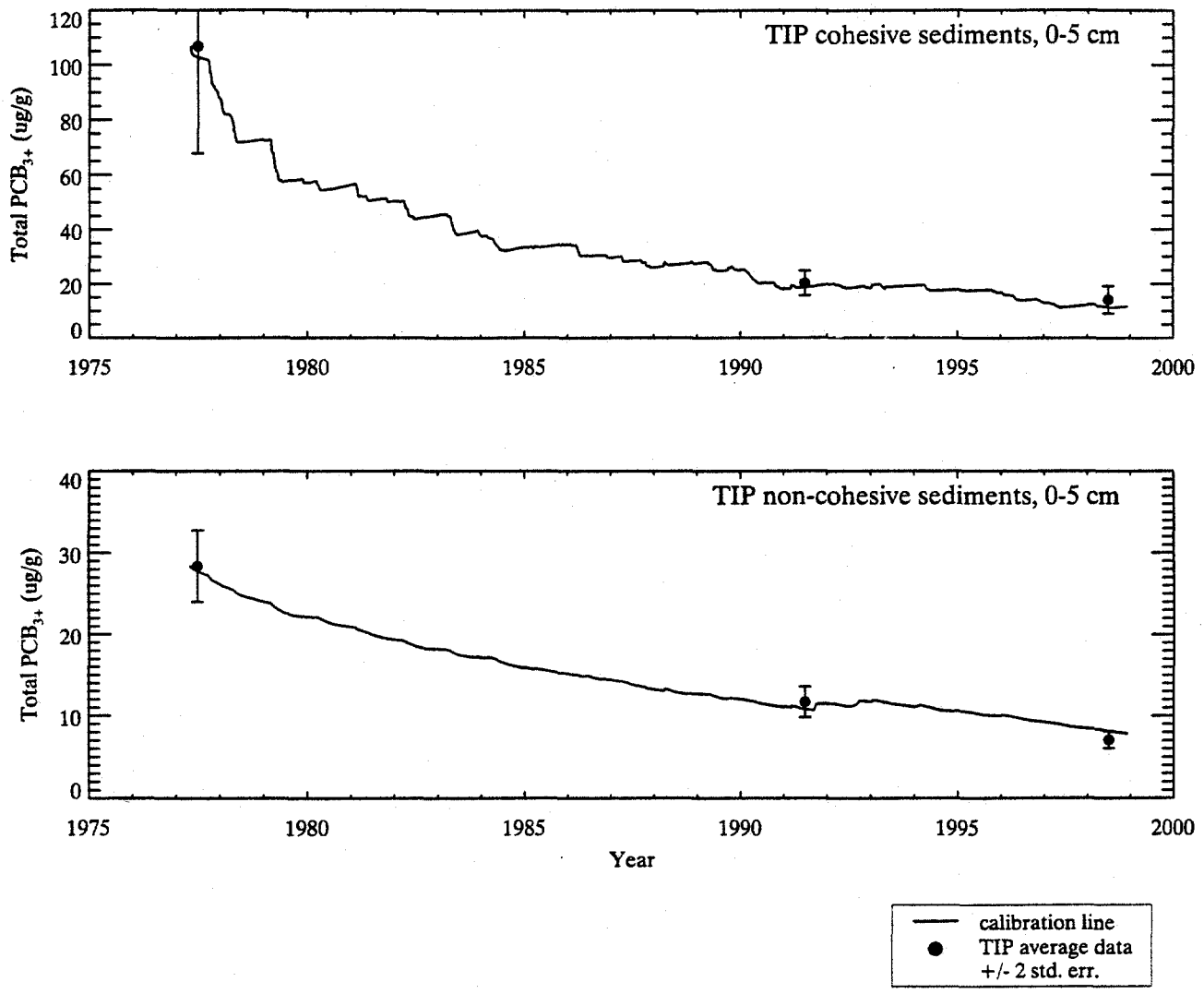

Figure 4-43. Predicted (line) and measured (symbols) average PCB_{3+} concentrations in surface sediments of the TIP using bounding calibration.

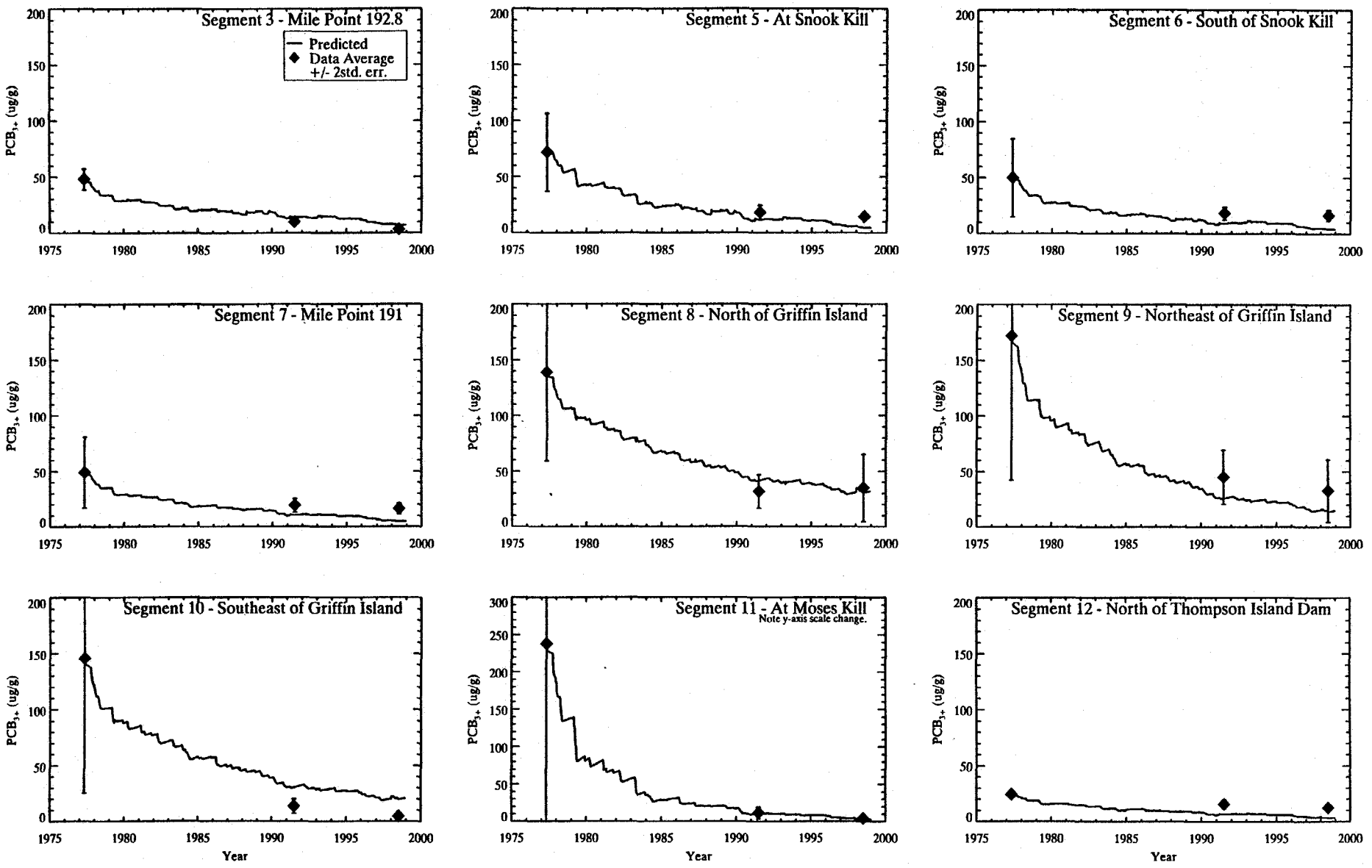

Figure 4-44. Data (symbols) to model (line) comparison of 0-5 cm cohesive surface PCB_{3+} sediment concentrations at nine select model segments in the TIP.

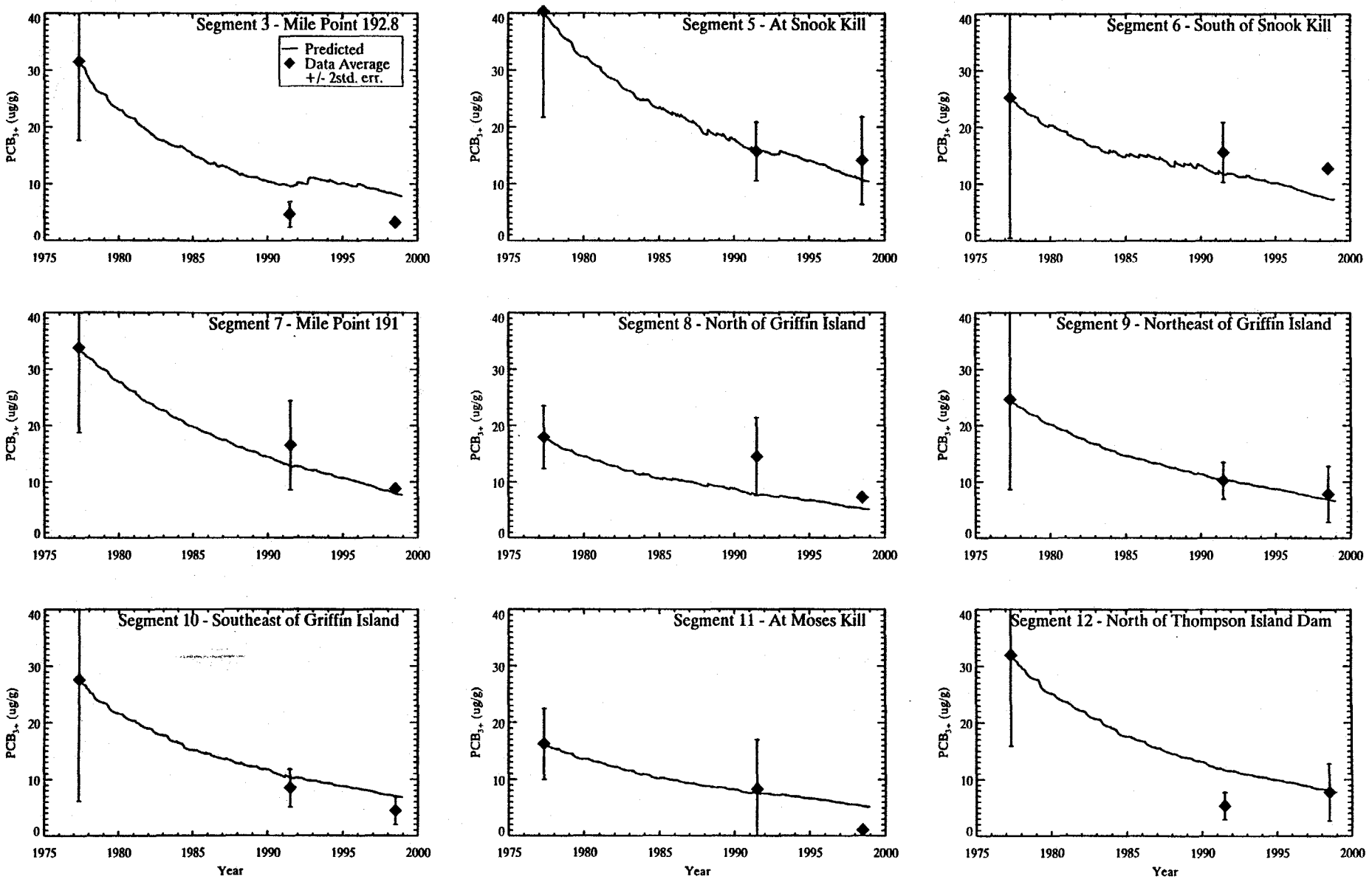

313980

Figure 4-45. Data (symbols) to model (line) comparison of 0-5 cm non-cohesive surface PCB_{3+} sediment concentrations at nine select model segments in the TIP.

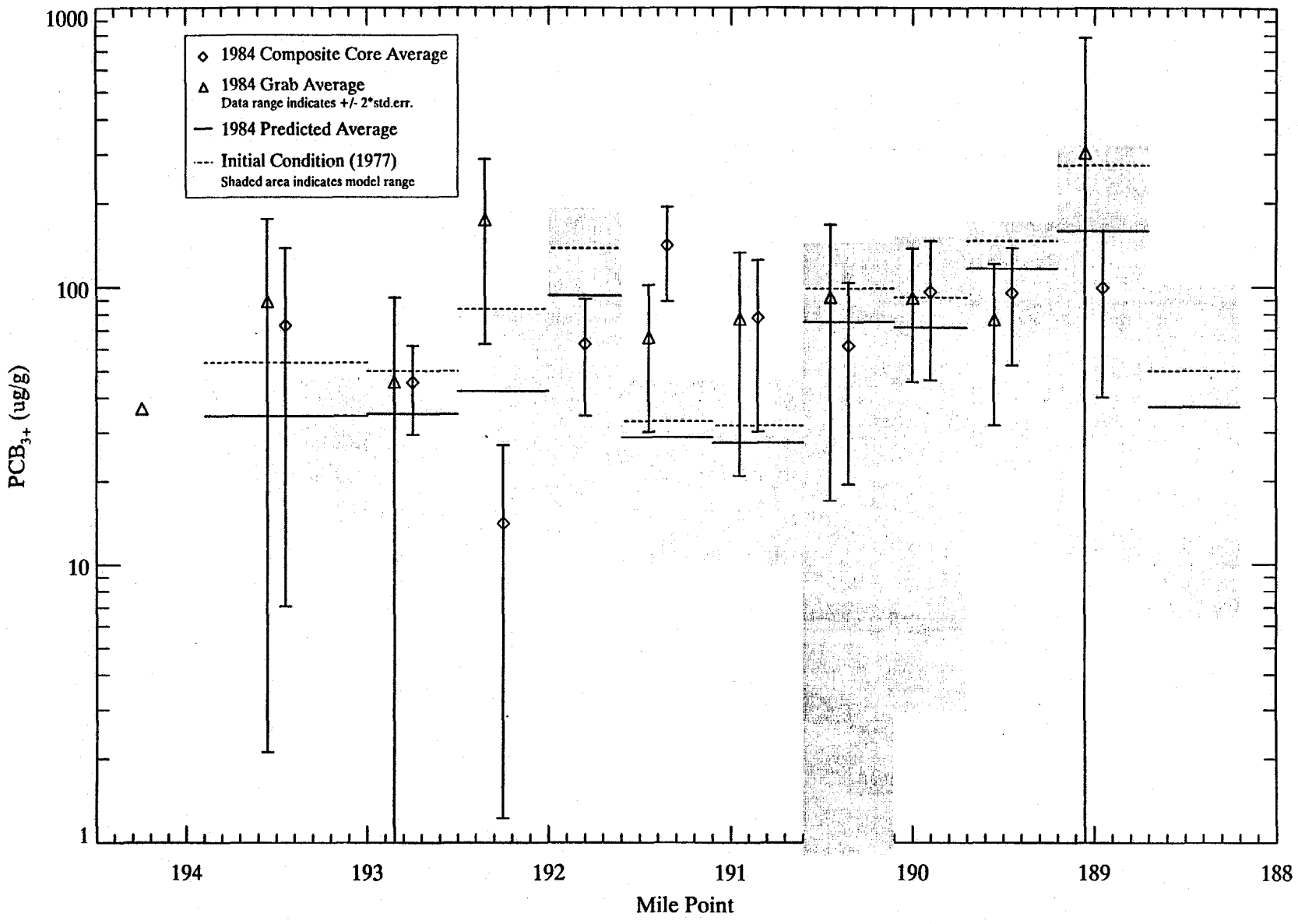

Note: 1977 levels used as initial conditions in the model are shown as dashed lines for comparison to the 1984 levels.

Figure 4-46. Spatial pattern of 0-25 cm cohesive sediment PCB_{3+} concentrations calculated by the model (lines) and measured (symbols) in 1984.

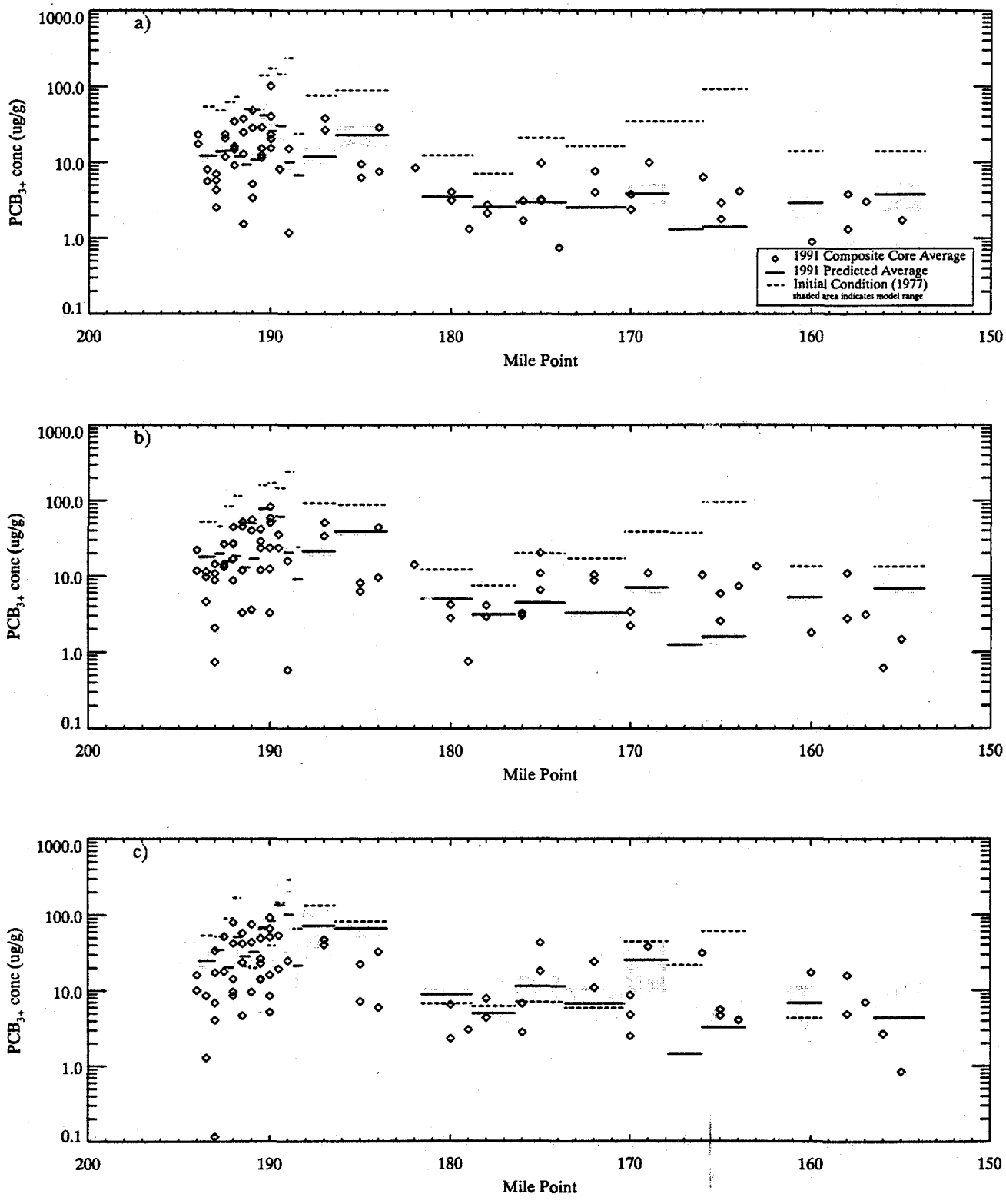

Note: 1977 levels used as initial conditions in the model are shown as dashed lines for comparison to the 1991 levels.

Figure 4-47. Spatial pattern of a) 0-5 cm, b) 5-10 cm, and c) 10-25 cm cohesive sediment PCB_{3+} concentrations calculated by the model (solid lines) and measured (symbols) in 1991.

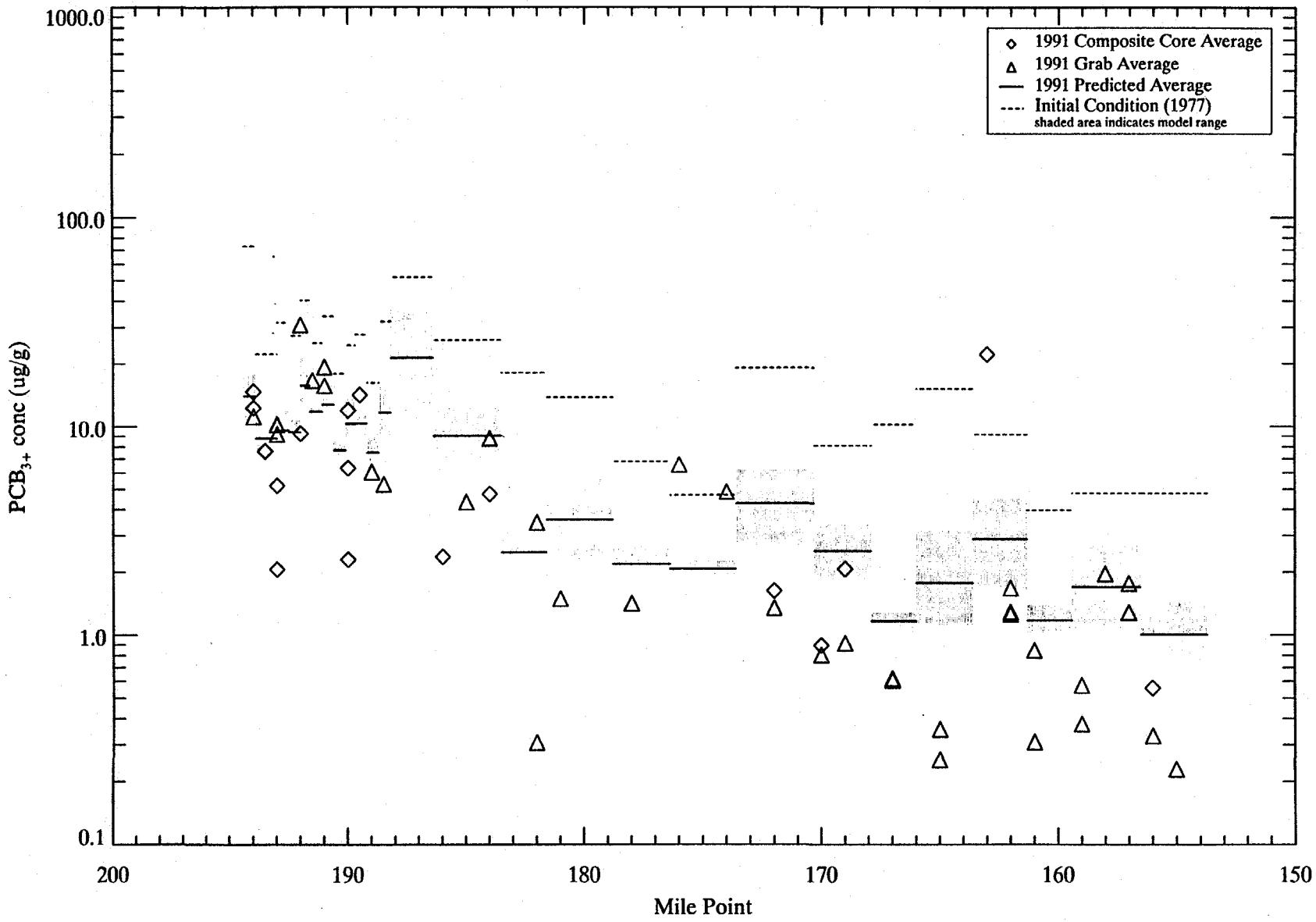

Note: 1977 levels used as initial conditions in the model are shown as dashed lines for comparison to the 1991 levels.

Figure 4-48. Spatial pattern of 0-5 cm non-cohesive sediment PCB_{3+} concentrations calculated by the model (solid lines) and measured (symbols) in 1991.

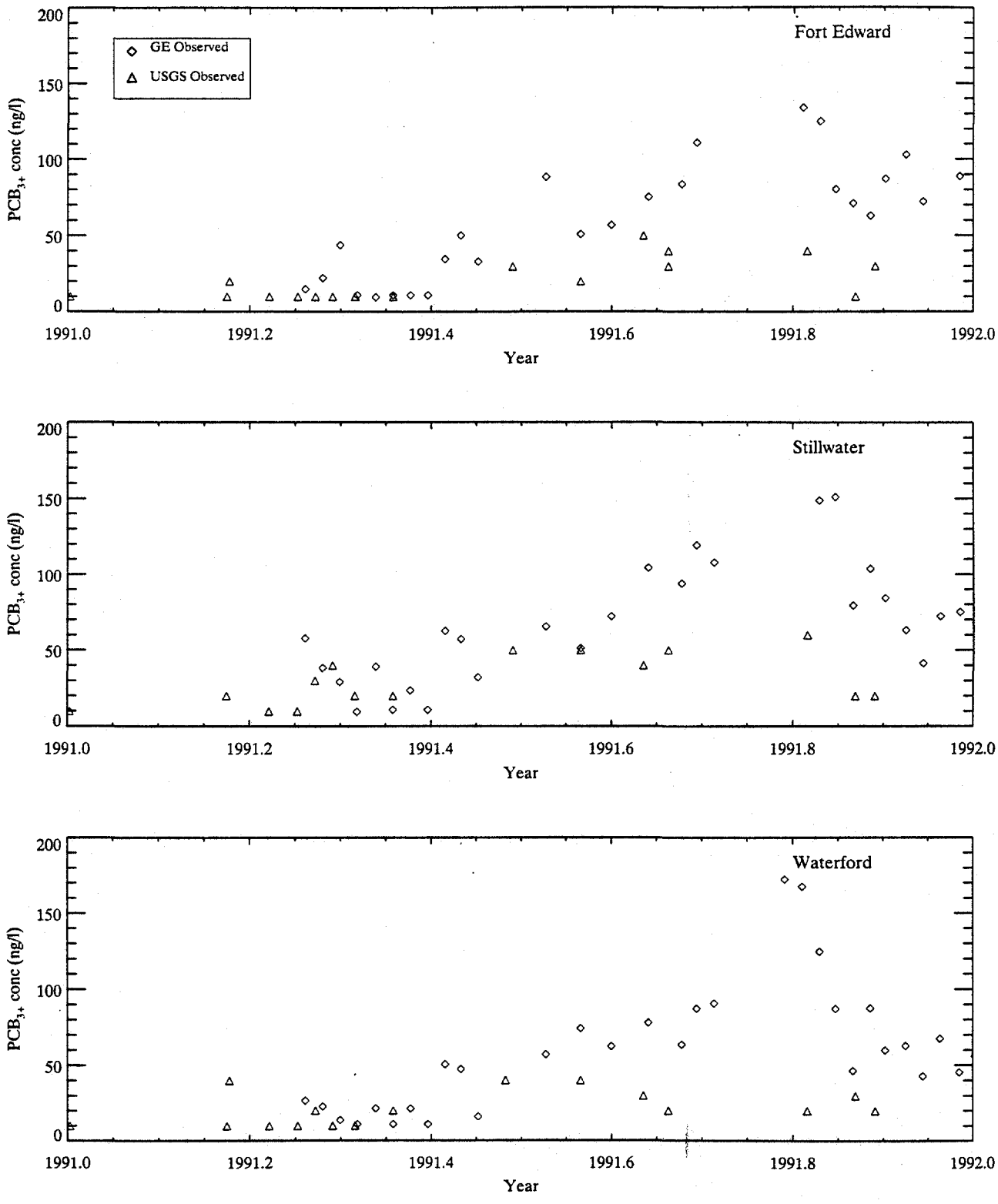

Figure 4-49. Comparison of observed water column PCB_{3+} measured by GE and USGS at Fort Edward, Stillwater, and Waterford.

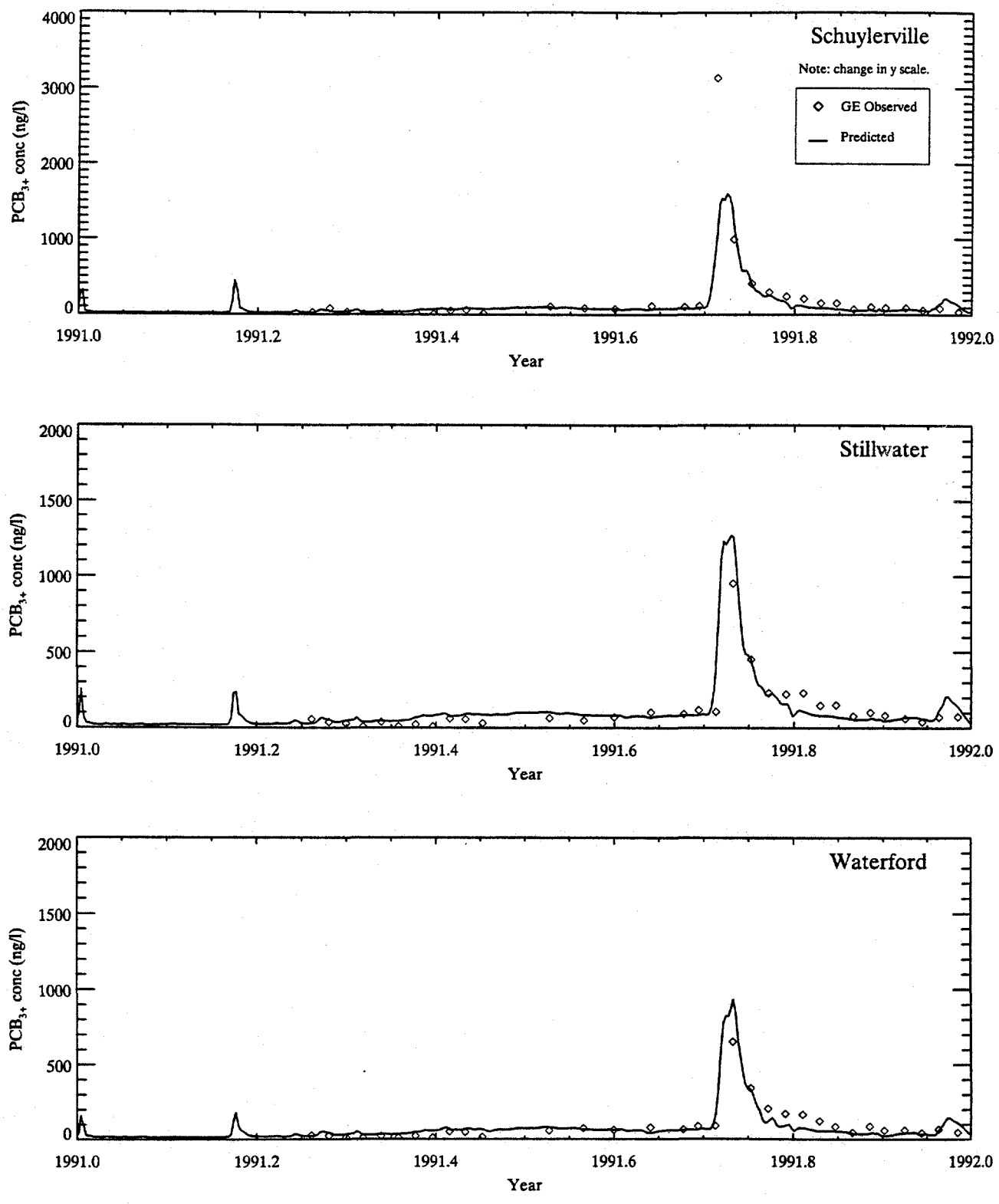

Figure 4-50. Comparison of predicted (lines) and measured (symbols) water column PCB_{3+} at Schuylerville, Stillwater, and Waterford.

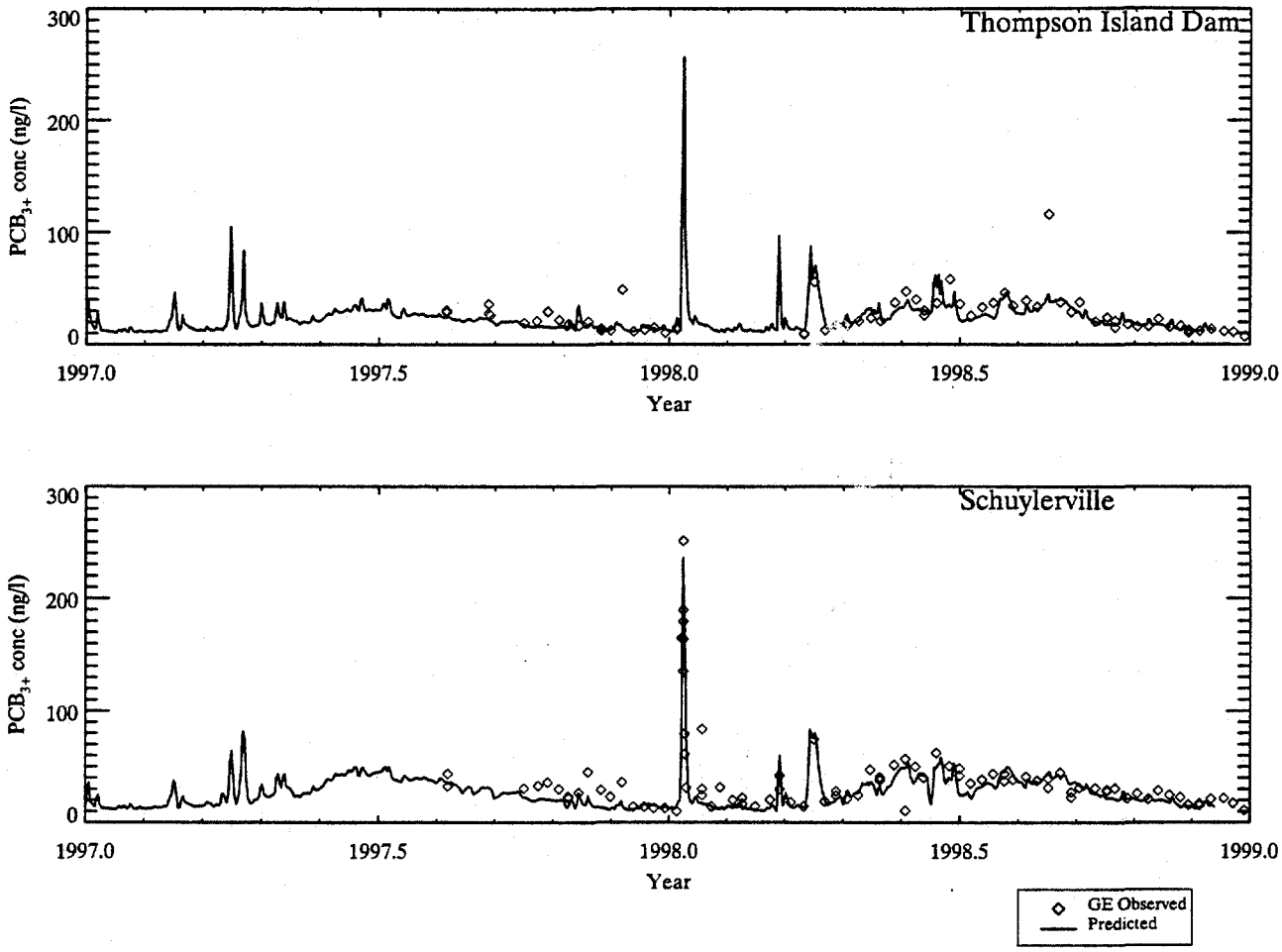

Figure 4-51. Comparison of predicted (line) using bounding calibration and measured (symbols) water column PCB_{3+} concentrations at Schuylerville and the Thompson Island Dam.

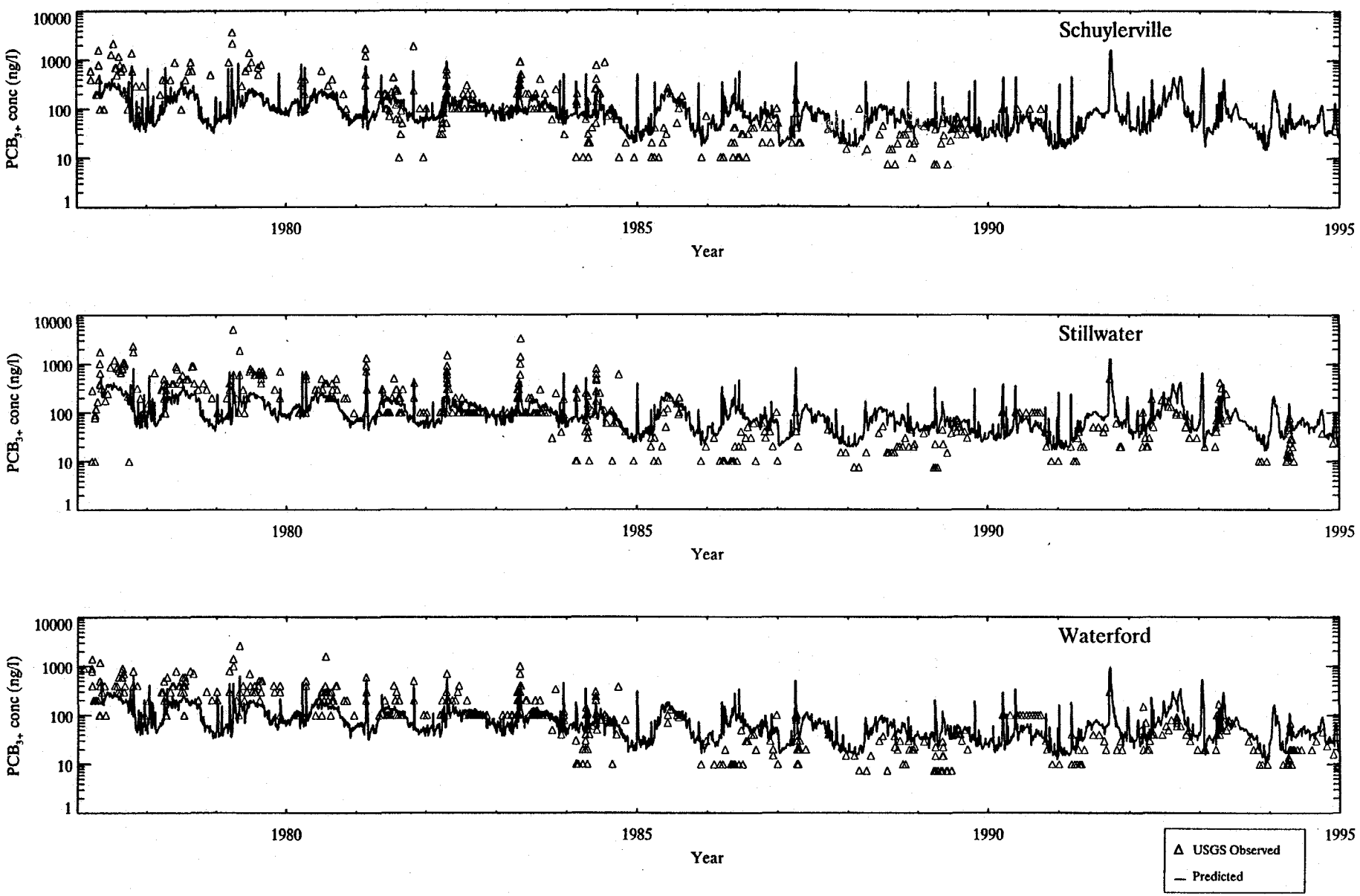

Figure 4-52. Comparison of predicted (line) and USGS measured (symbols) water column PCB_{3+} concentration at Schuylerville, Stillwater, and Waterford
for 1977 through 1994.

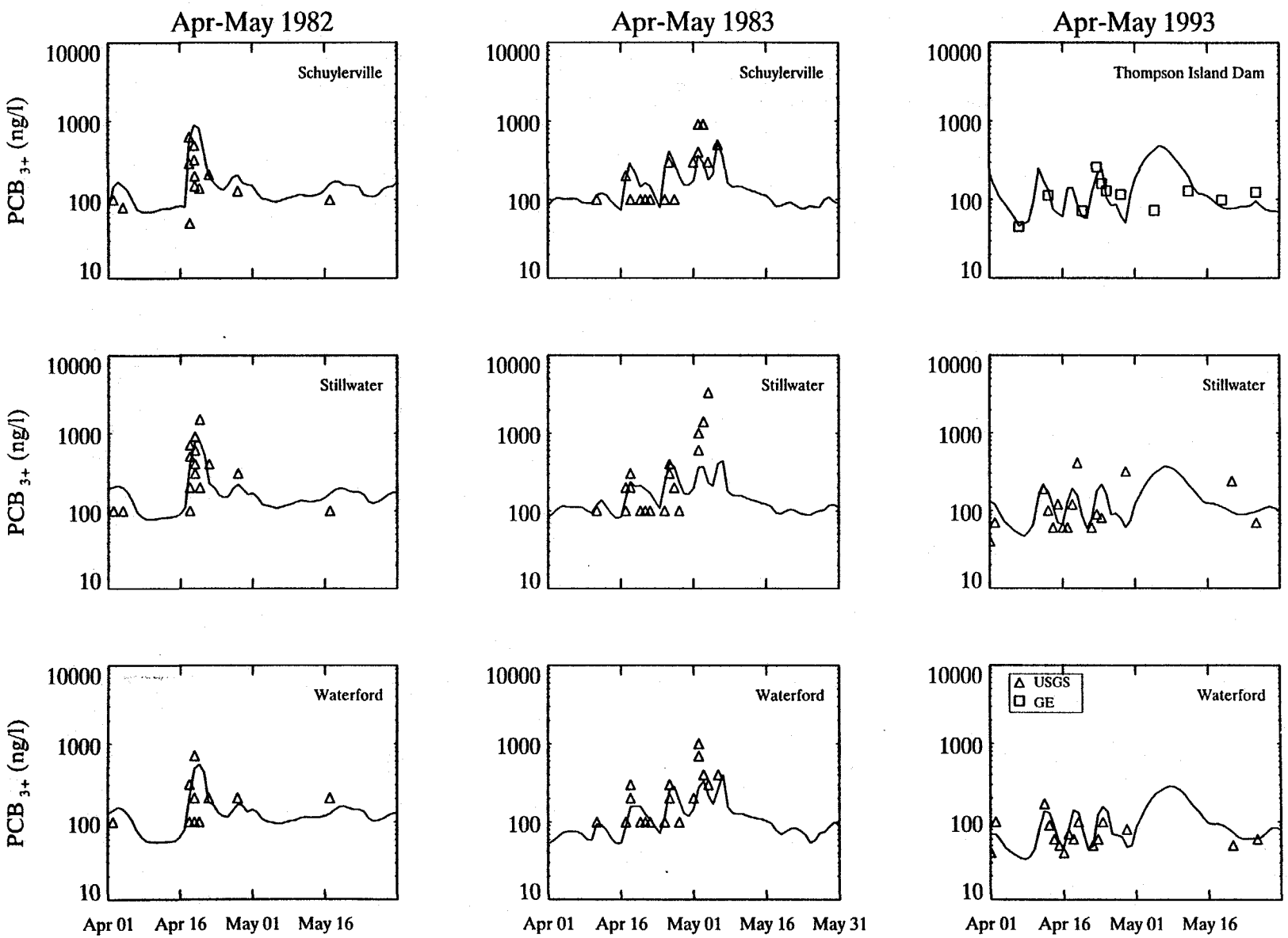

Figure 4-53. Comparison of predicted (lines) and measured (symbols) water column PCB_{3+} concentrations during three representative high flow periods.

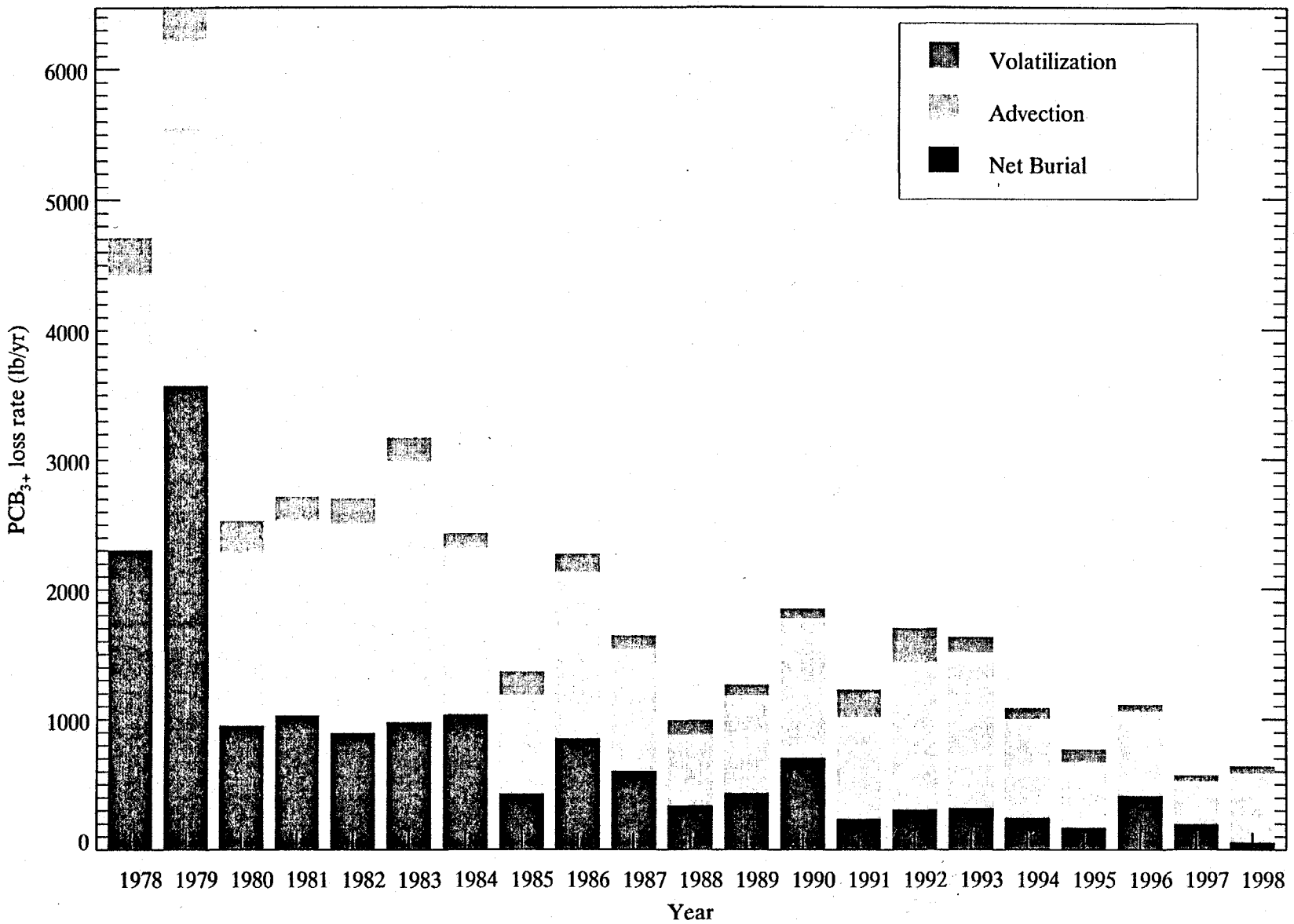

Figure 4-54. Hudson River PCB_{3+} loss mechanisms.

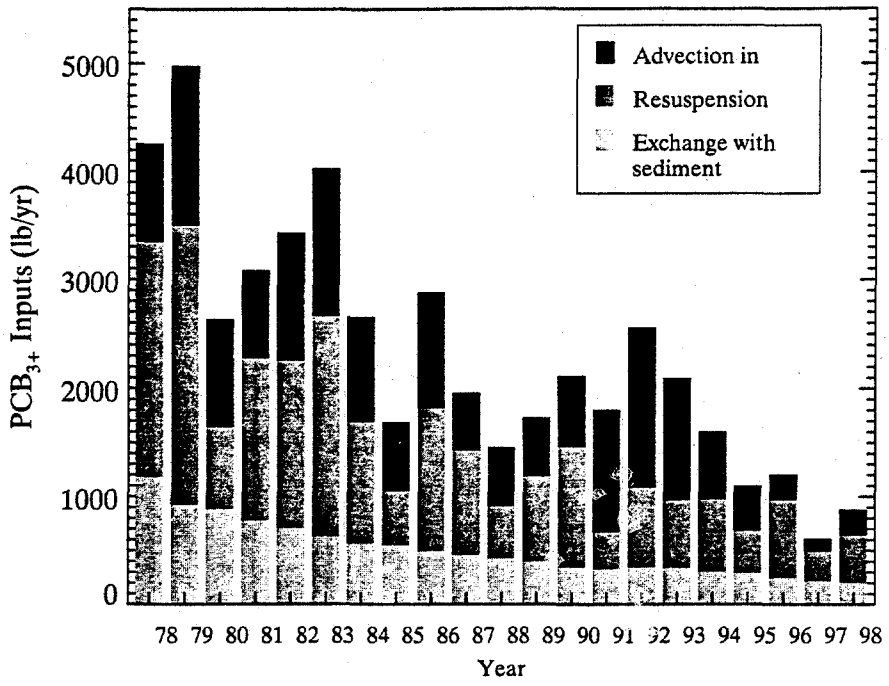

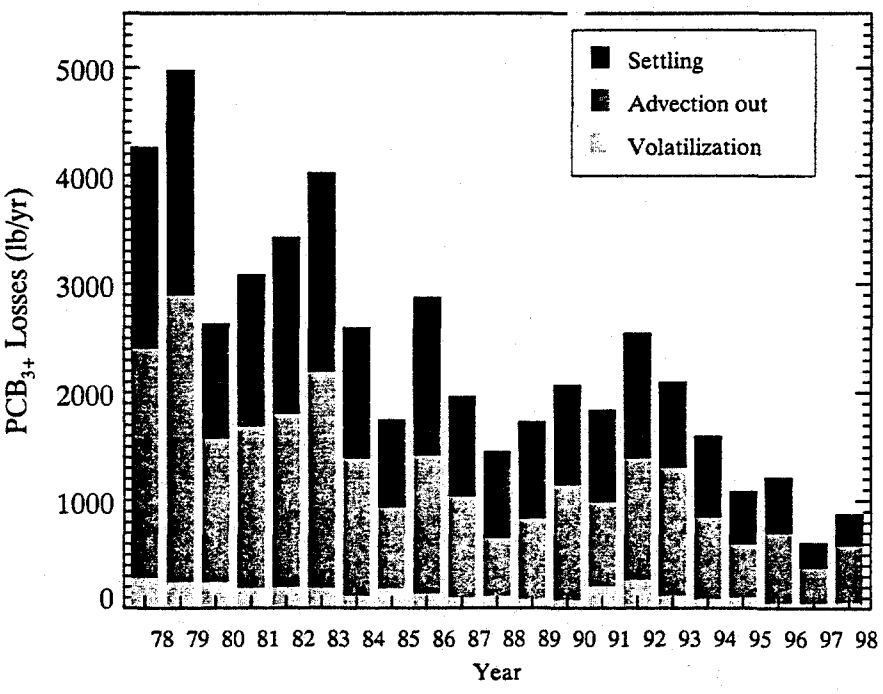

Figure 4-55. Water column PCB_{3+} sources and sinks.

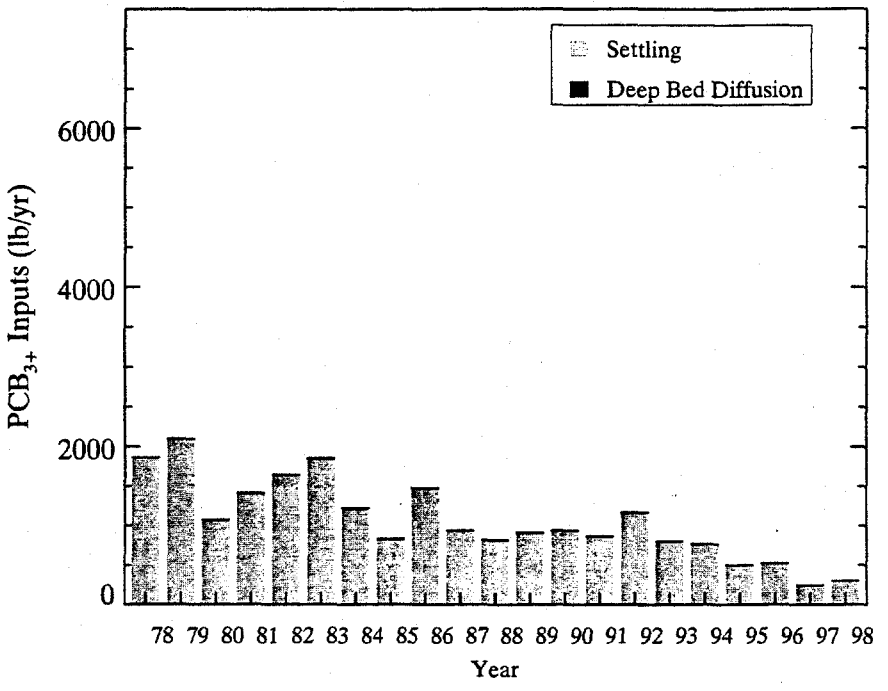

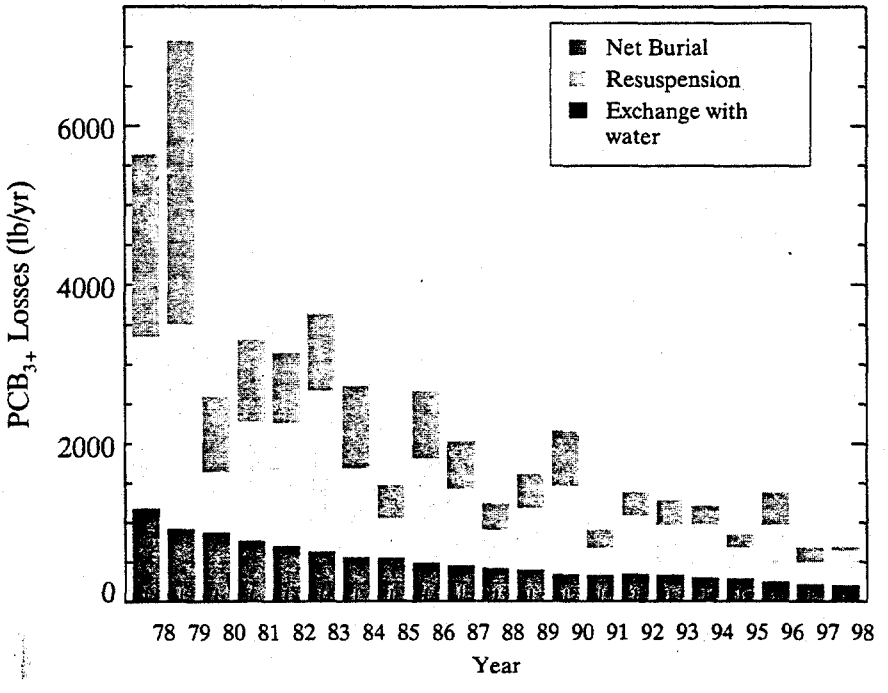

Figure 4-56. Sediment PCB $_{3+}$ sources and sinks.

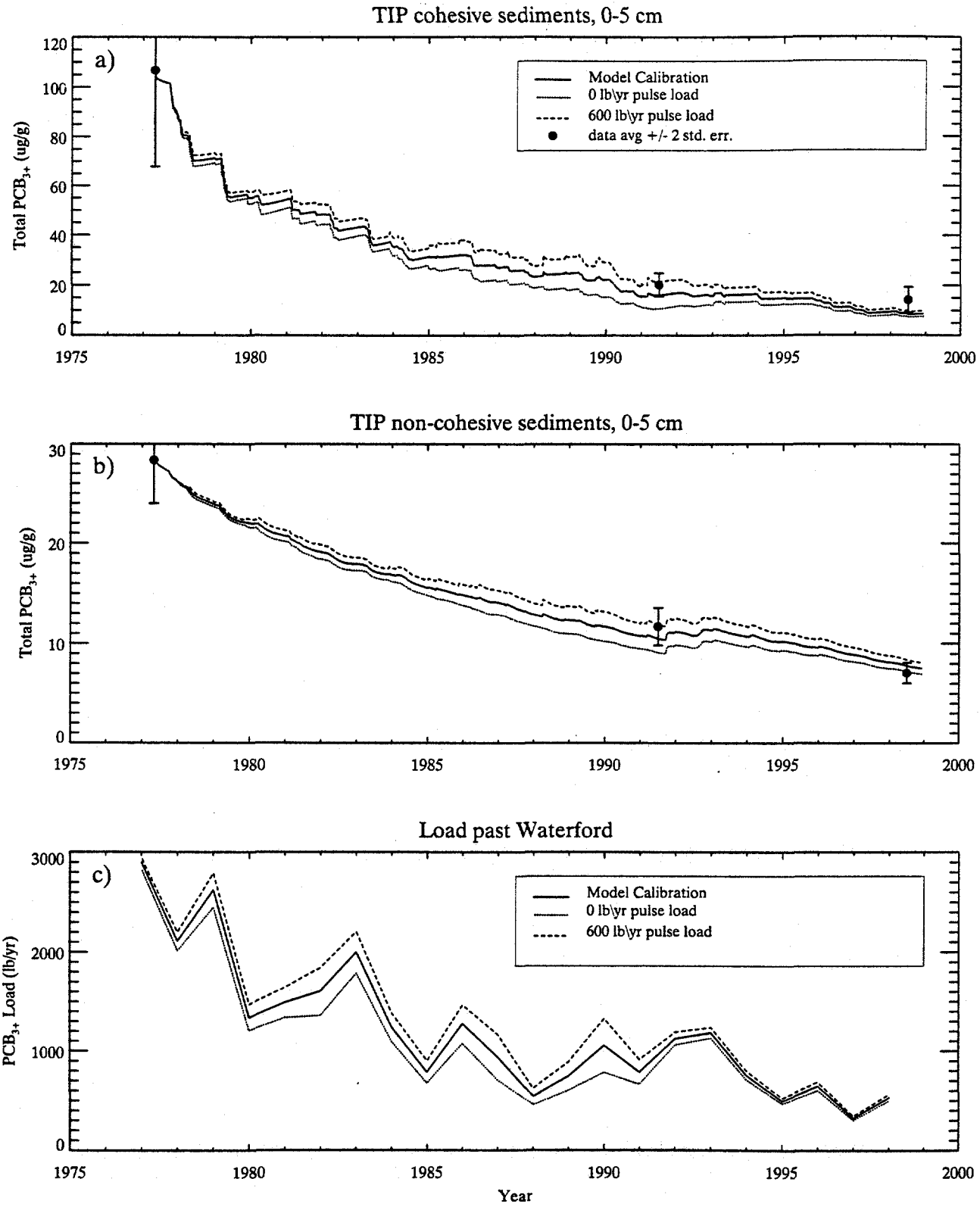

Figure 4-57. Comparison of average observed 0-5 cm cohesive and non-cohesive sediment PCB_{3+} concentration in the TIP and the load past Waterford with concentrations computed using alternate magnitudes of pulse loading.

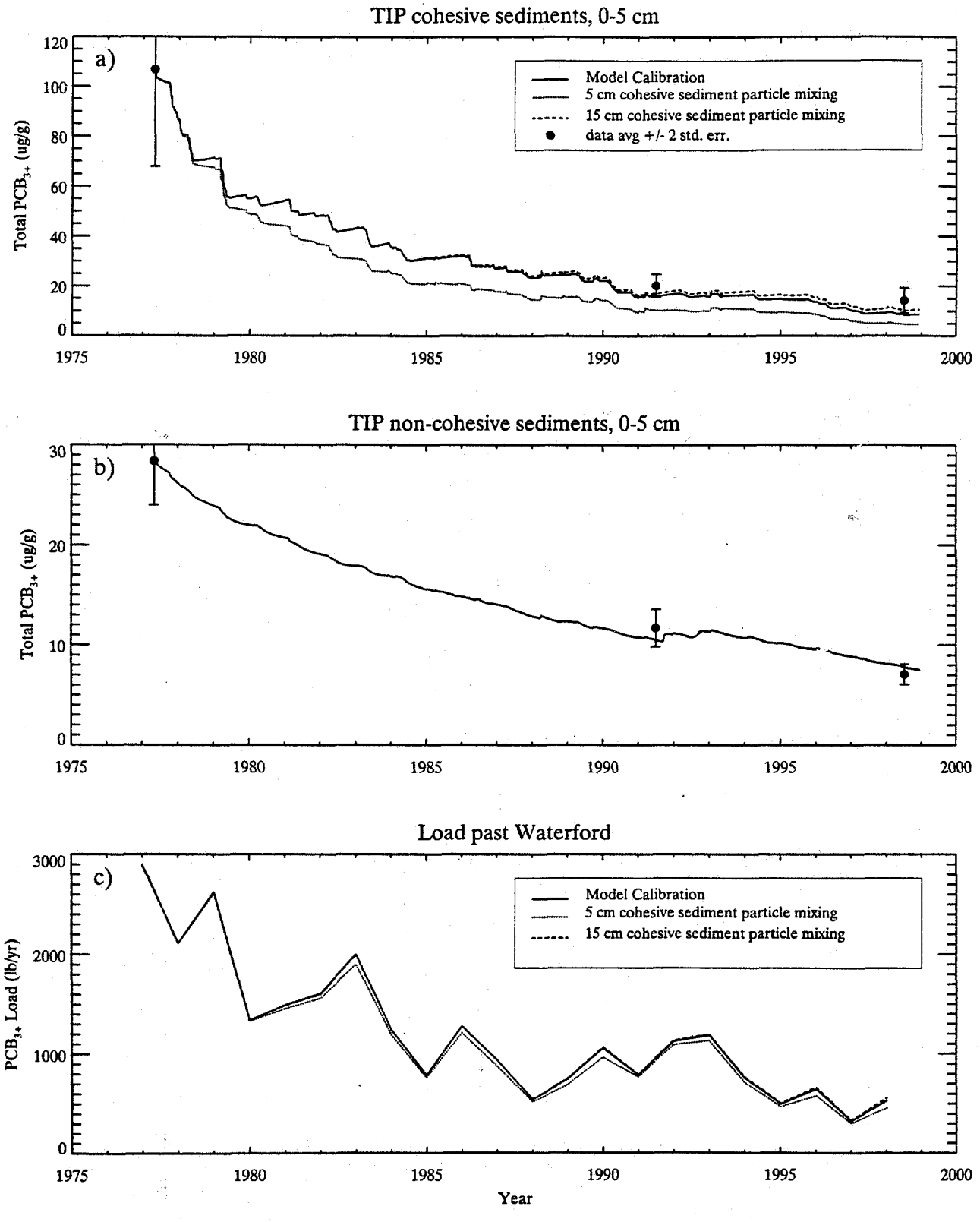

Figure 4-58. Comparison of average observed 0-5 cm cohesive and non-cohesive sediment PCB_{3+} concentration in the TIP and the load past Waterford with concentrations computed using alternate depths of particle mixing in cohesive sediments.

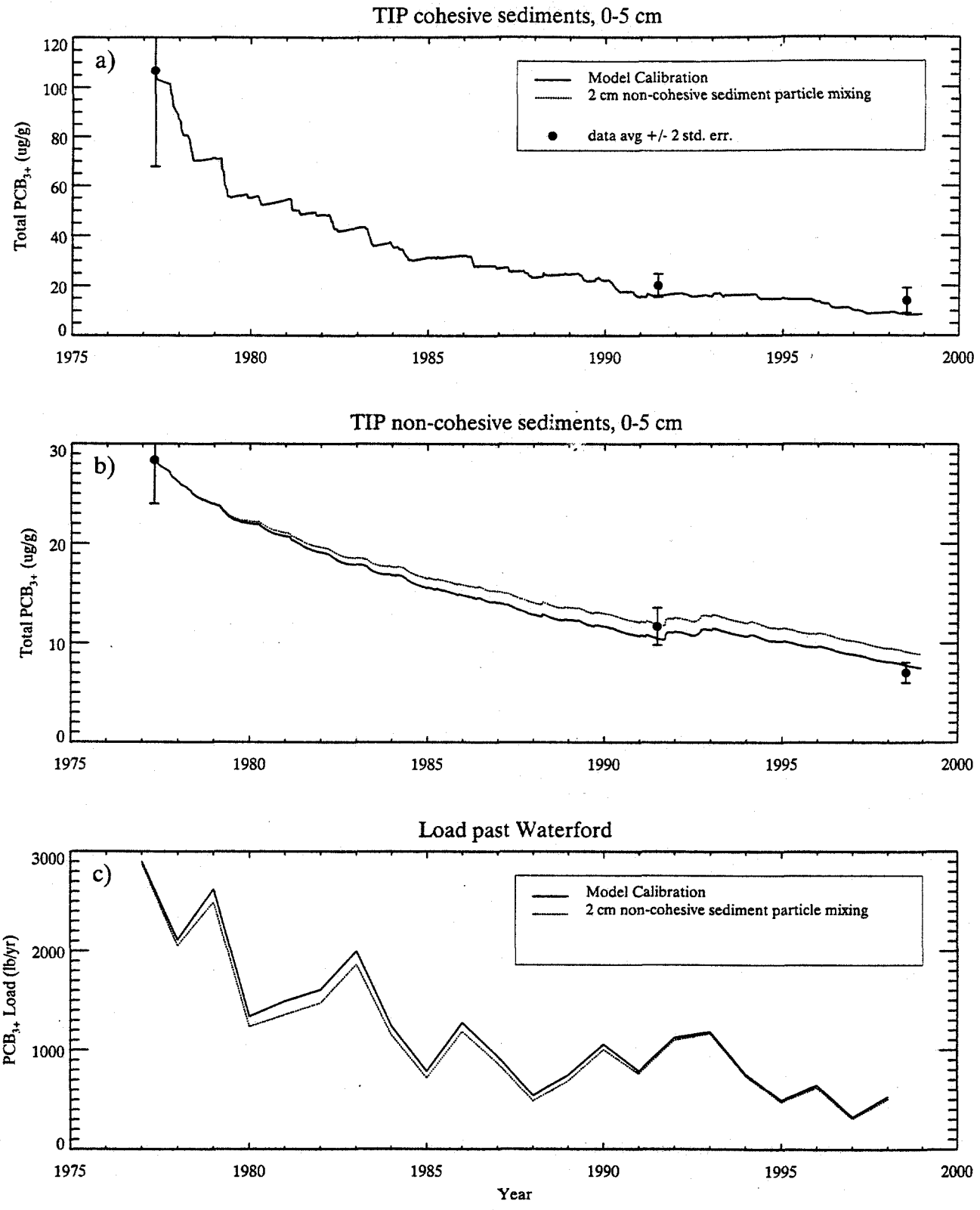

Figure 4-59. Comparison of average observed 0-5 cm cohesive and non-cohesive sediment PCB_{3+} concentration in the TIP and the load past Waterford with concentrations computed using alternate depths of particle mixing in non-cohesive sediments.

da - \\Poseidon\D_Drive\GENhud\Documents\Final_report\Vol_2\Section_4\fig4_57_66sens.pro
Tue Apr 13 13:52:21 1999

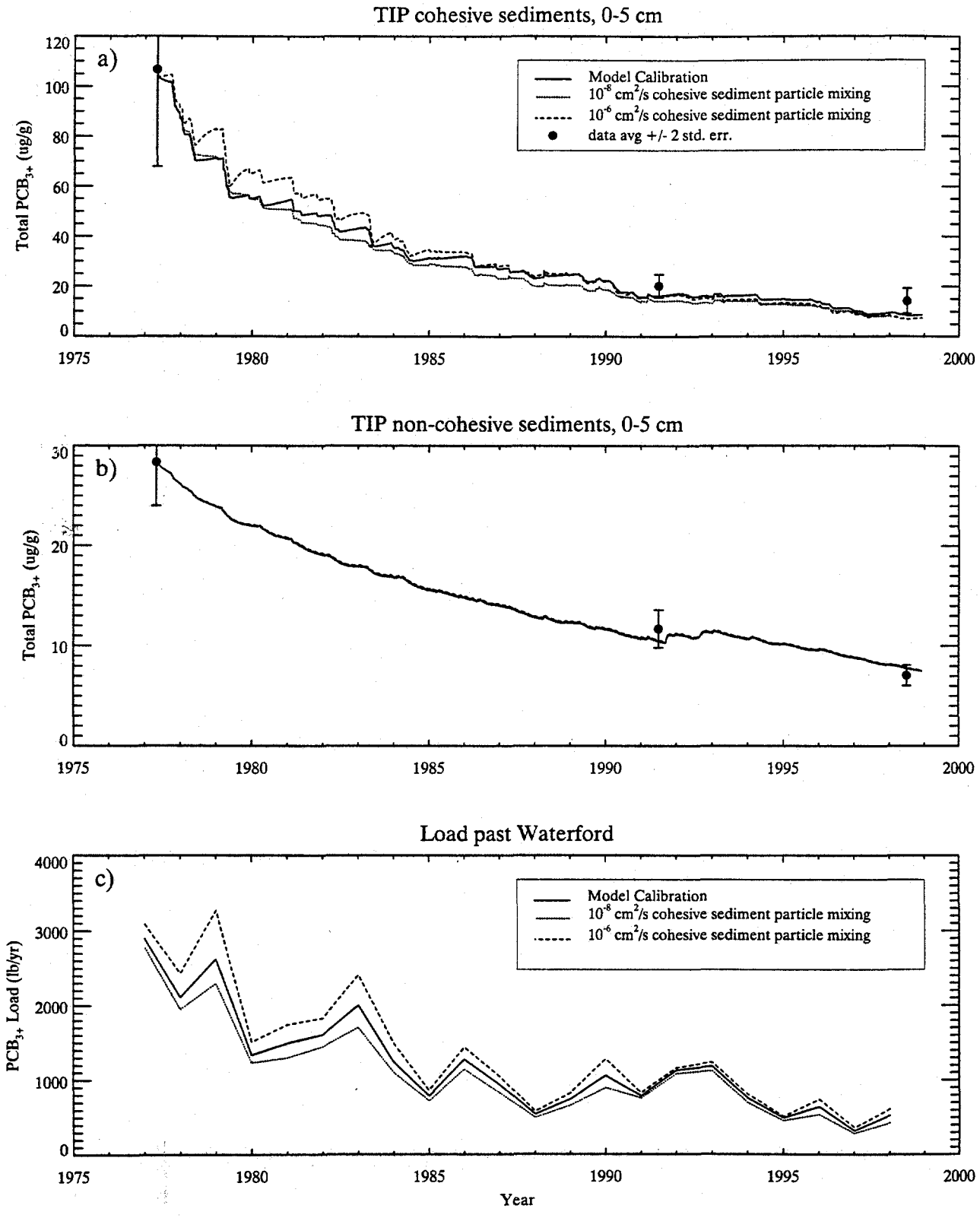

Figure 4-60. Comparison of average observed 0-5 cm cohesive and non-cohesive sediment PCB_{3+} concentration in the TIP and the load past Waterford with concentrations computed using alternate magnitudes of particle mixing in cohesive sediments

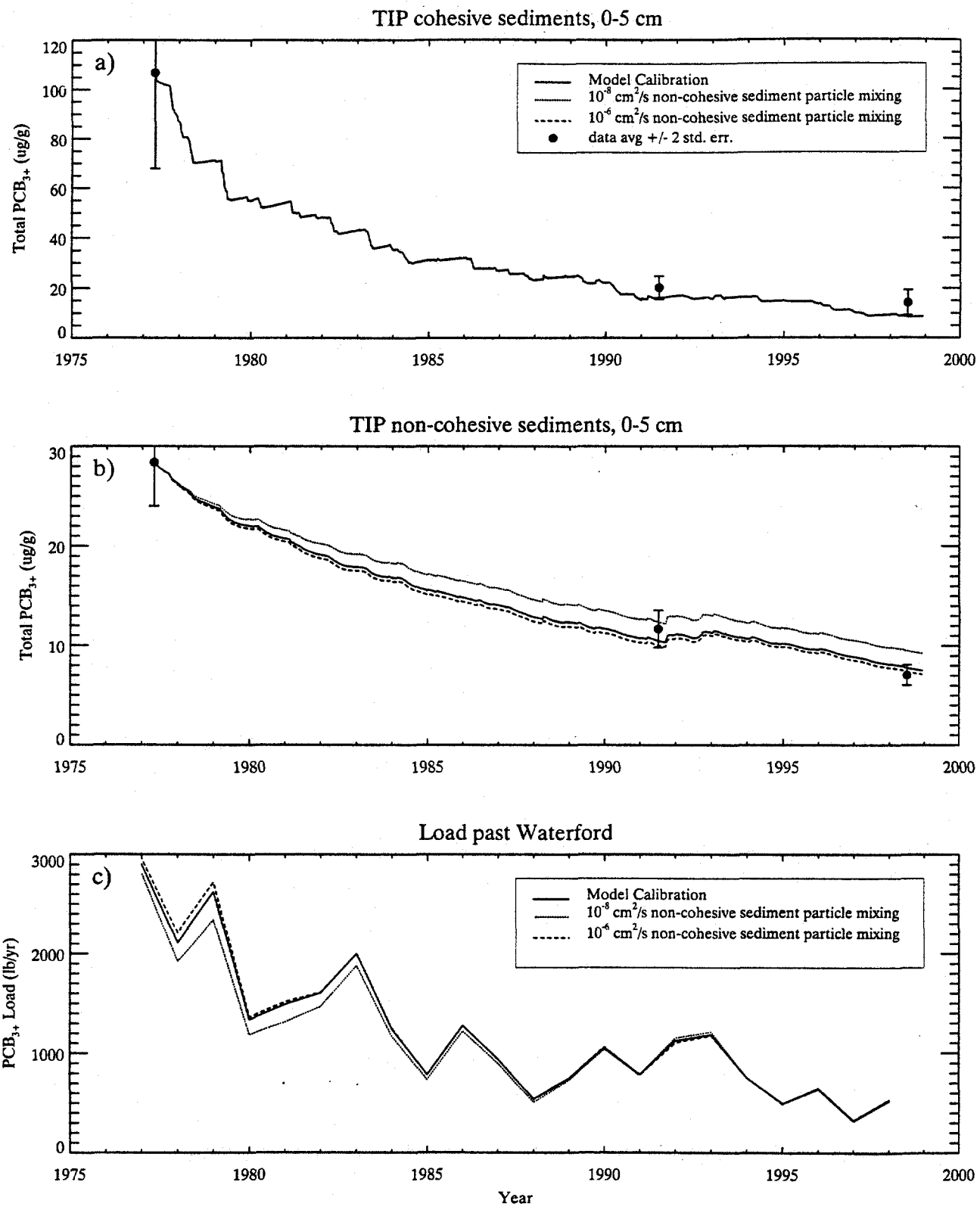

Figure 4-61. Comparison of average observed 0-5 cm cohesive and non-cohesive sediment PCB_{3+} concentration in the TIP and the load past Waterford with concentrations computed using alternate magnitudes of particle mixing in non-cohesive sediments.

da - \\Poseidon\D_Drive\GENhud\Documents\Final_report\Vol_2\Section_4\fig4_57_66sens.pro
Tue Apr 13 14:00:51 1999

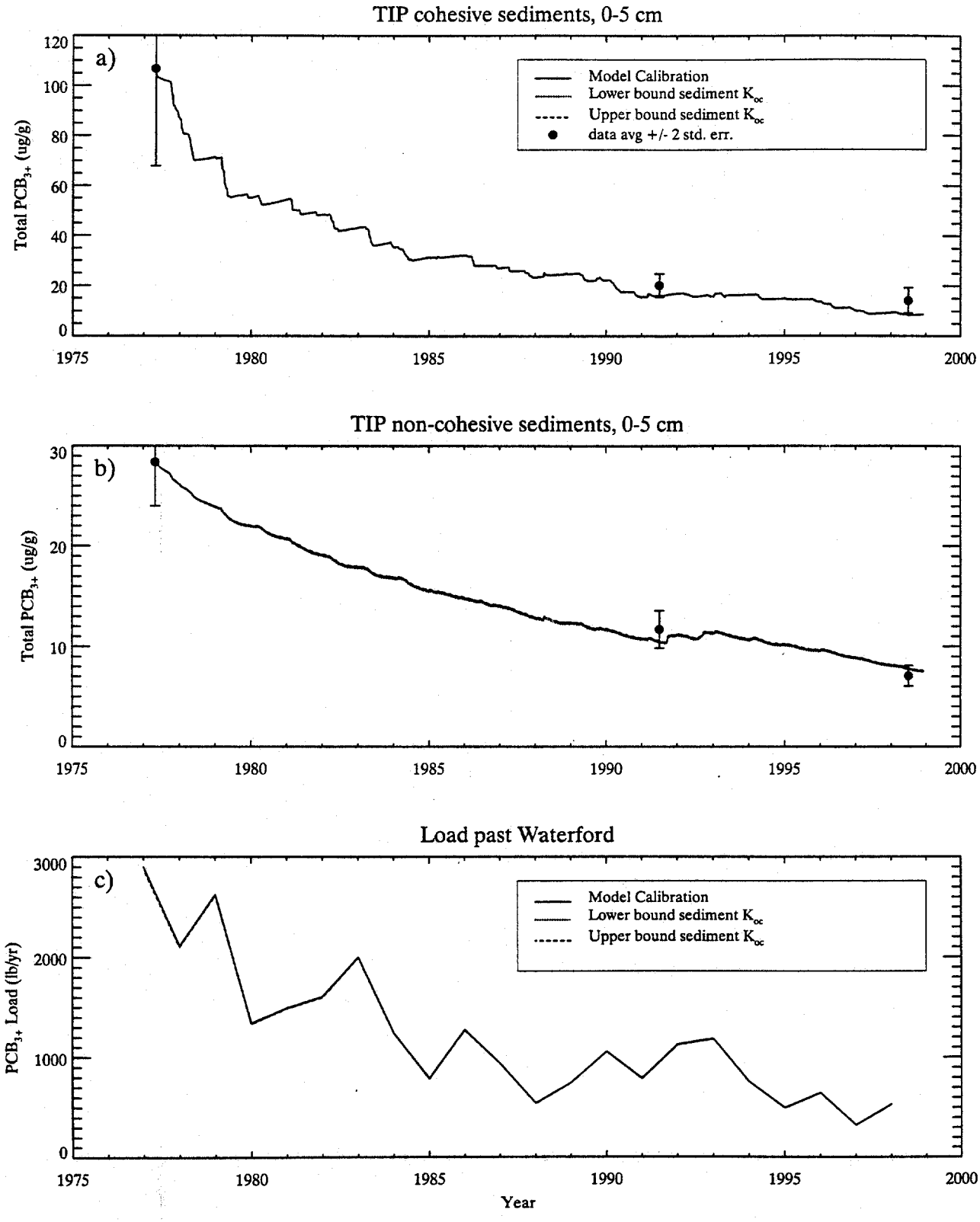

Figure 4-62. Comparison of average observed 0-5 cm cohesive and non-cohesive sediment PCB_{3+} concentration in the TIP and the load past Waterford with concentrations computed using alternate PCB partition coefficients in sediment.

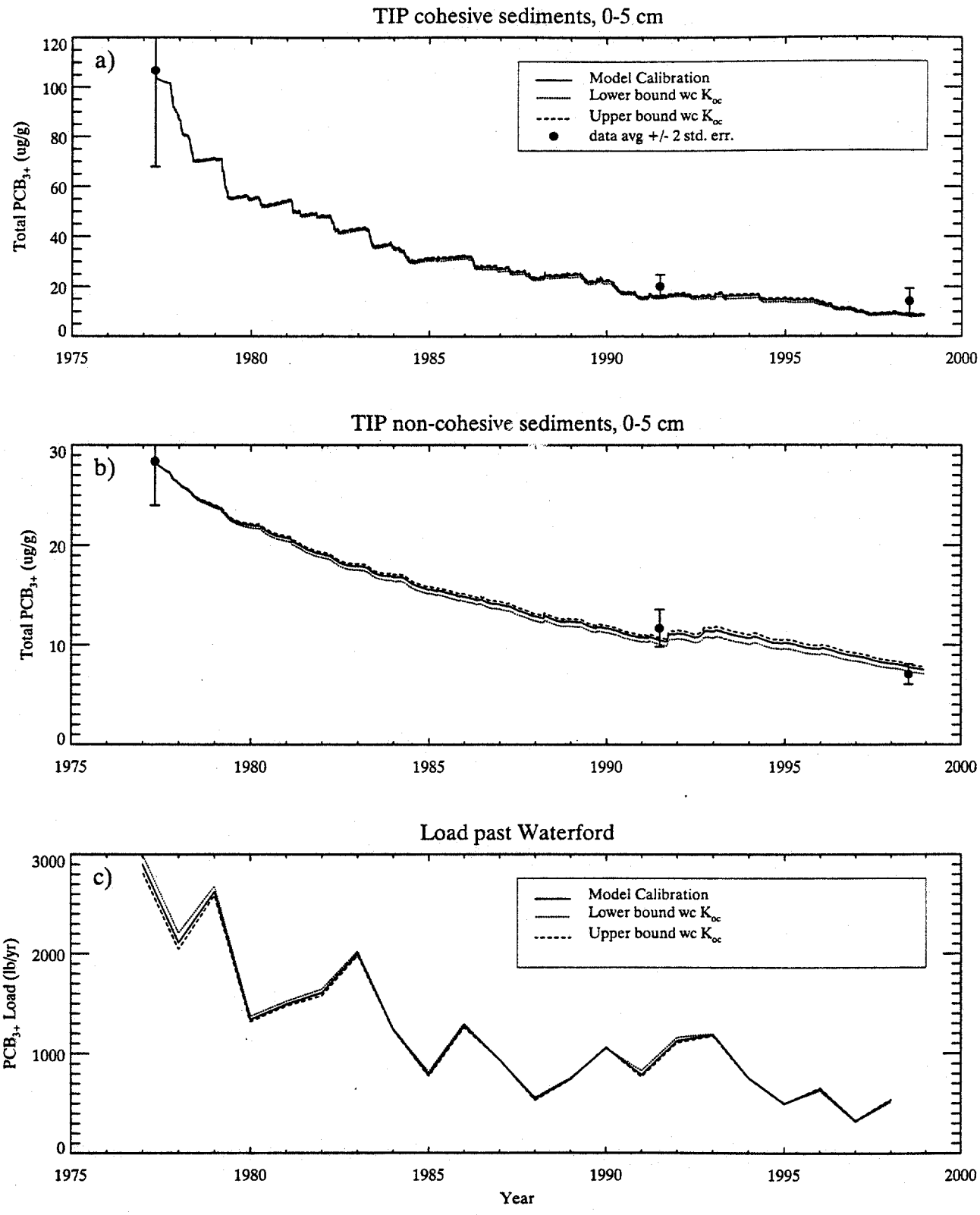

Figure 4-63. Comparison of average observed 0-5 cm cohesive and non-cohesive sediment PCB_{3+} concentration in the TIP and the load past Waterford with concentrations computed using alternate PCB partition coefficients in water.

da - \\Poseidon\D_Drive\GENhud\Documents\Final_report\Vol_2\Section_4\fig4_57_66sens.pro
Tue Apr 13 13:37:46 1999

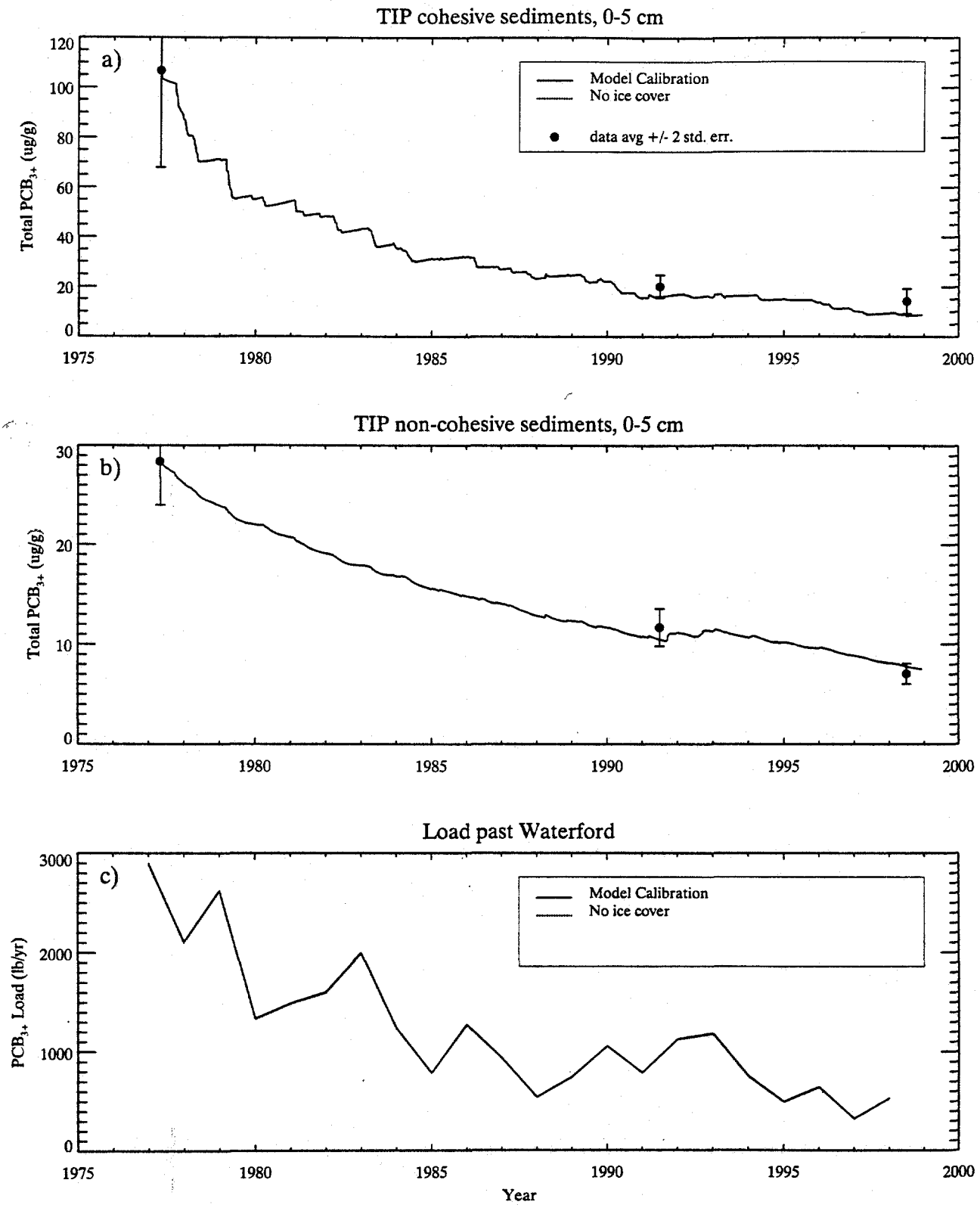

Figure 4-64. Comparison of average observed 0-5 cm cohesive and non-cohesive sediment PCB_{3+} concentration in the TIP and the load past Waterford with concentrations computed using alternate ice cover.

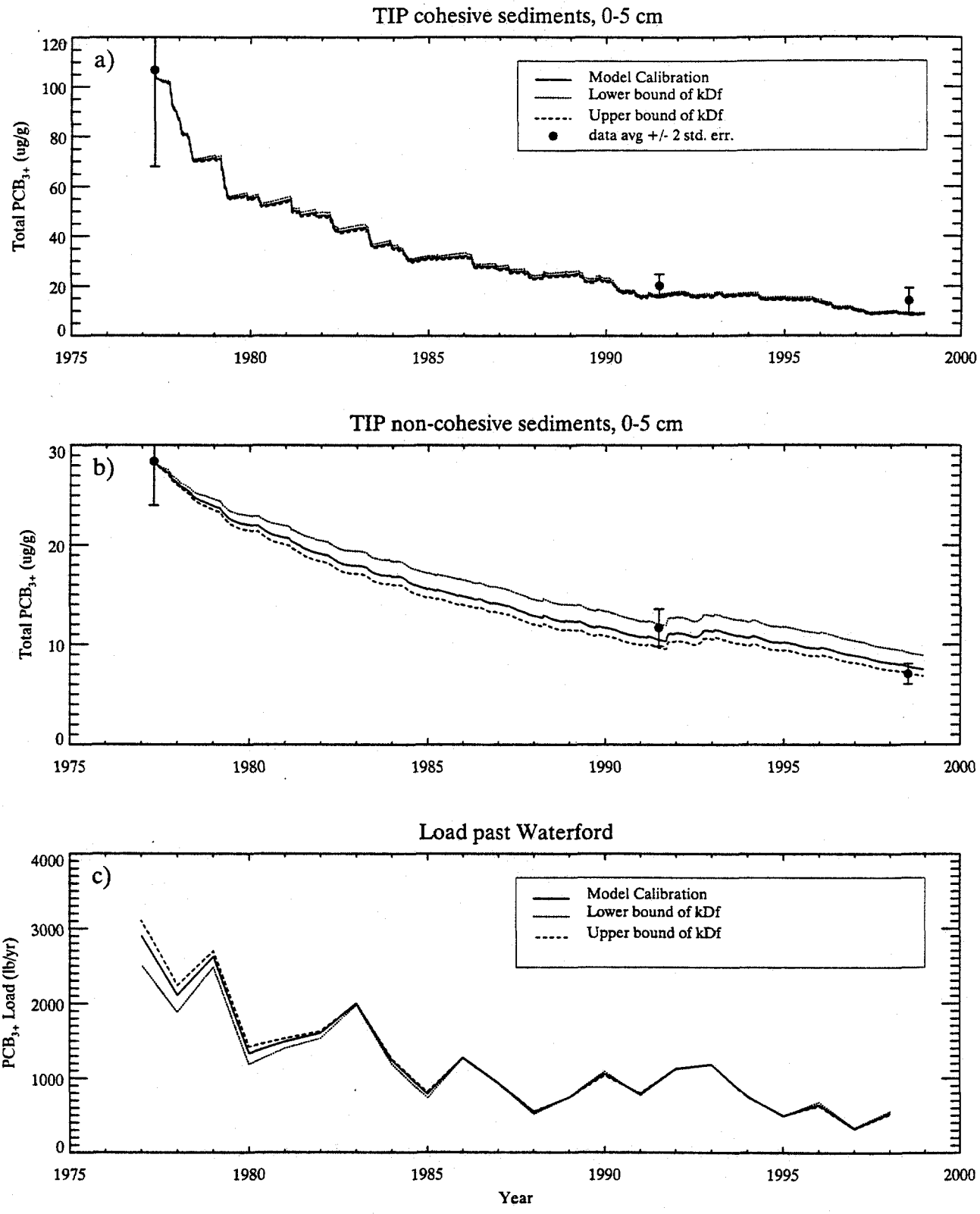

Figure 4-65. Comparison of average observed 0-5 cm cohesive and non-cohesive sediment PCB_{3+} concentration in the TIP and the load past Waterford with concentrations computed using the estimated range of mass transfer coefficients.

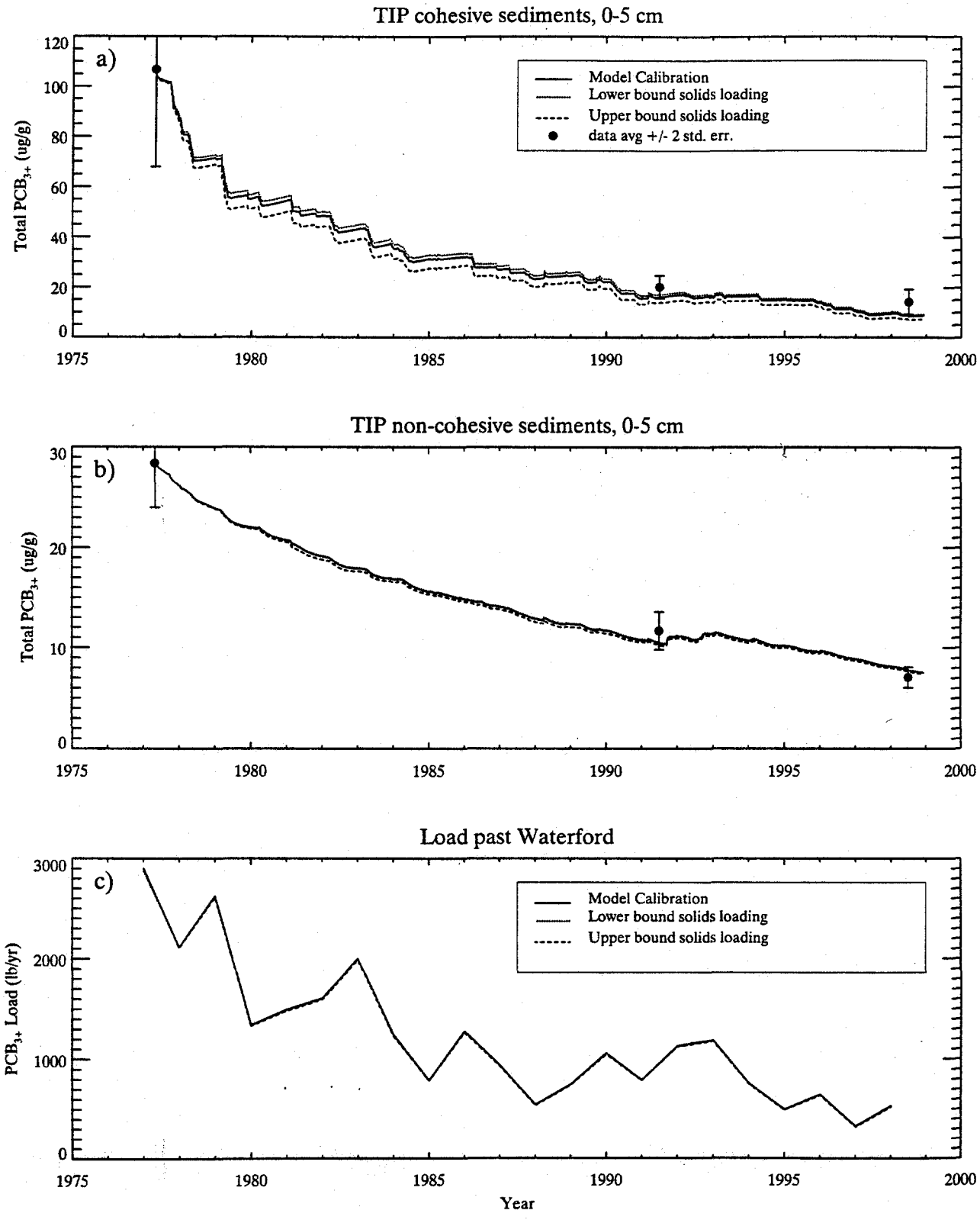

Figure 4-66. Comparison of average observed 0-5 cm cohesive and non-cohesive sediment PCB_{3+} concentration in the TIP and the load past Waterford with concentrations computed using the estimated range of solids loading.

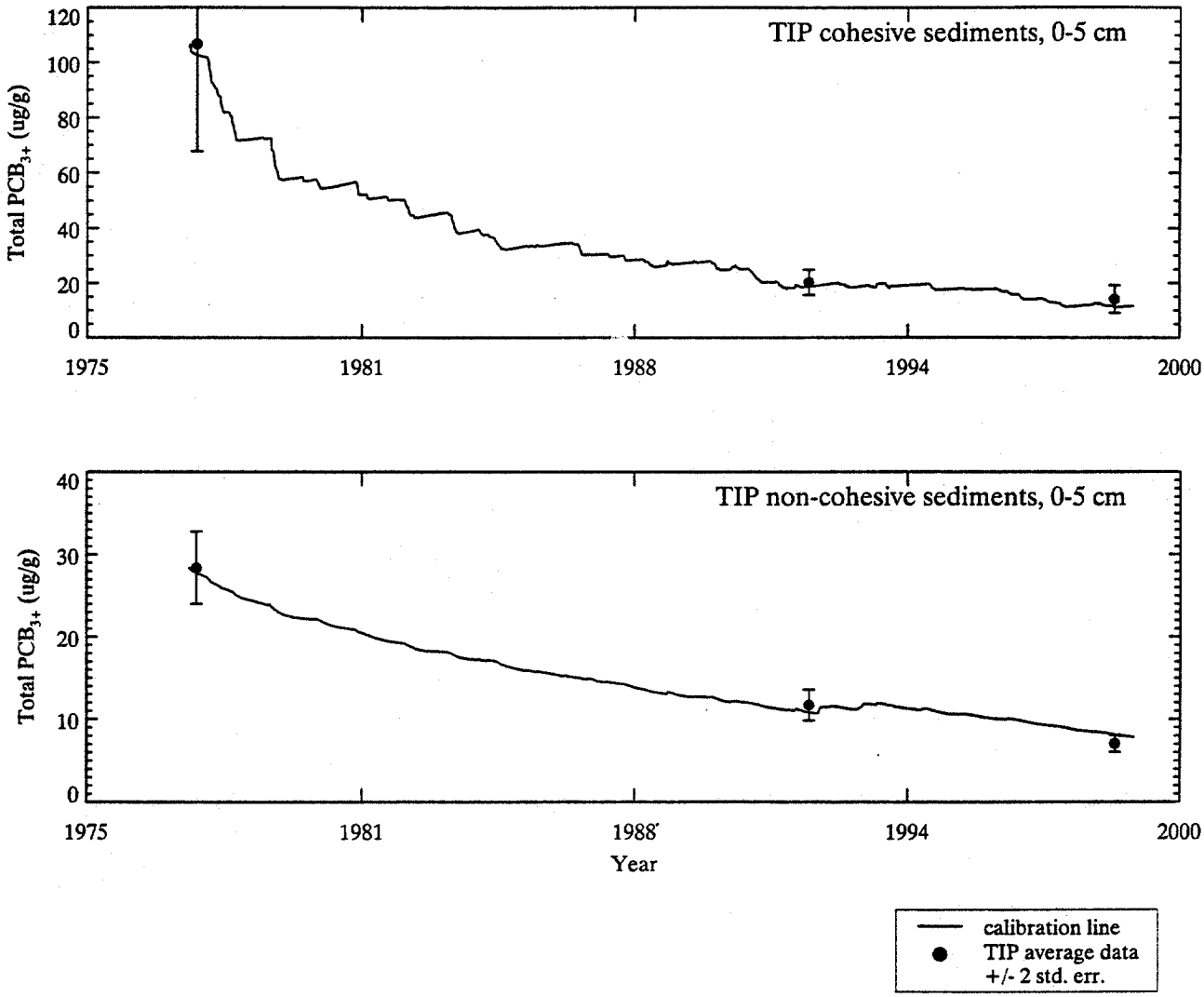

Figure 4-67. Predicted (line) and measured (symbols) average PCB_{3+} concentrations in surface sediments of the TIP using bounding calibration.

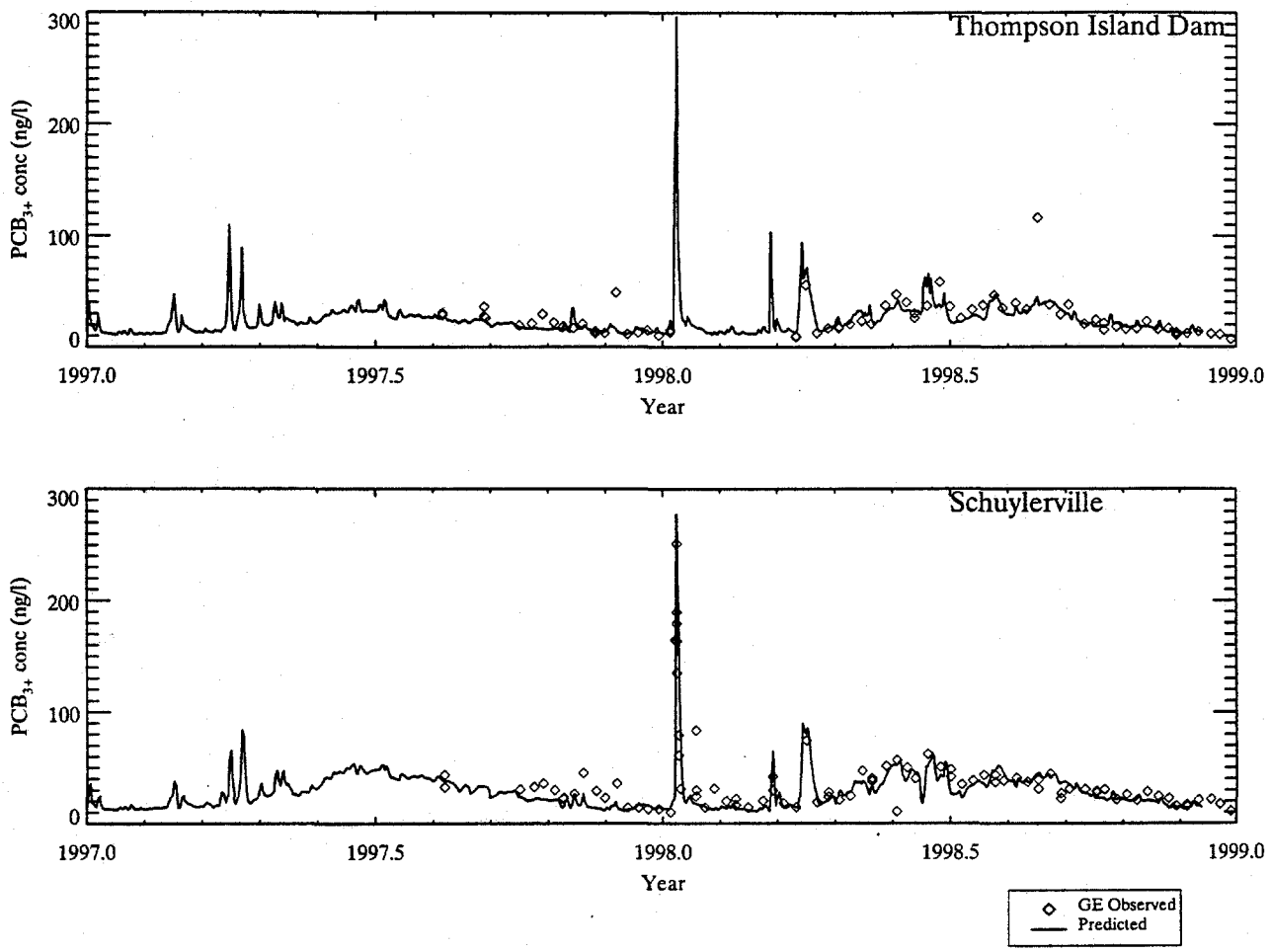

Figure 4-68. Comparison of bounding calibration computed (line) and measured (symbols) water column PCB_{3+} at Schuylerville and the Thompson Island Dam.

LOCATION MAP OF THE UPPER HUDSON RIVER

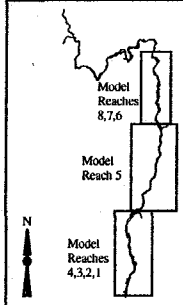

GRAPHIC SCALE

0.5 0 0.5 1 Miles

LEGEND

- Mile Markers
- Remnant Deposits (approx.)
- 1977 NYSDEC Hot Spots
- Fine Zones *
- Shoreline
- Dams and Locks

NOTES / DATA SOURCES

* Reaches 6-8 fine sediment defined by EPA side scan sonar.

Reaches 1-5 fine sediment defined by sediment transport bed mask (determined from field sampling).

GENERAL ELECTRIC COMPANY
Hudson River Project

PCBs in the Upper Hudson River Volume 2. A Model of PCB Fate, Transport, and Bioaccumulation.

Plate 4-1.

Cohesive sediment zones as defined by side scan sonar (reaches 6-8) and the sediment transport bed mapping (reaches 1-5).

QEA Quantitative Environmental Analysis, LLC

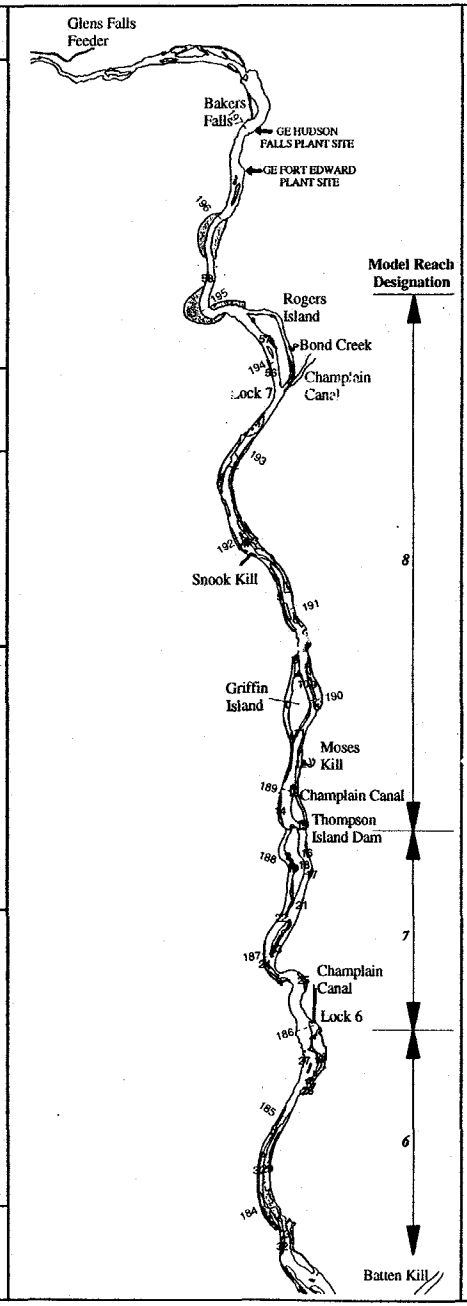

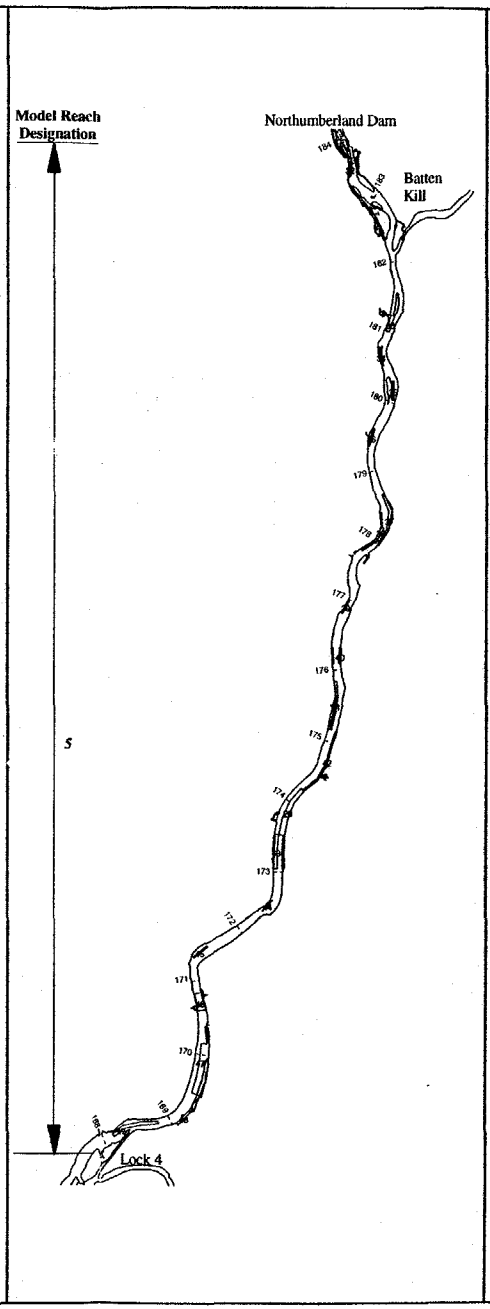

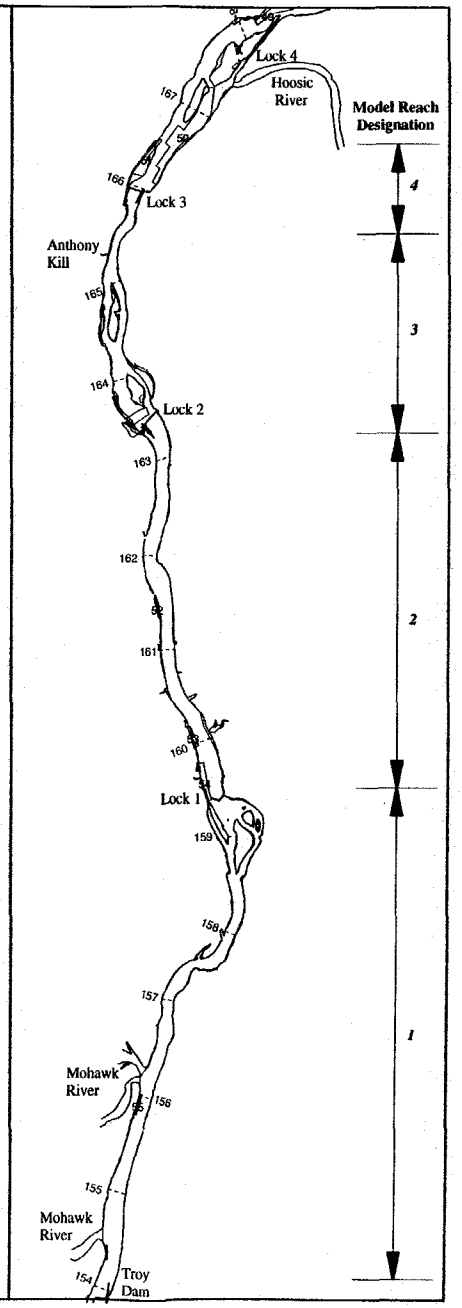

Bioaccumulation Model

Quantitative Environmental Analysis, LLC.

SECTION 5
BIOACCUMULATION MODEL

The bioaccumulation model is a mathematical description of the transfer of PCBs within the food web. The food web is comprised of the primary energy transfer pathways from the exposure sources, sediment and water, to the species of interest. The mathematical descriptions are generic (common to all aquatic food webs) and form the basis for the computer source code (Section 5.1). The parameters of the model were established in several ways:

- The food web was defined using a combination of general natural history information and site-specific studies (Section 5.2.1).
- The relative importance of sediment and water column exposure sources was explored using analyses of site-specific natural history studies and PCB data (Section 5.2.2).
- The depth within the sediment bed to which PCBs are bioavailable was estimated based on natural history and a model of the bioaccumulation of PCB homologs (Section 5.2.3).
- Bioaccumulation factors for the invertebrates at the base of the food web were based upon values measured in the Hudson River as well as values measured at other sites (Section 5.2.4).
- Respiration rates were based on species-specific laboratory studies (Section 5.2.5).
- Growth rates were calculated from site-specific field data for each species (Section 5.2.5).
- Toxicokinetic parameters (PCB assimilation efficiencies) were presumed to be generic to all aquatic food webs and were established from laboratory data and previous modeling studies (Section 5.2.6).

5.1 STRUCTURE AND EQUATIONS

5.1.1 Bioaccumulation Factors

The transfer of PCBs through the food web can be described in a number of ways. The simplest description is a bioaccumulation factor, or a ratio of the contaminant concentration in the species of interest to the concentration in the exposure source. Two bioaccumulation factors are used, one to describe accumulation from sediment (BSAF) and one to describe accumulation from the water column (BAF). Equation 5-1 describes the accumulation of PCBs from the water column:

$$BAF = \frac{v_L}{c}(1000) \qquad (5\text{-}1)$$

where:

BAF	=	bioaccumulation factor (L/kg lipid)
v_L	=	concentration of PCBs in the organism (mg/kg lipid)
c	=	concentration of PCBs dissolved in the water (µg/L)

Equation 5-2 describes the accumulation of PCBs from sediments:

$$BSAF = \frac{v_L}{r_{soc}} \qquad (5\text{-}2)$$

where:

BSAF	=	biota-sediment accumulation factor (kg organic carbon/kg lipid)
r_{soc}	=	concentration of PCBs on sediment particles (mg/kg organic carbon)

Concentrations in the sediments are represented on an organic carbon basis because PCBs preferentially associate with the organic matter fraction of the sediment bed and because benthic organisms derive their energy from sediment organic matter. Therefore, the amount of PCBs

ingested by the organism is proportional to the amount of PCBs present in the organic matter fraction, which is represented by r_{soc}.

Bioaccumulation factors are often used as screening-level descriptors of bioaccumulation for all aquatic biota. They are most useful in describing bioaccumulation in small, short-lived organisms that accumulate a chemical from one exposure source and that respond rapidly to changes in exposure concentrations. Examples of appropriate organisms include benthic and water column invertebrates. The Upper Hudson River bioaccumulation model uses bioaccumulation factors for these organisms.

The application of BAFs to simulate the bioaccumulation process is subject to a number of limitations. First, if both the water column and sediments contribute to overall exposure and if PCB concentrations in the two media change at different rates, then a single bioaccumulation factor may not predict concentrations in the biota accurately. Second, if exposure concentrations, organism physiology (especially lipid content) or the food web change on a time scale commensurate with the response time of the food web, then BAFs will not accurately describe the bioaccumulation process. Chemical levels in the organism cannot keep pace with changes in exposure levels that occur on a time scale similar to the response time of the organism. Under such conditions, they are not at steady state with respect to exposure levels and a time-variable modeling approach is required. These conditions are met in the Upper Hudson River: fish accumulate PCBs from both water and sediment, exposure concentrations vary on a range of time scales, and fish lipid contents change over time. Therefore, a time-variable model was used to simulate PCB bioaccumulation in Upper Hudson River fish. The model is mechanistic in that it is based upon basic toxicokinetic and bioenergetic principles.

5.1.2 Time-Variable Mechanistic Model Equations

Basic Equation

The accumulation of PCBs by aquatic animals is described by the following:

$$\frac{dv_i}{dt} = K_{ui}c + \alpha_c \sum_{j=1}^{n} C_{ij}v_j - (K_i + G_i)v_i \qquad (5\text{-}3)$$

where:

i & j	=	indices for predator and prey, respectively
υ_i	=	concentration of chemical in species i (µg/g(w) where g(w) is grams wet weight)
K_{ui}	=	rate constant for respiratory chemical uptake by species i (L/g(w)-d)
K_i	=	rate constant for excretion of chemical by species i (1/d)
α_c	=	efficiency at which ingested chemical is assimilated from prey
C_{ij}	=	predation or consumption rate of species i on species j (g(w)prey/g(w) predator-d)
G_i	=	growth rate of species i (g(w)/g(w)-d)
n	=	number of species (including different year classes of a single species) preyed upon by species i

The first term of Equation (5-3) represents the direct uptake of PCBs by the animal from water. The second term represents the flux of PCBs into the animal through feeding. The third term represents the loss of chemical due to diffusion across the gill and the change in concentration due to growth. The gill is the major site of depuration; the fecal elimination rate is much less than the growth rate and is not included in the model. The dynamic bioaccumulation model is applied to each fish species, accounting for species-specific differences in growth rate, consumption rate, and elimination rate.

The individual processes within Equation (5-3) have been discussed in detail elsewhere (Connolly 1991, Connolly *et al.* 1992) and are summarized and updated here.

Contaminant Mass Transfer at the Gill

The contaminant uptake rate constant K_{ui} is defined from a mass transfer coefficient k_{gi} and the active gill surface area A_{gi}:

$$K_u = \frac{k_{gl} A_{gl}}{W} \tag{5-4}$$

where W is the wet weight of the animal (g(w)). The index i representing an individual species is dropped for this discussion.

It is not necessary to explicitly define these parameters. Rather, K_u may be determined from the oxygen uptake rate constant, K_{uO_2}, and the ratio of the mass transfer coefficients of the contaminant and oxygen. Oxygen transfer rate is defined by the respiration rate of the animal and the oxygen concentration of the water (c_{O_2},gO_2/l):

$$K_{uO_2} = \frac{R}{c_{O_2}} \tag{5-5}$$

where R is the respiration rate in units gO_2/g(w)-d. Mechanistically this uptake rate may be described in term of a mass transfer rate constant at the gill (k_{glO_2}).

$$K_{uO_2} = \frac{k_{glO_2} A_{gl}}{W} \tag{5-6}$$

Equations (5-5) and (5-6) may be equated and solved for A_{gl}. Substituting this expression for A_{gl} in Equation (5-4) yields:

$$K_u = \frac{k_{gl}}{k_{glO_2}} \frac{R}{c_{O_2}} \tag{5-7}$$

The bioenergetic component of the model computes the respiration rate. The concentration of oxygen in the water is calculated assuming saturation, incorporating corrections for temperature and salinity. The ratio of chemical:oxygen mass transfer rates is estimated from experimental data, as described in section 5.2.4.

Within the body of fish, PCBs circulate in the blood and are stored in lipids within various tissues. Gill exchange involves diffusion between dissolved contaminant pools on either side of the gill membrane (e.g. Erickson and McKim 1990). Gill exchange (in units of μg/g(w)-day; without the subscript i denoting a specific species) is therefore given by:

$$Gill\ exchange = K_u(c - \upsilon_B) \qquad (5\text{-}8)$$

where:

ν_B = concentration of contaminant dissolved in blood (μg/L)

If lipid stores and blood equilibrate rapidly compared with gill exchange, then ν_B can be estimated by multiplying the contaminant concentration in lipid by a lipid/water partition coefficient. However, if the exchange between lipid stores and blood is relatively slow, then the kinetics of this transfer must be considered. Under these conditions, elimination is a two-step process, release from the storage compartment followed by release to the environment, and the elimination rate is controlled by the rate of mass transfer from the storage tissue to the blood.

There are several lines of evidence suggesting that elimination rates in chronically exposed fish are controlled by transfer from storage tissue to blood:

First, biphasic elimination of PCBs and other hydrophobic compounds from fish has been observed in laboratory experiments (Gooch and Hamdy 1982, Guiney *et al.* 1977, Guiney and Peterson 1980, Konemann and van Leeuwen 1980, Muir *et al.* 1980, Schrap and Opperhuizen 1988, Yamato *et al.* 1983). This refers to a change in the rate at which body burden declines (in units of 1/time) during a single elimination experiment. The observation of biphasic elimination suggests that there are two separate controls on excretion rate, one that produces a relatively rapid initial loss followed by a slower loss mechanism. This pattern is characteristic of a multi-compartment system (O'Flaherty 1981). With relatively short-term exposure, contaminant remains primarily in the "central" compartment(s), i.e. those with relatively rapid exchange with the blood. Contaminant transfer to the "deeper" storage compartments, i.e. those with relatively slow exchange, is minimal. During longer exposure, contaminant enters the deeper storage

compartments. During the first relatively rapid phase of biphasic elimination, the blood and the more central compartments depurate; during the second phase, the relatively slow exchange between deeper compartments and blood controls the overall elimination rate.

Second, elimination rates measured after long-term exposures are often lower than rates measured after shorter exposure periods (de Boer *et al.* 1994, Lieb *et al.* 1974, O'Connor and Pizza 1987, Sijm *et al.* 1992). This has also been ascribed to the relatively slow equilibration of contaminant within the deeper compartments during chronic exposure (O'Connor and Pizza 1987, de Boer *et al.* 1994, Spacie and Hamelink 1982).

Third, if contaminant in lipids exchanges rapidly with the blood, then reductions in lipid content should result in rapid increases in excretion. If lipid/blood exchange is rapid enough, then the concentration of contaminant in lipid should remain constant even though lipid content changes. Lieb *et al.* (1974) found that starvation of rainbow trout over a period of eight weeks led to an increase in PCB levels in lipid, not to increased elimination. PCB mass per fish did not change. This suggests that the transfer of PCBs from lipid to blood is slow, even relative to the transfer of lipids themselves.

Fourth, a two-compartment pharmacokinetic model of di-2-ethylhexyl phthalate (DEHP) in sheepshead minnow was developed and parameterized based upon a laboratory uptake experiment (Karara and Hayton 1984). The storage compartment was found to have relatively slow exchange with the central compartment. Model computations indicated that during longer exposure periods, the elimination of DEHP from the fish depended on its rate of transfer from the storage to the central compartment.

Fifth, chemical transport among tissues in people is generally perfusion-limited for lipid-soluble compounds for which diffusion and movement across lipoidal membrates should be relatively rapid (Gibaldi and Perrier 1982). Fat stores are in general poorly perfused (Gibaldi and Perrier 1982), suggesting the elimination may be controlled by tissue perfusion rates.

Thus, it appears that elimination in chronically-exposed fish is probably controlled by release from one or more deep compartments. The number of compartments can range from two, blood and lipid, to many. A multi-compartment model would include one central compartment, blood, along with multiple storage compartments, each with its own characteristic rate of contaminant transfer to the blood. There are probably several compartments in the body of a fish that can be distinguished on the basis of their mass transfer rates to and from blood, for example contaminant bound to lipoprotein in the blood, contaminant associated with triglycerides in muscle, liver and other tissues, and contaminant associated with phospholipids in body tissues. For illustrative purposes, the equations describing contaminant dynamics in the fish are developed assuming that the mass of PCBs resides in two compartments, dissolved in blood and associated with lipid (Figure 5-1). The inclusion of multiple compartments would change neither the form of the final equations nor the parameterization of the Hudson River bioaccumulation model.

The mass of contaminant in the whole body is equal to the sum of masses in the two compartments:

$$vm = v_B m_B + v_L m_L \tag{5-9}$$

where:

v	=	whole-body PCB concentration (μg/g(w))
v_L	=	PCB concentration in lipid (μg/g lipid)
m_B	=	mass of aqueous blood in the body (g blood)
m_L	=	mass of lipid in the body (g lipid)
m	=	whole body mass (g(w))

The rates of change of PCB mass in the blood and lipid are described by Equation 5-10 (Figure 5-1):

$$\frac{dv_B m_B}{dt} = k_u mc + \alpha_C m \sum_{j=1}^{n} C_{ij} v_j - k_1 v_B m_B - k_2 v_B m_B + k_3 v_L m_L \tag{5-10}$$

$$\frac{dv_L m_L}{dt} = k_2 v_B m_B - k_3 v_L m_L \qquad (5\text{-}11)$$

where:

k_u	=	uptake rate constant from water (1/d)
k_1	=	mass transfer constant from blood to water (1/d)
k_2	=	mass transfer constant from blood to lipid (1/d)
k_3	=	mass transfer constant from lipid to blood (1/d)

Summing Equations 5-10 and 5-11 results in an equation for the rate of change of PCB mass in the whole body containing only the first three terms of Equation 5-10. This whole-body equation is similar to Equation 5-3, except that it is formulated in units of mass rather than concentration. Reformulation in terms of concentration would result in the addition of the growth rate term (dm/dt) in Equation 5-3. Note that k_u in Equation 5-10 (units of 1/day) and K_u in Equation 5-3 (units of L/g(w)-d) are both used to calculate the exchange of contaminant across the gill surface, but they have different units.

Equations 5-10 and 5-11 have two additional rate constants, k_2 and k_3. A relationship between these can be developed by analyzing Equation 5-11 at steady state:

$$k_2 v_B m_B = k_3 v_L m_L \qquad (5\text{-}12)$$

We define a lipid/dissolved partition coefficient:

$$\frac{v_L}{v_B} = \pi_{LB} \qquad (5\text{-}13)$$

Then, Equations 5-12 and 5-13 can be substituted into Equations 5-10 and 5-11:

$$\frac{dv_B m_B}{dt} = k_u mc + \alpha_c m \sum_{j=1}^{n} C_{ij} \upsilon_j - k_1 v_B m_B - \pi_{LB} k_3 m_L v_B + k_3 v_L m_L \qquad (5\text{-}14)$$

$$\frac{dv_L m_L}{dt} = \pi_{LB} k_3 m_L v_B - k_3 m_L v_L \qquad (5\text{-}15)$$

The parameters in Equation 5-3 have counterparts in Equation 5-14: K_{ui} and k_u, the food consumption parameters, K_i and k_1. However, Equations 5-14 and 5-15 have one additional rate constant, k_3, that describes the rate of exchange with the storage compartment, as well as the lipid/blood partition coefficient, π_{LB}. Addition of more compartments would be done in a similar way and would add two additional parameters per compartment.

There is insufficient information to develop a full multi-compartment model and to estimate values for all of the necessary rate constants and partition coefficients. Therefore, in the bioaccumulation model, we account for the additional resistance due to the relatively slow transfer from deep compartments to blood by reducing the excretion rate below that calculated by diffusive exchange across the gill. The gill elimination rate, K_{gill}, is first computed assuming equilibration between lipid and blood, by substituting Equation 5-9 and 5-13 into the second term in Equation 5-8 (Connolly *et al.* 1992). Then, this rate is multiplied by a "resistance" factor, c_R, with a value between 0 and 1:

$$K_{gill} = K_u c_R v_B = K_u c_R \left(\frac{1}{f_B + \pi_{LB} f_L} \right) v \qquad (5\text{-}16)$$

where:

f_L = m_L/m = fraction lipid of the animal (g lipid/g(w))

f_B = m_B/m = fraction lipid of the animal (g blood/g(w))

c_R = factor accounting for the slow transfer of PCBs from lipid to blood

Three additional parameters must be estimated, π_{LB}, c_R and f_B.

Contaminant Mass Transfer at the Gut Wall

Contaminant mass transfer at the gut wall is determined by the amount of food consumed and the assimilation efficiency (Equation 5-3). The amount of food consumed is computed in the bioenergetics component of the model. The estimation of the assimilation efficiency is discussed in Section 5.2.5.

Analysis of laboratory data for chemicals with log (K_{ow}) between 4.5 and 8 indicates that elimination across the gut is of limited importance relative to overall elimination rate (Connolly *et al.* 1992). Gobas *et al.* (1989) presented data that showed fecal elimination rate to be below gill elimination rate until log (K_{ow}) was above about 7. In any event, the fecal elimination rate is much less than the growth rate and is not included in the model. Therefore, the gill is the major site of depuration (Gobas *et al.* 1989), and K_{gill} is equivalent to the whole-body loss rate (K_i in Equation 5-3).

Bioenergetics

Growth and respiration rates are required to calculate the total energy requirement, which is needed to calculate the rate of consumption of contaminated prey (Equation 5-3). In addition, the respiration rate is used to calculate the rate of diffusion of contaminant across the gill surface (Equation 5-7). Finally, the growth rate is used to calculate the dilution of contaminant within the body of the organism (Equation 5-3).

The model computes growth rates based upon a relationship between age and weight that is determined from data:

$$G = \frac{1}{W}\frac{dW}{dt} \qquad (5\text{-}17)$$

The respiration model is

$$R = \beta W^{\gamma} e^{\rho T} c_{act} \qquad (5\text{-}18)$$

where:

T	=	temperature (°C)
c_{act}	=	activity multiplier
β,γ,ρ	=	empirical coefficients determined by experiment

The model accounts for standard metabolism, that is, metabolism in the absence of feeding and activity, as well as the added impact of swimming. In addition, the effects of apparent specific dynamic action (ASDA) are incorporated. The ASDA consists of the heat produced during digestion as well as the energy required for absorption, digestion, transportation and deposition of food materials.

The rate of consumption of food, $\Sigma_j(C_{ij})$ is calculated from the rate of energy usage. Energy usage is estimated from the rates of production and metabolism. For the rest of this discussion, the index i representing an individual species is dropped. The rate of metabolism is computed from the respiration rate at time t (R_t, $gO_2/g(w)$-d), by stoichiometrically converting respiration to units of kJ/g(w)-d using a conversion factor λ_o = 13.7 kJ/g O_2 (Brett and Groves 1979). The rate of energy usage for production of body tissue is determined from the growth in mass and the change in lipid content. Given the energy density of the animal's tissue at time t (λ_t, kJ/g(w)), the energy usage rate at time t (P_t, kJ/g(w)-day), is then:

$$P_t = \lambda_o R_t + \left(\frac{W_{t+1}\lambda_{t+1} - W_t\lambda_t}{W_t} \right) \qquad (5\text{-}19)$$

where:

W_{t+1}	=	weight at time t+1 (g(w))

Note that the model computes P based upon field measurements of lipid content and weight/age relationships. The relationships among food availability, feeding behavior, growth and body composition are not modeled here.

Energy density is computed from the composition of the animal and the energy densities of lipid (39.5 kJ/g) and protein (20.08 kJ/g; Brett and Groves 1979):

$$\lambda = 39.5 f_L + 20.08 f_P \quad (5\text{-}20)$$

where:

f_P = fraction protein = f_L - f_D

f_D = fraction dry weight (g(d)/g(w))

The energy density of each organism changes over time in response to changes in lipid content. The fraction protein is assumed to remain constant.

Dividing the energy usage rate of species i, P_i by the fraction of ingested energy that is assimilated, α_F, yields the rate of energy intake by the animal. The rate of consumption of prey type j, C_{ij}, is the energy intake rate for that prey type, $f_{ij}P_i/\alpha_F$, divided by the energy density of the prey, λ_j:

$$C_{ij} = f_{ij} \frac{1}{\lambda_j} \frac{P_i}{\alpha_F} \quad (5\text{-}21)$$

where:

f_{ij} = fraction of the total energy consumed by predator i that consists of prey j.

Computer Code

The model computes the PCB concentration for each age class of each species on a daily basis as it advances from one age class to the next. Each day, the weight, lipid content, metabolic rate and PCB exposure for each model age class of each species change. Dietary composition can also change daily, although in the Upper Hudson River model the annual average dietary composition is used. The computer code has the ability to permit migration between sites with different exposure conditions. However, this feature is not used in the Upper

Hudson River model, because the fish are not considered capable of passing beyond dammed reaches on a regular basis.

5.2 APPLICATION TO THE UPPER HUDSON RIVER

5.2.1 Food Web Structure

Food resources enter the Upper Hudson River system through two pathways: 1) primary production by phytoplankton, periphyton and macrophytes within the river, and 2) transport of detritus from upstream and from nearby terrestrial ecosystems. Water column and sediment particulate matter are the first trophic level of the food web (TL1). These resources are consumed by invertebrates that reside in the water column as well as within and on the surface of the sediment bed (TL2). Invertebrates are consumed by fish (TL3), which in turn can be consumed by larger predatory fish (TL4; Figure 5-2).

5.2.1.1 Top Predators (Trophic Level 4)

The fish community of the Upper Hudson River is composed of more than 30 species (Figure 5-3, Law Environmental 1991, Exponent 1998a, NYSDEC 1998). The most common species in the TIP are smallmouth bass, largemouth bass, rock bass, yellow perch, pumpkinseed, spottail shiner, tessellated darter and fall fish.

Largemouth bass, smallmouth bass, northern pike, and chain pickerel are the most commonly collected top predators in the Upper Hudson River. Because top predators represent an important potential exposure source for people who catch and eat fish from the river, a top predator is included in the model. The model food web includes largemouth bass as a representative top predator, primarily because a large historical database of PCB concentrations is available (NYSDEC 1998). PCB levels in top predators should be among the highest in the aquatic biota. Indeed, largemouth bass have PCB levels higher than fish sampled from trophic level 3 in the Upper Hudson River (Figure 5-4).

To examine the degree to which largemouth bass is representative of top predators, total PCB levels and PCB composition were compared among the species. Annual average total PCB levels measured by NYSDEC (1998) were computed by location and year for all top predators. Average values in largemouth bass were matched by location and year with average values measured in other species and plotted (Figure 5-5). Largemouth bass values are correlated with values for other predators. There is no clear bias in the relationship. Values measured in other top predators generally lie within a factor of two of values measured in largemouth bass. A simple measure of PCB composition is the average number of chlorines per biphenyl (Cl/BP). Values measured in several top predators in the 1990s are presented in Figure 5-6 (data of USEPA, NOAA, Exponent and Law Environmental). The average largemouth bass value lies in the middle of the values for predators. Thus, based upon total PCB concentration and PCB composition, largemouth bass is a reasonable representative of the top predators of the Upper Hudson River.

Many piscivorous fish species, including those present in the Upper Hudson River, are generally opportunistic feeders, meaning that they consume prey species roughly in proportion to their availability, within an appropriate size range (Carlander 1971, Wootton 1990, Smith 1985, Hambright 1991). The guts of a limited number of largemouth bass collected in the Upper Hudson River included at least 11 species of fish (Figure 5-7). The most common species in the largemouth diet was the spottail shiner, a common component of the forage fish community. On the other hand, two species found in the guts of largemouth bass were not found in fish collections conducted in the same area, season and year (eastern silvery minnow, bluntnose minnow). Thus, largemouth bass appears to consume both relatively common and relatively rare fish species. Because largemouth bass are opportunistic and consume a variety of species, the relative contribution of benthic and water column-based PCBs to their diet depends on the composition and feeding behavior of the forage fish (TL3) are discussed in Section 5.2.1.2.

Insofar as predators are opportunistic, spatial and temporal trends in PCB levels in one predator should be representative of all predators. To provide the information needed for human health and ecological risk assessment, average PCB levels in other predatory fish species can be computed based upon the modeled average largemouth bass concentration and measured relationships among species.

In the model, yearling and older largemouth bass consume only fish. Young-of-the-year largemouth bass consume 50% invertebrates (Carlander 1977), equally split between water column and benthic species. The mixture of forage fish consumed by the largemouth bass was estimated based upon analyses of the forage fish community (Section 5.2.1.2) and by model calibration.

5.2.1.2 Forage Fish (Trophic Level 3)

There are at least 30 species of fish that are available prey for TL4 fish (Figure 5-3), including the young of piscivorous fish. Published information on dietary composition of the more abundant species is presented next.

Pumpkinseed is an opportunistic feeder that consumes many kinds of invertebrates (Thorp *et al.* 1989, Keast and Fox 1990, Domermuth and Reed 1980). The diet changes in the presence of other fish species (Osenberg *et al.* 1992), varies between night and day (Collins and Hinch 1993), and changes with age (Osenberg *et al.* 1992). Pumpkinseed is unusual in that it has strong pharyngeal teeth capable of crushing snail shells, providing a relative advantage in feeding on molluscs. Adults can be found to specialize on snails (Feldman 1992, Ringler and Johnson 1982, Osenberg *et al.* 1992), but also feed upon many other organisms. Young pumpkinseed are more likely to be important forage for predators, and these do not consume as high a proportion of snails. Feldman (1992) found primarily chironomids and ostracods in the guts of yearling pumpkinseed from the Upper Hudson River.

Brown bullheads are omnivorous, feeding at night with the aid of barbels (Werner 1980). They have been observed to consume insects, fish, fish eggs, molluscs crayfish, leeches, oligochaetes, bryozoans, amphipods and plants (Carlander 1969, Smith 1985). Crustacea were found to make up about 60% of the diet in northern Cayuga Lake, and chironomids were found to make up another 25% (Smith 1985).

Spottail shiner feeds on zooplankton and benthic organisms such as insect larvae, algae and eggs and larvae of its own species. Its undershot mouth suggests a benthic feeder (Smith 1985). This observation contrasts with the PCB composition information and field gut studies discussed below, which indicate a more water column-based existence than other forage fish.

Yellow perch feed opportunistically, both in the water column and the benthos (Werner 1980, Smith 1985). Major prey items include invertebrates such as chironomids, cladocerans, ostracods, amphipods, snails, and crayfish. Larger yellow perch (>130 mm) also feed on small fish including young yellow perch (Carlander 1997).

Fallfish are also opportunistic, feeding on algae, fish, insects, and crayfish, although insects and fish are the dominant prey items (Carlander 1969, Smith 1985).

Bluegills feed throughout the water column on plant material, insects, small crayfish, and small fish (Carlander 1977, Smith 1985).

Silvery minnow feed on organic bottom detritus and algae (Carlander 1969, Smith 1985).

The tessellated darter feed primarily on chironomids and mayflies. Organic bottom detritus can be found in its gut (Werner 1980, Smith 1985).

Thus, the forage fish component of the model food web is composed primarily of generalist, largely opportunistic, species. These species appear to specialize to some degree on feeding location (tessellated darter is relatively more associated with the sediment bed than bluegills), as well as taxonomically (adult pumpkinseed is morphologically adapted to consume snails). In general, TL3 are likely to consume carbon from a combination of both water column invertebrates (phytophilous macroinvertebrates, or PMI) and benthic macroinvertebrates (BMI).

Pumpkinseed and brown bullhead are the two representative trophic level 3 fish in the Upper Hudson River bioaccumulation model, largely because an extensive historical PCB database exists for these species (NYSDEC 1998). Based upon published natural history information, both species are likely to consume a mixture of water column- and sediment-based

invertebrates and are therefore representative of TL3 fish as a whole. Brown bullhead may forage more on the bottom than pumpkinseed. Both pumpkinseed and brown bullhead were found in largemouth bass guts collected in the Upper Hudson River (Figure 5–7). However, it is unlikely that these two species are the dominant prey of largemouth bass, based in part on the diversity of fish found in the guts (Figure 5-7). In fact, they may not even be frequent prey of the largemouth bass. In the model, pumpkinseed and brown bullhead *represent* the forage fish community, which is composed of many species. Next, we present evidence that indicates that their total PCB level, PCB composition and feeding behavior is similar to that of other TL3 fish, that is, that they are indeed appropriate representatives.

First, total PCB levels measured in brown bullhead and pumpkinseed were compared with levels measured in other forage fish. Annual average concentrations for each location were computed from the NYSDEC database, and the brown bullhead and pumpkinseed values were matched up with values for other TL3 fish by location and year (Figure 5-8), similar to the analysis performed for the largemouth bass (Figure 5-5). Total PCB levels measured in brown bullhead generally lie within a factor of two of levels measured in other species (Figure 5-8a). Below 600 μg/g lipid, levels in brown bullhead are generally unbiased with respect to levels in other forage fish. Above 600 μg/g lipid, brown bullhead levels are as much as two to three times higher than levels in pumpkinseed, goldfish and carp. As for the brown bullhead, levels in pumpkinseed are usually within a factor of 2 of levels in other forage fish. Below a concentration of 600 μg/g lipid they are generally unbiased (Figure 5-8b). Above 600 μg/g lipid, levels in pumpkinseed are for the most part lower than in other TL3 fish, but still within a factor of two. Thus, together, brown bullhead and pumpkinseed provide a reasonable representation of the range of total PCB levels found in the TL3 fish community.

Second, PCB composition in TL3 fish was explored. PCBs in the surface sediments of the TIP are generally more dechlorinated than PCBs collected on water column particles (Figure 5-9). The water column samples contained an average of 3.6 Cl/BP, and sediment samples contained an average of 2.7 Cl/BP. Therefore, TL3 fish that are more closely associated with the sediments should have PCBs that are, on average, less chlorinated than fish that are more closely associated with the water column; the homolog distribution in TL3 fish provides an indication of

PCB source. PCBs in predatory fish may be more chlorinated than in TL3 fish because of selective accumulation of higher chlorinated congeners from their prey.

The average Cl/BP varies among TL3 species from the TIP (Figure 5-6). Species that prefer benthic prey have relatively lower Cl/BP values (white sucker, tessellated darter and carp). Spottail shiner has a relatively high value for a TL3 fish (4.25), suggesting a more water column-based PCB source. Most species of TL3 fish, including pumpkinseed and brown bullhead, have values between 4.0 and 4.2 Cl/BP, indicating a mixed diet. Yellow bullhead should be a TL3 fish, based on published natural history information (Smith 1985, Werner 1980, Carlander 1969). However, its value of 4.6 Cl/BP is inconsistent with this, being higher than any other TL3 fish, and even higher than predators. Exponent (1998a,b) found fish in 65% of the yellow bullhead stomachs they sampled, indicating that this species belongs in TL4 in the Upper Hudson River, which is more consistent with the PCB composition data.

The extent to which the model food web might be biased due to the exclusion of a more water column-based fish such as the spottail shiner was explored by comparing pumpkinseed and spottail shiner total PCB concentrations. PCB levels in TIP surface sediments are approximately eight-fold greater than PCB levels on water column particles (Figure 5-10; data collected by USEPA in 1992 and 1993). Therefore, the exposure of spottail shiner to relatively more water column-based PCBs should result in lower PCB concentrations than pumpkinseed. This was not observed. The average total PCB level in spottail shiner collected in TIP in 1993 by USEPA was 20.2 μg/g(w) (standard error of the mean=3.4, n=18). The average total PCB level measured in pumpkinseed collected in TIP in 1993 by NYSDEC was 22.7 μg/g(w) (standard error of the mean=2.5, n=21). This is not consistent with a large difference in exposure concentrations, and suggests that spottail shiner and pumpkinseed consume similar proportions of BMI and PMI, and therefore that the difference between these species in Cl/BP is not indicative of a large difference in diet.

The extent to which the model food web might be biased due to the exclusion of a more sediment-based fish such as the carp was explored by comparing brown bullhead and carp total PCB concentrations. Brown bullhead total PCB levels are within a factor of two of carp levels,

and are actually higher than carp levels at total PCB concentrations greater than 600 µg/g lipid (Figure 5-7a). Thus, PCB levels in the brown bullhead are representative benthic species.

In summary, forage fish are opportunistic. Most TL3 fish in the Upper Hudson River feed upon a mixture of PMI and BMI. Some forage fish are more closely associated with benthic carbon sources (white sucker, tessellated darter, carp), and there is evidence that one species is more closely associated with the water column (spottail shiner). However, PCB levels in these species are similar to levels in brown bullhead and pumpkinseed, suggesting that their diets are also similar. Thus, PCB levels in the brown bullhead and pumpkinseed are representative of PCB levels in the forage fish community as a whole.

Field Studies of Forage Fish Diets

To further refine estimates of the relative importance of water column and sediment carbon and PCBs to the food web, field studies of fish diets in the Upper Hudson River were conducted. Exponent (1998a,b) sampled BMI, PMI, and the gut contents of several species of TL3 fish in the Upper Hudson River simultaneously. The results of the field study consisted of the numbers of each invertebrate taxon in the guts of several species of forage fish and in the samples of BMI and PMI collected in the same vicinity at the same time. Samples were identified to the lowest taxonomic level that was possible with reasonable effort, ranging from species to order. This study provided information on both the availability of prey in the BMI and PMI and the actual feeding behavior of the fish.

Two analyses were performed to estimate the relative importance of BMI and PMI in the diets of the forage fish. First, the invertebrate taxa that were found only in BMI or only in PMI were used as indicators of feeding behavior. For example, the presence of taxa in the diet of a forage fish that were unique to the BMI would suggest that this species feeds to some extent on the BMI. This analysis used the data at the lowest taxonomic level reported. These indicator taxa comprised 1 to 25% of the total items found in the guts.

Every fish species sampled was found to have fed on some invertebrates that were unique to the BMI and some that were unique to the PMI (Table 5-1). This suggests that none of the

sampled forage fish species feeds exclusively on either BMI or PMI. The importance of BMI in the diets was greater in Spring than in Fall, due to the lack of macrophytes at the time of the Spring 1998 sampling.

For the second analysis, all of the data were aggregated to the taxonomic level of order. The goal of this analysis was to estimate the relative importance of BMI and PMI in the diet by comparing the relative abundance of each order in the BMI and PMI samples with its relative abundance in the guts of the forage fish. The analysis was designed to take into consideration both opportunistic feeding by the fish as well as possible specialization on certain invertebrate orders.

The first step in this analysis was to compute an expected order composition in the fish diet from the PMI and BMI order composition, based on two assumptions. (1) The fish feed opportunistically, so that the proportion that a given order comprises in the environment should equal the proportion in the observed diet. (2) The fish accumulate a proportion of their carbon from the PMI ($f_{Diet,PMI}$) and from the BMI (1- $f_{Diet,PMI}$). Under these assumptions, the expected diet was:

$$f_{Diet,i} = f_{Diet,PMI} f_{PMI,i} + (1 - f_{Diet,PMI}) f_{BMI,i} \qquad (5\text{-}22)$$

where:

$f_{Diet,i}$	=	proportion of order i expected in the diet of the fish
$f_{Diet,PMI}$	=	proportion of PMI in the diet
$f_{PMI,i}$, $f_{BMI,i}$	=	average proportion of order i in all PMI or BMI samples

Table 5-1. Diets of Fish in the Upper Hudson River.
Individual Taxa in the Diets Which are Unique to the BMI or PMI. Data Collected by Exponent (1998b, 1998c)

	Pumpkinseed		Spottail shiner		Log perch		Yellow perch		Brown bullhead		Yellow bullhead		Redbreasted sunfish	
	BMI	PMI	BMI	PMI	BMI	PMI	BMI	PMI	BMI	PMI	BMI	PMI	BMI	PMI
Fall 1997														
Number of unique taxa[1]	24	8	12	6	16	9	7	7	5	4	3	4	3	4
Percent of individual items in the guts that belong to unique taxa	6.5	1.9	0.81	9.1	1.7	22.	1.1	9.8	2.9	1.7	2.4	1.9	13.	9.0
Spring 1998														
Number of unique taxa[1]			9	1			14	4	30	5	6	0		
Percent of individual items in the guts that belong to unique taxa			3.7	0.3			1.5	0.6	18.	2.2	12.	0.		

[1]Entries represent the number of taxa that are found in the stomachs of the indicated fish species and are only found in either the BMI or the PMI in all environmental samples collected in the Upper Hudson River.

For example, if a fish species feeds opportunistically and solely from the BMI, and $f_{Diet,PMI}$ is set to zero, then a graph of the order composition within the BMI *vs.* the order composition in the diet should exhibit a positive correlation, with a slope equal to 1:1 and an intercept at zero. Thus, the graphical comparison of the computed vs. the observed diets provides an indication of the degree to which the fish feed opportunistically.

The second step involved optimizing the value of $f_{Diet,PMI}$ to obtain the best agreement between computed and observed diet. The optimization was conducted by graphical comparison of the computed diet with the observed gut contents for several values of $f_{Diet,PMI}$. This analysis provided two types of information: what value of $f_{Diet,PMI}$ results in the best characterization of actual diet (i.e., the best overall relationship between observed and expected diet), and what orders are preferred (consistently above the 1:1 line) or avoided or unavailable (consistently below the 1:1 line). For this analysis, orders that were absent from either environmental samples or the stomach contents were placed on the appropriate axis, at an arbitrary value of 0.0001. Data sufficient to perform this analysis were available for pumpkinseed, spottail shiner and brown bullhead.

The diet of the pumpkinseed appeared to be opportunistic: in general, those orders that were more common in the environment were more common in the diet (Figure 5-11). One order, tubificid oligochaetes, was underrepresented in the guts of pumpkinseed relative to their abundance in both the PMI and BMI. This could have been due to a tendency to avoid tubificids, tubificids' ability to avoid predation, or to a sampling bias; oligochaetes are generally difficult to observe in gut samples. Without tubificids (the value indicated by the open square in Figure 5-11), the best overall relationship between computed and observed diets was observed for a mix of sediment- and water column–based invertebrates ranging between 25 and 75% of each. Thus, these results indicate that the pumpkinseed are opportunistic feeders and consume a mix that is likely to contain between 25 and 75% PMI. This information was used to constrain model calibration.

Cladocera appeared to be relatively abundant in the diet of the brown bullhead, comprising 12% overall, but were uniformly low in abundance in both PMI and BMI (Figure 5-

12). Cladocera are generally present in the water column, and therefore were likely to have been missed in both samplings. This suggests that the brown bullhead consumes some food from the water column. Without Cladocera (the value indicated by the open square in Figure 5-12), the values for six of the invertebrate orders lie within a few percent of the 1:1 line if the diet is assumed to be composed only of BMI, whereas values are generally below the 1:1 line if PMI contribute to the diet. This suggests that brown bullhead prefer BMI. The proportion PMI in its diet cannot be estimated from these data. Therefore, the diet of the brown bullhead in the model was determined by calibration and was also considered in the uncertainty analysis.

Cladocera were also consistently over-represented in the diet of the spottail shiner compared with their abundance in the PMI and BMI samples, while tubificids and mesogastropods (limpets) were consistently underrepresented (Figure 5-13). The apparent preference for Cladocera and the relative lack of tubificids in the diet suggest a preference for water column-based invertebrates. To explore the opportunistic the component of the spottail shiner diet, the analysis was repeated without these three groups (values indicated by open squares in Figure 5-13). Without these groups, the spottail shiner appeared to consume relatively more PMI than pumpkinseed: the relationship that shows the least bias with respect to the 1:1 line is observed with 100% PMI. However, the uncertainty associated with this relationship is relatively large. Thus, based upon the observed preference for Cladocera, the relative lack of oligochaetes in the diet, and the relationship between observed and expected diets, the spottail shiner is likely to be consuming relatively more PMI than BMI.

The conclusion that PMI are relatively more important in the diet of the spottail shiner than in the diets of the pumpkinseed and brown bullhead is consistent with the observation that the average Cl/BP value is greater in spottail shiner (Figure 5-6). However, the difference is likely to be small, based upon two lines of evidence. First, total PCB levels measured in pumpkinseed and spottail shiner in 1993 were similar (see previous discussion). Second, the evidence based upon the analysis of taxa unique to the BMI and PMI was equivocal. Based on the number of unique taxa in the diet, spottail shiner did not appear to consume relatively more PMI than BMI. In addition, the Spring 1998 data did not show a striking difference between

brown bullhead and spottail shiner. This suggests that the spottail shiner preference for PMI is not a strong preference.

Three potential refinements to the food web analysis were explored. First, some orders of invertebrates, for example Diptera, include both species that are found primarily in the PMI and species that are found primarily in the BMI. Important information regarding the feeding locations of individual species was lost in the analysis performed at the level of order. Therefore, the analysis was repeated at the taxonomic level of genus. For all three species of TL3 fish, there was greater scatter in the graphical relationship between the expected and observed diets, and correlations were either not evident or were not as clear as in the analyses performed at the level of order (results not shown). Thus, the biological refinement provided by performing the analysis at a lower taxonomic level was overwhelmed by the additional statistical uncertainty probably due to smaller sample sizes for each genus. As a result, the genus-based analysis did not provide additional information regarding the dietary preferences of these fish.

These analyses were repeated for each habitat type, that is, each macrophyte species, as well as for each sampling location (*Vallisneria* habitat only). The results exhibited a great deal of scatter, and correlations were generally not evident. Thus, these analyses did not provide additional information regarding the dietary preferences of the fish.

In conclusion, the TL3 community consists of generalized, opportunistic species. Pumpkinseed and brown bullhead are representative of the TL3 community both in total PCB level and PCB composition. There are fish that consume relatively greater proportions of sediment or water column carbon and PCBs than brown bullhead and pumpkinseed, but the differences are small. Pumpkinseed likely consumes between 25 and 75% PMI, and brown bullhead consumes somewhat greater percentage of BMI.

Finally, fish predation is size-dependent; larger largemouth bass consume larger prey fish (Lewis *et al.* 1974, Hamilton and Powles 1983, Keast 1985). In addition, the shape of the prey affects the preference of the predator (Hambright 1991). In the model, older age classes of largemouth bass consume progressively greater proportions of older forage fish. The age classes

of TL3 fish consumed by model TL4 fish are based upon Hambright (1991; Table 5-2). Note that we do not assert that older largemouth bass consume age 3 and 4 brown bullhead, only that brown bullhead of this age range are representative of largemouth bass prey with a more benthic tie.

Table 5-2. Age-Specific Predation by Largemouth Bass on Pumpkinseed and Brown Bullhead

Largemouth Bass		PMI	BMI	Pumpkinseed					
				Age					
				1	2	3	4	5	6
Age	Weight Range (g)			Weight range (g)					
				1-20	20-30	30-76	76-144	144-190	190-220
1	1-35	0.25	0.25	0.50					
2	35-171			1.00					
3	171-330			1.00					
4	330-509			1.00					
5	509-813			0.60	0.40				
6	813-1050			0.40	0.40	0.20			
7	1050-1270			0.20	0.60	0.20			
8	1270-1525				0.50	0.50			
9	1525-1775				0.40	0.60			
10	1775-2100				0.30	0.65	0.05		
Largemouth Bass		PMI	BMI	Brown Bullhead					
				Age					
				1	2	3	4	5	6
Age	Weight Range (g)			Weight range (g)					
				1-14	14-77	77-201	201-322	322-417	417-506
1	1-35	0.25	0.25	0.50					
2	35-171			1.00					
3	171-330			0.60	0.40				
4	330-509			0.50	0.50				
5	509-813			0.30	0.70				
6	813-1050			0.25	0.70	0.05			
7	1050-1270			0.10	0.70	0.20			
8	1270-1525				0.70	0.30			
9	1525-1775				0.50	0.50			
10	1775-2100				0.30	0.65	0.05		

Note: The values for pumpkinseed and brown bullhead in this table represent the proportion of each in the largemouth bass diet assuming each species constitutes all of the fish prey. If, for example, brown bullhead and pumpkinseed are consumed in equal proportions, then the proportions given in this table were multiplied by 0.5 (except for the invertebrates). Thus, age 1 largemouth bass would consume 25% PMI, 25% BMI, 25% pumpkinseed and 25% brown bullhead.

5.2.1.3 Invertebrates (Trophic Level 2)

The invertebrate fauna of the Upper Hudson River includes species that inhabit the sediment bed (e.g. oligochaetes and several species of chironomid larvae), species that live on the surfaces of macrophytes (e.g. Rheotanytarsus sp.; Exponent 1998a,b,c), and species that feed within the water column (e.g. Cladocera). Two types of studies of the invertebrate fauna have been conducted: surveys using multiplate samplers and direct surveys of the benthic and macrophyte-associated invertebrates.

Multiplate samplers consist of a stack of small hardboard plates separated by spacers and held together with an aluminum turnbuckle. They are suspended in the water column for several weeks. After removal from the river, the biological community that colonized the plates is analyzed for species composition. In the Upper Hudson River, PCB concentrations have been measured in material scraped from multiplate samplers. In the multiplate studies conducted on the Upper Hudson River, the most abundant taxa were chironomids and oligochaetes (Simpson 1976, Hetling *et al.* 1978, Novak *et al.* 1988, Bode 1979).

There have been three studies in which the invertebrate fauna of the Upper Hudson River has been sampled directly. Law Environmental sampled the benthic fauna with a Petite Ponar sampler at three sites in TIP and at one site in the river reach above the TIP in November, 1990 (Law Environmental 1991). Samples were dominated by oligochaetes (38% by numbers) and chironomids (23%).

Feldman (1992) sampled BMI as well as PMI in the TIP. Chironomids dominated both BMI and PMI. Cladocera, gastropods, amphipods and caddisflies were also important components of the PMI. Oligochaetes were rare in the PMI and constituted up to 15% of the BMI.

Exponent (1998a,b,c) sampled both BMI and PMI in surveys conducted at two locations in the TIP and one in the Stillwater Pool. The most common taxa were Diptera (40% of all sampled organisms, composed of 99% chironomids), followed by snails, limpets, mayflies and oligochaetes (Figure 5-14).

Thus, the invertebrate fauna of the Upper Hudson River is typical of temperate-zone freshwater ecosystems, being dominated by chironomids. Chironomids are the larvae of small flies called midges. They have a variety of feeding habits and are likely to consume either particles derived from the water column or particles from the surface of the sediment bed. Their diet can include living organisms such as algae, bacteria and higher plants (Pennak 1978).

Chironomid larvae are known to be an important resource for maintaining fish populations in general (Pennak 1978) and this is borne out in samples of fish guts from the Upper Hudson River. Exponent (1998a,b) found that chironomids comprised 32% of the total number of individual prey items identified in the stomachs of fish from the Upper Hudson River. Cladocera comprised 34%, and all other orders comprised less than 8% each. Oligochaetes were less than 0.1% of the total. Chironomids were present in 79% of the 709 fish stomachs that were analyzed, Cladocera in 61%, and oligochaetes in less than 2%.

Oligochaetes are also common in the benthos, but are relatively unimportant components of fish diets. They are close relatives of and ecologically similar to earthworms. Oligochaetes burrow in sediments and consume the particles of the bed directly, extracting microbial biomass and other organic material for nutrition. These worms mix the upper layer of the bed by their movement and feeding activities.

Cladocera were usually (but not always) rare in BMI and PMI samples, which is to be expected because they are generally found in the water column. However, they were relatively common in fish stomachs and therefore probably represent a source of water column-based PCBs to the food web.

For the purpose of quantifying PCB transfer, the invertebrates are distinguished by their exposure source (water column vs. sediment) and their degree of bioaccumulation. In the model, both BMI and PMI are represented. One type of invertebrate is modeled for each exposure route. That is, one generic BMI organism and one generic PMI organism are represented. The model BMI represents chironomids as well as other benthic species that are of less importance in the diet of the fish, including oligochaetes. The model PMI represents chironomids, Cladocera and

other species of invertebrates that accumulate PCBs from the water column. Individual taxa are not modeled, primarily because of a lack of the data necessary to develop invertebrate models that would significantly improve the accuracy of the overall model. The relative importance of BMI and PMI in the diet of the forage fish is a calibration parameter, subject to the constraints discussed in Section 5.2.1.2.

5.2.2 Bioavailable Depth within the Sediment Bed

Both the depth to which sediment mixing occurs as well as the degree of mixing within the bed are important determinants of chemical fate and bioaccumulation. The depth of mixing and the burial rate determine the speed with which natural recovery occurs. The degree of mixing within the surface sediments determines the chemical concentration that is available near the sediment/water interface, both for diffusion and resuspension into the water column as well as for consumption by benthic invertebrates.

Particle mixing is the result of both physical and biological processes. Cycles of deposition and resuspension result in mixing near the sediment/water interface. The feeding activity of invertebrates results in mixing at a greater depth.

The depth to which mixing occurs in the Upper Hudson River was estimated based upon three lines of evidence:

Published natural history information. As described in Section 4.3.4, there is likely to be some degree of mixing to a depth of five cm in the sediment bed. Most chironomids are concentrated in the upper 2-4 cm of lake mud (Milbrink 1973, Ford 1962). Tubificids penetrated lake muds to 15 cm, with maximum abundance from 2- 4 cm (Milbrink 1973). In a lake sediment core in which some degree of mixing was observed to 3 cm, the peak abundance of oligochaetes occurred at 1-3 cm (Krezoski *et al.* 1978). In another core, some mixing was found to 6 cm, but the depth of maximum abundance was 2-3 cm. Thus, most of the population of benthic organisms is found closer to the surface than the maximum depth of occurrence and the depth to which mixing is observed (Milbrink 1973, McCall and Tevesz 1982).

Use of dechlorination to fingerprint PCBs. Deeply buried PCBs are generally dechlorinated in the Upper Hudson River, and the available data indicate that surface PCBs are relatively undechlorinated. Because dechlorination is mediated by bacterial action in the environment and does not occur to an appreciable degree within fish, the PCB composition of the fish gives an indication of the dechlorination status of their exposure sources; fish exposed to dechlorinated PCBs are enriched in lower chlorinated congeners relative to fish exposed to fresh PCBs. This provides a marker that we use to estimate the bioavailable depth. Two analyses were performed based upon this premise: an analysis of measured congener concentration ratios *vs.* depth, and simulations using a homolog bioaccumulation model.

Ratios of selected congener concentrations provide a measure of dechlorination. For example, congener 56 (233'4') is dechlorinated relatively rapidly, while congener 49 (242'5') is dechlorinated to a much lesser degree. Both have similar K_{OW}'s and therefore similar partitioning and bioaccumulation properties. A ratio of the concentrations of the two congeners provides a measure of dechlorination: a high value is characteristic of undechlorinated PCBs, and a low value indicates dechlorination. The value of this ratio in sediments within the top 5 cm of the sediment bed is high and similar to the value in Aroclor 1242 (Figure 5-15) and decreases with depth. The value of this ratio is also relatively high in fish and similar to values observed in sediments within 5 cm of the surface. This indicates that the fish are exposed to undechlorinated sediments that originate within the top 5 cm of the bed.

PCB homolog model. The PCB_{3+} model was extended to model PCB homologs in the three species of fish collected in the TIP in the late 1980s. The dietary compositions estimated during the calibration of the total PCB model were used. The measured distribution of PCB homologs in the fish was compared with distributions computed by the model, based upon exposure to three different homolog distributions in the sediments, representative of 0-2 cm, 0-5 cm and highly dechlorinated PCBs. The computed fish distributions matched the data best if the fish were exposed to PCBs with a homolog distribution characteristic of 0-2 cm, suggesting that the food web is exposed to sediments on the order of 2 cm deep, and probably not as deep as 5 cm. The development and results of the homolog models are discussed in Section 5.5.

Summary. No direct estimates of mixing depth in rivers were found in the literature. Based on the lake data, we have concluded that the benthic organisms may be capable of mixing sediments to a depth of 6 – 9 cm, but are likely to be doing most of their feeding at a shallower depth. In the fate model, vertical mixing occurs to 5 cm. The depth to which BMI feed was estimated to be 2 cm, based upon the natural history information and the results of the homolog model described in Section 5.5.

5.2.3 Bioaccumulation Factors for the Base of the Food Web

Benthic Invertebrates

The model computes food consumption by fish on an energy basis (in units of kJ/g(w)-day). This permits the model to account for differences in energy density among prey and predators. Therefore, an energy-based BSAF was computed from the USEPA benthic invertebrate data collected in 1993 (in units of [ug/kJ] / [ug/gOC]). The energy-based BSAF is equal to:

$$BSAF_e = BSAF\left(\frac{f_L}{\lambda_{inv}}\right) \qquad (5\text{-}23)$$

where:

$BSAF_e$	=	energy-based BSAF (gOC/kJ)
BSAF	=	lipid-based BSAF (gOC/glipid)
λ_{inv}	=	energy density of the invertebrate sample (kJ/g(w))

BSAF was estimated using data collected by the USEPA in the Upper Hudson River (USEPA 1998). At each of four stations in the Upper Hudson River, the USEPA measured PCB levels in several samples of benthic invertebrates and in several nearby sediment samples. BSAF values for each station were calculated using the average of all invertebrate samples and the average of all sediment samples collected at the station. The reported "unsorted total" value was

used, representing the average PCB concentration and lipid content of all organisms in a sample (Limno-Tech, Inc. *et al.* 1996). The average BSAF for total PCBs was 1.4 gOC/glipid. This value is similar to the average value of 1.5 calculated by Tracey and Hansen (1996). The average BSAF computed for PCB_{3+} based upon the EPA data, 1.55, was used in the model.

The inverse of the term in parentheses in Equation 5-23 is equal to (see Equation 5-20):

$$\frac{\lambda_{inv}}{f_L} = 19.42 + 20.08\left(\frac{f_D}{f_L}\right) \qquad (5\text{-}24)$$

Thus, the lipid content of the invertebrate prey on a dry weight basis (f_L/f_D, in units of glipid/gdry) is required. This was estimated in several species of invertebrates (Herbreteau *et al.* 1994, Nalepa *et al.* 1993, Wilcock *et al.* 1993, Oliver 1984, Klump 1987, Swindoll and Applehans 1987, Leversee *et al.* 1982, Gerould *et al.* 1983, van de Guchte *et al.* 1988). From these data, average energy density were computed for four major groups: crustacea, chironomids, molluscs, and annelids. These averages were weighted according to the overall contribution of each group to the diets of all fish sampled by Exponent (1998b), and an average energy density of the invertebrate prey of TL3 fish was computed (190 kJ/g lipid). Thus, $BSAF_e$ equals (1.55 gOC/glipid) / (190 kJ/g lipid) = 0.0082 gOC/kJ.

Water Column Invertebrates

Water column invertebrates accumulate their PCBs from particles associated with plant surfaces and particles in the water. Thus, they are at the same trophic level as the BMI, which accumulate their PCBs from sediment particles. In addition, the composition of the invertebrate fauna is generally similar in the PMI and BMI. For example, 87% of all organisms sampled by Exponent (1998b) belonged to taxa that were found in both the PMI and the BMI.

However, the PCBs associated with water column particles are likely to be more bioavailable than the PCBs associated with sediments, for two reasons. First, PCBs on water column particles are probably more bioavailable than PCBs on sediment particles. Water

column particles probably include a significant proportion of biological material, based on the observation of average carbon contents of 15 to 30% during flows less than or equal to the annual average (see Section 4). For comparison, phytoplankton contain an average of 40% carbon on a dry weight basis, and sediment bed particulates generally contain 1 to 5% carbon. The particulate carbon in the water column is not likely to have originated in the local contaminated sediments of the Upper Hudson River, based on the difference in f_{OC} and the general lack of resuspension during most of the growing season. Therefore, sorption of the PCBs to water column particulates is likely to have occurred relatively recently and within the water column. Similarly, the material consumed by invertebrates feeding on macrophyte surfaces probably includes a high proportion of periphyton, which is live biological material. PCBs found in periphyton must also have sorbed recently, certainly within the current growing season. In contrast, the PCBs present on sediment particles are likely to have been in contact with those sediments for longer periods of time.

Bioavailability declines as the sediment/PCB contact time increases (Landrum 1989). This suggests that the recently sorbed PCBs on water column particles should be more bioavailable than the aged PCBs on sediment particles.

Second, biological carbon is likely to be more digestible, or bioavailable, than aged carbon on sediment particles. Aged carbon contains a relatively high proportion of high molecular weight humic materials, which are not readily digestible. Greater bioavailability of carbon results in greater bioavailability of the associated PCBs, because digestion of the carbon liberates PCBs.

The accumulation factor from water column particles to PMI was determined based upon PCB measurements in phytoplankton and zooplankton conducted in Green Bay as part of the Green Bay Mass Balance Study (Connolly *et al.* 1992, HydroQual 1995b). This data set includes a large number of pairs of phytoplankton and zooplankton samples collected over much of the year, providing what is probably the most extensive set of measured water column invertebrate accumulation factors available. For each sampling, phytoplankton and zooplankton samples were collected in the same bottle. Average trophic transfer factors ([µg PCB/g lipid]/[µg PCB/g

organic carbon]) for each congener in Green Bay ranged from 2 to 4. A value of 3 was used in the model. This is two times the trophic transfer factor used for the benthos.

5.2.4 Species Bioenergetics

Growth

The species-specific relationships between age and weight were estimated using fish collected from the Upper Hudson River in November, 1990 (Law Environmental 1991). Fish were collected from nine reaches upstream of the Troy Dam by electrofishing from a boat. For every fish, weight, length, and the number and radius of annual growth rings on scales were measured. PCB levels were measured in a subset of these fish.

Age-specific weights were calculated in two ways. First, the weights of individual fish were plotted against the ages of the fish. These weights were measured in November, which was after the 1990 growing season, but before the formation of the scale annulus, which is generally in early Spring (Crawford *et al.* 1989). Thus, for example, a fish that has lived through two growing seasons would have one annulus. Therefore, the age of each fish was equal to the number of scale annuli+1. This provided a weight/age relationship for all ages of largemouth bass and pumpkinseed and all ages of brown bullhead except young-of-the-year and yearlings (symbols in Figure 5-16). The weight values used in the model were determined by smoothing these data visually (represented by the lines in Figure 5-16).

The direct measurements of the weight/age relationship for brown bullhead were supplemented with back-calculated weights based upon measurements of spine annuli. Based on a comparison of back-calculated weights and directly measured weights for ages 3 through 7, the back-calculated weights for young-of-the-year and yearlings were used in the model. First, the relationship between fish age and length was determined by back-calculation. This method is based on the observation that the width of each annual growth ring on a spine is proportional to the annual change in length of the fish (Jearld 1983). The total length of each fish at each age was given by:

$$L_{T,i} = \frac{L_T}{R_S} R_{S,i} \qquad (5\text{-}25)$$

where:

$L_{T,i}$	=	total length of the fish at age i, back-calculated (mm)
L_T	=	total length of the fish (mm)
R_S	=	radius of the spine (mm)
$R_{S,i}$	=	radius of annulus i of the spine (mm)

The relationship between age and mean length in brown bullhead determined by back-calculation is presented in Figure 5-17a.

Next, the relationship between fish length and wet weight was determined using all brown bullhead collected by Law Environmental (1991; Figure 5-17b). Finally, mean wet weight at each age was calculated from the age-length and the length-weight relationships (open symbols in Figure 5-17c). Figure 5-17c also includes the average weights measured in fish of each age (from Figure 5-16, filled symbols), as well as the values used in the model (represented by the line).

The values in Figures 5-16 and 5-17 represent the weights at the end of each year's growing season, which are also the weights at the beginning of the following year's growing season. The weights at the start of the first year of life were arbitrarily set to 1.0 g. The growth rate for each age class was calculated by integrating Equation 5-17, using the appropriate beginning and ending weight values. In the model, each year's growth occurs between mid-May and the end of September, when water temperatures are above 10°C in the Upper Hudson River (Adams *et al.* 1982, Carline 1987).

Respiration

Species-specific measurements of standard, or quiescent, metabolism were available for all three model species. The rate of standard respiration by largemouth bass was based on a study by Beamish (1970) and an associated bioenergetics model (Rice 1981). This bioenergetics model was tested against field data by Rice and Cochran (1984), who found that predicted and measured cumulative food consumption agreed well. The rate of respiration by pumpkinseed was studied experimentally by Evans (1984), Burns (1975) and Brett and Sutherland (1965). Evans (1984) performed separate experiments to determine weight and temperature relationships with respiration, and these were combined mathematically in the present study to yield parameter estimates for the food chain bioaccumulation model. He found that the results of the previous investigators were similar to his results. Respiration rates in brown bullhead were estimated based upon the laboratory studies of Beamish (1964) and Saunders (1962).

Active metabolism is greater than standard metabolism (Peters 1989). In the pumpkinseed, routine metabolism, defined as metabolism during normal activity, was found to equal approximately 1.16 times the standard metabolism (Evans 1984). This is similar to the value estimated by Rice (1981) for the largemouth bass, 1.10. These values were used in the model. No direct estimates of the relationship between standard and active metabolism were found for the brown bullhead. Therefore, the average of the other two values, 1.13, was used. Parameters of the bioenergetics component of the model are given in Table 5-3.

Apparent specific dynamic activity is equal to approximately 15% of the total food consumption (Beamish 1974). Therefore, the sum of growth and respiration was multiplied by 1.15 to give total food consumption.

The efficiency with which food energy is assimilated (α_F in Equation 5-10) was set equal to 0.8 (Beamish 1974). Note that the ratio of α_c/α_F is required by the model (see section 5.2.5).

Table 5-3. Bioenergetic Parameters for Fish				
	β	y	ρ	Activity Multiplier
Largemouth Bass	0.113	-0.355	0.0313	1.10
Pumpkinseed	0.022	-0.269	0.0589	1.16
Brown bullhead	0.034	-0.075	0.0834	1.13

Lipid content

In the model, the lipid content of each fish species varied year to year. Values were calculated directly from the NYSDEC data set (Figures 5-18 and 5-19). The greatest variation was observed in the largemouth bass; annual average lipid contents ranged over approximately one order of magnitude during the calibration period. Due to the effect of lipid content on the rate of loss of PCBs across the gill surface, this variation had a significant impact on PCB levels in the fish (based on model results not shown).

No yearling pumpkinseeds were collected in 1991 or 1992. Average lipid contents measured in 1991 in older pumpkinseeds in Stillwater and Thompson Island Pool were 0.58 and 0.72%, respectively, considerably lower than values measured in yearlings in the 1980s and early 1990s. These data, along with the corroborating low values measured in largemouth bass and brown bullhead, were used to estimate lipid contents for yearling pumpkinseed in 1991.

5.2.5 Toxicokinetics

Gut transfer

The fraction of ingested contaminant that is transferred across the gut wall and into the animal is termed the assimilation efficiency (α_c in Equation 5-3). A compilation of experimental estimates of assimilation efficiency of various PCB congeners has shown that values ranges from about 0.1 to 1 (Connolly *et al.* 1992, Parkerton 1993). To examine these data, multiple values from individual studies were averaged to give all studies equal weight; the data were then grouped into half log unit K_{ow} bins (eg., 4.25 to 4.75) and displayed as box plots (Figure 5-20). Congeners with

log (K_{ow}) values below 6.75 (generally mono- to pentachlorobiphenyl) have similar assimilation efficiencies, although a slight decline with increasing K_{ow} is evident. Median values range between 0.75 and 0.85. As log (K_{ow}) increases beyond 6.75 a more dramatic decline occurs.

The differences in assimilation efficiency among studies reflect various factors including measurement error, residence time in the gut, digestibility of the portion of the ingested prey that contains most of the contaminant (for hydrophobic organic chemicals this is fat tissue) and the physical-chemical mechanisms responsible for moving the chemical across the gut wall. Of the biological and chemical factors, the digestibility of the prey appears to have the greatest impact. Studies indicate that the assimilation efficiency of hydrophobic contaminants is closely linked to dietary assimilation of lipids (Van Veld 1990). This is supported by experimental studies with metals and radionuclides which indicate a direct correspondence between the uptake of contaminant by zooplankton and the fraction in the digestible component of the algal diet (Reinfelder and Fisher 1991). The median assimilation efficiencies presented in Figure 5-20 (0.75 to 0.85 up to log (K_{ow}) 6.5) are similar to the food assimilation efficiency of 0.8 measured in largemouth bass by Beamish (1974). In addition, previous modeling studies have suggested that assimilation efficiency of hydrophobic organics with log (K_{ow}) values below about 6 to 6.5 is similar to that of food energy and is perhaps equal. Based on the above information, we have maintained equality between contaminant and food assimilation efficiency for PCB_{3+}. Note that the model requires only the ratio of these coefficients and not their absolute values. Substituting Equation 5-21 into the second term in Equation 5-3, which represents the dose of contaminant received by the fish from its prey:

$$Dose = \frac{\alpha_c}{\alpha_F} P_i \sum_{j=1}^{n} f_{ij} \frac{v_j}{\lambda_j} \qquad (5\text{-}26)$$

Gill Transfer

The rate of transfer of contaminants between blood and water across the gill epithelia is determined from the transfer rate of oxygen and a ratio between the uptake efficiencies of contaminant and oxygen (Equation 5-7). Based upon laboratory studies summarized in Figure 5-21 (Connolly *et al.* 1992), the ratio of uptake efficiencies is approximately 1.0. This value is used in the model.

Computation of the elimination rate requires estimation of the lipid/blood partition coefficient, π_{LB}. K_{ow} is used as an estimate of π_{LB} in the model, resulting in an inverse relationship between log (K_{ow}) and log (elimination rate), as found by Erickson and McKim (1990). In Equation 5-16, $f_B << \pi_{LB} f_L$. Therefore, the average elimination rate for total PCBs is approximately equal to:

$$K_{gill} = K_u c_R v_B \approx \left(\frac{K_u c_R v}{f_L} \right) \sum_{c=1}^{n} \frac{f_c}{K_{OW,c}} \qquad (5\text{-}27)$$

where:

f_c = weight fraction that congener c comprises in fish

$K_{ow,c}$ = octanol/water partition coefficient for congener c

Thus, estimation of the total PCB elimination rate requires the harmonic mean K_{ow}. This was calculated using the congener composition of all fish collected from Stillwater to the Route 197 Bridge at Rogers Island from 1990 to 1996, along with the congener-specific K_{ow} values reported by Hawker and Connell (1988). The resulting Log (K_{ow}) value was 5.81.

The mass proportion of blood in the body (f_B) is set equal to 0.05. Uncertainty in this value has no significant impact on model calculations, because $f_B << \pi_{LB} f_L$ (Equation 5-16).

The factor that accounts for the reduction in elimination rates due to the slow transfer from storage tissues (c_R) was estimated as follows. A value of 0.25 was found to be necessary for calibration of a PCB bioaccumulation model for the pelagic food web of Green Bay, Wisconsin (Connolly *et al.* 1992, HydroQual 1995b). The results of the Green Bay PCB model compared favorably with data over a spatial gradient of total PCB concentrations measured in five species of fish, for PCB congeners with log (K_{ow}) values ranging from 5.0 to 7.5. This value represented the best estimate prior to calibration of the Upper Hudson River model. Because the experimental data is insufficient to estimate a value for c_R, it was treated as a calibration

parameter, and the sensitivity of model results to variation in the value of c_R around the best estimate of 0.25 was explored.

5.3 CALIBRATION/VALIDATION STRATEGY

5.3.1 Overall Approach

Model simulations were performed for pumpkinseed, brown bullhead and largemouth bass at Stillwater and in the TIP for the period from May 1, 1977 to December 8, 1998. Model results were presented for the period from 1980 to 1998, because the uncertainty associated with the data in the late 1970s, including the initial conditions, increased the uncertainty of the simulations before this time. Total PCB concentrations measured in fish on an Aroclor basis (NYSDEC 1998) were compared with model results that were computed based upon PCB_{3+} exposure concentrations in sediments and water. This leads to a bias of less than 5% in model results, because mono- and dichlorobiphenyl comprise less than 5% of total PCBs in fish from the Upper Hudson River.

Model results and data collected by NYSDEC (1998) were compared on an age-specific basis, based on the age/weight relationships developed by Law Environmental (1991). Brown bullhead and largemouth bass were primarily age 4 and older, and pumpkinseed were primarily young-of-the-year and yearlings.

Calibration of the models involved adjusting the elimination resistance factor, c_R, starting with the initial best estimate of 0.25. This affects all 3 species. In addition, calibration of the pumpkinseed and brown bullhead models involved adjusting the mix of PMI and BMI in the diet (subject to consistency with the dietary composition data discussed in Section 5.2.1.2). Calibration of the largemouth bass model involved adjusting the proportions of pumpkinseed and brown bullhead in its diet.

5.3.2 Exposure Concentrations

The food web was exposed to PCBs in the cohesive sediments. Exponent (1998d) surveyed the vegetation of the Thompson Island Pool and found that of 587 locations in which vegetation was found, fine sediments were observed in 543 (93%), sand in 124 (21%), gravel in 95 (16%), cobble in 60 (10%), wood in 37 (6%), and rock in 6 (1%). Thus, vegetation is associated with fine sediments, and therefore the PCB concentrations in cohesive sediments computed by the fate model were used to represent the sediment exposure levels for the benthic component of the food web.

The food web was exposed to PCBs within the top 2 cm of the sediment bed, based upon the analyses presented in Section 5.2.2 and the result of the homolog model (Section 5.5).

The extent to which fish move within each dammed reach is not known. To explore the degree to which exposure levels may vary within each reach, total PCB concentrations in largemouth bass, pumpkinseed, brown bullhead and yellow bullhead were collected by Exponent in September, 1997 in two locations within Thompson Island Pool, near Griffin Island ("GI") and just north of Snook Kill ("NTIP"). For comparison, NYSDEC monitoring program in the Thompson Island Pool involved collections in Spring near Griffin Island exclusively. Average concentrations measured in largemouth bass, pumpkinseed and yellow bullhead in the two locations were statistically indistinguishable (Figure 5-22; Student's t-test, $P>0.05$), suggesting that these species either move throughout the pool on a regular basis or are local but are exposed to similar PCB concentrations. Based on this analysis, the model largemouth bass is exposed to forage fish that are in turn exposed to pool-wide average concentrations. In contrast, levels in brown bullhead were significantly greater at GI than at NTIP (Student's t-test, $P<0.01$; samples sizes 9 at GI and 15 at NTIP). Therefore, it is possible that subpopulations of brown bullhead experience differing local exposure levels. The possibility of locally exposed subpopulations is considered when interpreting the calibration results.

Because the sediment and water column exposure levels used in the bioaccumulation model were determined by the fate model, inaccuracy in the fate model calibration affects the

bioaccumulation model calibration. The most apparent inaccuracy in the fate model was an over-estimate of the water column PCB concentration in the mid-1980s (Figure 5-23). To correct this inaccuracy, PCB_{3+} concentrations computed by the fate model at both Thompson Island Pool and Stillwater from 1984 through 1989 were divided by two. The resulting exposure levels used in the bioaccumulation model are presented in Figure 5-23.

5.3.3 Fish Data

The model was calibrated using total PCB concentrations measured in largemouth bass, pumpkinseed and brown bullhead, at Thompson Island Pool and Stillwater, that were collected as part of NYSDEC monitoring program (Figures 5-24 through 5-27). Adult largemouth bass and brown bullhead samples were collected in Spring, while small pumpkinseed were collected in late Summer or early Fall. The data from the later 1970s and early 1980s were corrected following Butcher *et al.* (1997). These data are compared with re-analyses of DEC samples and additional samplings conducted by GE in 1997. Only years with more than 2 samples per species and location are presented. This affects data collected in the 1970s, as well as 2 largemouth bass collected in Thompson Island Pool in 1983. Data collected since 1980 are compared with model results.

Trends differ on lipid and wet weight bases (Figures 5-24 through 5-27). In addition, total PCB levels are generally correlated with lipid content (Figure 5-28), which means that with similar exposure levels, fatter fish tend to have more PCBs. Trend analysis must separate out variation in lipid content from changes in exposure level. Lipid-normalized data better reflect trends in exposure than do wet weight-based data. For example, while lipid-based levels in largemouth bass from Stillwater declined from the late 1970s to the late 1990s, consistent with trends in pumpkinseed and brown bullhead, the wet weight-based levels increased and decreased during this period in a manner that followed the changes in lipid content (compare Figures 5-24, 5-25 and 5-18).

However, even the lipid-based trends may not represent changes in exposure completely accurately if fish lipid contents change dramatically and rapidly. The gill elimination rate is

controlled by the lipid content (Equation 5-16). Elimination can track gradual changes in lipid content, and consequently, lipid-based PCB levels do not vary with gradual changes in lipid content; a good example is the largemouth bass at Stillwater in the 1980s. On the other hand, PCBs in adult fish have long half-lives (de Boer *et al.* 1994, Lieb *et al.* 1974, O'Connor and Pizza 1987, Sijm et al. 1992), which means that the excretion rate cannot track sudden large changes in lipid content. Such sudden changes can lead to changes in the lipid-based contaminant concentration, even in the absence of variation in exposure level (for example, Lieb *et al.* 1974). The bioaccumulation model provides the best way to fully evaluate the trends in fish PCB levels, because it accounts in a dynamic, mechanistic fashion for changes in both exposure and lipid content. Nonetheless, an evaluation of the data that is independent of the model is essential.

For the most part, changes in lipid content in the Upper Hudson River fish were relatively gradual (Figures 5-18 and 5-19). Therefore, while it may not provide a perfect representation of changes in exposure level, especially in the largemouth bass, the evaluation of long-term trends is best performed on a lipid basis. For the rest of this discussion, trends in exposure levels are explored on a lipid basis. Model calibration results are compared with both wet weight- and lipid-normalized data.

PCB concentrations in fish from both Stillwater and Thompson Island Pool have been declining since the late 1970s (Figures 5-24 through 5-27). The rate of decline has not been constant, but a consistent pattern emerges from the data (Figure 5-24, 5-26): a relatively rapid decline from the late 1970s to the early 1980s, followed by a slower rate from approximately 1982 to 1993/5, and then by a return to the more rapid rates of the late 1970s since 1993/5. The patterns in each species at each location are discussed next.

Stillwater

Lipid-based total PCB concentrations in largemouth bass declined in phases from the late 1970s to 1997 (Figure 5-24). A relatively rapid decline was observed between 1977 and 1982 (0.36 per year, equivalent to a half-life of 1.9 years). A slower decline was observed between

1982 and 1994 (0.050 per year, half-life = 15 years). The data collected since 1995 appear to exhibit a more rapid rate of decline is now more rapid than in the 1980s and early 1990s (0.19 per year, half-life =3.6 years). These trends suggest that there has been more than one mechanism controlling PCB fate in the Upper Hudson River in the last 20 years, possibly involving ongoing PCB sources to the river from the early 1980s to the mid-1990s.

Total PCB levels in pumpkinseed also exhibit three phases: levels declined relatively rapidly from 1979 to 1982 (Figure 5-24; 0.45 per year, half-life =1.5 years) and again from 1995 to 1997 (0.76 per year, half-life =0.92 years). Levels declined at a considerably slower rate between 1982 and 1995 (0.023 per year, half-life =30 years).

The three-phase pattern is also evident in the brown bullhead data: relatively rapid declines from 1977 to 1982 (0.34 per year, half-life =2.1 years) and from 1993 to 1997 (0.16 per year, half-life =4.5 years), with a relatively slow decline from 1982 to 1993 (0.06 per year, half-life =12 years). An alternative interpretation is that concentrations declined between 1986 and 1991, rose in 1992, and then declined thereafter. The increase from 1991 to 1992 would be contemporaneous with the Allen Mill event and similar to the trends observed in Thompson Island Pool brown bullhead (Figure 5-26).

The high average brown bullhead level with large error bars measured by Exponent in 1997 (Figure 5-24) consists of three samples, one of which contained an uncharacteristically low lipid content, lower than any other value in the Exponent brown bullhead data set (0.3%). In comparison, the wet weight-based values are consistent with NYSDEC data (Figure 5-25). This value was removed from the annual average in subsequent analyses.

Thompson Island Pool

The Thompson Island Pool pumpkinseed exhibit no clear trend between 1988 and 1991 (Figure 5-26). Levels declined in 1994-1997, as in Stillwater, with a rate of 0.37 per year (half-life=1.9 years). Levels in brown bullhead declined consistently from 1986 to 1991 with a rate of 0.15 per year (Figure 5-26; half-life = 4.7 years). The average concentration then increased

approximately 3-fold from 1991 to 1992. Brown bullhead is sampled in Spring, so the 1992 sampling was the first after the Allen Mill event. Levels again declined from 1992 to 1997 with a rate of 0.30 per year (half-life=2.3 years). PCB levels in the largemouth bass in the Thompson Island Pool in the 1980s declined from 1984 through 1988 (Figure 5-26; 0.11 per year, half-life= 6.2 years). Levels then increased in 1990, remained high through 1993, and declined from 1994 to 1997 (0.29 per year, half-life= 2.4 years).

There are two aspects of the largemouth bass data that are not consistent with PCB measurements in other species and in water. First, lipid-based levels in Thompson Island Pool largemouth bass increased 85% from 1988 to 1990. In contrast, there is considerable evidence that the average exposure levels did not change dramatically over this period: such increases were not observed in brown bullhead, pumpkinseed or water column PCB levels. In addition, the increase in 1990 occurred considerably before the Allen Mill event. Second, the wet weight-based 1993 average is considerably greater than both the 1992 and 1994 values (Figure 5-27), and the decline from 1993 to 1994 is inconsistent with our understanding of PCB uptake and loss rates (Figures 5-26 and 5-27). Lipid-based levels in brown bullhead and pumpkinseed declined 20 to 30%, while levels in the largemouth bass declined to a greater degree, 40%. Such a rapid change in the largemouth bass might be possible if their exposure to PCBs declined to near zero in 1994; however this was clearly not the case. Levels in a top predator should change at a slower rate than levels in TL3 fish, because of the relatively long half-life of PCBs in large fish.

In addition, there is considerable uncertainty associated with the 1997 largemouth bass values. GE reanalyzed several of the samples collected in Spring, 1997 by NYSDEC, and Exponent sampled fish in the fall of that year (Figures 5-26 and 5-27). The average computed from the GE re-analyses was very close to the average computed by NYSDEC, but both were greater than the Exponent average and exhibited relatively large standard errors. These characteristics of the data make recent trends unclear.

Therefore, the largemouth bass PCB data collected in the late 1980s and the 1990s were explored in greater detail. Total PCB concentration (µg/g wet weight) is positively correlated with percent lipid (Figure 5-28), but the scatter in the relationship varies considerably. In some

years, for example 1988, there is a relatively tight relationship; in others, for example 1992, the data are more scattered. In a few cases, almost all of the data are clustered, with one or two points lying outside of the cluster. These points are indicated in Figure 5-28 with open squares. The 1997 sample with a high PCB concentration (Figure 5-28) was reanalyzed by GE, and the high concentration was verified. The five values indicated in Figure 5-28 (six with the GE reanalysis of the high 1997 value) were excluded from calculations of population means in all subsequent analyses, although the excluded values are presented individually on all figures.

Without these largemouth bass values, the 1993 wet weight-based average is now more consistent with the other data collected in the 1990s (Figure 5-29). In addition, the 1997 NYSDEC/GE samples are now consistent with the Exponent data, and there appears to be a continuous downward trend from 1993 to 1997. However, the increase from 1988 to 1990 is still apparent. This is discussed further in the context of the model calibration.

In summary, the data suggest that the mechanisms controlling PCB fate and bioaccumulation have changed over time. Based upon the half-lives computed from the log regressions presented in Figures 5-24 through 5-27 and 5-29, relatively rapid declines were observed from the late 1970s until 1982 and from 1993/5 to 1997 (Figure 5-30). Slower declines were observed in the period between these years. One possible interpretation of these data is that the natural rate of decline in the Upper Hudson River is characterized by the rates of change observed in the late 1970s and mid-1990s. During the 1980s/early 1990s, the decline was slowed due to ongoing PCB sources to the river.

The averages presented in Figures 5-24 through 5-27 are used to calibrate the bioaccumulation model, except for the largemouth bass in Thompson Island Pool, for which the data presented in Figure 5-29 are used.

5.4 CALIBRATION RESULTS

Based upon graphical comparisons of model results and data, the best calibration was achieved with the following food web structure: pumpkinseed consumed 75% PMI and 25%

BMI, yearling and older brown bullhead consumed 50% BMI and 50% PMI, and yearling and older largemouth bass consumed 50% pumpkinseed and 50% brown bullhead (Figures 5-31 through 5-34). Based on the observation that young largemouth bass consume invertebrates before becoming essentially completely piscivorous, young-of-the-year largemouth bass diets consisted of 25% BMI and 25% PMI, in addition to 25% pumpkinseed and 25% brown bullhead (Smith 1985).

Comparisons of computed and observed PCB concentrations in Stillwater fish are presented in Figures 5-31 and 5-32. For all three species, the model reproduces the observed temporal trends in fish PCB concentrations reasonably well on both lipid-normalized and wet-weight bases. This is especially true for largemouth bass. The model exhibits the three phases of decline observed in the lipid-based data: rapid until the early 1980s, slower to 1995, and more rapid again after 1995. The model also captures the various rises and falls observed in the wet weight data throughout the entire 18-year period. The model reproduces the trends in the pumpkinseed data, and computed PCB concentrations are within 50 percent of the data. As in the largemouth bass, PCB levels declined relatively rapidly in the early 1980s and mid-1990s and slower in between. During the more rapid declines, the model exhibits year-to-year discrepancies with respect to observed levels. This could be due to the relative sensitivity of young fish to short-term (within-year) changes in their exposure and physiology, changes that may not be simulated accurately by the model. Finally, the model captures the trends in the brown bullhead. It under-estimates the average PCB levels in the mid- to late 1980s and over-estimates levels observed in the 1990s, but remains within two standard errors of the wet weight-based means throughout both periods.

Both model and data exhibit little or no trend in the Thompson Island Pool pumpkinseed during the late 1980s (Figure 5-33 and 5-34). Following a rise due to the Allen Mill event, the computed levels decline through the mid-1990s. No yearling pumpkinseeds were collected in 1991 and 1992, so the immediate response to the Allen Mill event was not observed. Both observed and computed levels declined from 1993 to 1997, although the rate of decline appears to be somewhat slower in the model. As at Stillwater, the model sometimes over-estimates and sometimes under-estimates each year's data.

Both computed and observed brown bullhead concentrations decline during the late 1980s, rise in the early 1990s and then resume their decline. The computed values lie generally within the error bars of the data. However, the precise timing of the changes in the trends is different in model and data. Measured lipid-based values decline from 1986 to 1987, while computed concentrations increase. Measured lipid-based values decrease to 1991 and then increase from 1991 to 1992, while computed concentrations increase from 1990 to 1991 and then decline. Both of these discrepancies occurred following relatively large declines in lipid content (Figure 5-19). They may be caused in part by inaccurate descriptions in the model of the time courses of these declines during the year.

Computed PCB concentrations in the Thompson Island Pool largemouth bass reproduce the gradual downward trend observed in the 1980s, over-estimating the average observed levels by 1 to 55% (Figures 5-33 and 5-34). Except for a temporary increase in 1991, computed lipid-based levels continue to decline through 1997. The increase in the lipid-based levels observed in 1990 is not reproduced by the model. The model matches the observed mean in 1991 and then under-estimates the means observed in 1992 through 1995. By 1996 the computed and observed values are again similar.

The under-estimation of the TIP largemouth bass levels in the early 1990s by the model is not likely due to the under-estimation of the average overall exposure of the largemouth bass population. This conclusion is based on the observation that the model results for the brown bullhead and pumpkinseed are similar to the data during this period.

On the other hand, changes in the distribution of exposure levels among the individual sampled largemouth bass may account for both the patterns in the data and the differences between the model and the data. As discussed in Section 5.3.3, wet weight-based PCB concentrations in fish are in general positively correlated with percent lipid (Figure 5-28), with individual values scattered randomly about a central relationship. However, in some years, the Hudson River largemouth bass data appear to cluster into distinct relationships. For example,

most of the largemouth bass data collected in 1990 and 1993 appear to cluster about two relationships (Figure 5-35; lines drawn by eye).

The observation of more than one cluster of individual values within a single year suggests that the largemouth bass population may be segregated into sub-populations with differing exposure levels. Such segregation could be caused by limited movement and heterogeneous surface sediment concentrations. Between 1990 and 1995, the inclusion in the data averages of sub-populations exposed to higher sediment PCB concentrations would explain several observations: the increase in the average measured largemouth bass lipid-based levels between 1990 and 1993 that is inconsistent with trends in TL3 fish and in water, the increases in measured variability during this period (larger error bars on Figures 5-33 and 5-34), as well as the under-estimation by the model. Similarly, the existence of brown bullhead sub-populations may explain the concentration difference between the northern Thompson Island Pool and Griffin Island samples that was observed by Exponent (Figure 5-22). It should be recognized that while this hypothesis provides a plausible explanation of the patterns in the data and the model results, the field data necessary to test it directly are not available.

Overall, the model exhibits no bias with respect to the data. On a graph of average computed *vs.* measured concentrations, values line up along the 1 to 1 line (Figure 5-36). In addition, 90% of the computed wet weight-based PCB concentrations are within a factor of two of the data (92% on a lipid basis). Some of the year-to-year variation in the model/data relationship is due to uncertainty in the data (*cf.* error bars on Figures 5-31 through 5-34). The uncertainty due to the model itself is therefore likely to be considerably less than a factor of two.

In summary, the model represents average PCB levels in the population as a whole both at Stillwater and Thompson Island Pool generally without bias and within a factor of two. Temporal trends as well as the spatial gradient between Thompson Island Pool and Stillwater are reproduced. While there may be some sub-populations exposed to lower or higher local sediment concentrations, the model can provide realistic projections of PCB concentrations for the population as a whole under natural recovery and alternative remediation scenarios.

5.5 HOMOLOG MODEL

5.5.1 Objective

The PCB homolog model was developed to assess the depth to which PCBs are available within the sediment bed. This assessment was possible, because the degree of dechlorination generally increases with depth in the Upper Hudson River (Figure 5-15), and the degree of bioaccumulation varies among homologs.

The model was used in a diagnostic fashion to estimate the most likely homolog composition of the sediment exposure source given the homolog distribution in the fish. The model food web was exposed to three different sediment homolog distributions, representative of 0-2 cm, 0-5 cm, and deeply buried, highly dechlorinated sediments in the TIP. For each exposure scenario, the computed homolog distribution in the fish was compared with the measured homolog distribution. The simulation results most similar to the data indicate the sediment homolog distribution to which the food web was most likely exposed.

5.5.2 Model Development

The homolog model was based upon the calibrated PCB_{3+} model described above. Additional information required to develop the homolog model consisted of homolog distributions in the sediments and water to which the fish were exposed, homolog-specific values for several model parameters (invertebrate BSAF, K_{ow}, chemical assimilation efficiencies at the gut surface, and chemical uptake efficiencies at the gill surface), and observed homolog distributions in fish. A steady-state model was developed for TIP for the 1990s, based on the observation that homolog distributions observed in fish exhibited little variation over this period (error bars in panels A-C of Figures 5-38, 5-39 and 5-40).

Exposure Concentrations

Three different homolog compositions were used for the sediments:

- the average composition of the 0-2 cm slices from high-resolution cores HR19, HR20 and HR23 collected by USEPA in the TIP in 1992,
- the pool-wide average composition of the 0-5 cm slices from the cores collected by GE in the TIP in 1991, and
- the average composition of the sediment slices with less than 2.0 chlorines/biphenyl from high-resolution cores HR19, HR20 and HR23.

The sediment homolog distribution characteristic of the 0-2 cm layer of the high-resolution cores is similar to Aroclor 1242 (panel D of Figures 5-38 through 5-40). The homolog distribution characteristic of highly dechlorinated sediments is composed almost entirely of mono- and dichlorobiphenyl (panel F of Figures 5-38 through 5-40). The homolog distribution measured in the 0-5 cm layer is intermediate.

The average homolog compositions of dissolved and particulate PCBs in the water column were estimated using water samples collected by USEPA at the TID and at Lock 7 (MP 193.7, June through August 1993; n=7; Figure 5-37). PCBs at the TID are enriched in lower chlorinated congeners relative to samples collected at Lock 7. The average exposure of fish collected in the TIP was estimated by averaging the distributions measured at both locations (lines in Figure 5-37).

The total PCB levels in the surface sediments and in the water column were estimated by averaging the results of the fate model computed during the growing season (temperature >= 10 degrees C) for the period from 1990 through 1998. Values were 50 ng/L dissolved in the water column, 46 ug/g OC on water column particles, and 491 ug/g OC on sediment particles.

Toxicokinetic Parameters

Bioaccumulation factors from particles to invertebrates were calculated based upon measurements made by USEPA in the Upper Hudson River, using the method described in Section 5.2.4. Lipid-based BSAF values for the homologs are presented in Table 5-4. In addition, separate simulations were performed using average values computed by Tracey and Hansen (1996) based on a review of literature. These values were used for both PMI and BMI.

Table 5-4. Homolog-Specific Parameter Values Used in the Bioaccumulation Model

Homolog	Log(K_{OW})	Invertebrate BSAF		Assimilation efficiency	
		USEPA Hudson River data	Tracey and Hansen (1996)	Gut – PCBs	Gill- PCB:O_2 Ratio
	L/Kg lipid	gOC/glipid	gOC/glipid		
1	4.50	0.79	0.30	0.90	1.00
2	5.15	1.47	0.42	0.85	1.00
3	5.65	1.27	0.70	0.82	1.00
4	5.76	1.89	0.92	0.81	1.00
5	6.12	1.82	1.38	0.78	1.00
6	6.55	1.95	1.80	0.75	1.00
7	7.08	2.68	1.80	0.70	1.00

Log (K_{ow}) values for each homolog were estimated using the same method as for the total PCB model. The resulting K_{ow} values are given in Table 5-4.

Median PCB assimilation efficiencies in the gut decline with increasing log (K_{ow}), ranging from 0.86 at log (K_{ow})=4.5 to 0.70 at log (K_{ow})=7.0 (Figure 5-20). A line was fit visually through the medians of these data to provide values for use in the model (Table 5-4).

Ratios of PCB:oxygen assimilation efficiencies in the gill do not exhibit a trend for log (K_{ow}) values ranging from approximately 3 to 7 (Figure 5-21). The value used in the PCB_{3+} model (1.00) was used for all homologs (Table 5-4).

Homolog distributions in the fish

PCB congener concentrations in fish were measured in the TIP in 1990 by Law Environmental, in 1992 by O'Brien & Gere, in 1993 by the USEPA and by NOAA, and in 1997 by Exponent. Fish collected during these sampling programs were combined to compute the

average weight proportion of each homolog for each model species. Combining the data from these sampling programs was valid, because the homolog distributions exhibited little variation (error bars in Figures 5-38, 5-39 and 5-40).

5.5.3 Model Results

The average measured fish homolog distributions are represented by the bars in panels A, B and C of Figures 5-38 through 5-40 (weight proportions +/- two standard errors). The computed fish homolog distributions (lines in panels A, B and C of Figures 5-38 through 5-40) are most similar to the data if the fish are exposed to sediments characteristic of the 0-2 cm layer of the high-resolution cores (panel A of Figures 5-38 through 5-40). These results indicate that the food web is probably exposed to PCBs within approximately the top 2 cm of the sediment bed. They are unlikely to be exposed to a layer 0-5 cm thick, and very unlikely to be exposed to highly dechlorinated sediments. This conclusion supports the use of the PCB_{3+} concentrations computed by the fate model for the 0-2 cm layer in the PCB_{3+} bioaccumulation model. Use of the BSAF values reported by Tracey and Hansen (1996) do not change these conclusions (results not shown).

5.6 MODEL SENSITIVITY AND UNCERTAINTY

The bioaccumulation model is useful for projecting future PCB levels in the fish insofar as: 1) it is able to reproduce PCB levels measured in the fish during the calibration period, and 2) it provides an accurate estimate of the relative importance of surface sediment and water column PCBs to the biota. The latter determines the response of the PCB levels in the fish to natural recovery processes and to remediation activities. Confidence in the realism of the projections derives from the quality of the calibration, the mechanistic structure of the model, previous successful experience using the model, and the constraints placed on parameter values by site-specific data (e.g. growth rate, lipid content, food web), species-specific data (e.g. respiration rates), as well as more general biological information.

The process of calibration involves minimizing the difference between model and data by adjusting the values of parameters, while remaining within reasonable limits determined by independent information concerning those parameters. Alternative calibrations are possible to the degree that two or more parameters can be changed simultaneously while maintaining an acceptable relationship between model and data. Model uncertainty arises when alternative calibrations result in different projections.

Alternative sets of calibration parameter values will result in significantly different projections only if the relative importance of sediment and water column PCBs to the food web changes. Thus, for the purpose of predicting PCB levels in fish, the most important uncertainty associated with the bioaccumulation model is just this property of the model, namely, the proportion of dose received by the food web from surface sediments and from the water column. Uncertainties in other components of the model, in particular the parameters that affect the degree of bioaccumulation in each organism and the depth of bioavailable sediment, are important only if changes in those components result in alternative calibrations with different proportions of PCB dose received from sediments and water.

The surface sediments are the dominant PCB source to the food web in much of the Upper Hudson River: spatial gradients in fish PCB levels follow the spatial gradients in sediment and not in water (Figure 5-41; data collected in 1991, before the Allen Mill event). That is, lower sediment concentrations in downstream locations lead to lower fish levels, in spite of the fact that water column concentrations change little, if at all. Therefore, the uncertainty analysis of the bioaccumulation model focused on developing a bounding calculation for the calibration that maximized the contribution of the PMI, and therefore water column PCBs, to the food web. To develop a bounding calculation, model parameters were divided into two groups, those that affect the degree of trophic transfer, and those that specify dietary composition.

One constraint on dietary composition was employed. The minimum contribution of BMI to the pumpkinseed diet was specified based on the following information. In the model calibration, pumpkinseed consumes 75% PMI. The comparison of predicted and observed diets indicated that the pumpkinseed probably consumes between 25 and 75% PMI (Figure 5-11). The

gut contents of pumpkinseed included some taxa unique to the BMI (Table 5-1). In addition, the spottail shiner consumes a greater proportion of PMI than pumpkinseed, yet still consumes an observable proportion of BMI (Table 5-1). Therefore, the proportion PMI was considered to be possibly greater than 75% but appreciably less than 100%. A value of 90% was chosen.

Any change in a parameter that increases the degree of trophic transfer requires a greater contribution from PMI in the calibration. With more bioaccumulation at each trophic level, the computed PCB levels in the fish will rise above the data; only by increasing the relative contribution of water column carbon will PCB levels in the fish drop to within the data. The parameter with the greatest uncertainty was c_R, the factor accounting for the slow transfer of PCBs from lipid to blood. A reduction in this parameter effectively reduces the rate at which PCBs are released from storage lipids and eliminated, and thereby increases fish PCB levels.

Therefore, the process of developing a bounding calculation involved adjusting the pumpkinseed diet to 90%PMI/10%BMI, then reducing c_R until the computed pumpkinseed concentrations compared favorably with the data. Next, the brown bullhead model was re-calibrated by adjusting its diet. Finally, the impacts of changes in the largemouth bass diet were explored. It should be noted that the process would be the same and the results similar if another toxicokinetic or bioenergetic parameter had been modified, instead of c_R.

Table 5-5. Parameters of the Bioaccumulation Model Changed in the Alternative Calibration

Parameter	Calibration Value	Alternative Calibration Value
Diet of the brown bullhead	50% PMI, 50% BMI	65%PMI, 35%BMI
Diet of the pumpkinseed	75% PMI, 25% BMI	90% PMI, 10% BMI
Factor accounting for the slow lipid/blood mass transfer rate (c_R)	0.25	0.125

Results of the bounding calculation for the calibration are presented in Figures 5-42 through 5-44. Similar to the calibration results, computed PCB levels in pumpkinseed and brown bullhead reproduce the temporal trends in PCB concentrations observed at both locations (Figures 5-42 and 5-43). For largemouth bass, the model computes higher PCB levels in TIP,

resulting in a better fit with data collected in the 1990s. However, the model calibration at Stillwater is degraded; computed PCB levels are higher than observed values throughout most of the simulation. The relationship between computed and observed values is less tightly clustered about the 1 to 1 line than in the calibration, but the model still computes PCB levels that generally lie within a factor of two of the data (Figure 5-44).

The relative contribution of sediments to largemouth bass PCB body burdens was evaluated using the bioaccumulation model. Paired simulations were performed, one that included both sediment and water column PCB sources (the calibration or the bounding calculation) and one that included sediments as the only source of PCBs to the largemouth bass (the calibration or bounding calculation with water column exposures set to zero). The proportion of PCB dose received by the largemouth bass from sediments was equal to the ratio of the largemouth bass PCB levels computed in the sediment-only exposure to the levels computed using the complete exposures.

In the calibration simulation, the proportion of PCB dose received by the largemouth bass from surface sediments averaged 79 and 52 percent at TIP and Stillwater, respectively (1980-1998 average). Before the loadings of the 1990s, the sediment contributions were even greater; the dose from sediments averaged about 87 and 60 percent for TIP and Stillwater, respectively. In the bounding calculation, TIP sediments were still the dominant source of PCBs to the largemouth bass, accounting for about 68 percent of the estimated dose (1980-1998); at Stillwater, sediments were less important, averaging 38 percent of the dose. As in the calibration, sediment contributions prior to the loads in the 1990s were greater, accounting for about 77 and 46 percent of the largemouth bass PCB dose at TIP and Stillwater, respectively.

Thus, the surface sediments are the dominant source of PCBs to the largemouth bass in the Thompson Island Pool, and provide on the order of half of the PCB dose at Stillwater. Water column PCBs became the dominant source to the largemouth bass only at Stillwater in the 1990s. Pushing the model parameterization so as to maximize the contribution of water column PCBs does not change these conclusions qualitatively.

In conclusion, we consider the parameter set used in the bounding calibration to be less consistent with the available data than that used in the calibration, based upon the field studies of the forage fish diet as well as the model/data comparisons. Therefore, while the bounding calculation constitutes an assessment of model uncertainty, it is not as realistic a representation of bioaccumulation in the Upper Hudson River as the calibration.

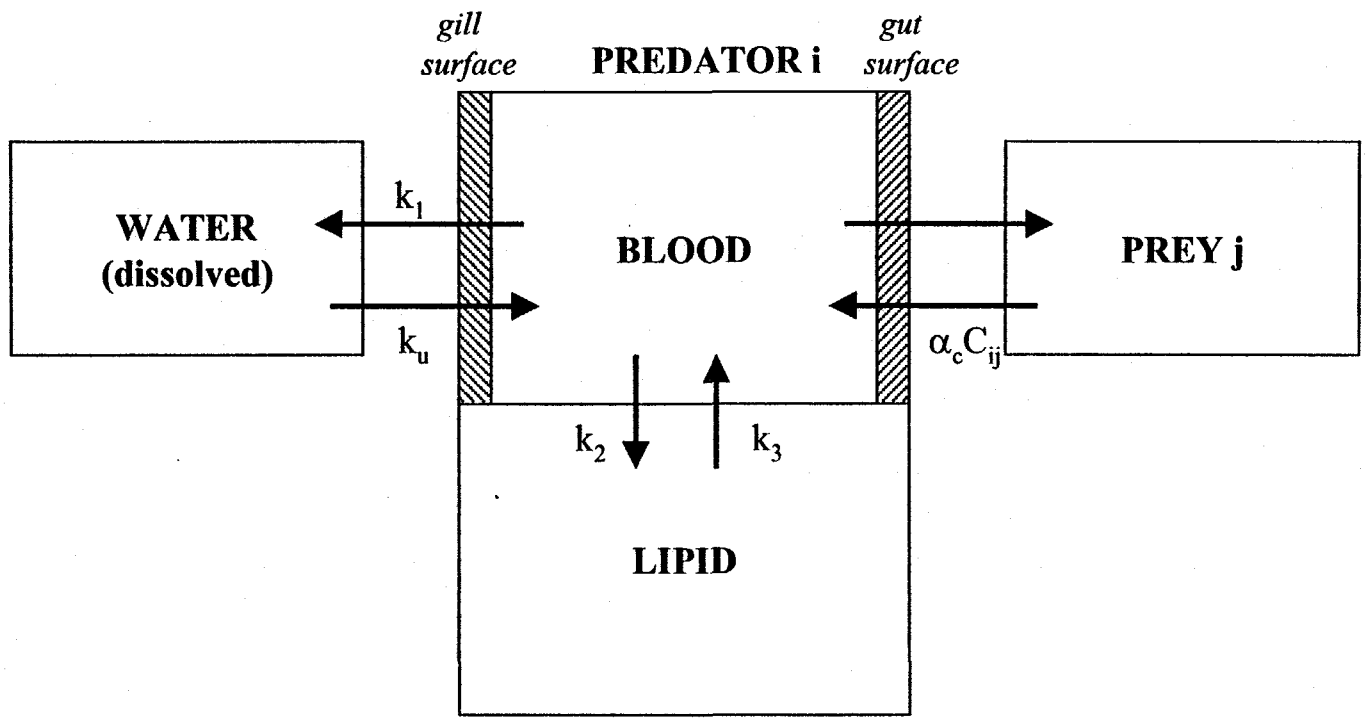

Figure 5-1. Schematic of the two-compartment bioaccumulation model. The rate constants are defined in equation 5-10.

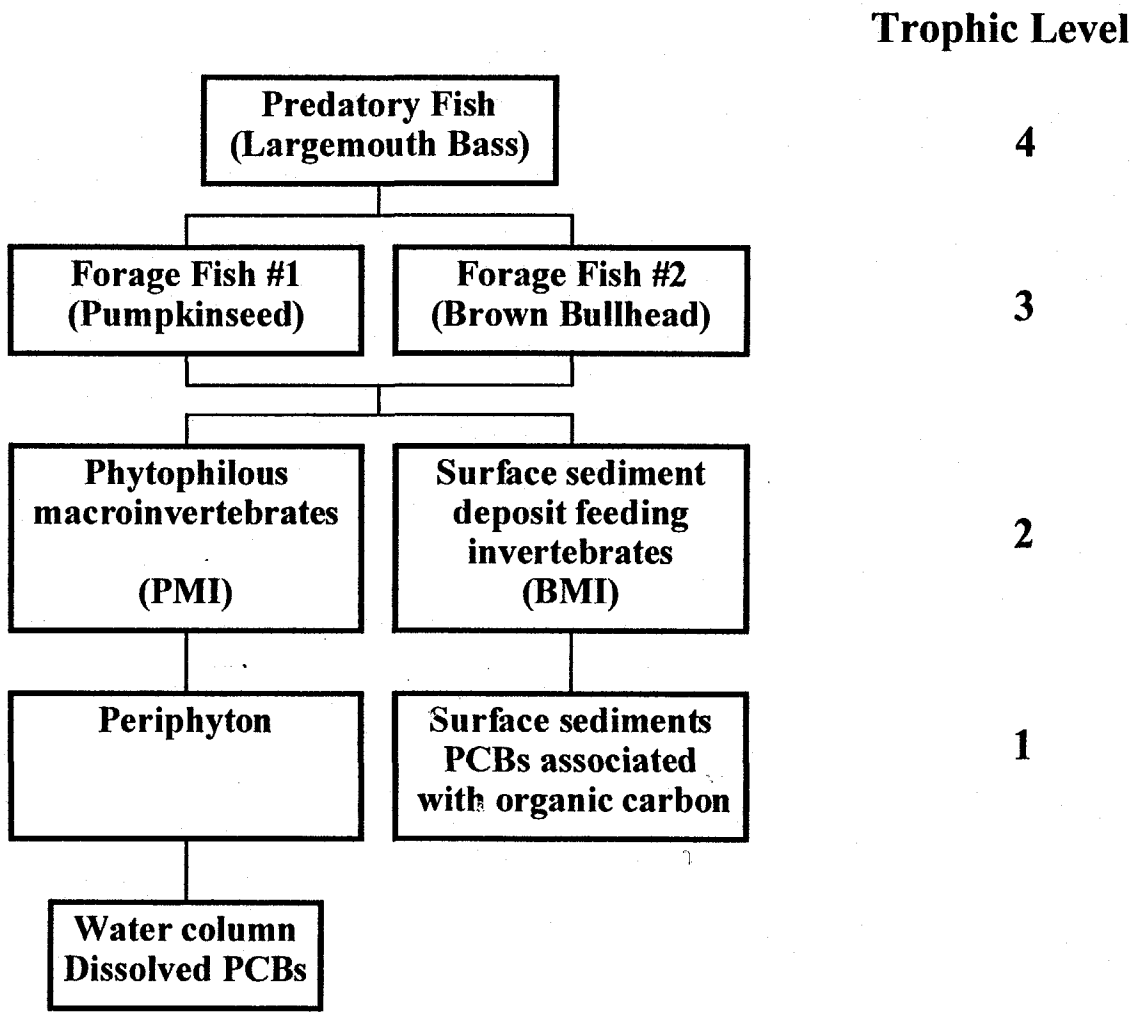

Figure 5-2. Food web structure in the bioaccumulation model of the Upper Hudson River.

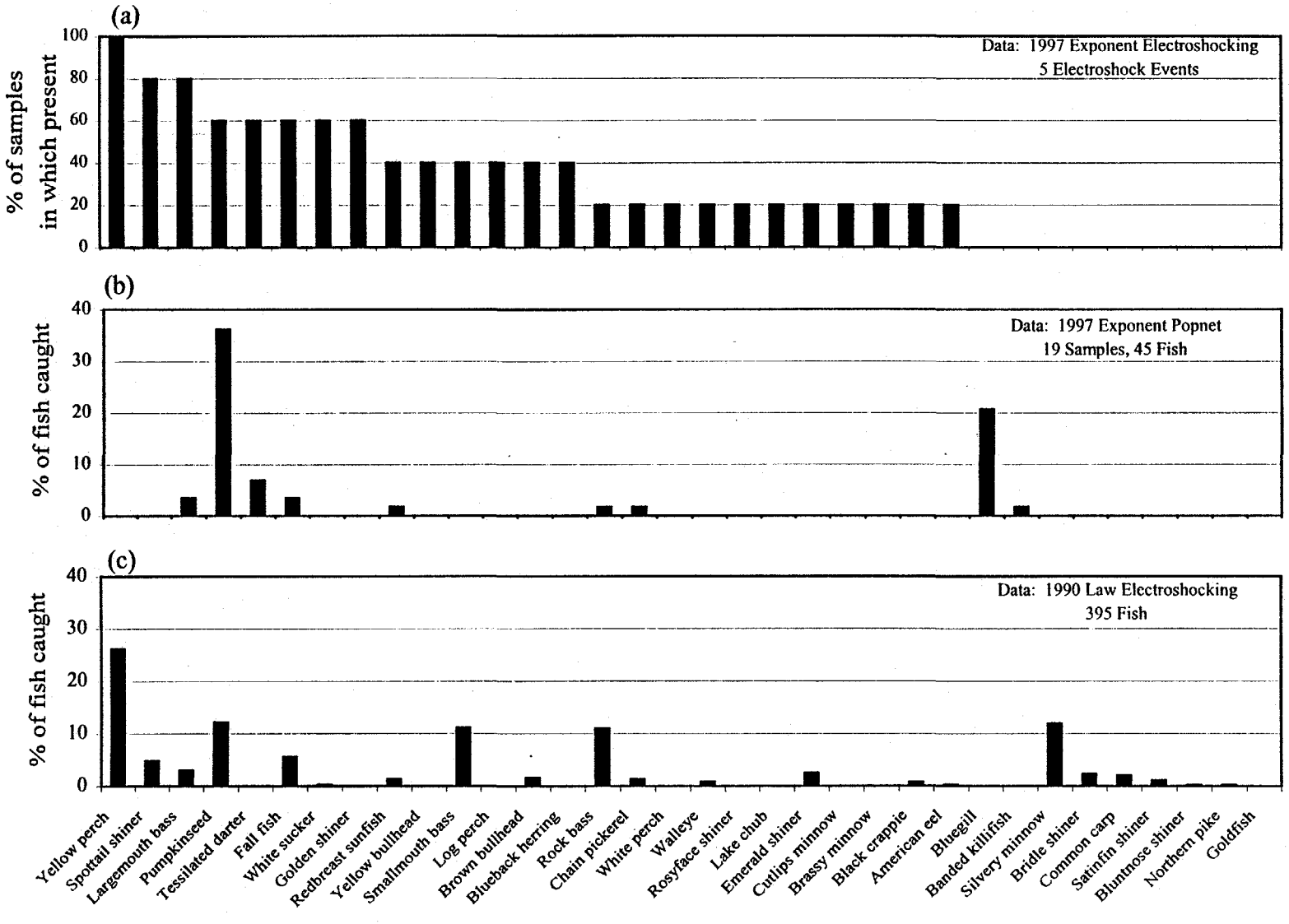

Figure 5-3. Composition of the fish community of the Upper Hudson River.

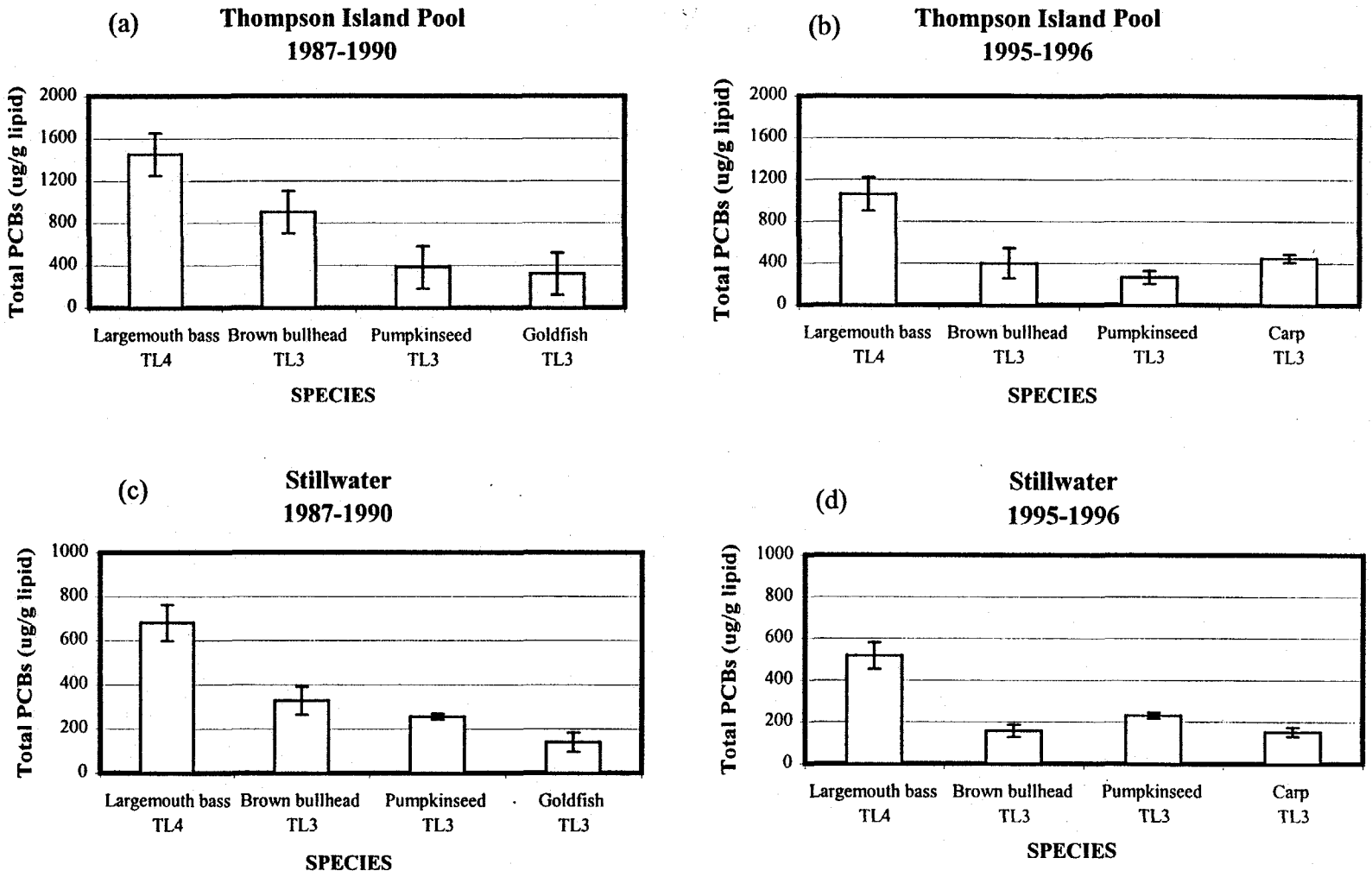

Data: NYSDEC

Figure 5-4. Average PCB levels (ug/g lipid) in fish at Thompson Island Pool in (a) 1987-1990 and (b) 1995-1996 and at Stillwater in (c) 1987-1990 and (d) 1995-1996. Data are averages of annual averages +/-2 Standard Errors. (Histogram).

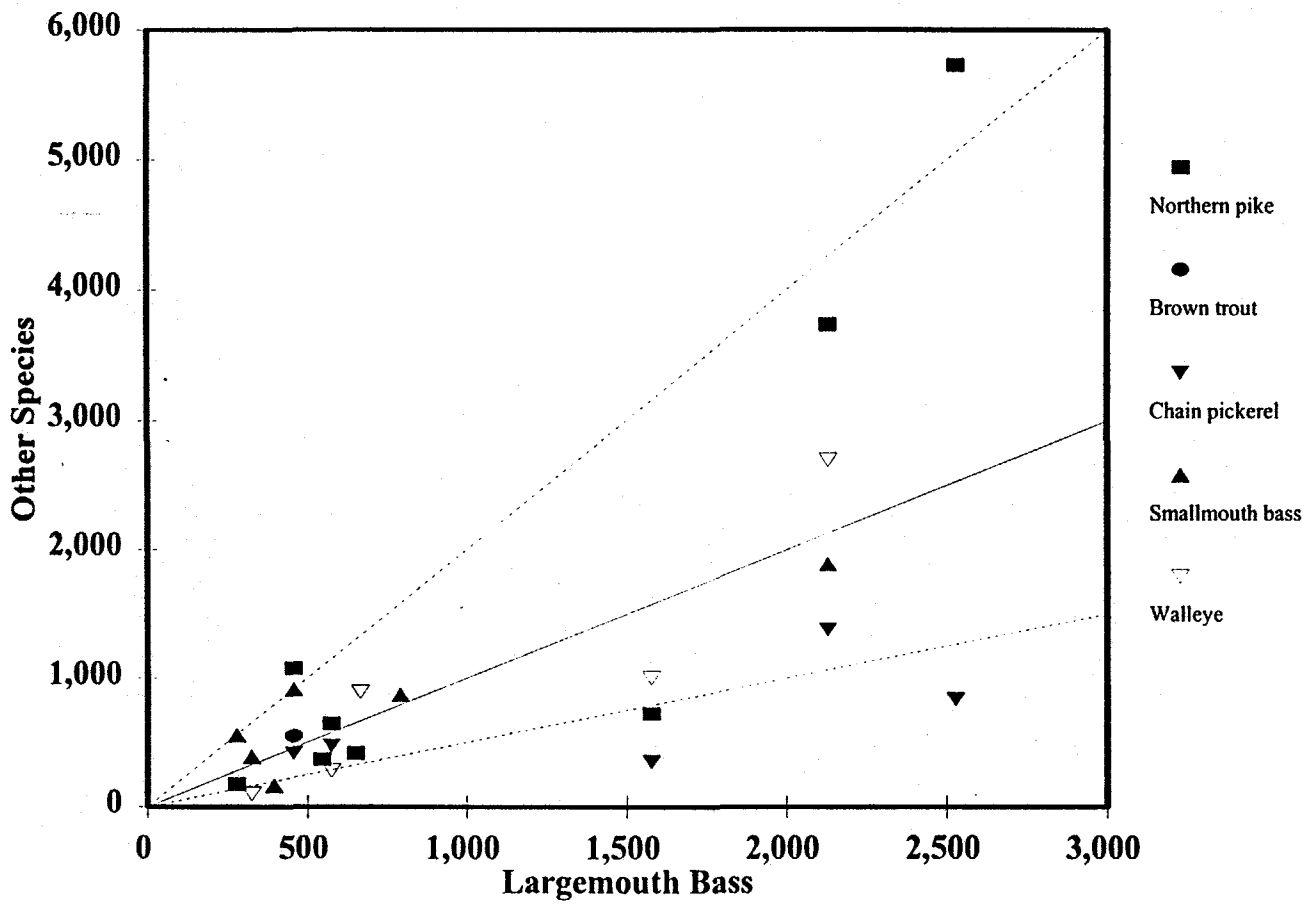

Lipid-based annual average concentrations (ug/g lipid)

Data collected by NYSDEC 1980-1997

Lines represent 0.5:1, 1:1, 2:1

Figure 5-5. Comparison of annual average total PCB levels in largemouth bass with other top predators.

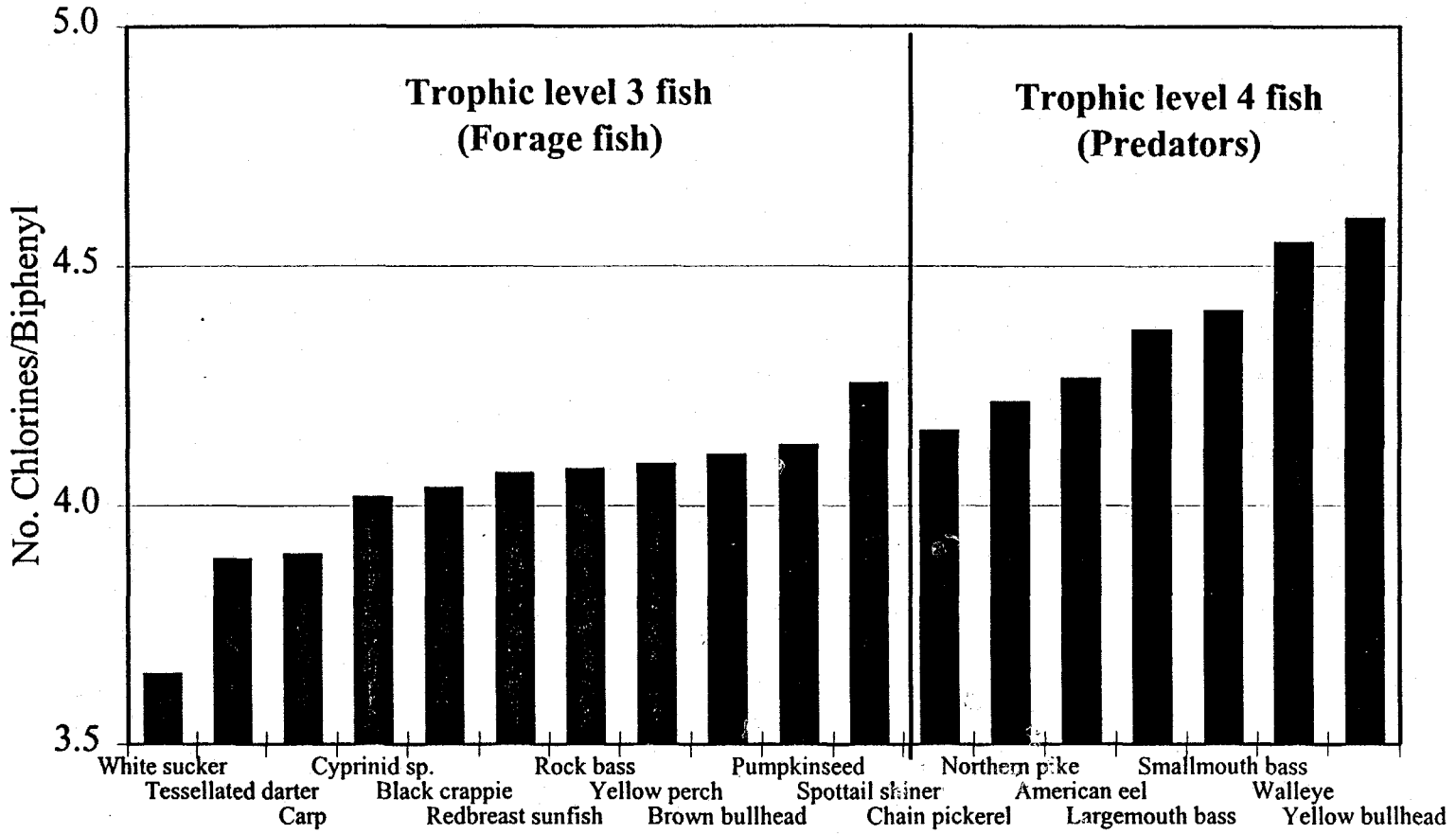

Data: USEPA, NOAA, Exponent, Law Environmental, 1990 to 1997

Figure 5-6. Number of chlorines per biphenyl in fish from the Thompson Island Pool.

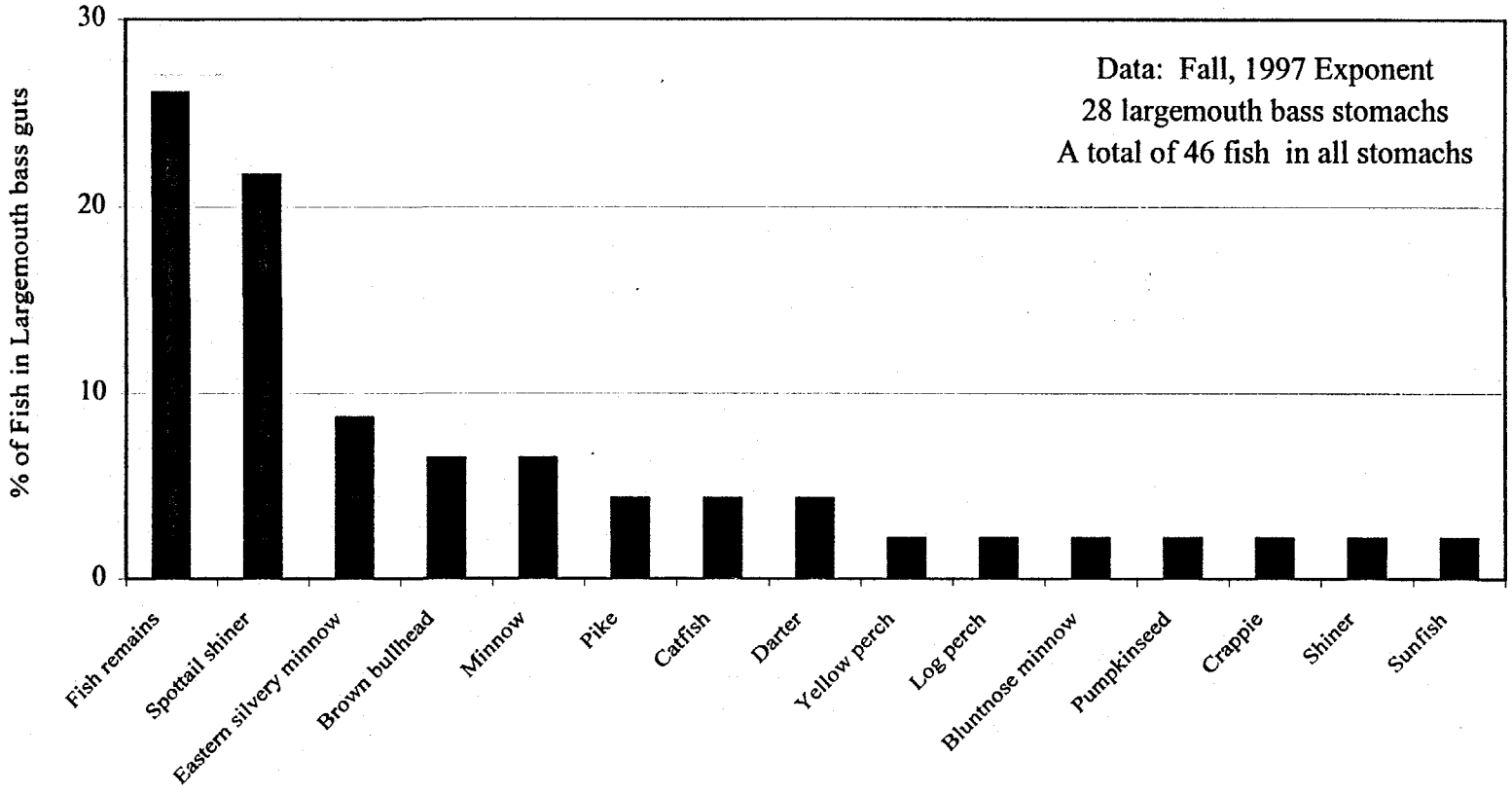

Figure 5-7. Prey consumed by the largemouth bass in Thompson Island Pool.

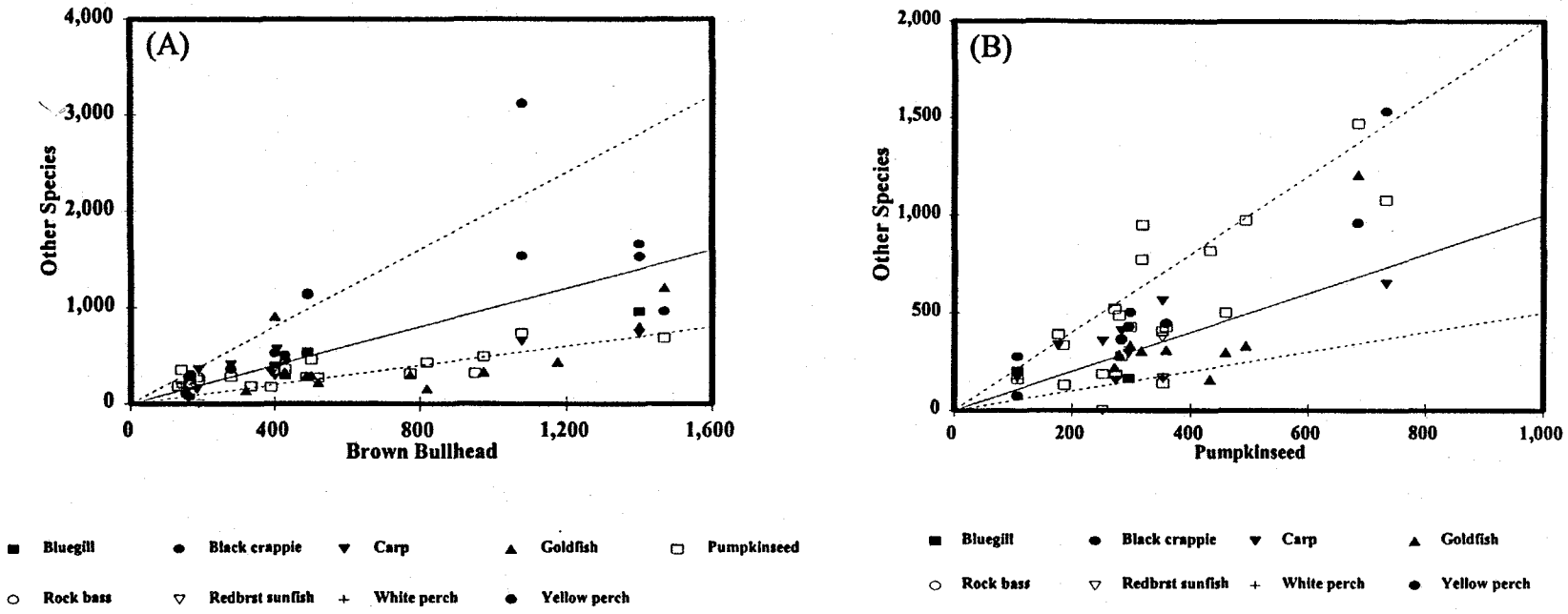

Lipid-based annual average concentrations (ug/g lipid)
Data collected by NYSDEC 1980-1997
Lines represent 0.5:1, 1:1, 2:1

Figure 5-8. Comparison of annual average total PCB levels in forage fish species with (a) brown bullhead and (b) pumpkinseed

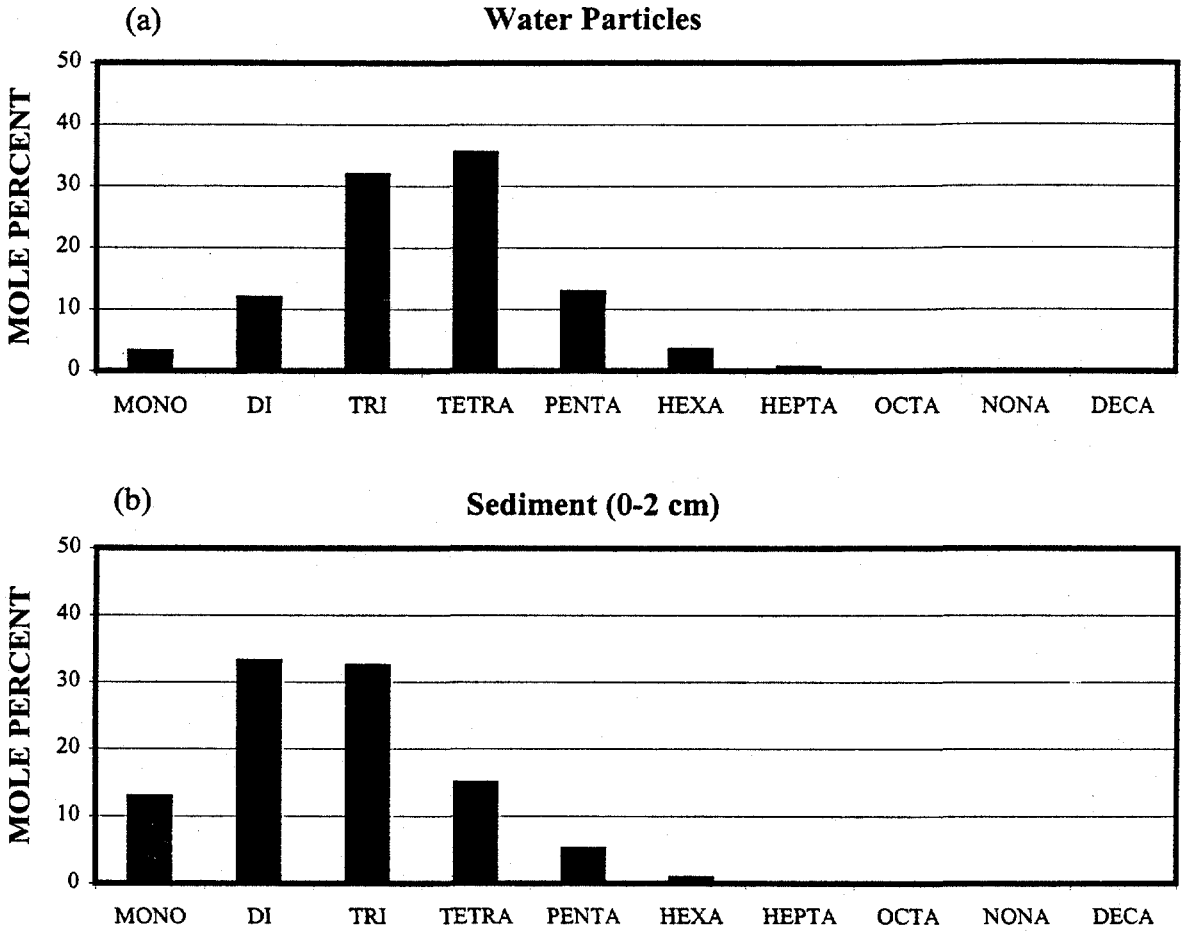

Water data: EPA, June-August 1993; Thompson Island Pool (RMs 188.5-193.7).
Sediment data: EPA, 1992; Thompson Island Pool, high resolution cores.

Figure 5-9. PCB homolog proportions on particulate matter from Thompson Island Pool. (a) water column; (b) sediments, 0-2 cm.

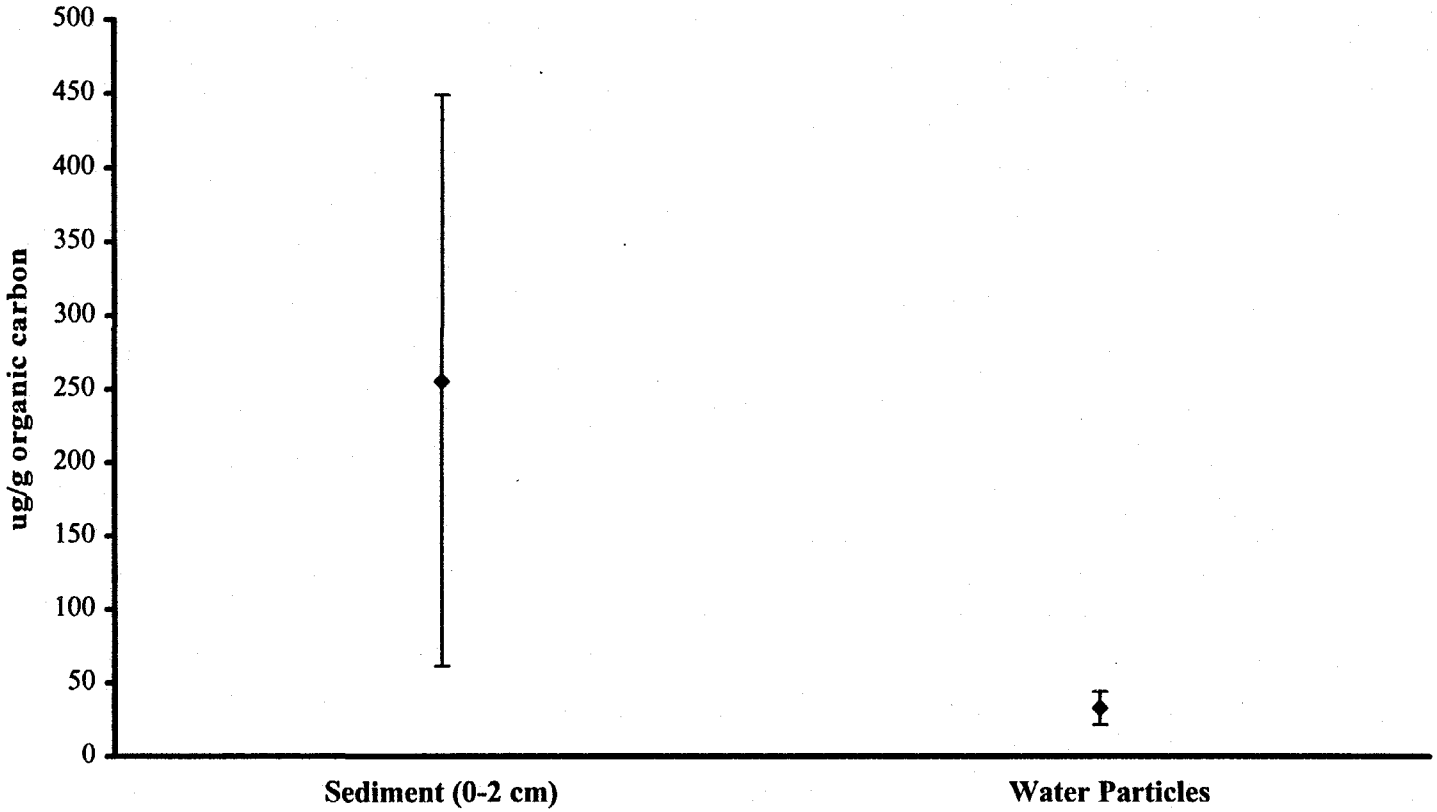

Water data: EPA, June-August, 1993.
Sediment data: EPA, high resolution cores, 1992.

Figure 5-10. Average PCB_{3+} concentrations on a carbon basis in sediments and on water column particles at Thompson Island Pool.

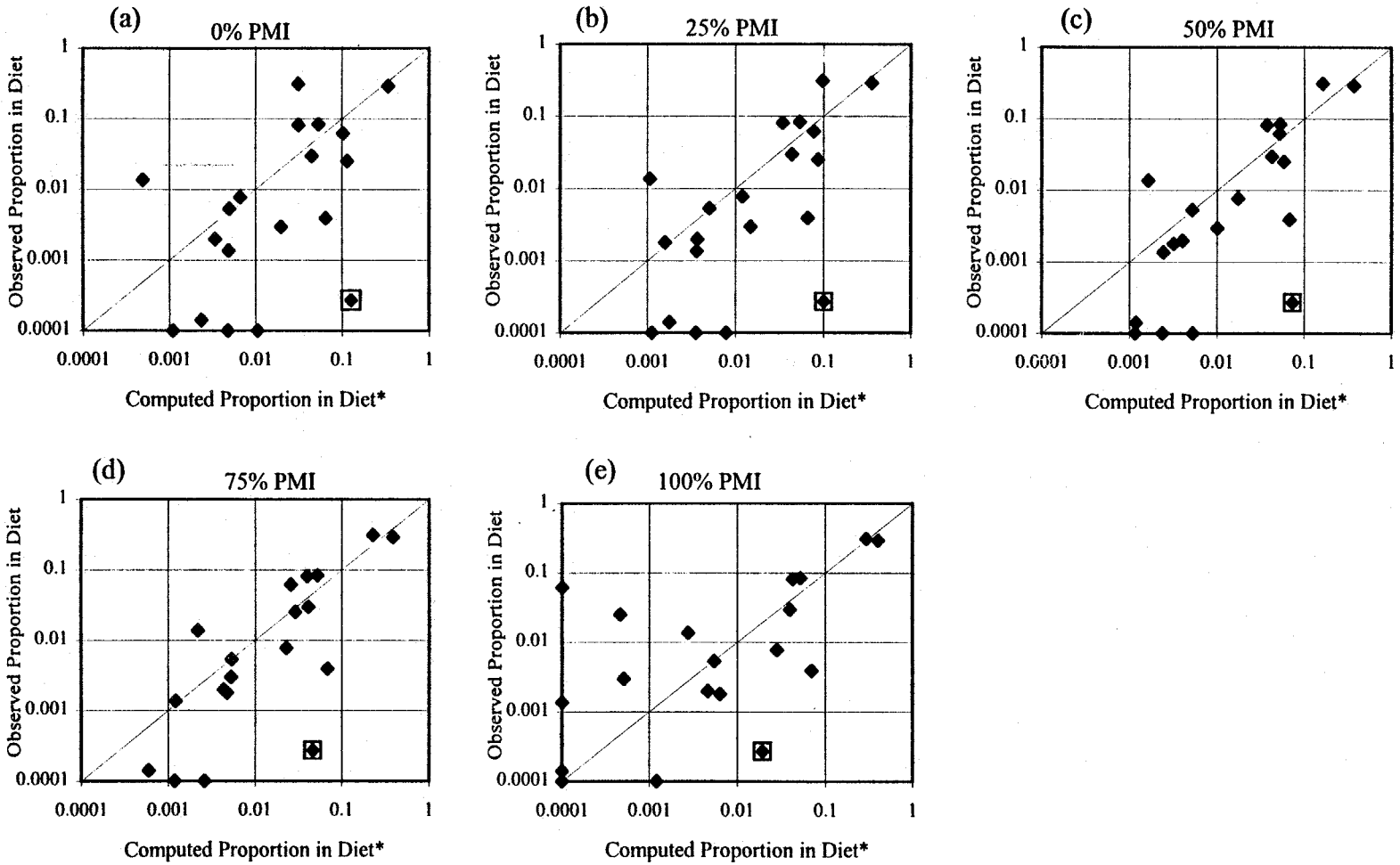

*Computed = $(f_{diet,PMI})$(% of all items in PMI) + $(1-f_{diet,PMI})$(% of all items in BMI)

Data: Exponent, Fall 1997

Figure 5-11. Observed *vs*. computed dietary composition of pumpkinseed. Percent PMI in the diet ranges from 0 (a) to 100 (e). Squares represent Tubificids.

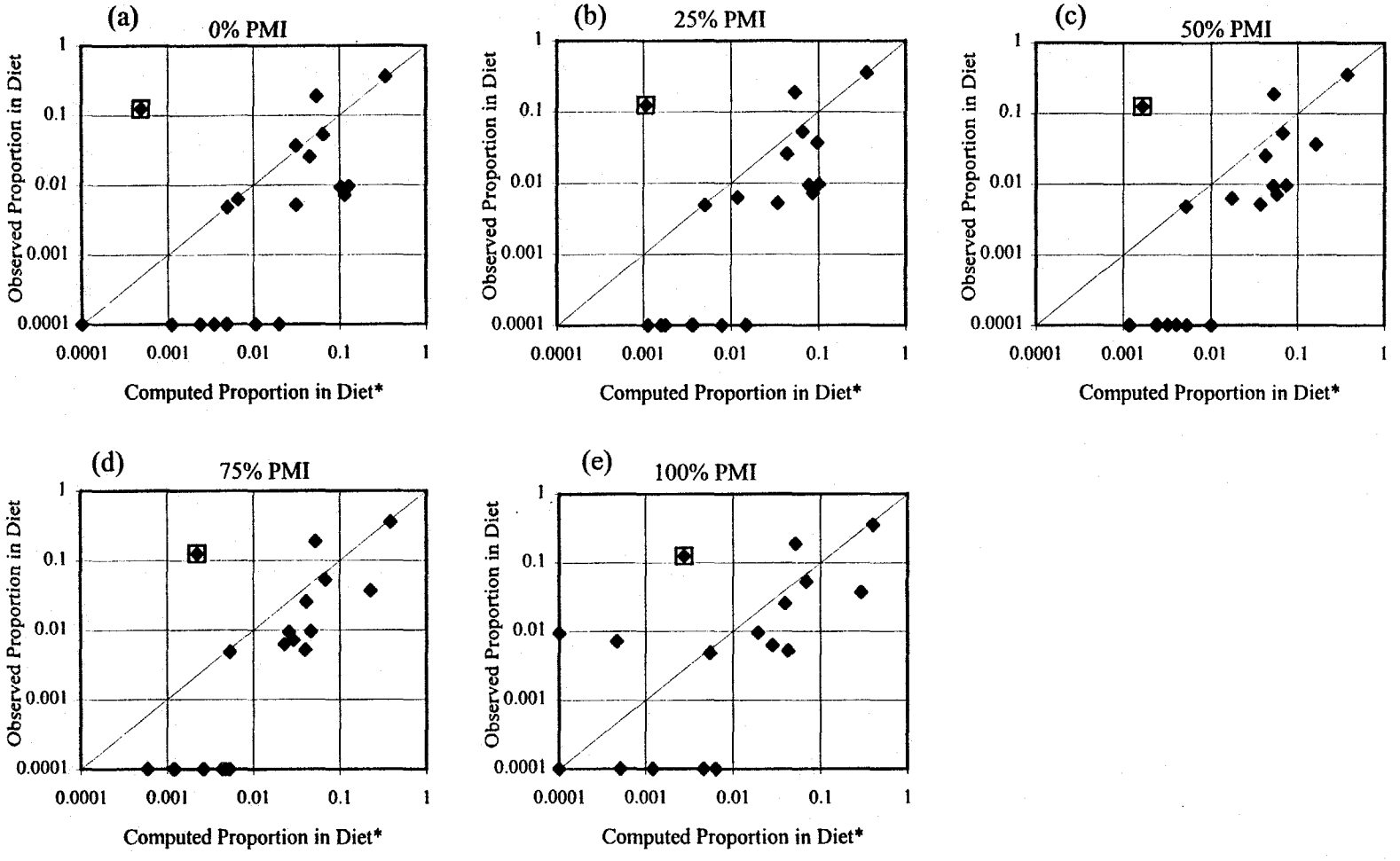

*Computed = $(f_{diet,PMI})$(% of all items in PMI) + $(1-f_{diet,PMI})$(% of all items in BMI)

Data: Exponent, Fall 1997

Figure 5-12. Observed *vs*. computed dietary composition of brown bullhead. Percent PMI in the diet ranges from 0 (a) to 100 (e). Squares represent Cladocera.

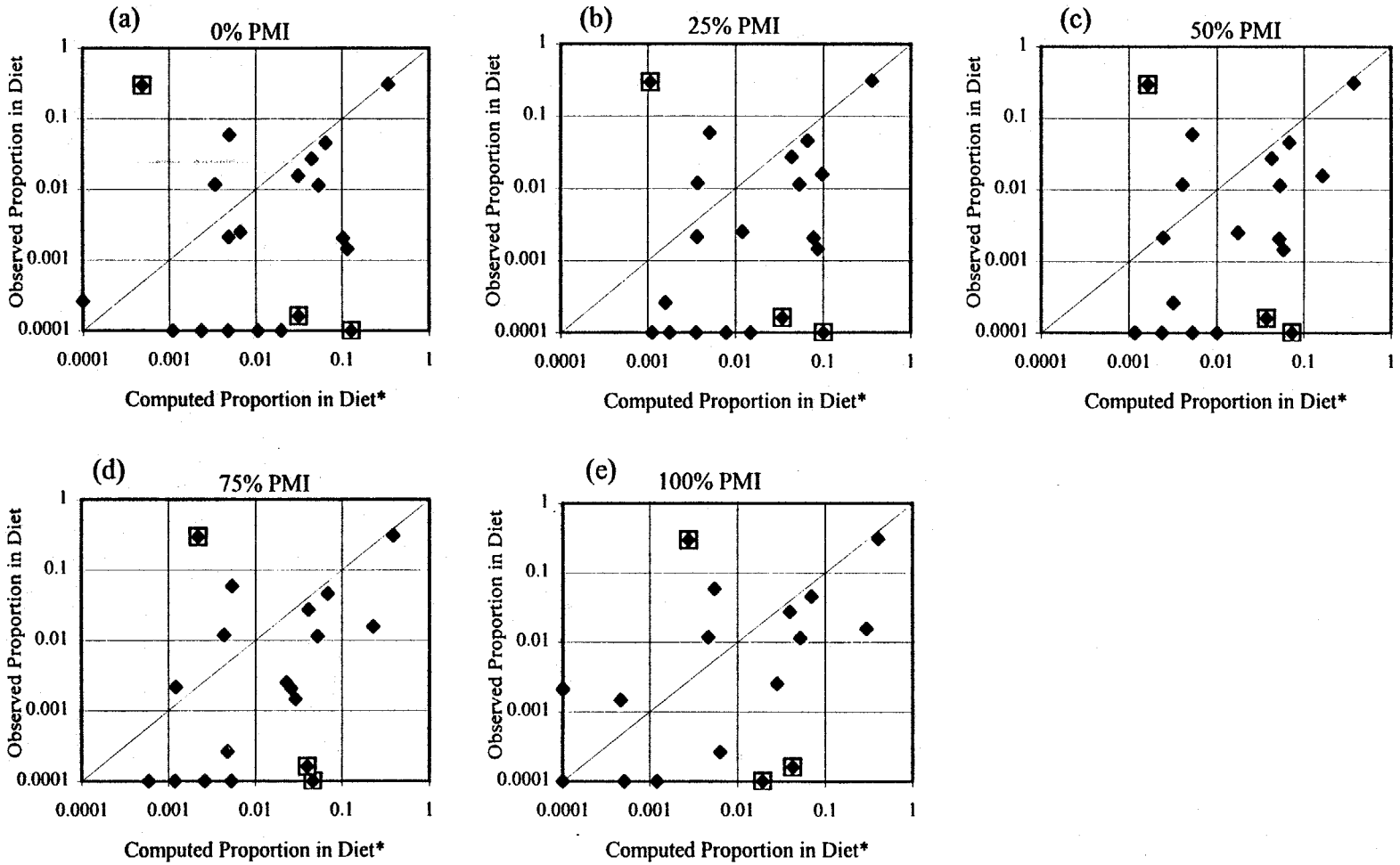

*Computed = $(f_{diet,PMI})$(% of all items in PMI) + $(1-f_{diet,PMI})$(% of all items in BMI)

Data: Exponent, Fall 1997

Figure 5-13. Observed *vs*. computed dietary composition of spottail shiner. Percent PMI in the diet ranges from 0 (a) to 100 (e). Squares represent Tubificids, Cladocera and Mesogastropoda.

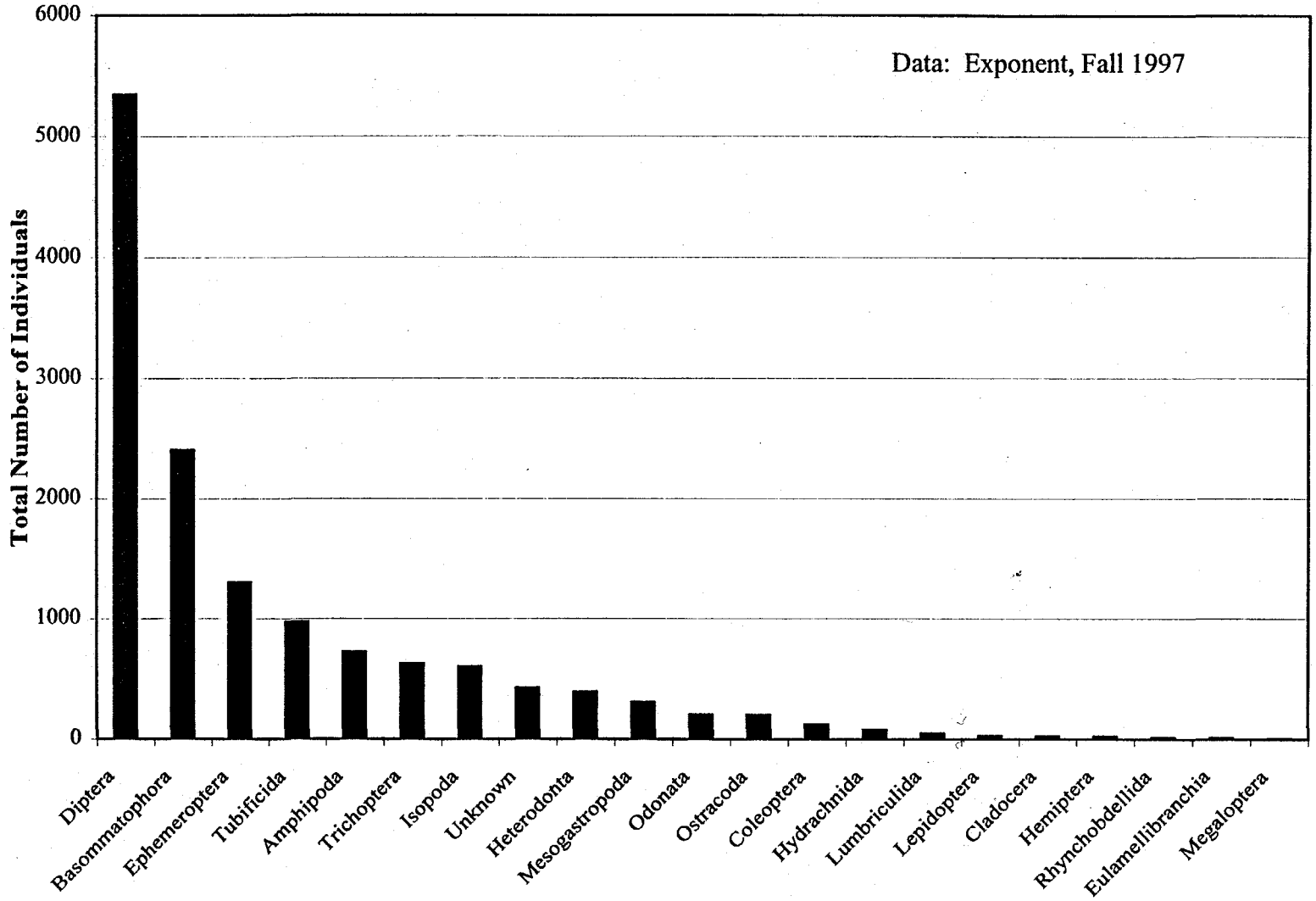

Figure 5-14. Relative Abundance of Invertebrates in the Upper Hudson River by Order.

JimQ - \\Poseidon\D_Drive\GENhud\Documents\Final_report\Vol_2\Section_5\fig5_14.xls Sheet2
4/12/99 PM

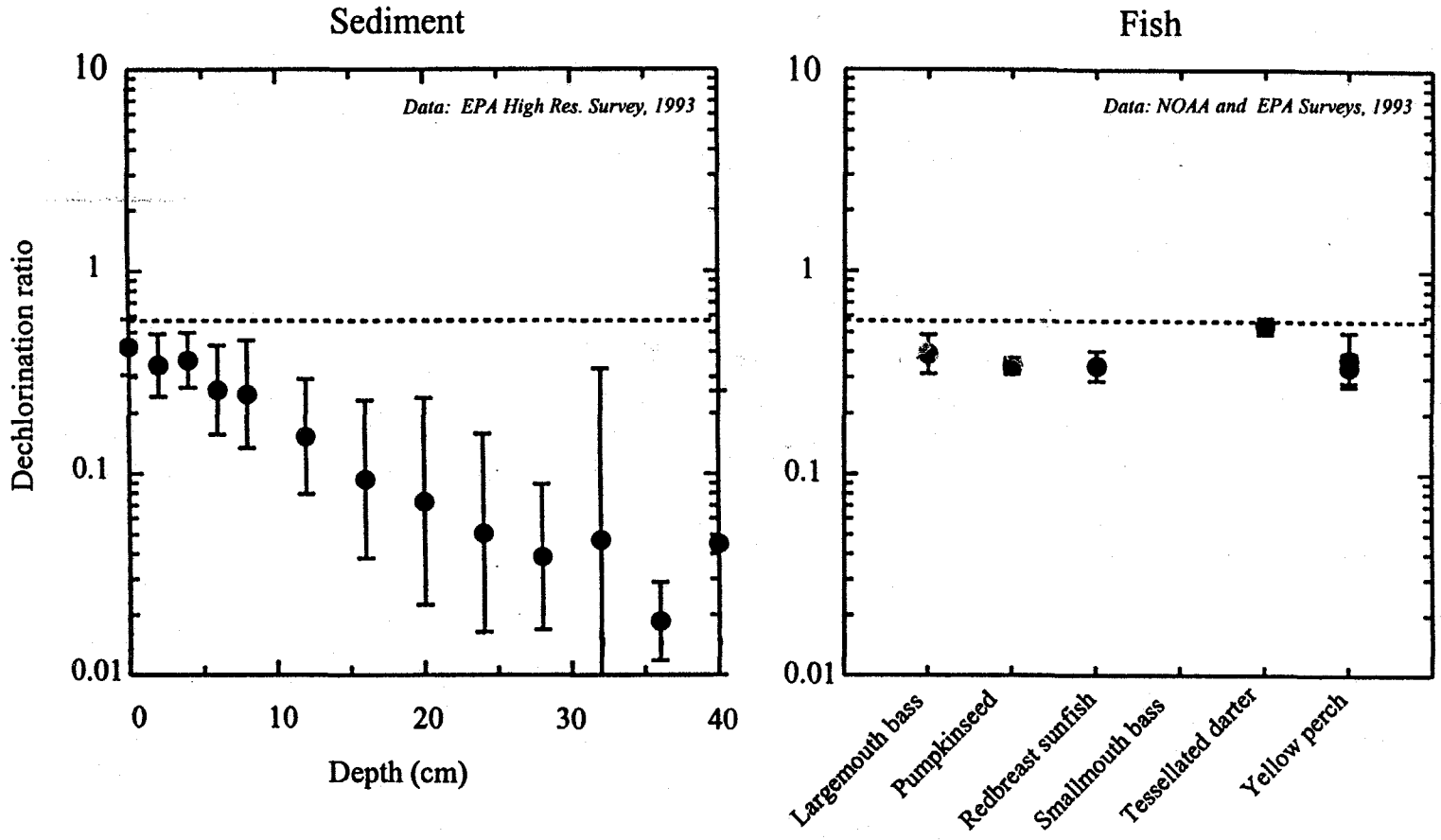

Note: dashed lines represent Aroclor 1242

Figure 5-15. Dechlorination ratios in fish and sediments of the Thompson Island Pool. The ratio of congener 56 to congener 49 is plotted in sediments against depth and for each species of fish.

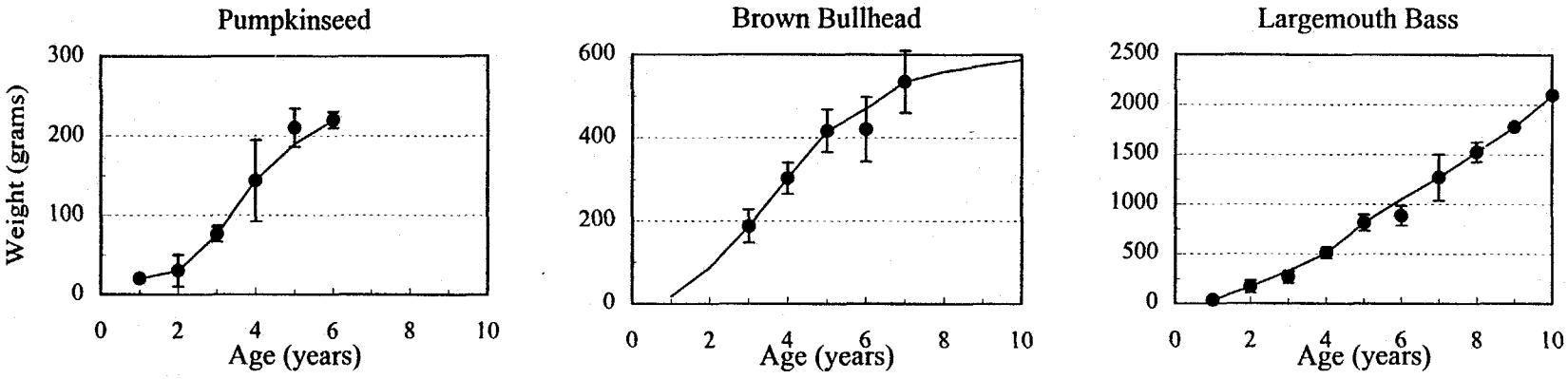

Circles represent data collected by Law Environmental (1991).
Data are arithmetic means (by age) +/- 2 standard errors.
Lines represent values used in bioaccumulation model.

Figure 5-16. Weight-age relationship for pumpkinseed, brown bullhead and largemouth bass collected in the Upper Hudson River.

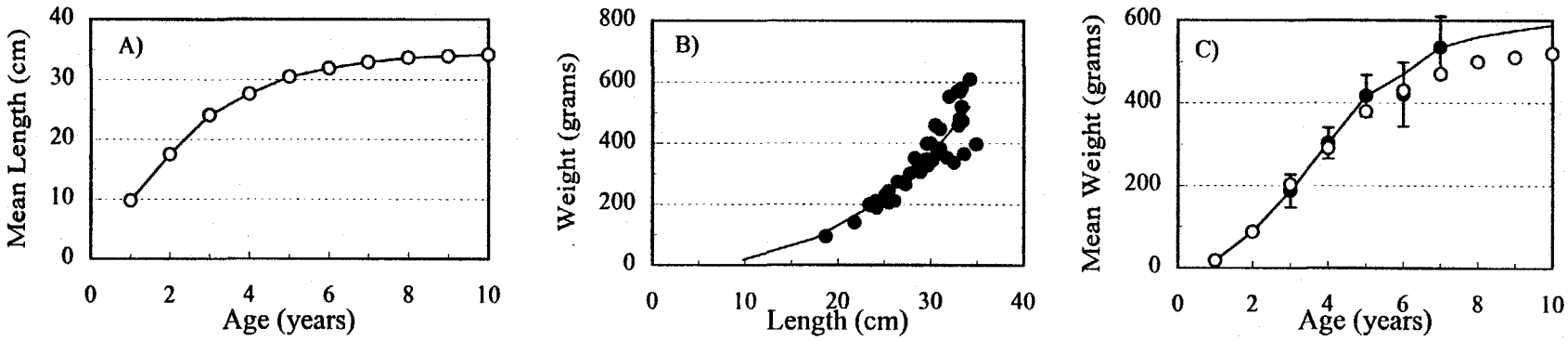

Open circles represent results of annuli analysis of Law Environmental (1991) data.
Closed circles represent data collected by Lawe (1991).
Data are arithmetic means (by age) +/- 2 standard errors.
Lines represent values used in bioaccumulation model.

Figure 5-17. Growth rate calculation for brown bullhead.

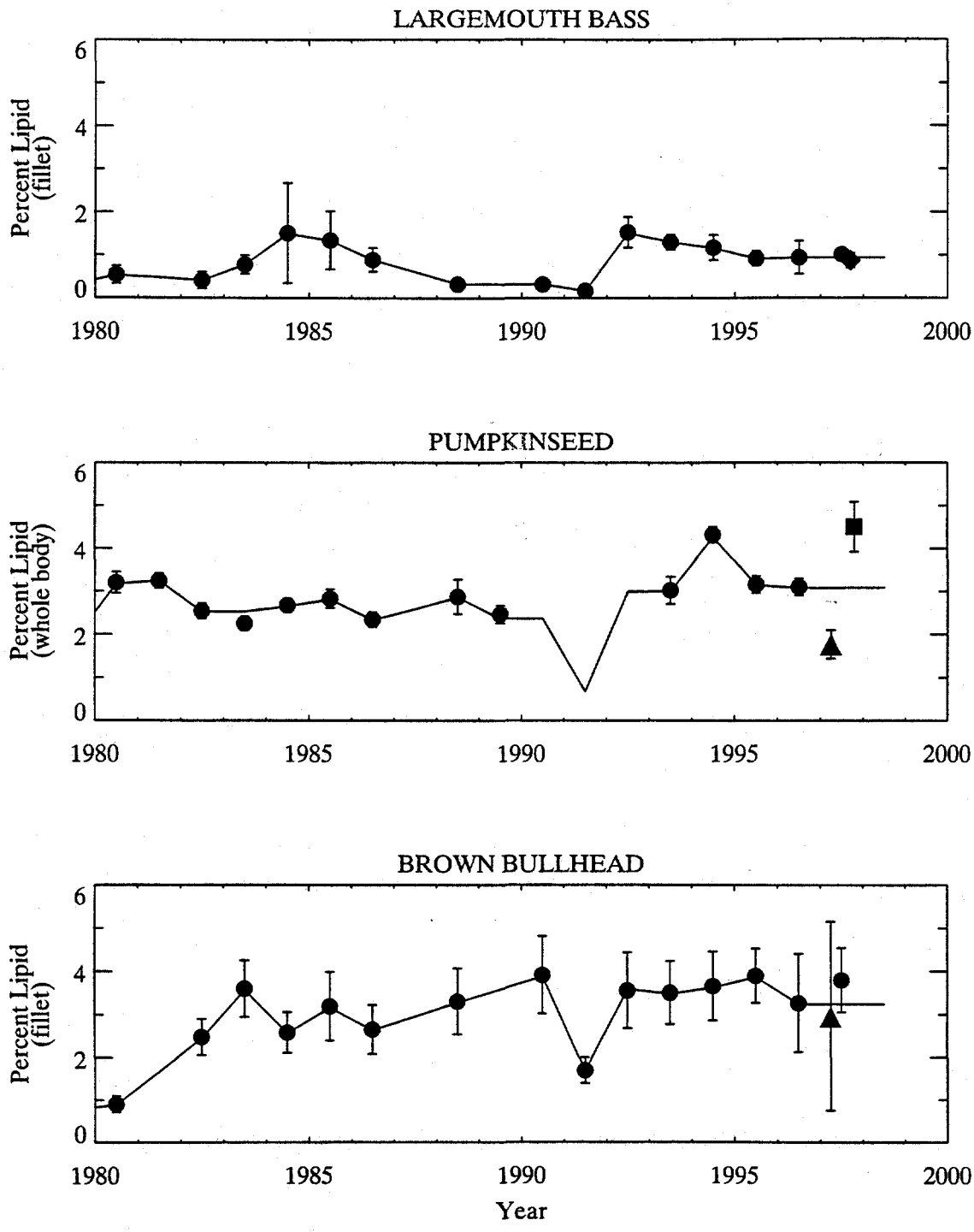

Solid lines indicate model results.
Data are arithmetic means +/- 2 standard errors.
Circles = NYSDEC, Squares = NYSDOH, Triangles = Exponent, Diamonds = GE.

Figure 5-18. Annual average lipid contents in resident fish collected from Stillwater Pool.

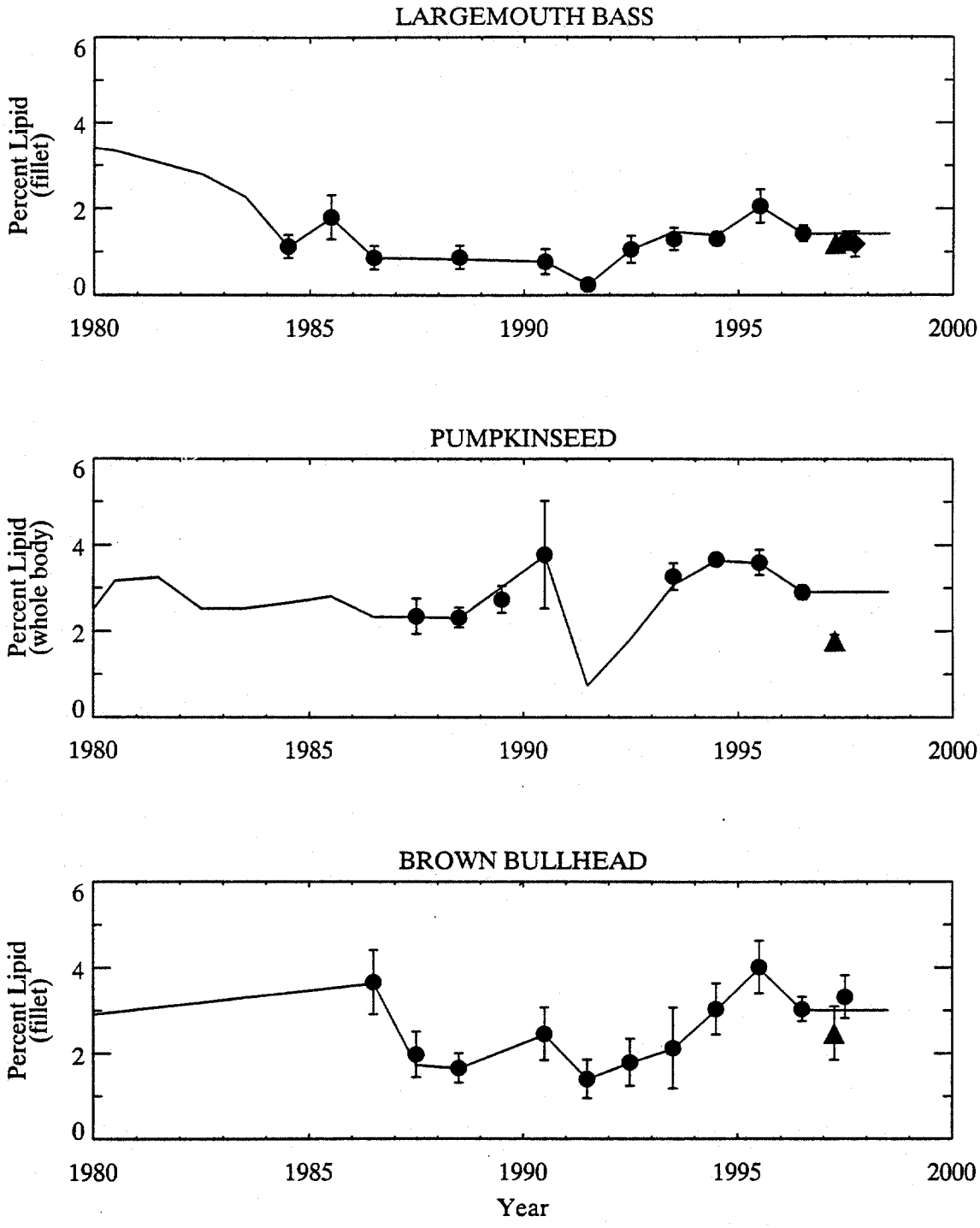

Solid lines indicate model results.
Data are arithmetic means +/- 2 standard errors.
Circles = NYSDEC, Triangles = Exponent, Diamonds = GE.

Figure 5-19. Annual average lipid contents in resident fish collected from Thompson Island Pool.

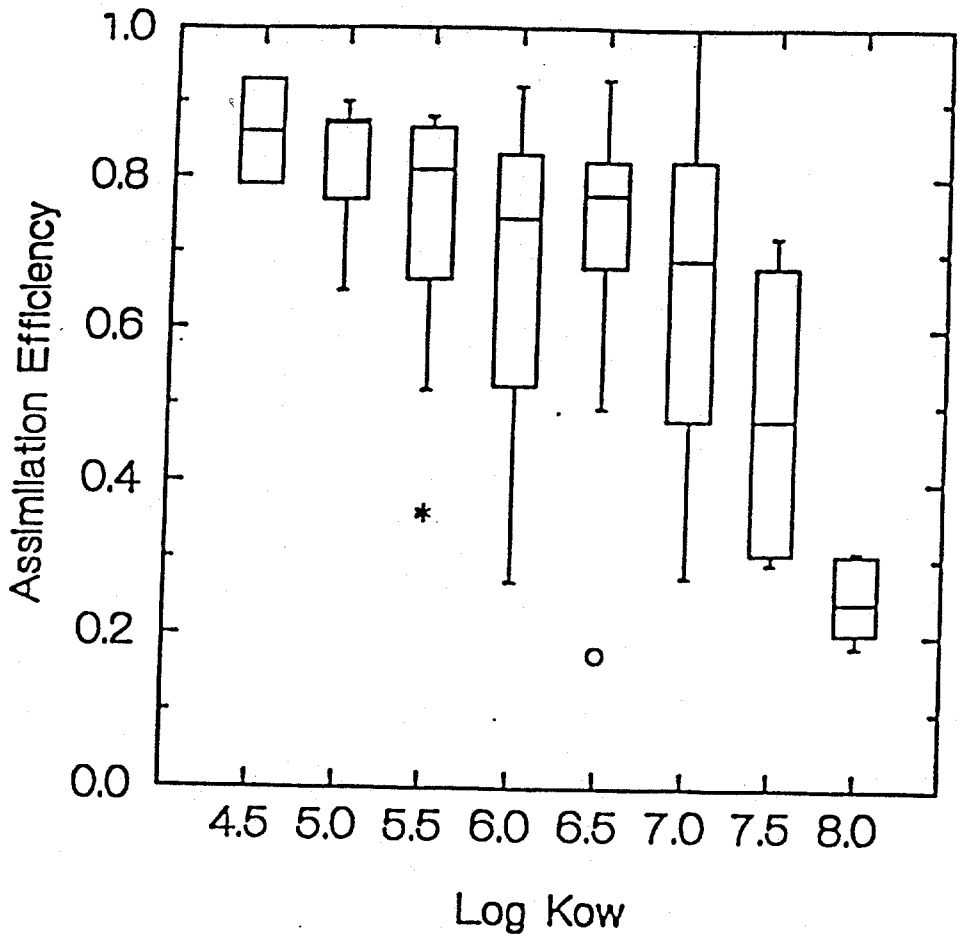

Data collected by Connolly et al. 1992, Parkerton 1993.

Figure 5-20. Dietary assimilation efficiencies of PCBs in fish (box plots).

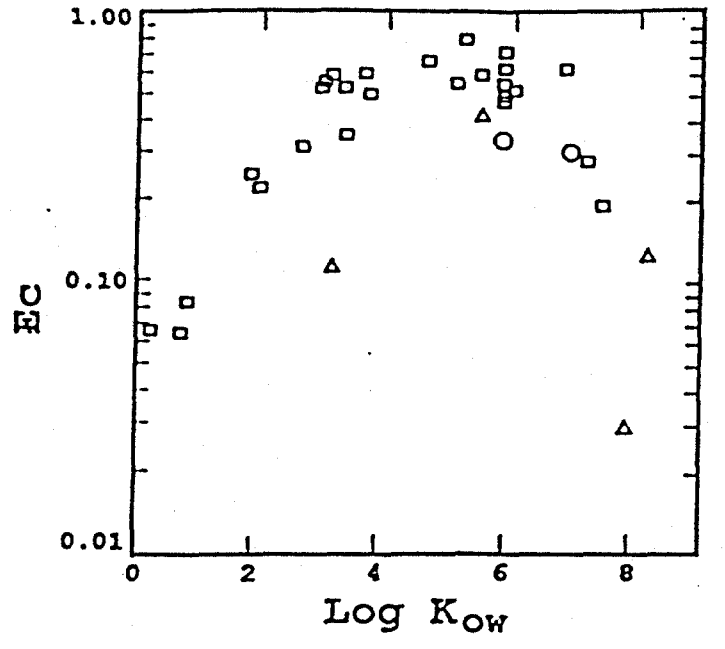

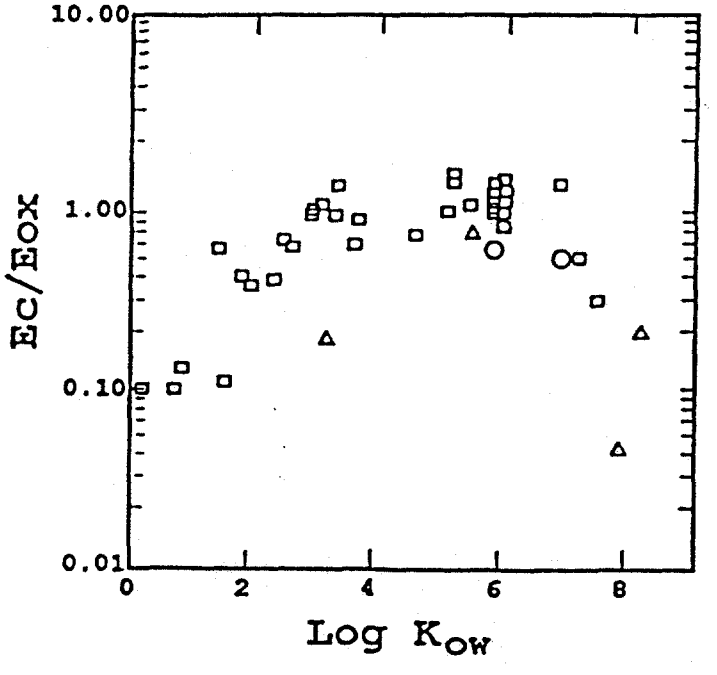

Data collected by Connolly et al. 1992.
Symbols: Circles < 10 g, Triangles 10-100 g, Squares > 100 g.

Figure 5-21. Ratio of PCB:oxygen uptake efficiencies at the gill (E_c/E_{ox}).

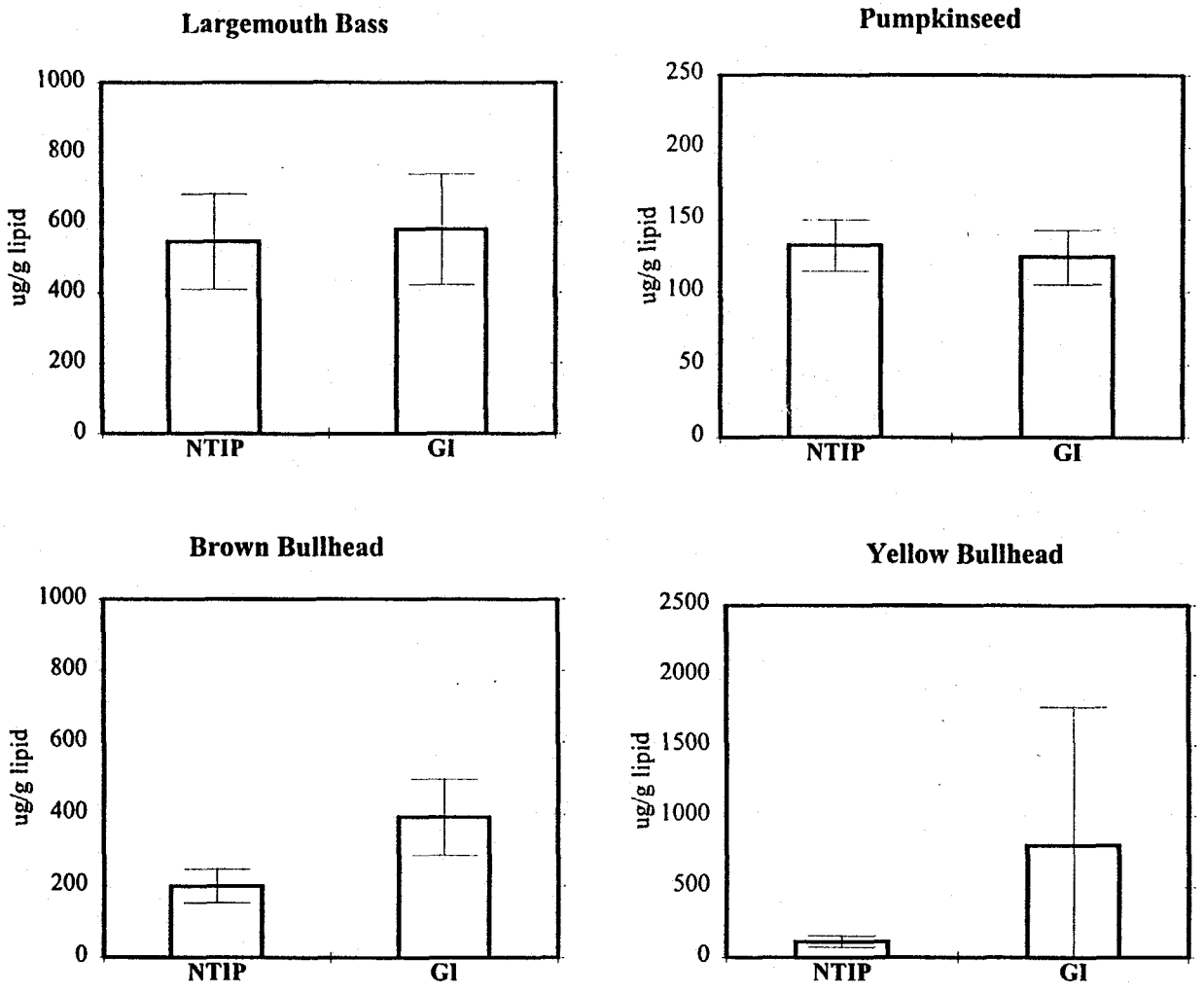

Mean +/- 2 standard errors
1997 Exponent Data

Figure 5-22. Spatial Patterns in Total PCB Concentrations in Fish Collected in TIP.

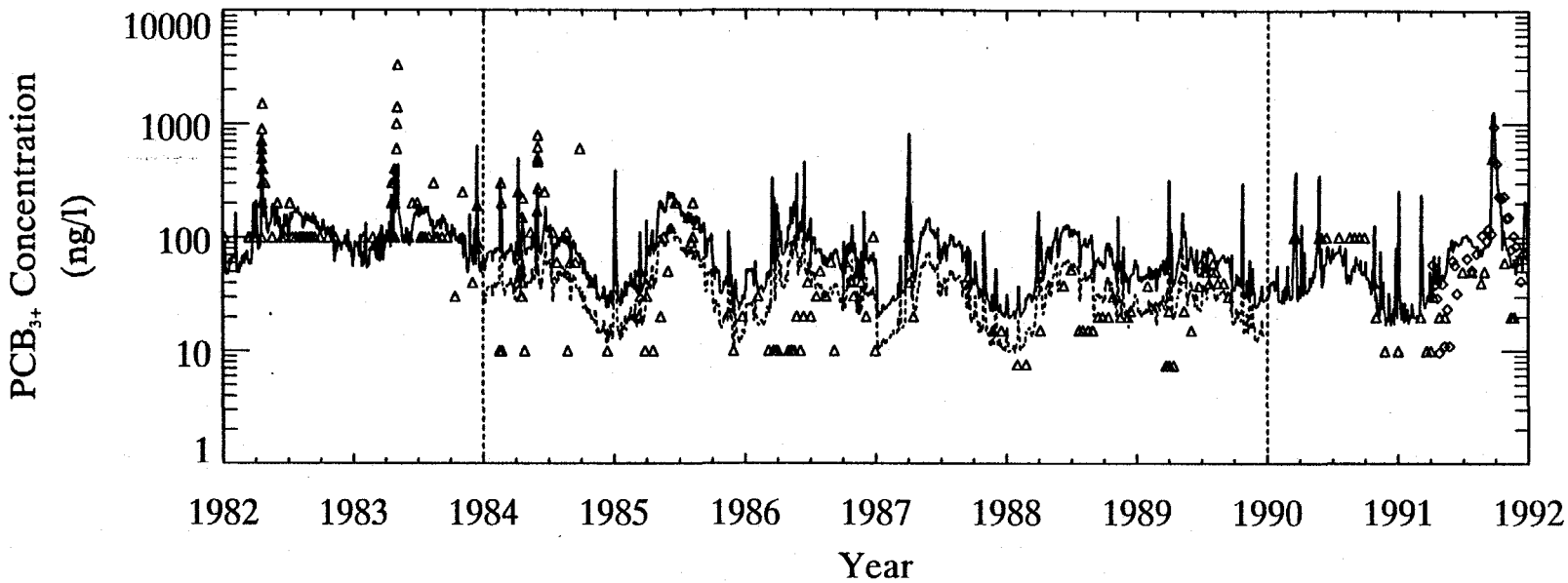

Symbols represent data collected by USGS (triangles) and GE (diamonds).
Solids lines represent levels predicted by fate model.
Dashed lines represent concentrations used in bioaccumulation model.

Figure 5-23. Predicted and adjusted water column PCB_{3+} concentrations at Stillwater from the PCB fate model. Adjusted values for 1984-1989 were used in the bioaccumulation model.

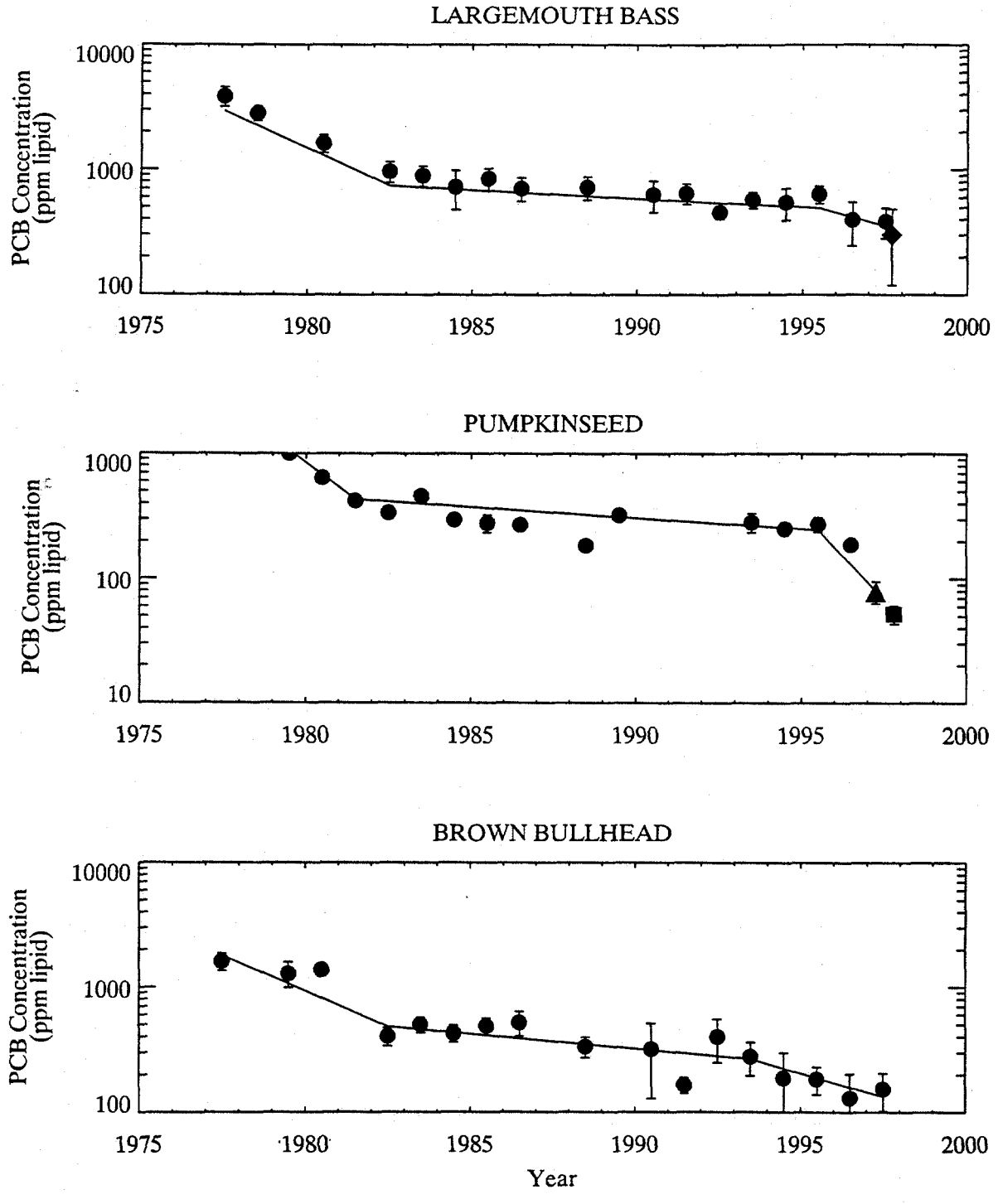

Solid lines represent logarithmic regressions of data.
Data are arithmetic means +/- 2 standard errors.
Circles = NYSDEC, Squares = NYSDOH, Triangles = Exponent, Diamonds = GE.
Crosses indicate values excluded from the annual averages.

Figure 5-24. Annual average PCB concentrations in resident fish of the Upper Hudson River. Lipid normalized, Stillwater Pool.

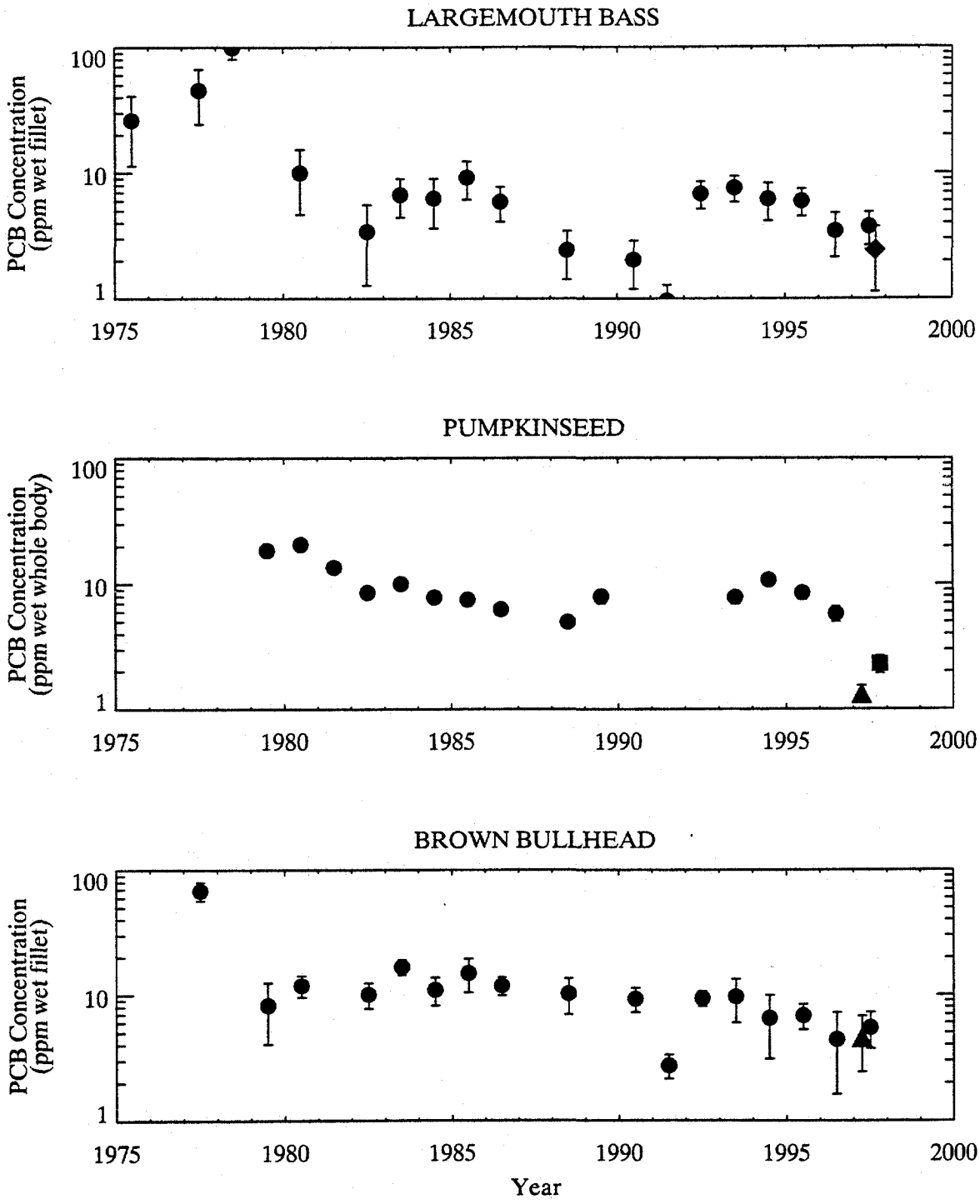

Data are arithmetic means +/- 2 standard errors.
Circles = NYSDEC, Squares = NYSDOH, Triangles = Exponent, Diamonds = GE.

Figure 5-25. Annual average PCB concentrations in resident fish of the Upper Hudson River. Wet-weight basis, Stillwater Pool.

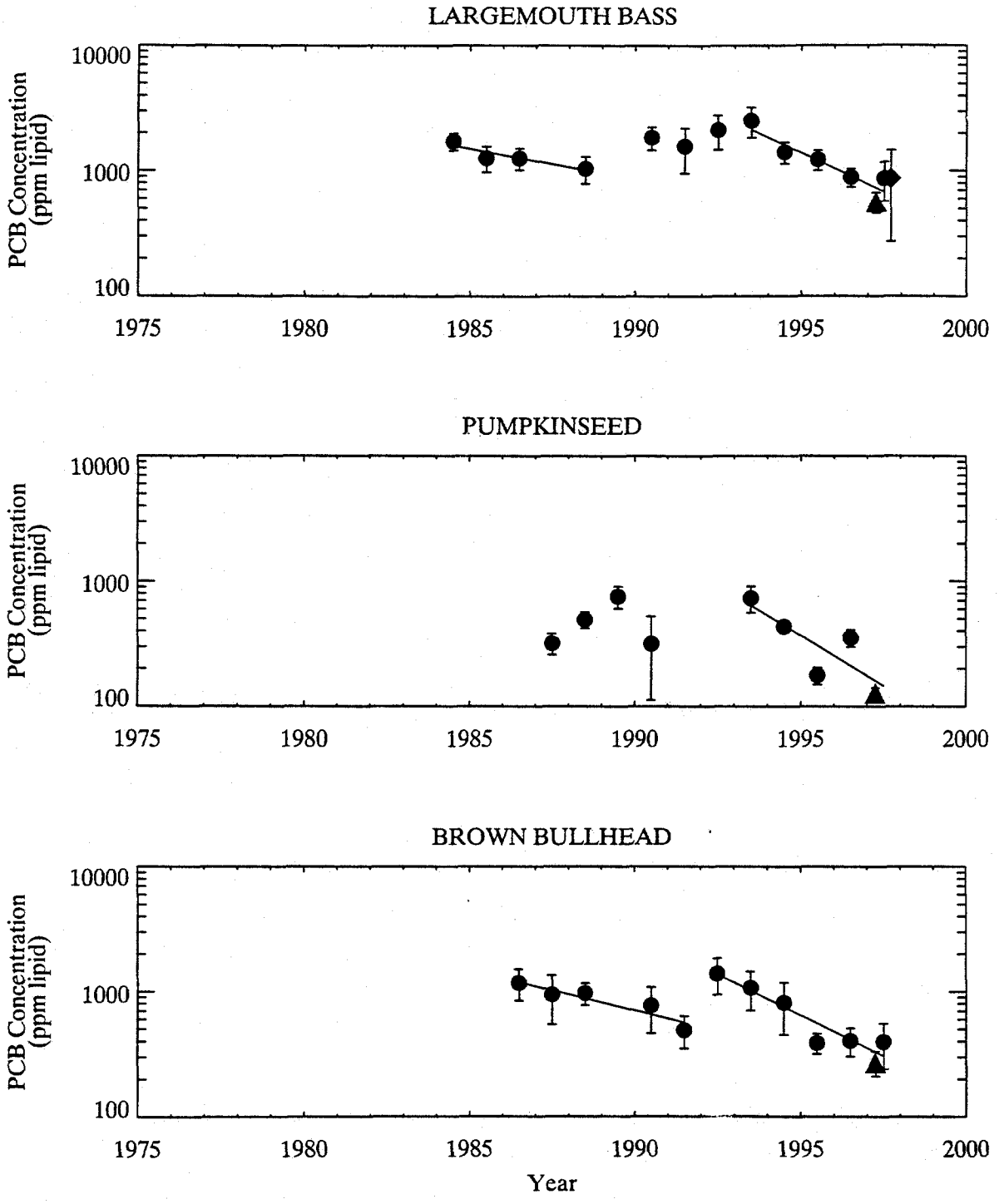

Solid lines represent logarithmic regressions of data.
Data are arithmetic means +/- 2 standard errors.
Circles = NYSDEC, Triangles = Exponent, Diamonds = GE.

Figure 5-26. Annual average PCB concentrations in resident fish of the Upper Hudson River. Lipid normalized, Thompson Island Pool.

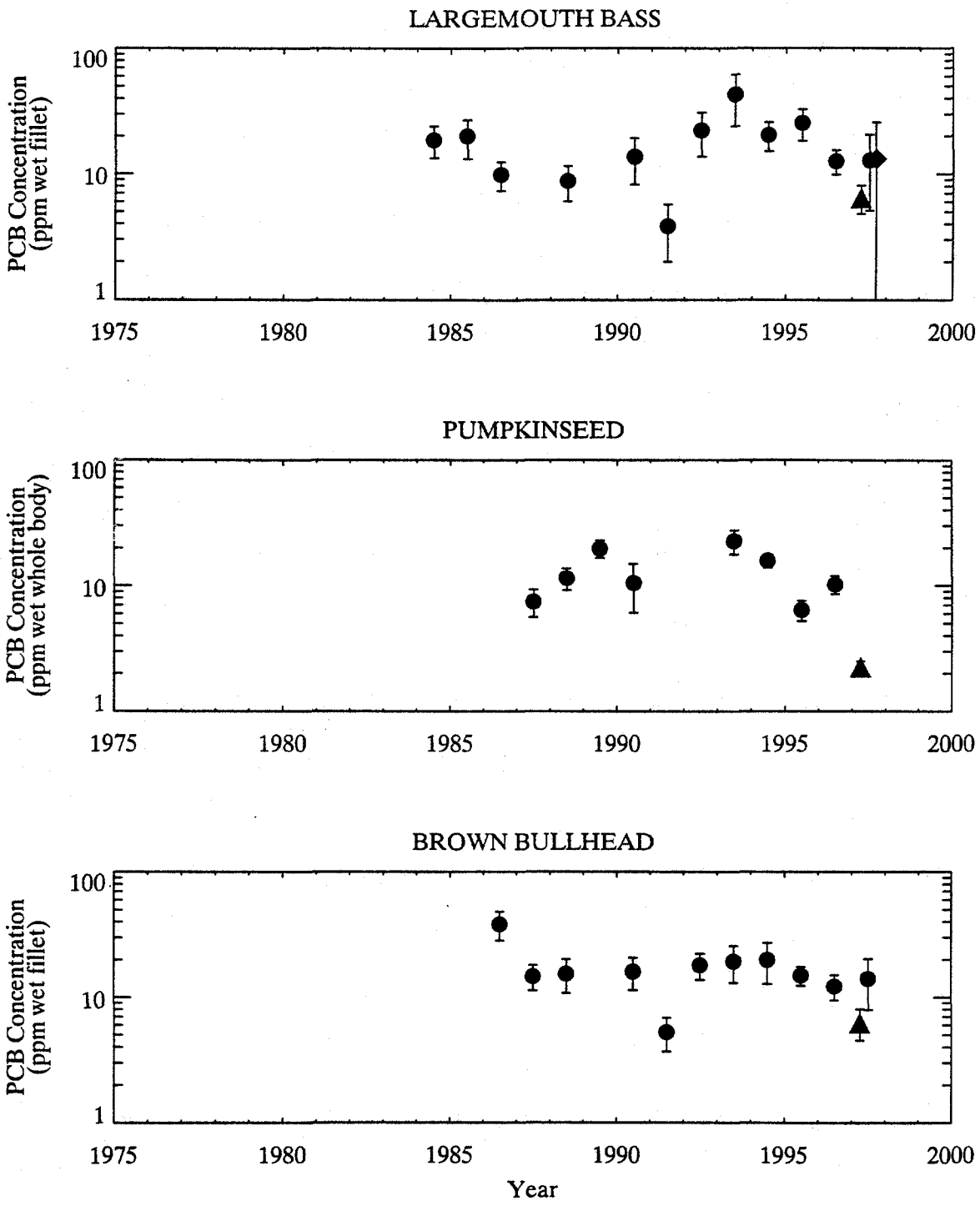

Data are arithmetic means +/- 2 standard errors.
Circles = NYSDEC, Triangles = Exponent, Diamonds = GE.

Figure 5-27. Annual average PCB concentrations in resident fish of the Upper Hudson River. Wet-weight basis, Thompson Island Pool.

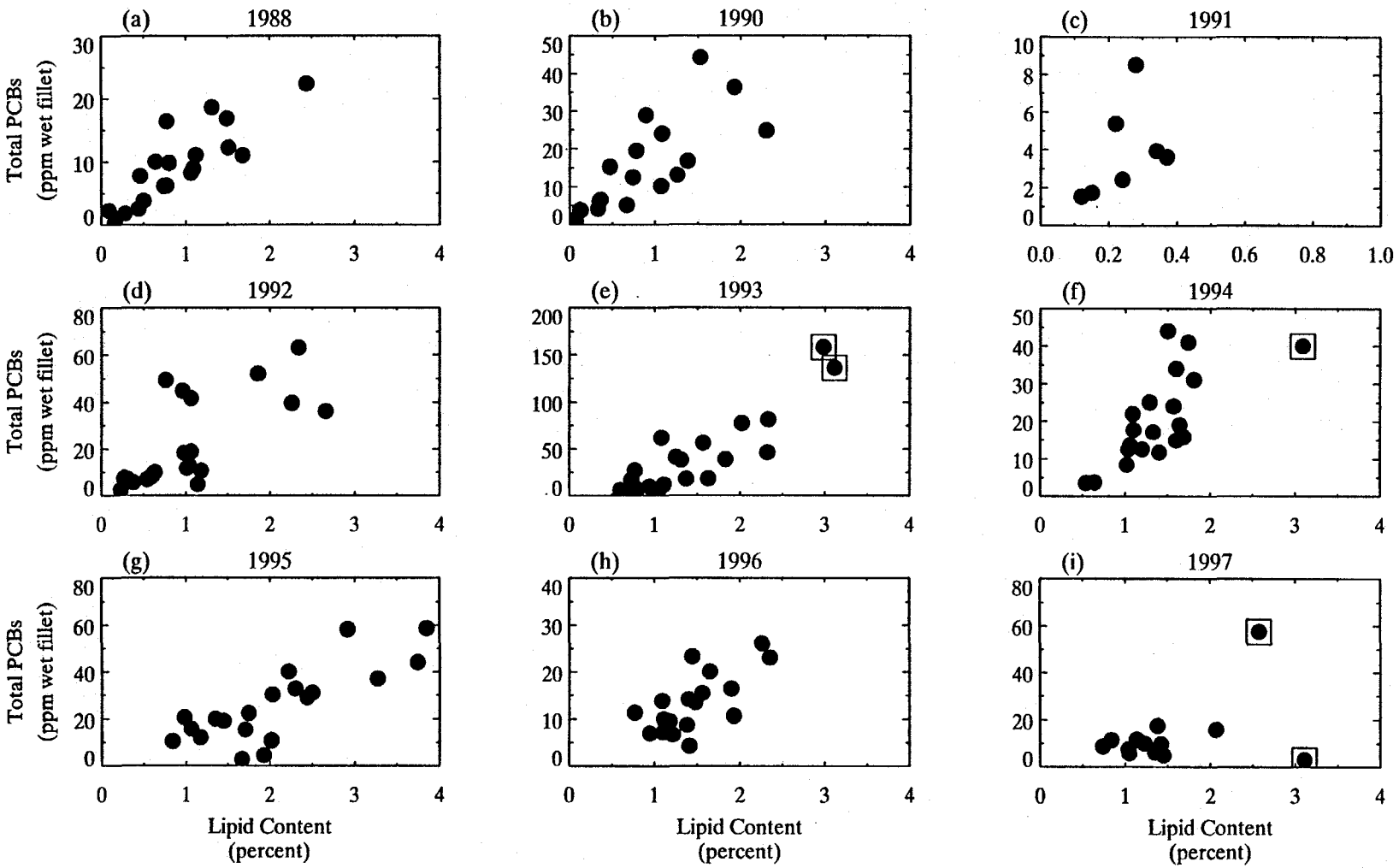

Data collected by NYSDEC.

Figure 5-28. Relationship between PCB concentrations and lipid levels in largemouth bass of Thompson Island Pool. Squares indicate values excluded from annual averages.

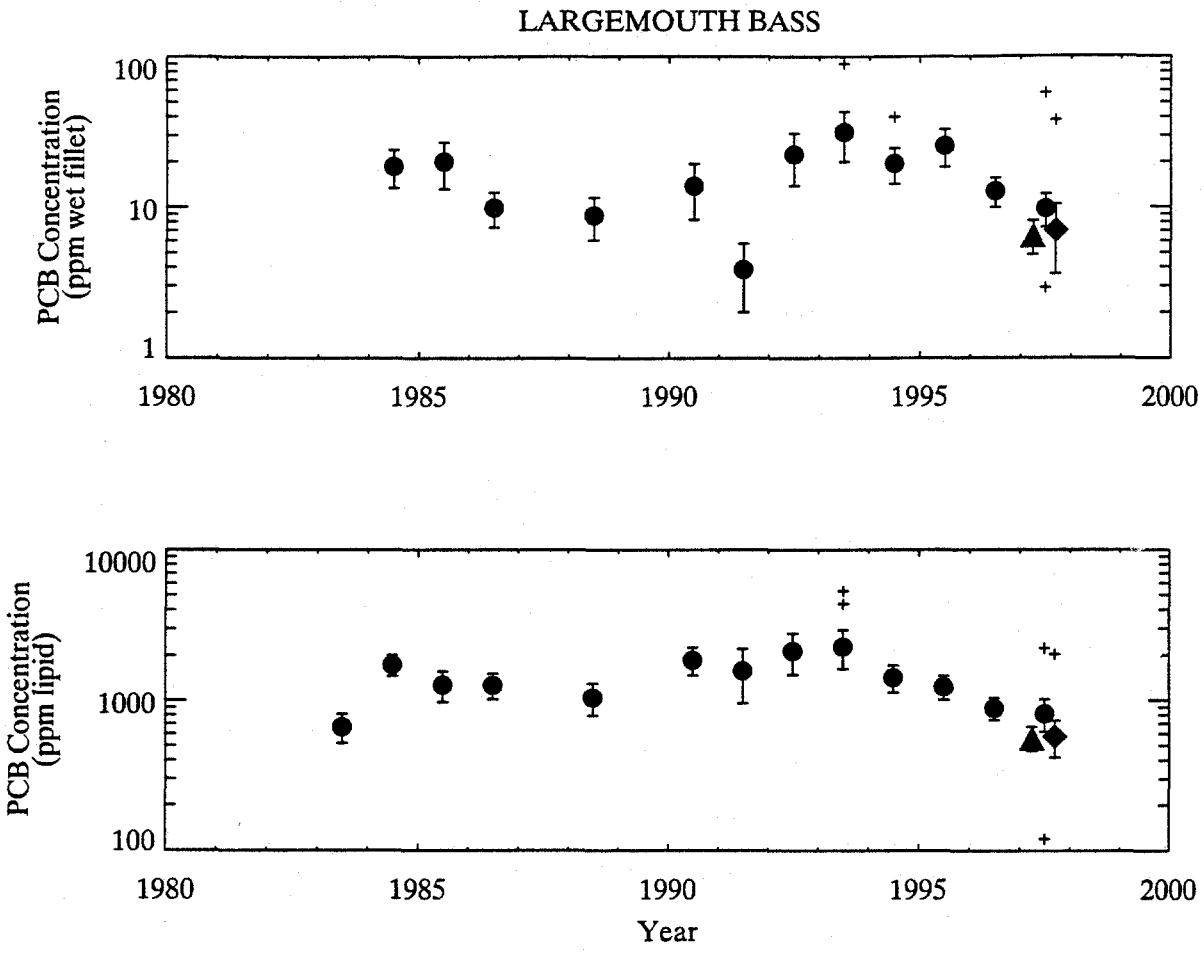

Data are arithmetic means +/- 2 standard errors.
Circles = NYSDEC, Triangles = Exponent, Diamonds = GE.
Crosses indicate data excluded from annual averages.
Crosses at top/bottom of axes represent values off of scale.

Figure 5-29. Annual average PCB concentrations in largemouth bass of the Thompson Island Pool. Six values were excluded from the annual averages.

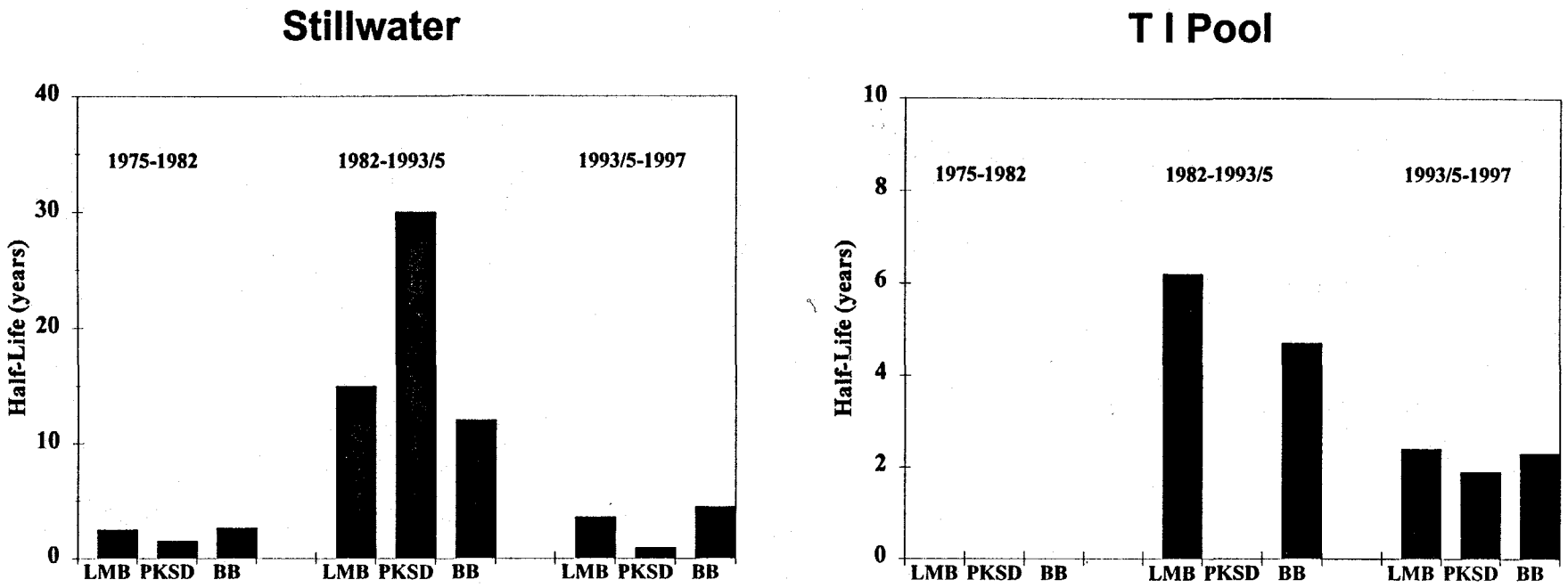

LMB: Largemouth bass

PKSD: Pumpkinseed

BB: Brown bullhead

Figure 5-30. Half-lives computed from trends in lipid-based total PCB concentrations measured in fish from the Upper Hudson River.

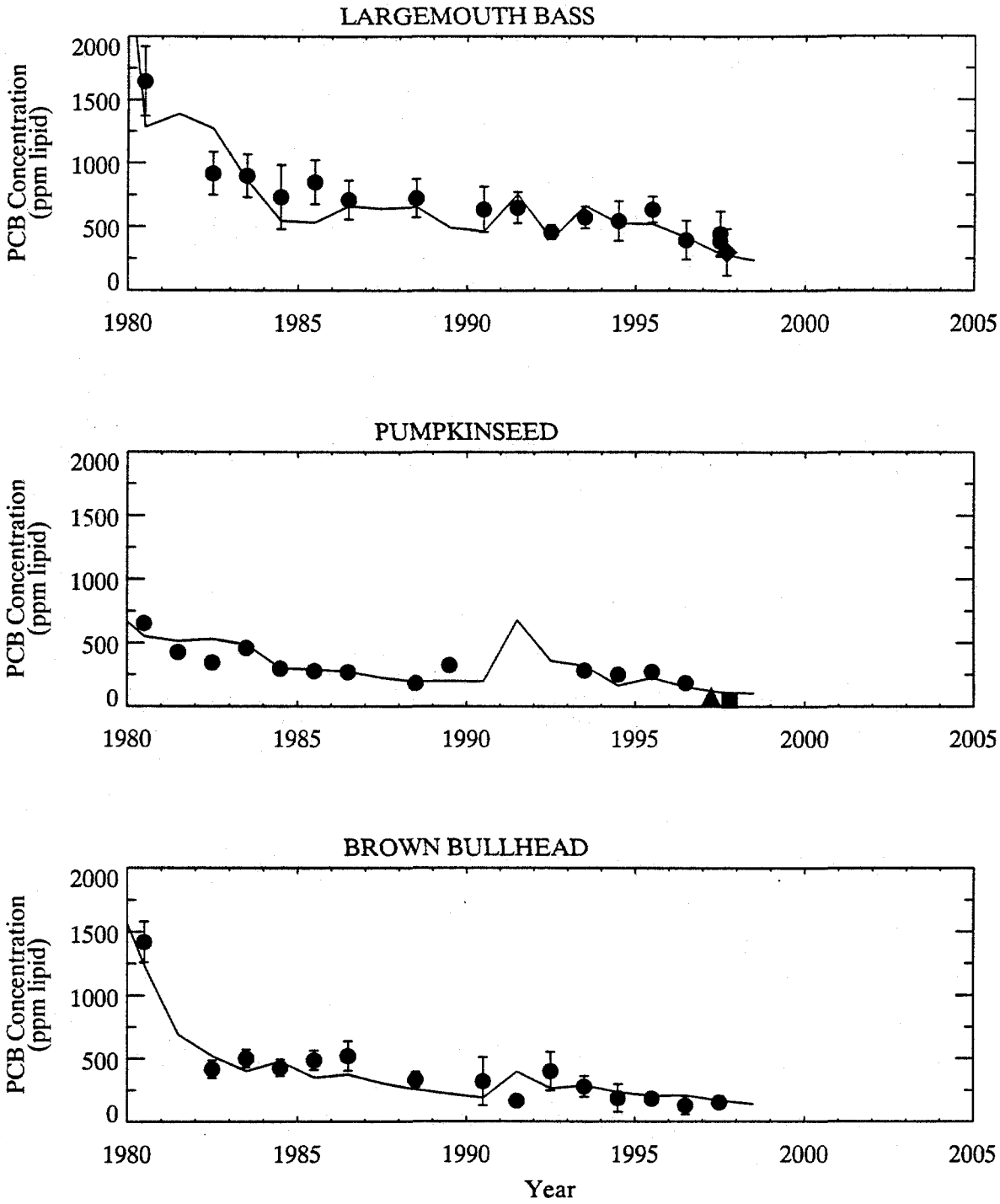

Solid lines indicate model results.
Data are arithmetic means +/- 2 standard errors.
Circles = NYSDEC, Squares = NYSDOH, Triangles = Exponent, Diamonds = GE.

Figure 5-31. Predicted (line) and measured (symbols) lipid-normalized PCB concentrations in largemouth bass, pumpkinseed and brown bullhead collected from Stillwater Pool.

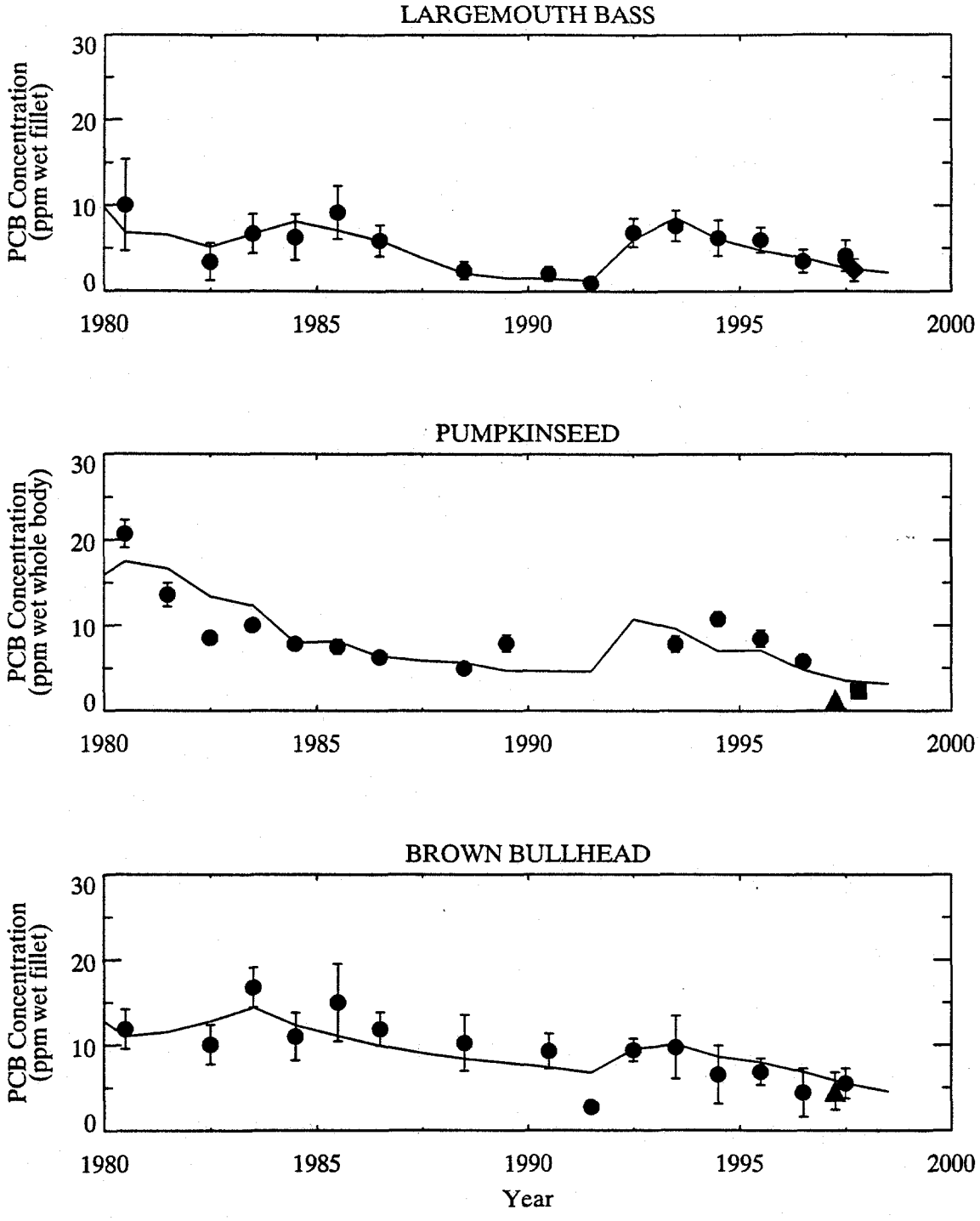

Solid lines indicate model results.
Data are arithmetic means +/- 2 standard errors.
Circles = NYSDEC, Squares = NYSDOH, Triangles = Exponent, Diamonds = GE.

Figure 5-32. Predicted (line) and measured (symbols) wet-weight PCB concentrations in largemouth bass, pumpkinseed and brown bullhead collected from Stillwater Pool.

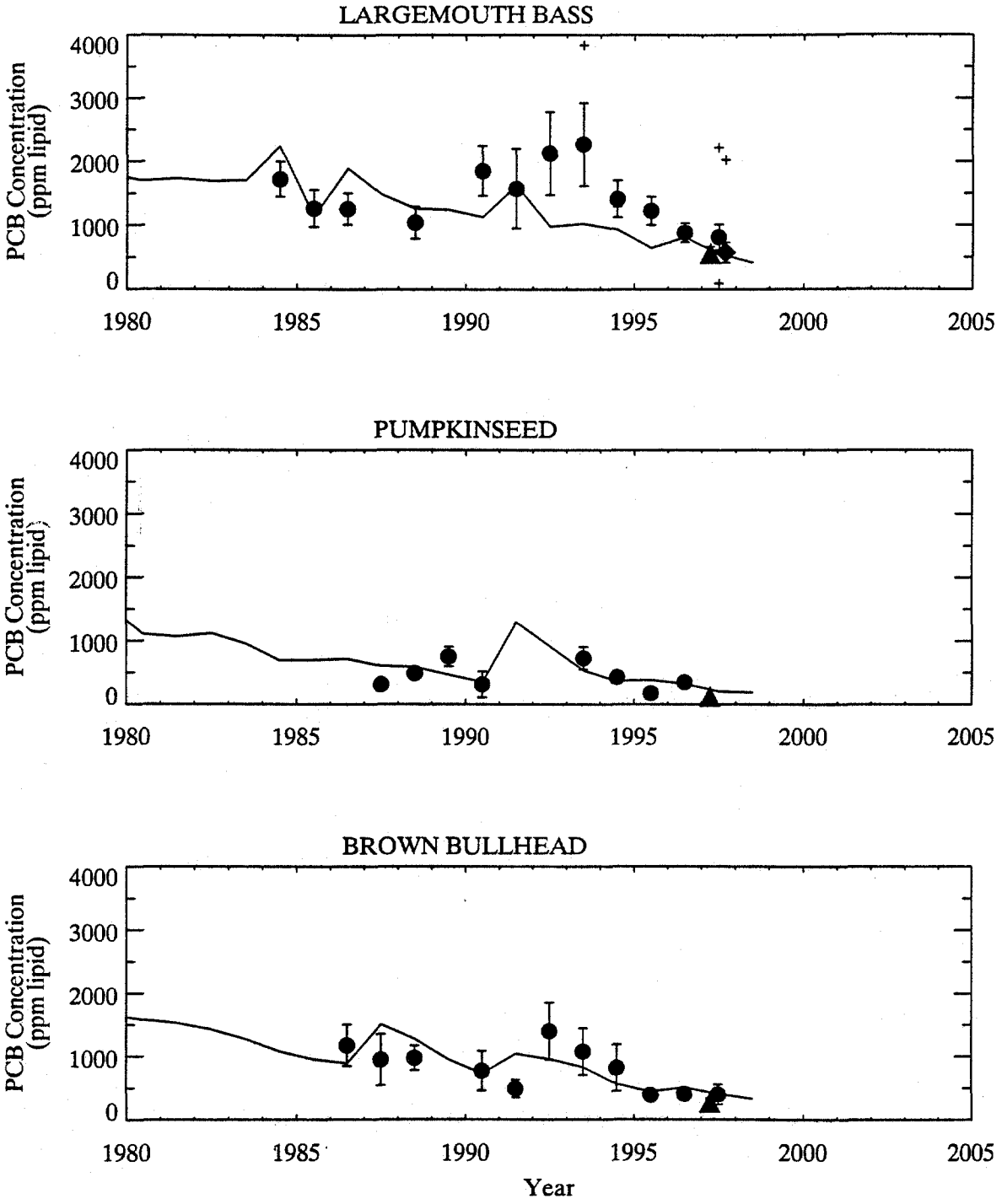

Solid lines indicate model results.
Data are arithmetic means +/- 2 standard errors.
Circles = NYSDEC, Triangles = Exponent, Diamonds = GE.
Crosses indicate data excluded from the annual averages.
Crosses at top of axes represent values off of scale.

Figure 5-33. Predicted (line) and measured (symbols) lipid-normalized PCB concentrations in largemouth bass, pumpkinseed and brown bullhead collected from Thompson Island Pool.

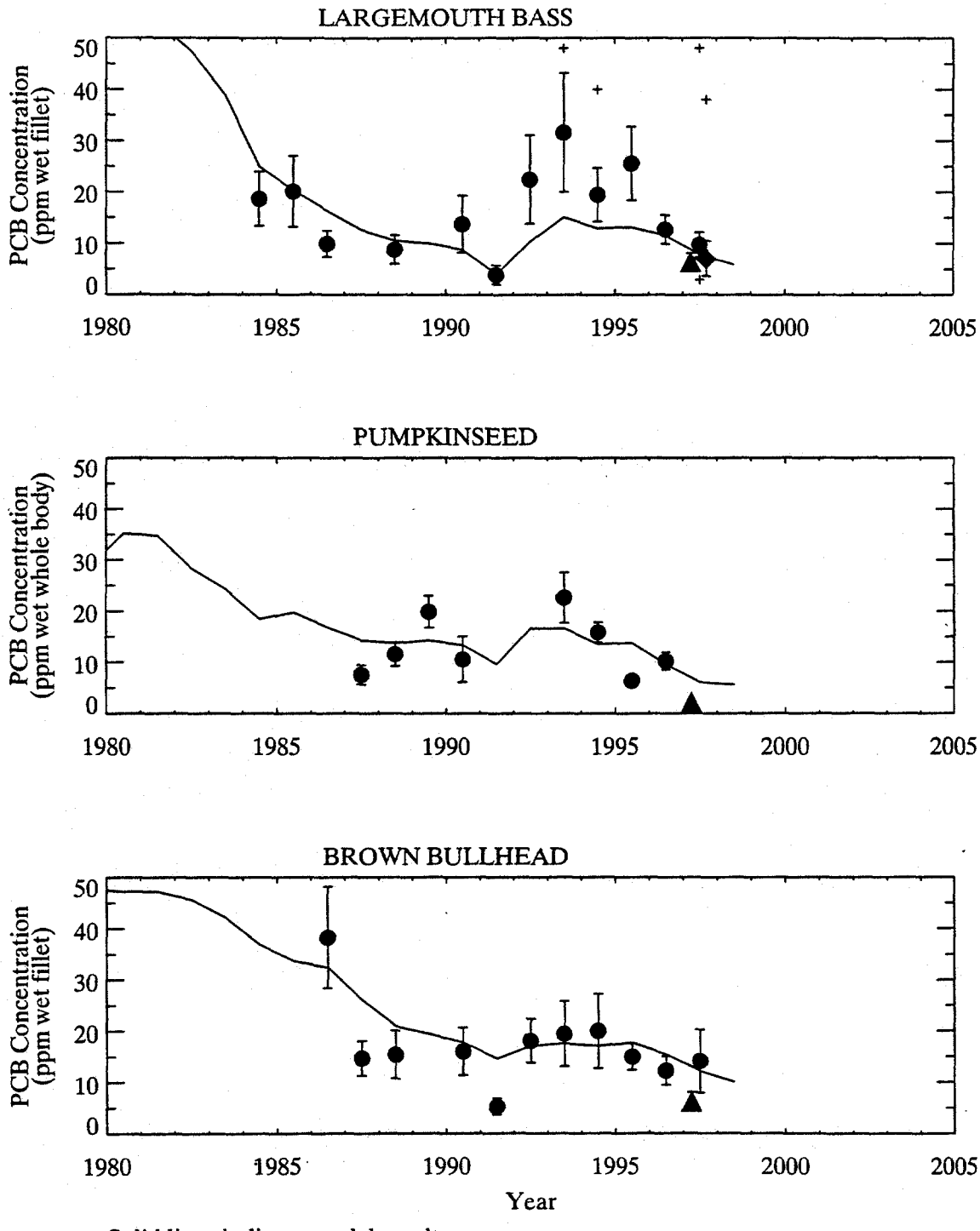

Solid lines indicate model results.
Data are arithmetic means +/- 2 standard errors.
Circles = NYSDEC, Triangles = Exponent, Diamonds = GE.
Crosses indicate values excluded from the annual averages.
Crosses at top of axes represent values off of scale.

Figure 5-34. Predicted (line) and measured (symbols) wet-weight PCB concentrations in largemouth bass, pumpkinseed and brown bullhead collected from Thompson Island Pool.

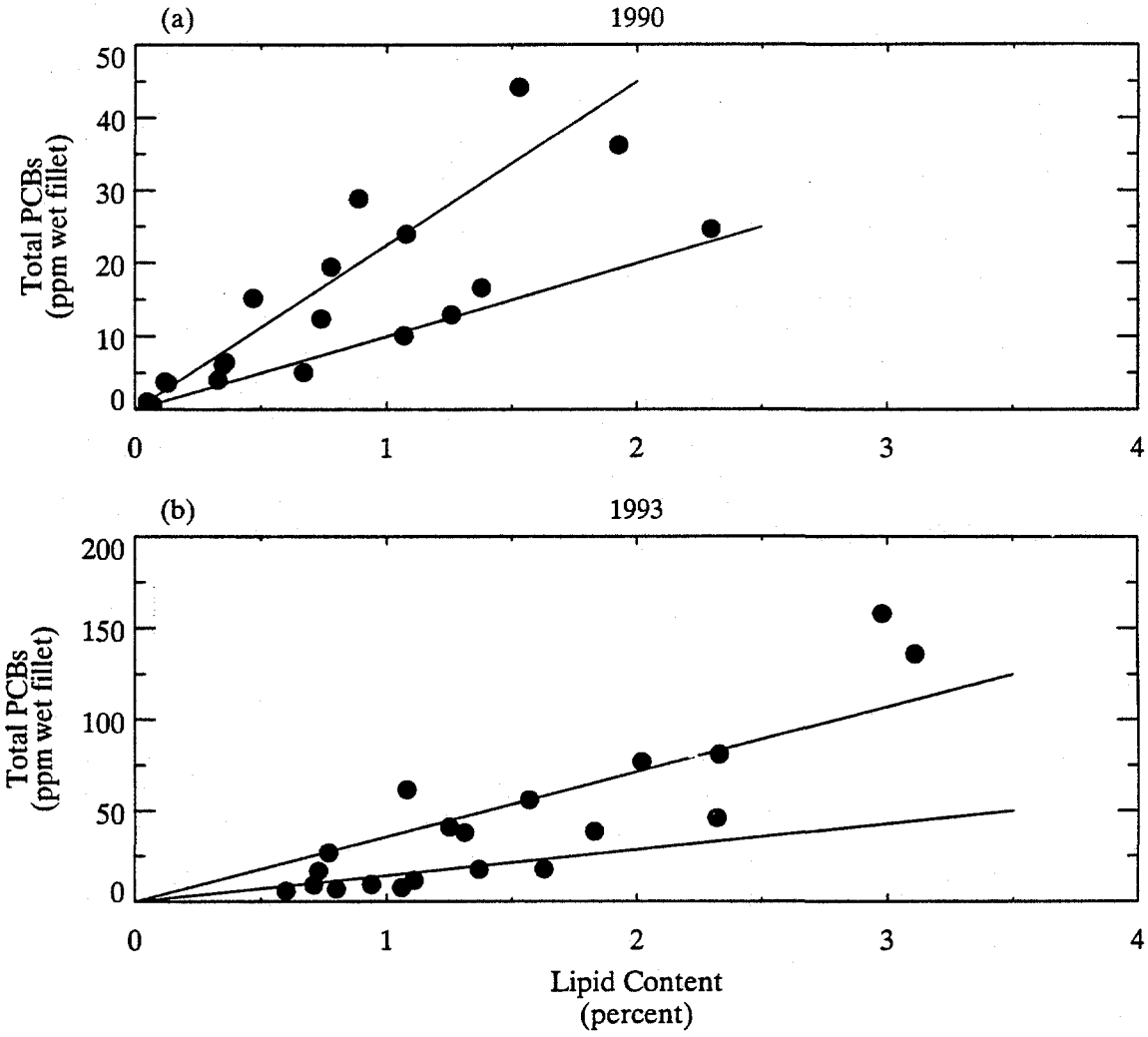

Data collected by NYSDEC.

Figure 5-35. Relationship between PCB concentrations and lipid levels in largemouth bass of Thompson Island Pool.

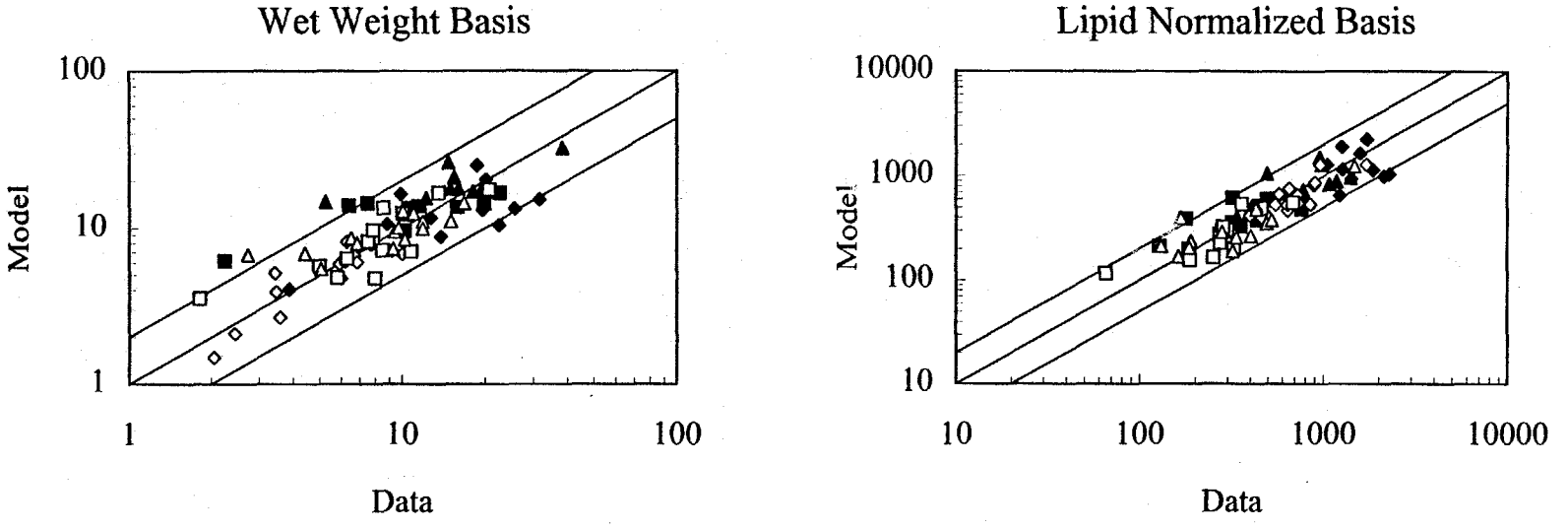

Diamonds = largemouth bass
Squares = pumpkinseed
Triangles = brown bullhead
Filled symbols = Thompson Island Pool values
Open symbols = Stillwater Pool values

Figure 5-36. Calibration of the food web model. Comparison of computed and observed PCB concentrations in fish.

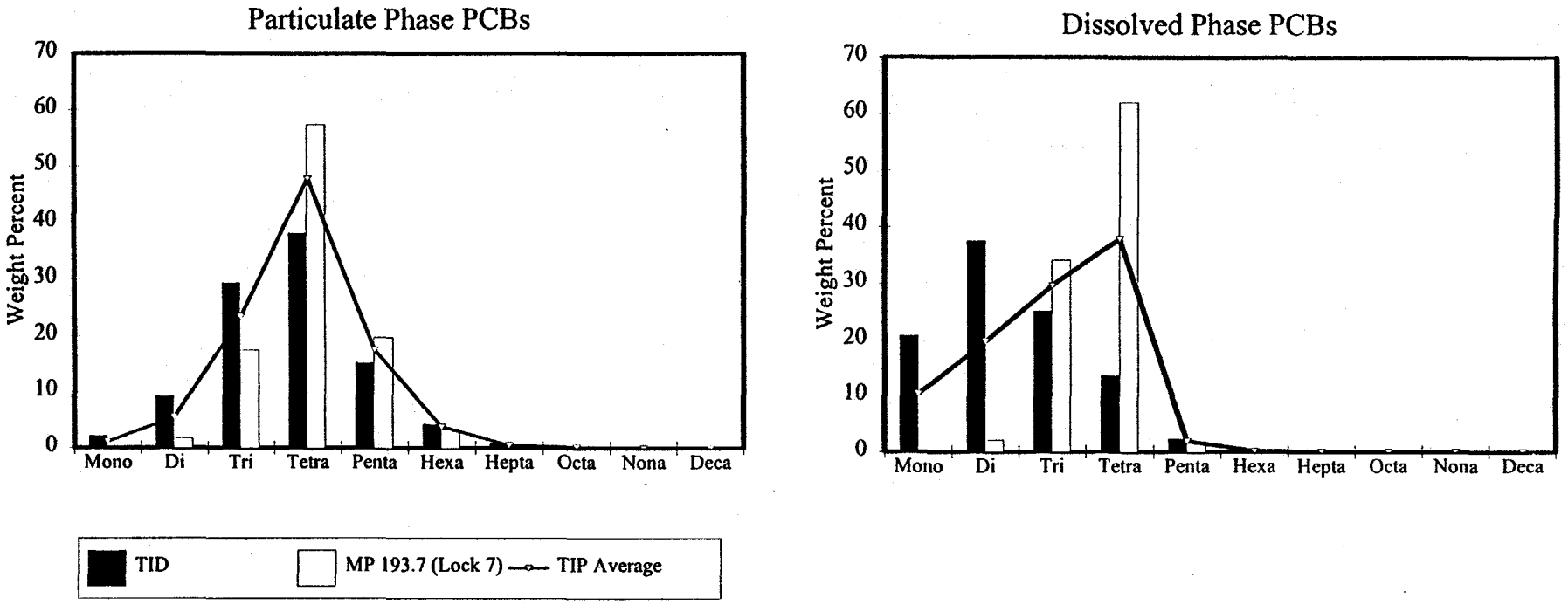

Data collected June-August 1993 by USEPA.

3140098

Figure 5-37. Homolog composition of dissolved and particulate water column PCBs in TIP.

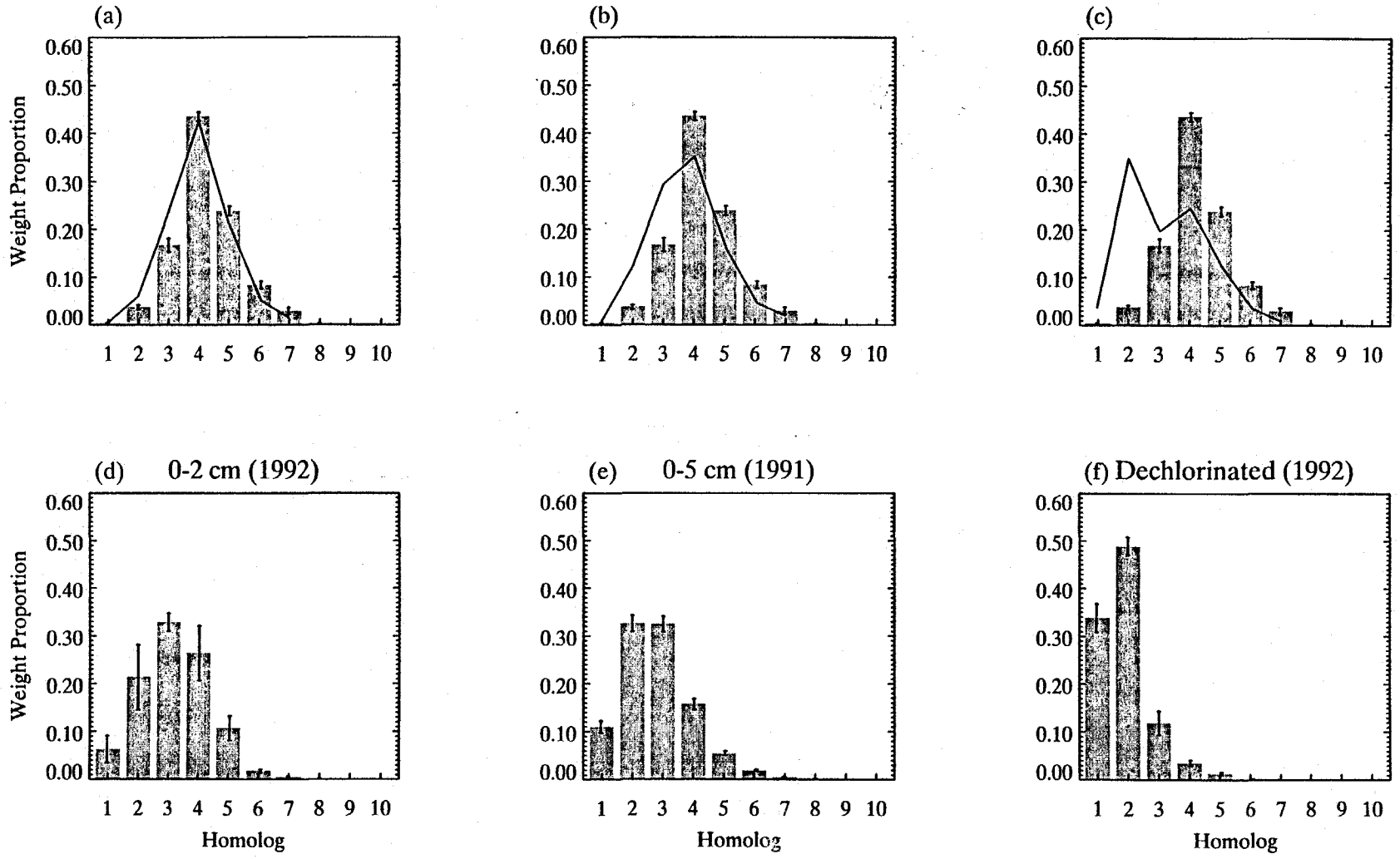

Bars represent data (arithmetic means +/- 2 standard errors).
Fish Data: USEPA, NOAA, Law Environmental, OBG and Exponent (panels a, b and c).
Sediment Data: USEPA (panels d and f) and GE (panel e).
Lines represent results of bioaccumulation model.

Figure 5-38. Food web homolog bioaccumulation model. Homolog compositions in pumpkinseed (panels a, b and c) and sediments (panel d, e and f) in the Thompson Island Pool.

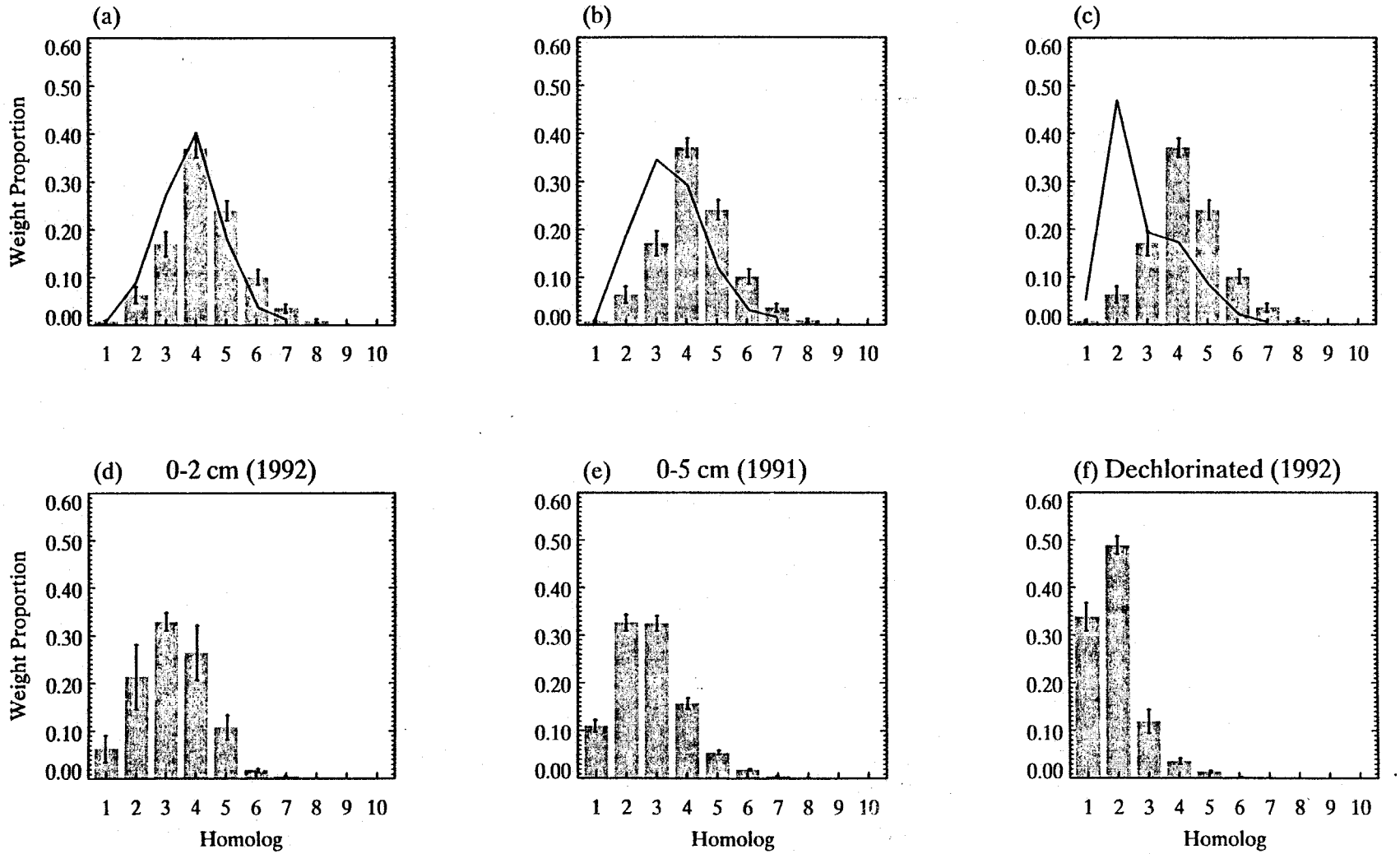

Bars represent data (arithmetic means +/- 2 standard errors).
Fish Data: USEPA, NOAA, Law Environmental, OBG and Exponent (panels a, b and c).
Sediment Data: USEPA (panels d and f) and GE (panel e).
Lines represent results of bioaccumulation model.

Figure 5-39. Food web homolog bioaccumulation model. Homolog compositions in brown bullhead (panels a, b and c) and sediments (panels d, e and f) in the Thompson Island Pool.

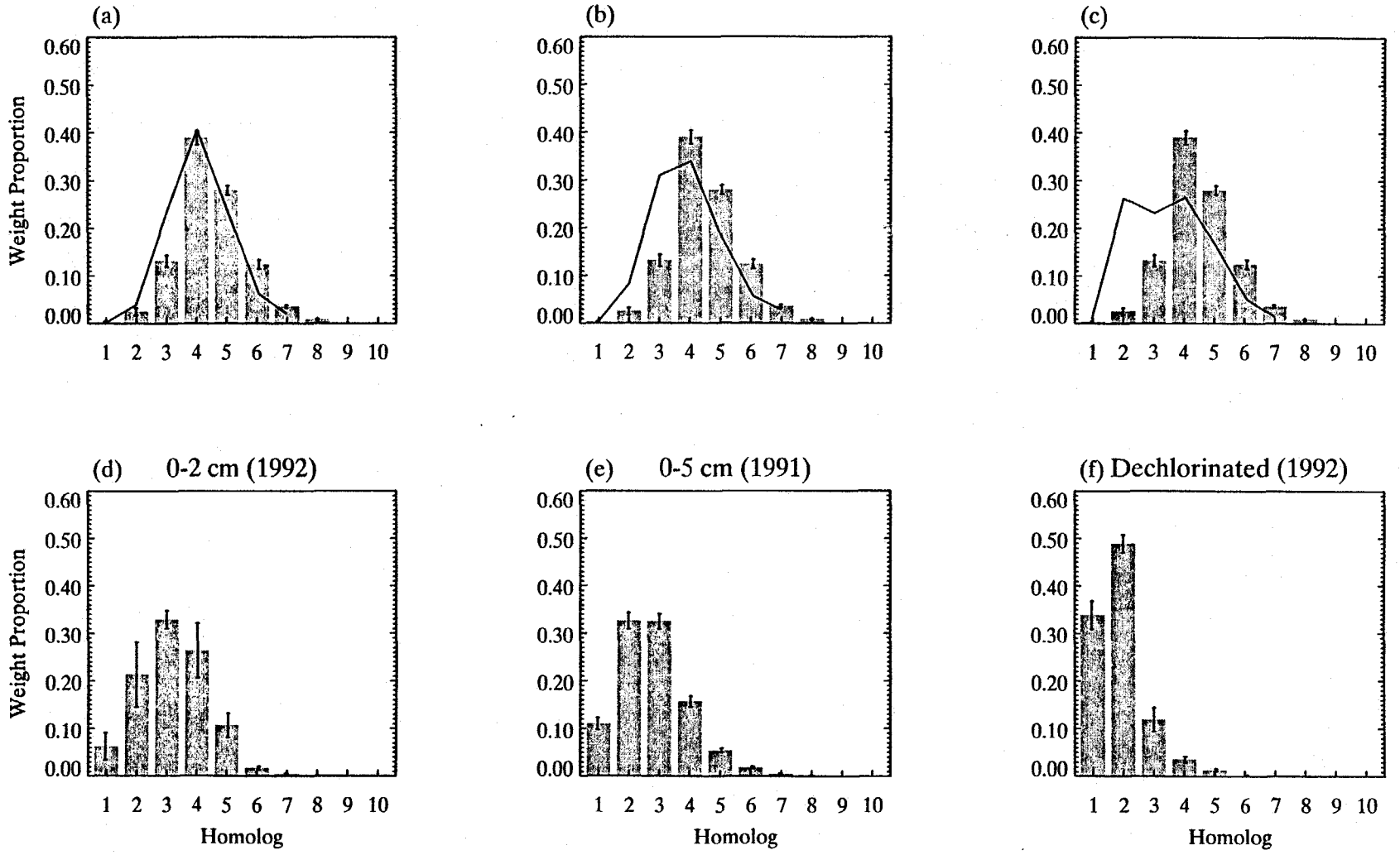

Bars represent data (arithmetic means +/- 2 standard errors).
Fish Data: USEPA, NOAA, Law Environmental, OBG and Exponent (panels a, b and c).
Sediment Data: USEPA (panels d and f) and GE (panel e).
Lines represent results of bioaccumulation model.

Figure 5-40. Food web homolog bioaccumulation model. Homolog compositions in largemouth bass (panels a, b and c) and sediments (panels d, e and f) in the Thompson Island Pool.

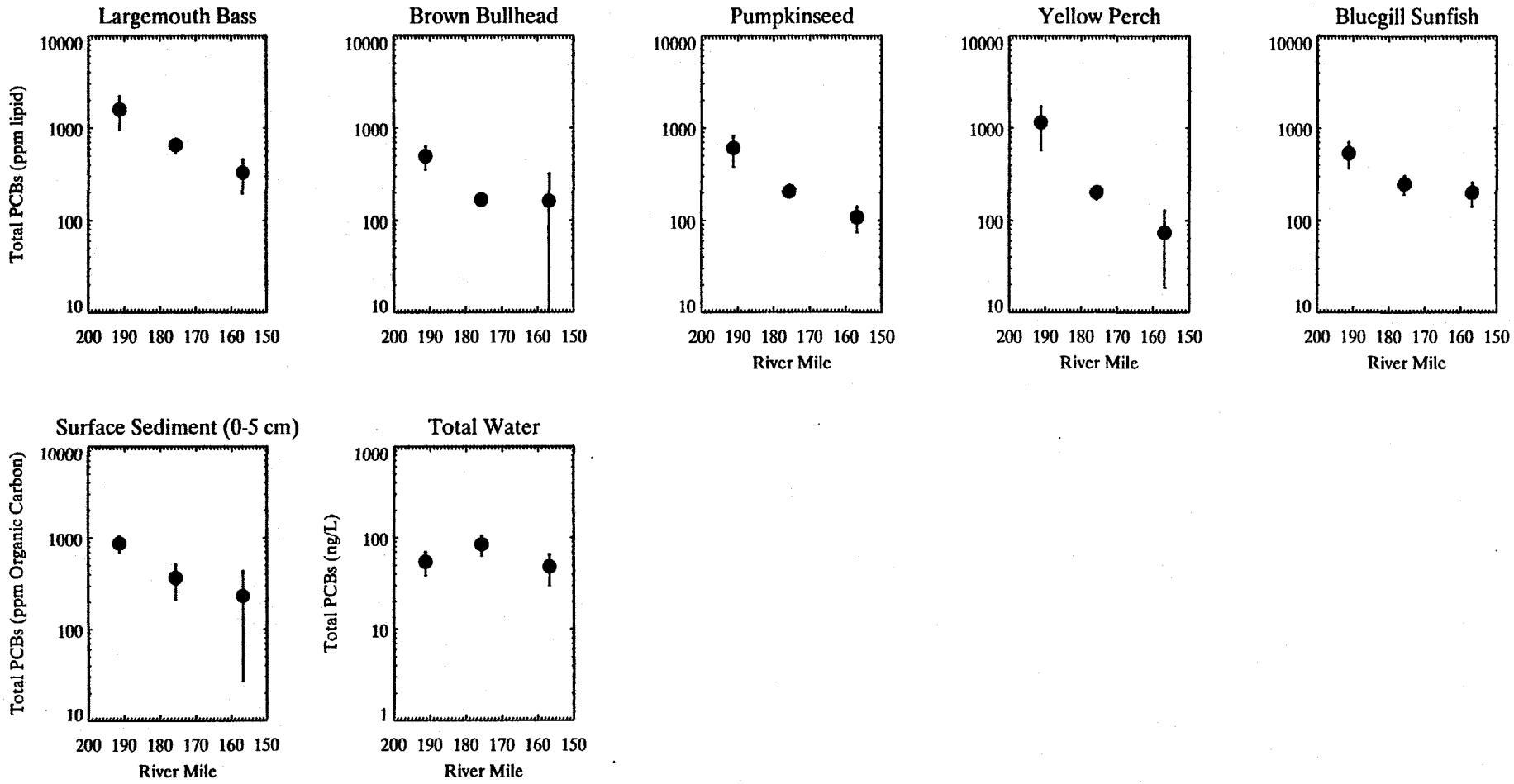

Annual Averages +/-2 Standard Errors
Surface sediment data: GE, 1991; PCB_{3+}, 0-5 cm.
Water data: GE, June-Sept., 1991; PCB_{3+}, whole water.
Fish data: NYSDEC, 1991; Total PCBs;

Figure 5-41. Spatial gradients in PCB concentrations in surface sediments, water, and fish.

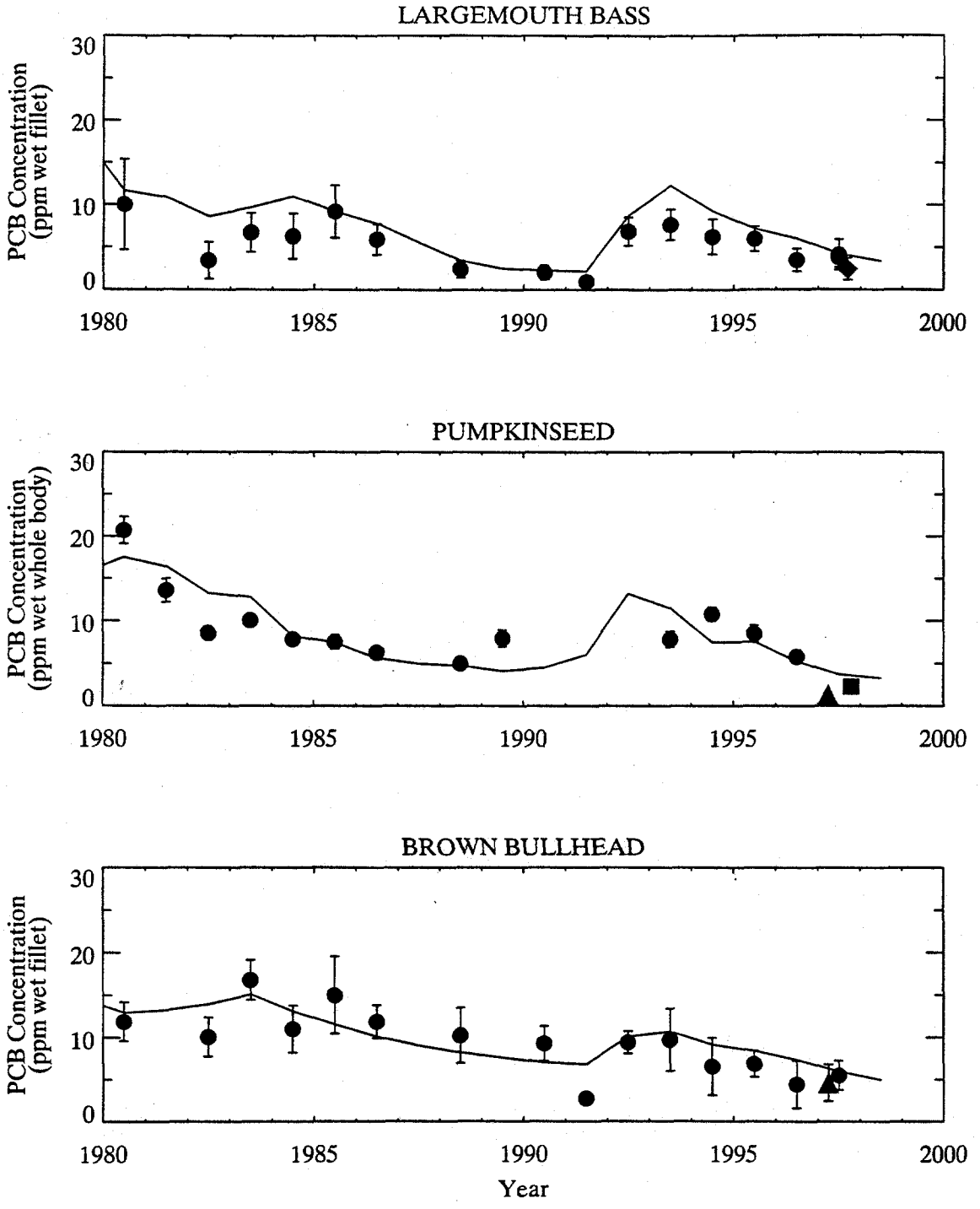

Solid lines indicate model results.
Data are arithmetic means +/- 2 standard errors.
Circles = NYSDEC, Squares = NYSDOH, Triangles = Exponent, Diamonds = GE.

Figure 5-42. Bounding calculation predicted (line) and measured (symbols) wet-weight PCB concentrations in largemouth bass, pumpkinseed and brown bullhead collected from Stillwater Pool.

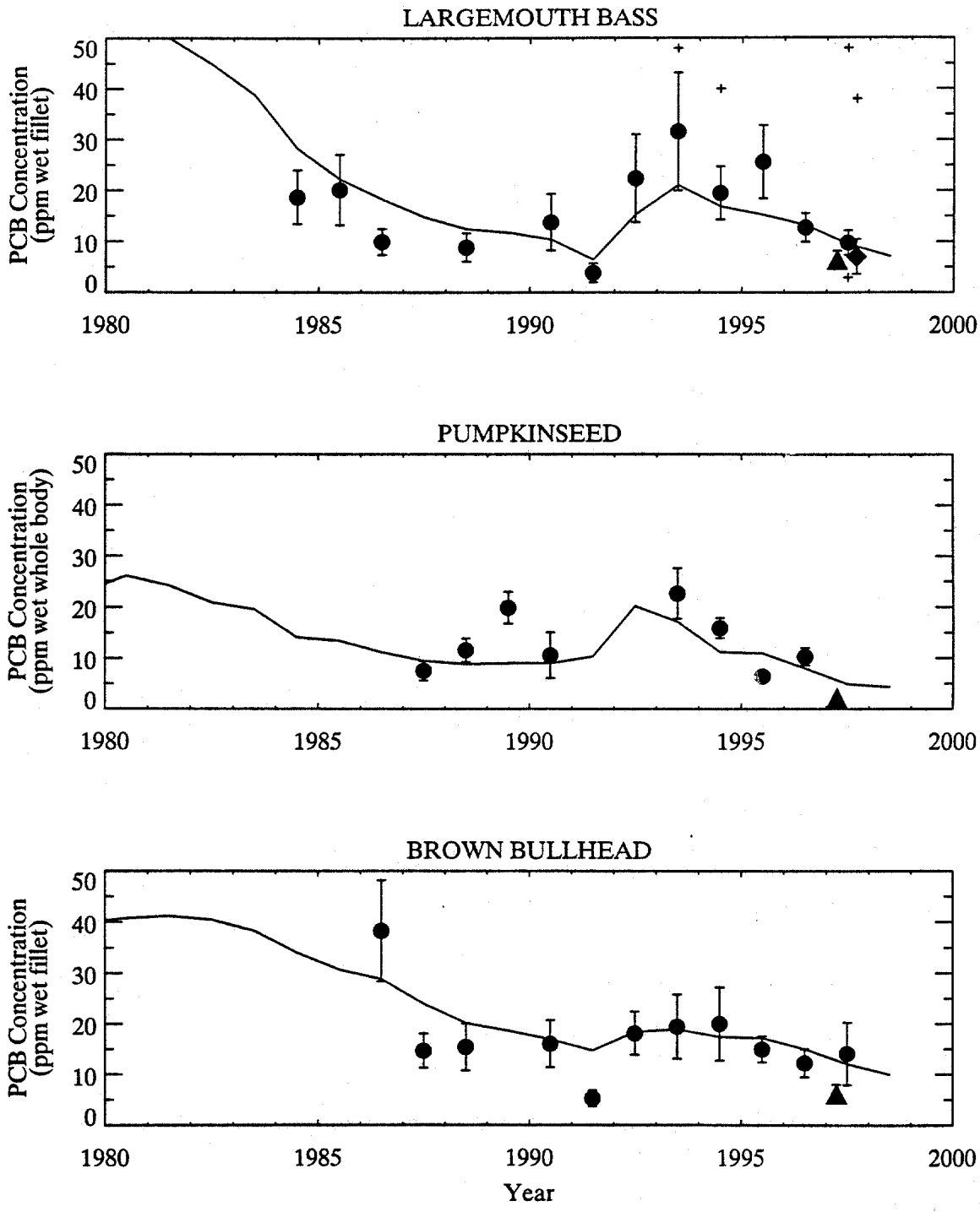

Solid lines indicate model results.
Data are arithmetic means +/- 2 standard errors.
Circles = NYSDEC, Triangles = Exponent, Diamonds = GE.
Crosses indicate values excluded from the annual averages.
Crosses at top of axes represent values off of scale.

Figure 5-43. Bounding calculation predicted (line) and measured (symbols) wet-weight PCB concentrations in largemouth bass, pumpkinseed and brown bullhead collected from Thompson Island Pool.

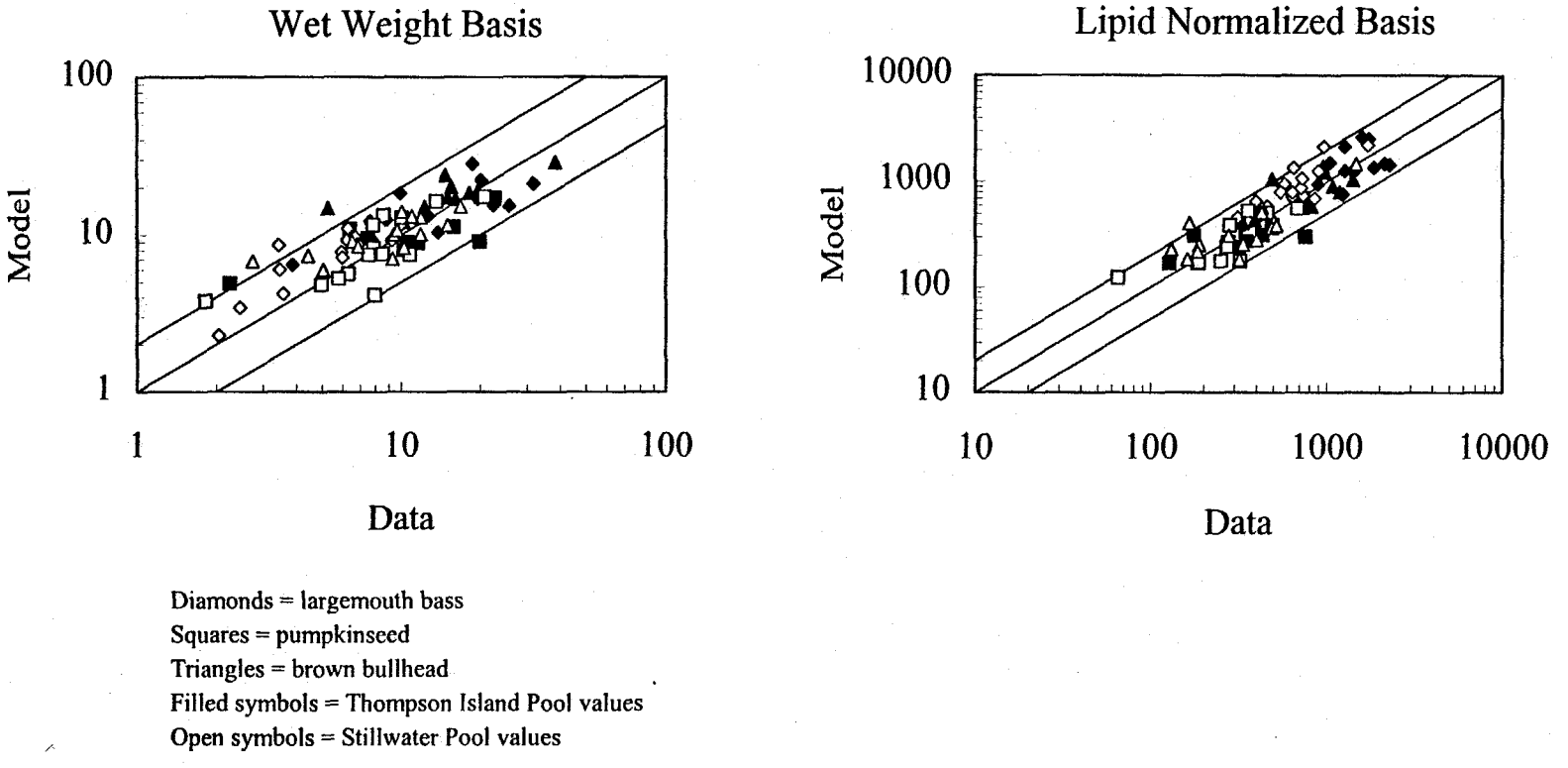

Figure 5-44. Bounding calculation for the calibration of the food web model. Comparison of computed and observed PCB concentrations in fish.

References

Quantitative Environmental Analysis, LLC

REFERENCES

Abromowicz, D.A., M.J. Brennan, H.M. Van Dort and E.L. Gallagher, 1993. "Factors influencing the rate of polychlorinated biphenyl dechlorination in Hudson River sediments." *Environ. Sci. Technol.*, 27:1125-1131.

Adams, S.M., R.B. McLean and J.A. Parrotta, 1982. "Energy partitioning in largemouth bass under conditions of seasonally fluctuating prey availability." *Tran. Amer. Fish. Soc.*, 111:549-558.

Amos, C.L., J. Grant, G.R. Daborn, and K. Black, 1992. "Sea carousel – A benthic, annular flume." *Estuar. Coast. and Shelf Sci.*, 34:557-577.

Ariathuria, R. and R.B. Krone, 1976. "Finite element model for cohesive sediment transport," *J. Hydr. Div., ASCE* 102(3):323-338.

Baker, J.R., J.R. Mihelcic, D.C. Luehrs and J.P. Hickey, 1997. "Evaluation of estimation methods for organic carbon normalized sorption coefficients." *Water Environ. Res.*, 69:136-145.

Barber, L.B. and J.H. Writer, 1998. "Impact of the 1993 flood on the distribution of organic contaminants in bed sediments of the Upper Mississippi River." *Environ. Sci. Tech.*, 32:2077-2083.

Beamish, F.W.H., 1974. "Apparent specific dynamic action of largemouth bass, *micropterus salmoides.*" *J. Fish. Res. Board Can.*, 31:1763-1769.

Beamish, F.W.H., 1970. "Oxygen consumption of largemouth bass, *micropterus salmoides*, in relation to swimming speed and temperature." *Can. J. Zool.*, 48:1221-1228.

Beamish, F.W.H., 1964. "Respiration of fishes with special emphasis on standard oxygen consumption, II. Influence of weight and temperature on respiration of several species." *Can. J. Zoology*, 42:177-188.

Bedard, D.L. and J.F. Quensen, III, 1995. "Microbial reductive dechlorination of polychlorinated biphenyls." In: *Microbial Transformation and Degradation of Toxic Organic Chemicals.* Eds. L.Y. Yound and C. Cerniglia, John Wiley & Sons, Inc.

Blumberg, A.F. and G.L. Mellor, 1983. "Diagnostic and prognostic numerical circulation studies of the South Atlantic Bight." *J. Geophys. Res.*, 88(C8):4579-4592.

Bode, R.W., 1979. DEC Tech. Memorandum (unpublished). A comparison of the 1972/73 and 1977 results, Hudson River.

Bopp, R.F., 1983. "Revised parameters for modeling the transport of PCB components across an air-water interface." *J. Geophys. Res.*, 88:2521-2529.

Borah, D.K., C.V. Alonso and S.N. Prasad, 1982. "Routing graded sediments in streams: formulations," *J. Hydr. Engrg., ASCE* 108(12):1486-1503.

Brett and Groves, 1979. "Physiological energetics," In: *Fish Physiology, Vol. VIII.* Academic Press. pp. 279-352.

Brett, J.R. and D.B. Sutherland, 1965. "Respiratory metabolism of pumpkinseed (*lepomis gibbosus*) in relation to swimmign speed." *J. Fish. Res. Bd. Canada*, 22:405-409.

Brown, J.F., D.L. Bedard, M.J. Brennan, J.C. Carnahan, H. Feng and R.E. Wagner, 1987a. "PCB dechlorination in aquatic sediments." *Science,* 236:709-712.

Brown, J.F., R.E. Wagner, H. Feng, D. Bedard, M. Brennan, J. Carnahan, and R. May, 1987b. "Environmental dechlorination of PCBs." *Environ. Tox. Chem.*, 6:579-593.

Brown, M.P., M.B. Werner, C.R. Carusone, and M. Klein, 1988. "Distribution of PCBs in the Thompson Island Pool of the Hudson River: Final Report of the Hudson River PCB Reclamation Demonstration Project Sediment Survey," NYSDEC, Albany, New York.

Brunner, S., E. Hornung, H. Santi, E. Wolff, O.G. Piringer, J. Altschuh and R. Brüggemann, 1990. "Henry's Law constants for polychlorinated biphenyls: experimental determination and structure-property relationships." *Environ. Sci. Technol.*, 24:1751-1754.

Burban, P.Y., Y.J. Xu, J. McNeil, and W. Lick, 1990. "Settling speeds of flocs in fresh water and seawater." *J. Geophys. Res.*, 95(C10):18,213-18,220.

Burkhard, L., D.E. Armstrong and A.W. Anderson, 1985. "Henry's Law constants for the polychlorinated biphenyls." *Environ. Sci. Technol.*, 19:590-596.

Burns, J.R., 1975, "Seasonal changes in the respiration of pumpkinseed, *lepomis gibbosus*, correlated with temperature, day length, and stage of reproductive development." *Physiol. Zool.*, 142-149.

Butcher, J.B. 1998a. Memorandum from J.B. Butcher of Tetra-Tech, Inc. to Doug Tomchuk of USEPA Region 2 regarding Preliminary Comments on GE Review of USGS Water Column Data dated February 13, 1998.

Butcher, J.B. 1998b. Memorandum from J.B. Butcher of Tetra-Tech, Inc. to Vic Bierman and Scott Heinz of Limno-Tech, Inc. and Ed. Garvey and Al DiBernardo of TAMS Consultants, Inc. regarding Historic Sediment PCB Data Conversions dated June 9, 1998.

Butcher, J.B. 1997a. Memorandum from J.B. Butcher of Tetra-Tech, Inc. to Vic Bierman and Scott Heinz of Limno-Tech, Inc. and Ed. Garvey and Al DiBernardo of TAMS Consultants, Inc. regarding Summary of PCB Data Issues for Modeling dated April 18, 1997.

Butcher, J.B. 1997b. Memorandum from J.B. Butcher of Tetra-Tech, Inc. to Hudson River Team regarding USGS PCB Data dated April 22, 1997.

Butcher, J.B. 1996a. Memorandum from J.B. Butcher of Tetra-Tech, Inc. to Vic Bierman and Scott Heinz of Limno-Tech, Inc. and Ed. Garvey of TAMS Consultants, Inc. regarding Interpretation of 1984 Sediment Data dated December 5, 1996.

Butcher, J.B. 1996b. Memorandum from J.B. Butcher of Tetra-Tech, Inc. to Vic Bierman and Scott Heinz of Limno-Tech, Inc. and Ed. Garvey of TAMS Consultants, Inc. regarding USGS Water Column Data: GE Splits dated December 11, 1996.

Butcher, J.B., T.D. Gauthier and E.A. Garvey, 1997. "Use of historical PCB Aroclor measurements: Hudson River fish data," *Environmental Toxicology and Chemistry*, 16(8):1618-1623.

Cardenas, M., J. Gailani, C.K. Ziegler, and W. Lick, 1995. "Sediment transport in the lower Saginaw River." *Mar. Freshwater Res.*, 46:337-347.

Carlander, K.D., 1997. *Handbook of Freshwater Fishery Biology: Life History Data on Freshwater Fishes of the United States and Canada, Exclusive of the Perciformes: Volume 3.* The Iowa State University Press, Iowa.

Carlander, K.D., 1977. *Handbook of Freshwater Fishery Biology: Life History Data on Freshwater Fishes of the United States and Canada, Exclusive of the Perciformes: Volume 2.* The Iowa State University Press, Iowa.

Carlander, K.D., 1969. *Handbook of Freshwater Fishery Biology: Life History Data on Freshwater Fishes of the United States and Canada, Exclusive of the Perciformes: Volume 1.* The Iowa State University Press, Iowa.

Carline, R.F., 1987. "Simplified method based on bioenergetics modeling to estimate food consumption by largemouth bass and northern pike." *Trans. Amer. Fish. Soc.*, 116:224-231.

Carroll, K.M., M.R. Harkness, A.A. Bracco and R.R. Balcarcel, 1994. "Application of a permeant/polymer diffusional model to the desorption of polychlorinated biphenyls from Hudson River sediments." *Environ. Sci. Technol.*, 28:253-258.

Cheng, N.S., 1997. "Simplified settling velocity formula for sediment particle." ASCE *J. Hydr. Engr.*, 123(2):149-152.

Cirpka, O. P. Reichert, O. Wanner, S.R. Müller and R. Schwarzenbach, 1993. "Gas exchange at river cascades: field experiments and model calculations." *Environ. Sci. Technol.*, 27:2086-2097.

Cohn, T.A., D.L. Caulder, E.J. Gilroy, L.D. Zynjuk, and R.M. Summers, 1992. "The validity of a simple statistical model for estimating fluvial constituent loads: an empirical study involving nutrient loads entering Chesapeake Bay." *Water Resour. Res.*, 28(9):2353-2363.

Collins, N.C. and S.G. Hinch, 1993. "Diel and seasonal variation in foraging activities of pumpkinseeds in an Ontario pond." *Trans. Amer. Fish. Soc.*, 122:357-365.

Connolly, J.P., 1991. "Application of a Food Chain Model to Polychlorinated Biphenyl Contamination of the Lobster and Winter Flounder Food Chains in New Bedford Harbor." *Environ. Sci. & Tech.*, 25:760-770.

Connolly, J.P., T.F. Parkerton, J.D. Quadrini, S.T. Taylor and A.J. Thuman, 1992. "Development and Application of a Model of PCBs in the Green Bay, Lake Michigan Walleye and Brown Trout and Their Food Webs." Report for Large Lakes Research Station, U.S. Environmental Protection Agency, Grosse Ile, Michigan 48138, Cooperative Agreement CR-815396.

Connolly, J.P. and R.P. Winfield, 1984. "WASTOX, a Framework for Modeling Toxic Chemicals in Aquatic Systems." U.S. Environmental Protection Agency, Gulf Breeze, Florida. EPA 600/3-84-077.

Crawford, S., W.S. Coleman and W.F. Porak, 1989. "Time of annulus formation in otoliths of Florida largemouth bass." *N. Amer. J. Fish. Man.*, 9:231-233.

Darby, S.E. and C.R. Thorne, 1996. "Predicting stage-discharge curves in channels with bank vegetation." *ASCE J. Hydr. Engr.*, 122(10):583-586.

de Boer, J., F. van der Valk, M.A.T. Kerhoff and P. Hagel, 1994. "8-year study on the elimination of PCBs and other organochlorine compounds from eel (*Anguilla anguilla*) under natural conditions," *Environ. Sci. Technol.* 28:2242-2248.

DiToro, D.M. and L.M. Horzempa, 1982. "Reversible and resistant components of PCB adsorption-desorption: isotherms." *Environ. Sci. Technol.*, 16:594-602.

Domermuth, R.B. and R.J. Reed, 1980. "Food of juvenile american shad, *alosa sapidissima,* juvenile blueback herring, *alosa aestivalis*, and pumpkinseed, *lepomis gibbosus*, in the Connecticut River below Holyoke Dam, Massachusetts." *Estuaries*, 3:65-68.

Dunnivant, F..M. and A.W. Elzerman, 1988. "Aqueous solubility and Henry's Law constant data for PCB congeners for evaluation of quantitative structure-property relationships (QSPRs)." *Chemosphere*, 17:525-541.

Erickson, M., 1998. "Preliminary development of sediment PCB initial conditions in 1977 for the historical HUDTOX simulation period." Technical memorandum. Limno Tech, Inc., Ann Arbor, MI.

Erickson, R.J. and J.M. McKim, 1990. "A model for exchange of organic chemicals at fish gills: flow and diffusion limitations." *Aquatic Toxicology*, 18:175-198.

Evans, D.O., 1984. "Temperature independence of the annual cycle of standard metabolism in the pumpkinseed." *Trans. Amer. Fish. Soc.*, 113:494-512.

Evans, H.E., 1988. "The binding of three PCB congeners to dissolved organic carbon in freshwaters." *Chemosphere*. 17:2325-2338.

Exponent, 1998a. "Food web structure of submerged aquatic vegetation beds and unvegetated habitats of the Upper Hudson River." Prepared for General Electric Company, Albany, New York.

Exponent, 1998b. "Data Report - Macroinvertebrate Communities and Diets of Selected Fish Species in the Upper Hudson River, Volume I." Prepared for General Electric Company, Albany, New York.

Exponent, 1998c. "Draft – Macroinvertebrate Communities and Diets of Selected Fish Species in the Upper Hudson River, Spring 1998: Data Report." Prepared for General Electric Company, Albany, New York.

Exponent, 1998d. "Data Documentation and Interpretation Report – Submerged Aquatic Vegetation and Fish Community Analysis." Prepared for General Electric Company, Albany, New York.

Federal Emergency Management Agency, 1995. "Flood Insurance Study, Saratoga County, New York (All Jurisdictions)." August 16, 1995.

Feldman, R.S., 1992. "PCB accumulation in Hudson River pumpkinseed sunfish and bullhead: influences of invertebrate prey." Ph.D. dissertation, Dept. of Biological Sciences, State University of New York at Binghamton.

Fish, K.M., 1996. "Influence of Aroclor 1242 concentration on polychlorinated biphenyl transformation in Hudson River test tube microcosms." *Appl. Environ. Microbiol.*, 62:3014-3016.

Flood, R.D., 1993. "Analysis of Side Scan Sonar, Bathymetric, Subbottom, and Sediment Data from the Upper Hudson River Between Bakers Falls and Lock 5." Hudson River PCB Reassessment RI/FS. EPA Work Assignment 013-2N84. EPA Contract No. 68-59-2001. SUNY Stony Brook.

Ford, J.B., 1962. "The vertical distribution of larval chironomidae (dipt.) in the mud of a stream." *Hydrobiologia*, 19:262-272.

Gailani, J., C.K. Ziegler, and W. Lick, 1991. "Transport of suspended solids in the Lower Fox River." *J. Great Lakes Res.*, 17(4):479-494.

Gailani, J., W. Lick, C.K. Ziegler, and D. Endicott, 1996. "Development and calibration of a fine-grained sediment transport model for the Buffalo River." *J. Great Lakes Res.*, 22:765-778.

Garcia, M. and G. Parker, 1991. "Entrainment of bed sediment into suspension," *J. Hydr. Engrg., ASCE* 117(4):414-435.

General Electric Company, 1998. "Monthly Reports to NYSDEC Under Order on Consent (Index #C5-0001-85-06) Documenting PCB DNAPL Collected from the Hudson Falls Plant Site."

General Electric Company, 1997. Monthly Reports to NYSDEC Under Order on Consent (Index #C5-0001-85-06) Documenting PCB DNAPL Collected from the Hudson Falls Plant Site."

Gerould, S., P. Landrum and J.P. Giesy, 1983. "Anthracene bioconcentration and biotranformation in chironomids: effects of temperature and concentration." *Environ. Pollut.*, 30:175-188.

Gibaldi, M. and D. Perrier, 1982. "Pharmacokinetics" Second edition, Marcel Dekker, Inc., New York.

Gobas, F.A.P.C., D.C.G. Muir and D. Mackay, 1989. "Dynamics of dietary bioaccumulation and fecal elimination of hydrophobic organic chemicals in fish." *Chemosphere*, 17:943-962.

Gooch, J.A. and M.K. Hamdy, 1982. "Depuration and biological half-life of ^{14}C-PCB in aquatic organisms," *Environ. Contam. Toxicol.*, 28:305-312.

Graham, D.I., P.W. James, T.E.R. Jones, J.M. Davies, and E.A. Delo, 1992. "Measurement and prediction of surface shear stress in annular flume." *ASEC J. Hydr. Engr.*, 118(9):1270-1286.

Guiney, P.D. and R.E. Peterson, 1980. "Distribution and elimination of a polychlorinated biphenyl after acute dietary exposure in yellow perch and rainbow trout," *Arch. Environ. Contam. Toxicol.*, 9:667-674.

Guiney, P.D., R.E. Peterson, M.J. Melancon and J.J. Lech, 1977. "The distribution and elimination of 2,5,2',5'-[^{14}C]Tetrachloro-biphenyl in rainbow trout (*Salmo gairdneri*)," *Toxicology and Applied Pharmacology*, 39:329-338.

Hambright, K.D., 1991. "Experimental analysis of prey selection by largemouth bass: role of predator mouth width and prey body depth." *Trans. Amer. Fish. Soc.*, 120:500-508.

Hamilton, J.G. and P.M. Powles, 1983. "Fish predation and other distinctive features in the diet of Nogies Creek, Ontario, largemouth bass, *micropterus salmoides.*" *Canadian Field-Naturalist*, 97:47-56.

Hawker, D.W. and D.W. Connell, 1988. "Octanol-water partition coefficients of polychlorinated biphenyls congeners." *Environ. Sci Tech.*, 22:382-385.

Hawley, N., 1991. "Preliminary observations of sediment erosion from a bottom resting flume." *J. Great Lakes Res.*, 17(3):361-367.

Hayduk, W. and H. Laudie, 1974. "Prediction of diffusion coefficients for non-electrolytes in dilute aqueous solutions." *AIChE, J.* 20:611-615.

Hayter, E.J. and A.J. Mehta, 1986. "Modelling cohesive sediment transport in estuarial waters," *Appl. Math. Modelling* 10:294-303.

Herbreteau, F, L. Coiffard, A. Derrien, and Y. Deroeckholtzhauer, 1994. "Determination of the fatty acid composition of the lipids of the flesh of *Crepidula fornicata* L – Laboratory Note." *Revue Francaise Des Corps Gras* 41:119-121.

Hetling, L., E. Horn and J. Tofflemire, 1978. "Summary of Hudson River PCB Study Results," Technical Paper #51. NYS Department of Environmental Conservation.

Hillary, B.R., I. Basu, C.W. Sweet and R.A. Hites, 1997. "Temporal and Spatial Trends in a Long-Term Study of Gas-Phase PCB Concentrations Near the Great Lakes." *Environ. Sci. Technol.*, 31:1811-1816.

Hoff, R.M., D.C.G. Muir, and N.P. Grift, 1992. "Annual Cycle of Polychlorinated Biphenyls and Organohalogen Peticides in Air in Southern Ontario. 1. Air Concentration Data." *Environ. Sci. Technol.*, 26:266-275.

HydroQual, Inc., 1998. Memoradum from J.R. Rhea to M. Schweiger and J. Haggard of General Electric Company, Corporate Environmental Programs regarding Evaluation of Analytical Bias in the USGS Water Column Database [Phase I] dated January 29, 1998.

HydroQual, 1997a. "Analysis of Sediment Loading to the Upper Hudson River during the April 1994 high flow event." HydroQual report.

HydroQual, 1997b. "Hudson River PCB DNAPL Transport Study." Prepared by HydroQual, Inc. for the General Electric Company, Corporate Environmental Programs, Albany, New York.

HydroQual, Inc., 1995a. "The Erosion Properties of Cohesive Sediments in the Upper Hudson River." HydroQual report.

HydroQual, Inc., 1995b. "Addendum to Green Bay Final Report, Food Chain Model Projections." Prepared for the USEPA, Gross Ile, Michigan.

Jain, S.C. and I. Park, 1989. "Guide for estimating riverbed degradation," *J. Hydr. Engrg., ASCE* 115(3):356-366.

Jearld, Jr., A., 1983. "Age determination," In: *Fisheries Techniques*, Eds. L.A. Nielson and D.L. Johnson. American Fisheries Society, Bethesda, Maryland, pp. 301-324.

Jepsen, R., J. Roberts, and W. Lick, 1997. "Effects of Bulk Density on Sediment Erosion Rates," *Water, Air, Soil Poll.*, 99:21-31.

Kan, A.T., G. Fu, M.A. Hunter and M.B. Tomson, 1997. "Irreversible adsorption of naphthalene and tetrachlorobiphenyl to Lula and surrogate sediments." *Environ. Sci. Technol.*, 2176-2185.

Karara, A.H. and W.L. Hayton, 1984. "Pharmacokinetic model for the uptake and disposition of di-2-ethylhexyl phthalate in sheepshead minnow (*Cyprinodon variegatus)*," *Aquatic Toxicology*, 5:181-195.

Karickhoff, S.W., 1984. "Organic pollutant sorption in aquatic system." *J. Hydr. Eng.* 110:707-735.

Karickhoff, S.W., 1981. "Semi-empirical estimation of sorption of hydrophobic pollutants on natural sediments and soils." *Chemosphere*, 10:833-846.

Karim, M.F. and F.M. Holly, 1986. "Armoring and sorting simulation in Alluvial Rivers," *J. Hydr. Engrg., ASCE* 112(8):705-715.

Karim, M.F. and J.F. Kennedy, 1981. "Computer-Based Predictors for Sediment Discharge and Friction Factor of Alluvial Streams." IIHR Report No. 242, Univ. of Iowa, Iowa City, Iowa.

Keast, A., 1985. "The piscivore feeding guild of fishes in small freshwater ecosystems." *Environmental Biology of Fishes*, 12:119-129.

Keast, A. and M.G. Fox, 1990. "Fish community structure, spatial distribution and feeding ecology in a beaver pond." *Environmental Biology of Fishes*, 27:201-214.

Klump, J.V., J.R. Krezoski, M.E. Smith and J.L. Kaster, 1987. "Dual tracer studies of the assimilation of an organic contaminant from sediments by deposit feeding oligochaetes." *Can. J. Fish. and Aquatic Sci.*, 44:1574-1583.

Konemann, H. and K. van Leeuwen, 1980. "Toxicokinetics in fish: accumulation and elimination of six chlorobenzenes by guppies," *Chemosphere*, 9:3-19.

Krezoski, J.R., S.C. Mozley and J.A. Robbins, 1978, "Influence of benthic macroinvertebrates on mixing of profundal sediments in southeastern Lake Hurton." *Limnol. Oceanogr.*, 23:1011-1016.

Krone, R.B., 1962. "Flume Studies of the Transport of Sediment in Estuarial Processes." Final Report, Hydraulic Engineering Laboratory and Sanitary Engineering Research Laboratory, Univ. of Calif., Berkeley, Calif.

Landrum, P.F., 1989. "Bioavailability and toxicokinetics of polycyclic aromatic hydrocarbons sorbed to sediments for the amphipod *pontopereia hoyi*," *Environ. Sci. Technol.*, 23:588-595.

Landrum, P.F., S.R. Nihart B.J. Eadie and L.R. Herche, 1987. "Reduction in bioavailability of organic contaminants to the amphipod *Pontoporeia hoyi* by dissolved organic matter of sediment interstitial waters." *Environ. Tox. Chem.*, 6:11-20.

Landrum, P.F., M.D. Reinhold, S.R. Nihart and B.J. Eadie, 1985. "Predicting the bioavailability of organic xenobiotics to *Pontoporeia hoyi* in the presence of humic and fulvic materials and natural dissolved organic matter." *Environ. Tox. Chem.*, 4:459-467.

Law Environmental, Inc., 1991. "Upper Hudson River Study Fish Age and Growth Data: Report for Fall 1990 Sampling." Project No. 41-0613 submitted to: John Mancini Consultants, Inc.

Lerman, A., 1978. "Chemical exchange across sediment-water interface." *Ann. Rev. Earth Planet*, 6:281-303.

Leversee, G.J., J.P. Giesy, P.F. Landrum, S. Gerould, J.W. Bowling, T.E. Fannin, J.D. Haddock and S.M. Bartell, 1982. "Kinetics and biotransformation of benzo(a)pyrene in *Chironomus riparius*." *Arch. Environ. Contam. Toxicol.*, 11:25-31.

Lewis, W.M., R. Heidinger, W. Kirk, W. Chapman and D. Johnson, 1974, "Food intake of the largemouth bass." *Trans. Amer. Fish. Soc.*, 2:277-280.

Lick, W., J. Lick and C.K. Ziegler, 1994. "The resuspension and transport of fine-grained sediments in Lake Erie," *J. Great Lakes Res.*, 20(4):599-612.

Lieb, A.J., D.D. Bills and R.O. Sinnhuber, 1974. "Accumulation of dietary polychlorinated biphenyls (Aroclor 1254) by rainbow trout (*Salmo gairdneri*)," *Agr. Food Chem.* 22:638-642.

Limno-Tech, Inc., 1998. Preliminary tributary flow estimates for the Upper Hudson River between Fort Edward and Waterford for the USEPA mass balance modeling. Technical Memorandum from Mike Erickson, to Doug Tomchuk.

Limno-Tech, Inc., 1997. Details of LTI's sediment dry bulk density estimation for HUDTOX. Technical memorandum from Mike Erickson to Kirk Ziegler.

Limno-Tech, Inc., Menzie Cura and Associates, Inc. and the Cadmus Group, Inc., 1996. "Phase 2 Report – Further Site Characterization and Analysis. Volume 2B – Preliminary Model Calibration Report, Hudson River PCBs reassessment RI/FS." Prepared for the USEPA, Region II.

MacIntyre, S., W. Lick, and C.H. Tsai, 1990. "Variability of entrainment of cohesive sediments in freshwater." *Biogeochemistry*, 9:187-209.

Mackay, D., W.Y. Shiu and K.C. Ma, 1992. *Illustrated handbook of physical-chemical properties and environmental fate for organic chemicals: Volume 1, monoaromatic hydrocarbons, chlorobenzenes and PCBs.* Lewis Publishers, Chelsea, MI. 697 p.

McCall, P.L. and M.J.S. Tevesz, 1982. "The effects of benthos on physical properties of freshwater sediments." In: *Animal-Sediment Relations: The Biogenic Alterations of Sediments.* Eds. P.L. McCall and M.J.S. Tevesz. Plenum Press, New York.

McGroddy, S.E., J.W. Farrington and P.M. Gschwend, 1996. "Comparison of the *in Situ* and desorption sediment-water partitioning of polycyclic aromatic hydrocarbons and polychlorinated biphenyls." *Environ. Sci. Technol.*, 30:172-177.

McLachlan, M., D. Mackay and P.H. Jones, 1990. "A conceptual model of organic chemical volatilization at waterfalls." *Environ. Sci. Technol.*, 24:252-257.

McNulty, A.K., 1997. "In-situ anaerobic dechlorination of polychlorinated biphenyls in Hudson River sediments." Master of Science Thesis submitted to Rensselaer Polytechnic Institute, Troy, New York, August, 1997.

Milbrink, G., 1973. "On the Vertical Distribution of Oligochaetes in Lakes Sediments." Institute of Freshwater Research, Fishery Board of Sweden, Report No. 53.

Muir, D.C.G, N.P. Grift, A.P. Blouw and W.L. Lockhart, 1980. "Environmental dynamics of phosphate esters. I. Uptake and bioaccumulation of triphenyl phosphate by rainbow trout," *Chemosphere*, 9:525-532.

Murphy, T.J., M.D. Mullin and J.A. Meyer, 1987. "Equilibration of polychlorinated biphenyls and toxaphene with air and water." *Environ. Sci. Technol.*, 21:155-162.

Nalepa, TF. J.F. Cavaletto, M. Ford, W.M. Gordon and M. Wimmer, 1993. "Seasonal and annual variation in weight and biochemical content of the zebra mussel, *dreissena-polymorpha*, in Lake St.-Clair." *J. Gr. Lakes Res.* 19:4541-552

Novak, M.A., A.A. Reilly and S.J. Jackling, 1988. "Long-term monitoring of polychlorinated biphenyls in the Hudson River (New York) using caddisfly and other macroinertebrates." *Arch. Environ. Contam. Toxicol.*, 17:699-711.

NYSDEC, 1998. "Database of historic and current fish PCB monitoring data collected in the Upper Hudson River." Received from Dennis Keane.

O'Brien & Gere Engineers, Inc. 1998. "1996-1997 Thompson Island Pool Studies." Prepared for General Electric Company, Corporate Environmental Programs, Albany, New York.

O'Brien & Gere Engineers, Inc. 1996. "Hudson Falls, Operable Unit 3, Interim Remedial Measures Report." O'Brien & Gere Engineers, Inc. Prepared for the General Electric Company Corporate Environmental Programs, Albany, N.Y.

O'Brien & Gere Engineers, Inc. 1994. "Bakers Falls Operable Unit 3, Remedial Investigation Report." Syracuse, N.Y. O'Brien & Gere Engineers, Inc. Prepared for the General Electric Company Corporate Environmental Programs, Albany, N.Y.

O'Brien & Gere Engineers, Inc. 1993a. "1991 Sediment Sampling and Analysis Program." Prepared for General Electric Company Corporate Environmental Programs, Albany, New York.

O'Brien & Gere Engineers, Inc., 1993b. "Hudson River Project, Sampling and Analysis Program, 1991 Hydrographic Survey of the Upper Hudson River." Prepared for General Electric Company Corporate Environmental Programs, Albany, New York.

O'Brien & Gere Engineers, Inc., 1978. "PCB Analysis: Final Report: Hudson River Samples." Prepared for the New York State Department of Environmental Conservation. Syracuse, New York.

O'Connor, D.J., 1983. "The effect of wind on the gas-liquid transfer coefficients." *J. Environ. Eng. Div. ASCE*, 109:731-752.

O'Connor, D.J., 1984. "The significance of gas exchange in water quality assessment and planning." In: *Gas Transfer at Water Surfaces*, Eds. W. Brutsaert, and G.H. Jirka, D. Reidel Publishing Company, pp. 559-576.

O'Connor, D.J. and W.E. Dobbins, 1958. "Mechanisms of reaeration in natural streams." *Trans. Am. Soc. Civ. Eng.*, 123:641-684.

O'Connor, J.M. and J.C. Pizza, 1987. "Dynamics of polychlorinated biphenyls in striped bass from the Hudson River. III. Tissue disposition and routes for elimination," *Estuaries*, 10:68-77.

O'Flaherty, E.J., 1981. "Toxicants and Drugs: Kinetics and Dynamics. John Wiley and Sons, New York.

Oliver, B.G., 1984. "Uptake of chlorinated organics from anthropogenically contaminated sediments by oligochaete worms." *Can. J. Fish. Aquat. Sci.*, 41:878-883.

Olsen, C.R., H.J. Simpson, T.H. Peng, R.F. Bopp and R.M. Trier, 1981. "Sediment mixing and accumulation rate effects on radionuclide depth profiles in Hudson estuary sediments." *J. Geophys. Res.*, 86:11020.

Osenberg, C.W., G.G. Mittelbach, P.C. Wainwright, 1992. "Two-stage life histories in fish: the interaction between juvenile competition and adult performance." *Ecology*, 73:255-267.

Paola, C., G. Parker, R. Seal, S.K. Sinha, J.B. Southard and P.R. Wilcock, 1992. "Downstream fining by selective deposition in a laboratory flume," *Science*, 258:1757-1760.

Paola, C. and R. Seal, 1995. "Grain Size Patchiness as a Cause of Selective Deposition and Downstream Fining," *Water Resour. Res.*, 31(5):1395-1407.

Parchure, T.M. and A.J. Mehta, 1985. "Erosion of soft cohesive sediment deposits." *ASCE J. Hydr. Engr.*, 111(10):1308-1326.

Parkerton, T.F., 1993. "Estimating toxicokinetic parameters for modeling the bioaccumulation of non-ionic organic chemicals in aquatic organisms." Ph.D. dissertation thesis, Rutgers University.

Partheniades, E., 1992. "Estuarine sediment dynamics and shoaling processes." In: *Handbook of Coastal and Ocean Engineering, Volume 3.* Ed. J. Herbick, pp.985-1071.

Partheniades, E., 1965. "Erosion and deposition of cohesive sediments," *J. Hydr. Div., ASCE,* 91(1):105-139.

Pennak, R.W., 1978. *Fresh-water Invertebrates of the United States.* John Wiley & Sons, Inc., New York.

Peters, R.H., 1989. *The Ecological Implications of Body Size*, 4th Edition. Cambridge University Press, New York.

Phillips, P.J. and Hanchar, D.W., 1996. "Water-Quality Assessment of the Hudson River Basin in New York and Adjacent States – Analysis of Available Nutrient, Pesticide, Volatile Organic Compound, and Suspended-Sediment Data, 1970-90," U.S. Geological Survey, Water-Resources Investigations Report 96-4065.

Pignatello, J.J. and B. Xing, 1996. "Mechanisms of slow sorption of organic chemicals to natural particles." *Environ. Sci. Technol.*, 30:1-11.

Quantitative Environmental Analysis, LLC, 1999. Memorandum from J. Rhea to Angus Macbeth, "Phase 2 Evaluation of Analytical Bias in the USGS Water Column Database" dated January 8, 1999.

Quantitative Environmental Analysis, LLC, 1998a. "Sediment Bed Mapping study of the Upper Hudson River from Northumberland Dam to Troy Dam." Final report submitted to General Electric Company, New York.

Quantitative Environmental Analysis, LLC, 1998b. "Thompson Island Pool Sediment PCB Sources." Final report. Prepared for General Electric Company.

Quantitative Environmental Analysis, LLC, 1998c. "Thompson Island Pool Sediment Coring Program - Field Sampling Plan." Prepared for General Electric Company.

Rahuel, J.L., F.M. Holly, J.P. Chollet, P.J. Belleudy and G. Yang, 1989. "Modeling of riverbed evolution for bedload sediment mixtures." *J. Hydr. Engrg.*, ASCE, 115(11):1521-1542.

Reinfelder, J.R. and N.S. Fisher, 1991. "The assimilation of elements ingested by marine copepad." *Science*, 251:794-796.

Rice, J.A., 1981. "Derivation and application of a bioenergetics model for largemouth bass (*micropterus salmoides*)" Master thesis, University of Wisconsin – Madison.

Rice, J.A. and P.A. Cochran, 1984. "Independent evaluation of a bioenergetics model for largemouth bass." *Ecology*, 65:732-739.

Ringler, N.H. and J.H. Johnson, 1982. "Diet composition and diel feeding periodicity of some fishes in the St. Lawrence River." *New York Fish and Game Journal*, 29:65-74.

Roberts, J., R. Jepsen, D. Gotthard, and W. Lick, 1998. "Effects of Particle Size and Bulk Density on Erosion of Quartz Particles," *ASCE J. Hydr. Engr.*, 124(12):1261-1267.

Saunders, R.L., 1962. "The irrigation of the gills in fishes, II. Efficiency of oxygen uptake in relation to respiratory flow activity and concentrations of oxygen and carbon dioxide." *Can. J. Zoology*, 40:817-862.

Schrap, S.M. and A. Opperhuizen, 1988. "Elimination kinetics of two unmetabolized polychlorinated biphenyls in *Poecilla reticulata* after dietary exposure," *Bull. Environ. Contam. Toxicol.*, 40:381-388.

Schweiger, M.B., J.G. Haggard and J.P. Connolly, 1997. "Comments of the General Electric Company: Phase 2 Report – Review Copy: Further Site Characterization and Analysis Volume 2C Data Evaluation and Interpretation Report." General Electric Company, Albany, New York.

Shen, H.W. and J.Y. Lu, 1983. "Development and prediction of bed armoring," *J. Hydr. Engrg., ASCE*, 109(4):611-629.

Sijm, D.T.H.M., W. Seinen and A. Opperhuizen, 1992. "Life-cycle biomagnification study in fish," *Environ. Sci. Technol.*, 26:2162-2174.

Simpson, K.W., 1976. "A Water Quality Evaluation of the Hudson River, Based on the Collection and Analysis of Macroinvertebrate Communities." Presented at Fourth Symposium on Hudson River Ecology, New York.

Smith, C.L., 1985. *The Inland Fishes of New York State.* The New York State Department of Environmental Conservation, New York.

Soil Conservation Service, 1974. "Erosion and Sediment Inventory, New York," U.S. Department of Agriculture.

Sokol, R.C., C.M. Bethoney and G-Y. Rhee, 1998a. "Reductive dechlorination of preexisting sediment polychlorinated biphenyls with long-term laboratory incubation." *Environ. Toxicol. Chem.*, 17:982-987.

Sokol, R.C., C.M. Bethoney and G-Y. Rhee, 1998b. "Effect of Aroclor 1248 concentration on the rate and extent of polychlorinated biphenyl dechlorination." *Environ. Toxicol. Chem.*, 17:1922-1926.

Spacie, A. and J.L. Hamelink, 1982. "Alternative models for describing the bioconcentration of organics in fish," *Environmental Toxicology and Chemistry*, 1:309-320.

Steinberg, L.J., K.H. Reckhow and R.L. Wolpert, 1996. "Bayesian model for fate and transport of polychlorinated biphenyl in Upper Hudson River." *J. Environ. Eng.*, 122:341-349.

Swindoll, C.M. and F.M. Applehans, 1987. "Factors influencing the accumulation of sediment-sorbed hexachlorobiphenyl by midge larvae" *Bull. Environ. Contam. Toxicol.*, 39:1055-1062.

Task Committee of ASCE on Fine Sediment Transport Processes, 1989. "Cohesive sediment transport Part II: Application." *J. Hydr. Engr., ASCE* 115(8):1094-1112.

Tateya, S., S. Tanabe and R. Tatsulawa, 1988. "PCBs on the Globe: Possible trend of future levels in the open ocean environment." In: *Toxic Contamination in Large Lakes.* Ed. N.W. Schmidtke, Vol. III, pp 237-281.

ten Hulscher, Th.E.M., L.E. van der Velde and W.A. Bruggeman, 1992. "Temperature dependence of Henry's Law constants for selected chlorobenzenes, polychlorinated biphenyls and polycyclic aromatic hydrocarbons." *Environ. Tox. Chem.*, 11:1595-1603.

Thoms, S.R., G. Matisoff, P.L. McCall and X. Wang, 1995. "Models for alteration of sediments by benthic organisms." Water Environmental Research Foundation Project 92-NPS-2, Alexandria, VA.

Thorp, J.H., L.D. Goldsmith, J.A. Polgreen and L.M. Mayer, 1989. "Foraging patterns of nesting and nonnesting sunfish (*centrarchidae: lepomis-auritus and l. gibbosus).*" *Can. J. Fish. Aquat. Sci.*, 46:1342-1346.

Tofflemire, T.J. and S.O. Quinn, 1979. "PCB in the Upper Hudson River: Mapping and Sediment Relationships." New York State Department of Environmental Conservation Technical Report No. 56.

Tofflemire, T.J., S.O. Quinn, and P.R. Hague, 1979. "PCB in the Hudson River: Mapping, Sediment Sampling, and Data Analysis." New York State Department of Environmental Conservation Technical Report 57.

Tracey, G.A. and D.J. Hansen, 1996. "Use of biota-sediment accumulation factors to assess similarity of nonionic organic chemical exposure to benthically-coupled organisms of differing trophic mode." *Archives of Environmental Contamination and Toxicology* 30 (4): 467-475.

Tsai, C.H. and W. Lick, 1987. "Resuspension of sediments from Long Island Sound." *Wat. Sci. Tech.*, 21(6/7):155-184.

U.S. Army Corps of Engineers, 1990. "Status and new capabilities of computer program HEC-6: Scour and deposition in rivers and reservoirs," Technical Paper No. 129, Hydrologic Engineering Center.

U.S. Army Corps of Engineers, 1976. "HEC-6 scour and deposition in rivers and reservoirs," Hydrologic Engineering Center.

U.S. Environmental Protection Agency, 1998. Database for the Hudson River PCBs Reassessment RI/FS. Release 4.1.

U.S. Environmental Protection Agency, 1997. "Phase 2 Report – Review Copy: Further Site Characterization and Analysis - Volume 2C Data Evaluation and Interpretation Report." Hudson River PCBs Reassessment RI/FS. USEPA, Region 2. New York, New York.

U.S. Environmental Protection Agency, 1996. "Phase 2 Report – Review copy: Further Site Characterization and Analysis – Volume 2B Preliminary Model Calibration Report." Hudson River PCBs Reassessment RI/FS. Volume 2B, Book 1 of 2. USEPA, Region 2, New York, New York.

U.S. Environmental Protection Agency, 1995. "Phase 2 Report - Review Copy: Further Site Characterization and Analysis - Database Report." Hudson River PCBs Reassessment RI/FS. USEPA, Region 2, New York, New York.

U.S. Environmental Protection Agency, 1992. "Final Phase 2 Work Plan and Sampling Plan. Hudson River PCB Reassessment RI/FS." Prepared by Tams Consultants, Inc. and Gradient Corporation for Region II. New York, New York.

U.S. Environmental Protection Agency, 1984. "Feasibility Study, Hudson River PCB Site, New York." Volume 1. Prepared by NUS Corporation.

Van De Guchte, C., G. Niebeek and J. Botterweg, 1988. "Chironomid's uptake of chlorobenzenes from contaminated sediments," presented in Hamburg, Federal Republic of Germany.

Van Niekerk, A., K.R. Vogel, R.L. Slingerland, and J.S. Bridge, 1992. "Routing of heterogeneous sediments over movable bed: model development." *ASCE J. Hydr. Engr.*, 118(2):246-279.

van Rijn, L.C., 1984a. "Sediment transport, Part I: Bed load transport," *J. Hydr. Engrg., ASCE* 110(10):1431-1456.

van Rijn, L.C., 1984b. "Sediment transport, Part II: Suspended load transport," *J. Hydr. Engrg., ASCE* 110(11):1612-1638.

van Rijn, L.C., 1984c. "Sediment transport, Part III: Bed forms and alluvial roughness," *J. Hydr. Engrg, ASCE* 110(12):1732-1754.

Van Veld, P.A., 1990. "Absorption and metabolism of dietary xenobiotics by the intenstines of fish." *Rev. Aquat. Sci.*, 2:185-203.

Walling, D.E. and P.W. Moorehead, 1989. "The particle size characteristics of fluvial suspended sediments: an overview," *Hydrobiologia*, 176/177:125-149.

Werner, R.G., 1980. *Freshwater Fishes of New York State*. Syracuse University Press, New York.

Wilcock, R.J., T.J. Smith, R.D. Pridmore, S.F. Thrush, V.J. Cummings and J.E. Hewitt, 1993. "Bioaccumulation and elimination of chlordane by selected intertidal benthic fauna." *Environmental Toxicology and Chemistry*, 12:733-742.

Wootton, R.J., 1990. *Ecology of Teleost Fishes*. Chapman and Hall, London.

Yamato, Y., M. Kiyonaga, T. Watanabe, 1983. "Comparative bioaccumulation and elimination of HCH isomers in short-necked clam (*Venerupis japonica*) and guppy (*Poecilia reticulata*)," *Bull. Environ. Contam. Toxicol.*, 31:352-359.

Van Rijn, L.C., M.W.C. Nieuwjaar, T. van der Kaay, E. Nap and A. van Kampen, 1993. "Transport of fine sands by currents and waves," *ASCE J. Water. Port, Coast., Ocean Engr.*, 119(2):123-143.

Ziegler, C.K. and W. Lick, 1986. "A numerical model of the resuspension, deposition, and transport of fine-grained sediments in shallow water," UCSB Report ME-86-3.

Ziegler, C.K. and B.S. Nisbet, 1995. "Long-term simulation of fine-grained sediment transport in large reservoir." *ASCE J. Hydr. Engr.*, 121(11):773-781.

Ziegler, C.K. and B.S. Nisbet, 1994. "Fine-grained sediment transport in Pawtuxet River, Rhode Island." *ASCE J. Hydr. Engr.*, 120(5):561-576.

Zimmie, T.F., 1985. "Assessment of Erodibility of Sediments in the Thompson Island Pool of the Hudson River," Final Report, NYSDEC, RPI Project No. 5-25360.

Appendices

Quantitative Environmental Analysis, LLC.

Appendix A

Modeling Suspended Load Transport of Non-Cohesive Sediments in the Upper Hudson River

Appendix A is a report prepared by
HydroQual, Inc., Mahwah, NJ
for
General Electric Company, Albany, NY
June 1997

CONTENTS

FIGURES

SECTION 1

INTRODUCTION

The sediment bed of the Upper Hudson River can generally be separated into two distinct bed types: cohesive and non-cohesive. Cohesive bed deposits are primarily composed of fine-grained sediments, e.g., clay, silt and fine sand, with the median particle diameter (D_{50}) typically being less than 200 μm. The non-cohesive bed is coarser (D_{50} ranging from $\sim$200 μm to over 4,000 μm) and this bed type generally contains significant fractions of non-suspendable sediment, i.e., coarse sand and gravel. In addition, the organic carbon content of cohesive sediment deposits is usually greater than that of the non-cohesive bed.

Analysis of side-scan sonar data collected in the Upper Hudson River shows that the non-cohesive bed comprises at least 50% of the total bed area in each of the three reaches between Fort Edward and Northumberland Dam. Deposition and resuspension from the non-cohesive bed should thus be included in a sediment transport model of the Upper Hudson River because this bed type accounts for a majority of the surface area in the river. A previous study has shown the importance and viability of simulating both cohesive and non-cohesive transport processes in a riverine system (Ziegler and Nisbet, 1994).

The non-cohesive suspended load transport model developed by Ziegler and Nisbet (1994) and applied to the Pawtuxet River, which is located in Rhode Island, has been modified and enhanced for application to the Upper Hudson River. A detailed discussion of the structure of the model, and the formulations used in it, is presented herein. The following section describes the method used to determine resuspension and deposition fluxes at the sediment-water interface for a non-cohesive bed that is composed of a relatively uniform mix of sand particles. Because the non-cohesive sediment bed in the Upper Hudson River is typically graded (heterogeneous) and contains significant fractions of non-suspendable sediments (coarse sand and gravel), the effects of bed armoring must be considered and formulations for simulating non-cohesive bed armoring are presented in Section 3. The fourth section of the report presents a detailed computational procedure for the model and also a discussion on how to calibrate and apply the model.

SECTION 2

NON-COHESIVE SUSPENDED LOAD TRANSPORT MODEL

2.1 INTRODUCTION

Numerous laboratory and field studies have been conducted on the erosion and deposition properties of non-cohesive sediments (e.g., see Vanoni (1975) and van Rijn (1993) for overviews). These investigations have lead to the development of various formulations for quantification of non-cohesive suspended load transport in a riverine system such as the Upper Hudson River. Several investigators have evaluated the accuracy of different quantitative approaches using laboratory and field data (Garcia and Parker, 1991; Voogt et al., 1991; van den Berg and van Gelder, 1993). The results of these investigations have shown that the formulations developed by van Rijn (1984a,b,c) provide one of the best methods for calculating suspended load transport of non-cohesive sediments. The van Rijn equations have also been successfully used in sediment transport modeling studies of riverine (Ziegler and Nisbet, 1994) and estuarine (van Rijn et al., 1990) systems.

Based upon these findings, the van Rijn method for non-cohesive suspended load transport is an appropriate modeling framework for application to the Upper Hudson River. A detailed review of the van Rijn suspended load equations will now be given. For convenience, equation numbers in the original van Rijn publications will be referred to as (VR84a,b,c Eq. _).

An important assumption in the van Rijn procedure is that the sediment bed is composed of relatively homogeneous fine sands so that the following equations apply to the entire sediment bed. As discussed in Section 1, the sediment bed of the Upper Hudson River is heterogeneous, with a significant fraction of the bed being composed of coarse sands ($D > 500\ \mu m$) and gravels ($D > 2000\ \mu m$) which are not transported as suspended load. Modifications that have to be made to the van Rijn equations to account for the effects of non-suspendable bed sediments, i.e., bed armoring, are discussed in Section 3.

2.2 NON-COHESIVE RESUSPENSION

Following the van Rijn method, the equations presented below are used to calculate the suspended load transport rate for a given particle size-class k of suspended sediment, which can be represented by an effective particle diameter (D_k).

The critical bed-shear velocity for initiation of bed load transport ($u_{*,cr}$) is calculated using the Shields criteria (see Figure 1 in VR84a):

$$u_{*,cr} = [(s-1)g\ D_k\ \theta_{cr}]^{1/2} \tag{2-1}$$

where θ_{cr} = critical mobility parameter. For suspendable sands, D_k is less than 500 μm (see Figure 1 in VR84a) and θ_{cr} is calculated as follows:

$$\theta_{cr} = \begin{cases} 0.24\ D_*^{-1} & , \quad D_* \le 4 \\ 0.14\ D_*^{-0.64} & , \quad 4 < D_* \le 10 \\ 0.04\ D_*^{-0.10} & , \quad 10 < D_* \le 20 \end{cases} \tag{2-2}$$

where D_* = non-dimensional particle parameter (VR84b, Eq. 1):

$$D_* = D_k \left[\frac{(s-1)g}{\nu^2}\right]^{1/3} \tag{2-3}$$

where s = specific density of particle (assumed to be 2.65 for sand particles); g = acceleration of gravity; and ν = kinematic viscosity of water.

Experiments on non-cohesive resuspension have shown that the critical bed-shear velocity for initiation of suspension ($u_{*,crs}$) is proportional to the settling speed of particle size-class k ($W_{s,k}$). Laboratory experiments conducted at the Delft Hydraulics Laboratory indicated that (VR84b, Eq. 8 and 9):

$$u_{*,crs} = \begin{cases} 4\,\dfrac{W_{s,k}}{D_*} & , \quad 1 < D_* \le 10 \\ 0.4\,W_{s,k} & , \quad D_* > 10 \end{cases} \tag{2-4}$$

Note that if $u_{*,crs}$ is less than $u_{*,cr}$, i.e., the critical shear velocity for bed load calculated using Equation (2-1), then $u_{*,crs} = u_{*,cr}$.

The settling speed of a sand particle is related to the particle diameter, representing size-class k, as follows (Cheng, 1997):

$$W_{s,k} = \frac{\nu}{D_k}\left[(25 + 1.2D_*^2)^{1/2} - 5\right]^{1.5} \tag{2-5}$$

The dependence of $W_{s,k}$ on D_k is illustrated in Figure 2-1, which shows that the settling speeds of suspended sand particles (i.e., $62 < D_k < 500$ μm) range from about 2,300 to 59,000 μm/s (~200 to 5,000 m/day).

Once it has been determined that the bottom shear velocity (i.e., bottom shear stress) exceeds the critical values for suspension (i.e., $u_* > u_{*,cr}$ and $u_* > u_{*,crs}$)[1], then an equilibrium reference concentration at a reference height z = a above the sediment bed is calculated (VR84b, Eq. 38):

$$C_{eq} = 0.015\,\frac{D_k\,T^{1.5}}{a\,D_*^{0.3}} \tag{2-6}$$

---

[1]Bottom shear velocity is calculated as

$$u_* = \left(\frac{\tau_b}{\rho}\right)^{1/2}$$

where τ_b = bottom shear stress and ρ = water density.

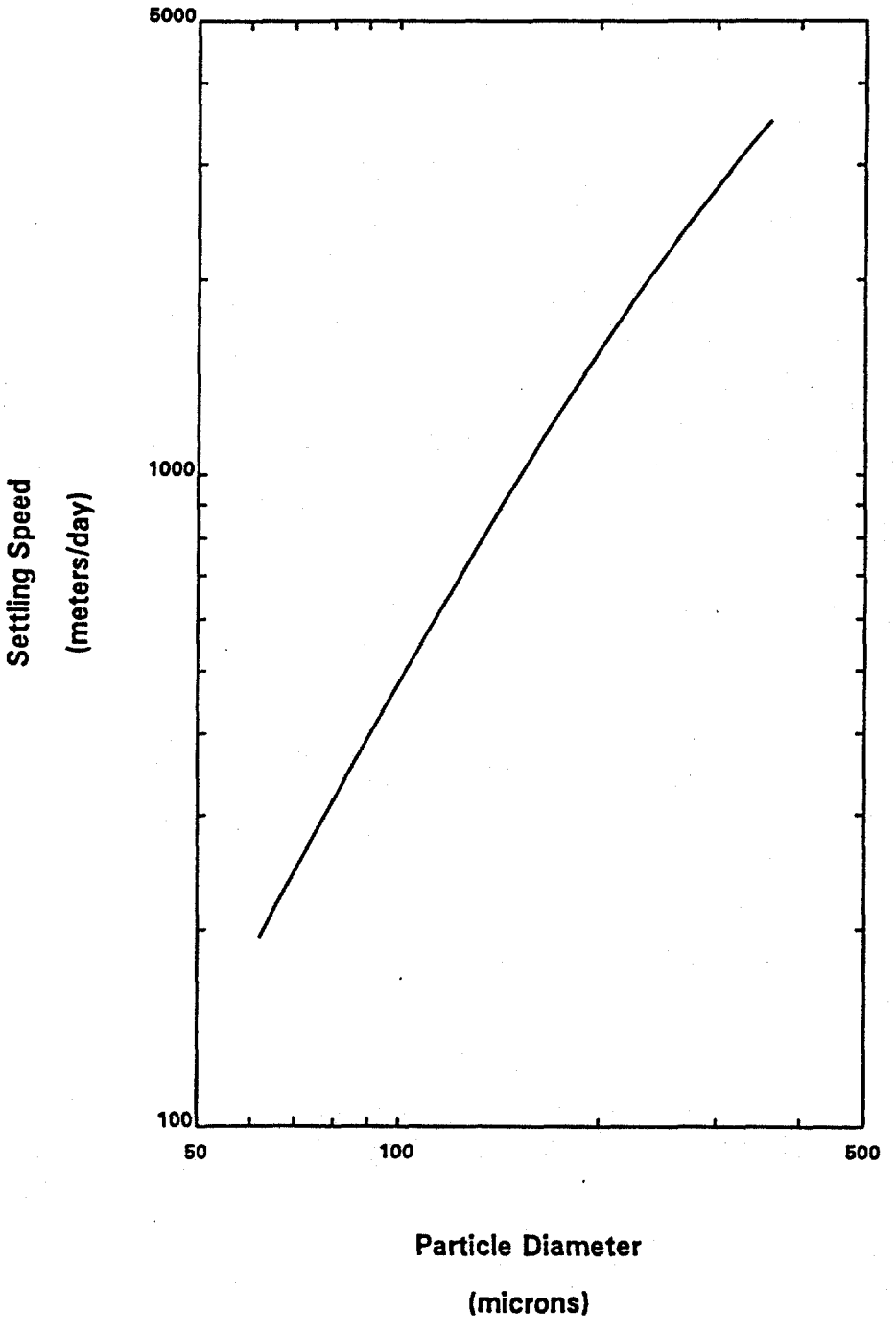

Figure 2-1. Settling speed of sand as function of particle diameter.

where C_{eq} is a volumetric concentration (i.e., solids volume/unit fluid volume) and T is the transport stage parameter, which is determined using $u_{*,cr}$ (VR84b, Eq.2):

$$T = \left(\frac{u_*}{u_{*,cr}}\right)^2 - 1 \qquad (2\text{-}7)$$

To convert C_{eq} to a mass concentration (i.e., g/cm^3), which is needed for calculating resuspension fluxes, multiply C_{eq} by the sediment particle density (ρ_s). Note that the maximum volumetric concentration ($C_{eq,max}$) is 0.65 or 1.72 g/cm^3 (1,720,000 mg/l) (van Rijn, 1984b). Variation in C_{eq} as a function of τ_b, for different D_k values, is shown on Figure 2-2.

The reference height (a) is given by (VR84b, Eq. 37):

$$a = MAX\ (0.5\ \Delta,\ k_s,\ 0.01d) \qquad (2\text{-}8)$$

where Δ = bed-form height, k_s = equivalent roughness height of Nikuradse and d = local water depth. The bed-form height, where bed-forms are characterized as ripples and dunes, is estimated using (VR84c, Eq. 14):

$$\Delta = 0.11\ d^{0.7}\ D_{50}^{0.3}\ (1 - e^{-0.5T})\ (25 - T) \qquad (2\text{-}9)$$

where D_{50} = median particle diameter of the sediment bed. A plane bed exists when T is greater than 25, i.e., ripples and dunes are washed out and the bed-form height is zero (van Rijn, 1984c).

The resuspension flux is calculated using (van Rijn, 1993):

$$E_{ss,k} = -W_{s,k}\ (C_{a,k} - C_{eq}) \qquad (2\text{-}10)$$

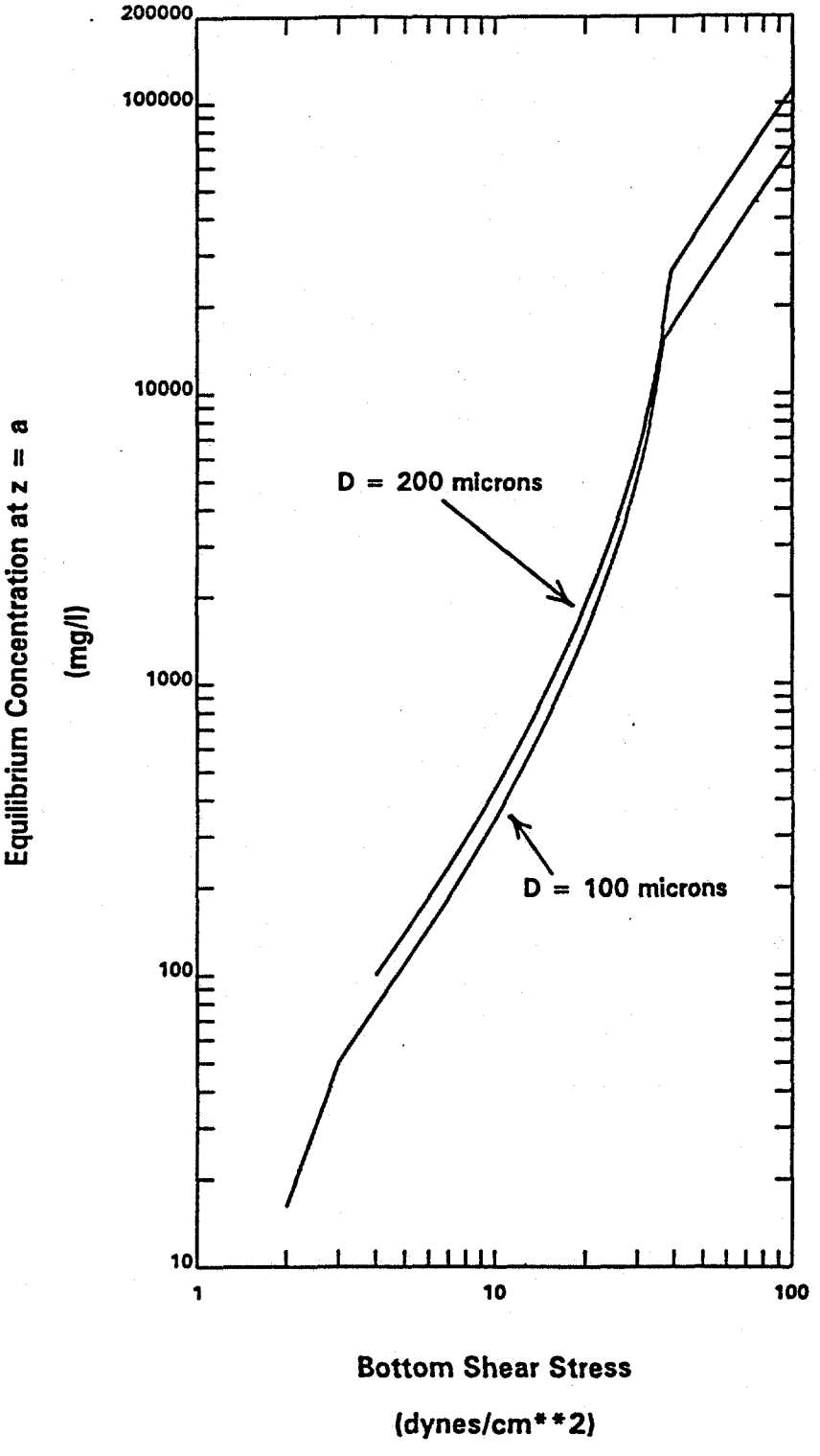

Figure 2-2. Equilibrium concentration at z = a (C_{eq}) as function of bottom shear stress for different particle diameters.

where $E_{na,k}$ = net resuspension flux of size-class k for non-armoring sediment bed and $C_{a,k}$ = suspended sediment concentration of size-class k at z=a. A maximum sediment concentration, represented by C_{eq}, can be transported in the water column for a given bed shear velocity (which is equivalent to a certain level of turbulence in the water column). If $C_{a,k} < C_{eq}$, additional sediment can be carried by the flow, so that erosion occurs and $E_{na,k} > 0$. Conversely, if $C_{a,k} > C_{eq}$, the carrying capacity of the water column at a particular bed shear velocity has been exceeded, which means that $E_{na,k} < 0$ and deposition can occur, even though the critical bed shear velocity has been exceeded. Thus, $C_{a,k}$ needs to be calculated before $E_{na,k}$ can be determined, the consequences of which will be discussed in Section 4.

Most sediment transport models applied to riverine systems have used a vertically-averaged approximation of the vertical distribution of sediment in the water column (e.g., Ziegler and Nisbet, 1994). This approach assumes that particles are uniformly distributed throughout the water column, which is a good approximation for cohesive sediments due to their lower settling velocities (ca. 100 μm/s). The high settling speeds of suspended sands cause significant stratification to occur, with order of magnitude increases in concentration typically occurring between the top and bottom of the water column. Thus, simulation of suspended sand transport with a vertically-averaged model necessitates the use of a correction factor (Γ) to account for effects of concentration stratification.

This correction factor will relate the vertically-averaged sediment concentration of size-class k ($C_{m,k}$), which is calculated by the sediment transport model, to $C_{a,k}$ and it is developed as follows. The vertical distribution of non-cohesive sediment in the water column can be calculated using (VR84b, Eq. 19a,b):

$$C_K(z) = \begin{cases} C_{a,k}\left[\left(\frac{a}{d-a}\right)\left(\frac{d}{z} - 1\right)\right]^{\zeta} & , \quad \frac{z}{d} < 0.5 \\ C_{a,k}\left(\frac{a}{d-a}\right)^{\zeta} e^{-4\zeta\left(\frac{z}{d} - 0.5\right)} & , \quad \frac{z}{d} \geq 0.5 \end{cases} \tag{2-11}$$

where z = vertical coordinate (z=0 at sediment-water interface and z=d at water surface) and ζ = suspension parameter (originally denoted as Z in VR84b) defined by (VR84b, Eq. 3):

$$\zeta = \frac{W_{s,k}}{\beta \kappa u_*} \tag{2-12}$$

where κ = von Karman constant (assumed to be 0.4) and the β-factor, which is related to the vertical diffusion of particles, is given by (VR84b, Eq. 22):

$$\beta = 1 + 2\left(\frac{W_{s,k}}{u_*}\right)^2 \quad , \quad 0.1 < \frac{W_{s,k}}{u_*} < 1 \tag{2-13}$$

The vertically-averaged concentration, $C_{m,k}$, is defined as:

$$C_{m,k} = \frac{1}{d}\int_a^d C_k(z)\, dz \tag{2-14}$$

Using Eq. (2-11) in the above integral yields:

$$C_{m,k} = \frac{C_{a,k}}{d}\left(\frac{a}{d-a}\right)^{\zeta}\left\{\int_a^{0.5d}\left(\frac{d}{z}-1\right)^{\zeta} dz + \int_{0.5d}^{d} e^{-4\zeta\left(\frac{z}{d}-0.5\right)} dz\right\} \tag{2-15}$$

The integrals in this equation will be evaluated separately. The first integral does not have a closed form solution. Approximating the solution using the trapezoidal rule (Carnahan et al., 1969) and three segments between z = a and z = 0.5 d, i.e., δz = (0.5 d - a)/3, yields:

$$\int_a^{0.5d}\left(\frac{d}{z}-1\right)^{\zeta} dz = \frac{1}{3}(0.5d-a)\left[0.5\left(\frac{d}{a}-1\right)^{\zeta} + \left(\frac{d}{a+\delta z}-1\right)^{\zeta} + \left(\frac{d}{a+2\delta z}-1\right)^{\zeta} + 0.5\right] \tag{2-16}$$

The second integral has the following solution:

$$\int_{0.5d}^{d} e^{-4\zeta\left(\frac{z}{d}-0.5\right)}\,dz = \frac{d}{4\zeta}\left(1 - e^{-2\zeta}\right) \qquad (2\text{-}17)$$

Inserting Equations (2-16) and (2-17) into Equation (2-15) and solving for C_a produces:

$$C_{a,k} = \Gamma\, C_{m,k} \qquad (2\text{-}18)$$

where:

$$\Gamma = \left(\frac{d}{a}-1\right)^{\zeta}\left\{\frac{1}{4\zeta}\left(1-e^{-2\zeta}\right) + \frac{1}{3}\left(0.5-\frac{a}{d}\right)\left[0.5\left(\frac{d}{a}-1\right)^{\zeta} + \left(\frac{d}{a+\delta z}-1\right)^{\zeta} + \left(\frac{d}{a+2\delta z}-1\right)^{\zeta} + 0.5\right]\right\}^{-1} \qquad (2\text{-}19)$$

The correction factor, Γ, as a function of $W_{s,k}/u_*$, for various values of a/d, is presented on Figure (2-3).

2.3 NON-COHESIVE DEPOSITION

When the bed-shear velocity is less than the critical value, the resuspension rate is zero and non-cohesive sediments in the water column can be deposited on the sediment bed. The deposition flux for sediments of size-class k (DEP_k) under this condition is:

$$DEP_k = P_{dep}\, W_{s,k}\, C_{a,k} \qquad (2\text{-}20)$$

where P_{dep} = probability of deposition of non-cohesive sediment. The probability of deposition parameter (P_{dep}) accounts for the effects of near-bed turbulence and particle size variations on deposition. In quiescent water, the bottom shear stress will be zero and P_{dep} will equal one. As the bottom shear stress increases, the probability of deposition decreases. The dependence of P_{dep} on bottom shear stress was investigated by Gessler (1967), who determined that P_{dep} could be described by a Gaussian distribution:

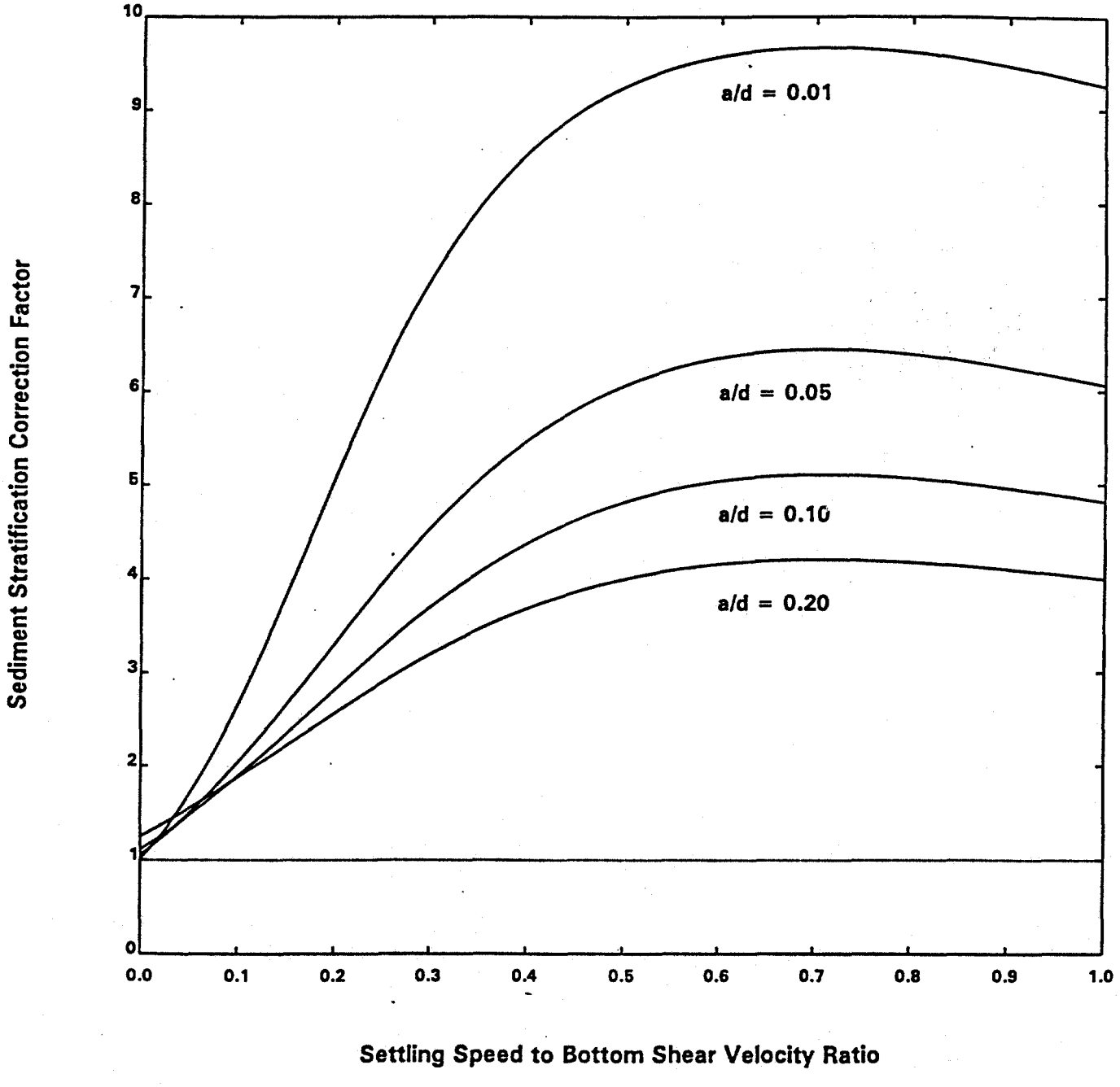

Figure 2-3. Sediment stratification correction factor (Γ) as function of W_s/u_* for various reference heights (normalized with respect to water depth).

$$P_{dep} = \frac{1}{(2\pi)^{1/2}} \int_{-\infty}^{Y} e^{-\frac{1}{2}x^2} dx \qquad (2\text{-}21)$$

where:

$$Y = \frac{1}{\sigma}\left(\frac{\tau_{c,k}}{\tau_b} - 1\right) \qquad (2\text{-}22)$$

and $\tau_{c,k}$ = critical shear stress for size-class k, with

$$\tau_{c,k} = \rho\ [\text{MAX}\ (u_{*,cns}\ ,\ u_{*,cr})]^2 \qquad (2\text{-}23)$$

and σ = standard deviation of the Gaussian distribution for incipient motion. Based upon experimental results, Gessler (1967) determined that σ was equal to 0.57.

An approximation to the probability integral in Equation (2-21), with an error of less than 0.001%, is (Abramowitz and Stegun, 1972):

$$P_{dep}(Y) = 1 - F(Y)\ (0.4362X - 0.1202X^2 + 0.9373X^3), \qquad Y > 0 \qquad (2\text{-}24)$$

where:

$$F(Y) = \frac{1}{(2\pi)^{1/2}} e^{-\frac{1}{2}Y^2} \qquad (2\text{-}25)$$

$$X = (1 + 0.3327Y)^{-1} \qquad (2\text{-}26)$$

For $Y < 0$:

$$P_{dep}(Y) = 1 - P_{dep}(|Y|) \tag{2-27}$$

The dependence of P_{dep} on bottom shear, for different particle sizes, is illustrated on Figure (2-4).

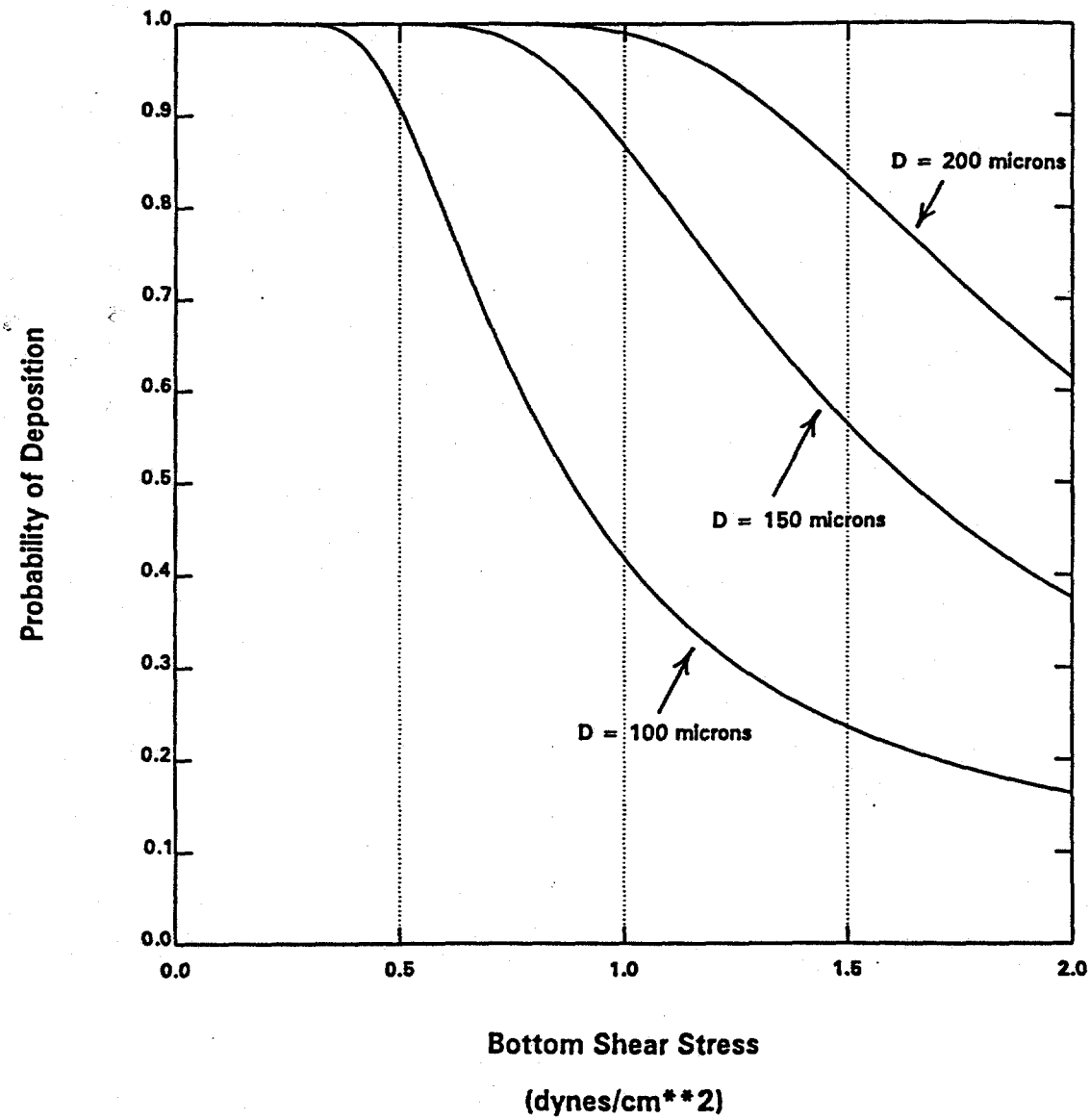

Figure 2-4. Probability of deposition (P_{dep}) of sand as function of bottom shear stress for different particle diameters.

SECTION 3

SIMULATION OF NON-COHESIVE BED ARMORING

3.1 INTRODUCTION

A non-cohesive sediment bed that contains a wide range of particle sizes, from fine sands that are suspendable to coarse sands and gravels that are only transported as bed load, will experience a phenomenon known as bed armoring during a resuspension event. Bed armoring occurs when fine sands are eroded from a heterogeneous sediment bed and the coarser material that cannot be resuspended remains on the bed surface. As the erosion process continues, the suspendable sediments in the near-surface layer, referred to as the active layer, are depleted and a layer of coarse, non-suspendable sediments forms. Continuous depletion of suspendable sediments in the active layer will eventually reduce the erosion rate to zero, at which point the active layer is composed entirely of non-suspendable sediments, and the sediment bed has become armored (Shen and Lu, 1983; Karim and Holly, 1986; Jain and Park, 1989; Rahuel et al., 1989; van Niekerk et al., 1992).

Non-cohesive areas of the sediment bed in the Upper Hudson River typically contain a significant fraction of non-suspendable material. For example, coarse sand and gravel comprises approximately 50% of the non-cohesive bed in the Thompson Island Pool. In addition, an analysis of sediment loading data in the Thompson Island Pool showed that bed armoring occurred on the rising limb of the hydrograph during a high flow event in 1994 (HydroQual, 1997). Thus, the effects of bed armoring must be accounted for in any non-cohesive sediment transport model applied to this reach, or other reaches of the Upper Hudson River. Erosion rates will be significantly overestimated if bed armoring effects are not considered during a sediment transport simulation of a flood event.

3.2 BED ARMORING MODEL

The bed armoring process has been modeled by assuming that the sediment bed is composed of an active layer, which interacts with the water column, and a parent bed layer, which is below the active layer, see Figure 3-1 (Karim and Holly, 1986; van Niekerk et al., 1992). Sediment bed data can be used to determine the initial grain size distribution in the parent bed. The parent bed is aggregated into K size-classes of suspendable sediment (D_k <

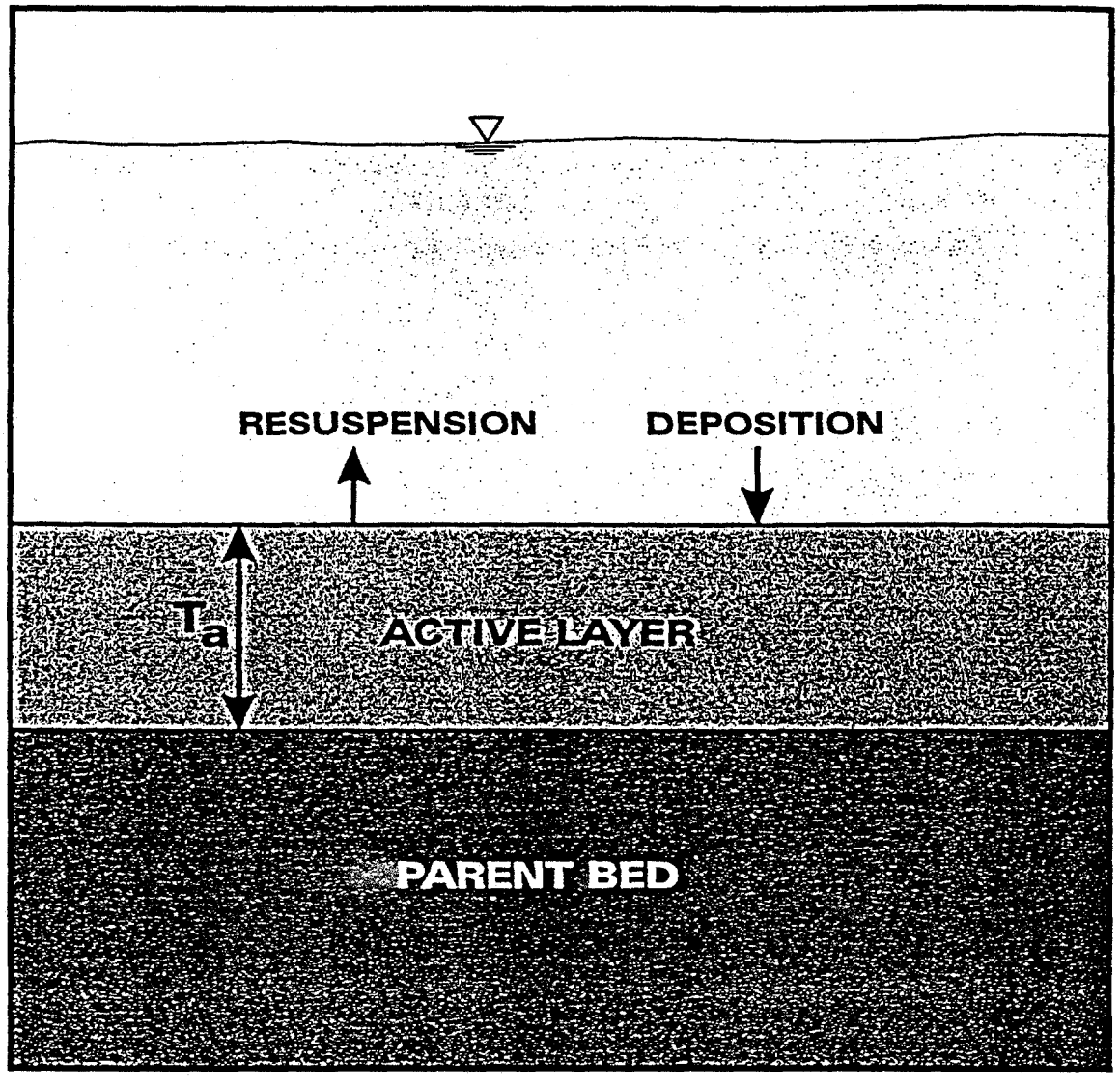

Figure 3-1. Conceptual model of non-cohesive sediment bed.

500 μm, k= 1, K). The fraction of suspendable sediment of size-class k in the parent bed ($f_{p,k}$) is determined from grain size distribution data.

Large, non-suspendable particles in the bed provide voids where smaller, suspendable particles can be shielded from the main flow in the water column. For example, the localized bottom shear stress immediately downstream of a very fine pebble (2,000 μm < D < 4,000 μm) could be much lower than the mean bed shear stress, which might provide a small area in which fine sands (D < 250 μm) could exist without being resuspended. This geometrical effect reduces the suspendable sediment of size-class k below that given by $f_{a,k}$. The reduction factor is referred to as the hiding factor and it is defined as (Karim and Kennedy, 1981; Rahuel et al., 1989):

$$H_k = \left(\frac{D_k}{D_{50}}\right)^m \tag{3-1}$$

where H_k = hiding factor for size-class k and m = site-specific exponent. Karim and Kennedy (1981) set m equal to 0.85, however, Rahuel et al. (1989) stated that the value of m may depend upon local conditions in a particular riverine system. Note that H_k is less than one for an armoring bed.

Interactions between the parent bed, active layer and water column cause the grain size distributions in the parent bed and active layer to change with time. Changes in the active layer grain size distribution control the bed armoring process and, hence, the resuspension flux. The non-cohesive resuspension flux formulation developed in Section 2 assumes that the entire sediment bed is composed of suspendable sediment. Thus, Equation (2-10) must be modified to account for bed armoring effects.

For a non-armoring bed, erosion occurs when the bed shear velocity (u_*) is greater than both the critical shear velocities for bed load ($u_{*,cr}$) and suspended load ($u_{*,crs}$) transport. Both of these critical shear velocities are functions of particle size, see Equations (2-1), (2-4) and (2-5). Bed load transport will be initiated in an armoring bed when the bed shear velocity exceeds the critical shear velocity for the entire bed ($u_{*,cr,bed}$), which is a function of the median particle diameter of the parent bed (D_{50}). The assumption is made that resuspension from an armoring

bed can occur after the initiation of bed load, i.e., $u_* > u_{*,cr,bed}$, provided $u_* > u_{*,crs}$. The value of $u_{*,cr,bed}$ is calculated using Equation (2-1), but with D_{50} replacing D_k.

The fraction of size-class k in the active layer will affect the resuspension rate of that class because sediments are resuspended from the active layer. In addition, the hiding factor will also reduce the resuspension flux, so that (Rahuel et al., 1989):

$$E_k = H_k \, f_{a,k} \, E_{na,k} \tag{3-2}$$

where E_k = net resuspension flux for size-class k and $f_{a,k}$ = fraction of size-class k sediment in the active layer, which will change with time.

Calculating temporal changes of $f_{a,k}$ requires construction of a sediment bed model that tracks compositional changes in the active layer and the parent bed. Size-class k sediment is removed from the active layer at the rate determined by Equation (3-2). The bed model transfers sediment from the parent bed to the active layer at the same rate, but that material has the particle size distribution of the parent bed (Karim and Holly, 1986). This process causes the active layer to become enriched in non-suspendable sediment and eventually it becomes armored; size-class k sediment is resuspended from the active layer at a faster rate than that sediment type is transported into the active layer from the parent bed.

Various expressions have been proposed for the active layer thickness (e.g., Borah et al., 1982; Karim and Holly, 1986; van Niekerk et al., 1992). The Borah et al. (1982) formulation is:

$$T_a = \frac{D_{50}}{(1 - p)\,(1 - \sum f_{a,k})} \tag{3-3}$$

where T_a = active layer thickness, p = bed porosity and $(1 - \Sigma f_{a,k})$ = fraction of the active layer composed of non-suspendable sediment. Initial testing of a Thompson Island Pool sediment transport model has indicated that it may be difficult to adequately calibrate the model using the Borah formulation. These results are probably due to the non-dynamic form of

Equation (3-3), i.e., T_a only depends upon bed properties and it is insensitive to variable hydrodynamic conditions.

An alternative expression for the active layer thickness has been developed by van Niekerk et al. (1992) that is a linear function of the local bottom shear stress. A modified form of their formulation is proposed for application to the Upper Hudson River:

$$T_a = \begin{cases} 2D_{50} & , \ \tau_b < \tau_{c50} \\ 2D_{50}\left[B\left(\frac{\tau_b}{\tau_{c50}}\right) + (1-B)\right] & , \ \tau_b \geq \tau_{c50} \end{cases} \quad (3\text{-}4)$$

where τ_{c50} = critical shear stress for initiation of bed load, based upon parent bed D_{50} and B = adjustable constant. Note that Equation (3-4) reduces to the original van Niekerk et al. (1992) equation when B = 1. A potential advantage of Equation (3-4) is that varying hydrodynamic conditions affect the active layer thickness, with T_a increasing as the current velocity (and τ_b) increases, which causes the amount of sediment that is available for resuspension to increase. The dependence of T_a on τ_b is not well known and the constant (B) in Equation (3-4) can be adjusted during model calibration to account for local conditions.

The approach developed by Karim and Holly (1986) to model changes in the active layer and parent bed composition is used as follows. Sediment volumes are tracked in both layers of the bed model to ensure conservation of mass. The fraction of suspendable sediment, size-class k, in the active layer is defined as:

$$f_{a,k} = \frac{V_{a,k}}{V_{a,tot}} \quad (3\text{-}5)$$

where $V_{a,k}$ = volume of size-class k sediment in the active layer and $V_{a,tot}$ = total volume of sediment in the active layer. The active layer thickness, T_a, is converted to a sediment volume using:

$$V_{a,tot} = (1-p)\, T_a\, A_{ref} \tag{3-6}$$

where A_{ref} = reference area, which is the area of a specific grid element in a numerical model. Similarly, for the parent bed:

$$f_{p,k} = \frac{V_{p,k}}{V_{p,tot}} \tag{3-7}$$

where $f_{p,k}$ = fraction of size-class k sediment in the parent bed layer, $V_{p,k}$ = volume of size-class k sediment in the parent bed layer and $V_{p,tot}$ = total volume of sediment in the parent bed layer and:

$$V_{p,tot} = (1-p)\, T_p\, A_{ref} \tag{3-8}$$

where T_p = thickness of parent bed layer.

Tracking volume changes in the active and parent bed layers with a numerical model is accomplished using the framework proposed by Karim and Holly (1986). It is assumed that the state of the active and parent bed layers are known at some time t^n (i.e., T_a^n, T_p^n, $f_{a,k}^n$, $f_{p,k}^n$, etc. have been calculated or specified). Erosion occurs during the next timestep in the calculation, i.e., $\delta t = t^{n+1} - t^n$, and changes in bed composition need to be determined at t^{n+1}. The mass of size-class k sediment, on a mass/unit area basis, removed from the active layer ($M_{e,k}^{n+1}$) during this timestep is:

$$M_{e,k}^{n+1} = \delta t\, E_k \tag{3-9}$$

where the resuspension rate, E_k, is calculated using Equation (3-2). This mass is converted to a volume for the reference area:

$$V_{e,k}^{n+1} = \frac{A_{ref}}{\rho_s} M_{e,k}^{n+1} \quad (3\text{-}10)$$

where ρ_s = particle density (assumed to be 2.65 g/cm^3 for sand particles).

The total sediment bed thickness (T_{tot}) decreases due to erosion:

$$T_{tot}^{n+1} = T_{tot}^{n} - \frac{\sum V_{e,k}^{n+1}}{(1-p)\, A_{ref}} \quad (3\text{-}11)$$

where $\Sigma V_{e,k}^{n+1}$ = total eroded volume, i.e., summation for all suspendable size-classes (k = 1, K). Volume changes of size-class k in the active and parent bed layers for a timestep during which erosion occurs also need to account for variations in the active layer thickness (Karim and Holly, 1986). The active layer thickness at t^{n+1} (T_a^{n+1}) is calculated using Equation (3-4). Thickness of the parent bed at t^{n+1} is given by:

$$T_p^{n+1} = T_{tot}^{n+1} - T_a^{n+1} \quad (3\text{-}12)$$

The above equations are used to calculate volumes of size-class k in the active and parent bed layers at t^{n+1} for increasing active layer thickness ($V_a^{n+1} > V_a^n$):

$$V_{a,k}^{n+1} = V_{a,k}^{n} + f_{p,k}^{n} (V_a^{n+1} - V_a^n) - V_{e,k}^{n+1} + f_{p,k}^{n} \sum V_{e,k}^{n+1} \quad (3\text{-}13)$$

$$V_{p,k}^{n+1} = V_{p,k}^{n} - f_{p,k}^{n} (V_a^{n+1} - V_a^n) - f_{p,k}^{n} \sum V_{e,k}^{n+1} \quad (3\text{-}14)$$

or decreasing/constant active layer thickness ($V_a^{n+1} \leq V_a^n$):

$$V_{a,k}^{n+1} = V_{a,k}^{n} + f_{a,k}^{n} (V_s^{n+1} - V_s^{n}) - V_{c,k}^{n+1} + f_{p,k}^{n} \sum V_{c,k}^{n+1} \quad (3\text{-}15)$$

$$V_{p,k}^{n+1} = V_{p,k}^{n} - f_{a,k}^{n} (V_s^{n+1} - V_s^{n}) - f_{p,k}^{n} \sum V_{c,k}^{n+1} \quad (3\text{-}16)$$

Equations (3-5) and (3-7) are then used to calculate $f_{a,k}^{n+1}$ and $f_{p,k}^{n+1}$, respectively, using $V_{a,k}^{n+1}$, $V_{p,k}^{n+1}$, $V_{a,tot}^{n+1}$ and $V_{p,tot}^{n+1}$. See Figure 3 of Karim and Holly (1986) for a diagram that illustrates the erosional process and changes in active layer content during a particular timestep.

When depositional conditions occur, as calculated using Equation (2-20), the total depositional volume for each size-class during a timestep is added to the active layer:

$$V_{a,k}^{n+1} = V_{a,k}^{n} + f_{a,k}^{n} \left(V_s^{n+1} - V_s^{n}\right) + \frac{\delta t}{\rho_s} A_{ref} (DEP_k - f_{a,k}^{n} \sum DEP_k) \quad (3\text{-}17)$$

$$V_{p,k}^{n+1} = V_{p,k}^{n} - f_{a,k}^{n} (V_s^{n+1} - V_s^{n}) + \frac{\delta t}{\rho_s} A_{ref} f_{a,k}^{n} \sum DEP_k \quad (3\text{-}18)$$

where the active layer thickness is either decreasing (transition from erosional to depositional conditions) or constant (pure deposition).

SECTION 4

MODEL APPLICATION AND CALIBRATION

4.1 INTRODUCTION

The objective of this section is to suggest procedures that should be followed to ensure that the non-cohesive transport model is used in a consistent and correct manner. First, a step-by-step computational procedure for applying the model is outlined. A discussion on applying the model to the Upper Hudson River, including data requirements and calibration procedures, concludes this section.

4.2 COMPUTATIONAL PROCEDURE

The non-cohesive modeling framework discussed in Sections 2 and 3 is used to calculate resuspension and deposition fluxes across the sediment-water interface. These fluxes are used as a boundary condition in a sediment transport model that transports suspended sediments, of various size-classes, in the water column.

The computational procedure used to calculate sediment flux across the sediment-water interface at a particular location and time (i.e., grid element in a numerical model and at timestep t^{n+1}) assumes that the following information is known at time t^n:

1. Hydrodynamic parameters: u_*, τ_b, d, ν
2. Bed properties: D_{50}, p, ρ_s
3. Active and parent bed composition: $f_{a,k}$, $f_{p,k}$
4. Sediment transport parameter: $C_{m,k}$
5. Numerical parameters: A_{ref}, δt

It is assumed that the sediment bed contains K classes of suspendable sediment, with each size-class k represented by an effective particle diameter, D_k ($D_k < 500\ \mu m$). Note that this necessitates calculating the water column transport of K classes of sediment, with each class having a corresponding vertically-averaged water column concentration at t^n ($C_{m,k}$). Calculating the resuspension or deposition flux of size-class k for a specific location (grid element) at time t^{n+1} proceeds as follows:

1. Calculate D_* for size-class k, Eq. (2-3) using D_k
2. Calculate θ_{cr} for size-class k, Eq. (2-2)
3. Calculate $u_{*,cr}$ for size-class k, Eq. (2-1) using D_k
4. Calculate D_* for parent bed, Eq. (2-3) using D_{50}
5. Calculate θ_{cr} for parent bed, Eq. (2-2)
6. Calculate $u_{*,cr,bed}$ for parent bed, Eq. (2-1) using D_{50}
7. Calculate $W_{s,k}$ for size-class k, Eq. (2-5) using D_k
8. Calculate $u_{*,crs}$ for size-class k, Eq. (2-4)
9. Determine if resuspension or deposition occurs:

   a. If $u_* > MAX(u_{*,cr}, u_{*,cr,bed}, u_{*,crs}) \Rightarrow$ resuspension

   b. If $u_* \leq MAX(u_{*,cr}, u_{*,cr,bed}, u_{*,crs}) \Rightarrow$ deposition

For resuspension conditions:

1. Calculate T for size-class k, Eq. (2-7)
2. Calculate Δ, Eq. (2-9) using D_{50}
3. Calculate a, Eq. (2-8)
4. Calculate C_{eq} for size-class k, Eq. (2-6)
5. Calculate β for size-class k, Eq. (2-13)
6. Calculate ζ for size-class k, Eq. (2-12)
7. Calculate $\delta z = (0.5d - a)/3$
8. Calculate Γ for size-class k, Eq. (2-19)
9. Calculate $C_{a,k}$, Eq. (2-18)

10. Calculate $E_{na,k}$, Eq. (2-10)
11. Calculate H_k, Eq. (3-1)
12. Calculate E_k, Eq. (3-2)
13. Calculate $M_{e,k}^{n+1}$, Eq. (3-9)
14. Calculate $V_{e,k}^{n+1}$, Eq. (3-10)
15. Calculate T_{tot}^{n+1}, Eq. (3-11)
16. Calculate T_a^{n+1}, Eq. (3-4)
17. Calculate T_p^{n+1}, Eq. (3-12)
18. Calculate $V_{a,tot}^{n+1}$, Eq. (3-6)
19. Calculate $V_{p,tot}^{n+1}$, Eq. (3-8)
20. Calculate $V_{a,k}^{n+1}$, Eq. (3-13) or (3-15)
21. Calculate $V_{p,k}^{n+1}$, Eq. (3-14) or (3-16)
22. Calculate $f_{a,k}^{n+1}$, Eq. (3-5)
23. Calculate $f_{p,k}^{n+1}$, Eq. (3-7)

For deposition conditions:

1. Calculate β for size-class k, Eq. (2-13)
2. Calculate ζ for size-class k, Eq. (2-12)
3. Calculate $a = 0.01d$
4. Calculate $\delta z = (0.5d - a)/3$
5. Calculate Γ for size-class k, Eq. (2-19)
6. Calculate $C_{a,k}$, Eq. (2-18)
7. Calculate $\tau_{c,k}$, Eq. (2-23)
8. Calculate Y, Eq. (2-22)
9. Calculate F(Y), Eq. (2-25)
10. Calculate X, Eq. (2-26)
11. Calculate P_{dep}, Eq. (2-24) or (2-27)
12. Calculate DEP_k^{n+1}, Eq. (2-20)
13. Calculate T_{tot}^{n+1}, Eq. (3-11)
14. Calculate T_a^{n+1}, Eq. (3-4)

15. Calculate T_p^{n+1}, Eq. (3-12)
16. Calculate $V_{a,tot}^{n+1}$, Eq. (3-6)
17. Calculate $V_{p,tot}^{n+1}$, Eq. (3-8)
18. Calculate $V_{a,k}^{n+1}$, Eq. (3-17)
19. Calculate $V_{p,k}^{n+1}$, Eq. (3-18)
20. Calculate $f_{a,k}^{n+1}$, Eq. (3-5)
21. Calculate $f_{p,k}^{n+1}$, Eq. (3-7)

4.3 MODEL APPLICATION AND CALIBRATION

Successful application of the non-cohesive suspended load formulations developed in the preceding sections to the Upper Hudson River requires careful development, calibration and validation of the model. First, bed property data in the non-cohesive areas of a particular reach, e.g., Thompson Island Pool, must be analyzed to determine the appropriate bed parameters for use as model input, e.g., D_{50}, p, ρ_s and $f_{p,k}$ for K classes of suspendable sediment. Analysis of non-cohesive bed property data from the Thompson Island Pool indicates the presence of a wide range of D_{50} (from ~200 to 9,000 μm) and $f_{p,k}$ (for 75 μm < D_k < 425 μm, which are fine and medium sands, f_p ranges from 0.06 to 0.85). Judicious examination of the data must be carried out to generate a credible spatial distribution of D_{50} and f_p values throughout this reach.

Once bed property values have been determined, TSS data collected during a high flow event must be used to calibrate the model. The April 1994 high flow event (HydroQual, 1997) yielded a set of TSS data that can be used to calibrate the model in the Thompson Island Pool. The calibration process is important because it demonstrates model accuracy and establishes a certain level of scientific credibility which is necessary before the sediment transport model can be used as a predictive tool.

Use of this model also requires performing time-dependent simulations of water column sediment transport, which can be accomplished using a high flow event for calibration. Time-

dependent calculations are necessary because the resuspension flux, as defined by Equations (2-10) and (3-2), at a particular non-cohesive bed location depends upon the local suspended sediment concentration, as well as various bed properties. Without a time-dependent simulation that calculates suspended sediment concentrations, the non-cohesive resuspension flux cannot be calculated and, hence, scour depths in non-cohesive bed areas cannot be predicted with any confidence.

While the non-cohesive suspended load model developed in this report is based upon formulations presented in peer-reviewed publications, uncertainty exists in some model parameters due to data limitations. Model parameters that cannot be determined using Upper Hudson River data can serve as calibration variables for the model. Calibration of the model in this context means adjustment of various input parameters until the best agreement between model results and data is achieved, e.g., comparison between predicted and observed TSS at one or more locations. However, it must be emphasized that parameter adjustment during calibration cannot be done arbitrarily nor should a large number of parameters be varied in an independent and inconsistent manner. A small number of model parameters, i.e., less than four, need to be adjusted such that the final parameter values are realistic and consistent with data collected from the Upper Hudson River, other riverine systems or laboratory experiments. For the model developed here, the two parameters that are not well known in the Upper Hudson River are: (1) D_k, effective particle diameter of size class k and (2) B, the constant in the active layer thickness formulation expressed in Equation (3-4). These two parameters could be used as the primary calibration parameters for the non-cohesive suspended transport model when it is applied to various reaches in the Upper Hudson River.

Additional testing of the model needs to be done after calibration is completed. This validation is accomplished by simulating other high flow events for which TSS data exist in a particular reach of the Upper Hudson River, e.g., April 1993 and Spring 1997 in the Thompson Island Pool. Model parameters are set at the same values used during calibration and are not adjusted during validation runs; the only model inputs changed are flow rates and solids loadings at the upstream and tributary inflow boundaries.

Confidence in the ability of this model to realistically and accurately simulate non-cohesive suspended load transport, and associated bed armoring, is dependent upon credible calibration and validation results. The uncertainty associated with input and parameter values for this model, or any similar non-cohesive modeling framework, are large enough that successful calibration and validation are necessary before the model can be used as a predictive tool, e.g., simulating the impacts of a 100-year flood. Without direct model-data comparisons, which demonstrate that the model adequately simulates suspended sediment concentrations during at least one high flow event, the model cannot be used as a management tool with any scientific credibility. In other words, an uncalibrated non-cohesive suspended transport model is of questionable value because the uncertainties in the input parameters are so great that an unacceptably low level of confidence will be associated with the model predictions.

Fortunately, adequate data sets exist for the Thompson Island Pool to develop, calibrate and validate the non-cohesive suspended load model described in this report. The model has been applied to this reach of the Upper Hudson River and initial modeling efforts indicate that successful calibration and validation can be achieved using the available data. Thus, this model will be able to be used as a management tool to evaluate the impacts of a 100-year flood or other issues related to sediment transport in the Thompson Island Pool.

SECTION 5

MODEL NOTATION

The following symbols are used in this report:

a = reference height
A_{ref} = reference area
B = constant in Equation (3-4)
$C_{a,k}$ = suspended sediment concentration of size-class k at z = a
$C_{m,k}$ = vertically-averaged suspended sediment concentration of size-class k
C_{eq} = equilibrium concentration at reference height z = a
$C_{eq,max}$ = maximum volumetric concentration (0.65)
$C_k(z)$ = suspended sediment concentration of size-class k at z
d = water depth
D_{50} = median particle diameter of the sediment bed
D_* = non-dimensional particle parameter
D_k = effective particle diameter of size-class k
DEP_k = deposition flux for sediments of size-class k
E_k = net resuspension flux of size-class k for armoring sediment bed
$E_{na,k}$ = net resuspension flux of size-class k for non-armoring sediment bed
$f_{a,k}$ = fraction of size-class k sediment in the active layer
$f_{p,k}$ = fraction of size-class k sediment in the parent bed
$F(Y)$ = probability of deposition parameter
g = acceleration of gravity
H_k = hiding factor for size-class k
k_s = equivalent roughness height of Nikuradse
m = site-specific exponent for hiding factor
$M_{e,k}$ = mass of size-class k sediment eroded from the active layer
p = bed porosity
P_{dep} = probability of deposition of non-cohesive sediment
s = specific density of particle (assumed to be 2.65 for sand)
T = transport stage parameter
T_a = active layer thickness
T_p = parent bed layer thickness

T_{tot} = total sediment bed thickness
u_* = bed shear velocity
$u_{*,cr}$ = critical bed-shear velocity for initiation of bed load transport (based on D_k)
$u_{*,cr,bed}$ = critical bed-shear velocity for initiation of bed load transport (based on D_{50})
$u_{*,crs}$ = critical bed-shear velocity for initiation of suspension
$V_{a,k}$ = volume of size-class k sediment in the active layer
$V_{a,tot}$ = total volume of sediment in the active layer
$V_{e,k}$ = volume of size-class k sediment eroded from the active layer
$V_{p,k}$ = volume of size-class k sediment in the parent bed
$V_{p,tot}$ = total volume of sediment in the parent bed
$W_{s,k}$ = settling speed of particle size-class k
X = probability of deposition parameter
Y = probability of deposition parameter
z = vertical coordinate (z = 0 at sediment-water interface and z = d at surface)
β = β-factor
Γ = sediment stratification correction factor
δt = $t^{n+1} - t^n$ (timestep in numerical model)
δz = (0.5d - a)/3
Δ = bed form height
ζ = suspension parameter (originally denoted as Z in VR84b)
θ_{cr} = critical mobility parameter
κ = von Karman constant (0.4)
ν = kinematic viscosity of water
ρ = water density
ρ_s = sediment particle density (2.65 g/cm^3)
σ = standard deviation of the Gaussian distribution for incipient motion (0.57)
τ_b = bottom shear stress
$\tau_{c,k}$ = critical shear stress for size-class k
τ_{c50} = critical shear stress based on D_{50}

SECTION 6

REFERENCES

Abramowitz, M. and Stegun, I.A., 1972. *Handbook of Mathematical Functions*, National Bureau of Standards, Applied Mathematics Series 55, Washington, D.C.

Borah, D.K., Alonso, C.V. and Prasad, S.N., 1982. Routing Graded Sediments in Streams: Formulations, *J. Hydr. Engrg.*, ASCE, 108(12):1486-1503.

Carnahan, B., Luther, H.A. and Wilkes, J.O., 1969. *Applied Numerical Methods*, John Wiley & Sons, New York.

Cheng, N.S., 1997. Simplified Settling Velocity Formula for Sediment Particle, *J. Hydr. Engrg.*, ASCE, 123(2):149-152.

Garcia, M. and Parker, G., 1991. Entrainment of Bed Sediment Into Suspension, *J. Hydr. Engrg.*, ASCE, 117(4):414-435.

Gessler, J., 1967. *The Beginning of Bedload Movement of Mixtures Investigated as Natural Armoring in Channels*, W.M. Keck Laboratory of Hydraulics and Water Resources, California Institute of Technology, Translation T-5.

HydroQual, 1997. *Analysis of Sediment Loading to the Upper Hudson River During the April 1994 High Flow Event*, HydroQual report.

Jain, S.C., and Park, I., 1989. Guide for Estimating Riverbed Degradation, *J. Hydr. Engrg.*, ASCE, 115(3):356-366.

Karim, M.F. and Holly, F.M., 1986. Armoring and Sorting Simulation in Alluvial Rivers, *J. Hydr. Engrg.*, ASCE, 112(8):705-715.

Karim, M.F. and Kennedy, J.F., 1981. *Computer-Based Predictors for Sediment Discharge and Friction Factor of Alluvial Streams*, IIHR Report No. 242, Univ. of Iowa, Iowa City, Iowa.

Rahuel, J.L., Holly, F.M., Chollet, J.P., Belleudy, P.J. and Yang, G., 1989. Modeling of Riverbed Evolution for Bedload Sediment Mixtures, *J. Hydr. Engrg.*, ASCE, 115(11):1521-1542.

Shen, H.W. and Lu, J.Y., 1983. Development and Prediction of Bed Armoring, *J. Hydr. Engrg.*, ASCE, 109(4):611-629.

van den Berg, J.H. and van Gelder, A., 1993. Prediction of Suspended Bed Material Transport in Flows Over Silt and Very Fine Sand, *Water Resour. Res.*, 29(5):1392-1404.

van Niekerk, A., Vogel, K.R., Slingerland, R.L. and Bridge, J.S., 1992. Routing of Heterogeneous Sediments Over Movable Bed: Model Development, *J. Hydr. Engrg.*, ASCE, 118(2):246-279.

Vanoni, V.A., 1975. *Sedimentation Engineering*, ASCE, New York.

van Rijn, L.C., 1984a. Sediment Transport, Part I: Bed Load Transport, *J. Hydr. Engrg.*, ASCE, 110(10):1431-1456.

van Rijn, L.C., 1984b. Sediment Transport, Part II: Suspended Load Transport, *J. Hydr. Engrg.*, ASCE, 110(11): 1612-1638.

van Rijn, L.C., 1984c. Sediment Transport, Part III: Bed Forms and Alluvial Roughness, *J. Hydr. Engrg.*, ASCE, 110(12): 1732-1754.

van Rijn, L.C., 1993. *Principles of Sediment Transport in Rivers, Estuaries and Coastal Seas*, Aqua Publications, The Netherlands.

van Rijn, L.C., van Rossum, H. and Termes, P., 1990. Field Verification of 2-D and 3-D Suspended-Sediment Models, *J. Hydr. Engrg.*, ASCE, 116(10): 1270-1288.

Voogt, L., van Rijn, L.C. and van den Berg, J.H., 1991. Sediment Transport of Fine Sands at High Velocities, *J. Hydr. Engrg.*, ASCE, 117(7): 869-890.

Ziegler, C.K. and Nisbet, B., 1994. Fine-Grained Sediment Transport in Pawtuxet River, Rhode Island, *J. Hydr. Engrg.*, ASCE, 120(5): 561-576.

Appendix B

The Erosion Properties of Cohesive Sediments in the Upper Hudson River

Appendix B is a report prepared by
HydroQual, Inc., Mahwah, NJ
for
General Electric Company, Albany, NY
October 1995

CONTENTS

FIGURES

TABLES

SECTION 1
INTRODUCTION

The transport and fate of PCBs in the Upper Hudson River are greatly affected by sediment transport processes. Cohesive sediments are particularly important when considering the transport of PCBs in a riverine system because PCBs are hydrophobic and preferentially adsorb onto fine-grained particles, i.e., clay and silt. Another important factor that must be considered when studying sediment transport processes in a river is that the erosional properties of cohesive sediments (clay and silt) differ greatly from those of non-cohesive sediments (sand and gravel). Understanding and quantifying the long-term fate of PCBs in the Upper Hudson River therefore requires a realistic and accurate description of fine-grained sediment deposition and erosion processes in the river. As a step toward this goal, experimental studies have been conducted and the results analyzed in an effort to describe and quantify the erosion properties of cohesive sediments in this river.

The amount of sediment that can be eroded from a cohesive sediment bed, i.e., a bed primarily composed of clay, silt and organic matter, is generally referred to as *erosion potential* and has units of mass per unit area, e.g., milligrams per square centimeter (mg/cm^2). Erosion potential depends upon the properties of the bed and the shear stress applied to the bed, where shear stress is a measure of the force exerted on the bed by flowing water in a river. This information can then be used to estimate sediment erosion during various high flow events (floods). Previous studies of cohesive sediment transport in rivers, e.g., Fox River in Wisconsin (Gailani et al,. 1991) and Pawtuxet River in Rhode Island (Ziegler and Nisbet, 1994), have used laboratory and field data to determine parameter values that represent bed property effects on erosion. The results of these studies clearly indicate the need to obtain river-specific data if accurate predictions of cohesive sediment bed erosion are to be realized.

The river-specific nature of erosion potential prompted General Electric to conduct field and laboratory studies on cohesive sediments from the Upper Hudson River. Data

from these studies have been used to derive relationships between erosion and bed shear stress for each of the eight reaches from Fort Edward to Troy Dam, i.e., the Thompson Island Pool and the pools behind the other seven downstream dams. This information is of importance when considering the fate of PCB-contaminated sediments in this river system.

A formulation that has been shown to accurately and realistically predict erosion potential is presented in Section 2, i.e., Equation (2-1). Laboratory data were used to determine parameter values in Equation (2-1) that are applicable to the Upper Hudson River system. The values of these river-specific parameters are: m = 0.5, $T_{d,max}$ = 7 days and τ_0 = 1 dyne/cm^2. Data collected during a field study, using a device called a shaker, were used to calculate values of the reach-specific parameter, a_0, for each of the eight reaches in the Upper Hudson River, see Table 1-1 and Figure 1-1. Based upon field study data, setting the exponent n in Equation (2-1) equal to three for all of the reaches is a valid approximation in this riverine system.

Table 1-1. Reach Average Values of a_0

Reach	Mean a_0 (mg-day$^{1/2}$/cm^2)
8	0.071
7	0.079
6	0.135
5	0.116
4	0.340
3	0.140
2	0.067
1	0.192

Section 2 of this report reviews experimental research on cohesive sediment resuspension processes and then presents an equation for predicting cohesive sediment erosion that has been successfully used in sediment transport studies on other rivers. An example that highlights the importance of using river-specific data when evaluating the

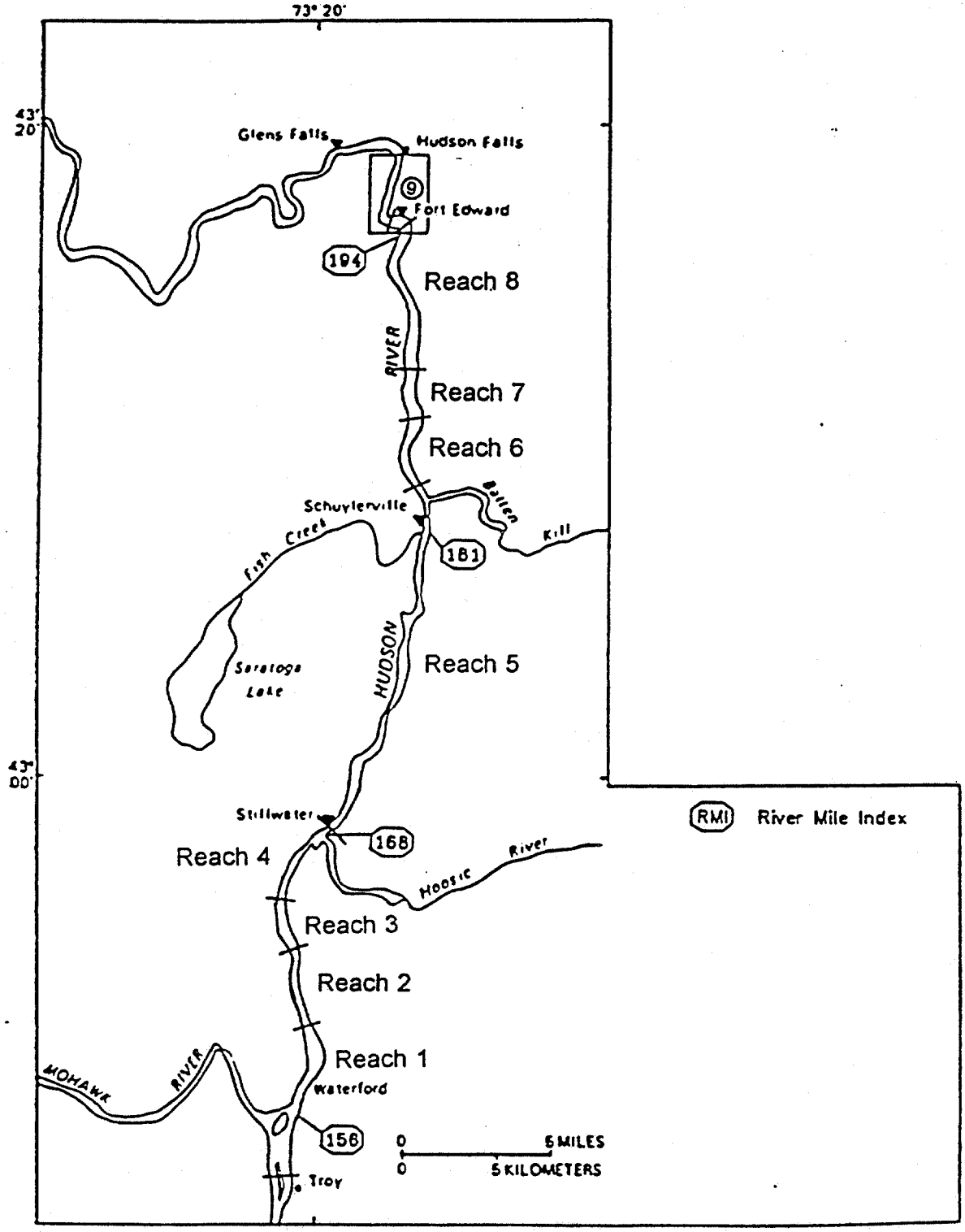

Figure 1-1. Reach identification for the Upper Hudson River.

erosional properties of cohesive sediments in the Upper Hudson River is also included in that section. Section 3 summarizes results of laboratory and field studies conducted on cohesive sediments from the Upper Hudson River. Based upon these experimental data, values of parameters in the resuspension formulation discussed in Section 2 have been determined for Upper Hudson River sediments. This report concludes with a summary of pertinent results.

SECTION 2
COHESIVE SEDIMENT RESUSPENSION PROCESSES

Laboratory and field studies on the resuspension properties of fine-grained, cohesive sediments have been conducted by a number of researchers during the last thirty to forty years, with important contributions being made by R.B. Krone (1962), E. Partheniades (1965), A.J. Mehta (1985) and W. Lick (1990). Results of this research have shown that resuspension from a cohesive sediment bed is significantly affected by the wide range of particle sizes, typically varying over two orders of magnitude in the bed of a river, and interparticle cohesion. Compaction effects increase with increasing depth in the bed, as indicated by a decrease in bed porosity with depth, causing surface sediments to be more easily resuspended than sediments buried deeper in the bed. Bed particle size heterogeneity and compaction effects cause bed armoring, which is the observed phenomenon that only a finite amount of sediment can be resuspended from a cohesive sediment bed at a particular bottom shear stress. Cohesive bed armoring has been observed and quantified in various laboratory (Parchure and Mehta, 1985; Tsai and Lick, 1987; Graham et al., 1992) and field studies (Hawley, 1991; Amos et al., 1992). This property of cohesive sediment beds does not extend to a bed composed of non-cohesive, uniform size sediments, e.g., sands, which have a constant erosion rate (Massion, 1982).

The amount of cohesive sediment resuspended at a specific bottom shear stress depends on the turbulent stress at the sediment-water interface and the state of compaction of the bed (Krone, 1962; Lee et al., 1981; Parchure and Mehta, 1985; Lick and Kang, 1987; Tsai and Lick, 1987; MacIntyre et al., 1990). Analysis of laboratory and field data has indicated that the following relationship is valid (Gailani et al., 1991)

$$\epsilon = \frac{a_o}{T_d^m}\left(\frac{\tau - \tau_o}{\tau_o}\right)^n, \qquad \tau \geq \tau_o \tag{2-1}$$

where ϵ = net mass of resuspended sediment per unit surface area (mg/cm^2); a_o = site-specific constant; T_d = time after deposition in days; m and n are dependent upon the

deposition environment; τ = bottom shear stress due to currents; and τ_0 = effective critical shear stress.

The resuspension properties of cohesive beds can differ substantially (Gailani et al., 1991; Ziegler and Nisbet, 1994). Variability of erosion characteristics between rivers is reflected in Equation (2-1) parameter values, with data from different rivers indicating that the exponent n can range from two to three and the constant a_0 may vary by an order of magnitude. As will be shown in Section 3, laboratory work on Upper Hudson River sediments has suggested that m in Equation (2-1), which accounts for compaction effects, may vary from 0.5 to 2, depending upon deposition environment.

The U.S. Environmental Protection Agency (USEPA) has proposed to use Equation (2-1) in their Upper Hudson River modeling effort, but with parameter values determined from other river systems (Rodgers and Bierman, 1993). This approach may result in significant errors in predictions of cohesive sediment erosion and it should not be considered. Instead, the results of laboratory and field studies on Upper Hudson River cohesive sediments that are presented in this report should be used.

The importance of using river-specific parameters when applying Equation (2-1) to the Upper Hudson River is illustrated by the following example. A comparison of the resuspension potential functions for the Thompson Island Pool, the Fox River in Wisconsin (Gailani et al.. 1991) and Pawtuxet River in Rhode Island (Ziegler and Nisbet, 1994) is shown on Figure 2-1. Data used to develop the erosion potential function for the Thompson Island Pool will be discussed in Section 3. The horizontal axis of the graph is bed shear stress (dynes/cm^2) and this quantity is related to river flow rate, i.e., as flow rate increases so does the bed shear stress at a given location. The vertical axis of the graph is erosion potential (mg/cm^2).

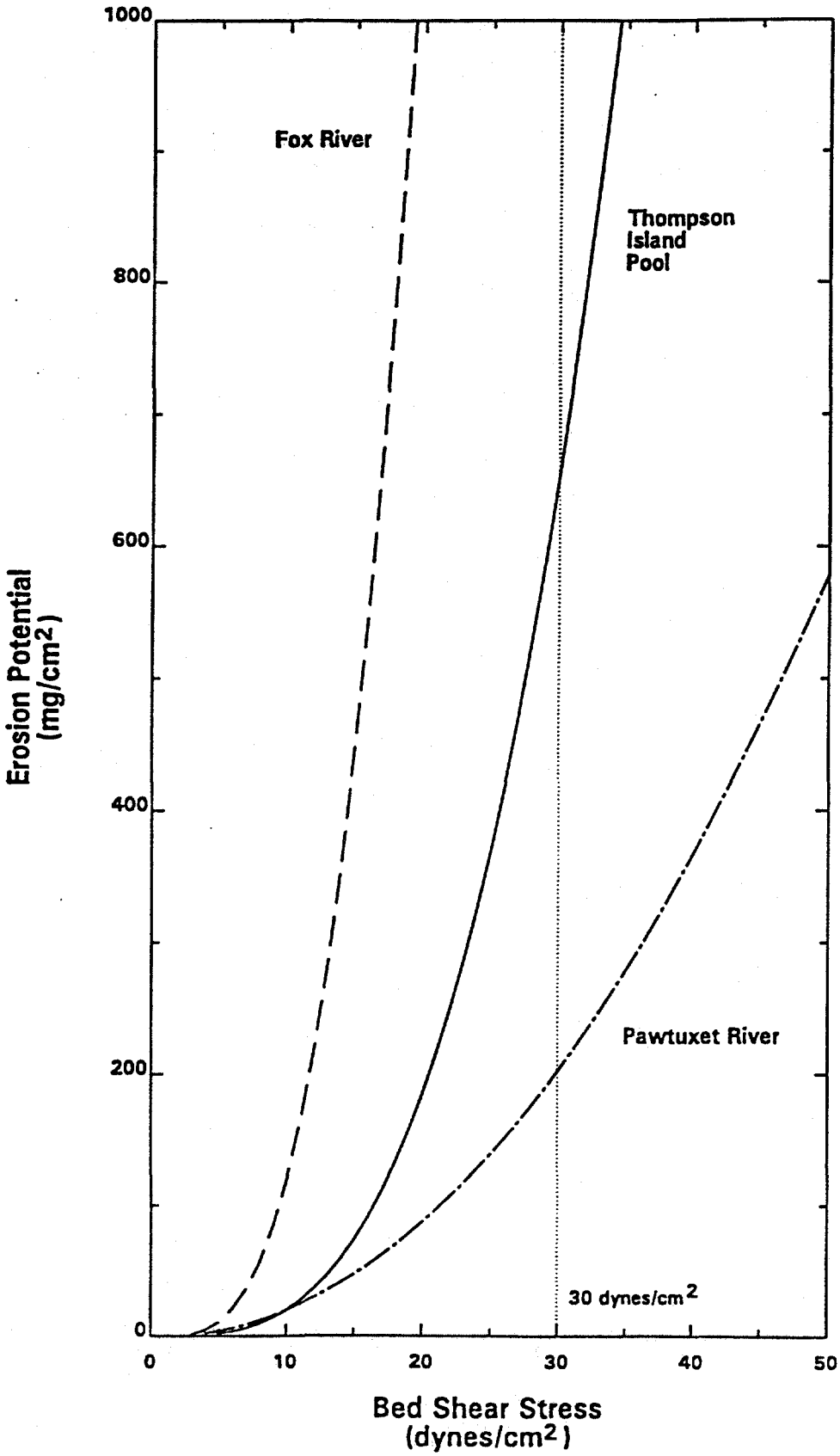

Figure 2-1. Comparison of resuspension potential functions for Thompson Island Pool, Fox River and Pawtuxet River.

The erosion potential functions for the three rivers shown on this figure all have the same functional form; the differences arise from the river-specific characteristics of the cohesive bed. To emphasize the importance of obtaining river-specific erosion potential data, consider the erosion potential predicted in the three different rivers at a bed shear stress of 30 dynes/cm^2. This bed shear stress approximately corresponds to the average bed shear stress in the Thompson Island Pool during a high flow event (flood). The predicted erosion potentials are 660, 3980 and 200 mg/cm^2, respectively, in the Thompson Island Pool, Fox River and Pawtuxet River. Using data from other riverine systems to predict erosion potential in the Thompson Island Pool could thus generate significant errors. In this case, using Fox River or Pawtuxet River data would result in errors of 600% (high) or -70% (low). Therefore, river-specific resuspension values, developed from Upper Hudson River data, should be used when applying Equation (2-1) if accurate predictions of erosion in this riverine system are to be realized.

SECTION 3
EROSION POTENTIAL DATA ANALYSIS

As discussed in Section 2, the resuspension properties of cohesive sediments can vary considerably from one riverine system to another. Hence, parameter values in Equation (2-1), e.g., a_0 and n, should be based upon data from field and laboratory studies on cohesive sediments from the Upper Hudson River. This section presents the results of studies on the erosion properties of Upper Hudson River sediments. Laboratory investigations, using an annular flume, were performed to study bed compaction effects on the resuspension of cohesive sediments deposited in a riverine environment and to estimate critical shear stress values. Measurements of in situ resuspension potential throughout the Upper Hudson River were made using established procedures applied in other river systems (Tsai and Lick, 1986; Gailani et al., 1991; Ziegler and Nisbet, 1994). Analyses of the field and laboratory data were also done to determine river-specific values of parameters in Equation (2-1).

3.1 Laboratory Study Results

Previous laboratory studies have used an annular flume to investigate various aspects of cohesive sediment resuspension (e.g., Tsai and Lick, 1987; MacIntyre et al., 1990). Annular flume studies were conducted to determine erosional properties of cohesive sediments in the Upper Hudson River. These flume studies were used to derive Upper Hudson River specific values of T_d, m and τ_0 in Equation (2-1). The procedure used to determine values of a_0 and n in that equation are described in the next sub-section.

Appendix A contains details on laboratory procedures, data presentation and subsequent analysis. The results of the flume studies indicate that the critical shear stress, τ_0, for Upper Hudson River sediments is approximately one dyne/cm^2, which is the same value used in other riverine sediment transport studies (Gailani et al., 1991; Ziegler and Nisbet, 1994). The maximum time of deposition, $T_{d,max}$, was found to be approximately seven days. This statement means that all cohesive sediments in the bed

with an age of seven days or greater will be assumed to be seven days old when applying Equation (2-1). Finally, results of the annular flume experiments indicated that the exponent m should have a value of 0.5 for cohesive sediment beds formed under continuous flow conditions, as is typically found in rivers.

3.2 Field Study Results

A field study was conducted during November, 1990 to measure the in situ resuspension potential of fine-grained, cohesive sediments in the Upper Hudson River. These measurements were made using a portable resuspension device, commonly called a shaker, and a procedure developed by Tsai and Lick (1986). The methods used in this study, a tabulation of the raw data and analysis of these data are presented in Appendix B.

The data analysis indicates that the exponent n in Equation (2-1) is approximately three for all of the eight reaches in the Upper Hudson River. However, the site-specific parameter, a_0, is spatially variable and needs to be specified as an average value for each of the eight reaches. The reach mean values of a_0 ranged from 0.067 to 0.340 mg-day$^{1/2}$/cm^2 and are tabulated in Table B-2.

SECTION 4
SUMMARY

A formulation that expresses the mass of sediment resuspended from a cohesive sediment bed as a function of bed shear stress, Equation (2-1), has been successfully applied in sediment transport studies on several river systems and the USEPA has indicated that it will also be used in their modeling effort on the Upper Hudson River. As discussed in Section 2, Equation (2-1) contains river-specific parameters which must be determined from resuspension studies of cohesive sediments in the Upper Hudson River.

This data requirement has been met as a result of laboratory and field studies. The results of these studies, which are discussed in detail in Appendices A and B, indicate that the parameters in Equation (2-1) should have the following values for all of the eight reaches in the Upper Hudson River: $m = 0.5$, $T_{d,max} = 7$ days, $n = 3$ and $\tau_o = 1$ dyne/cm^2. The reach-specific constant, a_o, needs to be specified as an average value for each of the eight reaches, see Table 1-1.

SECTION 5
REFERENCES

Amos, C.L., Grant, J. Daborn, G.R. and Black, K., 1992. Sea Carousel - A Benthic, Annular Flume, Estuarine, Coast. and Shelf Sci., 34:557-577.

Gailani, J., Ziegler, C.K. and Lick, W., 1991. The Transport of Suspended Solids in the Lower Fox River, J. of Great Lakes Res., 17(4):479-494.

Graham, D.I., James, P.W., Jones, T.E.R., Davies, J.M. and Delo, E.A., 1992. Measurement and Prediction of Surface Shear Stress in Annular Flume, ASCE J. Hydr. Engr., 118(9):1270-1286.

Hawley, N., 1991. Preliminary Observations of Sediment Erosion from a Bottom Resting Flume, J. Great Lakes Res., 17(3):361-367.

Krone, R.B., 1962. Flume Studies of the Transport of Sediment in Estuarial Processes, Final Report, Hydraulic Engineering Laboratory and Sanitary Engineering Research Laboratory, Univ. of California, Berkeley, California.

Lee, D.Y., Lick, W. and Kang, S.W., 1981. The Entrainment and Deposition of Fine-Grained Sediments, J. Great Lakes Res., 7:224-233.

Lick, W. and Kang, S.W., 1987. Entrainment of Sediments and Dredged Materials in Shallow Lake Waters, J. Great Lakes Res., 13(4):619-627.

Lick, W., Xu, Y.J. and McNeil, J., 1995. Resuspension Properties of Sediments from the Fox, Saginaw, and Buffalo Rivers, J. Great Lakes Res., 21(2):257-274.

MacIntyre, S., Lick, W. and Tsai, C.H., 1990. Variability of Entrainment of Cohesive Sediments in Freshwater, Biogeochemistry, 9:187-209.

Massion, E., 1982. The Resuspension of Uniform-Sized Fine-Grained Sediments, M.S. thesis, University of California, Santa Barbara.

Parchure, T.M. and Mehta, A.J., 1985. Erosion of Soft Cohesive Sediment Deposits, ASCE J. Hyd. Engr., 111(10):1308-1326.

Partheniades, E., 1965. Erosion and Deposition of Cohesive Sediments, J. Hydr. Div., ASCE, 91(1):105-139.

Rodgers, P.W. and Bierman, V.J., 1993. Proposed (Revised) Technical Approach for Short-Term Event Model for Thompson Island Pool, LTI Memorandum, October 4, 1993.

Tsai, C.H. and Lick, W., 1986. A Portable Device for Measuring Sediment Resuspension, J. of Great Lakes Res., 12(4):314-321.

Tsai, C.H. and Lick, W., 1987. Resuspension of Sediments from Long Island Sound, Wat. Sci. Tech., 21(6/7):155-184.

Xu, Y.J., 1991. Transport Properties of Fine-Grained Sediments, Ph.D. dissertation, University of California, Santa Barbara.

Ziegler, C.K. and Nisbet, B., 1994. Fine-Grained Sediment Transport in Pawtuxet River, Rhode Island, ASCE J. Hyd. Engr., 120(5):561-576.

APPENDIX A
LABORATORY STUDY METHODS AND RESULTS

A.1 Sediment Sample Collection

Cohesive sediment samples for the laboratory study were collected from three different locations in the Thompson Island Pool (Reach 8), see Figures A-1 and 1-1. Approximately twenty-five gallons of sediment were collected at each site on December 6, 1990. A Ponar grab sampler was used to collect surficial sediments. The sediments were placed in three separate plastic garbage cans and sealed.

Sediment sample 1 was collected in water four to six feet deep about five to fifteen feet from shore. This sediment had a grayish silty appearance and also contained some leaves. Sample 2 appeared to be very muddy and had a gelatinous consistency. This sediment was obtained in five to six feet of water at a distance of forty feet from shore. Sample 3 was taken about ten to fifteen feet east of the island shore in four to nine feet of water. This sample appeared to have a sand content lower than sample 1 but higher than sample 2. Subsequent grain size analysis of the samples showed that samples 1, 2 and 3 had average clay/silt contents of 55, 51 and 21 percent, respectively.

The sediments were allowed to compact and dewater in the garbage cans for approximately two weeks after collection. The sediments were then transferred to plastic containers, which were lined with plastic garbage sacks to prevent leakage, and shipped to the University of California at Santa Barbara (UCSB) on December 28, 1990.

A.2 Annular Flume Experiments and Results

An annular flume at UCSB was used to study the resuspension properties of the cohesive sediments collected from the Thompson Island Pool. An illustration of the flume is shown on Figure A-2. This flume has been used extensively to study the properties of

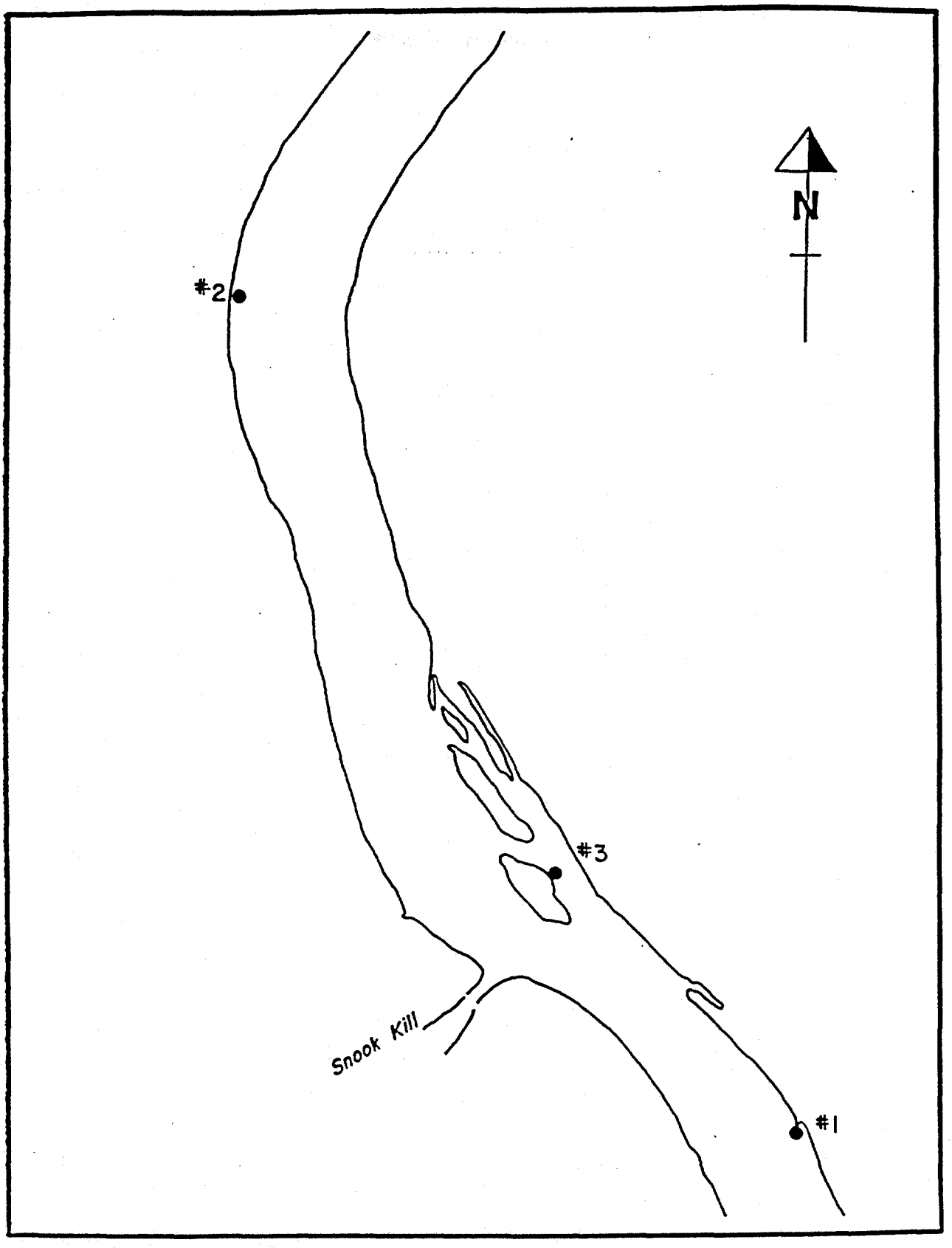

Figure A-1. Locations in the Thompson Island Pool of sediment samples used for flume experiments.

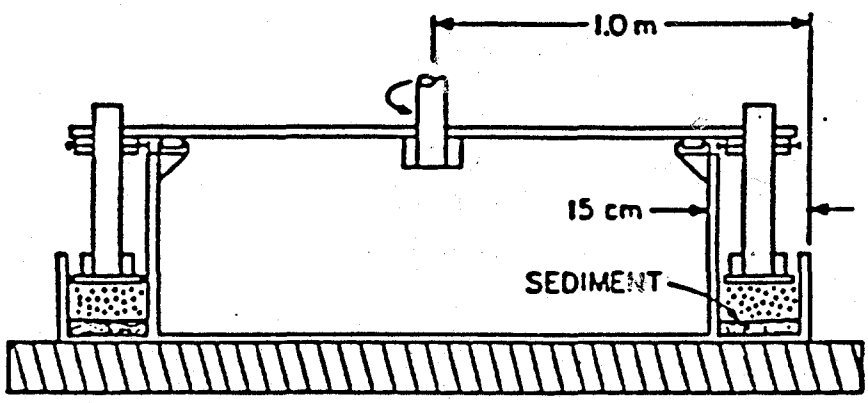

Figure A-2. Schematic of the annular flume.

cohesive sediments from other aquatic systems. Details of flume calibration and operating procedure are discussed in MacIntyre et al., 1990 and Xu, 1991.

The primary objective of the flume experiments was to investigate the effects of bed compaction of sediment resuspension. Two types of experiments were performed to study bed compaction: multiple shear stress tests and a continuous flow test. The procedures and results for these two investigations are presented in the next two sub-sections.

Another goal of these experiments was to estimate the critical shear stress, τ_0, of surficial sediments in the Upper Hudson River. This parameter, which is used in Equation (2-1), is difficult to measure directly. Typically, the value of τ_0 is estimated by observation in the following way. At the beginning of a flume experiment, the applied bed shear stress in the flume is slowly increased from zero until the point at which sediment is first observed to be resuspended from the bed. This shear stress is then estimated to be the critical shear stress for erosion of surficial sediments, which is what is used in Equation (2-1). Results of the flume tests on Thompson Island Pool sediments indicated a critical shear stress of approximately one dyne/cm^2.

A.2.1 Multiple Shear Stress Tests

Multiple shear stress tests were performed on each sediment sample using the following procedure. The flume was filled with sediment to a depth of approximately 6 cm and an overlying water depth of about 7.5 cm. After creating a sediment bed in the flume, the bed was allowed to compact for 1, 3 or 14 days prior to running the experiment. No shear stress was applied to the bed, i.e., the flume was not running, during the compaction period. A total of nine multiple shear stress tests were run; three compaction times were used for each of the three sediment samples.

At the end of the compaction time, the experiment was started by rotating the lid of the flume at a constant speed which corresponded to a bed shear stress of 1 dyne/cm^2.

Some sediment was resuspended and the sediment concentration in the flume water increased, rapidly at first and then more slowly until steady-state was reached. The suspended sediment concentration was measured every thirty minutes. After the sediment concentration reached steady-state, which took about two hours, the speed of the lid was increased until a shear stress of 3 dynes/cm^2 was reached and more sediment was resuspended. The sediment concentration sampling was continued at thirty minute intervals until steady-state was reached for a shear stress of 3 dynes/cm^2. The multiple shear stress test was continued by repeating this procedure for shear stresses of 5, 7, 9 and 11 dynes/cm^2.

Generally, no significant problems were encountered during these flume tests. However, gross bed erosion did occur during some of the tests, where gross bed erosion was defined as the formation in the sediment bed of channels with a depth greater than 1 cm. For sample 1 with one day compaction, the bed began to break down at 580 minutes and a shear stress of 11 dynes/cm^2. The bed was quite uneven and possibly eroded all the way to the bottom of the flume in spots. The sediment bed became non-uniform at 11 dynes/cm^2 for sample 1 with a three day compaction time. The multiple shear stress test for sample 2 had to be stopped at 7 dynes/cm^2 for compaction times of one and three days and at 9 dynes/cm^2 for fourteen days of compaction. Tests on sample 3 were concluded at 7 dynes/cm^2 with one day compaction and at 9 dynes/cm^2 for three day compaction. Gross bed erosion was the cause of the test stoppages for samples 2 and 3.

Measured suspended sediment concentrations for the multiple shear stress tests for samples 1, 2 and 3, with compaction times of 1, 3 and 14 days, are listed in Tables A-1, A-2 and A-3, respectively. Graphical plots of the data are presented on Figures A-3, A-4 and A-5.

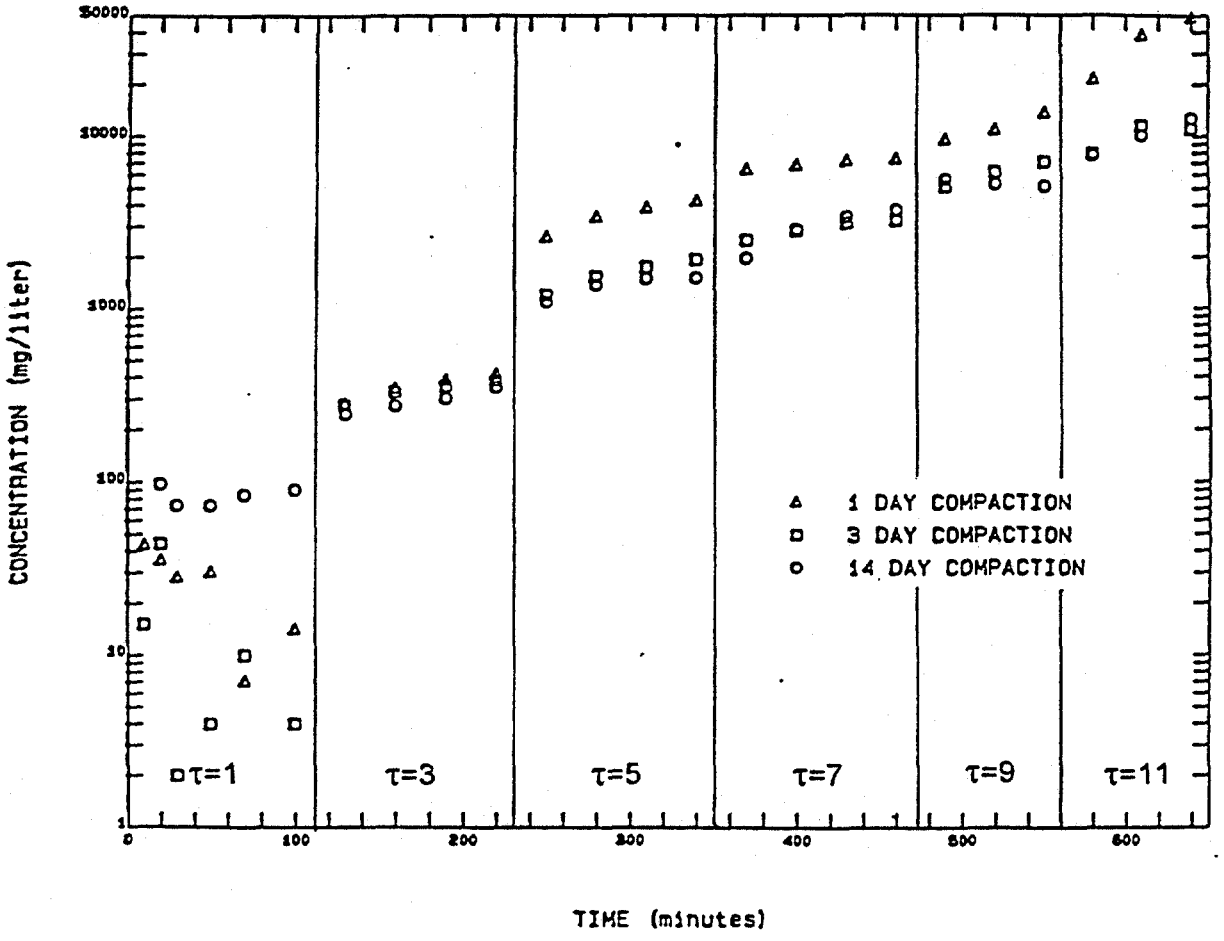

Figure A-3. Flume data from multiple shear stress tests for sample 1. Shear stress (τ) is in dynes/cm^2.

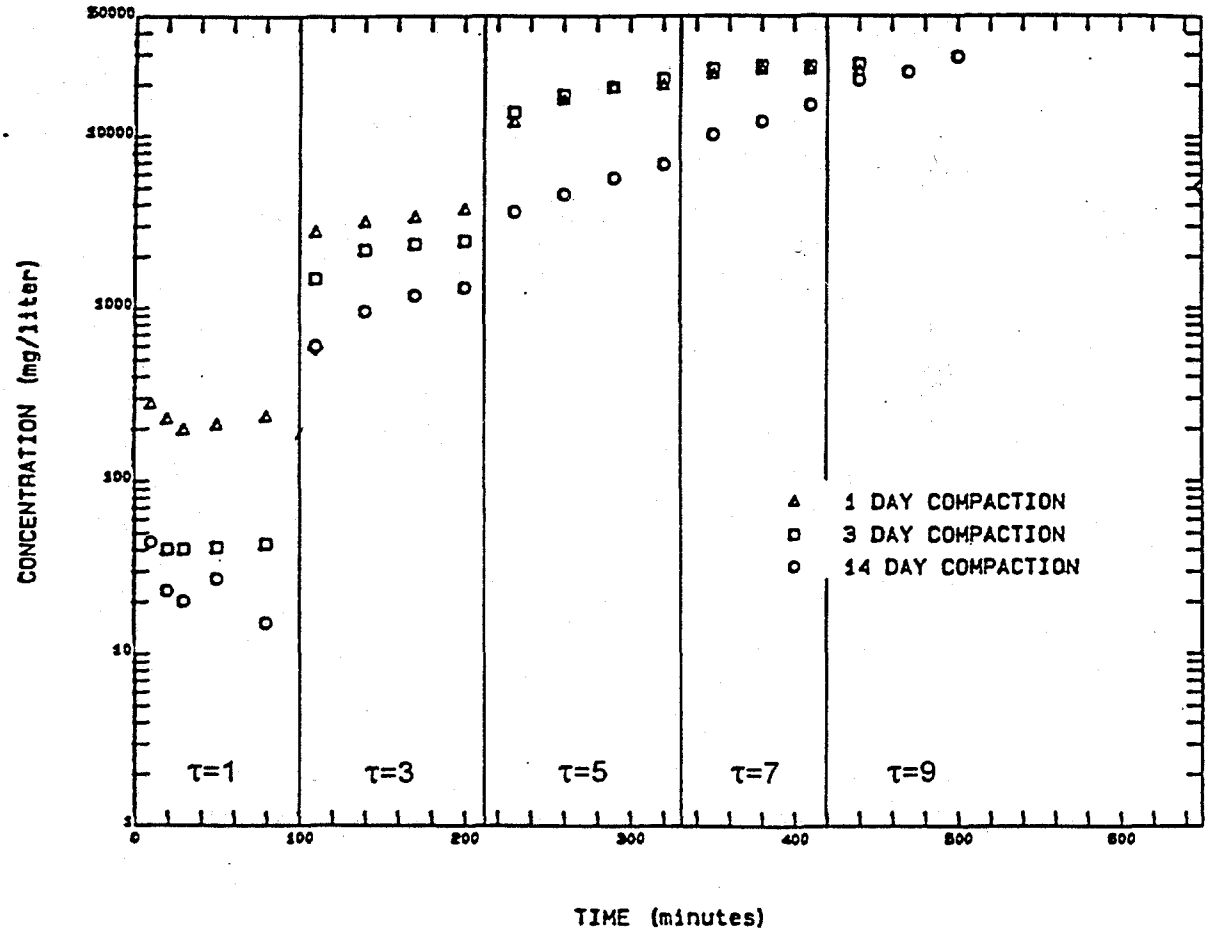

Figure A-4. Flume data from multiple shear stress tests for sample 2. Shear stress (τ) is in dynes/cm^2.

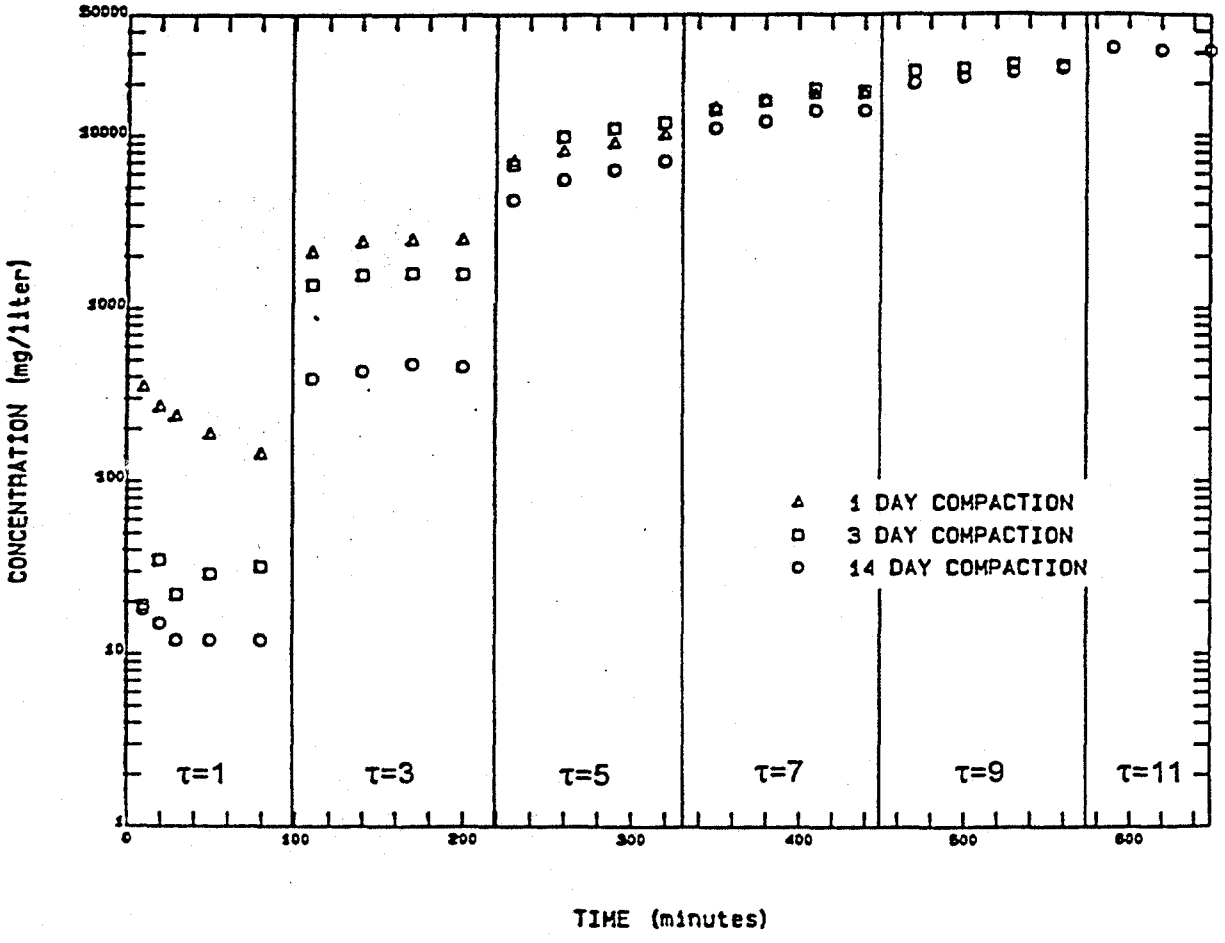

Figure A-5. Flume data from multiple shear stress tests for sample 3. Shear stress (τ) is in dynes/cm^2.

TABLE A-1. FLUME DATA FROM MULTIPLE SHEAR STRESS TESTS FOR SAMPLE 1 WITH COMPACTION TIMES OF 1, 3 AND 14 DAYS				
Shear Stress ($dynes/cm^2$)	Run time (minutes)	Concentration (mg/l)		
		1 day	3 days	14 days
1	10	43	15	--
	20	35	44	97
	30	28	2	73
	50	30	4	73
	70	7	10	84
	100	14	4	90
3	130	282	278	246
	160	344	330	274
	190	384	358	302
	220	414	384	350
5	250	2,596	1,204	1,102
	280	3,404	1,546	1,388
	310	3,852	1,760	1,510
	340	4,210	1,940	1,522
7	370	6,340	2,496	1,964
	400	6,720	2,830	2,876
	430	7,100	3,135	3,404
	460	7,270	3,235	3,725
9	490	9,440	5,110	5,590
	520	10,760	6,180	5,260
	550	13,540	7,100	5,140
11	580	21,280	7,960	7,700
	610	38,080	11,560	10,160
	640	48,400	11,120	12,780

TABLE A-2. FLUME DATA FROM MULTIPLE SHEAR STRESS TESTS FOR SAMPLE 2 WITH COMPACTION TIMES OF 1, 3 AND 14 DAYS				
Shear Stress ($dynes/cm^2$)	Run Time (minutes)	Concentration (mg/l)		
		1 day	3 days	14 days
1	10	277	--	44
	20	226	40	23
	30	196	40	20
	50	210	41	27
	80	234	43	15
3	110	2,774	1,490	606
	140	3,158	2,190	960
	170	3,373	2,363	1,183
	200	3,740	2,467	1,320
5	230	11,927	13,640	3,640
	260	16,220	17,280	4,595
	290	19,220	19,420	5,740
	320	19,850	21,590	6,880
7	350	22,900	24,570	10,160
	380	24,310	25,670	12,120
	410	24,190	25,340	15,110
9	440	23,980	26,340	21,260
	460	--	--	23,760
	490	--	--	29,020

TABLE A-3. FLUME DATA FROM MULTIPLE SHEAR STRESS TESTS FOR SAMPLE 3 WITH COMPACTION TIMES OF 1, 3 AND 14 DAYS				
Shear Stress ($dynes/cm^2$)	Run Time (minutes)	Concentration (mg/l)		
		1 day	3 day	14 days
1	10	350	19	18
	20	269	35	15
	30	237	22	12
	50	186	29	12
	80	143	32	12
3	110	2,100	1,368	390
	140	2,400	1,556	430
	170	2,476	1,596	474
	200	2,488	1,578	458
5	230	7,053	6,760	4,216
	260	8,033	9,750	5,520
	290	8,960	10,915	6,255
	320	10,067	11,795	7,065
7	350	14,450	14,067	11,040
	380	15,970	15,853	12,053
	410	17,140	18,527	13,907
	440	17,330	17,960	13,880
9	470	--	23,380	19,900
	500	--	24,180	21,640
	530	--	25,520	23,140
	560	--	25,140	24,320
11	590	--	--	31,930
	620	--	--	30,920
	650	--	--	30,950
	680	--	--	30,710

A.2.2 Continuous Flow Experiment

The multiple shear stress tests were performed on sediment beds in the flume that were compacted under zero flow conditions. Other flume research (Xu, 1991) has indicated that the flow environment under which bed compaction takes place affects the resuspension potential of fine-grained, cohesive sediments. A continuous flow, such as in a river, appears to slow the rate at which compaction effects modify the resuspension properties of cohesive sediments, when compared with similar sediments that undergo compaction in a quasi-quiescent flow, i.e., a lake. In an attempt to quantify these effects, a multiple shear stress test was conducted on a sediment bed that had been subjected to compaction under continuous flow conditions.

The sediment bed in the continuous flow experiment was prepared in the same manner as the previous multiple shear stress tests and sediment from sample location 2 was used. After initial formation of the bed, the flume was run continuously for 47 days, from July 20, 1991 until September 5, 1991, at a shear stress of about 1 dyne/cm^2. A short, medium-strength resuspension event was simulated on days 7, 21, 28 and 35 by increasing the shear stress to 5 dynes/cm^2 for two hours, after which the shear stress was decreased to 1 dyne/cm^2. On day 42, a complete multiple shear stress test was conducted, as described in Section A.2.1, with the exception that the maximum shear stress was 13 dynes/cm^2. The shear stress was then decreased to 1 dyne/cm^2 for five additional days and then a final 5 dyne/cm^2 shear test was conducted on day 47. The sediment concentration in the flume was measured daily during constant 1 dyne/cm^2 flow conditions. During the 5 dyne/cm^2 and multiple shear stress tests, water column concentrations were measured at thirty minute intervals. The sediment concentration data for this experiment are listed in Table A-4.

TABLE A-4. FLUME DATA FROM LONG TERM COMPACTION TEST			
Date	Sheer Stress (dynes/cm^2)	Run Time (minutes)	Concentration (mg/l)
7/21/91	1		66
7/22/92	1		120
7/23/91	1		164
7/24/91	1		172
7/25/91	1		292
7/26/91	1		246
7/27/91	1		312
	5	15	4,085
	5	30	5,440
	5	60	7,480
	5	90	8,267
	5	120	9,153
7/28/91	1		194
7/29/91	1		148
7/30/91	1		112
7/31/91	1		154
8/01/91	1		206
8/02/91	1		160
8/04/91	1		152
8/05/91	1		118
8/06/91	1		166
8/07/91	1		158
8/08/91	1		174
8/09/91	1		72
8/10/91	1		44
	5	15	1,383
	5	30	1,547
	5	60	1,767
	5	90	1,827
	5	120	1,947
8/11/91	1		396

TABLE A-4. FLUME DATA FROM LONG TERM COMPACTION TEST (continued)

Date	Sheer Stress ($dynes/cm^2$)	Run Time (minutes)	Concentration (mg/l)
8/12/91	1		290
8/13/91	1		234
8/14/91	1		242
8/15/91	1		162
8/16/91	1		160
8/17/91	1		134
	5	15	1,700
	5	30	1,807
	5	60	1,970
	5	90	2,010
	5	120	2,103
8/18/91	1		270
8/20/91	1		194
8/21/91	1		144
8/22/91	1		140
8/23/91	1		66
8/24/91	1		18
	5	15	1,623
	5	30	1,693
	5	60	1,913
	5	90	1,927
	5	120	1,957
8/25/91	1		98
8/26/91	1		82
8/27/91	1		112
8/28/91	1		78
8/29/91	1		96
8/30/91	1		52
8/31/91	1		60
	3	15	515
	3	30	590
	3	60	657

TABLE A-4. FLUME DATA FROM LONG TERM COMPACTION TEST (continued)			
Date	Sheer Stress ($dynes/cm^2$)	Run Time (minutes)	Concentration (mg/l)
	3	90	750
	3	120	777
	5	150	1,443
	5	180	1,600
	5	210	1,650
	5	240	1,740
	7	270	2,100
	7	300	2,155
	7	330	2,260
	7	360	2,250
	9	390	2,813
	9	420	3,113
	9	450	3,300
	9	480	3,373
	11	510	4,407
	11	540	4,780
	11	570	5,133
	11	600	5,333
	13	630	6,707
	13	660	7,187
	13	690	8,513
	13	820	9,213
9/3/91	1		198
9/5/91	5	15	1,623
	5	30	1,703
	5	60	1,773
	5	90	1,927
	5	120	1,920

No equipment malfunctions occurred during this experiment. Visual observations of the sediment bed in the flume indicated the presence of many small, thin worms, less than 1 cm in length, working the surface of the bed. The worms dug burrows into the bed

and their heads protruded out of the bed to feed. This bioturbation formed a loose, thin layer of sediment approximately 0.2 cm thick.

No gross bed erosion occurred during the multiple shear stress at day 42, which was significantly different than the previous multiple shear stress tests during which the bed typically became unstable at about 9 dynes/cm^2. The bed remained level, even at 11 dynes/cm^2. However, during the 13 dynes/cm^2 portion of the test, the bed became wavy and unstable. Examination of the bed after completion of the experiment indicated that the bed had a gelatinous consistency which was nearly uniform from top to bottom.

A.3 Data Analysis

The flume experiments described in Section A.2 produced data that can provide insight into the effects of compaction under continuous flow conditions. Sediment concentrations measured in the flume are directly related to the mass of sediment resuspended from the bed, so this data can be used to evaluate erosional effects due to compaction. The T_d^{-m} term in Equation (2-1) accounts for compaction effects; the mass of sediment resuspended decreases with increasing time after deposition, which is correlated with bed compaction. However, two questions about the T_d^{-m} term must be answered before applying Equation (2-1). First, at what time after deposition do compaction effects on resuspension of surficial sediments become negligible? Second, what is the value of the exponent m?

The continuous flow experiment results can be used to approximately answer the first question. Previous research has suggested that the effects of compaction on the resuspension of surficial cohesive sediments become insignificant approximately seven to fourteen days after deposition (Tsai and Lick, 1987; MacIntyre et al., 1990). Results of the continuous flow experiment indicate that bed compaction effects become negligible at seven days or less after deposition. This finding can be demonstrated by examining a time history plot of the water column sediment concentration data during the 47 day test period, see Figure A-6.

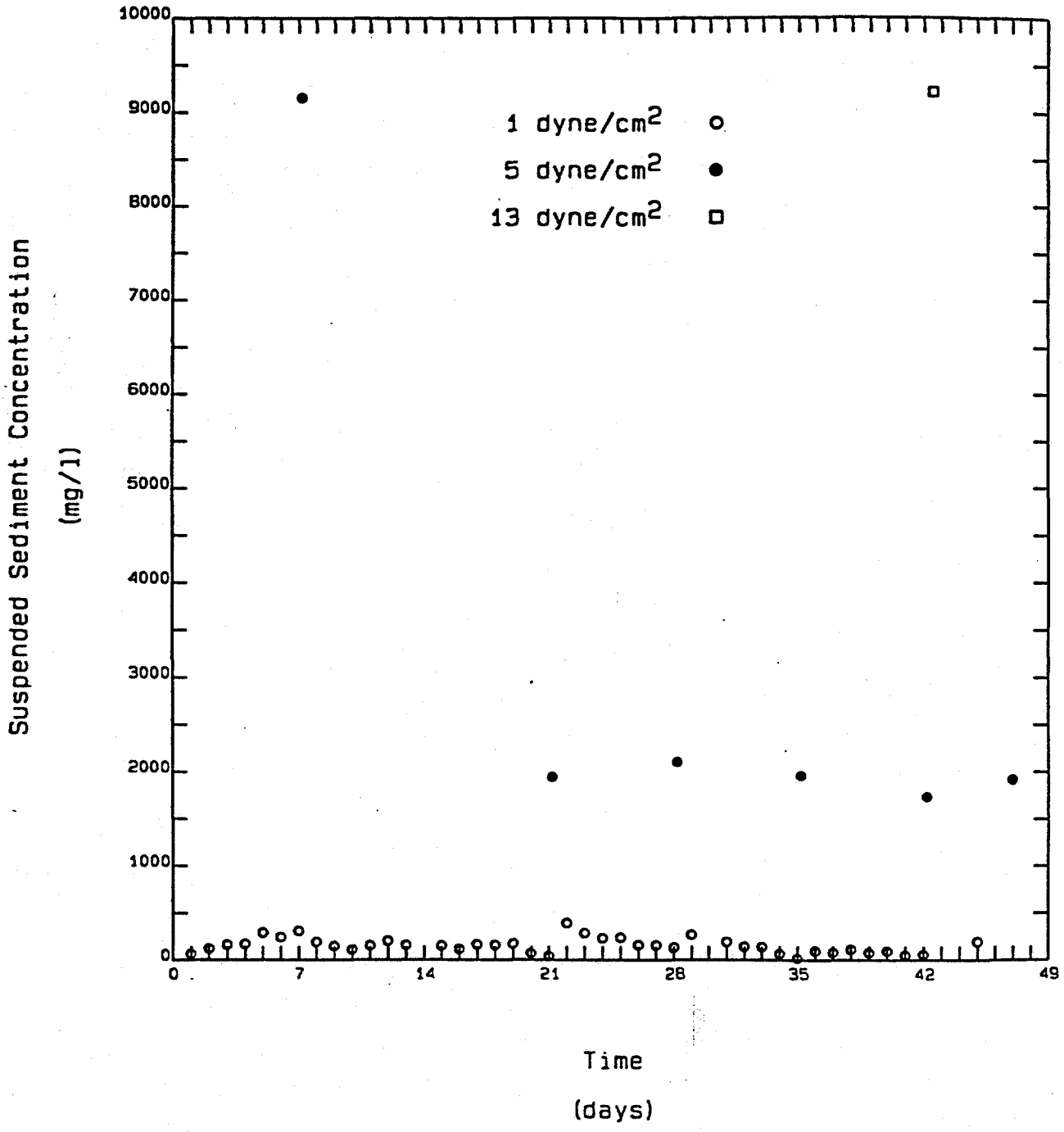

Figure A-6. Flume data from continuous flow experiment.

First, note that the sediment concentration at the 5 dyne/cm^2 shear stress test on day 7 is much higher than measured values at the same shear stress on days 14, 21, 28, 35, 42 and 47. After day 7, the sediment concentration for an applied shear stress of 5 dynes/cm^2 is very repeatable ($\pm$9% and coefficient of variation = 0.07). This result shows that the bed created in the flume has changed characteristics after the first 5 dyne/cm^2 resuspension event. As a result of the day 7 resuspension event, the sediment in the flume has changed from a bed created under static conditions to a bed formed in a depositional environment under continuous flow conditions.

The 5 dyne/cm^2 resuspension events on days 21, 28, 35, 42 and 47 had times of deposition of 14, 7, 7, 7 and 5 days, respectively. However, all five events had approximately the same mass of sediment resuspended in the flume. This result indicates that the effects of compaction on resuspension were about the same for sediments deposited for 5 , 7 or 14 days. Based on these data, a valid assumption when applying Equation (2-1) is that the maximum time of deposition, $T_{d,max}$, of a cohesive sediment bed in a riverine environment is seven days. This statement means that all sediments in the bed with an age of seven days or greater can be assumed to be seven days old when using Equation (2-1). These results are consistent with experimental work done by Lick et al. (1995) on the effects of consolidation on resuspension of fine-grained sediments from the Fox, Saginaw and Buffalo Rivers.

Earlier flume studies on sediments deposited in a quiescent environment have shown that exponent m in Equation (2-1) has a value of approximately two (Tsai and Lick, 1987). To determine if this value is appropriate for river sediments, the multiple shear stress data was plotted as a function of compaction time, see Figure A-7. The data on this plot has been normalized with respect to shear stress, i.e.,

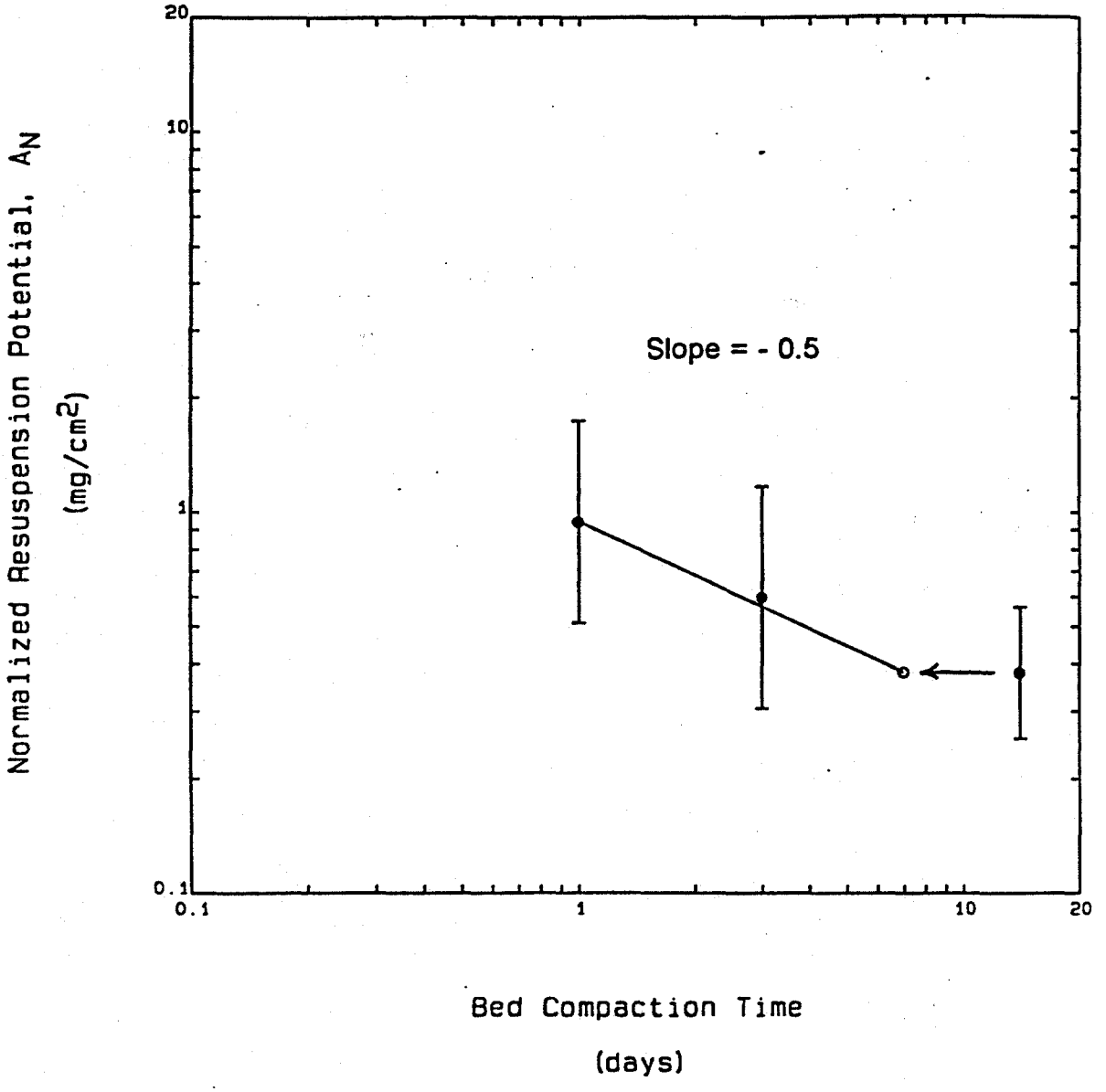

Figure A-7. Effect of bed compaction on resuspension of cohesive sediments deposited in a continuous flow environment.

$$A_N = \frac{a_o}{T_d^m} = \epsilon_M \left(\frac{\tau - \tau_o}{\tau_o}\right)^{-n} \qquad \text{(A-1)}$$

where A_N = normalized resuspension potential (mg/cm^2) and ϵ_M = measured mass of eroded sediment per unit area (mg/cm^2). This normalization allows resuspension data obtained at different shear stresses to be compared. Furthermore, the slope of a log linear regression line, for A_N as a function of T_d, corresponds to the exponent m, which can be seen from a log transform of A_N,

$$\log A_N = \log a_o - m \log T_d \qquad \text{(A-2)}$$

Using the finding from the continuous flow experiment that compaction effects are negligible after about seven days of deposition, the assumption can be made that the log mean of the fourteen day data from the multiple shear stress test is approximately equal to what would have been measured at seven days. Transferring the fourteen-day log mean value to seven days on Figure A-7 and then performing a linear regression analysis through the log means at 1, 3 and 7 days results in a slope of -0.5, or m = 0.5. Regressing a line through the 1,3 and 14 day log mean values would result in m = 0.35. Lick et al. (1995) reported values of m (which was denoted as n in that paper) ranging between 0.8 and 1.1 for Fox, Saginaw and Buffalo River sediments, providing further validation of the present analysis.

APPENDIX B
FIELD STUDY METHODS AND RESULTS

B.1 Field Study Description and Procedures

A field study was conducted during November, 1990 to measure the in situ resuspension potential of fine-grained, cohesive sediments in the Upper Hudson River. Surficial sediment cores were collected at twenty locations in the Thompson Island Pool (Reach 8), see Figure B-1. Samples were also collected at eight locations (two sampling sites per location) in the seven reaches downstream of the Thompson Island Pool, see Figure B-2. The cores were collected from shallow, nearshore areas where the sediment bed is primarily composed of cohesive sediments with varying amounts of fine sand. A five-inch diameter push core was used to collect the samples, which were typically six to eight inches long.

The cores were transported to shore within one hour of collection for testing in a portable resuspension device, commonly called a shaker, see Figure B-3. The procedure described in Tsai and Lick (1986) was used to measure the in situ resuspension potential of the collected cores in the following manner. Three surficial cores were collected at each sampling location and each of the three cores was tested at a different effective shear stress. Generally, the cores at each site were tested at shear stresses of 5, 9 and 11 dynes/cm^2. However, twelve of the sampling locations in the Thompson Island Pool were tested at shear stresses of 5, 7 and 9 dynes/cm^2. The in situ resuspension potential data resulting from this study are tabulated in Table B-1.

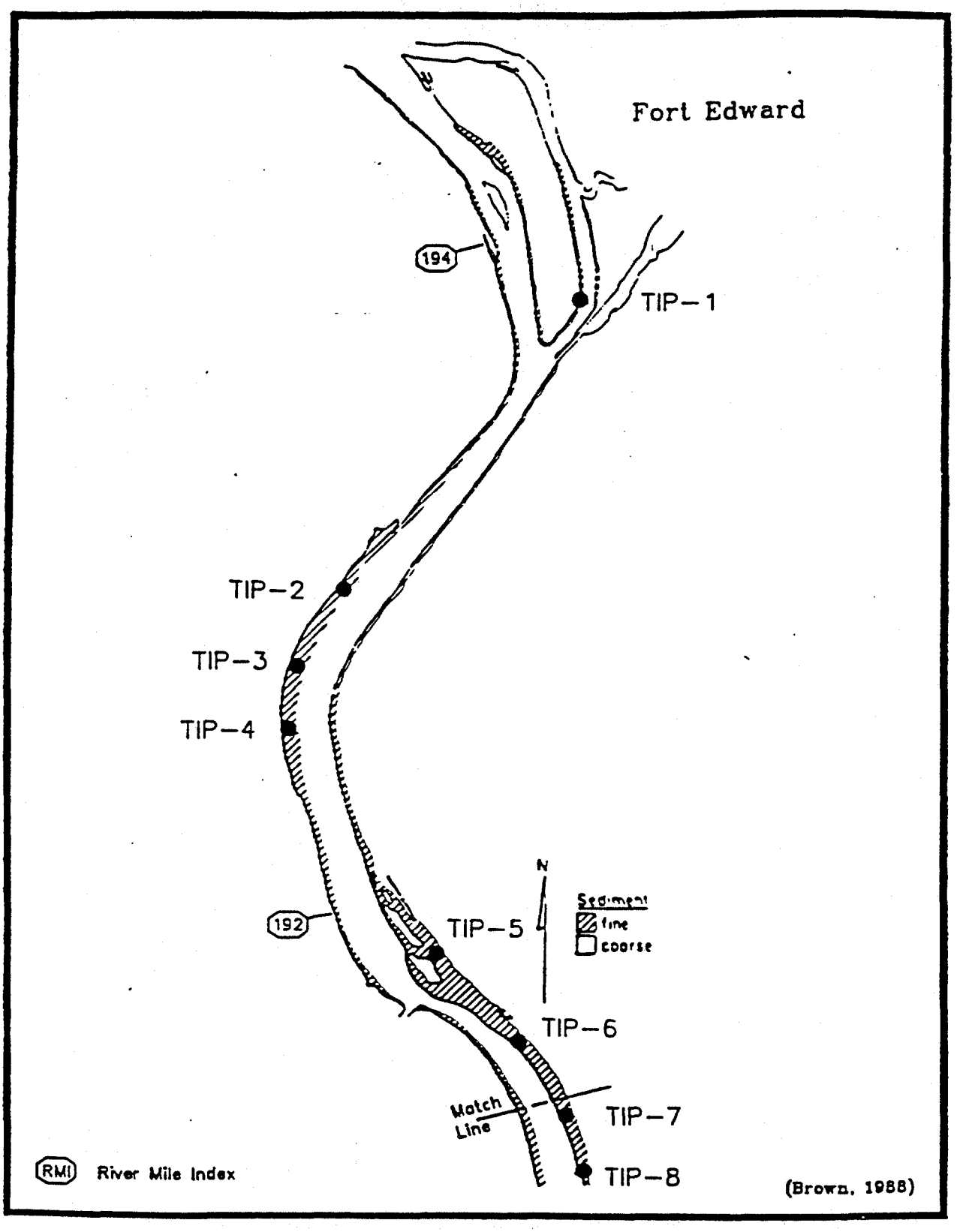

Figure B-1a. Locations of in situ resuspension potential stations in the Thompson Island Pool.

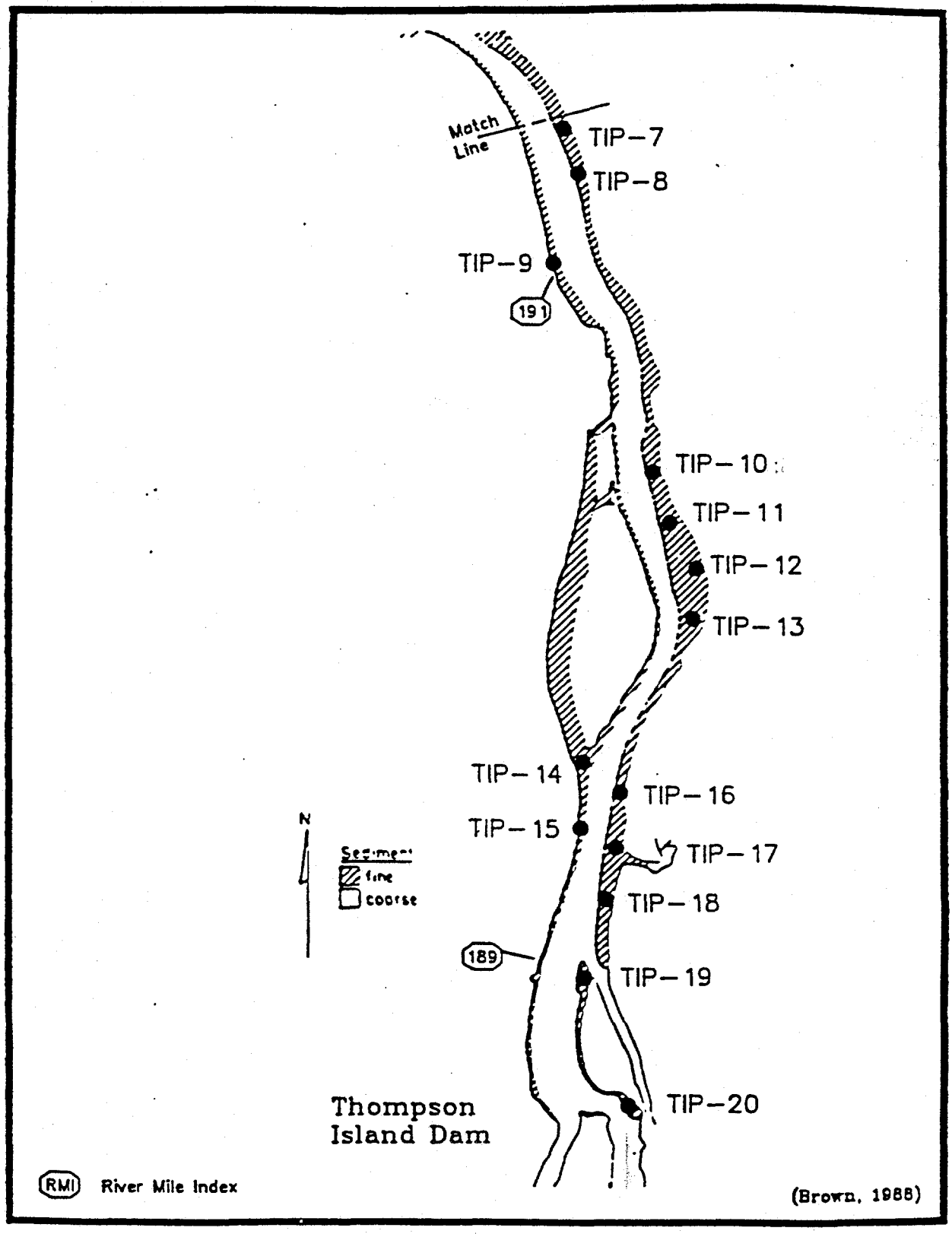

Figure B-1b. Locations of in situ resuspension potential stations in the Thompson Island Pool.

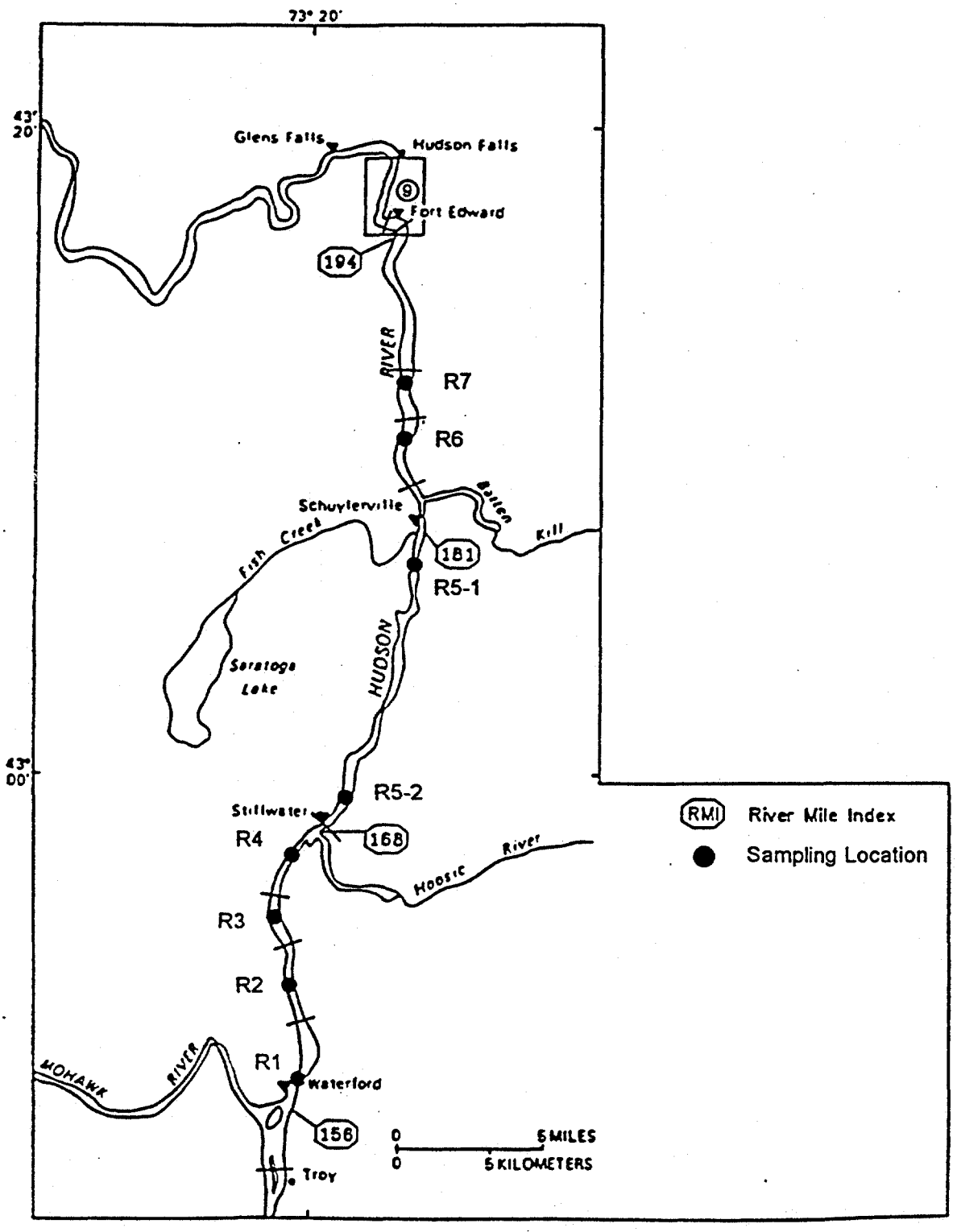

Figure B-2. Locations of in situ resuspension potential stations from Thompson Island Dam to Troy Dam .

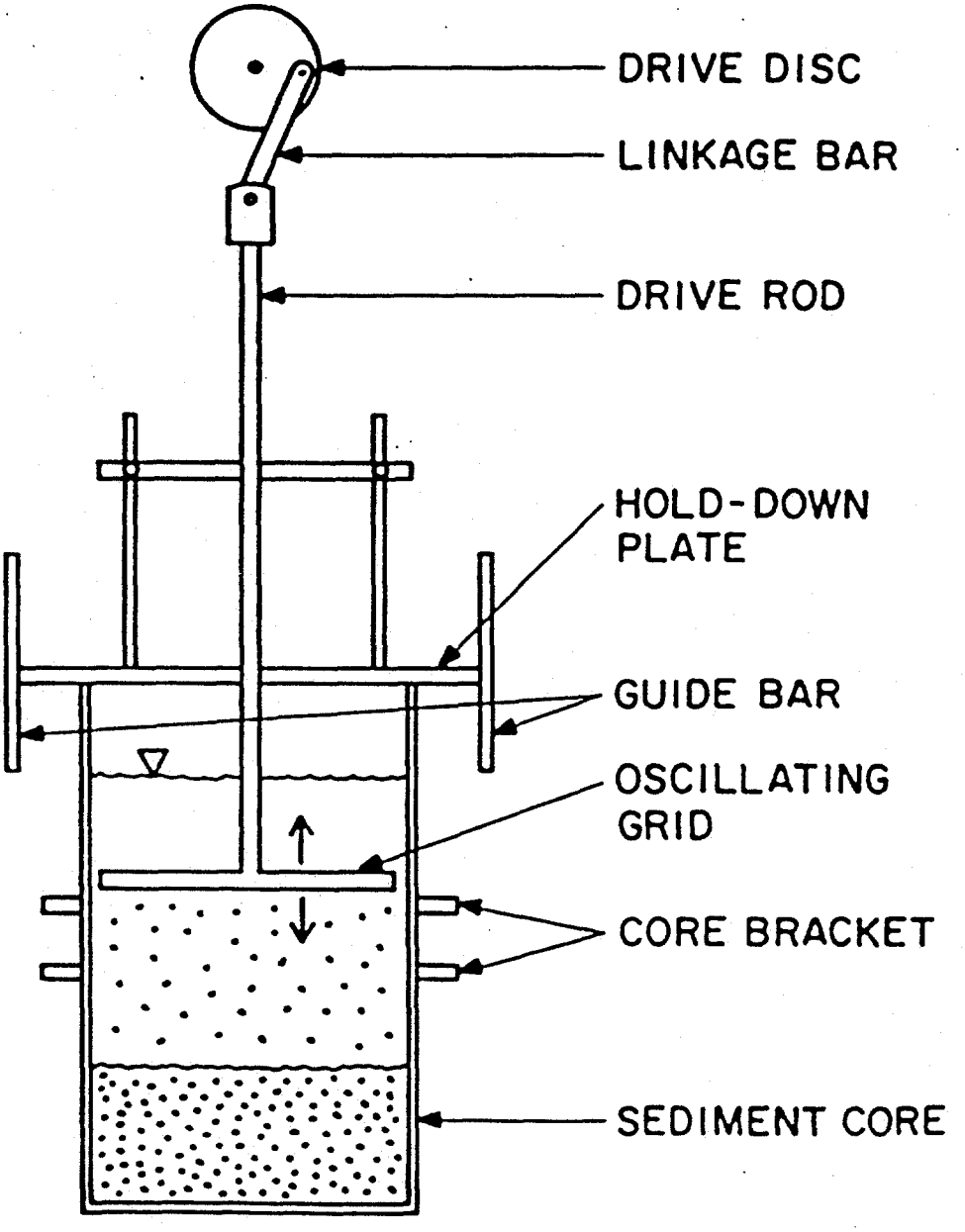

Figure B-3. Schematic of the shaker.

TABLE B-1. RESUSPENSION POTENTIAL STUDY SUMMARY

Station	Depth (Ft.)	Resuspension Potential (mg/cm^2) $r=5$	$r=7$	$r=9$	$r=11$	Sediment Description
TIP-1	5	0.11	-	3.76	13.24	Fine sand to silt, grass and weeds growing on bottom, very compact, difficult to core, most of the bottom was hard but not gravel.
TIP-2	5	0.41	-	2.05	7.20	Mixture of silt and sand with more silt on surface and more sand under surface. Some organic on surface, but not as much as TIP-4. ~80 percent sand in these cores.
TIP-3	5	1.06	-	3.70	13.91	Very soft fine sand to silt, lots of organic flocs on surface, resuspends very easily, cores taken on outer bend of river, very shallow area, lots of sediment deposition.
TIP-4	8	0.29	-	5.57	16.97	Soft mud, very silty, organic debris on surface, cohesive like a gel, lot of zooplankton, some sand mixed in.
TIP-5	6	0.68	-	3.54	8.95	Very silty, soft, lots of organic debris, not as much flocculation, a lot of fine sand mixed in, a few roots and some zooplankton.
TIP-6	10	0.35	-	4.33	22.18	Silt, some fine sand, lots of organics, fibers, loose flocs.
TIP-7	8	0.64	-	9.7	12.96	Silt, some organics and fiber.
TIP-8	5	0.06	-	3.71	0.47	Coarse sand, difficult to core, some gravel and organic debris, very little organic debris.
TIP-9	14	0.21	7.05	11.02	-	Soft mud, a lot of roots, loose flocs.
TIP-10	7	1.82	10.26	12.21	-	Soft mud, loose flocs, some zooplankton and wood fiber, easy to resuspend, sediment bed is patchy mud/gravel.
TIP-11	9	4.26	5.23	8.74	-	Soft mud, loose flocs.

TABLE B-1. RESUSPENSION POTENTIAL STUDY SUMMARY (continued)

Station	Depth (Ft.)	Resuspension Potential (mg/cm^2) $\tau=5$	$\tau=7$	$\tau=9$	$\tau=11$	Sediment Description
TIP-12	7	2.52	13.79	15.70	-	Very soft mud, loose flocs, small amount of fibers and wood, some zooplankton.
TIP-13	11	2.37	14.29	12.52	-	Soft mud, some bottom plants, zooplankton, some wood chips and fiber. Sediment bed has steep slope from shore and changes rapidly from mud to gravel.
TIP-14	6	3.48	8.44	21.37	-	Soft mud, loose flocs.
TIP-15	5	1.28	5.46	10.23	-	Soft mud, loose flocs, wood fibers, lots of organics, some zooplankton.
TIP-16	5	1.23	2.93	22.67	-	Soft mud, loose flocs, lots of zooplankton and worms, some wood fiber, resuspends very easily.
TIP-17	11	3.24	6.60	28.84	-	Soft mud, loose flocs, some wood fiber, small amount of dead grass, resuspends very easily.
TIP-18	8	1.14	12.68	9.74	-	Soft mud, loose flocs, easily resuspended, organic fibers perhaps which the flocs attach to; some organic debris, wood fibers and roots.
TIP-19	7	8.30	14.39	25.25	-	Soft mud with loose flocs, lots of organic debris including wood chips, fiber and dead weeds, very easily resuspended.
TIP-20	8	0.40	0.99	8.32	-	Soft mud, flocs, some wood fiber, tuberous roots throughout cores, low amount of resuspension, cores surface layers were very irregular due to roots, sediment was fairly compact at bottom of core.
R7-E	6	5.78	-	6.54	43.99	Fine sand, silty surface with some organic growth, some flocculation on surface, clay in lower portion of core. Some snails on surface. Clay has grey color.

TABLE B-1. RESUSPENSION POTENTIAL STUDY SUMMARY (continued)

Station	Depth (Ft.)	Resuspension Potential (mg/cm^2) $r=5$	$r=7$	$r=9$	$r=11$	Sediment Description
R7-W	12	1.16	-	2.36	9.29	Fine sand, not much flocculation, very little organic or growth. Very uniform core, fine sand with a little silt. No zooplankton, but some very small clams below the surface. Sand has reddish brown color.
R6-E	10	3.16	-	8.00	13.66	Loose flocs on surface, silt mixed with sand in upper inch, clay below that.
R6-W	7	8.85	-	19.63	-	Clay to silt, loose flocs, not much debris or organics, some small roots on surface, very soft.
R5-1E	7	0.88	-	6.80	60.78	Fine sand, leaf debris, dead weeds.
R5-1W	7	1.26	-	12.49	44.57	Clay to silt, leaf debris, dead weeds, a little organics.
R5-2E	5	4.87	-	25.44	47.81	Sandy, very fine, silt mixed in, very little organic debris.
R5-2W	-	4.12	-	36.24	38.54	Fine sand and silt, fairly soft, no organic debris, not much flocculation on surface.
R4-E	5	19.40	-	62.52	56.91	Fine sand with clay, fairly compact, not much organic debris.
R4-W	-	11.76	-	30.99	44.42	Fine sand and clay with a lot of organic debris mixed in.
R3-E	7	6.16	-	29.59	44.00	Fine sand with some fine silt or clay mixed in, not much organic debris.
R3-W	7	1.16	-	27.73	48.59	Fine sand with some clay. Lots of zooplankton and little shrimp, some organic debris and weeds growing.
R2-E	5	1.57	-	23.80	43.17	Fine sand in top layer with a light colored clay on the bottom layer.
R2-W	6	0.40	-	2.31	23.03	Sand and silt, not much organic on the surface, very little flocculation.
R1-E	6	12.04	-	20.35	94.91	Fine sand and silt.
R1-W	7	1.69	-	13.25	59.17	Sand and silt mixed together.

B.2 Data Analysis

The objective of the field study was to obtain data that could be used to determine values of a_o and n in Equation (2-1) that are appropriate for cohesive sediments in the Upper Hudson River. Studies in other rivers have shown that the exponent n can range from two to three (Gailani et al., 1991; Ziegler and Nisbet, 1994). Examination of the resuspension potential data from the eight reaches of the Upper Hudson River indicated that setting n equal to three for all of the reaches was a valid approximation.

The only remaining parameter in Equation (2-1) that must be determined is the site-specific constant, a_o. The flume experiments described in Appendix A were used to set values of τ_o, m and $T_{d,max}$. The assumption will be made that the depositional age of collected cores was seven days, i.e., $T_d = T_{d,max}$, in using the resuspension data to determine a_o in Equation (2-1). This assumption is valid because the cores were collected at a time when negligible deposition had occurred during the previous three to four weeks. Thus, the value of a_o for each of the collected cores was calculated using a manipulated version of Equation (2-1)

$$a_o = T_{d,max}^m \left(\frac{\tau - \tau_o}{\tau_o}\right)^{-n} \epsilon_M = 2.65\ (\tau - 1)^{-3}\ \epsilon_M \qquad \text{(B-1)}$$

where $T_{d,max}^m = 7^{0.5} = 2.65$ and ϵ_M = measured resuspension potential for a particular core (mg/cm^2).

As in any riverine system, variability in cohesive bed composition resulted in a_o values ranging over nearly two orders of magnitude for the cores tested in the Upper Hudson River. The goal then was to determine the mean value of a_o that was representative of cohesive sediments throughout the system; system average values have been used successfully in other sediment transport studies (Gailani et al., 1991; Ziegler and Nisbet, 1994). However, significant variation of a_o between the various reaches of the Upper Hudson River made it necessary to determine the mean value of a_o for each

reach instead of calculating a global average for the entire system. The reach average a_0 values for the Upper Hudson River are presented in Table B-2. Note that cores from ~~two~~ one stations in the Thompson Island Pool (TIP-8 ~~and TIP-10~~) ~~were~~ were not included in the averaging process because the a_0 values for the cores at ~~those~~ that locations appeared to be an outliers. Examination of the visual description of these cores supports this decision.

TABLE B-2. STATISTICAL INFORMATION ON a_0 VALUES BY REACH

Reach	Mean a_0 (mg-day$^{1/2}$/cm^2)	Standard Deviation	Sample Size
8	0.071	0.062	~~54~~ 57
7	0.079	0.087	6
6	0.135	0.135	5
5	0.116	0.058	12
4	0.340	0.266	6
3	0.140	0.067	6
2	0.067	0.047	6
1	0.192	0.165	6

Appendix C

List of Acronyms
List of Variables
List of Equations

List of Acronyms	
Name	**Acronym**
Adirondack Hydro Development Corporation	AHDC
apparent specific dynamic action	ASDA
benthic macroinvertebrates	BMI
biota-sediment accumulation factor	BSAF
Comprehensive Environmental Response, Compensation, and Liability Act	CERCLA
chlorine atoms per biphenyl molecule	Cl/BP
dense non-aqueous phase liquid	DNAPL
di-2-ethylhexyl phthalate	DEHP
dissolved or colloidal organic matter	DOM
Food and Drug Administration	FDA
gas chromatographic	GC
General Electric	GE
Geographic Information Systems	GIS
Griffin Island	GI
mean sea level	MSL
metric tons	MT
mile point	MP
minimum variance unbiased estimator	MVUE
New York State Department of Environmental Conservation	NYSDEC
New York State Department of Health	NYSDOH
north of Snook Kill	NTIP
organic carbon	OC
parts per million	ppm
phytophilous macroinvertebrates	PMI
polychlorinated biphenyl	PCB
tri and higher polychlorinated biphenyl	PCB_{3+}
Potentially Responsible Parties	PRPs
Quantitative Environmental Analysis	QEA
Reassessment Remedial Investigation/Feasibility Study	RRI/FS
Record of Decision	ROD
root mean square	RMS
Sediment transport model that was originally developed by Ziegler and Lick	SEDZL
TAMS Consultants, Inc.	TAMS
Thompson Island Dam	TID
Thompson Island Pool	TIP
total suspended solids	TSS
tropic level one through four of the food web	TL1-TL4
U.S. Environmental Protection Agency	USEPA
U.S. Geological Survey	USGS
Weight-loss-on-ignition	WLOI

List of Variables		
Symbol	**Definition**	**Equation #**
A	cross-sectional area (L^2) (in Chapters 2-4)	2-1, 4-22
A_{gl}	active gill surface area (L^2)	5-4, 5-6
A_s	sediment surface area in TIP (L^2)	4-28, 4-30, 4-31
A_{trib}	sediment rating curve coefficient	3-20
a_o	site-specific constant for resuspension potential eqn.	3-7
α_c	efficiency at which ingested chemical is assimilated from prey	5-3, 5-10, 5-14, 5-26
α_F	fraction of ingested energy that is assimilated (in Chapter 5)	5-21, 5-26
${}^k\alpha_{FS}$	drainage area proration adjustment factor for Fort Edward to Stillwater drainage basin, for month k	2-7, 2-10, 2-11
${}^k\alpha_{SW}$	drainage area proration adjustment factor for Stillwater to Waterford drainage basin, for month k	2-8, 2-10
$Aroclor_{1016}$	concentration of PCB Aroclor 1016 (M/M)	4-37
$Aroclor_{1254}$	concentration of PCB Aroclor 1254 (M/M)	4-37
b	reach-dependent exponent, dam rating curve	2-12
B	adjustable constant, active layer thickness eqn.	3-10
B_H	horizontal eddy viscosity (L^2/T)	2-4, 2-5
BAF	bioaccumulation factor (L^3/M lipid)	5-1
β_i	drainage area proration factor for tributary i between Fort Edward and Waterford	2-7, 2-8, 2-9, 2-10, 2-11
β,γ,ρ	coefficients of the relation among weight, temperature and respiration	5-18
BSAF	biota-sediment accumulation factor (M OC/M lipid)	5-2, 5-23
$BSAF_e$	energy-based BSAF (M OC/kJ)	5-23
c	concentration of PCBs dissolved in the water (M/L^3)	4-2, 4-3, 4-5, 4-7, 4-13, 4-14, 4-16, 4-23, 4-28, 5-1, 5-3, 5-8, 5-10, 5-14
c_{act}	activity multiplier for respiration	5-18
c_{air}	vapor phase PCB concentration in air (M/L^3)	4-23, 4-25
C_{avg_j}	average concentration of PCB in layer j (non-cohesive or cohesive) within a cohesive or non-cohesive area (M/M)	4-38, 4-39
c_d	downstream dissolved PCB concentration (M/L^3)	4-25
c_{dc3+}	concentration of dechlorinatable PCB_{3+} (M/L^3)	4-26
c_{dom}	concentration of PCB bound to DOM (M/L^3)	4-13, 4-14, 4-16, 4-28
C_f	spatially variable bottom friction factor	2-4, 2-5, 2-6
C_{FE}	suspended sediment-concentration at Fort Edward (M/L^3)	3-19
$C_{f,min}$	minimum bottom friction factor	2-6
c_i	concentration of PCB in sample i located within layer j (M/M)	4-38
c_i	concentration of PCB in cohesive zone i, for a given layer (M/M)	4-39
C_{ij}	predation or consumption rate of species i on species j (M-wet prey/M-wet predator·T)	5-3, 5-10, 5-14, 5-21

List of Variables		
Symbol	**Definition**	**Equation #**
C_k	concentration of suspended sediment of size-class k, k = 1 or 2 (M/L^3)	3-1, 3-2, 3-3, 3-6, 3-12
c_{o_2}	oxygen concentration of water ($M\ O_2/L^3$)	5-5, 5-7
c_R	chemical excretion multiplier	5-16, 5-27
c_T	total PCB concentration (M/L^3)	4-4, 4-5, 4-6, 4-13
$c_{T_{RI}}$	PCB_{3+} in the water column at Rogers Island (Rt. 197 Br. station) (M/L^3)	4-28, 4-30, 4-32
c_{s1999}	concentration of pore water PCB in sediment at year 1998 (M/L^3)	4-30, 4-31
c_{st}	concentration of pore water PCB in sediment at year t (M/L^3)	4-29, 4-30, 4-31
C_{trib}	tributary suspended sediment concentration (M/L^3)	3-20
c_{Ts1998}	total PCB concentration in the sediment in year 1998 (M/L^3)	4-31, 4-32
$c_{T_{st}}$	total PCB concentration in the sediment (M/L^3) in year t	4-31, 4-32
$c_{T_{TID}}$	PCB_{3+} concentration in the water column at TID (TID-PRW2 station) (M/L^3)	4-28, 4-30, 4-32
c_u	upstream concentration (M/L^3)	4-25
$(c+c_{dom})_s$	the average surface sediment pore water dissolved + DOM bound PCB_{3+} concentration in TIP (M/L^3)	4-14, 4-28
D	reach-dependent constant, dam rating curve	2-12
D_k	deposition flux of size-class k, k=1 or 2, ($M/L^2 \cdot T$)	3-1, 3-2, 3-6
d_{non}	effective particle size on non-suspendable bed material (L)	3-11
D_s	molecular diffusivity of the PCBs in sediment pore water (L^2/T)	4-16
D_{tot}	Depositional flux of solids (classes 1 + 2) calculated by the sediment transport model ($M/(L^2 \cdot T)$)	3-21, 4-4
D_w	molecular diffusivity of the PCBs in water (L^2/T)	4-34, 4-35
DA_{HR}	drainage area at Hoosic River gauge (L^2)	2-9
DA_i	drainage area for tributary i between Fort Edward and Waterford (L^2)	2-9
DA_{KC}	drainage area at Kayaderosseras Creek gauge (L^2)	2-9
d_{50}	median particle size of bed sediment (L)	3-10, 3-14, 3-15, 3-16, 3-17, 3-18
E_d	dispersion coefficient (L^2/T)	4-13
E_p	particle mixing coefficient (L^2/T)	4-13
$E_{x,y,z}$	dispersion coefficient along the x, y, or z axes, respectively (L^2/T)	4-2, 4-3, 4-4
E_x, E_y	horizontal eddy diffusivities along the x- and y-axes, respectively (comparable to E_x, E_y in Chapter 4) (L^2/T)	3-1
ϵ	net mass of resuspended sediment per unit surface area (M/L^2)	3-7, 3-8
η	water surface displacement from the reference depth (L)	2-2, 2-3, 2-4, 2-5
η_{DAM}	water surface elevation above dam crest (L)	2-12

List of Variables		
Symbol	**Definition**	**Equation #**
$f_{a,k}$	fraction of class k sediment that is suspendable in the active layer	3-11
f_B	weight fraction of whole body that is blood water	5-16
f_c	weight fraction that congener c comprises in fish	5-27
f_d	fraction of total PCB in dissolved form	4-5, 4-8, 4-10, 4-31
f_{dom}	fraction of total PCB sorbed to DOM	4-12
f_D	fraction dry weight of fish (M-dry/M-wet)	5-24
$f_{Diet,i}$	proportion of order i expected in the diet of the fish	5-22
$f_{Diet,PMI}$	proportion of PMI in the diet	5-22
f_i	fraction of cohesive zone i relative to total cohesive area within segment j	4-39
f_{ij}	fraction of the total energy consumed by predator i that consists of prey j	5-21, 5-26
f_k	fraction of class k sediment in the surficial layer of the bed that is suspendable, k = 1 or 2	3-9, 3-17
f_L, f_{Li}	fraction lipid of the species i (M-lipid/M-wet)	5-16, 5-20, 5-23, 5-24, 5-27
f_p	fraction of total PCB in particulate form	4-4, 4-6, 4-9, 4-11
f_P	fraction protein (f_L - f_D)	5-20
$f_{PMI,i}$, $f_{BMI,i}$	proportion of order i in all PMI or BMI samples	5-22
f_{sus}	fraction of suspended sediment (f_1 + f_2)	3-15
g	acceleration due to gravity (L/T^2)	2-2, 2-4, 2-5
G	water column shear stress (dynes/L^2)	3-3
G	entrained air flow rate (L^3/T)	4-25
G, G_i	growth rate of species i (M-wet/M-wet·T)	5-3, 5-17
Γ	class 2 stratification correction factor, deposition flux	3-6
h	total water depth ($h_o + \eta$) (L)	2-3, 2-4, 2-5, 2-6, 4-4, 4-15, 4-23, 4-34, 3-1, 3-13
H	dune height (L)	3-12
H	dimensionless Henry's Constant	4-23, 4-24, 4-25
h_o	reference water depth (L)	In definition of h
H_T	Henry's Constant at temperature, T (Pa*m^3/mol)	4-33
H_{veg}	vegetation height (L)	3-22, 3-23
ΔH°	net change in enthropy (heat content) of the reaction	4-17, 4-18, 4-20, 4-21, 4-22
J_D	areal flux rate due to diffusion ($M/L^2 \cdot T$)	4-14, 4-15
J_{Dt}	flux of PCB from the sediment to the water column at time t ($M/L^2 \cdot T$)	4-29, 4-30, 4-32
$J_{i,j}$	vertical pore water diffusive flux between elements i + j ($M/L^2 \cdot T$)	4-16
k	von Karman's constant (0.4)	2-6
k_1	chemical mass transfer coefficient from blood to the environment (1/T)	5-10, 5-14
k_2	chemical mass transfer coefficient from blood to lipid	5-10, 5-11, 5-12

List of Variables		
Symbol	**Definition**	**Equation #**
	(1/T)	
k_3	chemical mass transfer coefficient from lipid to blood	5-10, 5-11, 5-12, 5-14, 5-15
K_2	desorption coefficient (1/T)	4-2, 4-3
k_{dc}	first-order rate constant for dechlorination (1/T)	4-26
K_{doc}	the partition coefficient between PCBs sorbed to DOM and freely dissolved (L^3/M OC)	4-10, 4-11, 4-12
k_f	sediment pore water-water column mass transfer coefficient (L/T)	4-14, 4-28, 4-29
k_g	vapor phase mass transfer constant (L/T)	4-24
K_{gill}	gill elimination rate (M/MT)	5-16, 5-27
k_{gl}	mass transfer coefficient of the gill (L/T)	5-4, 5-7
k_{glO_2}	mass transfer coefficient of oxygen at the gill (L/T)	5-6, 5-7
K_i	rate constant for excretion of chemical by species i (1/T)	5-3
k_l	water phase mass transfer constant (L/T)	4-24, 4-34
k_L	volatilization mass transfer coefficient (L/T)	4-23, 4-24
K_o	adsorption coefficient (L^3/M·T)	4-2, 4-3
$K_{ow,c}$	octanol/water partition coefficient for congener c (L^3/M)	5-27
K_p	adsorption partition coefficient (L^3/M)	4-7, 4-8, 4-9, 4-10, 4-11, 4-12, 4-17, 4-18, 4-20
K_{p1}	partition coefficient at temperature T_1 (L^3/M)	4-21, 4-22
K_{p2}	partition coefficient at temperature T_2 (L^3/M)	4-21, 4-22
K_u, K_{ui}	rate constant for respiratory chemical uptake by species i (L^3/M-wet·T)	5-3, 5-4, 5-7, 5-8, 5-10, 5-14, 5-16, 5-27
K_{uo_2}	oxygen uptake rate (L/M-wet·T)	5-5, 5-6
l_i	weight assigned to sample i, indicating the fraction of sample within layer j	4-38
$l_{i,j}$	mixing length between adjacent sediment bed segments (L)	4-16
L_T	total length of the fish (L)	5-25
$L_{T,i}$	total length of the fish at age i, back-calculated (L)	5-25
λ	bed porosity	3-11
λ, $\lambda_{i \text{ or } j \text{ or } t}$	energy density of animal i or j's tissue or at time t (E/M-wet)	5-19, 5-20, 5-21, 5-26
λ_{inv}	energy density of the invertebrate sample (E/M-wet)	5-23, 5-24
λ_o	conversion factor representing the amount of energy made available during respiration of one gram of 0_2 = 13.7 kJ/g O_2	5-19
m	Concentration of the solids [M/L^3]	3-21, 4-1, 4-2, 4-3, 4-4, 4-8, 4-9, 4-10, 4-11, 4-12
m	mass of the organism (M-wet)	5-10, 5-14
m_{doc}	concentration of dissolved organic matter expressed in terms of organic carbon (M OC/L^3)	4-10, 4-11, 4-12

List of Variables		
Symbol	**Definition**	**Equation #**
mei	vegetation stiffness	3-22, 3-23
m_B	mass of blood in the organism (M)	5-9, 5-10, 5-11, 5-12, 5-14
m_L	mass of lipid in the organism (M)	5-9, 5-10, 5-11, 5-12, 5-14, 5-15
μ	viscosity of water (centipoise, 10^{-2} g/cm-s)	4-35, 4-36
n	Manning's coefficient ($T/L^{1/3}$)	2-2
n	shear stress exponent	3-7
N	consolidation exponent	3-7
N_{trib}	tributary rating curve exponent	3-20
v, $v_{i \text{ or } j}$	concentration of chemical in species i or j (M/M-wet)	5-3, 5-9, 5-10, 5-14, 5-16, 5-26, 5-27
v_B	concentration of chemical in blood (M/L^3)	5-8, 5-9, 5-10, 5-11, 5-12, 5-13, 5-14, 5-15, 5-16, 5-27
v_L	concentration of PCBs in the organism (M/M lipid)	5-1, 5-2, 5-9, 5-10, 5-11, 5-12, 5-13, 5-14, 5-15
%OC	percent organic carbon of particulate matter	4-27
p	particulate PCB concentration [M/L^3]	4-1, 4-2, 4-3, 4-6, 4-13
P	pressure ($M/L \cdot T^2$)	4-17
P_i, P_t	energy usage rate for species i or at time t (E/M-wet·T)	5-19, 5-21, 5-26
P_k	probability of deposition for sediment class k, k= 1 or 2	3-2, 3-4, 3-6
PCB_{3+}	concentration of PCB_{3+} (M/M)	4-37
π_{LB}	equilibrium partition coefficient of the contaminant between the lipid and aqueous blood (M-aqueous/M-lipid)	5-13, 5-14, 5-15, 5-16
q	resolved velocity vector $(u_x^2 + u_y^2)^{1/2}$ (L/T)	2-4, 2-5
Q	river flow rate (L^3/T)	4-25
Q_{DAM}	flow rate at dam (L^3/T)	2-12
Q_{FE}	Fort Edward flow rate (L^3/T)	3-19, 4-28, 4-30, 4-32
Q_{GC}	measured flow rate at Glowegee Creek gauge (L^3/T)	2-11
Q_{HR}	measured flow rate at Hoosic River gauge (L^3/T)	2-10
Q_i	estimated flow rate in tributary i between Fort Edward and Waterford (L^3/T)	2-10, 2-11
Q_{KC}	measured flow rate at Kayaderosseras Creek gauge(L^3/T)	2-10
Q_{trib}	tributary flow rate (L^3/T)	3-20
$\overline{Q}_{trib}$	mean flow rate of tributary (L^3/T)	3-20
${}^k\overline{Q}_{FE}$	mean flow rate at Fort Edward, for month k (L^3/T)	2-7
${}^k\overline{Q}_{HR}$	mean flow rate at Hoosic River gauge, for month k(L^3/T)	2-7, 2-8
${}^k\overline{Q}_{KC}$	mean flow rate at Kayaderosseras Creek gauge, for month k (L^3/T)	2-7
${}^k\overline{Q}_{ST}$	mean flow rate at Stillwater, for month k (L^3/T)	2-7, 2-8

List of Variables		
Symbol	**Definition**	**Equation #**
${}^{k}\overline{Q}_{WA}$	mean flow rate at Waterford, for month k (L^3/T)	2-8
r	mass of chemical/unit mass of solids (M/M) (in Chapter 4)	4-1, 4-7
R	hydraulic radius (L) (in Chapter 2)	2-2
R	universal gas constant (in Chapter 4)	4-17, 4-18, 4-20, 4-21, 4-22
R, R_t	respiration rate (at time t) ($MO_2/M \cdot T$)	5-7, 5-18, 5-19
R_k	resuspension (erosion) flux of size-class k, k = 1 or 2 ($M/L^2 \cdot T$)	3-1, 3-9
R, R_t	respiration rate (at time t) ($MO_2/M \cdot T$)	5-7, 5-18, 5-19
R_s	radius of the scale (L)	5-25
$R_{S,i}$	radius of annulus i of the scale (L)	5-25
r_{soc}	concentration of PCBs on sediment particles (M/M OC)	5-2
$R_{tot, coh}$	total resuspension rate (M/L^2-T)	3-8, 3-9
ρ_a	density of aqueous blood (M/L^3)	5-8, 5-19
ξ	fraction of area covered with non-moving particles	3-12
S	summation of all sources and sinks (M/L3·T or M/M·T)	4-4
S_b	sources and sinks, including dechlorination and biodegradation (M/L3·T or M/M·T)	4-13
S_D	PCB flux between sediment pore water and water column (M/L·T)	4-15
S_i	sources and sinks of PCB component i due to reactions, phase transfers and resuspension of contaminated bed sediment ($M/L^3 \cdot T$ or M/M·T)	4-2, 4-3
S_v	PCB flux due to volatilization (M/L·T)	4-23
t	time (T)	numerous
T	temperature (°C or °K depending on eqn)	4-17, 4-18, 4-21, 4-22, 4-19, 4-20, 4-33, 4-36, 5-18
T_a	active layer thickness (L)	3-10, 3-11, 3-12
T_d	time after deposition (T)	3-7
τ_b	Bottom shear stress (dynes/L^2)	3-5, 3-7, 3-10, 3-14, 3-22
$\tau_{b,min}$	bottom shear stress below which $P_1 = 1$ (dynes/L^2)	3-5
τ_{c50}	critical shear stress for initiation of bed load based upon the parent bed d_{50} (dynes/L^2)	3-10
τ_{cr}	effective critical shear stress (dynes/L^2)	3-7
τ_{max}	maximum bottom shear stress in non-cohesive bed area at a given flow rate (dynes/L^2)	In definition of τ_n
τ_n	normalized bottom shear stress (τ_b/τ_{max})	3-16, 3-18
θ	non-dimensional bottom shear stress	3-13, 3-14
θ	porosity (L^3 water/L^3 total)	4-8, 4-9, 4-10, 4-11, 4-12
u	velocity [L/T]	4-34
u_x, u_y, u_z	the velocities along the x-, y- and z-axes (L/T),	2-1, 2-3, 2-4, 2-5, 3-1,

List of Variables		
Symbol	**Definition**	**Equation #**
	respectively	4-2, 4-3, 4-4, 4-13
$\overline{V}$	the molar volume of the PCB (L^3/mol)	4-35
ΔV°	net change in volume of the system (L^3)	4-17
w	dummy integration variable	3-4
W, W_t	wet weight of the animal (at time t) (M-wet)	5-4, 5-6, 5-17, 5-18, 5-19
$W(t)_{base}$	average base load for a given year (M/T)	4-40
$W(t)_{pulse}$	estimated pulse load for the given time period, t (M/T)	4-40
$W(t)_{resuspension}$	r_{avg}·TSS·Q;r_{avg} is average PCB_{3+} particulate concentrations (M/M) for a given year during high flow events, TSS is the total suspended solids during the high flow event (M/L^3), and Q is the flow during the event (L^3/T)	4-40
$W(t)_{total}$	total load at Fort Edward for the given time period, t (M/T)	4-40
w_s	settling velocity of the particulates (L/T)	4-3
W_s	effective settling speed (L/T)	3-21
$W_{s,k}$	sediment settling speed of sediment class k, k = 1 or 2 (L/T)	3-2, 3-3, 3-6
$WLOI_{375}$	weight loss on ignition at 375°C (%)	4-27
$WLOI_{450}$	weight loss on ignition at 450°C (%)	4-27
y	probability of deposition parameter	3-5
z_o	effective bottom roughness (L)	2-6
$z_{o,fp}$	effective bottom roughness for a vegetated flood plain (L)	3-21

Note: M = mass, L = length, T = time, E = energy

LIST OF EQUATIONS

SECTION 2

$$\frac{\partial A}{\partial t} + \frac{\partial (u_x A)}{\partial x} = 0 \tag{2-1}$$

$$\frac{\partial u_x}{\partial t} + \frac{1}{2}\frac{\partial u_x^2}{\partial x} = -g\frac{\partial \eta}{\partial x} - g\frac{n^2}{R^{4/3}}u_x|u_x| \tag{2-2}$$

$$\frac{\partial \eta}{\partial t} + \frac{\partial (u_x h)}{\partial x} + \frac{\partial (u_y h)}{\partial y} = 0 \tag{2-3}$$

$$\frac{\partial (u_x h)}{\partial t} + \frac{\partial (u_x^2 h)}{\partial x} + \frac{\partial (u_x u_y h)}{\partial y} = -gh\frac{\partial \eta}{\partial x} - C_f q u_x + \frac{\partial}{\partial x}\left(hB_H\frac{\partial u_x}{\partial x}\right) + \frac{\partial}{\partial y}\left(hB_H\frac{\partial u_x}{\partial y}\right) \tag{2-4}$$

$$\frac{\partial (u_y h)}{\partial t} + \frac{\partial (u_x u_y h)}{\partial x} + \frac{\partial (u_y^2 h)}{\partial y} = -gh\frac{\partial \eta}{\partial y} - C_f q u_y + \frac{\partial}{\partial x}\left(hB_H\frac{\partial u_y}{\partial x}\right) + \frac{\partial}{\partial y}\left(hB_H\frac{\partial u_y}{\partial y}\right) \tag{2-5}$$

$$C_f = MAX\left[\frac{k^2}{\left(\ln\frac{h}{2z_o}\right)^2} \quad , \quad C_{f,\min}\right] \tag{2-6}$$

$${}^k\overline{Q}_{ST} - {}^k\overline{Q}_{FE} = {}^k\alpha_{FS}\left(\sum_{i=1}^{7}\beta_i\,{}^k\overline{Q}_{KC} + \sum_{i=8}^{9}\beta_i\,{}^k\overline{Q}_{HR}\right) \tag{2-7}$$

$${}^k\overline{Q}_{WA} - {}^k\overline{Q}_{ST} = {}^k\alpha_{SW}\sum_{i=10}^{15}\beta_i\,{}^k\overline{Q}_{HR} \tag{2-8}$$

$$\beta_i = \begin{cases} \dfrac{DA_i}{DA_{KC}} & , \quad i < 8 \\ \dfrac{DA_i}{DA_{HR}} & , \quad i \geq 8 \end{cases} \tag{2-9}$$

$$Q_i = \begin{cases} {}^k\alpha_{FS}\beta_i Q_{KC} & , \quad i \leq 7 \\ {}^k\alpha_{FS}\beta_i Q_{HR} & , \quad i = 8,9 \\ {}^k\alpha_{SW}\beta_i Q_{HR} & , \quad i > 9 \end{cases} \tag{2-10}$$

$$Q_i = {}^k\alpha_{FS}\beta_i \left(\frac{90}{26}\right) Q_{GC} \quad , \quad i \leq 7 \tag{2-11}$$

$$\eta_{DAM} = DQ_{DAM}^b \tag{2-12}$$

SECTION 3

$$\frac{\partial(hC_k)}{\partial t}+\frac{\partial(u_x hC_k)}{\partial x}+\frac{\partial(u_y hC_k)}{\partial y}=\frac{\partial}{\partial x}\left(hE_x\frac{\partial C_k}{\partial x}\right)+\frac{\partial}{\partial y}\left(hE_y\frac{\partial C_k}{\partial y}\right)+R_k-D_k \tag{3-1}$$

$$D_1 = P_1\ W_{s,1}\ C_1 \tag{3-2}$$

$$W_{s,1} = 3.3\left(C_1 G\right)^{0.12} \tag{3-3}$$

$$P_1 = 1-(2\pi)^{-1/2}\int_{-\infty}^{Y} e^{-\frac{w^2}{2}}\,dw \tag{3-4}$$

$$Y = 2.04\ln\left[0.25\left(\frac{\tau_b}{\tau_{b,\min}}-1\right)e^{1.27\tau_{b,\min}}\right] \tag{3-5}$$

$$D_2 = P_2 W_{s,2}\Gamma C_2 \tag{3-6}$$

$$\epsilon = \frac{a_o}{T_d^N}\left(\frac{\tau_b-\tau_{cr}}{\tau_{cr}}\right)^n \quad , \quad \tau_b \geq \tau_{cr} \tag{3-7}$$

$$R_{tot,coh} = \frac{\epsilon}{3600} \tag{3-8}$$

$$R_k = f_k R_{tot,coh} \tag{3-9}$$

$$T_a = \begin{cases} 2d_{50} & , \quad \tau_b < \tau_{c50} \\ 2d_{50}\left[B\left(\dfrac{\tau_b}{\tau_{c50}}\right)+(1-B)\right] & , \quad \tau_b \geq \tau_{c50} \end{cases} \tag{3-10}$$

$$T_a = \frac{d_{non}}{(1-\lambda)(1-\sum f_{a,k})} \tag{3-11}$$

$$T_a = \frac{1}{2} H(1 - C_1 \xi) \tag{3-12}$$

$$H = h(0.08 + 0.75\theta - 2.01\theta^2 + 2.63\theta^3 - 1.09\theta^4) \tag{3-13}$$

$$\theta = (6x10^{-4}) \frac{\tau_b}{d_{50}} \tag{3-14}$$

$$d_{50} = 135\, f_{sus}^{-1.67} \tag{3-15}$$

$$\begin{aligned} d_{50} &= 140\, e^{16.6\tau_n^2} \quad , \quad \tau_n < 0.45 \\ &= 9000\, \tau_n^{1.02} \quad , \quad \tau_n \geq 0.45 \end{aligned} \tag{3-16}$$

$$f_2 = 22\, d_{50}^{-0.66} \tag{3-17}$$

$$\begin{aligned} d_{50} &= 190\, e^{15.5\tau_n^2} \quad , \quad \tau_n < 0.45 \\ &= 6000\, \tau_n^2 \quad , \quad \tau_n \geq 0.45 \end{aligned} \tag{3-18}$$

$$\begin{aligned} C_{FE} &= 4.5\left(\frac{Q_{FE}}{10{,}000}\right)^{0.29} \quad , \quad Q_{FE} \leq 10{,}000 \\ &= 5.4\left(\frac{Q_{FE}}{10{,}000}\right)^{2.02} \quad , \quad Q_{FE} > 10{,}000 \end{aligned} \tag{3-19}$$

$$\begin{aligned} C_{trib} &= A_{trib} \quad , \quad Q_{trib} \leq \overline{Q}_{trib} \\ &= A_{trib}\left(\frac{Q_{trib}}{\overline{Q}_{trib}}\right)^{N_{trib}} \quad , \quad Q_{trib} > \overline{Q}_{trib} \end{aligned} \tag{3-20}$$

$$W_s = \frac{D_{tot}}{m} \tag{3-21}$$

$$z_{o,fp} = 1.3 H_{veg}^{-0.59} \left(\frac{mei}{\tau_b} \right)^{0.40} \tag{3-22}$$

$$mei = 25.4\ H_{veg}^{2.26} \tag{3-23}$$

SECTION 4

$$p = rm \tag{4-1}$$

$$\frac{\partial c}{\partial t} = \frac{\partial}{\partial x}\left(E_x \frac{\partial c}{\partial x}\right) + \frac{\partial}{\partial y}\left(E_y \frac{\partial c}{\partial y}\right) + \frac{\partial}{\partial z}\left(E_z \frac{\partial c}{\partial z}\right) - \frac{\partial}{\partial x}u_x c - \frac{\partial}{\partial y}u_y c - \frac{\partial}{\partial z}u_z c - K_o m c + K_2 p \pm S_1(s,y,z,t) \tag{4-2}$$

$$\frac{\partial p}{\partial t} = \frac{\partial}{\partial x}\left(E_x \frac{\partial p}{\partial x}\right) + \frac{\partial}{\partial y}\left(E_y \frac{\partial p}{\partial y}\right) + \frac{\partial}{\partial z}\left(E_z \frac{\partial p}{\partial z}\right) - \frac{\partial}{\partial x}u_x p - \frac{\partial}{\partial y}u_y p - \frac{\partial}{\partial z}u_z p + \frac{\partial}{\partial z}w_s p + K_o m c - K_2 p \pm S_2(s,y,z,t) \tag{4-3}$$

$$\frac{\partial c_T}{\partial t} = \frac{\partial}{\partial x}\left(E_x \frac{\partial c_T}{\partial x}\right) + \frac{\partial}{\partial y}\left(E_y \frac{\partial c_T}{\partial y}\right) - \frac{\partial u_x c_T}{\partial x} - \frac{\partial u_y c_T}{\partial y} - \frac{D_{tot}}{hm}\left(f_p c_T\right) \pm S \tag{4-4}$$

$$c = f_d c_T \tag{4-5}$$

$$p = f_p c_T \tag{4-6}$$

$$r = K_p c \tag{4-7}$$

$$f_d = \frac{\theta}{\theta + K_p m} \tag{4-8}$$

$$f_p = \frac{K_p m}{\theta + K_p m} \tag{4-9}$$

$$f_d = \frac{\theta}{\theta + K_p m + K_{doc} m_{doc}} \tag{4-10}$$

$$f_p = \frac{K_p m}{\theta + K_p m + K_{doc} m_{doc}} \tag{4-11}$$

$$f_{dom} = \frac{K_{doc} m_{doc}}{\theta + K_p m + K_{doc} m_{doc}} \tag{4-12}$$

$$\frac{\partial c_T}{\partial t} = \frac{\partial}{\partial z}\left(E_p \frac{\partial p}{\partial z}\right) + \frac{\partial}{\partial z}\left[E_d \frac{\partial (c + c_{dom})}{\partial z}\right] - \frac{\partial u_z (c + c_{dom})}{\partial z} \pm S_b \tag{4-13}$$

$$J_D = k_f \left[(c + c_{dom})_s - (c + c_{dom})_w\right] \tag{4-14}$$

$$S_D = \frac{J_D}{h} \tag{4-15}$$

$$J_{i,j} = \frac{D_s}{l_{i,j}}\left[(c + c_{dom})_i - (c + c_{dom})_j\right] \tag{4-16}$$

$$R\, d \ln K_p = \frac{\Delta H^\circ}{T^2} dT - \frac{\Delta V^\circ}{T} dP \tag{4-17}$$

$$\left(\frac{\partial \ln K_p}{\partial T}\right) = \frac{\Delta H^\circ}{RT^2} \tag{4-18}$$

$$d\left(\frac{1}{T}\right) = -\frac{dT}{T^2} \tag{4-19}$$

$$\frac{\partial \ln K_p}{\partial\left(\frac{1}{T}\right)} = \frac{\Delta H^\circ}{R} \tag{4-20}$$

$$\ln\frac{K_{p2}}{K_{p1}} = -\frac{\Delta H^\circ}{R}\left(\frac{1}{T_2} - \frac{1}{T_1}\right) \tag{4-21}$$

$$A = \frac{-\Delta H^\circ}{R} = \frac{\ln\frac{K_{p2}}{K_{p1}}}{\left(\frac{1}{T_2} - \frac{1}{T_1}\right)} \tag{4-22}$$

$$S_v = \frac{k_L}{h}\left(c - \frac{c_{air}}{H}\right) \tag{4-23}$$

$$k_L = \frac{k_g k_l}{k_g + \frac{k_l}{H}} \tag{4-24}$$

$$c_d = \left(\frac{1}{1+\frac{GH}{Q}}\right)c_u + \left(\frac{\frac{GH}{Q}}{1+\frac{GH}{Q}}\right)\frac{c_{air}}{H} \tag{4-25}$$

$$\frac{dc_{dc_{3+}}}{dt} = -k_{dc}c_{dc_{3+}} \tag{4-26}$$

$$\begin{aligned} \%OC &= 0.611 * WLOI_{375} \\ \%OC &= 0.528 * WLOI_{450} \end{aligned} \tag{4-27}$$

$$k_f = \frac{Q_{FE}\left(c_{T_{TD}} - c_{T_{RI}}\right)}{A_S(c + c_{dom})_s} \tag{4-28}$$

$$J_{D_t} = k_f c_{s_t} \tag{4-29}$$

$$J_{D_t} = \frac{\left|Q_{FE}(c_{T_{TID}} - c_{T_{RI}})\right|_{1998}}{A_s} \frac{c_{s_t}}{c_{s_{1998}}} \tag{4-30}$$

$$\frac{c_{s_t}}{c_{s_{1998}}} = \frac{f_d c_{T_{s_t}}}{f_d c_{T_{s_{1998}}}} \tag{4-31}$$

$$J_{D_t} = \frac{\left|Q_{FE}(c_{T_{TID}} - c_{T_{RI}})\right|_{1998}}{A_s} \frac{c_{T_{s_t}}}{c_{T_{s_{1998}}}} \tag{4-32}$$

$$\ln(H_T) = 22.57 - \frac{5753}{T} \tag{4-33}$$

$$k_l = \sqrt{\frac{D_w u}{h}} \tag{4-34}$$

$$D_w = \frac{13.26x10^{-5}}{\mu^{1.14}(\bar{V})^{0.589}} \tag{4-35}$$

$$\mu = 100\left[10^{\frac{1.301x10^3}{998.333+8.1855(T-20)+0.00585(T-20)^2}-3.30233}\right] \tag{4-36}$$

$$PCB_{3+} = 1.113*(Aroclor_{1016} + Aroclor_{1254}) \tag{4-37}$$

$$C_{avg_j} = \frac{\sum c_i l_i}{\sum l_i} \tag{4-38}$$

$$C_{avg_j} = \sum f_i c_i \tag{4-39}$$

$$W(t)_{total} = W(t)_{base} + W(t)_{resuspension} + W(t)_{pulse} \tag{4-40}$$

SECTION 5

$$BAF = \frac{v_L}{c}(1000) \tag{5-1}$$

$$BSAF = \frac{v_L}{r_{soc}} \tag{5-2}$$

$$\frac{dv_i}{dt} = K_{ui}c + \alpha_c \sum_{j=1}^{n} C_{ij}v_j - (K_i + G_i)v_i \tag{5-3}$$

$$K_u = \frac{k_{gl}A_{gl}}{W} \tag{5-4}$$

$$K_{uO_2} = \frac{R}{c_{O_2}} \tag{5-5}$$

$$K_{uO_2} = \frac{k_{glO_2}A_{gl}}{W} \tag{5-6}$$

$$K_u = \frac{k_{gl}}{k_{glO_2}}\frac{R}{c_{O_2}} \tag{5-7}$$

$$Gill\ exchange = K_u(c - \upsilon_B) \tag{5-8}$$

$$vm = v_B m_B + v_L m_L \tag{5-9}$$

$$\frac{dv_B m_B}{dt} = k_u mc + \alpha_C m \sum_{j=1}^{n} C_{ij}v_j - k_1 v_B m_B - k_2 v_B m_B + k_3 v_L m_L \tag{5-10}$$

$$\frac{dv_L m_L}{dt} = k_2 v_B m_B - k_3 v_L m_L \tag{5-11}$$

$$k_2 v_B m_B = k_3 v_L m_L \tag{5-12}$$

$$\frac{v_L}{v_B} = \pi_{LB} \tag{5-13}$$

$$\frac{dv_B m_B}{dt} = k_u mc + \alpha_c m \sum_{j=1}^{n} C_{ij} \upsilon_j - k_1 v_B m_B - \pi_{LB} k_3 m_L v_B + k_3 v_L m_L \tag{5-14}$$

$$\frac{dv_L m_L}{dt} = \pi_{LB} k_3 m_L v_B - k_3 m_L v_L \tag{5-15}$$

$$K_{gill} = K_u c_R v_B = K_u c_R \left(\frac{1}{f_B + \pi_{LB} f_L} \right) v \tag{5-16}$$

$$G = \frac{1}{W} \frac{dW}{dt} \tag{5-17}$$

$$R = \beta W^{\gamma} e^{pT} c_{act} \tag{5-18}$$

$$P_t = \lambda_o R_t + \left(\frac{W_{t+1} \lambda_{t+1} - W_t \lambda_t}{W_t} \right) \tag{5-19}$$

$$\lambda = 39.5 f_L + 20.08 f_P \tag{5-20}$$

$$C_{ij} = f_{ij} \frac{1}{\lambda_j} \frac{P_i}{\alpha_F} \tag{5-21}$$

$$f_{Diet,i} = f_{Diet,PMI} f_{PMI,i} + (1 - f_{Diet,PMI}) f_{BMI,i} \quad (5\text{-}22)$$

$$BSAF_e = BSAF\left(\frac{f_L}{\lambda_{inv}}\right) \quad (5\text{-}23)$$

$$\frac{\lambda_{inv}}{f_L} = 19.42 + 20.08\left(\frac{f_D}{f_L}\right) \quad (5\text{-}24)$$

$$L_{T,i} = \frac{L_T}{R_S} R_{S,i} \quad (5\text{-}25)$$

$$Dose = \frac{\alpha_c}{\alpha_F} P_i \sum_{j=1}^{n} f_{ij} \frac{\nu_j}{\lambda_j} \quad (5\text{-}26)$$

$$K_{gill} = K_u c_R \nu_B \approx \left(\frac{K_u c_R \nu}{f_L}\right) \sum_{c=1}^{n} \frac{f_c}{K_{OW,c}} \quad (5\text{-}27)$$